Summer School on
Micro- and Nano- structural characterization of materials
focused on electron microscopy

July 11-15, 2012, Thessaloniki, Greece

PROCEEDINGS

NetFISiC funded by the European Commission FP7 GA n.264613

netFISiC

ARISTOTLE UNIVERSITY OF THESSALONIKI

Table of contents

Lecturers' Presentations

Welcome and Introduction 4
Prof. Efstathios K. Polychroniadis
Aristotle University of Thessaloniki, Greece

Principles and design of the Transmission Electron Microscope (TEM) 12
Dr. Aria Andreadou
Aristotle University of Thessaloniki, Greece

Physical concepts of diffraction and electron crystallography 44
Dr. Alkyoni Mantzari
Aristotle University of Thessaloniki, Greece

Contrast and image formation in TEM 77
Dr. Andreas Delimitis
Centre for Research and Technology Hellas, Greece

High Resolution Electron Microscopy (HREM) 101
Prof. Christos Lioutas
Aristotle University of Thessaloniki, Greece

Application of transmission electron microscopy in solving some problems of shape memory alloys 120
Prof. Danuta Stróż
University of Silesia, Poland

Electron spectroscopy techniques for surface chemical analysis: XPS/AES/SAM 150
Prof. Panagiotis Patsalas
University of Ioannina, Greece

Highly performing semiconductor quantum dots, towards commercialization in optoelectronics and photovoltaics 177
Dr. Alexandros Stavrinadis
The Institute of Photonic Sciences, Spain

Micro- and nano-structural study of SiC, polytypes and stacking faults 180
Dr. Maya Marinova
University of Paris-Sud, France

SEM, basics and applications 214
Dr. Lori Nalbandian
Centre for Research and Technology Hellas, Greece

AFM, basics and applications 260
Prof. Nikos Frangis
Aristotle University of Thessaloniki, Greece

New techniques for nanocrystal structure determination by precession electron diffraction 281
Dr. Stavros Nicolopoulos
NanoMEGAS, Belgium

XRD for structural determination of materials, basics and applications 320
Prof. Tomasz Goryczka
University of Silesia, Poland

Electron microscopy for high-tech materials and structures: examples of work 359
Dr. Konstantinos P. Giannakopoulos
National Centre for Scientific Research "Demokritos", Greece

General introduction to European Funds 398
Cécile Le Duc
Lyon Ingénierie Projets, France

Dislocations in solids 412
Dr. Gabrielle Regula
Aix-Marseille University, France

Basic principles of optical investigation techniques 454
Prof. Jean Camassel
University of Montpellier 2, France

Optical investigation of as-grown stacking faults in SiC samples 489
Prof. Sandrine Juillaguet
University of Montpellier 2, France

SiC surfaces, interfaces and nanostructures: atomic structure, nanochemistry, and electronic & optical properties 516
Prof. Patrick Soukiassian
University of Paris-Sud, France

Evaluation and Closing 556
Prof. Efstathios K. Polychroniadis
Aristotle University of Thessaloniki, Greece

Participants' Presentations

Germanium incorporation inside 4H-SiC 8° off-axis seed 559
Kassem AlAssaad
Université Claude Bernard Lyon 1, France

Synthesis and characterization of SiC-SiO_2 core shell nanowires 565
Sathish Chander Dhanabalan
Istituto IMEM-CNR, Italy

Microstructural design of coatings produced by powder spraying 570
Dina Dudina
Russian Academy of Sciences, Russia

Heating efficacy of bimetallic FePt magnetic nanoparticles 572
Evangelos Makrygiannis
Aristotle University of Thessaloniki, Greece

Synthesis and characterization of silicon carbide nanowires 580
Marco Negri
Istituto IMEM-CNR, Italy


Summer School on
Micro- and Nano- structural characterization of materials
focused on electron microscopy
July 11-15, 2012, Thessaloniki, Greece
Welcome
NetFISiC funded by the European Commission FP7 GA n.264613
ARISTOTLE UNIVERSITY OF THESSALONIKI


Aristotle University of Thessaloniki
44 Departments
and numerous other units, laboratories, libraries, clinics, etc,
make it the largest university in Greece
http://www.auth.gr

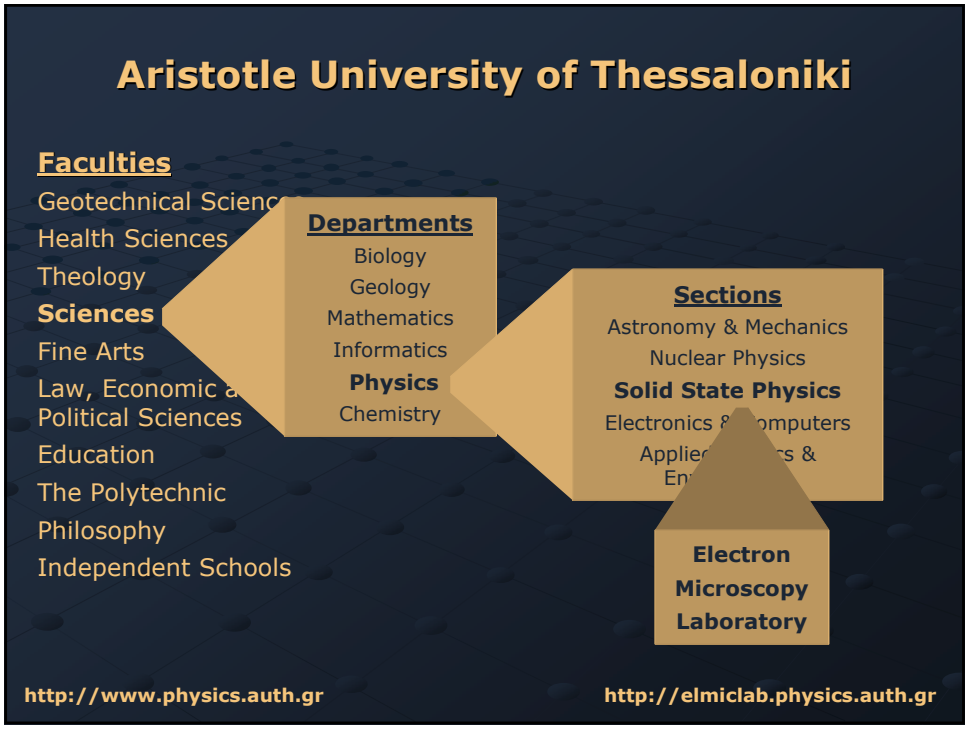
Aristotle University of Thessaloniki
Faculties
Geotechnical Scienc
Health Sciences
Theology
Sciences
Fine Arts
Law, Economic a
Political Sciences
Education
The Polytechnic
Philosophy
Independent Schools
Departments
Biology
Geology
Mathematics
Informatics
Physics
Chemistry
Sections
Astronomy & Mechanics
Nuclear Physics
Solid State Physics
Electronics &
Applie
En
Electron Microscopy Laboratory
http://www.physics.auth.gr
http://elmiclab.physics.auth.gr

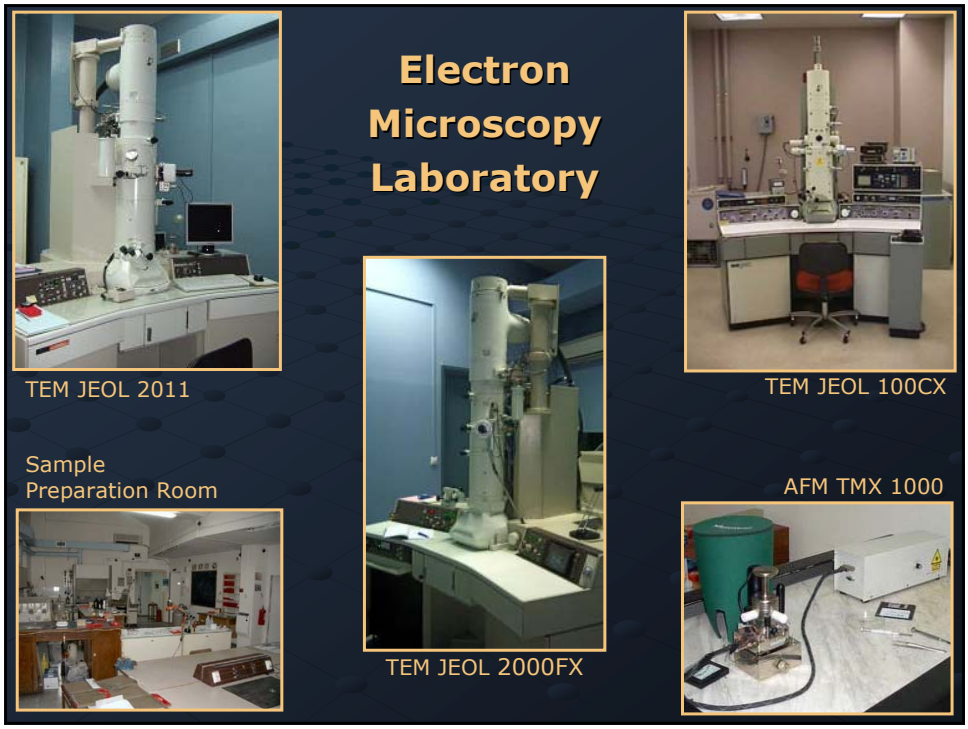
Electron Microscopy Laboratory
TEM JEOL 2011
TEM JEOL 100CX
Sample Preparation Room
TEM JEOL 2000FX
AFM TMX 1000

Electron Microscopy Laboratory

- oldest microscopy lab in Greece since 1965
- introduced microscopy to the Greek scientific community
- numerous Greek and European projects
- world class research work
  - in the last five years:
    - 100 journal papers
    - 240 conference announcements
    - 1200 third-party citations
- members today: 10 professors, 4 academic staff, numerous PhD candidates
- right now 13 PhD thesis are in progress

1933 Ernst Ruska

He built the first

electron microscope

Nobel Prize 1986

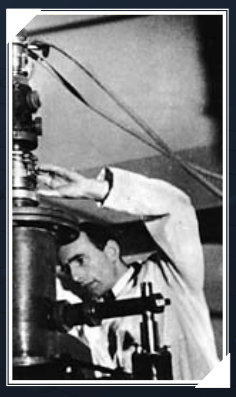

Ruska, E.: On a magnetic objective lens for the electron microscope. Dissertation of the Technological University of Berlin, submitted August 31, 1933.
Z. Physik 89, 90- 128 (1934), submitted March 5, 1934

Ruska, E.: On progress in the construction and performance of the magnetic electron microscope.
Z. Physik 87, 580-602 (1934), submitted December 12, 1933

1939 Siemens

The first commercial electron microscope

Borries, B.v., and Ruska, E.: Preliminary communication on advances in the construction and performance of the Ultramicroscope. Wiss. Veroeff. a.d. SiemensWerken 17, 99-106 (1938), submitted Feb 29, 1938

Borries, B.v., and Ruska, E.: An Ultramicroscope for industrial research. Naturwissenschaften 27, 577-582 (1939), submitted June 24, 1939

Resolution or Resolving power of a microscope

$$R.P. = \frac{0.61 \cdot \lambda_\alpha}{\mu \cdot \sin\alpha} = \frac{0.61 \cdot \lambda_\alpha}{NA}$$

- λ_α: wavelength of light in air
- μ: index of refraction of the object space
- α: half the aperture angle of the objective lens
- NA: numerical aperture of the objective lens

$$\lambda = \frac{h}{mv} \qquad \frac{1}{2}mv^2 = eV \qquad \Rightarrow \qquad \lambda = \frac{h}{\sqrt{2emV}} = \sqrt{\frac{1.5}{V(\text{Volts})}}\ \text{nm}$$

Resolution

	optical microscope	electron microscope
Wavelength	**750 nm (visible)**	**0.0037 nm (100kV)**
Resolution	**200 nm = 0.2μm**	**0.2 nm**

The best resolution achieved today with aberration-corrected TEM: **0.05 nm**

NetFISiC Joint Training Events

Kick-off meeting			Midterm meeting					Final meeting
2/11	12/11	3/12	7/12	9/12	5/13	10/13	4/14	9/14	10/14
	Training school 1		Training school 2		Workshop 2		Training school 3		Training courses
	Introduction to NetFISiC		**Structural characterization**		**Workshop 2 + Hetero-SiC'13**		**SiC Devices**		**Presentation & Job Fair**
	CNM **Barcelona** Introduction to SiC material and interfacial issues		**AUTH** **Thessaloniki** Microstructural charactrization of material focused on SiC		**NOVASiC,CNRS** **Nice** Heteroepitaxy, devices, surface preparation and industrial issues		**ACREO, LIU** **Stockholm** Devices based on SiC material		**IAP,INFINEON** **Erlangen** Young researchers meet industry
Meeting		Workshop 1		Tutorial day		Tutorial day		Tutorial day	
Kick-off meeting		**Power devices & R&D**		**Tutorial day + ECSCRM 2012**		**Tutorial day + ICSCRM 2013**		**Tutorial day + ECSCRM 2014**	
UCBL **Lyon** NETFISIC start, preparation of the recruitment procedure		**INFINEON** **Nuremberg** Basics on power devices and industrial R&D methods		**LIU, GIT** **St. Petersburg** SiC growth: from bulk to thin layers		**IAP, UCBL** **Japan** Advanced materials for high power electronic application		**CNR, GIT** **to be defined** Electrical and structural characte-rization of SiC at nanometer scale	


netFISiC
NetFISiC—Training NETwork on Functional Interfaces for SiC
Home >
NetFISiC - Training Network on Functional Interfaces for Silicon Carbide
Project abstract The main scientific objective of NetFISiC (ITN Marie Curie action) is to provide Silicon carbide material (of various polytypes) with improved and adequate functional interfaces for getting a step forward in electronic devices performance. Research efforts will be dedicated to solve the problems faced by important devices like MOSFET and Schottky diodes. Besides, some fundamental research will be performed both on the growth aspect and on new and innovating devices. Applications in high temperature, high power and harsh environment are targeted.
Based on this research program, the ambitious target of NeTFISiC partners is to train the next generation of researchers on various semiconductor related fields (such as physics, material science and engineering), taking the emerging SiC technology as an appropriate tool for study. This shall contribute to long-term strengthening of the European position on a technologically important semiconductor. 13 early stage researchers (ESR) and 2 experienced researchers (ER) will be recruited and trained within this network, on multi-disciplinary subjects like material growth, characterization and devices fabrication, with a particular focus on SiC.
For each of these young researchers, the individual training at the host institution will be enriched by specific shared training in other partner's institution and joint training activities (workshops, training schools, tutorial days) organized by the network. This shall give them the broad necessary background in order to understand the various aspect of semiconductor science.
! Upcoming Events!
Home
NetFiSic for all
NEtFiSic in a nutshell
Consortium
Fellows
Training Events
Vacant positions
Keydata
Links
Contact
Legal information
www.netfisic.eu


netFISiC

Scientific Program

The Basics of Transmission Electron Microscopy

Structural Imperfections and Applications

Other Techniques, New Achievements

Microstructural Study Using Optical Techniques

Management and Funding

Hands-on experimental training in the lab


Social Program
Welcome Reception
Thessaloniki City Tour
Excursion to the beaches of Chalkidiki and dinner by the sea
Excursion to the Archaeological Site of Vergina and lunch in a local tavern
Visit to the byzantine basilica of St. Demetrius
Goodbye Dinner in Thessaloniki


Summer School on
Micro- and Nano- structural characterization of materials
focused on electron microscopy
July 11-15, 2012, Thessaloniki, Greece
Have a nice stay in Thessaloniki and a nice time at the school

Principles and Design of Transmission Electron Microscope (TEM)

Dr. Ariadne Andreadou
Transmission Electron Microscopy Laboratory
Solid State Physics Section
Department of Physics
Aristotle University of Thessaloniki

fppt.com

Electron Microscope vs. Optical Microscope

(first one built in 1931 by Ruska and Knoll) (Leeuwenhoek in 17th century)

Electron vs. Photon

Electron: charged, has rest mass, not visible

Photon: neutral, has no rest mass, visible at the wavelength ~ 400 nm-760 nm.

Because of these differences, the microscope construction will also be different

What is the common property?

fppt.com

Comparison of EM and LM

A. Similarities (Arrangement and function of components are similar)

1) Illumination system: produces required radiation and directs it onto the specimen. Consists of a source, which emits the radiation, and a condenser lens, which focuses the illuminating beam (allowing variations of intensity to be made) on the specimen.

2) Specimen stage: situated between the illumination and imaging systems.

3) Imaging system: Lenses which together produce the final magnified image of the specimen. Consists of i) an objective lens which focuses the beam after it passes through the specimen and forms an intermediate image of the specimen and ii) the projector lens(es) which magnifies a portion of the intermediate image to form the final image.

4) Image recording system: Converts the radiation into a permanent image (typically on a photographic emulsion) that can be viewed.

fppt.com

Comparison of EM and LM

B. Differences

1) *optical lenses* made of glass with fixed focal lengths
magnetic lenses are constructed with ferromagnetic materials and focal length may be varied
2) The LM has a small depth of field, thus different focal levels can be seen in the specimen. The large (relative) depth of field in the TEM means that the entire (thin) specimen is in focus simultaneously.
3) Mechanisms of image formation vary (phase and amplitude contrast).
4) TEM is operated at high vacuum
5) TEMs can achieve higher magnification and better resolution than LMs.
6) Price tag!!! (~4$ for each electron volt of energy in the beam 100000-400000eV)

fppt.com

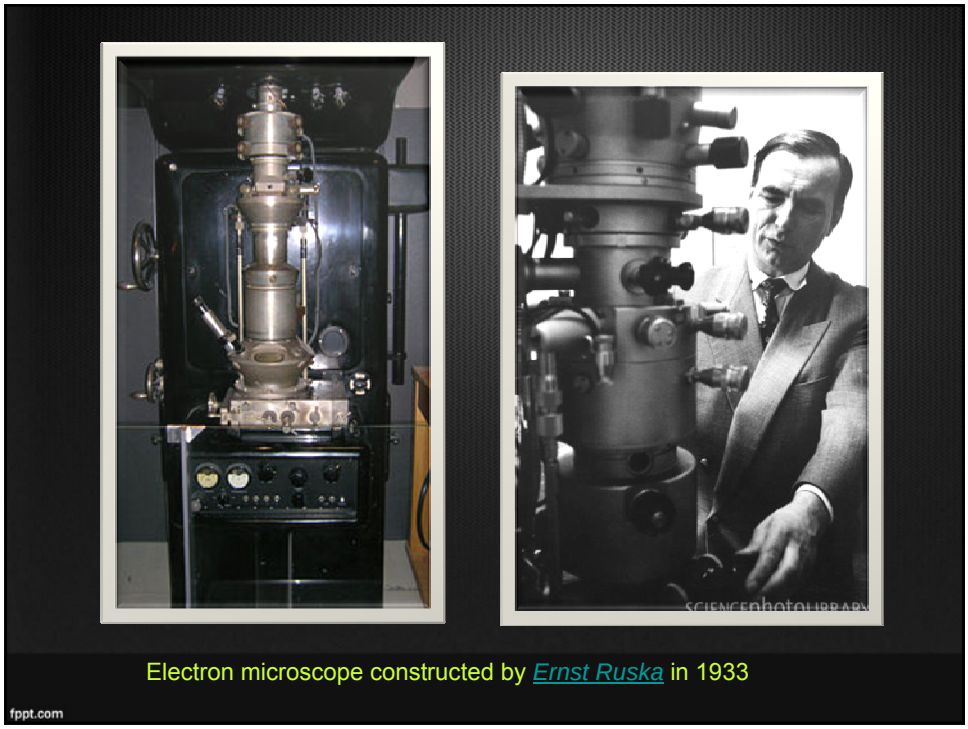
Electron microscope constructed by Ernst Ruska in 1933
fppt.com

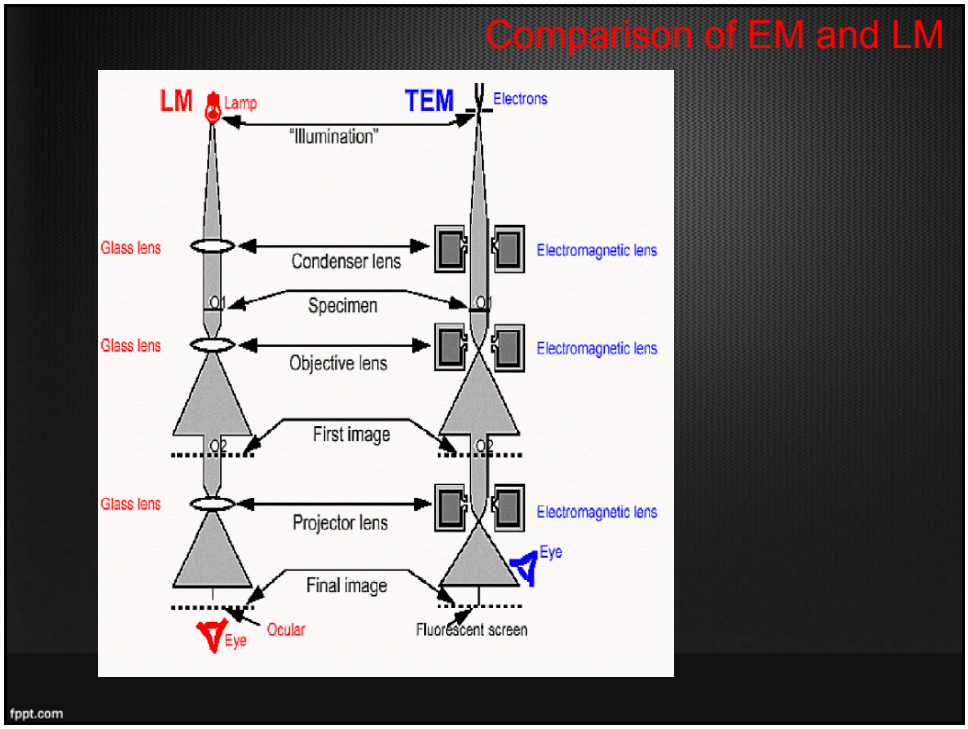
Comparison of EM and LM
LM
Lamp
TEM
Electrons
"Illumination"
Glass lens
Condenser lens
Electromagnetic lens
Specimen
Glass lens
Objective lens
Electromagnetic lens
First image
Glass lens
Projector lens
Electromagnetic lens
Eye
Final image
Eye
Ocular
Fluorescent screen
fppt.com

Concept of Resolution of a microscope

Resolving power: the smallest distance between two points that we can resolve

eyes resolution~0.1-0.2mm

Rayleigh criterion → $0.61\lambda/NA$

λ=wavelength of radiation

N.A. is the numerical aperture = $n(\sin\alpha)$~1

n: refractive index

α: semi-angle of collection of magnifying lens

LM resolution~300nm

~1000 atom diameters

De Broglie's eq → $\lambda \sim 1.22/E^{1/2}$

the electron's wavelength is related to their energy

TEM : 100keV e^- ⇨ λ~0.004nm

< atom diameter

There are other factors that limit the resolution!

fppt.com

The resolution is proportional to the wavelength!

Electron equivalent wavelength and accelerating voltage

The dualism wave/particle is quantified by the *De Broglie* equation:

$\lambda = h/p = h/mv$

λ : wavelength; h: Planck constant; p: momentum

The energy of accelerate electrons is equal to their kinetic energy:

$E = eV = m_0v^2/2$

V: acceleration voltage

e / m_0 / v: charge / rest mass / velocity of the electron

These equations can be combined to calculate the wave length of an electron with a certain energy:

$p = m_0v = (2m_0eV)^{1/2}$

$\lambda = h / (2m_0eV)^{1/2}$ ($\approx 1.22 / V^{1/2}$ nm)

At the acceleration voltages used in TEM, *relativistic effects* have to be taken into account (e.g. E>100 keV)

$\lambda = h / [2m_0eV\,(1 + eV/2m_0/c^2)]^{1/2}$

fppt.com

Resolution of a microscope

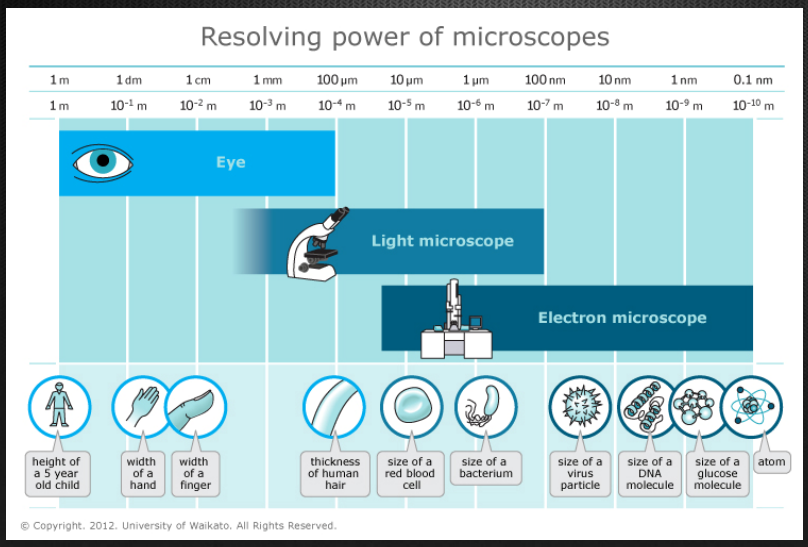

fppt.com

TEM Specimen Preparation

Specimen preparation is an important aspect of the transmission electron microscopy (TEM)

Objective: to make a TEM specimen which is

- representative of the material studied
- thin enough → electron transparent → <100nm (for HRTEM <50nm)

Methods: depend on both the type of material and the information to obtain.

fppt.com

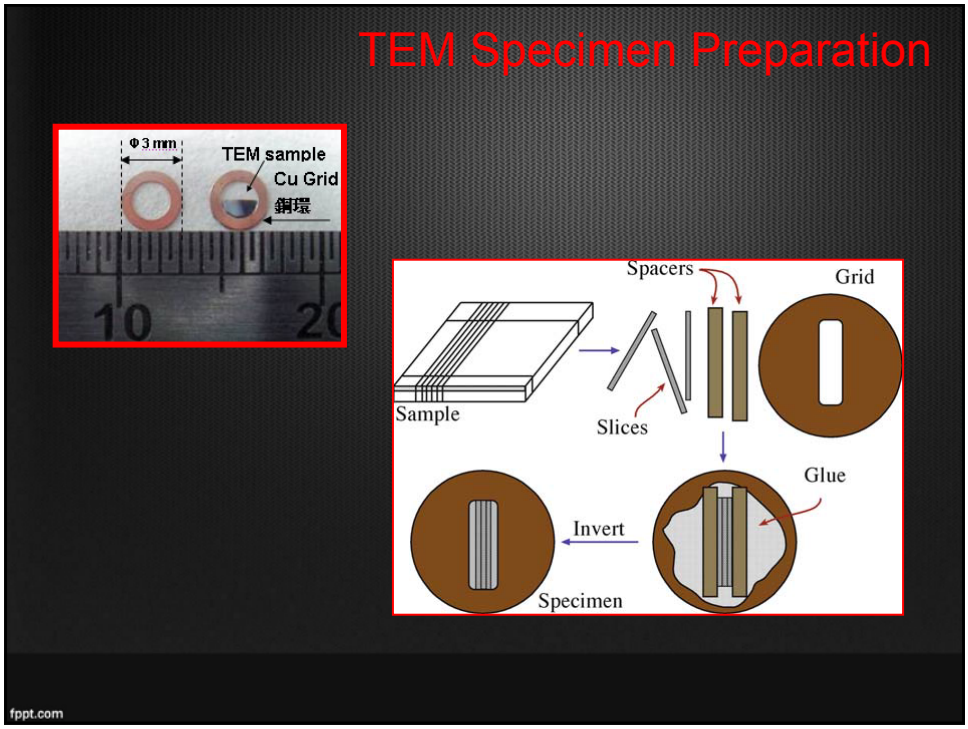
TEM Specimen Preparation
Φ3 mm
TEM sample
Cu Grid
銅環
10
Spacers
Grid
Sample
Slices
Glue
Invert
Specimen
fppt.com


Sample Holders
A
B
fppt.com

Sample Holders

- Once inside the microscope, the specimen sits right inside the objective lens and must therefore be small - typically less than 3 mm in diameter;
- It is necessary to align the specimen very accurately with the electron beam to achieve the required images;
- Common specimen holders allow rotation about two horizontal axes, along with lateral movement. Other holders might include heating elements or nano-indenters to deform the specimen as it is imaged.

fppt.com

electron-specimen interaction

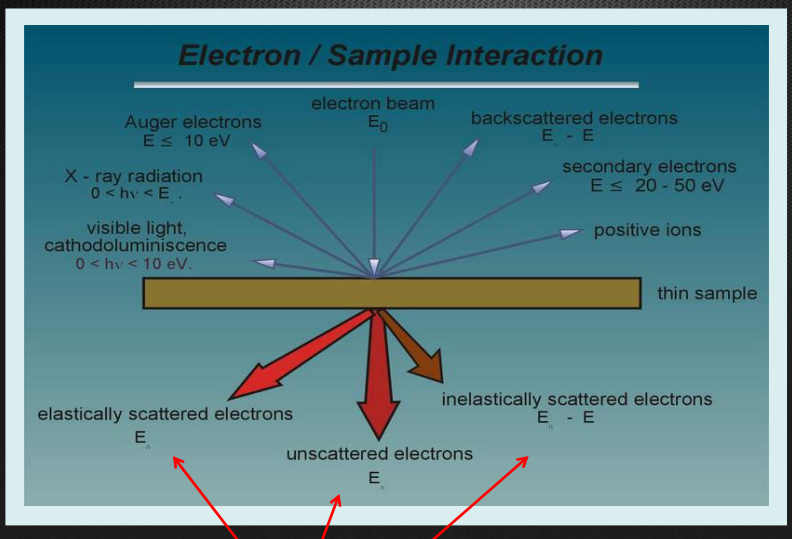

transmitted electrons

fppt.com

Electron-specimen interaction

electrons → "ionizing radiation"
→ wide range of secondary signals

Analytical Electron Microscopy (AEM)

- X-ray Energy Dispersive Spectrometry (XEDS)
- Electron Energy Loss Spectrometry (EELS)
- Scanning Transmission Electron Microscopy (STEM)

Methods	Information
EDXS	qualitative and quantitative element analysis
EELS	qualitative and quantitative element analysis. Bonding situation (energy-loss near-edge structure ELNES), coordination and interatomic distances (extended energy-loss fine structure EXELFS)
ESI	element distribution
STEM	element distribution

• Unscattered Electrons

Source

Incident electrons which are transmitted through the thin specimen without any interaction occurring inside the specimen.

Utilization

The transmission of unscattered electrons is inversely proportional to the specimen thickness. Areas of the specimen that are thicker will have fewer transmitted unscattered electrons and so will appear darker, conversely the thinner areas will have more transmitted and thus will appear lighter.

- **Elasticity Scattered electrons**

Source

Incident electrons that are scattered (deflected from their original path) by atoms in the specimen in an elastic fashion (no loss of energy). These scattered electrons are then transmitted through the remaining portions of the specimen.

Utilization

All electrons follow Bragg's Law and thus are scattered according to ml=2*d*sin q (angle of scattering). All incident electrons have the same energy (thus wavelength) and enter the specimen normal to its surface. All incidents that are scattered by the same atomic spacing will be scattered by the same angle. These "similar angle" scattered electrons can be collated using magnetic lenses to form a pattern of spots; *each spot corresponding to a specific atomic spacing (a plane)*. This pattern can then yield information about the orientation, atomic arrangements and phases present in the area being examined.

fppt.com

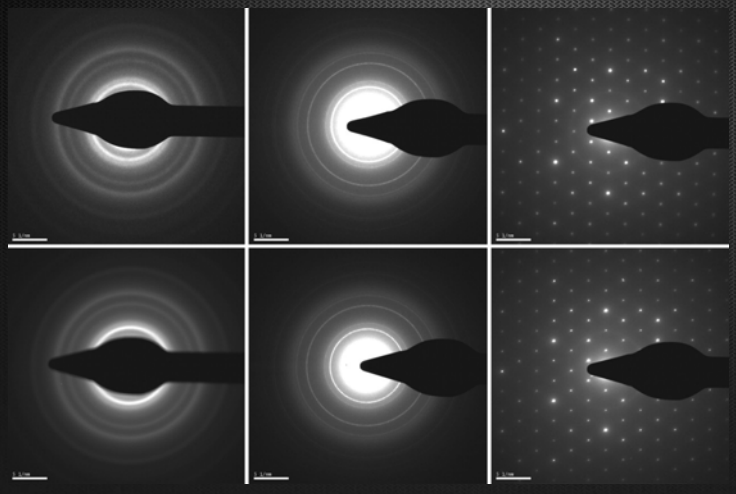

The diffraction pattern is highly dependable on the structure of the specimen

Dr. A. Mantzari will have a lecture dedicated to diffraction

fppt.com

• Inelastically Scattered Electrons

Source

Incident electrons that interact with specimen atoms in a inelastic fashion, loosing energy during the interaction. These electrons are then transmitted trough the rest of the specimen

Utilization

Inelastically scattered electrons can be utilized two ways

Electron Energy Loss Spectroscopy (EELS): The inelastic loss of energy by the incident electrons is characteristic of the elements that were interacted with. These energies are unique to each bonding state of each element and thus can be used to extract both compositional and bonding (i.e. oxidation state) information on the specimen region being examined.

Kikuchi Bands: Bands of alternating light and dark lines that are formed by inelastic scattering interactions that are related to atomic spacings in the specimen. These bands can be either measured (their width is inversely proportional to atomic spacing) or "followed" like a roadmap to the "real" elasticity scattered electron pattern.

fppt.com

Specimen interaction volume

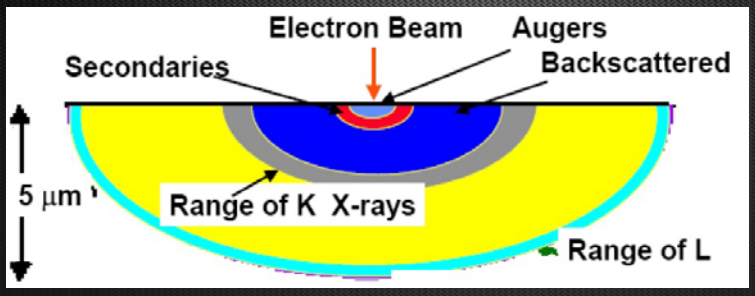

- Atomic number of the material being examined; higher atomic number materials absorb or stop more electrons and so have a smaller interaction volume.
- Accelerating voltage being used; higher voltages penetrate further into the sample and generate larger interaction volumes
- Angle of incidence for the electron beam; the greater the angle (further from normal) the smaller the volume

fppt.com

The *Depth of Field* Concept

Depth of Field: how much of the object we are looking remains "in focus" at the same time

- like *resolution*, this property is governed by the lenses
- the best electron lens is not a good one
- to overcome the problem we use *apertures*
  a. *narrowing the beam down*
  b. *increasing the "depth of focus"*

Depth of Field → refers to the specimen

Depth of Focus → refers to the image

fppt.com

Types of Electron Microscope

- **Transmission Electron Microscope** (TEM) uses a wide beam of electrons passing through a thin sliced specimen to form an image. This microscope is analogous to a standard upright or inverted light microscope
- **Scanning Electron Microscope** (SEM) uses focused beam of electrons scanning over the surface of thick or thin specimens. Images are produced one spot at a time in a grid-like raster pattern.
- **Scanning Transmission Electron Microscope** (STEM) uses a focused beam of electrons scanning through a thin sliced specimen to form an image. The STEM looks like a TEM but produces images as does an SEM (one spot at a time). It is most commonly used for elemental analysis of samples.

fppt.com

Top to Bottom

- Electron gun
  - *Electron Source*
  - *Electron Accelerator*
  - *Gun alignment Deflection Coils*
- Condenser Lenses
- Condenser Aperture
- Alignment (Scan) Coils

Illumination System

- Objective Lens
- Lens Stigmators
- More Apertures for Microscopy
- Deflector Coils (Tilt Scan)

Image Forming

- Projector Lens
- Screen/Camera/Detectors

Image Process

- Vaccum System

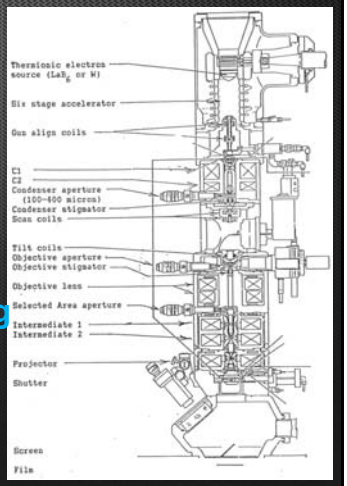

fppt.com

High Vacuum

electron beam must be generated and used in a high vacuum of 10^{-4} mbars or less.

This ensures that:

- The electrons are not deflected by gas molecules;
- The filament and specimen are not contaminated.

Three different pumps are used for that reason.

fppt.com

pumps

Rotary Pumps (RP)
Used for preliminary evacuation and to back up the other pumps.
It is a simple mechanical pump that sweeps gas out using rotating vanes immersed in an oil tank.
This reduces air pressure to about 10^{-1} to 10^{-3} mbars.

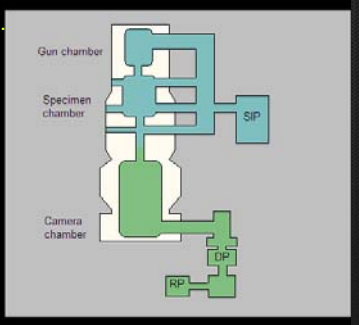

Diffusion Pump (DP)
Works by heating oil or mercury until it gives off vapor.
Gas molecules from the microscope diffuse into a fast moving stream of vapor and are 'swept away'.
This reduces air pressure to about 10^{-4} to 10^{-7} mbars.

Sputter Ion Pump (SIP)
Ion pumps act by attracting ionised gases towards an electrode.
They generate an oil-free, ultra high vacuum of < 10^{-7} mbars.

fppt.com

What does a TEM look like?

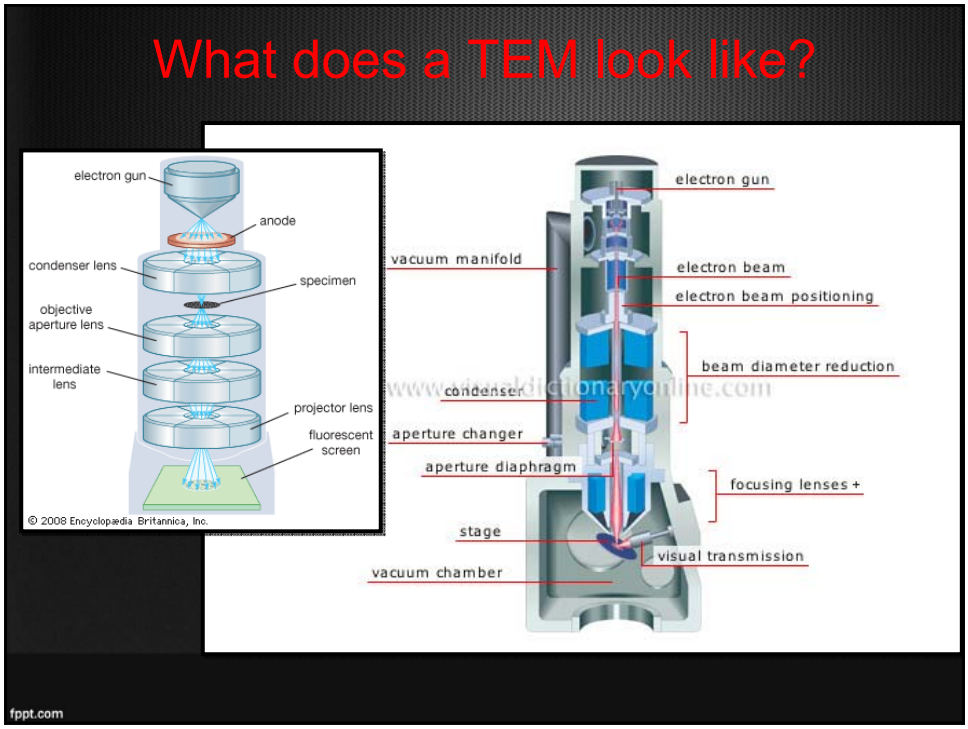
What does a TEM look like?
electron gun
anode
condenser lens
specimen
objective aperture lens
intermediate lens
projector lens
fluorescent screen
© 2008 Encyclopædia Britannica, Inc.
electron gun
vacuum manifold
electron beam
electron beam positioning
beam diameter reduction
condenser
aperture changer
aperture diaphragm
focusing lenses +
stage
visual transmission
vacuum chamber
fppt.com

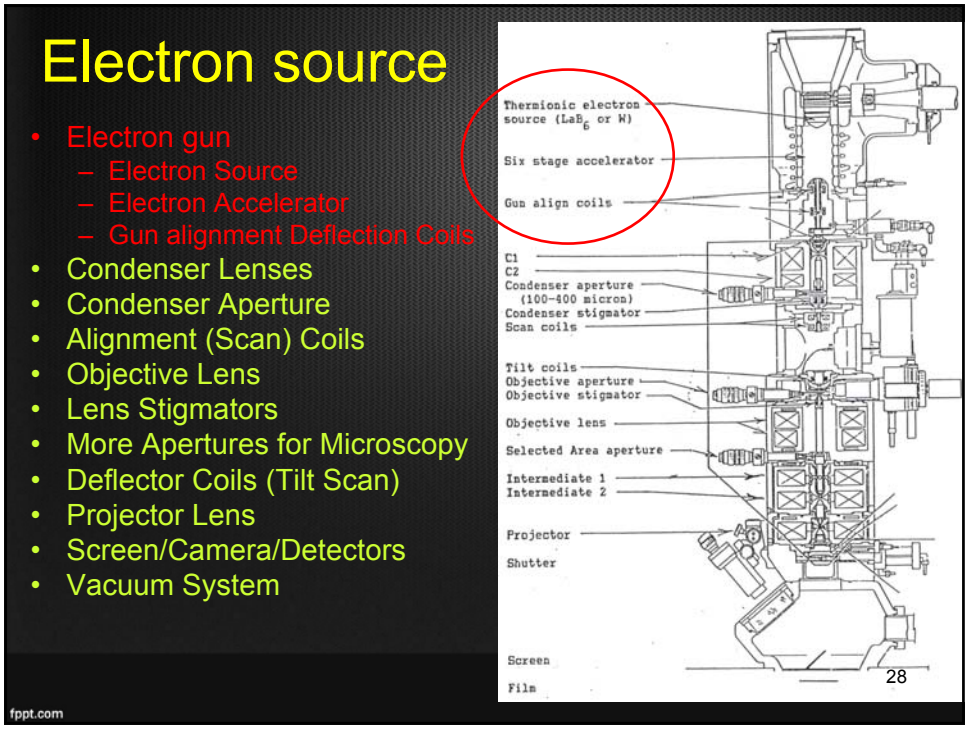
Electron source
Electron gun
Electron Source
Electron Accelerator
Gun alignment Deflection Coils
Condenser Lenses
Condenser Aperture
Alignment (Scan) Coils
Objective Lens
Lens Stigmators
More Apertures for Microscopy
Deflector Coils (Tilt Scan)
Projector Lens
Screen/Camera/Detectors
Vacuum System
Thermionic electron source (LaB6 or W)
Six stage accelerator
Gun align coils
C1
C2
Condenser aperture (100-400 micron)
Condenser stigmator
Scan coils
Tilt coils
Objective aperture
Objective stigmator
Objective lens
Selected Area aperture
Intermediate 1
Intermediate 2
Projector
Shutter
Screen
Film
28
fppt.com

Electron Gun

Thermionic Emission

W-wire hairpin

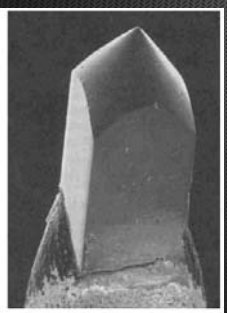

LaB_6 oriented single crystal

Field Emission

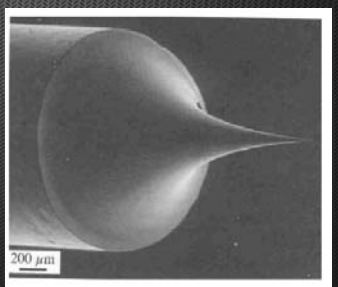

Electrochemically polished textured W wire

Field emission guns are around twice as expensive as thermionic electron guns, and must be used under ultra-high vacuum conditions.
They are favorable for applications in which a high brightness and low energy-spread of incident electrons is needed. (eg. HRTEM, FEG.)

29

fppt.com

Electron Gun Types

Heated tungsten (W)
A heated filament made from the metal tungsten. Much in the way that an incandescent lightbulb works, the high voltage that is fed through the filament causes electrons to be kicked off the filament. The amount of energy required is known as the work function.

Lanthanum hexaboride (LaB_6)
The LaB_6 filament is also a thermal filament. However, its work function is lower than for a tungsten filament, so it is more efficient.

Tungsten field emission gun (FEG)
The FEG gun is not a thermal filament. Instead, electrons are expelled by applying a very powerful electric field very close to the filament tip. The size and proximity of the electric field to the electron reservoir in the filament causes the electrons to tunnel out of the reservoir.

W hairpin

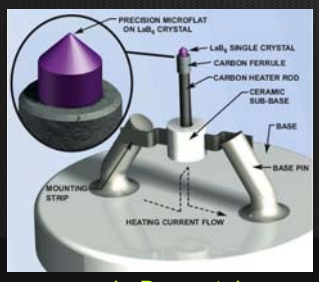

LaB_6 crystal

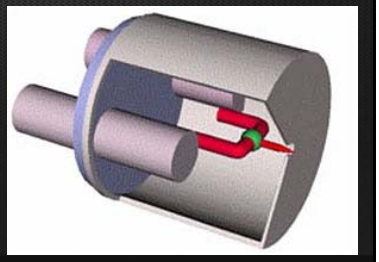

FEG

fppt.com

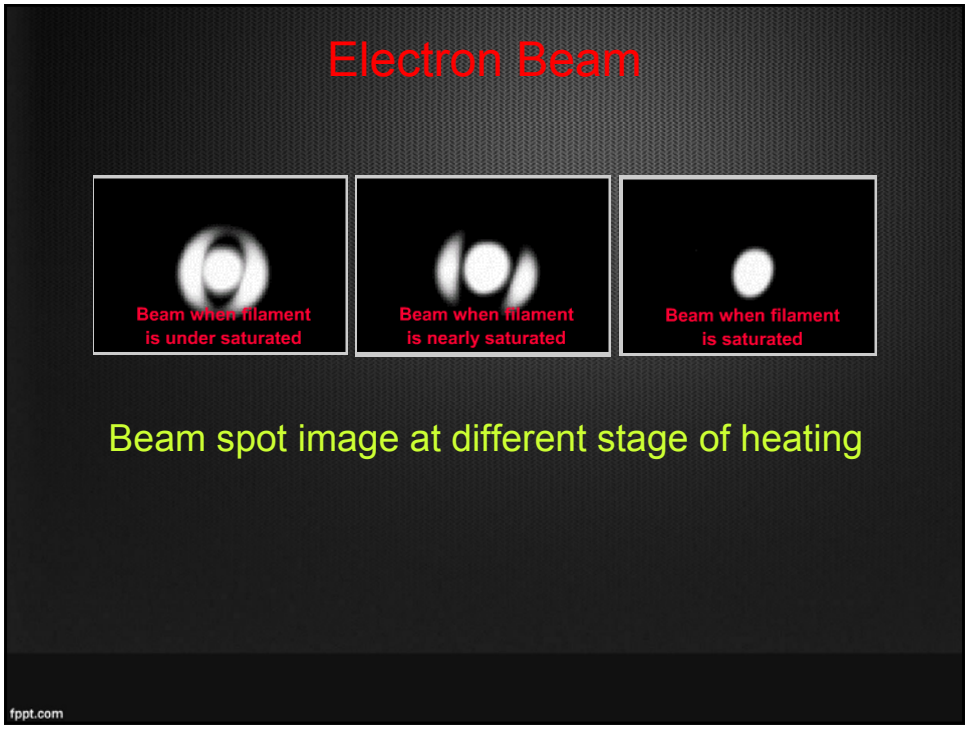
Electron Beam
Beam when filament is under saturated
Beam when filament is nearly saturated
Beam when filament is saturated
Beam spot image at different stage of heating
fppt.com

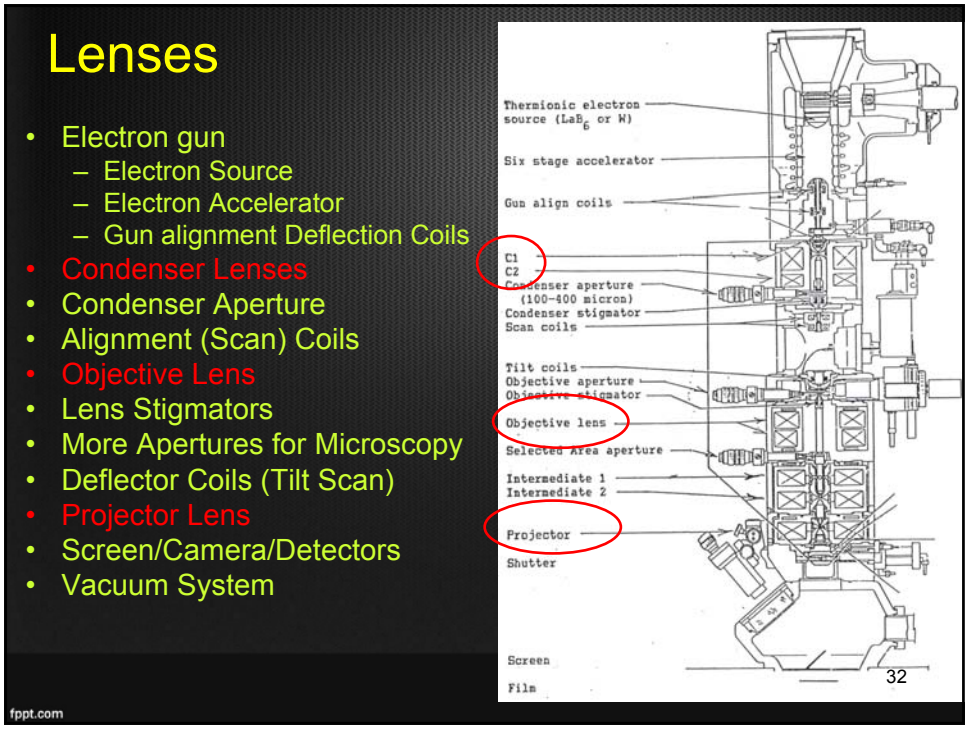
Lenses
• Electron gun
– Electron Source
– Electron Accelerator
– Gun alignment Deflection Coils
• Condenser Lenses
• Condenser Aperture
• Alignment (Scan) Coils
• Objective Lens
• Lens Stigmators
• More Apertures for Microscopy
• Deflector Coils (Tilt Scan)
• Projector Lens
• Screen/Camera/Detectors
• Vacuum System
Thermionic electron source (LaB6 or W)
Six stage accelerator
Gun align coils
C1
C2
Condenser aperture (100-400 micron)
Condenser stigmator
Scan coils
Tilt coils
Objective aperture
Objective stigmator
Objective lens
Selected Area aperture
Intermediate 1
Intermediate 2
Projector
Shutter
Screen
Film
32
fppt.com

Electromagnetic lens

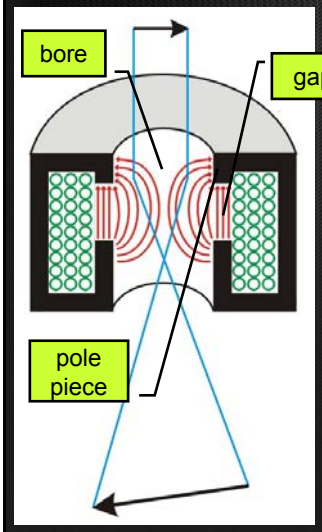

- A magnetic lens consists of a coil of copper wires inside the iron pole pieces. A current through the coils creates a magnetic field in the bore of the pole pieces;
- The rotationally symmetric magnetic field is inhomogeneous
- Electrons close to the center are less strongly deflected than those passing the lens far from the axis. The overall effect is that a beam of parallel electrons is focused into a spot (cross-over);
- The focusing effect of a magnetic lens therefore increases with the magnetic field B, which can be controlled via the current flowing through the coils;
- The resulting force **F** is perpendicular **v** and **B**. This leads to a helical trajectory of the electrons and to the magnetic rotation (image is rotated in respect of the object).

fppt.com

Electromagnetic lens

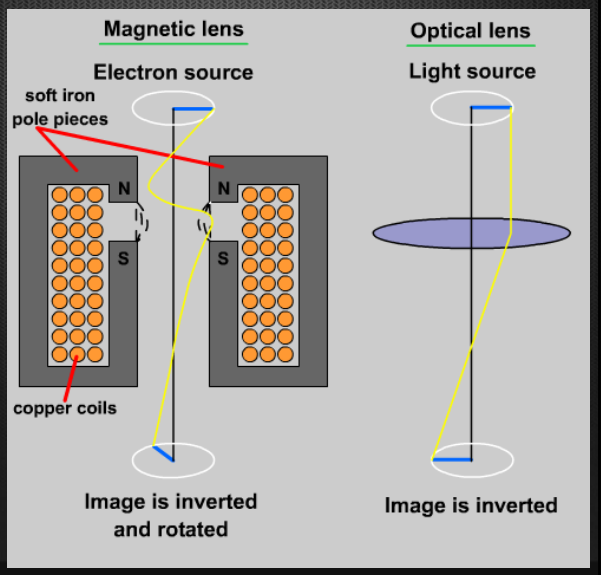

fppt.com

Apertures

- Electron gun
  - Electron Source
  - Electron Accelerator
  - Gun alignment Deflection Coils
- Condenser Lenses
- Condenser Aperture
- Alignment (Scan) Coils
- Objective Lens
- Lens Stigmators
- More Apertures for Microscopy
- Deflector Coils (Tilt Scan)
- Projector Lens
- Screen/Camera/Detectors
- Vacuum System

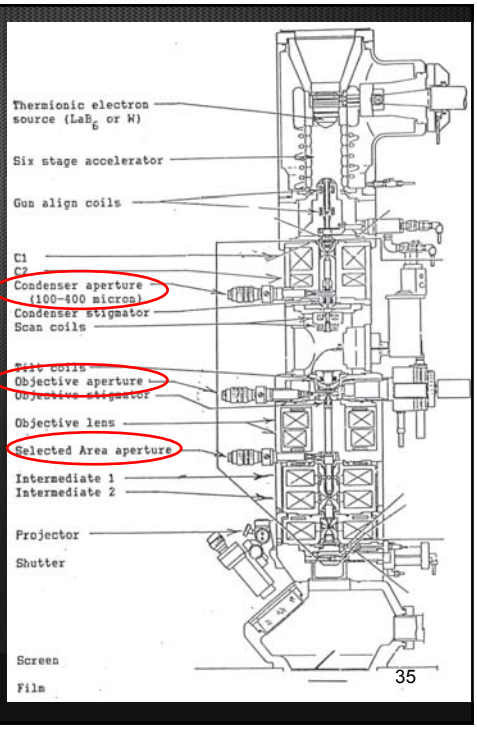

35

fppt.com

Apertures and Diaphragms

- Aperture = hole
  - allows radiation through
- Diaphragm = blocking material
  - stops radiation from passing

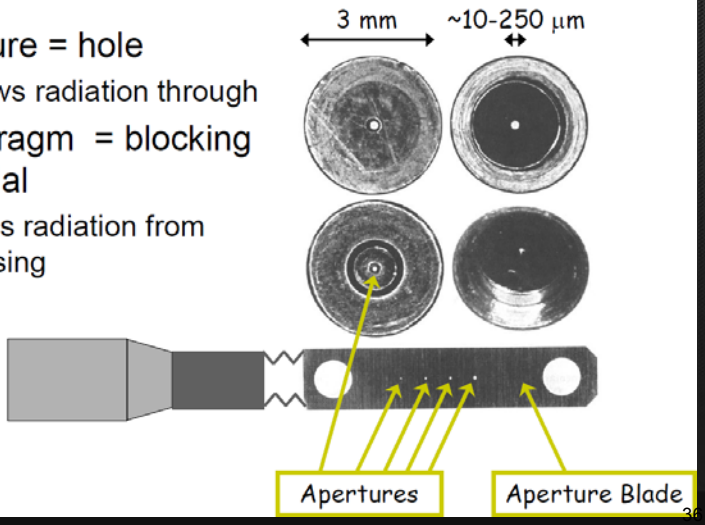

fppt.com

Lens and Apertures

- A lens takes the radiation emanating from a point (the source) and brings it together at another point (the image).
- Same for light or charged particles, although e- lenses use a magnetic field instead of glass.
- An aperture blocks some of this radiation.
- Useful because of *aberrations*, or to create contrast.

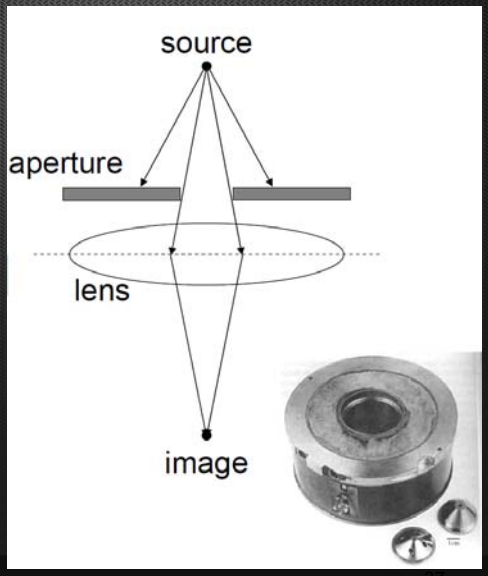

37

fppt.com

Illumination System

- Electron gun
- Illumination Systems
  - Condenser Lenses
  - Condenser Aperture
  - Alignment (Scan) Coils
- Objective Lens
- Lens Stigmators
- More Apertures for Microscopy
- Deflector Coils (Tilt Scan)
- Projector Lens
- Screen/Camera/Detectors
- Vacuum System

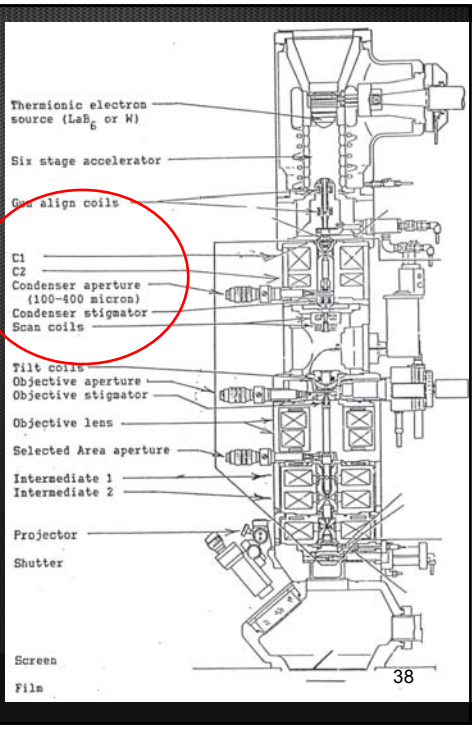

38

fppt.com

Condenser-lens system

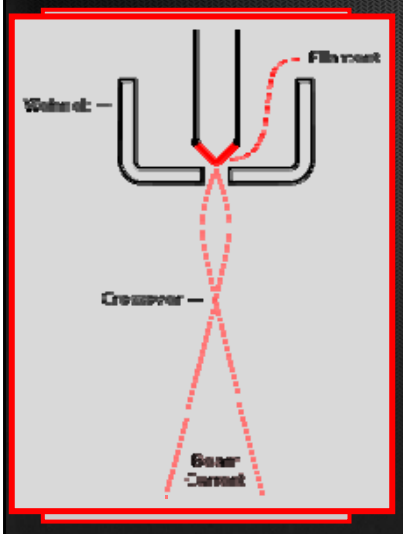

- The Wehnelt (or 2nd anode in a FEG) focuses the beam to a crossover which is accelerated down the column;
- The first condenser de-magnifies the crossover to give a smaller point source – this is referred to as C_1 or spot size;
- The second condenser lens (C2) is used to either converge or spread the beam of illumination on the sample;
- A condenser aperture is placed in the beam path to remove electrons far from the optic axis which would reduce resolution;
- The smaller the aperture the better the resolution, but there is an associated decrease in brightness – need to compromise.

fppt.com

Image Forming System

- Electron gun
- Illuminations System
- Image Forming System
  - Objective Lens
  - Lens Stigmators
  - Tilt Coils
  - Samples
  - Selected Area and Objective Apertures
- Projector Lens
- Screen/Camera/Detectors
- Vacuum System

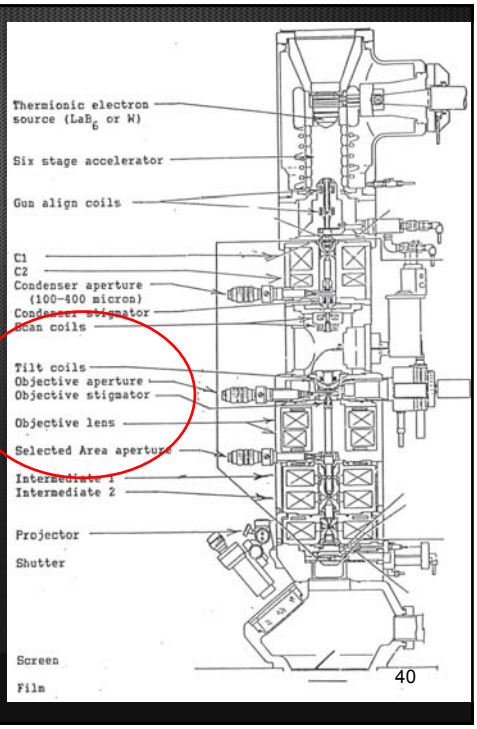

40

fppt.com

Objective Lens

- By far the strongest lens in electron microscope;
- Its resolution limit defines the resolution of the whole microscope;
- The objective lens forms an inverted *initial image*, which is subsequently magnified;
- In the back focal plane of the objective lens a *diffraction pattern* is formed. The objective aperture can be inserted here.

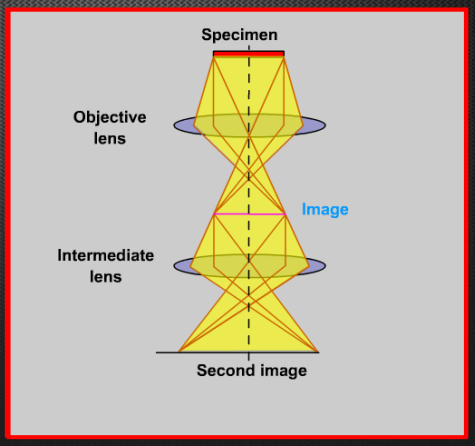

41

fppt.com

Objective Lens

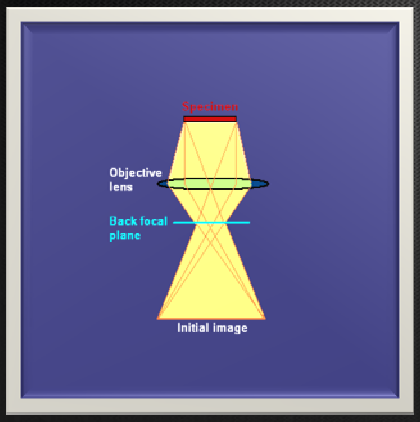

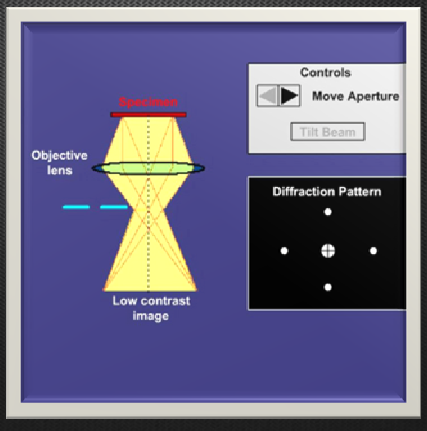

fppt.com

TEM imaging modes

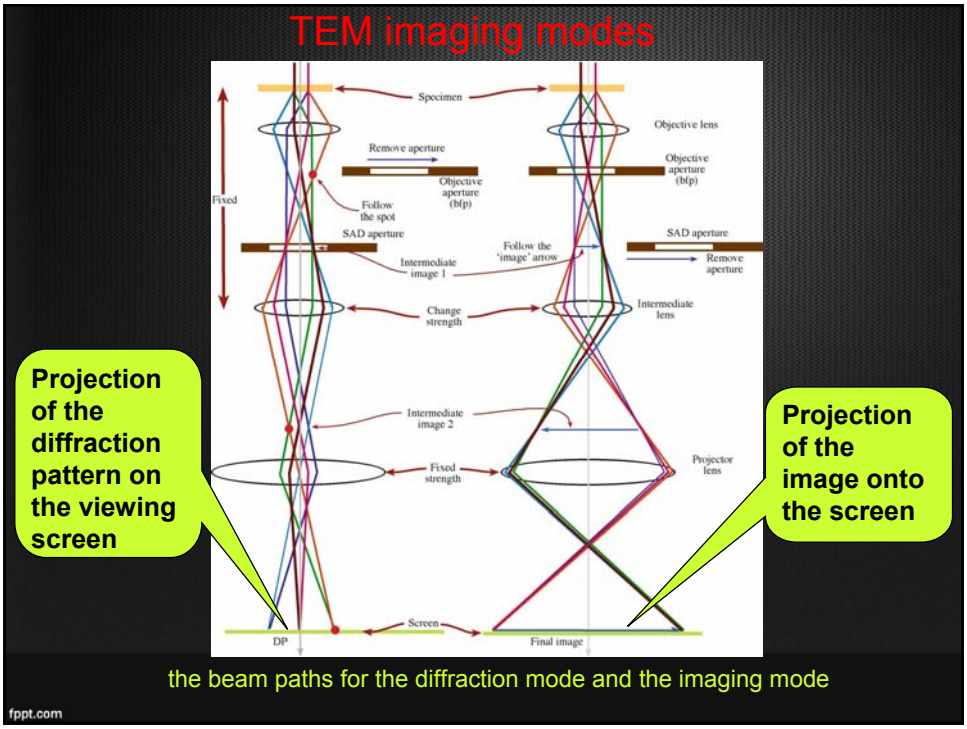

the beam paths for the diffraction mode and the imaging mode

fppt.com

TEM imaging modes

in order to investigate an electron microscope image, we first observe the DP;

by inserting an aperture (selected area aperture), adjusting the lenses, and focusing on a specific area that we are interested in, we will get a DP of the area;

this kind of observation mode is the selected area diffraction;

then by passing the transmitted beam or one of the diffracted beams through a selected aperture and changing to the imaging mode, we can get the image with enhanced contrast.

fppt.com

Image Forming System

we either form an image using the central spot, or we use some or all of the scattered electrons;

how ⇨ by inserting an aperture into the back focal plane of the objective lens;

thus, blocking out most of the diffraction pattern except that which is visible through the aperture;

if the direct beam is selected we call the resultant image a *bright-field image*, and if we select scattered electrons of any form, we call it a *dark-field image*.

fppt.com

Bright-field and Dark-field imaging

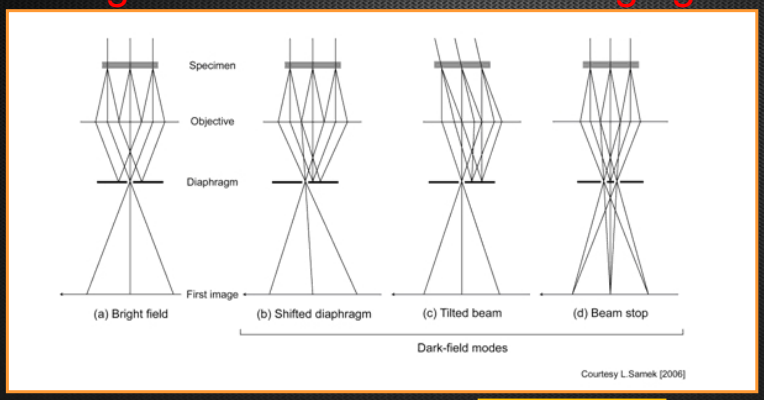

Bright field (BF)

Dark field (DF)

fppt.com

Deflectors

- Electron gun
  - Electron Source
  - Electron Accelerator
  - Gun alignment Deflection Coils
- Condenser Lenses
- Condenser Aperture
- Alignment (Scan) Coils
- Objective Lens
- Lens Stigmators
- More Apertures for Microscopy
- Deflector Coils (Tilt Scan)
- Projector Lens
- Screen/Camera/Detectors
- Vacuum System

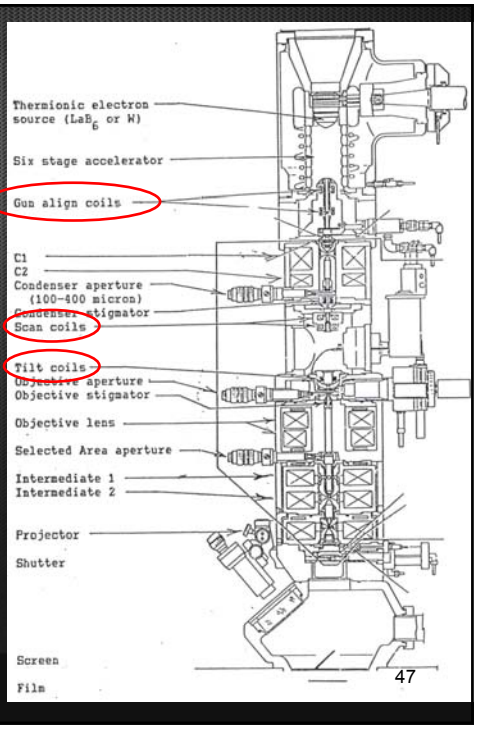

47

fppt.com

Deflectors

- Actually two sets of magnetic coils to:
  - shift / translate beam from side of side
  - tilt it / change beam angle
- Used for:
  - aligning the beam with the optic axis or minimum aberration path
  - adjusting which part of the sample is illuminated at what angle / scanning the beam
  - moving the image onto a particular detector

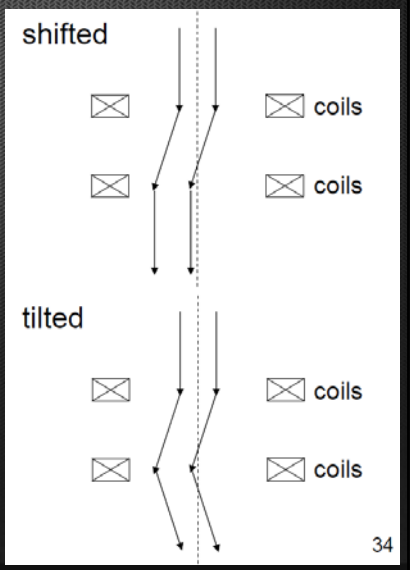

48

fppt.com

Stigmators

- Electron gun
  - Electron Source
  - Electron Accelerator
  - Gun alignment Deflection Coils
- Condenser Lenses
- Condenser Aperture
- Alignment (Scan) Coils
- Objective Lens
- Lens Stigmators
- More Apertures for Microscopy
- Deflector Coils (Tilt Scan)
- Projector Lens
- Screen/Camera/Detectors
- Vacuum System

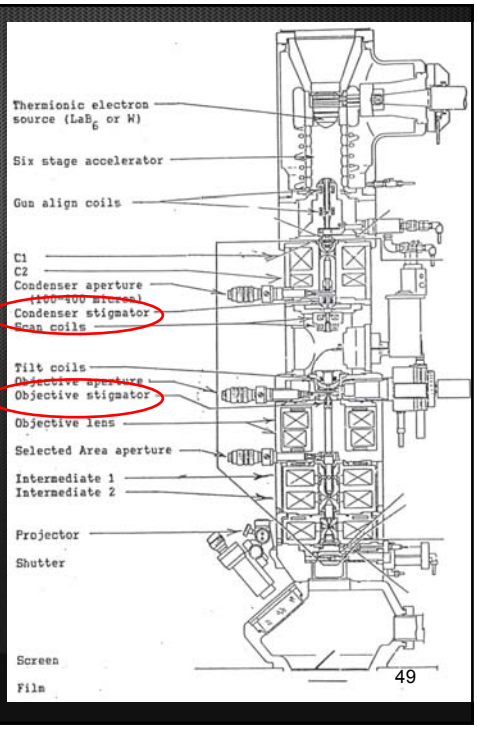

49

fppt.com

Stigmators

- Astigmatism is a directional defocus: image features are in focus in one direction, but out of focus in the perpendicular direction;
- Astigmatism occurs when the electrons sense a non-uniform magnetic field as they spiral round the optic axis;
- This defect arises because we can't machine the soft-iron polepieces to be perfectly cylindrically symmetrical down the bore;
- Common imperfection (aberration) of electron lenses;
- Correctable with quadrapole lenses called stigmators.

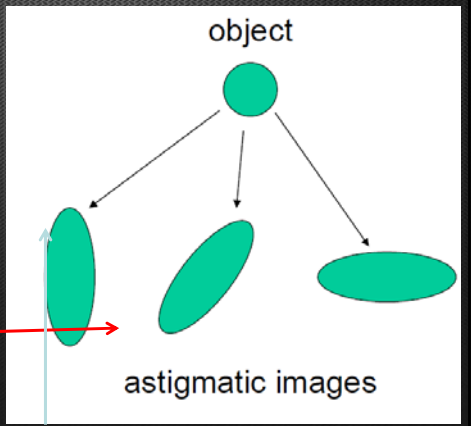

fppt.com

Projector System

- Electron gun
- Illumination System
- Image Formation System
  - 2-5 additional lenses below the objective lens
  - Mostly there to magnify, magnify and magnify
  - also control whether a diffraction pattern or image appears on the detector
- Vacuum System

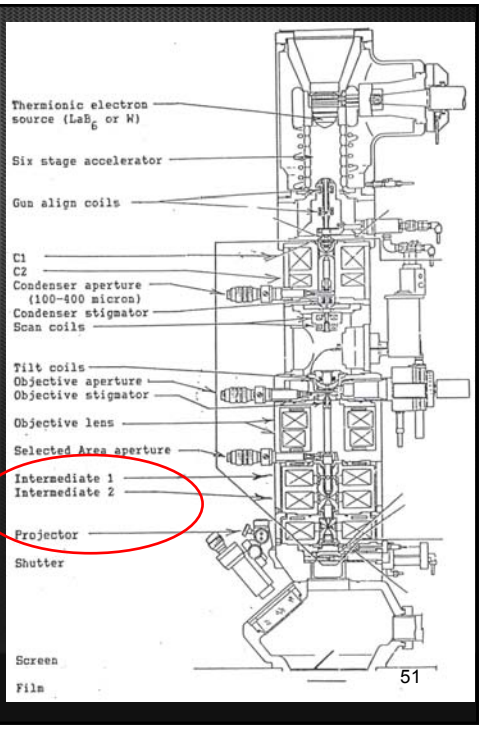

fppt.com

Projector System

- magnifies the images or diffraction patterns formed from the specimen and focuses images in the plane of the screen;
- the electron density is converted into light-optical images for the microscopist to see;
- here effects of spherical and chromatic aberrations in the lenses are most significant;

fppt.com

aberrations

Spherical Aberration

This defect occurs when the lens field behaves differently for off-axis rays;

For electromagnetic lenses, the further off axis the electron is, the more strongly it is bent back toward the axis;

As a result, a point object is imaged as a disk of finite size, which limits our ability to magnify detail because the detail is degraded by the imaging process;

We can correct this aberration, but it still limits the resolution of most TEMs so we need to examine it carefully.

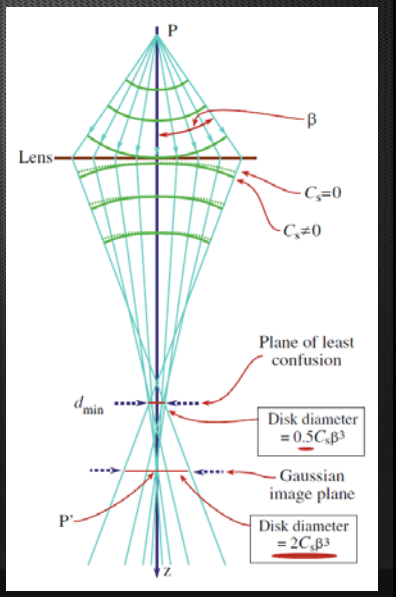

fppt.com

aberrations

Chromatic Aberration

This term is related to the 'color' (i.e., frequency, wavelength, or energy) of the electrons;

We've assumed that the electrons are monochromatic, but they aren't really;

Depending on the electron source the actual energy spread in the beam may vary from 0.3 eV (cold FEG) to1 eV(LaB_6);

This range is still so small that we generally don't have to worry about chromatic aberration affecting the image resolution.

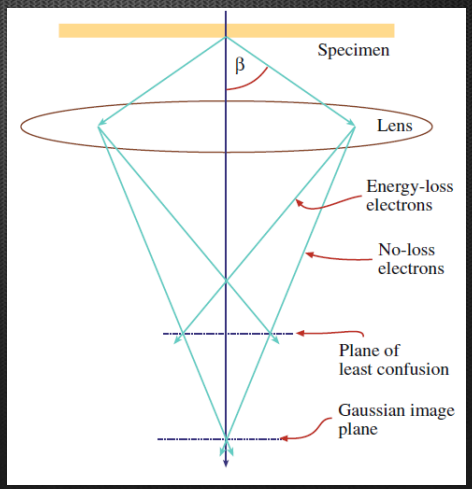

fppt.com

Magnification in TEM

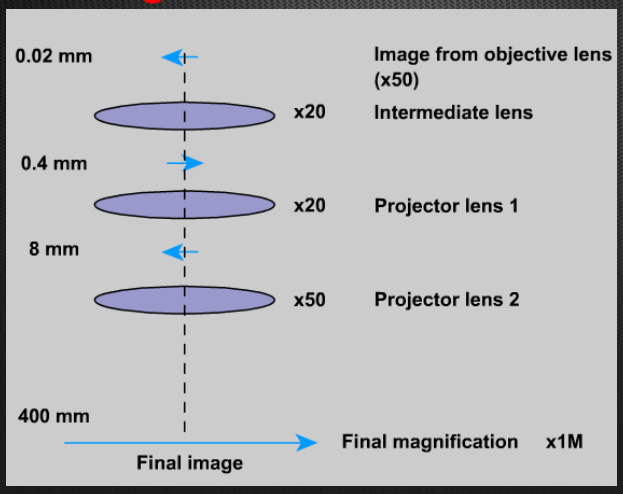

$M_{ob} \times M_{int} \times M_{proj}$ = Total Mag

Depending on the magnification, some lens may not be used

fppt.com

Detector Systems

- Electron gun
- Condenser Lenses
- Condenser Aperture
- Alignment Coils
- Objective Lens
- Lens Stigmators
- More Apertures for Microscopy
- Deflector Coils (Tilt Scan)
- Projector Lens
- Screen/Camera/Detectors
- Vacuum System

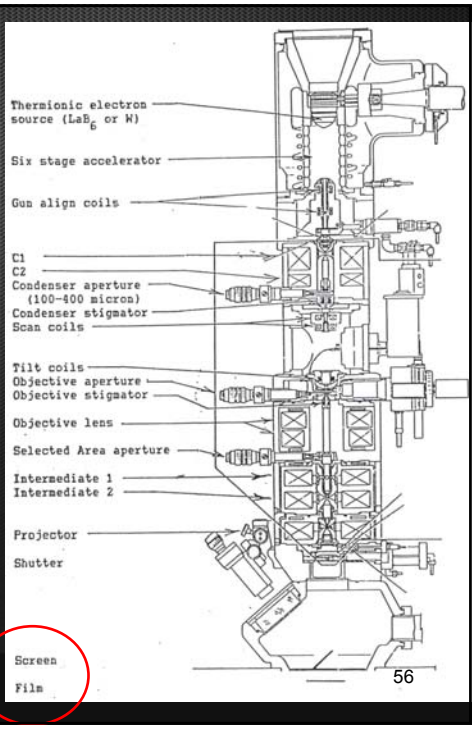

fppt.com

Detector Systems

- Analog imaging:
  - phosphorescent screen for viewing by eye
  - photographic film for permanent recording
- Digital imaging:
  - TV camera and VCR for real-time alignment and dynamic experiments
  - slow-scan CCD for permanent recording
  - image plates for high pixel density, high dynamic range permanent recording
- Analytical detectors:
  - energy-dispersive x-ray spectroscopy detector (EDS)
  - bending magnet electron spectrometer

57

Screen

Beneath all the lenses is a phosphorescent screen that glows when it is struck by electrons, displaying the image or diffraction pattern. The screen is viewed through a lead-glass window.

• In the electron microscope, we cannot usually see the effect of the wavelength of the electrons (the "colour") in each image, so we only have "black and white" images.

• Hence, the information contained in an electron micrograph is solely due to the difference in the flux of electrons through each point in the image - the contrast.

Screen

The electron microscopist must understand the reasons for contrast in order to gather information from the sample.
Briefly with the main sources of contrast are the following:

Mass absorption contrast

On passing through matter, a beam of electrons is gradually attenuated. The degree of attenuation increases with the thickness of the specimen and its mass, so variations of mass and thickness across the sample give rise to contrast in the image.

Diffraction contrast

Diffraction of electrons from Bragg planes causes a change in their direction of travel. Hence, contrast can arise between adjacent grains or between different regions near the core of a dislocation.

Phase contrast

Scattering mechanisms often cause a change in the phase of the scattered electrons, as well as a change in direction. Interference between electrons of different phase which are incident on the same part of the image will cause a change in intensity and give rise to contrast.

Limitations of TEM

Interpreting transmission images

- TEM present us with 2D images of a 3D specimen, viewed in transmission.
- One aspect of this particular drawback is that a single TEM images has no depth sensitivity. There often is information about the top and bottom surfaces of the specimen, but this is not immediately apparent.
- There has been progress in overcoming this limitation, by the development of electron tomography, which uses a sequence of images taken at different angles.
- In addition, there has been improvement in specimen-holder design to permit full 360° rotation and, in combination with easy data storage and manipulation.

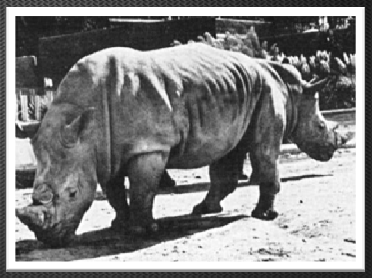

In projection, this photograph of two rhinos appears as one two-headed beast, because sometimes people have difficulty to translate a 2D image to a 3D image.
Adapted from D. B. Williams and C. B. Carter, *Transmission Electron Microscopy*: A Textbook for Material Science, 2nd Ed., Springer, New York (2009).

Limitations of TEM

Electron beam damage

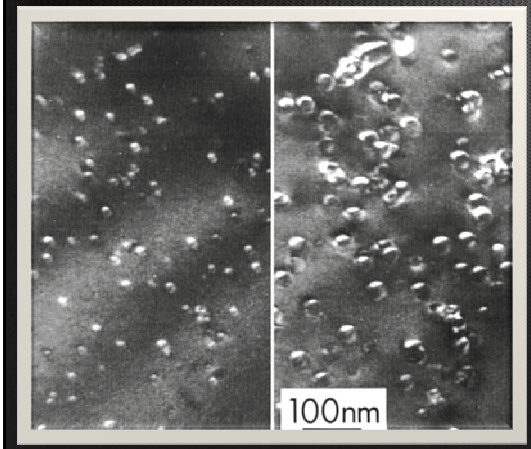

A detrimental effect of ionizing radiation is that it can damage the specimen;'
Some aspects of beam damage made worse at higher voltages;

However, the combination of more intense electron sources with more sensitive electron detectors, and the use computer enhancement of noisy images, can be used to minimize the total energy received by the sample.

Beam damage (bright bubble-like regions) in quartz after bombardment with 125 keV electrons. With increasing time from (A) to (B) the damaged regions increase in size.

fppt.com

Limitations of TEM

Sampling

- we only look at a small part of the specimen
- the higher the resolution → the worse sampling abilities
- before TEM study we must examine the specimen with poorer resolution techniques (eyes, OM, SEM…)
- know the forest before start looking at the tree leaves!

fppt.com

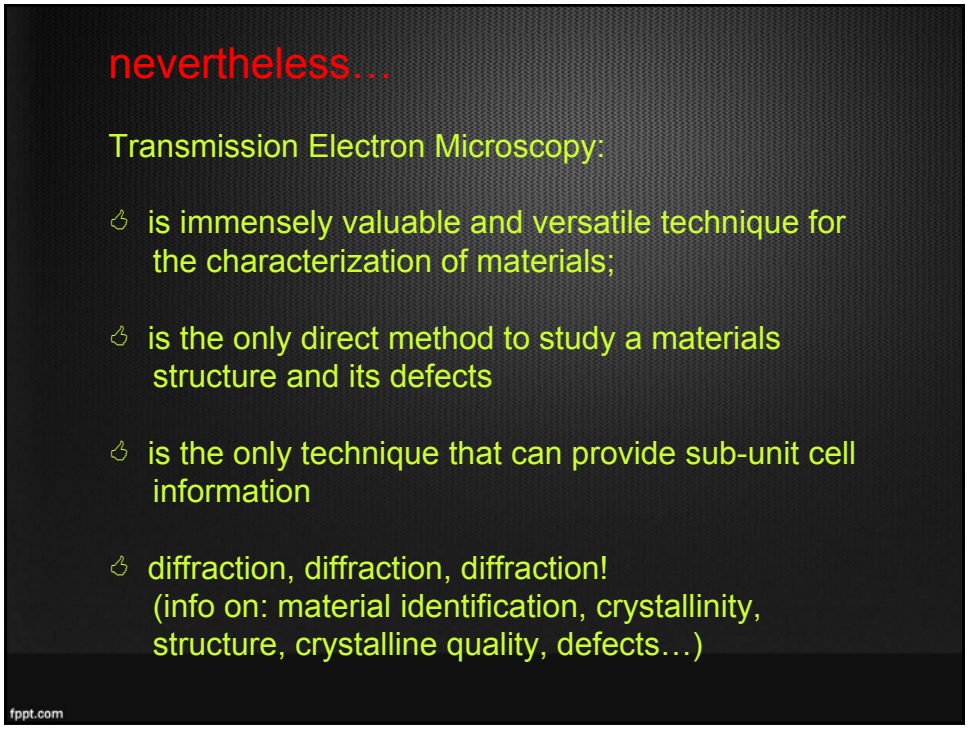
nevertheless…
Transmission Electron Microscopy:
is immensely valuable and versatile technique for the characterization of materials;
is the only direct method to study a materials structure and its defects
is the only technique that can provide sub-unit cell information
diffraction, diffraction, diffraction!
(info on: material identification, crystallinity, structure, crystalline quality, defects…)
fppt.com

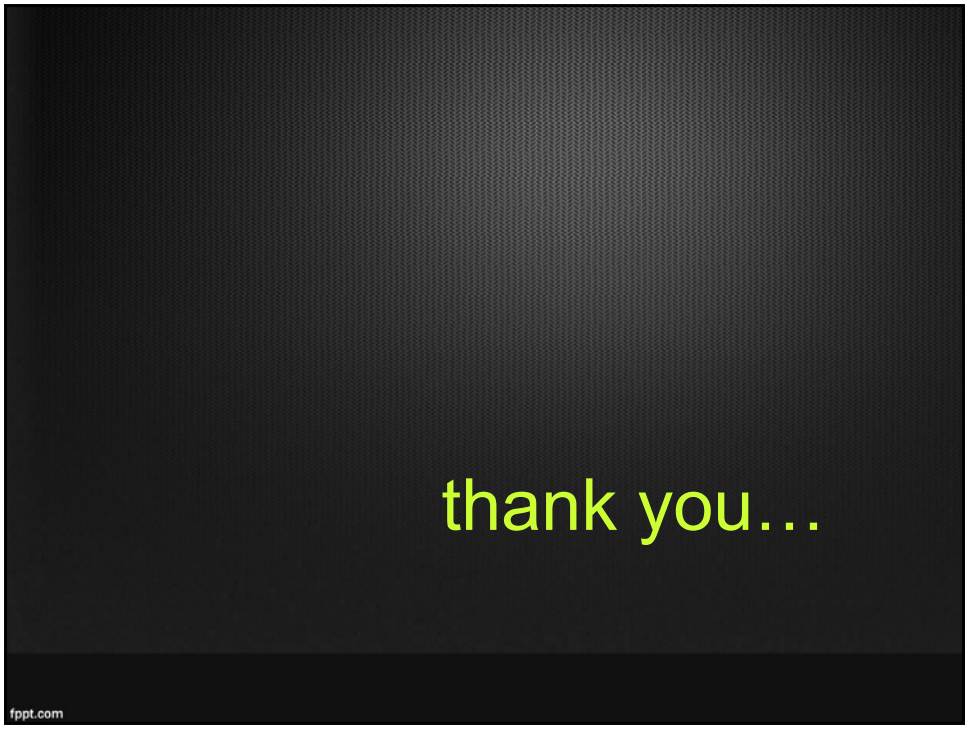
thank you…
fppt.com

Summer school on Micro- and Nano- structural characterization of materials
July 11-15, 2012, Thessaloniki, Greece

Physical concepts of diffraction and electron crystallography

Alkyoni Mantzari, Dr
Physics Department, Aristotle University of Thessaloniki

Outline

- Basics of crystallography
- Electron Crystallography
- Diffraction

Basics of crystallography

- Have an understanding of the basic concepts of crystallography, i.e. lattices, motifs, symmetry elements etc.
- Be able to identify lattices and symmetry elements within those lattices.
- Know about the different types of unit cells.
- Understand the idea of close-packing and packing efficiency.
- Be familiar with the different crystal systems and Bravais lattices.

Lattices

- Crystalline materials are characterised by a regular atomic structure that repeats itself in all three dimensions. In other words the structure displays **translational symmetry**.
- The periodic nature of the structure can be represented using a lattice.
- To generate the lattice from any repeating pattern, we choose an arbitrary reference point and examine its environment. We then simply mark in all the points in the pattern that are identical to the chosen reference point. The set of identical points is the **lattice**, and each point within it is a **lattice point**.

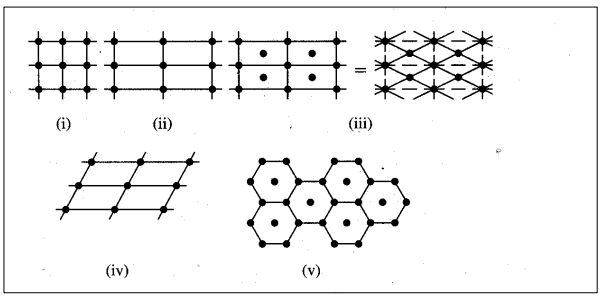

2-D lattices

(i) Simple square
(ii) Simple rectangle
(iii) Area centered rectangle (or rhombus)
(iv) Parallelogram
(v) Area centered hexagon

http://www.doitpoms.ac.uk/tlplib/crystallography3/lattice.php

Unit cell

- The building block of a crystal that when repeated in three dimensions composes the crystal structure is the unit cell.
- In three dimensions the unit cell is any parallelepiped whose vertices are lattice points, in two dimensions it is any parallelogram whose vertices are lattice points → infinite number of possible unit cells.
- The unit cell is chosen such that it is the smallest unit cell that reflects the symmetry of the structure.
- Primitive unit cells contain only one lattice point, which is made up from the lattice points at each of the corners.
- Non-primitive unit cells contain additional lattice points, either on a face of the unit cell or within the unit cell, and so have more than one lattice point per unit cell
- When a primitive unit cell does not reflect the symmetry of the crystal structure, a suitable non-primitive unit cell is picked.

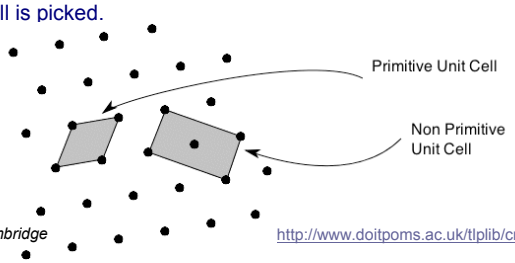

 http://www.doitpoms.ac.uk/tlplib/crystallography3/unit_cell.php

Most common types of unit cells

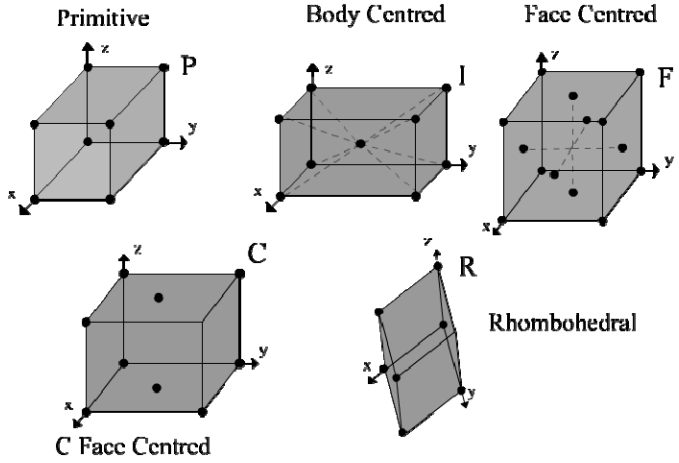

Lattice geometry

Lattice parameters
The length of the unit cell along the x, y, and z direction are defined as a, b, and c. Alternatively, we can think of the sides of the unit cell in terms of vectors **a**, **b**, and **c**. The angles between the crystallographic axes are defined by:
α = the angle between **b** and **c**
β = the angle between **a** and **c**
γ = the angle between **a** and **b**
a, b, c, α, β, γ are collectively known as the **lattice parameters** (often also called 'unit cell parameters', or just 'cell parameters').

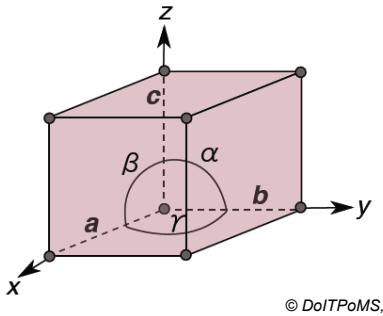

Lattice vectors

A lattice vector is a vector joining any two lattice points. Any lattice vector can be written as a linear combination of the unit cell vectors **a**, **b**, and **c**:
t = U **a** + V **b** + W **c**
In shorthand, lattice vectors are written in the form:
t = [UVW]

Negative values are not prefixed with a minus sign. Instead a bar is placed above the number to denote that the value is negative:
t = −U **a** + V **b** − W **c**
This lattice vector would be written in the form: $\mathbf{t} = [\bar{U}V\bar{W}]$

http://www.doitpoms.ac.uk/tlplib/crystallography3/parameters.php

Indexing lattice directions - zone axis symbols

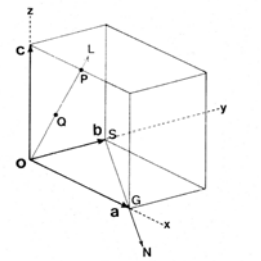

- The direction whose symbol is to be determined must pass through the origin of the unit cell
- Coordinates of P in terms of fractions of the lengths a, b and c: ½, 0, 1
- The above fractions expressed as the ratio of whole numbers is the direction or zone axis for OL: [102]
- For the direction SN the origin must be shifted from O to S → $[1\bar{1}0]$
- The general symbol for a direction is [uuw] or written as a vector:

$$\mathbf{r}_{uuw} = u\mathbf{a} + u\mathbf{b} + w\mathbf{c}$$

- For the unit cell edge vectors **a**, **b** and **c** the direction symbols are: [100], [010], [001]

Crystal structure

The **lattice type** defines the location of the lattice points within the unit cell.
The **lattice parameters** define the size and shape of the unit cell.
The **motif** is a list of the atoms associated with each lattice point, along with their fractional coordinates relative to the lattice point. Since each lattice point is, by definition, identical, if we add the motif to each lattice point, we will generate the entire structure.

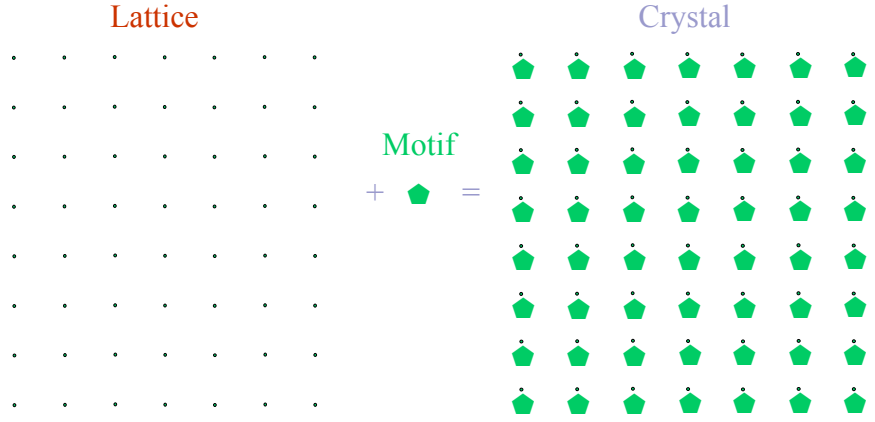

Packing of atoms

Understanding of simple crystal structures by considering the ways in which atoms can be packed together

Hard sphere model: representation of the structures arising from the packing together of atoms

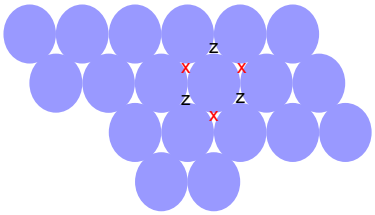

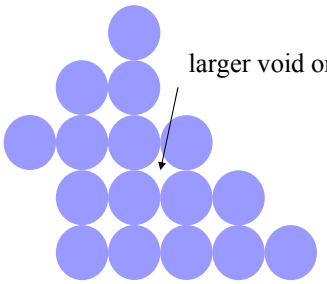

atoms are packed in a close-packed hexagonal arrangement – the most compact way which is possible

I. Constructing crystals from closed packed hexagonal layers of atoms

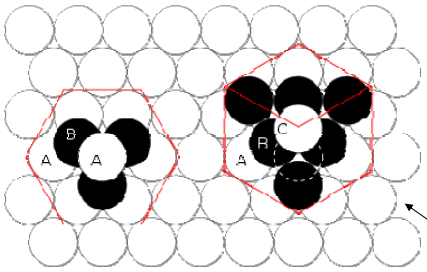

ABABAB…stacking sequence → **hexagonal close-packed (hcp) structure**

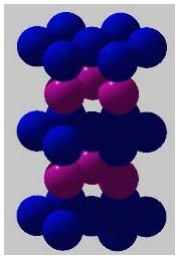

ABCABC…stacking sequence → **cubic close-packed (ccp) structure**

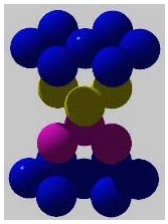

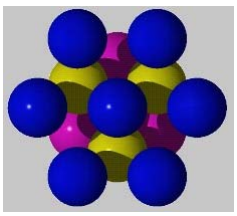

http://www.doitpoms.ac.uk/tlplib/crystallography3/packing.php

Unit cells of the hcp and ccp structures

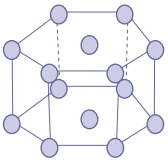

Simple hexagonal structure with AAA…stacking sequence

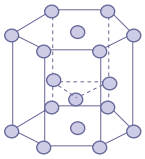

hcp structure with ABAB…stacking sequence

CCP Structure

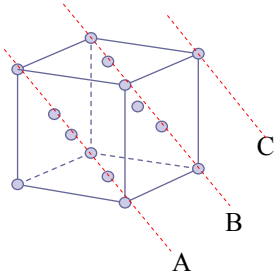

Cubic cell

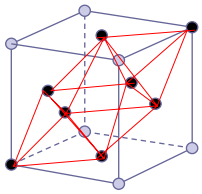

Rhombohedral cell

The close-packed layers lie perpendicular to the body diagonal of the cube. 4 body diagonals → 4 different sets of close-packed layers

II. Constructing crystals from square layers of atoms

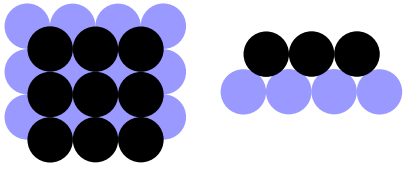

Stacking sequence of ABAB…
→ close-packed layers

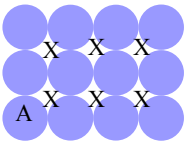

The next layer can only be put in site X or site A.

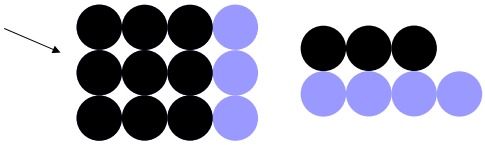

Stacking sequence of AAAA…→ **simple cubic structure** (α-polonium)

III. Constructing body-centered cubic (bcc) crystals

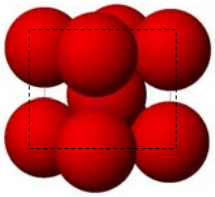

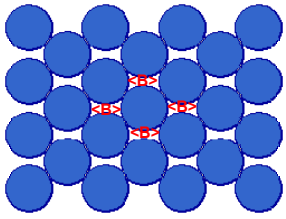

- Not close- packed atoms at corners and body center of cube.
- The atoms are only in contact along the body diagonal where they are most (not fully) "closely packed".
- ABAB…type of stacking sequence.

Plan view of the "closest-packed" plane of atoms where the positions of atoms in alternate layers are marked B. The arrows indicate possible slip directions from these positions.

Comparing the hexagonal close-packed plane and BCC close packed plane

Some important bcc ⇔ ccp and bcc ⇔ hcp transformations are thought to occur.

Interstitial structures

Different structures of many compounds arise from the different numbers and sizes of interstices which occur in the simple hexagonal, hcp, ccp, simple cubic and bcc structures and from the ways in which the "small" atoms distribute themselves among these interstices.

Interstices in ccp structure

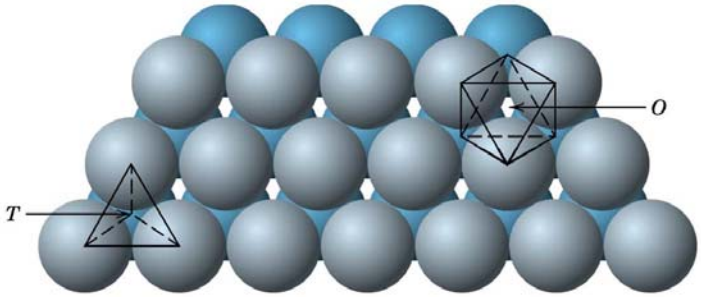

Tetrahedral (T_d) sites

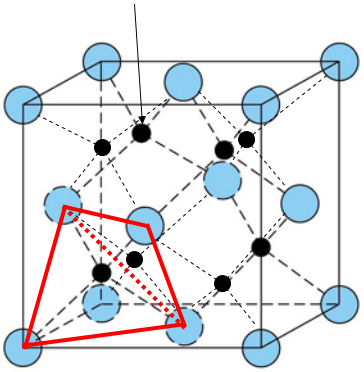

$r_x / r_a = 0.225$

Octahedral (O_h) sites

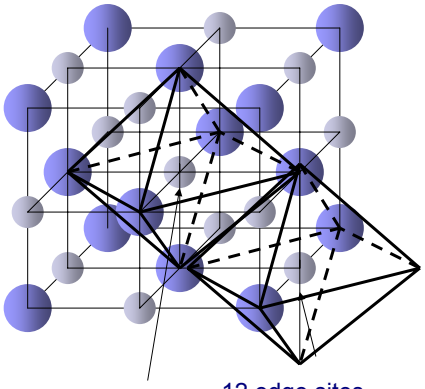

1 at the center

12 edge sites
(each shared by 4 cells)

$r_x / r_a = 0.414$

r_x=radius of the interstitial atoms X

r_A= radius of the large atoms A

Silicon Carbide-SiC

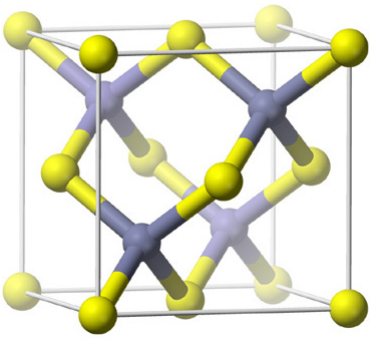

Zinc blende structure / 3C-SiC stacking sequence is ABCABC… or tetrahedral stacking in the pattern of CCP

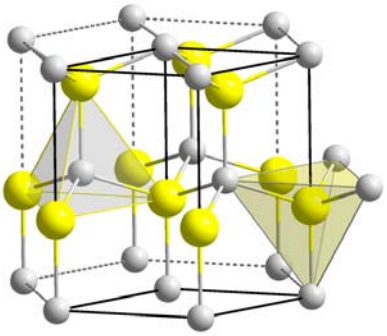

Wurtzite structure / 2H-SiC stacking sequence is ABABAB… or tetrahedral stacking in the pattern of HCP

Packing Efficiency

The packing efficiency of a crystal structure tells us how much of the available space is being occupied by atoms. It is usually represented by a percentage or volume fraction.
The packing efficiency is given by the following equation:

$$\frac{\text{(number of atoms per cell) * (volume of one atom)}}{\text{volume of unit cell}}$$

c.c.p.: 74%

h.c.p.: 74%

b.c.c.: 68%

Symmetry

Types of symmetry:

- translation
- rotation axes
- mirror planes
- centre of symmetry
- inversion axes (combination of rotation and centre of symmetry operations)

An n fold rotational symmetry operation rotates an object by 360°/n. Only n = 1, 2, 3, 4, and 6 are permitted in a periodic lattice

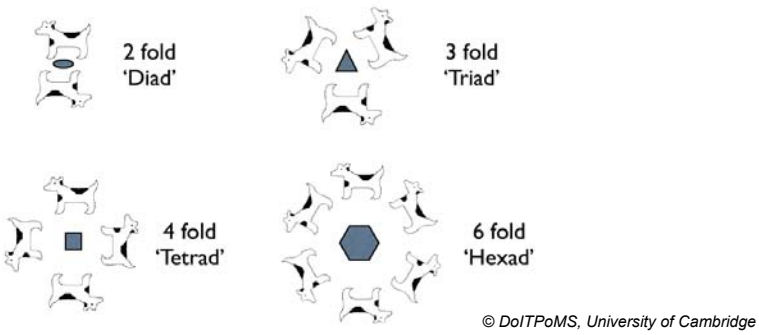

An object has mirror symmetry if reflection of the object in a plane brings it into coincidence with itself

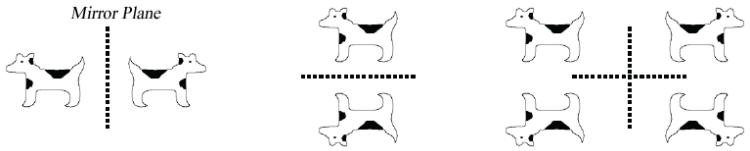

Some objects have special symmetry about an origin such that, for any point at position x, y, z, there is an exactly similar point at $-x$, $-y$, $-z$. The origin is called a centre of symmetry ("inversion centre"). Such an object is said to be centrosymmetric.

An n-fold inversion axis is a combination of a rotation by 360/n followed by a centre of symmetry operation.

There are only 32 permitted combinations of mirror planes, rotation axes, centres of symmetry and inversion axes. These are known as the 32 **point groups**. Each point group is a finite set of mutually compatible symmetry elements. When the symmetry elements of a point group are operated on each other, they simply generate one of the other elements within the group.

Crystal systems

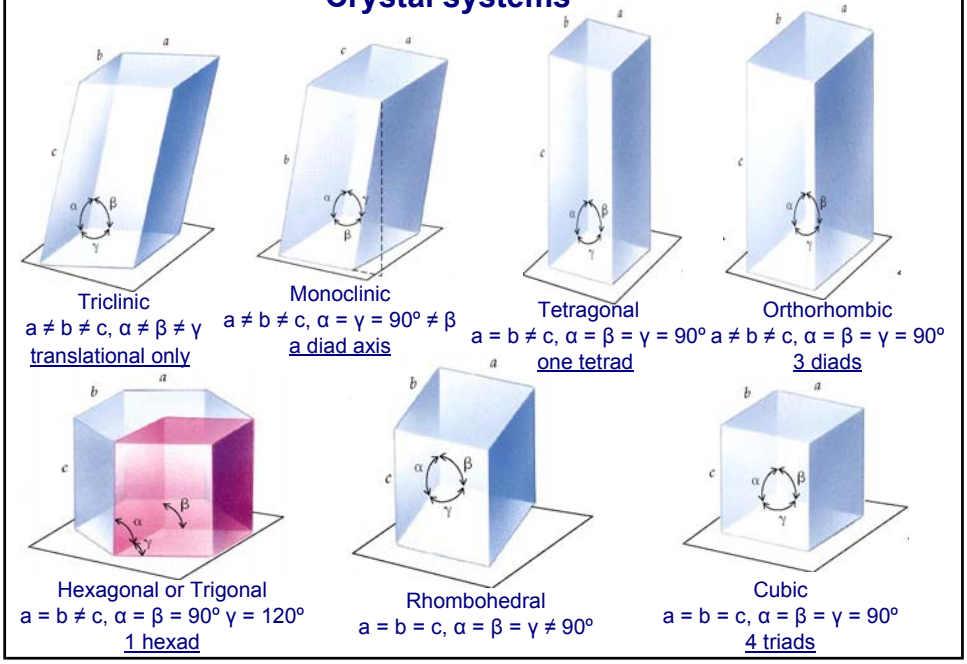

Triclinic
$a \neq b \neq c$, $\alpha \neq \beta \neq \gamma$
translational only

Monoclinic
$a \neq b \neq c$, $\alpha = \gamma = 90^\circ \neq \beta$
a diad axis

Tetragonal
$a = b \neq c$, $\alpha = \beta = \gamma = 90^\circ$
one tetrad

Orthorhombic
$a \neq b \neq c$, $\alpha = \beta = \gamma = 90^\circ$
3 diads

Hexagonal or Trigonal
$a = b \neq c$, $\alpha = \beta = 90^\circ$ $\gamma = 120^\circ$
1 hexad

Rhombohedral
$a = b = c$, $\alpha = \beta = \gamma \neq 90^\circ$

Cubic
$a = b = c$, $\alpha = \beta = \gamma = 90^\circ$
4 triads

Types of Unit Cell:

P=primitive

I=body-centered

F=face centered

C=one face centered

+ 7 crystal classes

→ **14 Bravais lattices**

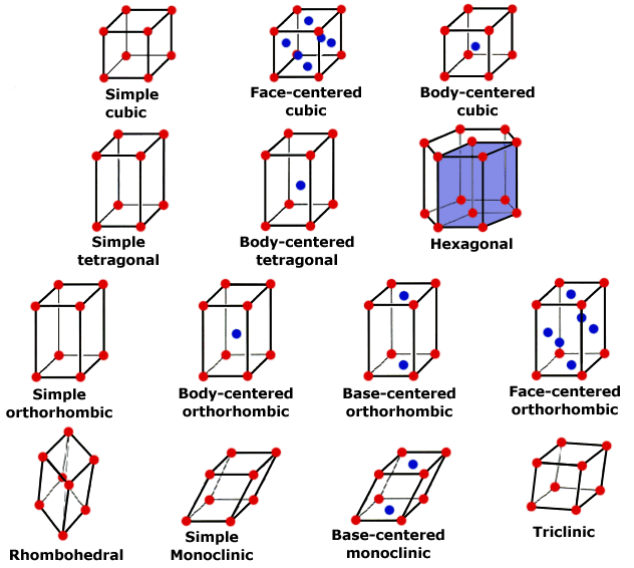

Indexing lattice planes - Miller indices

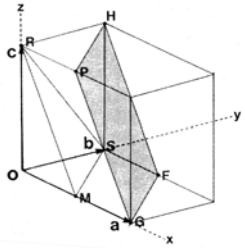

- The lattice plane whose index is to be determined must not pass through the origin of the unit cell or the origin must be shifted to a corner of the cell which doesn't lie in the plane.
- **RMS** is a plane belonging to a family of identical, parallel planes passing through the crystal, with the next plane "up" being PGFH
- For **RMS**, the plane nearest the origin, the *intercepts* of the plane on the unit cell vectors **a**, **b** and **c** are: 1/2a,1b, 1c
- Expressed as fractions of the cell edge lengths we have: ½, 1, 1
- By taking the *reciprocals* of these fractions and putting the whole numbers into round brackets the **Miller index** of the plane is defined as (211)

- The general index for a lattice plane is (hkl), the first plane in the family from the origin makes intercepts a/h, b/k, c/l on the axes → h planes are intercepted in passing from one corner of the unit cell to the next along x-axis, k planes along y-axis and l planes along z-axis.
- When a crystal plane // axis, its intercept is infinity → the reciprocal is zero

  e.g the "top" face of a crystal which intercepts only the z-axis is (001)

Miller indices and zone axis symbols in cubic crystals

- The positive and negative directions of the crystal axes x, y, z are:

$$[100],[\bar{1}00],[010],[0\bar{1}0],[001],[00\bar{1}]$$

- In the cubic system the axes are crystallographically equivalent and interchangeable → also all the above 6 directions which can be expressed collectively as <100> implying all 6 permutations of 1, 0, 0.
- The triad axis corner to corner directions are: <111>
- The diad axis edge to edge directions are: <110>

- The 6 faces of a cube (with the origin at the centre) are:

$$(100),(\bar{1}00),(010),(0\bar{1}0),(001),(00\bar{1})$$

These can be expressed collectively as planes of the form {100}

- In cubic crystals, directions are perpendicular to planes with the same numerical indices e.g direction [111] is perpendicular to the plane (111), which does not apply to crystals of lower symmetry except in special cases.

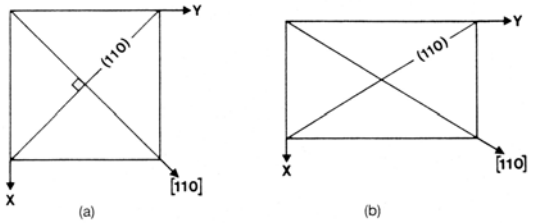

Plans of (a) cubic and (b) orthorhombic unit cells perpendicular to the z-axis, showing the relationship between planes and zone axes of the same numerical indices.

Spacings between the lattice planes (d-spacings)

A large number of lines may be drawn which contain a number of atoms

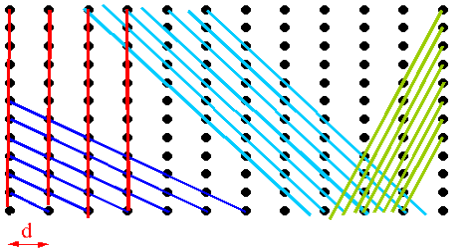

d-spacings= spacings between the individual planes, in these sets of parallel planes → d_{hkl} spacing between (hkl) planes

Electron diffraction determines the orientation relationship between the various sets of planes.

Lattice plane spacings, Miller indices and Laue indices

- Lattice plane spacing d_{hkl}= length of the normal ON
- $A\bar{O}N = a$ (angle between normal and x-axis)
- $O\hat{N}A = 90^{\circ}$

Thus

OA cosα= ON → (a/h)cosα= d_{hkl} → **cosα= (h/a) d_{hkl}**

Similarly **cosβ= (k/b) d_{hkl}** and **cosγ= (l/c) d_{hkl}**

where β, γ are the angles between ON and the y- and z- axes respectively

For orthogonal axes:

$\cos^2\alpha + \cos^2\beta + \cos^2\gamma = 1$

and for a cubic crystal **a = b = c**

So:

$$\frac{1}{d_{hkl}^2} = \frac{h^2 + k^2 + l^2}{\alpha}$$

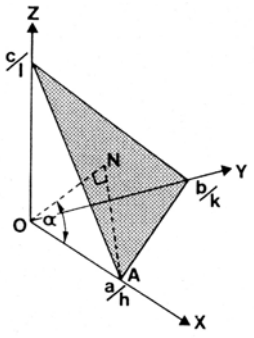

d-spacings formulae for the seven crystal systems

System	
Cubic	$\left[\frac{1}{a^2}(h^2+k^2+l^2)\right]^{-1/2}$
Tetragonal	$\left[\frac{h^2+k^2}{a^2}+\frac{l^2}{c^2}\right]^{-1/2}$
Orthorhombic	$\left[\frac{h^2}{a^2}+\frac{k^2}{b^2}+\frac{l^2}{c^2}\right]^{-1/2}$
Hexagonal	$\left[\frac{4}{3a^2}(h^2+hk+k^2)+\frac{l^2}{c^2}\right]^{-1/2}$
Rhombohedral	$\left[\frac{1}{a^2}\frac{(h^2+k^2+l^2)\sin^2\alpha+2(hk+kl+lh)(\cos^2\alpha-\cos\alpha)}{1-2\cos^3\alpha+3\cos^2\alpha}\right]^{-1/2}$
Monoclinic	$\left[\frac{\frac{h^2}{a^2}+\frac{l^2}{c^2}-\frac{2hl\cos\beta}{ac}}{\sin^2\beta}+\frac{k^2}{b^2}\right]^{-1/2}$
Triclinic	$\left[\frac{\frac{h^2}{a^2}\sin^2\alpha+\frac{k^2}{b^2}\sin^2\beta+\frac{l^2}{c^2}\sin^2\gamma+\frac{2hk}{ab}(\cos\alpha\cos\beta-\cos\gamma)+\frac{2kl}{bc}(\cos\beta\cos\gamma-\cos\alpha)+\frac{2lh}{ca}(\cos\gamma\cos\alpha-\cos\beta)}{1-\cos^2\alpha-\cos^2\beta-\cos^2\gamma+2\cos\alpha\cos\beta\cos\gamma}\right]^{-1/2}$

What is Electron Crystallography?

Electron crystallography is the quantitative use of different information by electron scattering to study crystal structures.

Why electrons?

- **10^{4-5} times stronger interaction with matter compared with X-ray**
  - *single crystal data on powder sample*
  - *short data collection time*
- **Phases are present in high resolution electron microscopy (HREM) images**
  - *for nano- and micro-sized crystals*

Transmission Electron Microscopy

Diffraction	Imaging	Chemical analysis
selected area, nano and convergent beam electron diffraction	**conventional, High resolution**	**EDS and EELS**

- **SAED – Selected Area Electron Diffraction**
- **CBED – Convergent Beam Electron Diffraction**

The questions that we can address using DPs obtained in the TEM include the following:

•Is the specimen crystalline? Crystalline and amorphous materials have very different properties.

•If it is crystalline, then what are the crystallographic characteristics (lattice parameter, symmetry, etc.) of the specimen?

•Is the specimen monocrystalline? If not, what is the grain morphology, how large are the grains, what is the grain-size distribution, etc.?

Diffraction phenomenon

- **Diffraction** is normally taken to refer to various phenomena which occur when a wave encounters an obstacle. It is described as the apparent bending of waves around small obstacles and the spreading out of waves past small openings.
- Diffraction effects are generally most pronounced for waves where the wavelength is roughly similar to the dimensions of the diffracting objects. If the obstructing object provides multiple, closely spaced openings, a complex pattern of varying intensity can result.
- Electrons are charged particles and interact strongly with all atoms. So electrons with an energy of a few eV would be completely absorbed by the specimen. In order that an electron beam can penetrate into a specimen, it necessitates a beam of very high energy (50 keV to 1MeV) as well as the specimen must be thin (~100 nm).
- The wavelength of high energy electron is about 0.0037 nm at 100 keV;
  The bond of atoms (distance of two adjacent atoms) is about 0.08 – 0.2 nm.

The crystal is the best "barrier" to observe the diffraction of electrons and X-rays!

- Transmitted beam electrons & elastically scattered electrons retain their initial energy (energy of the e^- from the incident beam) → same wavelength
- Rutherford scattering: elastically scattered e^- due to Coulomb interactions between the incident e^- and the atoms nuclei.
- Scattering probability of one e^- with energy E_0 from one atom at angle θ is:

$$p(\theta) \propto 1/E_0^2 \sin^4\theta$$

- high probability of small angle scattering
- Small probability with increase of the e^- energy

- atoms of a crystal structure → diffraction phenomena → diffraction patterns with intensity maxima.

What is an electron diffraction pattern?

Single crystal DP

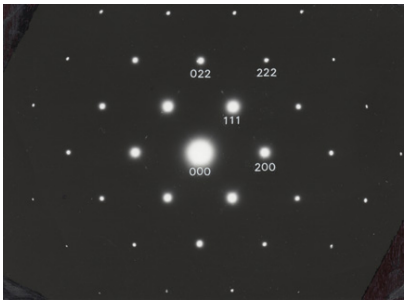

Electron DP taken from an epitaxial Au single crystal film with (001) orientation and [110] incidence of the electron beam.

- Single crystals consist of atoms arranged in an orderly lattice.
- An electron beam passing through a single crystal will produce a pattern of spots. The arrangement of the spots depends upon the orientation of the atomic array in the electron microscope.
- Determination of structure type, lattice parameter and crystal orientation.

Polycrystalline material

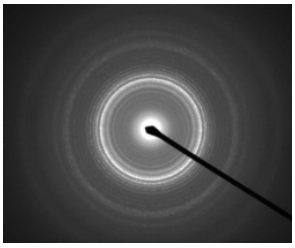

- Specimen with large number of small discrete areas, each with exactly the same atomic array, but at different orientations to each other.
- DP superposition of single crystal spot patterns: a series of concentric rings resulting from many spots very close together at various rotations around the centre beam spot.
- Determination of structure type and lattice parameter.

Amorphous material

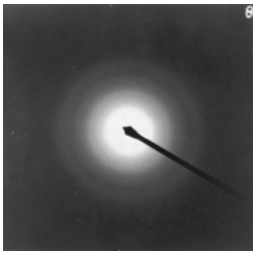

- Atoms arrangement entirely random and without any distinct repeating structure.
- Electron DP with fuzzy rings of light on the fluorescent screen. The diameters of these rings of light are related to average nearest neighbour distances in the material.

ANALYSIS OF THE ELECTRON DIFFRACTION PATTERN

Two basic type of information in the diffraction pattern:

(a) Spatial arrangement, that is, distances R, between the central spot and the other diffraction spots or rings, and the angles φ, between lines joining the central spot to each diffraction spot.

(b) Intensities, in comparative values between the central spot and the other diffraction maxima.

Physical concept of electron diffraction

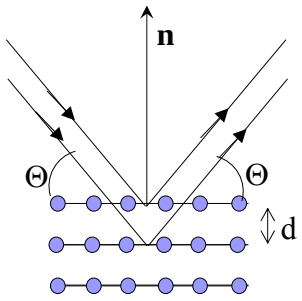

The Bragg equation states that constructive interference occurs when the path length difference associated with reflections from adjacent crystal planes is an integral number of wavelengths:

$$n\lambda = 2d_{hkl}\sin\theta$$

where n is the order of reflection, λ is the wavelength, d_{hkl} is the lattice plane spacing and θ is the angle of incidence/reflection to the lattice planes.

Important to distinguish between lattice planes and reflecting planes:

- Indices for lattice planes do not have common factors except in cases of non-primitive cells.
- Indices for reflecting planes frequently do have common factors. They are called **Laue indices** and are usually written without brackets.

Bragg' s law for (111) lattice planes in a crystal:

First order reflection (n=1): $\mathbf{1\lambda = 2d_{111}\sin\theta_1}$

Second order reflection (n=2): $\mathbf{2\lambda = 2d_{111}\sin\theta_2} \rightarrow$

$$\mathbf{1\lambda = 2(d_{111}/2)\sin\theta_2}$$

which can be regarded **as first-order reflections from planes of half the spacing $d_{111}/2$.** These are 222 planes with $d_{222}=d_{111}/2$ (imaginary planes in the sense that half of them pass through lattice points)

Useful fiction in the sense that the order of reflection, n in Bragg's law, can be omitted.

Third-order reflections from (111) planes can be regarded as **first-order reflections from the 333 reflecting planes**.

Only in the case of centred lattices where lattice planes have common factors reflecting planes are also lattice planes.

Derivation of the basic formula, Rd=λL

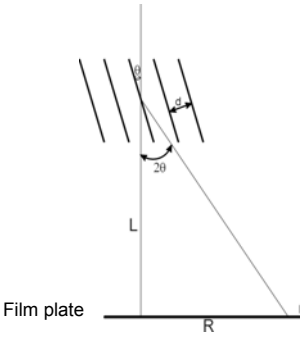

tan2θ=R/L
θ=1°-2 °
→ tan2θ=2sinθ → 2sinθ=R/L
Bragg law: λ=2dsinθ
→ R/L=λ/d

$$\mathbf{d_{hkl}=\lambda L/R}$$

Indexing a simple diffraction pattern from a known specimen

Indexing of diffraction spots or rings: assigning Miller indices of the lattice planes from which they arise.

Determining the d-spacings

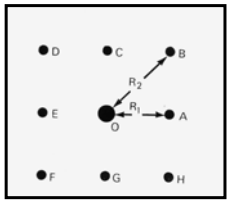

Schematic diffraction pattern from a single crystal specimen with a simple cubic structure, of lattice parameter, α=0.25 nm.

A, C, E and G at the same distance from the centre as B, D, F and H → measurement of only R_1 and R_2:

R_1=12.8 mm, R_2=18.1 mm

Accelerating voltage in the microscope: 80kV, for which λ=0.004 nm and

Camera length: L=800 mm (in practice the camera length λL is determined experimentally using known standards).

$$d_1 = \frac{\lambda\,(nm) x L(mm)}{R_1(mm)} = \frac{0.004\,x\,800}{12.8} = 0.25\ nm \qquad d_2 = \frac{0.004\,x\,800}{18.1} = 0.177\ nm$$

Assigning Miller indices

For the cubic system: $\frac{1}{d^2} = \frac{h^2+k^2+l^2}{\alpha^2}$

α=0.25 nm

Spot A

$$h_1^2 + k_1^2 + l_1^2 = \frac{\alpha^2}{d_1^2} = \frac{(0.25)^2}{(0.25)^2} = 1$$

Spot B

$$h_2^2 + k_2^2 + l_2^2 = \frac{\alpha^2}{d_2^2} = \frac{(0.25)^2}{(0.177)^2} = 2$$

But h, k and l must be whole numbers, so

$h_1k_1l_1$ must be {100}, i.e. (100), (010) or (001)

and

$h_2k_2l_2$ must be {110}, i.e. (110), (101) or (011)

Indexing procedure

(i) Index the central spot as (000).

(ii) Assign, quite arbitrarily, since they are all equivalent, one of the three possibilities for ($h_1k_1l_1$) as the index for spot A, say (100).

(iii) Assign one of the three possibilities for ($h_2k_2l_2$) as the index for spot B. Indices of all spots consistent with vectorial addition of the individual indices.

Since h_1=1 → step in the OA direction adds 1 to the *h* index

→ B may be either (110) or (101), but not (001).

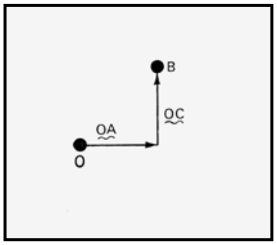

If B is (110)

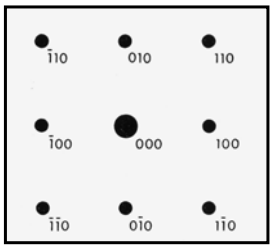

Since k_2=1 → step in the OC direction adds 1 to the *k* index

(a) In going along any straight line of spots, if a change in the *h*, *k* or *l* index occurs in one step, a similar change must also occur on the next step.

(b) Spots equidistant either side of the central spot, along a straight line, are the negative of each other.

(c) Vectorial addition, for example (010) + (100) → (110)

Checking the interplanar angles

The interplanar angle formulae

Crystal system	*Angle ϕ between $(h_1k_1l_1)$ and $(h_2k_2l_2)$*

Cubic

$$\cos\phi = \frac{h_1h_2 + k_1k_2 + l_1l_2}{\sqrt{[(h_1^2 + k_1^2 + l_1^2)(h_2^2 + k_2^2 + l_2^2)]}}$$

Tetragonal

$$\cos\phi = \frac{\left(\frac{h_1h_2 + k_1k_2}{a^2}\right) + \left(\frac{l_1l_2}{c^2}\right)}{\sqrt{\left\{\left[\frac{(h_1^2 + k_1^2)}{a^2} + \frac{l_1^2}{c^2}\right]\left[\frac{(h_2^2 + k_2^2)}{a^2} + \frac{l_2^2}{c^2}\right]\right\}}}$$

Orthorhombic

$$\cos\phi = \frac{\frac{h_1h_2}{a^2} + \frac{k_1k_2}{b^2} + \frac{l_1l_2}{c^2}}{\sqrt{\left[\left(\frac{h_1^2}{a^2} + \frac{k_1^2}{b^2} + \frac{l_1^2}{c^2}\right)\left(\frac{h_2^2}{a^2} + \frac{k_2^2}{b^2} + \frac{l_2^2}{c^2}\right)\right]}}$$

Hexagonal

$$\cos\phi = \frac{h_1h_2 + k_1k_2 + \left(\frac{h_1k_2 + k_1h_2}{2}\right) + \frac{3a^2}{4c^2}l_1l_2}{\sqrt{\left[\left(h_1^2 + k_1^2 + h_1k_1 + \frac{3a^2}{4c^2}l_1^2\right)\left(h_2^2 + k_2^2 + h_2k_2 + \frac{3a^2}{4c^2}l_2^2\right)\right]}}$$

Rhombohedral, Monoclinic, Triclinic: (Complex–see Andrews, K. W., D. J. Dyson and S. R. Keown (1971), Interpretation of electron diffraction patterns (Hilger and Watts, London).

Important for higher order reflections!

Indexing a diffraction pattern with many diffraction spots

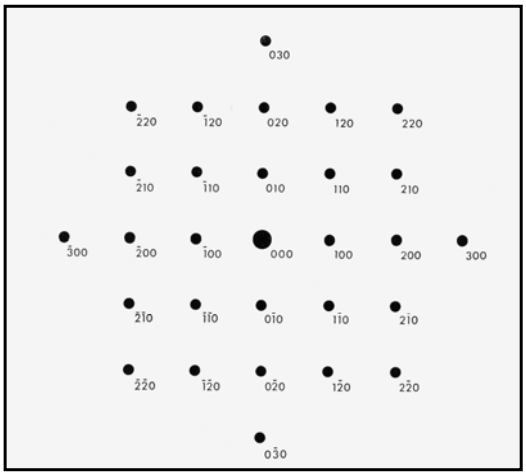

(i) A step in the OA direction adds 1 to the *h* index

(ii) A step in the OC direction adds 1 to the *k* index

(iii) The *l* index is always zero, in this particular diffraction pattern

Determining the zone axis of the diffraction pattern

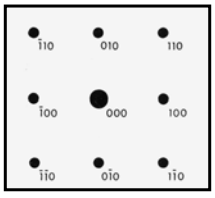

l=0 for all diffraction spots → the planes do not intersect the z axis → planes // to z axis

Electron beam diffracted from those planes must strike at a very shallow angle, less than 1º-2 º → beam traveling down the z axis

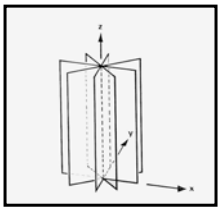

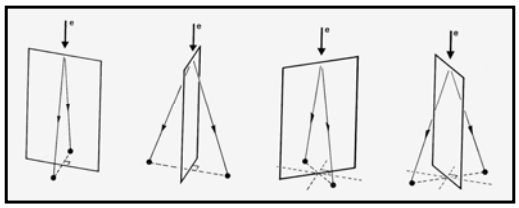

Sample oriented with the electron beam parallel to the z axis → perpendicular to (001) planes → **zone axis of the diffraction pattern is [001]**

Zones, zone axes and the zone law

The zone law (or Weiss zone law)

If a plane (hkl) lies in a zone [uuw] (i.e the direction [uuw] is parallel to the plane (hkl)) then:

$$hu + ku + lw = 0$$

Zone axis at the intersection of two planes

The line or direction of intersection of two planes ($h_1k_1l_1$) and ($h_2k_2l_2$) gives the zone axis [uuw] where: **$u=(k_1l_2-k_2l_1)$ $v=(l_1h_2-l_2h_1)$ $w=(h_1k_2-k_1h_2)$**

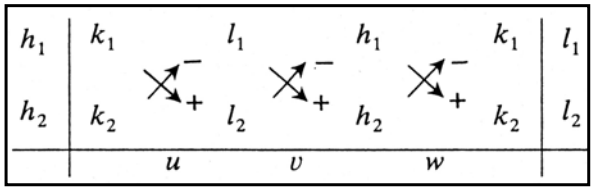

Plane parallel to two directions

To find the plane lying parallel to two directions [$u_1v_1w_1$] and [$u_2v_2w_2$], use this memogram:

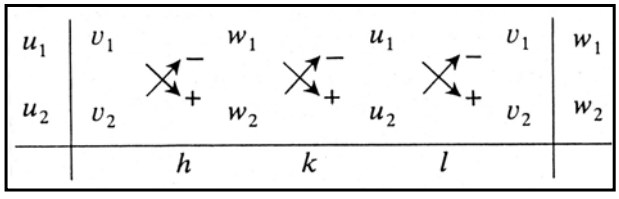

***h*=(v_1w_2-v_2w_1)** ***k*=(w_1u_2-w_2u_1)** ***l*=(u_1v_2-v_1u_2)**

Forbidden diffraction spots

Forbidden reflections= expected diffraction spots that may not occur

Diffraction pattern with [001] zone axis for an f.c.c. specimen.

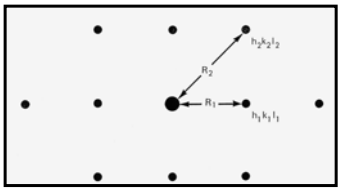

Schematic diffraction pattern from a single crystal nickel specimen, α= 0.35 nm

$(h_1^2+k_1^2+l_1^2)=4$ and $(h_2^2+k_2^2+l_2^2)=8$

$h_1k_1l_1$ of {200} type

$h_2k_2l_2$ of {220} type

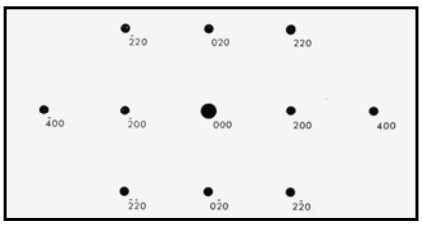

Alternate diffraction spots are now absent and are termed **forbidden reflections**.

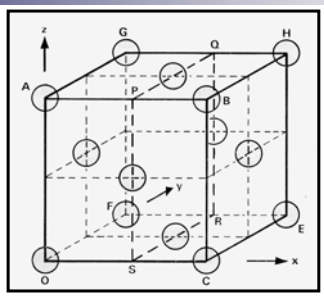

Unit cell of the face-centered cubic lattice

- Extra (200) plane PQRS, containing the face-centering atoms.
- Number and arrangement of atoms the same as in the (100) planes OAGF and CBHE and in half way between them.
- Electron beam cannot distinguish the two planes → twice the number of planes, indexed as (200) planes at $a/2$ lattice spacing and (100) planes no longer exist as separate entities → type {100} **forbidden reflections.**

Selection rules for cubic system allow reflections to appear only when:

for f.c.c. lattice h, k and l are ALL EVEN

for b.c.c. lattice $(h+k+l)$ is EVEN

Superlattice reflections

- For a binary alloy where the atoms of one element occupy one particular site in the unit cell, while the atoms of the other occupy another discrete site → ordered specimen with **superlattice** structure.
- Ordering occurs usually when the fractional amounts of the elements are simple numbers like 1:1, 2:1, 3:1… (f.c.c. superlattice for Cu_3Au and b.c.c. superlattice for CsCl)

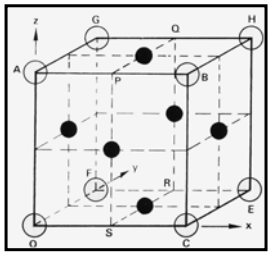

f.c.c. superlattice, Cu_3Au

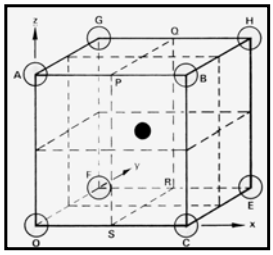

b.c.c. superlattice, CsCl

● Cu atoms 6x1/2=3

○ Au atoms 8x1/8=1

- {200} planes

  OAGF, CBHE: equal number of Cu and Au atoms

  SPQR: only Cu atoms

- different scattering efficiency of the different set of planes → electron beam sees two types of planes, one with spacing a from the origin, that is {100}, and one with spacing $a/2$ from the origin, that is {200} → [001] diffraction pattern of an f.c.c. structure with the intermediate spots of the simple cubic structure.
- Spot intensities determined by F_{Cu}-F_{Au}.
- Forbidden reflections reappear!

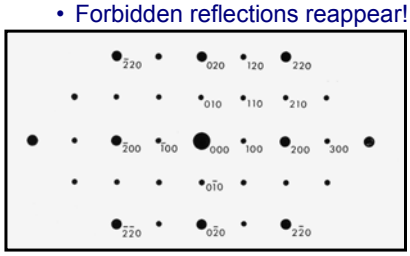

Schematic [001] diffraction pattern from the f.c.c. superlattice specimen, Cu_3Au

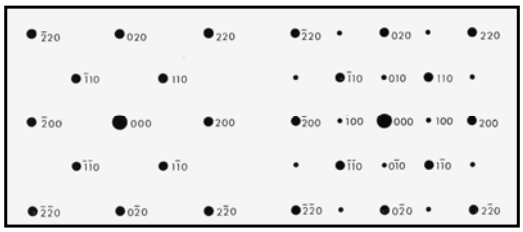

Schematic [001] diffraction pattern from the basic b.c.c. structure and the b.c.c. superlattice, CsCl

Indexing in the hexagonal systems: Weber symbols and Miller-Bravais indices

- Outline unit cells using the easily recognized hexagonal layers as the "base" of the cells and with the z-axis perpendicular thereto
- Three choices of unit cell commonly made in the hexagonal lattice:

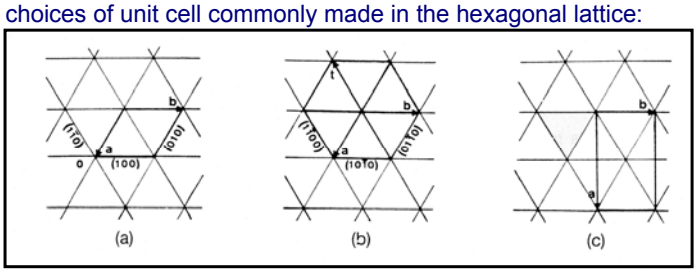

Hexagonal net of the hexagonal P lattice showing (a) primitive hexagonal unit cell with the traces of the six prism faces indexed {hkl}, (b) hexagonal (four-index) unit cell with the traces of the six prism faces indexed {hkil}, (c) orthohexagonal unit cell

- The primitive hexagonal unit cell doesn't reveal the hexagonal symmetry of the lattice.
- A fourth axis – the u-axis – is inserted at 120° to both the x- and y- axes

Miller-Bravais axes x, y, u, z (vectors **a, b, t, c**)

Miller-Bravais indices (hkil) where h +k + i =0

Zone axis symbols – **Weber symbols** <UVTW> where U + V + T = 0

Transformation from [uuw] to [UVTW] is given by the identities:

U=1/3(2u-u) V=1/3(2u-u) T= - (U + V) W=w

Zone axis symbols for x-, y- and u- axes are $[2\bar{1}\bar{1}0], [\bar{1}2\bar{1}0], [\bar{1}\bar{1}20]$

Reverse transformation from [UVTW] to [uuw] is given by the identities:

u= (U – T) u= (V – T) w=W

Zone law: hU + kV + iT + lW = 0

- The orthohexagonal unit cell doesn't also reveal the hexagonal symmetry of the lattice.
- Ratio of the length of the edges, a/b= $\sqrt{3}$
- Advantage from the orthogonal axes in showing relationships between crystals with similar structures but where small distortions can change the symmetry from hexagonal to orthorhombic.

Transforming Miller indices and zone axis symbols

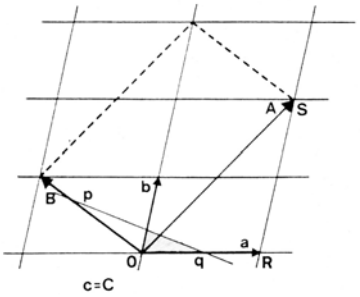

Plan view of a lattice with two possible unit cells. (hkl) and [uuw] refer to the primitive cell **a, b, c** and (HKL) and [UVW] refer to the "large" unit cell **A, B, C** (**c=C**)

The unit cell vectors **A, B, C** can be expressed as components of **a, b, c**:

$$\mathbf{A} = 1\mathbf{a} + 2\mathbf{b} + 0\mathbf{c}$$
$$\mathbf{B} = \bar{1}\mathbf{a} + 1\mathbf{b} + 0\mathbf{c}$$
$$\mathbf{C} = 0\mathbf{a} + 0\mathbf{b} + 1\mathbf{c}.$$

Equations expressed as:

Column matrices

$$\begin{pmatrix} \mathbf{A} \\ \mathbf{B} \\ \mathbf{C} \end{pmatrix} = \begin{pmatrix} 1 & 2 & 0 \\ \bar{1} & 1 & 0 \\ 0 & 0 & 1 \end{pmatrix} \begin{pmatrix} \mathbf{a} \\ \mathbf{b} \\ \mathbf{c} \end{pmatrix}$$

or as row matrices

$$(\mathbf{A} \quad \mathbf{B} \quad \mathbf{C}) = (\mathbf{a} \quad \mathbf{b} \quad \mathbf{c}) \begin{pmatrix} 1 & \bar{1} & 0 \\ 2 & 1 & 0 \\ 0 & 0 & 1 \end{pmatrix}$$

pq: trace of the first plane from the origin from a family of planes.

h: number of planes intersected along **a**

k: number of planes intersected along **b** → 2k: number of planes intersected along 2**b**

Thus, h+2k: total number of planes intersected along 1**a**+2**b**

Since **A**= 1**a**+2**b** →

$$H = 1h + 2k + 0l$$
$$K = \bar{1}h + 1k + 0l$$
$$L = 0h + 0k + 1l,$$

Equations expressed as row matrices

$$(HKL) = (hkl) \begin{pmatrix} 1 & \bar{1} & 0 \\ 2 & 1 & 0 \\ 0 & 0 & 1 \end{pmatrix}.$$

vector **r** in the lattice: **r**= u**a** + υ**b** +w**c** = U**A** + V**B** + W**C**

$$u = 1U + \bar{1}V + 0W$$
$$v = 2U + 1V + 0W$$
$$w = 0U + 0V + 1W.$$

Equations expressed as column matrices

$$\begin{pmatrix} u \\ v \\ w \end{pmatrix} = \begin{pmatrix} 1 & \bar{1} & 0 \\ 2 & 1 & 0 \\ 0 & 0 & 1 \end{pmatrix} \begin{pmatrix} U \\ V \\ W \end{pmatrix}.$$

Reverse relationships from the inverse of the matrix:

$$\begin{pmatrix} 1 & \bar{1} & 0 \\ 2 & 1 & 0 \\ 0 & 0 & 1 \end{pmatrix}^{-1} = \frac{1}{3}\begin{pmatrix} 1 & 1 & 0 \\ \bar{2} & 1 & 0 \\ 0 & 0 & 3 \end{pmatrix};$$

So: $(hkl) = (HKL)\frac{1}{3}\begin{pmatrix} 1 & 1 & 0 \\ \bar{2} & 1 & 0 \\ 0 & 0 & 3 \end{pmatrix}$ and $\begin{pmatrix} U \\ V \\ W \end{pmatrix} = \frac{1}{3}\begin{pmatrix} 1 & 1 & 0 \\ \bar{2} & 1 & 0 \\ 0 & 0 & 3 \end{pmatrix}\begin{pmatrix} u \\ v \\ w \end{pmatrix}.$

Transformation matrices for trigonal crystals with rhombohedral lattices

$$(HKL) = (hkl)\begin{pmatrix} 1 & 0 & 1 \\ \bar{1} & 1 & 0 \\ 0 & \bar{1} & 1 \end{pmatrix}; \quad \begin{pmatrix} u \\ v \\ w \end{pmatrix} = \begin{pmatrix} 1 & 0 & 1 \\ \bar{1} & 1 & 0 \\ 0 & \bar{1} & 1 \end{pmatrix}\begin{pmatrix} U \\ V \\ W \end{pmatrix}$$

$$(hkl) = (HKL)\begin{pmatrix} \frac{2}{3} & \frac{\bar{1}}{3} & \frac{\bar{1}}{3} \\ \frac{1}{3} & \frac{1}{3} & \frac{\bar{2}}{3} \\ \frac{1}{3} & \frac{1}{3} & \frac{1}{3} \end{pmatrix}; \quad \begin{pmatrix} U \\ V \\ W \end{pmatrix} = \begin{pmatrix} \frac{2}{3} & \frac{\bar{1}}{3} & \frac{\bar{1}}{3} \\ \frac{1}{3} & \frac{1}{3} & \frac{\bar{2}}{3} \\ \frac{1}{3} & \frac{1}{3} & \frac{1}{3} \end{pmatrix}\begin{pmatrix} u \\ v \\ w \end{pmatrix}$$

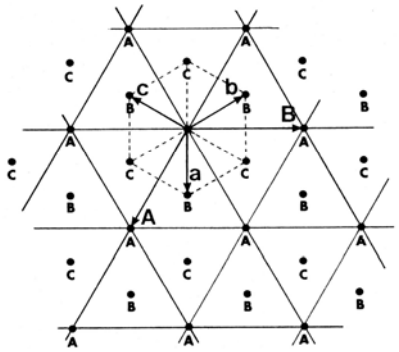

Plan view of hexagonal layers of lattice points stacked in the rhombohedral ABC… sequence

- primitive rhombohedral unit cell with **a, b, c** vectors
- non-primitive hexagonal unit cell with **A, B, C** vectors

The reciprocal lattice

Josiah Willard Gibbs first made the formalisation of reciprocal lattice vectors in 1881. The reciprocal vectors lie in "reciprocal space", an imaginary space where planes of atoms are represented by reciprocal points, and all lengths are the inverse of their length in real space.

Construction of reciprocal lattice by drawing a normal to each set of planes in the real lattice and marking off points along these normals at distances 1/d, from the origin, where d is the interplanar spacing of each set of planes.

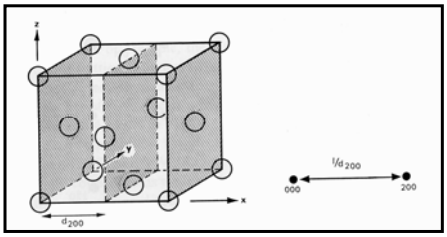

(200) Planes in the f.c.c. unit cell and the corresponding reciprocal lattice point.

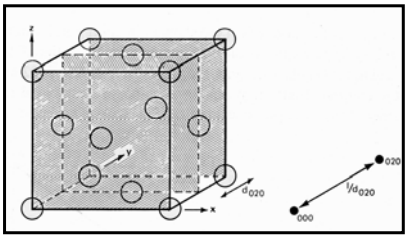

(020) Planes in the f.c.c. unit cell and the corresponding reciprocal lattice point.

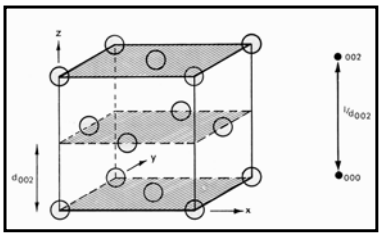

(002) Planes in the f.c.c. unit cell and the corresponding reciprocal lattice point.

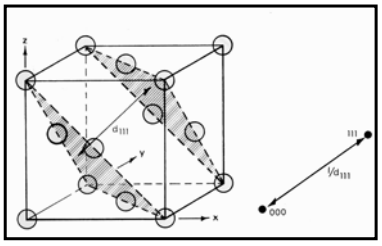

(111) Planes in the f.c.c. unit cell and the corresponding reciprocal lattice point.

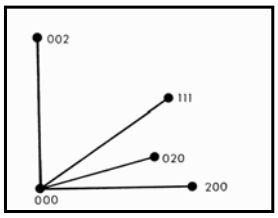

The basic array of the f.c.c. reciprocal lattice.

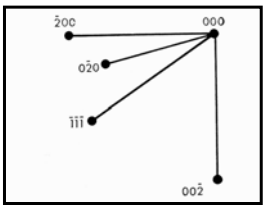

Reciprocal lattice points corresponding to the reverse sides of the planes.

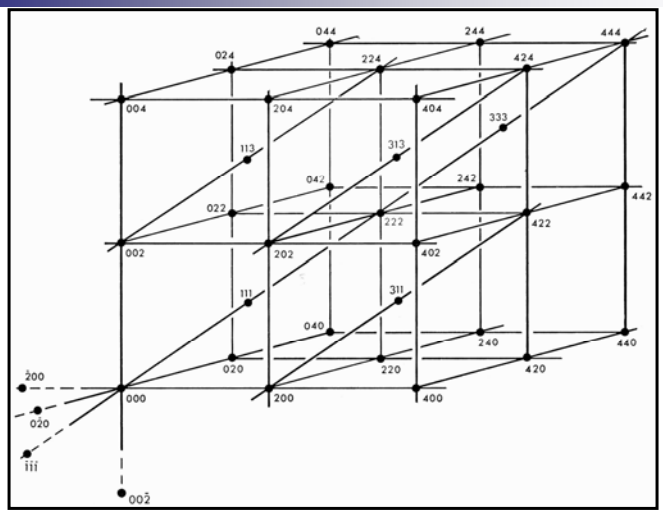

A sector of the full f.c.c. reciprocal lattice. The other sectors can be imagined extending in the directions of the dotted lines.

The **f.c.c. reciprocal lattice** is identical to a **real b.c.c. lattice**, with the atom positions substituted by reciprocal lattice points!!!

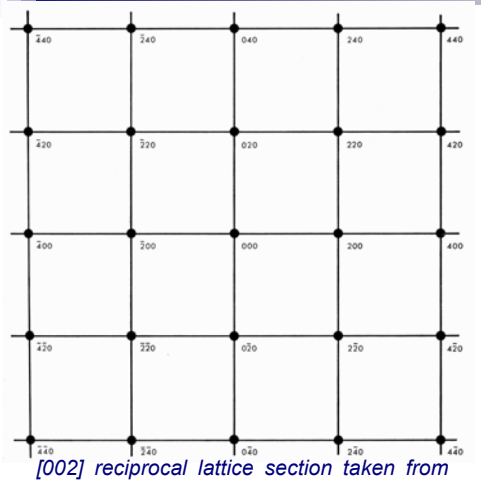

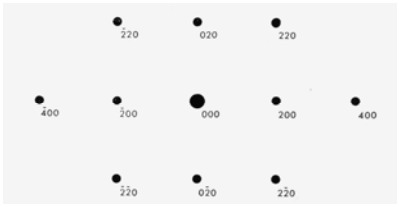

[002] reciprocal lattice section taken from the full reciprocal lattice.

The diffraction pattern is a section from the reciprocal lattice!!

Any diffraction pattern can be indexed by choosing the reciprocal lattice section with an identical spatial arrangement of points to that of the spots in the diffraction.

In general, the periodicity in the reciprocal lattice is given by:

$$\rho_{hkl}^{*} = \frac{1}{d_{hkl}}$$

In vector form, the general reciprocal lattice vector for the (h k l) plane is given by

$$s_{hkl} = \frac{n_{hkl}}{d_{hkl}}$$

where $\mathbf{n}_{hkl}$ is the unit vector normal to the (h k l) planes.
This concept can be applied to crystals, to generate a reciprocal lattice of the crystal lattice. The units in reciprocal space are $Å^{-1}$ or nm^{-1}

reciprocal lattice vectors

$$\mathbf{a}^* = \frac{\mathbf{b}\times\mathbf{c}}{\mathbf{a}.\mathbf{b}\times\mathbf{c}} \qquad \mathbf{b}^* = \frac{\mathbf{c}\times\mathbf{a}}{\mathbf{a}.\mathbf{b}\times\mathbf{c}} \qquad \mathbf{c}^* = \frac{\mathbf{a}\times\mathbf{b}}{\mathbf{a}.\mathbf{b}\times\mathbf{c}}$$

Ewald sphere

In 1913, P. P. Ewald demonstrated the use of the Ewald sphere together with the reciprocal lattice to understand diffraction. It geometrically represents the conditions in reciprocal space where the Bragg equation is satisfied.

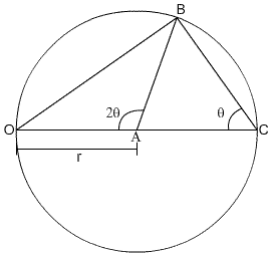

By using simple trigonometry: $\sin\theta = \frac{OB}{2r}$

If this geometry is constructed in reciprocal space, then it has some important implications.
The radius can be set to 1/λ, where λ is the experimental wavelength.
If O is the (0 0 0) reciprocal lattice point, and B is a general point (h k l), then the distance OB is $1/d_{hkl} = S_{hkl}$ The reciprocal vector between the points, S, increases in magnitude with increasing 2θ, Hence

$$\sin\theta = \frac{\frac{1}{d_{hkl}}}{\frac{2}{\lambda}} \quad \rightarrow \quad \lambda = 2\, d_{hkl} \sin\theta$$

Bragg's conditions are satisfied when the Ewald sphere cuts a reciprocal lattice point specified by the indices of the reflecting plane.

http://www.doitpoms.ac.uk/tlplib/reciprocal_lattice/ewald.php

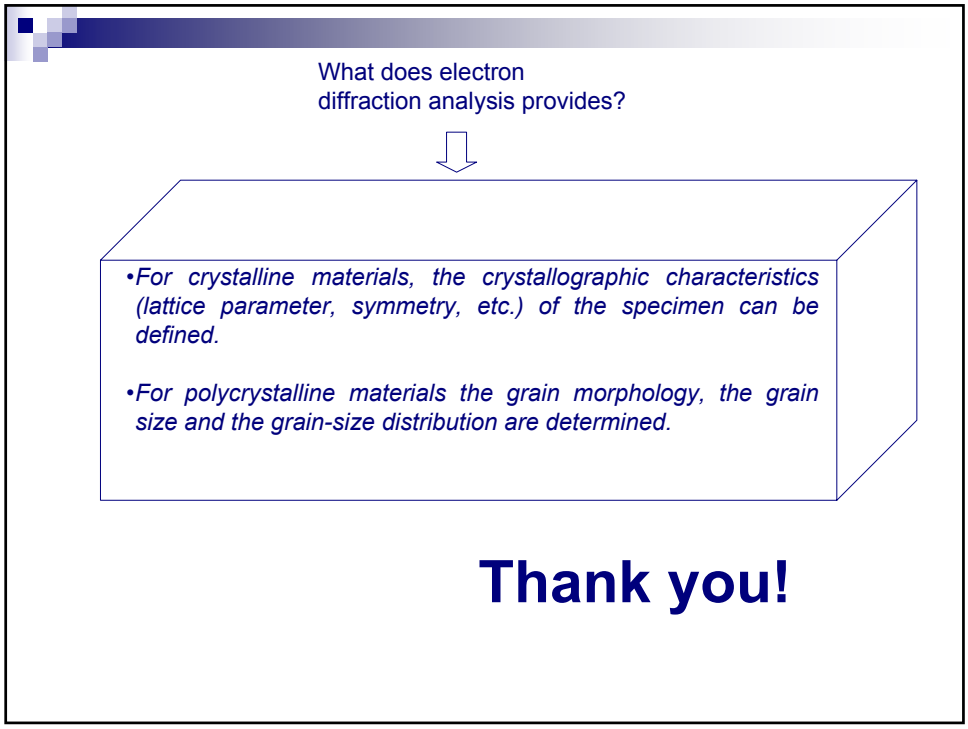
What does electron
diffraction analysis provides?
•For crystalline materials, the crystallographic characteristics (lattice parameter, symmetry, etc.) of the specimen can be defined.
•For polycrystalline materials the grain morphology, the grain size and the grain-size distribution are determined.
Thank you!

CONTRAST AND IMAGE FORMATION IN TEM

Dr. Andreas Delimitis

Chemical Process and Energy Resources Institute (CPERI)
Centre for Research & Technology - Hellas (CERTH)

Presentation Outline

- Defining image contrast in TEM
- TEM operation modes
- TEM imaging modes → BF, DF, WB imaging
- Principles of image contrast
- Mass - Thickness
- Diffraction contrast
  - Kinematic Theory of image contrast
  - Dynamical Theory of image contrast
  - Imaging of structural defects: dislocations, SFs, twins, grain boundaries
- Phase Contrast
  - HRTEM imaging
  - Moiré Contrast
  - Fresnel Contrast

Definition of Image Contrast

- What is image contrast?

$$\text{Contrast} = (I_1 - I_0)/I_0 = \Delta I/I_0$$

i.e. the relative difference in intensity between two areas in a TEM specimen

* Contrast # Intensity ⟶ inversely proportional !!

increased brightness brings upon reduced contrast details

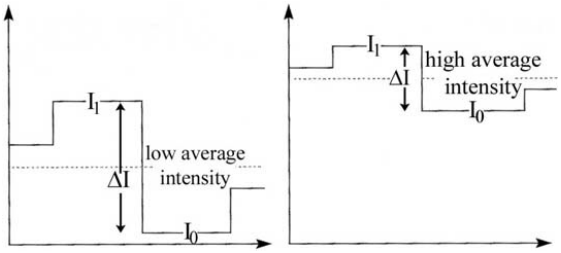

Transmission Electron Microscope

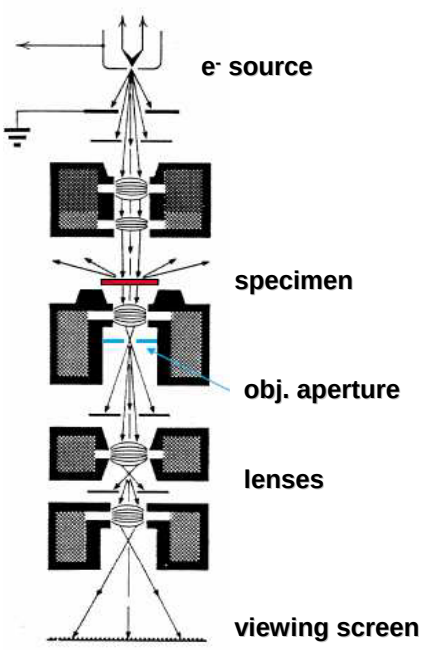

Presentation Outline

- Defining image contrast in TEM
- TEM operation modes
- TEM imaging modes → BF, DF, WB imaging
- Principles of image contrast
- Mass - Thickness
- Diffraction contrast
  - Kinematic Theory of image contrast
  - Dynamical Theory of image contrast
  - Imaging of structural defects: dislocations, SFs, twins, grain boundaries
- Phase Contrast
  - HRTEM imaging
  - Moiré Contrast
  - Fresnel Contrast

TEM Operation Modes

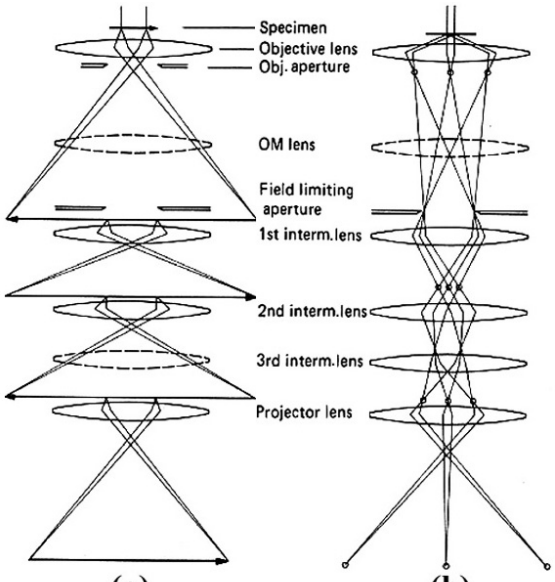

(a) Magnified TEM image

(b) Electron diffraction pattern

TEM Images:

- diffraction pattern
- objective aperture
- manipulate brightness

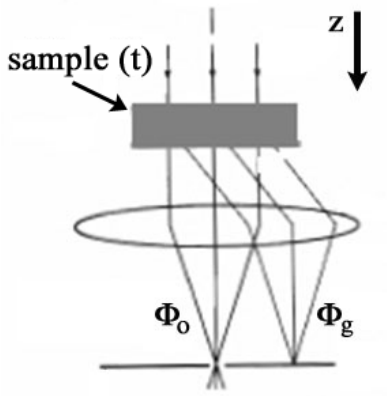

Variations in TEM images

Imaging between different materials could be tricky!!

Imaging and SAD patterns: strongly related!!!

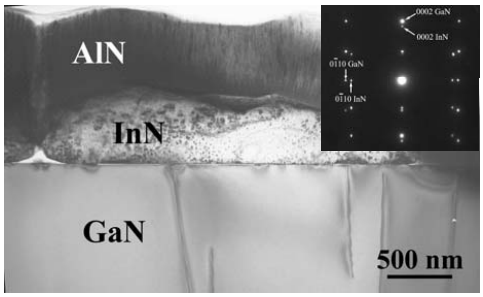

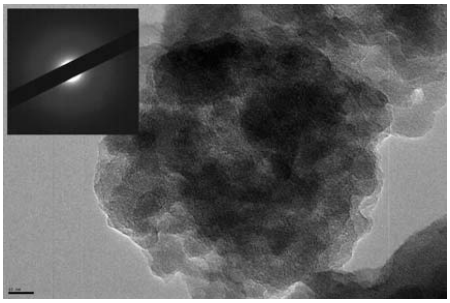

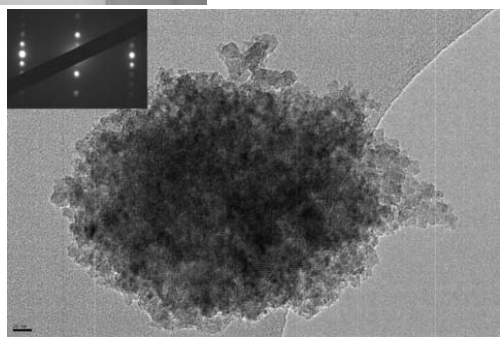

Presentation Outline

- Defining image contrast in TEM
- TEM operation modes
- TEM imaging modes
  - BF, DF, WB imaging
- Principles of image contrast
- Mass – Thickness contrast
- Diffraction contrast
  - Kinematic Theory of image contrast
  - Dynamical Theory of image contrast
  - Imaging of structural defects: dislocations, SFs, twins, grain boundaries
- Phase Contrast
  - HRTEM imaging
  - Moiré Contrast
  - Fresnel Contrast

TEM Imaging

 What does a TEM image depend on?

- Specimen
  - thickness
  - crystalline state
  - physical properties (e.g. magnetic materials)

- TEM accelerating voltage
  - contrast inversely proportional to E_0

- Objective aperture
  - direct and/or number of diffracted e^- beams allowed
  - * resolution !!

- Brightness and coherency of illumination system

- Lens aberrations HRTEM

TEM Imaging Modes

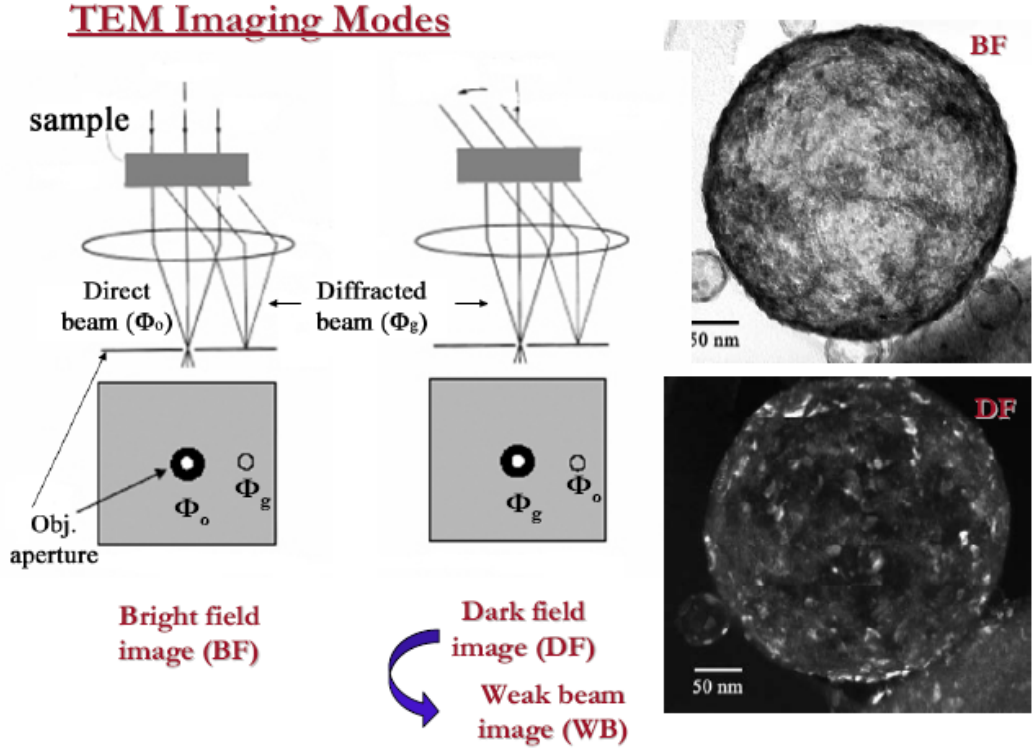

Bright Field (BF) Imaging

- Image is formed by the direct beam (Φ_o)
- Objective aperture excludes all diffracted beams
- Direct beam is on the microscope optical axis

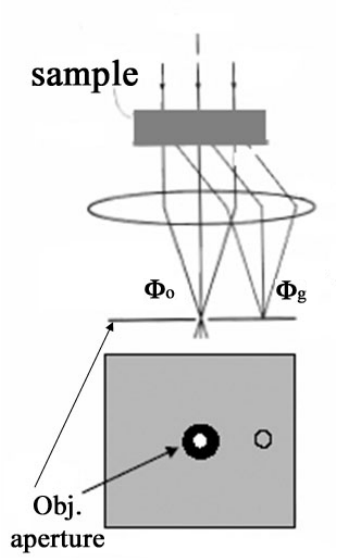

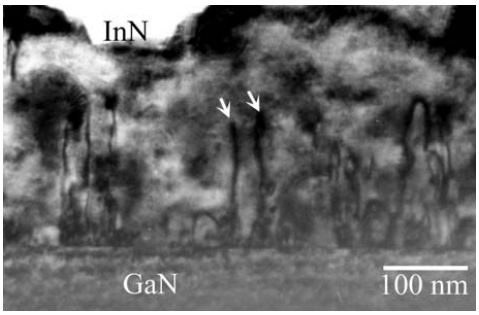

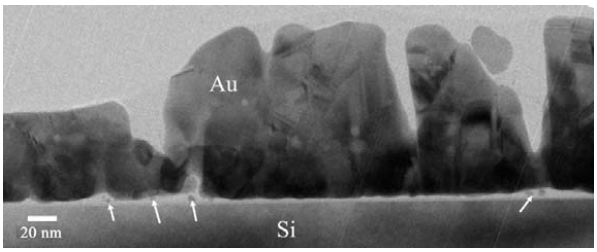

Dark Field (DF) Imaging

- Image is formed by one diffracted beam (Φ_g)
- Objective aperture excludes all other diffracted beams and the direct beam
- The diffracted beam is *usually* on the microscope optical axis
- Image is complementary to BF

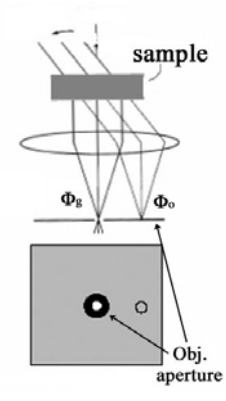

Centered DF image (DF)

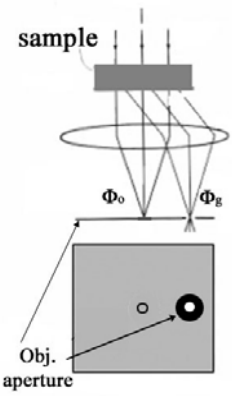

Displaced DF image

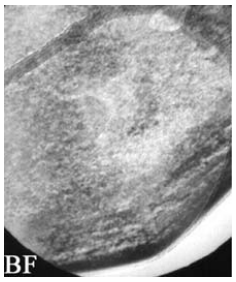

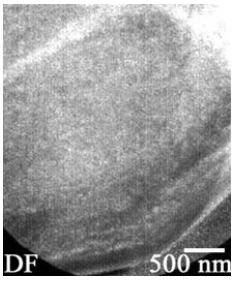

** lens aberrations !!*

Dark Field (DF) Imaging

Why form DF images??

- higher contrast → details resolved
- reveal differences in crystal orientation
- distinguish between various *crystallographically* different regions or phases
- distinguish between various *chemically* different phases
- reveal and identify structural defects

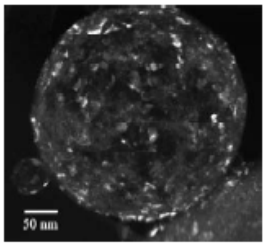

ZnO particles

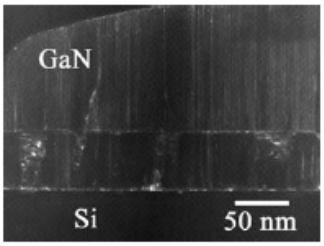

GaN/Si epitaxy

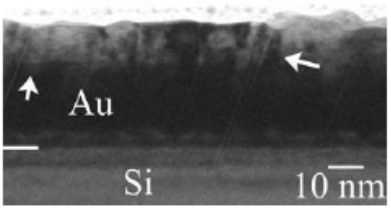

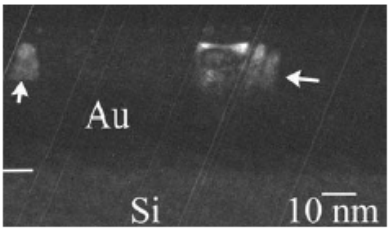

Au nano-islands on Si substrate

BF & DF Imaging in Two-Beam Conditions

- On-axis images often contain too much information
- Lattice defect analysis is greatly facilitated

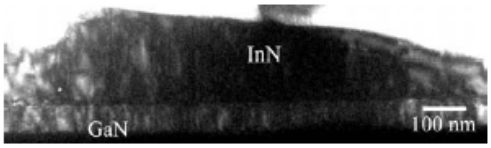

on axis

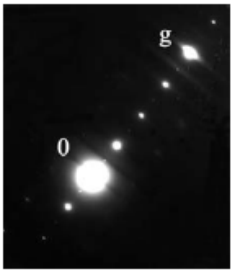

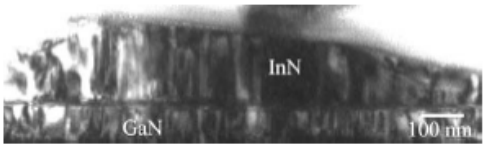

2-beam BF

2-beam BF, different g

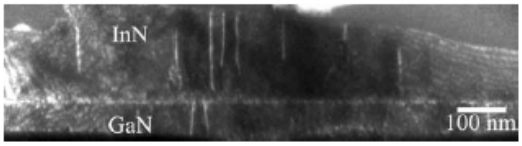

2-beam DF, different g

Weak Beam (WB) Imaging

- Image is formed by one diffracted beam (Φ_{-g}) → DF image!
- Objective aperture excludes all other diffracted beams and the direct beam
- The diffracted beam is on the microscope optical axis
- Image is complementary to BF
- Setting up requires two-beam imaging conditions

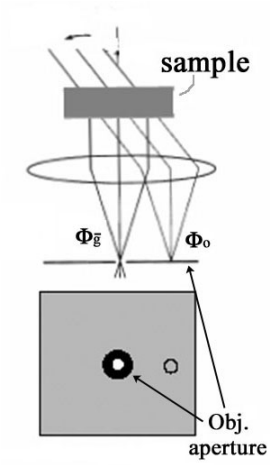

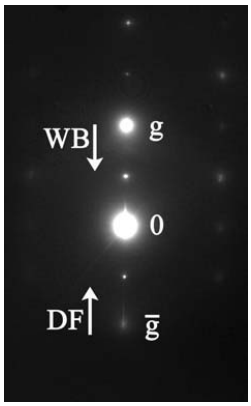

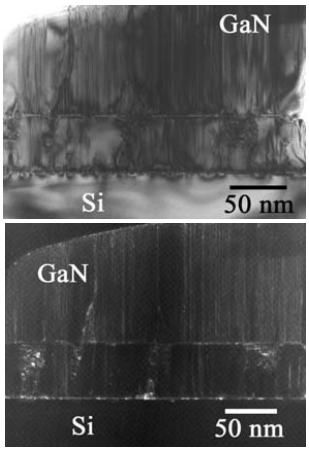

Weak Beam (WB) Imaging

Why form WB images??

- higher contrast → details resolved
- reveal and identify structural defects in crystalline materials
- image sharpness is greatly improved

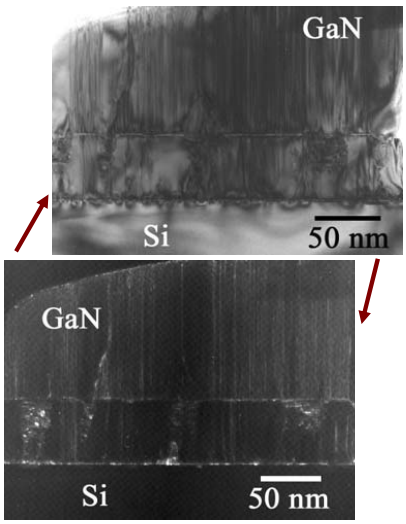

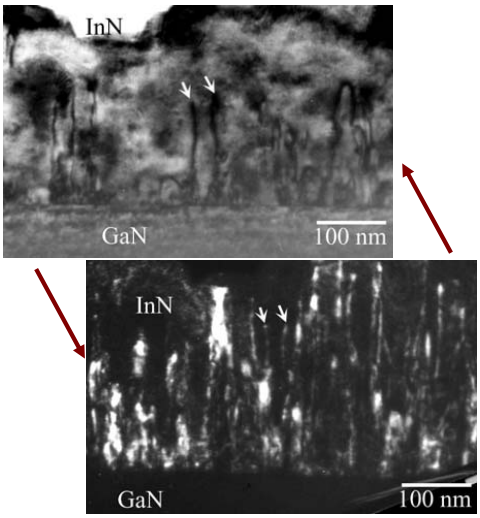

Presentation Outline

- Defining image contrast in TEM
- TEM operation modes
- TEM imaging modes
  BF, DF, WB imaging
- Principles of image contrast
- Mass – Thickness contrast
- Diffraction contrast
  Kinematic Theory of image contrast
  Dynamical Theory of image contrast
  Imaging of structural defects: dislocations, SFs , twins, grain boundaries
- Phase Contrast
  HRTEM imaging
  Moiré Contrast
  Fresnel Contrast

Principles of Image Contrast

Mass-Thickness contrast (Z, t) ← amplitude contrast → Diffraction contrast (Φ_o, Φ_g)

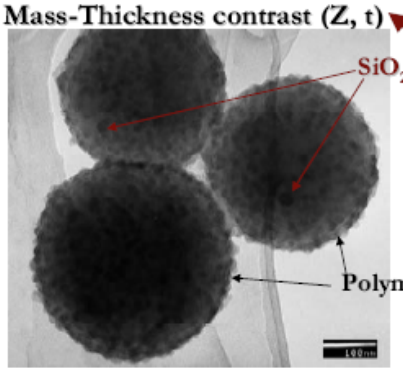

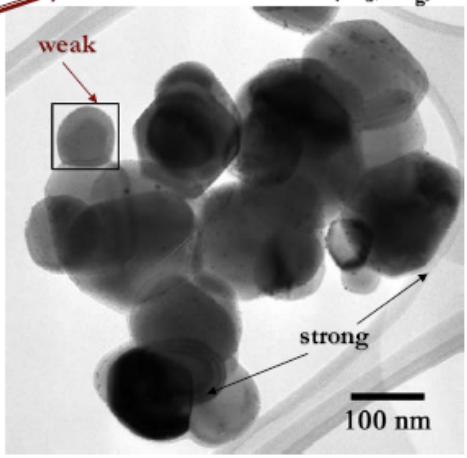

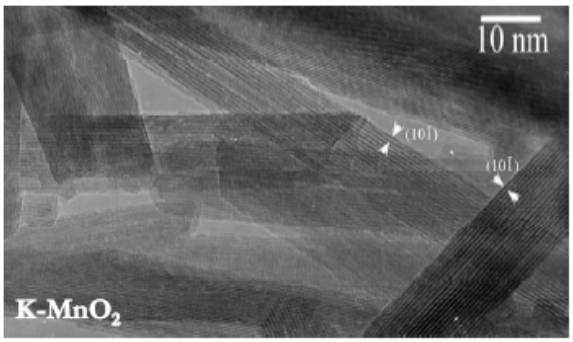

Phase contrast (Φ_o, Φ_{g1}, Φ_{g2} Φ_{g3},…)

Mass – Thickness Contrast

- Dominant contrast mechanism for poorly / non-crystalline materials
- Amplitude contrast
- Important for biological specimen

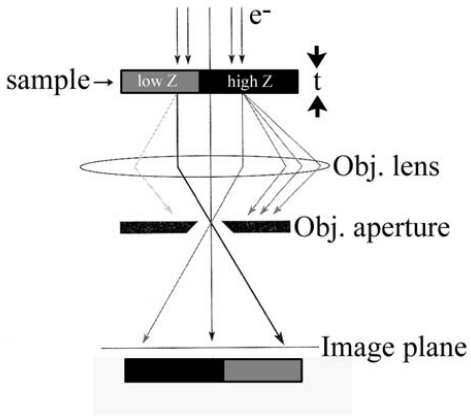

* Thicker areas (t) in a sample scatter more e^- → darker images
* Heavier elements (Z) in a sample scatter stronger → darker images

- Mass – thickness contrast on a TEM depends on:
1. accelerating voltage
2. objective aperture size

Mass – Thickness Contrast

- Incoherent (Rutherford) elastic scattering of the e^- beam

- Dependence on thickness t (Δt)

$$\text{Contrast} = \Delta I/I = 1-\exp(-Q\Delta t) \approx Q\Delta t = (N_0\sigma(\theta)\varrho/A)\,\Delta t$$

Q the total elastic scattering cross-section
N_0 Avogadro's number
$\sigma(\theta)$ the single atom scattering cross-section
ϱ the density
A the atomic weight

- Dependence on atomic number Z

Rutherford differential scattering cross-section:

$$d\sigma(\theta)/d\Omega = e^4Z^2 / 16(E_0)^2 \sin^2\theta/2$$

E_0 the energy of the electron beam
θ the scattering angle

* $\sigma(\theta)$:
- proportional to Z
- inversely proportional to θ, E_0

Atomic scattering factor $f(\theta)$: ($|f(\theta)|^2 = d\sigma(\theta)/d\Omega$)

$$f(\theta) = [(1+E_0/m_0c^2)/8\pi^2a_0]\,(\lambda/\sin\theta/2)^2\,(Z-f_x)$$

m_0 the rest mass of e^-
a_0 the Bohr radius of the scattering atom
f_x the X-rays scattering factor

* $f(\theta)$:
- proportional to Z, λ
- inversely proportional to θ

$$F(\theta) = \Sigma_i f_i e^{2\pi i(hxi+kyi+lzi)}$$

Mass – Thickness Contrast Examples

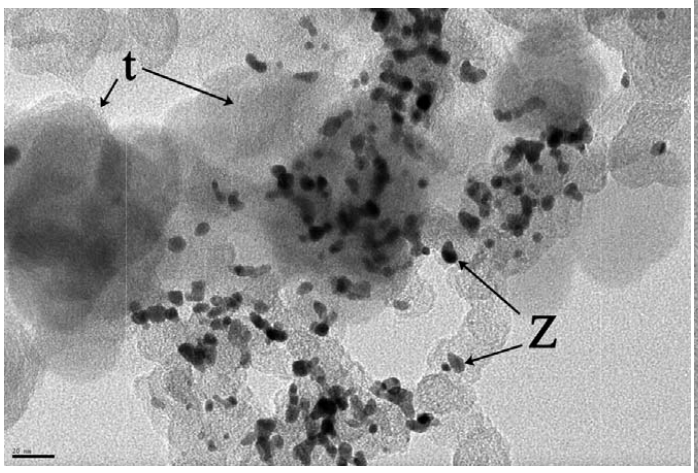

Pt particles on amorphous C black

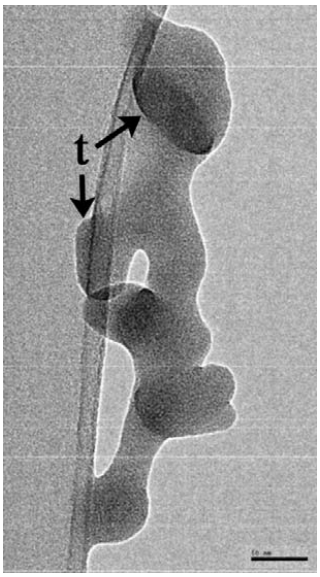

Biological sample

Presentation Outline

- Defining image contrast in TEM
- TEM operation modes
- TEM imaging modes
  - BF, DF, WB imaging
- Principles of image contrast
- Mass – Thickness contrast
- Diffraction contrast
  - Kinematic Theory of image contrast
  - Dynamical Theory of image contrast
  - Imaging of structural defects: dislocations, SFs, twins, grain boundaries
- Phase Contrast
  - HRTEM imaging
  - Moiré Contrast
  - Fresnel Contrast

Diffraction Contrast

- Amplitude contrast
- Coherent elastic scattering

Bragg's Law: $n\lambda = 2d_{hkl}\sin\theta$

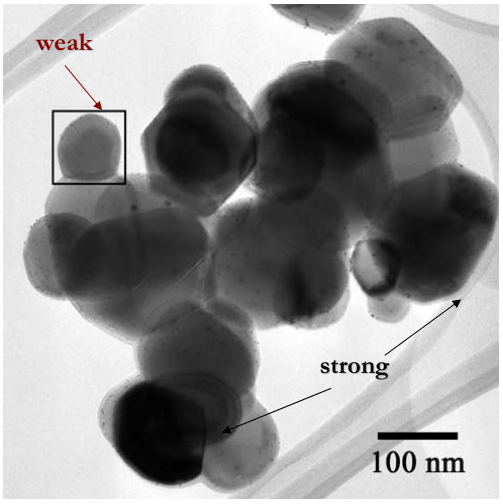

Areas diffracting strongly

Dark contrast in BF TEM images
Bright contrast in DF TEM images

Objective aperture !!

Kinematic Theory of Electron Diffraction

Assumptions:

- monochromatic e^- beam
- defect-free specimen
- small fraction of e^- beam scattered
- no absorption effects - elastic scattering
- only two beams considered (Φ_o, Φ_g)

* 2-beam conditions

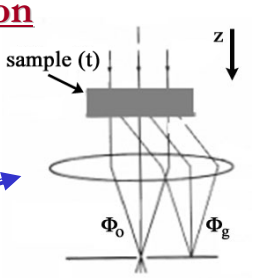

- Intensity of the diffracted beam g

$$I_g = |\Phi_g|^2 = (\pi/\xi_g)^2 [(\sin^2\pi t s_g)/(\pi s_g)^2]$$

$$I_g = 1\text{-}I_0 = 1\text{-}|\Phi_0|^2$$

* I_0 and I_g are complementary
* periodic (sinusoidal) dependence of intensity on t and s_g

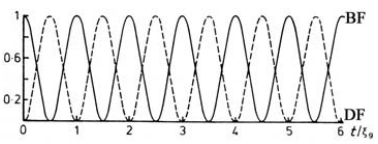

t the thickness of the crystal
s_g the excitation error
$\xi_g = \pi V_c \cos\theta/\lambda F_g$ the extinction distance for the reflection g
V_c the volume of the unit cell
λ the e^- beam wavelength
F_g the structure factor for reflection g

Thickness Fringes and Bend Contours

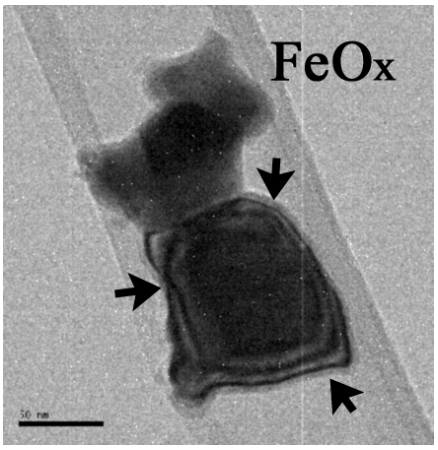

Thickness fringes: t variable and s_g constant

$I_g = |\Phi_g|^2 = (\pi/\xi_g)^2 [(\sin^2\pi t s_g)/(\pi s_g)^2]$

$ts_g = 0,1,2, \ldots ,n$

$\downarrow$

$\sin^2\pi t s_g = 0$

$\downarrow$

$I_g = 0$

* $s_g = 0$????

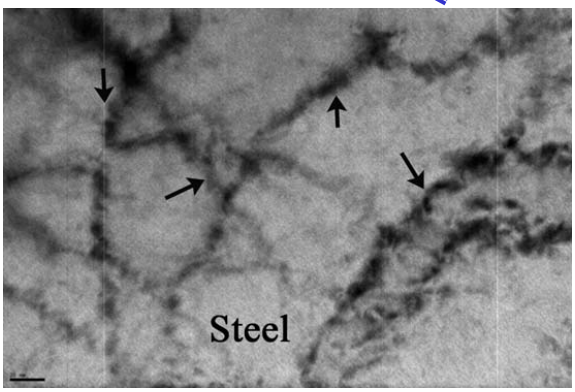

Bend contours: s_g variable and t constant

Dynamical Theory of Electron Diffraction

Real TEM conditions:

- considerable specimen thickness
- stronger diffracted beam ($\Phi_g > \Phi_o$)
- multiple diffraction events
- beam absorption effects

Dynamical theory

- only two beams considered (Φ_o, Φ_g)
- crystal divided into thin columns

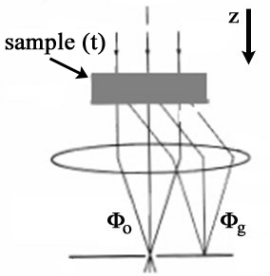

* 2-beam conditions

Howie – Whelan Equations

$$\frac{d\phi_0}{dz} = \frac{\pi i}{\xi_0}\phi_0 + \frac{\pi i}{\xi_g}\phi_g e^{2\pi i s z}$$

$$\frac{d\phi_g}{dz} = \frac{\pi i}{\xi_g}\phi_0 e^{-2\pi i s z} + \frac{\pi i}{\xi_0}\phi_g$$

* Dynamical coupling of Φ_o and Φ_g
* changes in Φ_g depend both in Φ_g and Φ_o

Intensity of the diffracted beam g

$I_g = |\Phi_g|^2 = (\pi t/\xi_g)^2 [(\sin^2\pi t s_g^{eff})/(\pi t s_g^{eff})^2]$

$I_g = 1 - I_0 = 1 - |\Phi_0|^2$

Effective excitation error:

$s_g^{eff} = (s_g^2 + 1/\xi_g^2)^{1/2}$

$s_g^{eff} \neq 0$

Dynamical Theory of Electron Diffraction

Absorption and inelastic scattering from crystals:

$$1/\xi_g \rightarrow 1/\xi_g + i/\xi_g'$$

* I_0 and I_g are complementary
* periodic (sinusoidal) dependence of intensity on t and s_g^{eff} but, finite!

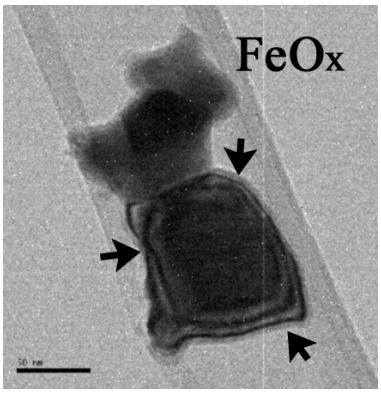

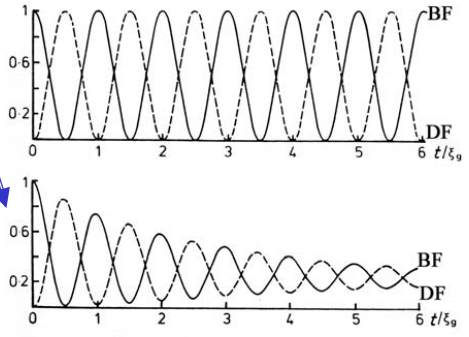

Dynamical Theory of Electron Diffraction

Existence of lattice defects

Howie – Whelan Equations

$$\frac{d\phi_0}{dz} = \frac{i\pi}{\xi_0}\phi_0 + \frac{i\pi}{\xi_g}\phi_g \exp[2\pi i(sz + \mathbf{g}\cdot\mathbf{R})]$$

$$\frac{d\phi_g}{dz} = \frac{i\pi}{\xi_g}\phi_0 \exp[-2\pi i(sz + \mathbf{g}\cdot\mathbf{R})] + \frac{i\pi}{\xi_0}\phi_g$$

R the displacement vector associated with the lattice defect

materials' properties !!

Line defects: dislocations
- edge
- screw
- mixed

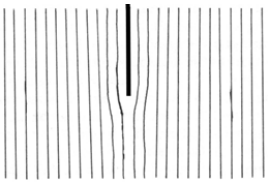

Twins

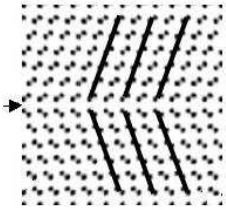

Planar defects

Stacking faults

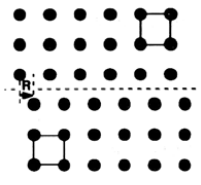

Grain boundaries

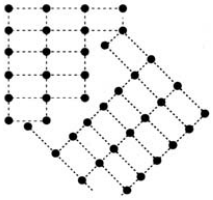

Line Defects: Dislocations

* *increased bending of lattice planes near the dislocation core → strong diffraction contrast*

Parameters defining a dislocation:

- dislocation line *l*
- Burger's vector *b*
- glide plane

Types of dislocations:

edge → Burger's vector *b* perpendicular to dislocation line ($b \perp l$)
screw → Burger's vector *b* parallel to dislocation line ($b // l$)
mixed → with edge and screw components

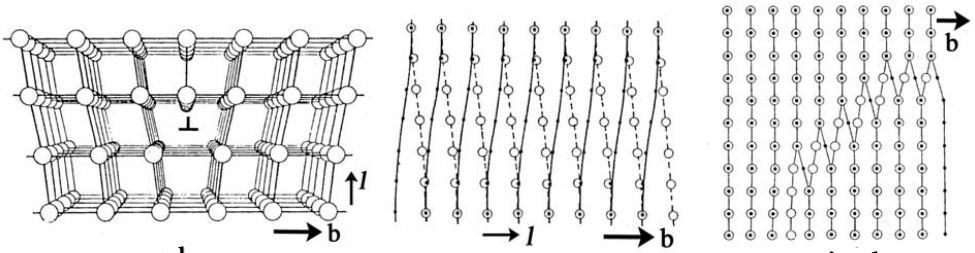

Line Defects: Dislocations

* Burger's vector determination ⇒ Invisibility criterion: $g_n \cdot R = 0$
$R // (g_1 \times g_2)$

Displacement vector R:

$$R = (1/2\pi)\{b\varphi + 1/4(1-\nu)[b_e + b \times u(2(1-2\nu)\ln r + \cos 2\varphi)]\}$$

(polar coordinates, r & φ)
where b_e the edge component of Burger's vector
u the unit vector along the dislocation line
ν Poisson's ratio

- Screw dislocation: $b_e = 0$ and $b // u \rightarrow R = b\varphi/2\pi$, then $g \cdot R = 0$ when $g \cdot b = 0$
- Edge/mixed dislocation: $b = b_e$ and $b \times u \neq 0$, then $g \cdot R = 0$ when $g \cdot b = 0$ and $g \cdot b \times u = 0$

Dislocation Examples

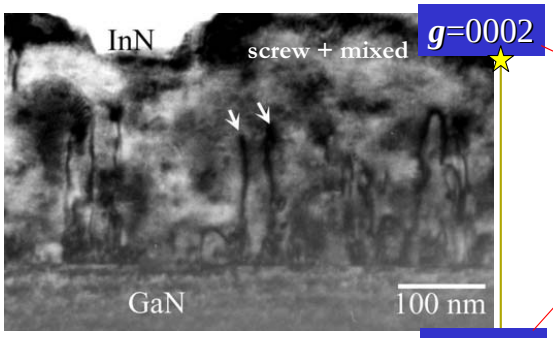

Threading dislocations in InN/GaN films

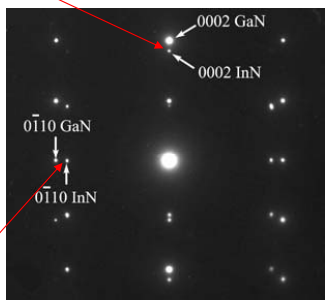

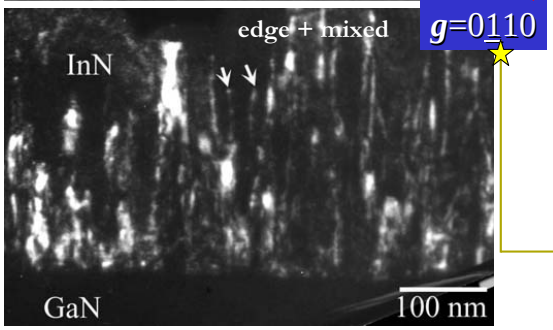

Imaging with two different vectors g reveals the character and density of dislocations

* DF / WB images !!

Planar Defects: Stacking Faults

- Distortions of stacking sequence in crystalline materials (SF)

missing plane → intrinsic SF
added plane → extrinsic SF

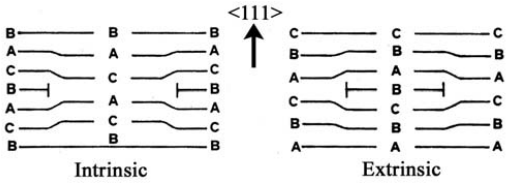

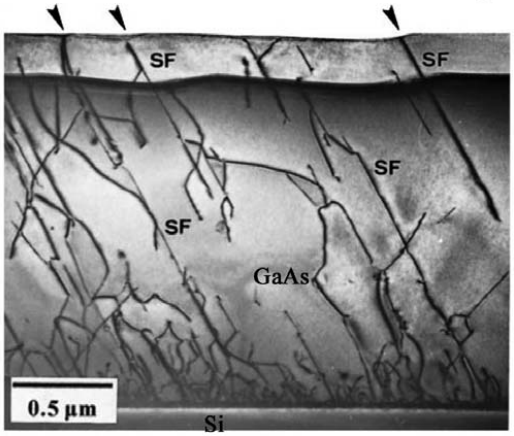

* SF displacement vector determination

Invisibility criterion: $g_n \bullet R=0$

Planar Defects: Stacking Faults

- *Imaging in BF and DF conditions enables identification of SFs*

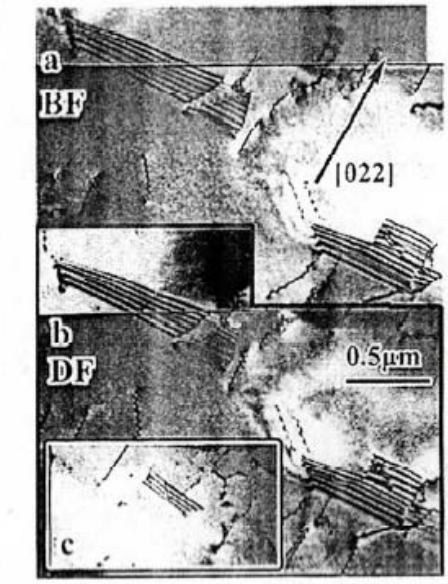

- *TEM contrast of stacking faults:*

α-fringes parallel to intersection of SF with specimen surface

* α-fringes in TEM images:
- BF symmetric
- DF asymmetric

Asymmetric (not complementary) contrast between BF and DF images

Planar Defects: Twins

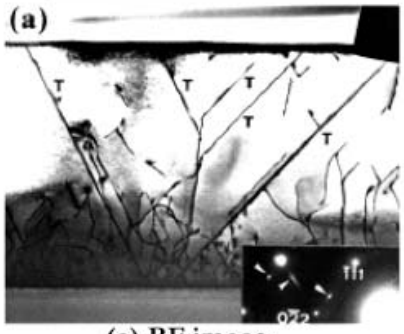

(a) BF image

Crystal divided into two symmetrical parts

Twin plane

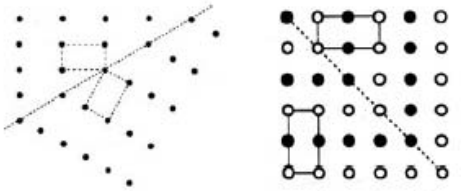

twin ordered twin

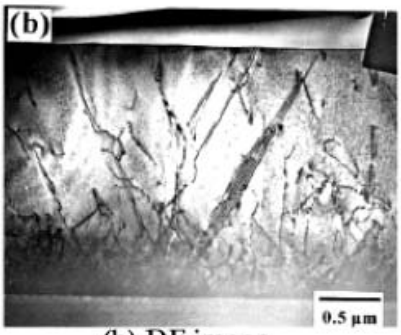

(b) DF image

- TEM imaging in BF/DF conditions

Twin identification by:
- δ-fringes in BF and DF images
- SAD patterns

* δ-fringes in TEM images:
- BF asymmetric
- DF symmetric

Planar Defects: Grain Boundaries

- Planes bounding grains of different crystallographic orientations or various phases in materials

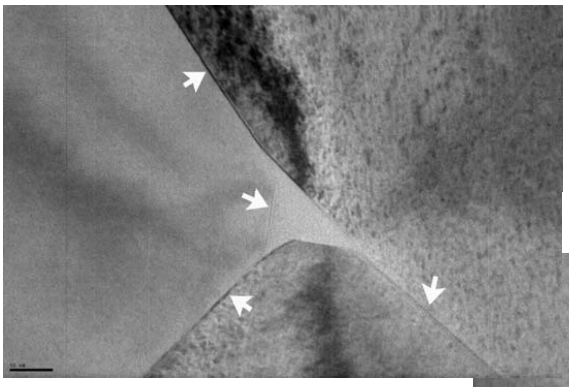

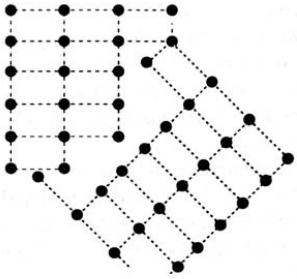

Edge-on

Inclined

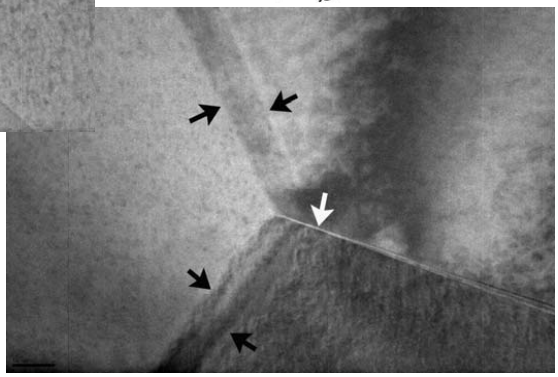

Planar Defects: Grain Boundaries

* Diffraction conditions are often quite distinct between adjacent grains

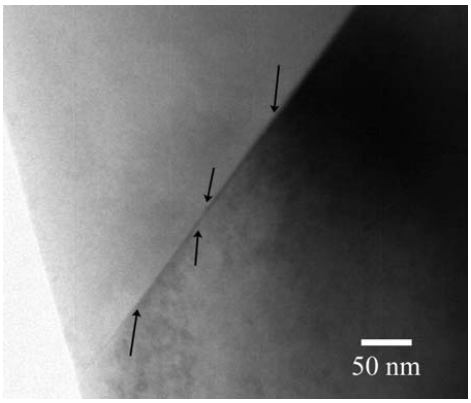

* Distinguishable by the intense strain contrast associated with high defect concentration

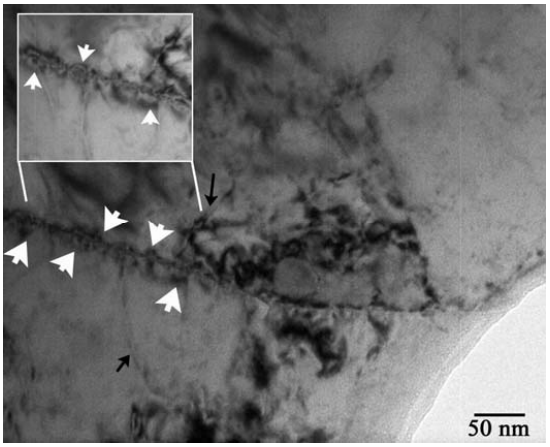

* Often imaged as α-, δ- or thickness fringes, depending on their defect type

Presentation Outline

- Defining image contrast in TEM
- TEM operation modes
- TEM imaging modes
  BF, DF, WB imaging
- Principles of image contrast
- Mass – Thickness contrast
- Diffraction contrast
  Kinematic Theory of image contrast
  Dynamical Theory of image contrast
  Imaging of structural defects: dislocations, SFs, twins, grain boundaries
- Phase Contrast
  HRTEM imaging
  Moiré Contrast
  Fresnel Contrast

Phase Contrast

- Contrast arises when e^- waves with different phases pass through the objective aperture
- Image formed using multiple e^- beams

use of large objective apertures in TEM !!

* image formed using one set of g

Lattice fringe image

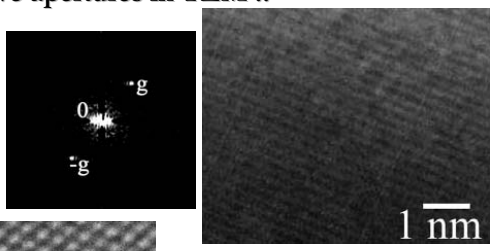

* image formed using many sets of g

Structure image

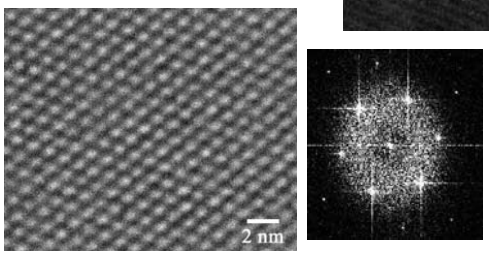

Phase Contrast

- Lattice fringe image creation

  two beam interference (Φ_0 and Φ_g)

  e^- wavefunction: $\Psi = \Phi_0 exp2\pi i(k_1 \cdot r) + \Phi_g exp(2\pi i k_D \cdot r)$

  $k_D = k_1 + g + s_g$ wave vectors

  intensity: $I = \Phi_0^2 + B^2 + 2\Phi_0 B cos(2\pi(g+s_g)\cdot r - \pi t s_{eff} + \pi/2)$

  $B = sin(\pi t s_{eff}) / \xi_g s_{eff}$

  * periodic oscillation of I normal to $(g+s_g)$ fringes
  * periodicity depends on s_g and t
  * fringe separation is $1/g$ (interplanar spacing)

- Calculations extended in many -beam case atomic structure images

HRTEM Images

- contributions of many e^- beams
- oriented in a low-index zone axis
- large objective apertures
- imaging of crystalline structure down to atomic level

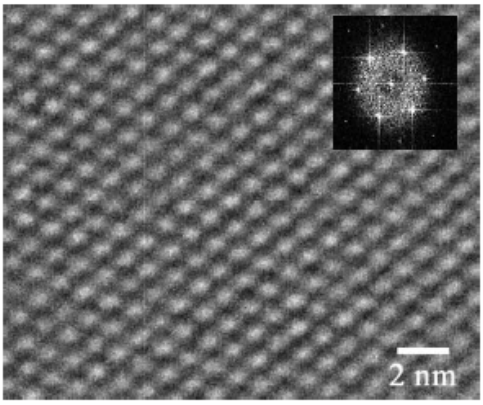

HRTEM images depend on:

- thickness t [crystal potential $V(r)$]
- monochromatic, coherent e^- sources
- defocus conditions Δf
- TEM lens aberrations (C_s)

HRTEM image simulation is a requirement

- Contrast Transfer Function, CTF

$H(u)=A(u)\,E(u)\,exp[-i\chi(u)]$, $\chi(u)=\pi\Delta f\lambda u^2+(1/2)\pi C_s\lambda^3 u^4$

Required: $H(u) \gg \& \neq 0$ → $\Delta f_{Sch} = -(1.33 C_s \lambda)^{1/2}$ Scherzer Defocus

HRTEM Images

VPO industrial catalyst, after reaction:

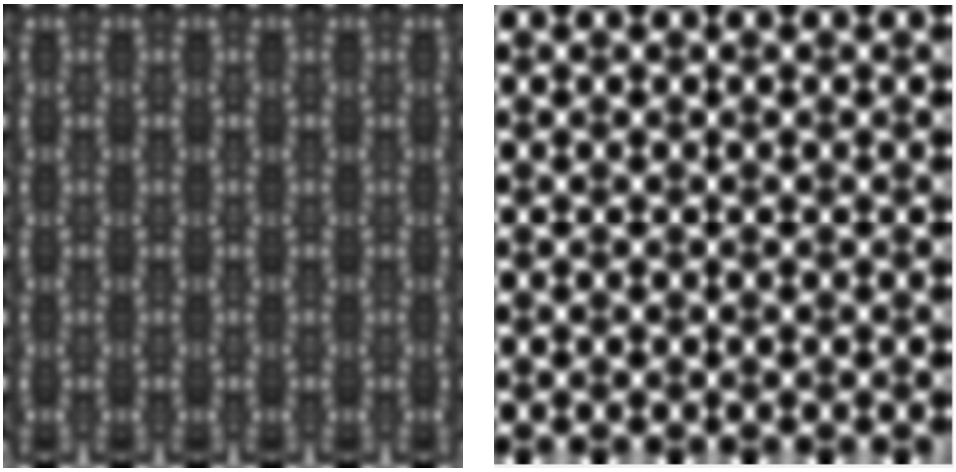

* **Which are the different catalyst phases in the two HRTEM images?**

HRTEM Images

* **Both images represent the same phase, $(VO)_2P_2O_7$!!!**

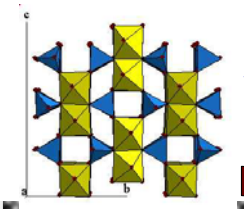

1. Structure creation
2. Calculation of HRTEM simulated images
3. HRTEM maps

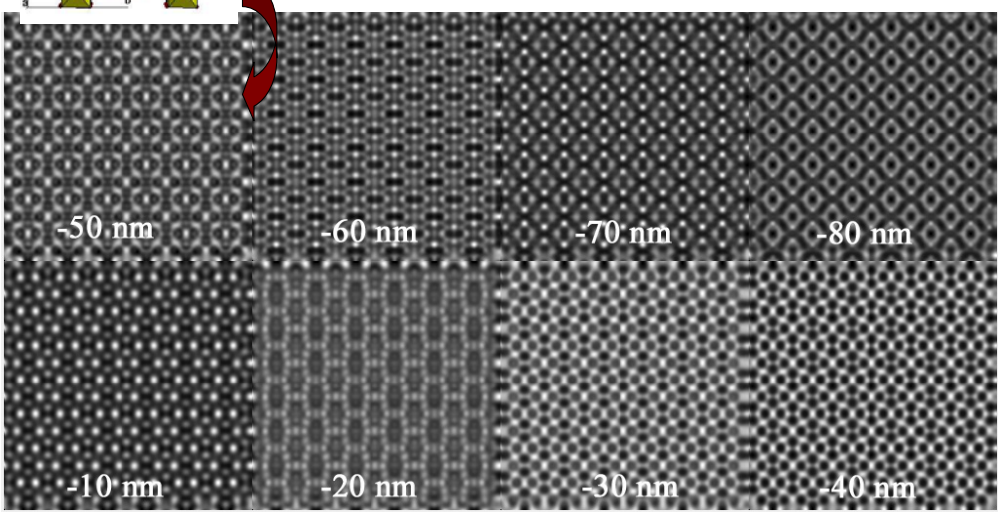

Moiré Fringes

- Formed by interference of two sets of lines with closed periodicities

↓ lattice planes

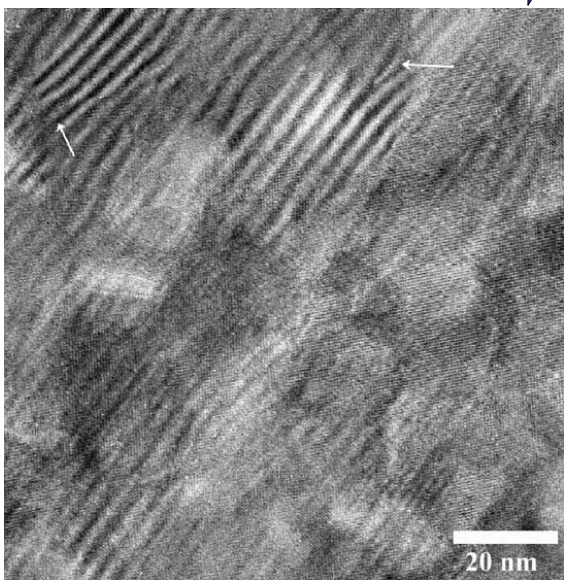

- Coarser than lattice fringes
- superposition of two crystalline lattices
- highly sensitive on even tiny misorientations in the two crystal structures superimposed
- imaging *does not* require HRTEM conditions

Moiré Fringes

- Types of Moiré fringes:

1. Translational → lattice planes parallel & with different spacings (d_1, d_2)

↓

Moiré fringes parallel

$$d_{tm} = d_1 d_2/(d_1-d_2)$$

2. Rotational → lattice planes rotated through angle α & with equal spacing d

↓

Moiré fringes perpendicular to their average direction

$$d_{rm} = d/2\sin\alpha/2$$

3. Mixed → lattice planes rotated through angle α & with different spacings (d_1, d_2)

↓

Moiré fringes direction not straightforward

$$d_{mm} = d_1 d_2/(d_1^2+d_2^2-2d_1 d_2\cos\alpha)^{1/2}$$

$$\sin\theta_{mm} = d_1\sin\alpha/(d_1^2+d_2^2-2d_1 d_2\cos\alpha)^{1/2}$$

Moiré Fringes

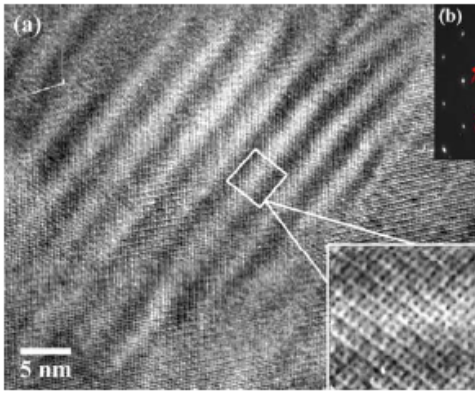

* co-existence of more than one type of Moiré fringes
* phase identification facilitated in complex systems

* misfit dislocations presence in epitaxial systems
* local variations of lattice constants
* residual strain estimations

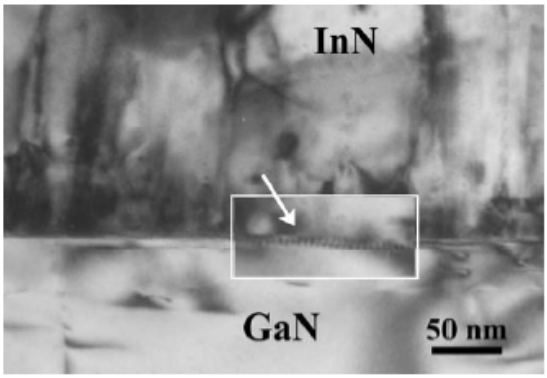

Fresnel Fringes

- Imaged as black or white fringes at the edges of specimen or within holes
- Visualization requires out of focus images !!

- underfocused image → white fringe
- overfocused image → black fringe

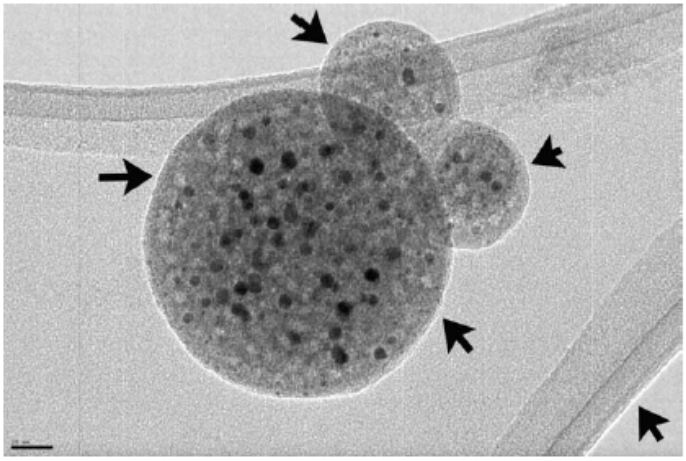

** objective lens astigmatism correction*

Further Reading

D.B Williams and C.B. Carter, *Transmission Electron Microscopy* vols. I-IV, Plenum Publishing Corporation, New York (1996)

P. Hirsch, A. Howie, R.B. Nicholson, D.W. Pashley and M.J. Whelan, *Electron Microscopy of Thin Crystals*, 2nd edition, Krieger, Huntington, New York (1977)

P.J. Goodhew and F.J. Humphreys, *Electron Microscopy and Analysis*, 2nd edition, Taylor & Francis (1988)

J.M. Cowley, *Electron Diffraction Techniques* 1 & 2 (ed. J.M. Cowley), Oxford University Press, New York (1992)

D. Van Dyck, *Electron Microscopy in Materials Science*, World Scientific, River Edge, New Jersey (1992)

M.H. Loretto and R.E. Smallman, *Defect Analysis in Electron Microscopy*, Chapman and Hall, London (1975)

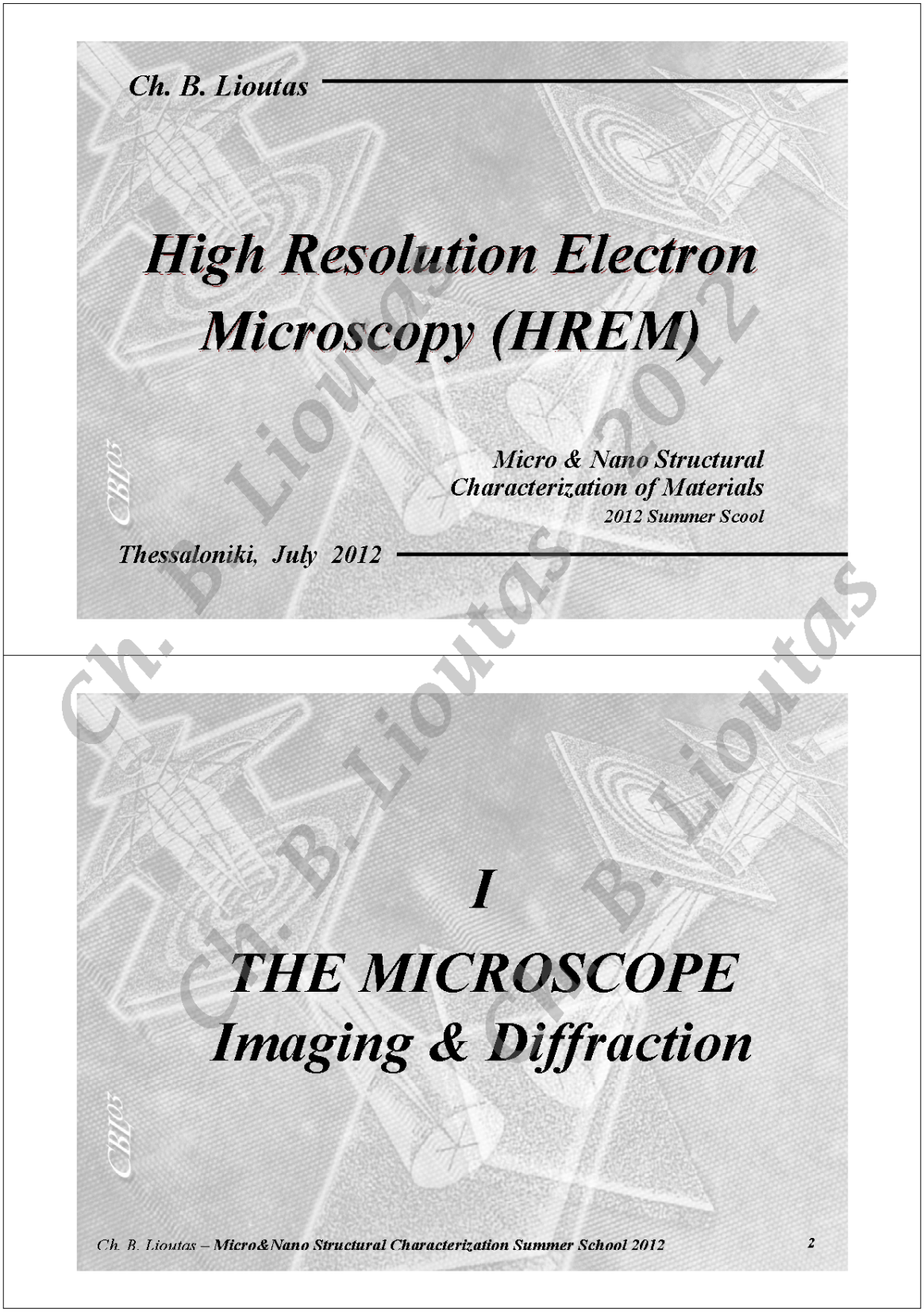
Ch. B. Lioutas
High Resolution Electron Microscopy (HREM)
Micro & Nano Structural Characterization of Materials
2012 Summer Scool
Thessaloniki, July 2012
CBL05
I
THE MICROSCOPE
Imaging & Diffraction
CBL05
Ch. B. Lioutas – Micro&Nano Structural Characterization Summer School 2012
2

The Optical Microscope (linear optics)

Geometrical optics
Dual character of electrons
ELECTRON-OPTICS
Description completely analogous to the light rays

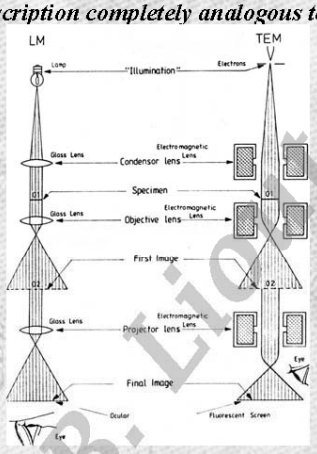

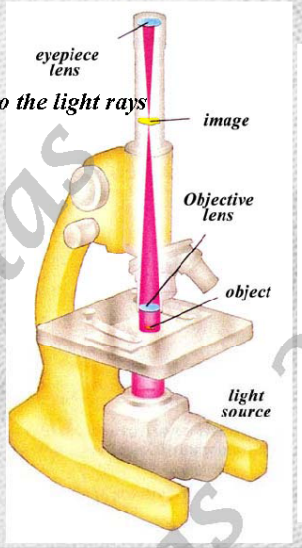

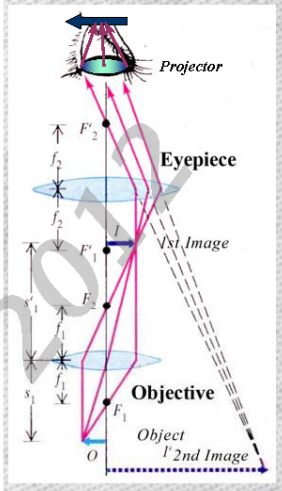

Diffraction

Diffraction

general effect of wave phenomena occurring whenever a portion of a wavefront (elastic, electromagnetic or matter wave) is obstructed in some way

The wavefront is modified from one point to the next one

Final Result on the observed image

Deviation of the intensity distribution that is predicted from the linear propagation

Increasing or decreasing of the intensity at "unexpected" points that give rise to bright or dark fringes

Diffraction (Huygens – Fresnel Principle)

Every unobstructed point of a primary wavefront, at a given instant in time, serves as the source of spherical secondary wavelets that advance with a speed and frequency equal to that of the primary wavefront. Moreover, the primary wavefront at some later time is the envelope of the secondary wavelets

The amplitude of the resulting wave at a point beyond P is the superposition of all of these waves (considering their amplitudes and relative phases). The calculation requires the integration of the elementary wavelets dy_s over all the diffracting space

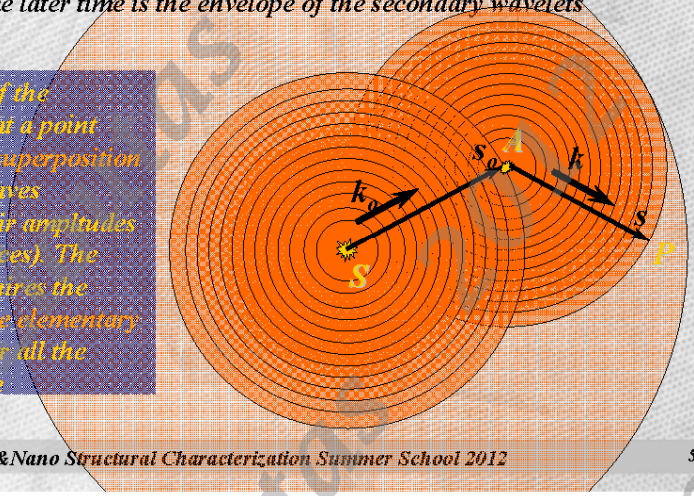

Ch. B. Lioutas – Micro&Nano Structural Characterization Summer School 2012 5

Electron diffraction (basic formula)

Diffraction result from the interaction of the secondary wavelets "produced" from every scattering point of the obstacle (Huygens-Fresnel Principle)

We must calculate the optical path-length difference (or phase difference) for every wavelet in relation to an arbitrary origin

$\Delta\varphi = 2\pi/\lambda(OB+OC)$

Fraunhofer approximation : large distances wavelets become plane waves

$2\pi/\lambda(r\cos\theta_1 + r\cos\theta_2)$

$2\pi(k_o\, r\cos\theta_1 + k\, r\cos\theta_2) =$

$2\pi(-\mathbf{k}_o\,\mathbf{r} + \mathbf{k}\,\mathbf{r})$

$2\pi(-\mathbf{k}_o + \mathbf{k})\,\mathbf{r} = 2\pi\,\mathbf{K}\,\mathbf{r}$

$1/\lambda = |k| = |k_o|$ και $\mathbf{K} = \mathbf{k} - \mathbf{k}_o$

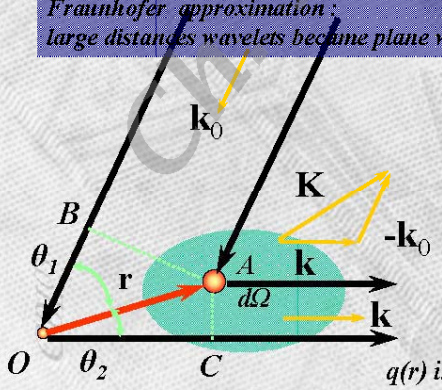

q(r) the amplitude scattered per volume unit the secondary wavelet from point A

$$q(\mathbf{r})\,d\Omega\,\exp[i2\pi\mathbf{K}\cdot\mathbf{r}]$$

q(r) is analog to the V(r) the potential in point A

Ch. B. Lioutas – Micro&Nano Structural Characterization Summer School 2012 6

Electron diffraction (basic formula)

Diffraction result from the interaction of the secondary wavelets "produced" from every scattering point of the obstacle (Huygens-Fresnel Principle)

We must calculate the optical path-length difference (or phase difference) for every wavelet in relation to an arbitrary origin

$$\Delta\varphi = 2\pi/\lambda(OB+OC)$$

$$2\pi/\lambda(r\cos\theta_1 + r\cos\theta_2)$$

$$2\pi(k_o\, r\cos\theta_1 + k\, r\cos\theta_2) =$$

$$2\pi(-\mathbf{k}_o\,\mathbf{r} + \mathbf{k}\,\mathbf{r})$$

$$2\pi(-\mathbf{k}_o + \mathbf{k})\,\mathbf{r} = 2\pi\,\mathbf{K}\,\mathbf{r}$$

$$1/\lambda = |k| = |k_o| \;\kappa\alpha\iota\; \mathbf{K} = \mathbf{k} - \mathbf{k}_o$$

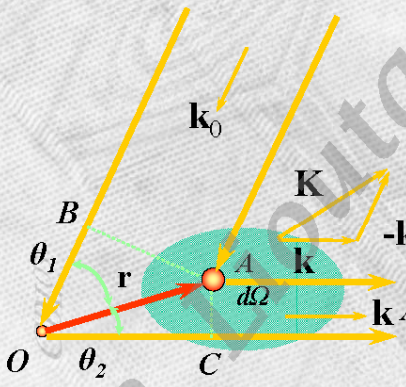

Superposition of the secondary wavelets triple integral over all diffraction space (Ω)

$$A(\theta) = \iiint_{\Omega} \frac{2\pi m_o e}{h^2} V(\mathbf{r}) \exp[i 2\pi \mathbf{K}\cdot\mathbf{r}]\, d\Omega$$

e charge & m_o rest mass of electron, h Plank's constant, V(r) the potential in point A

Electron diffraction (Fourier Transform)

$$A(\theta) = \frac{2\pi m_o e}{h^2} \iiint_{\Omega} V(\mathbf{r}) \exp[i 2\pi \mathbf{K}\cdot\mathbf{r}]\, d\Omega$$

The integral gives the Fourier Transform of the function that describes the potential of the material that induces the electrons' diffraction

The intensity of every diffracted beam in Fraunhofer diffraction conditions is proportional to Fourier Transform and is observed on the back focal plane of the imaging lens

A lens visualizes

the Fourier Transform of the function that describes the imaging object

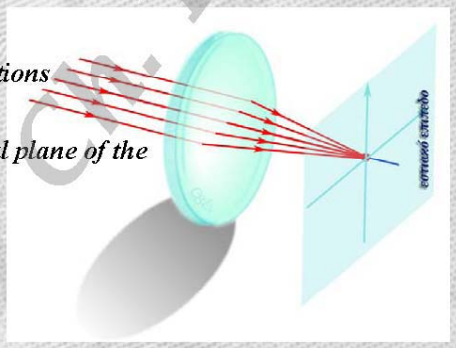

Electron diffraction (Inverse Fourier Transform)

$$A(\mathrm{K}) = \frac{2\pi m_o e}{h^2} \iiint_{\Omega} V(\mathbf{r}) \exp[i 2\pi \mathbf{K}\cdot\mathbf{r}] d\Omega$$

The integral gives the Fourier Transform of the function that describes the potential of the material that induces the electrons' diffraction

According to J.B. Fourier:
A periodic function V(x) with period a can be written as a sum of harmonic functions A(u)
Fourier components with frequencies u=n/a
Every Fourier component contains information about the details of order a/n of V(x)

For crystals V(r) is a periodic function in three dimensions
A(K) are Fourier components – spatial frequencies corresponding to diffracted beams

The electron Microscope (working modes)

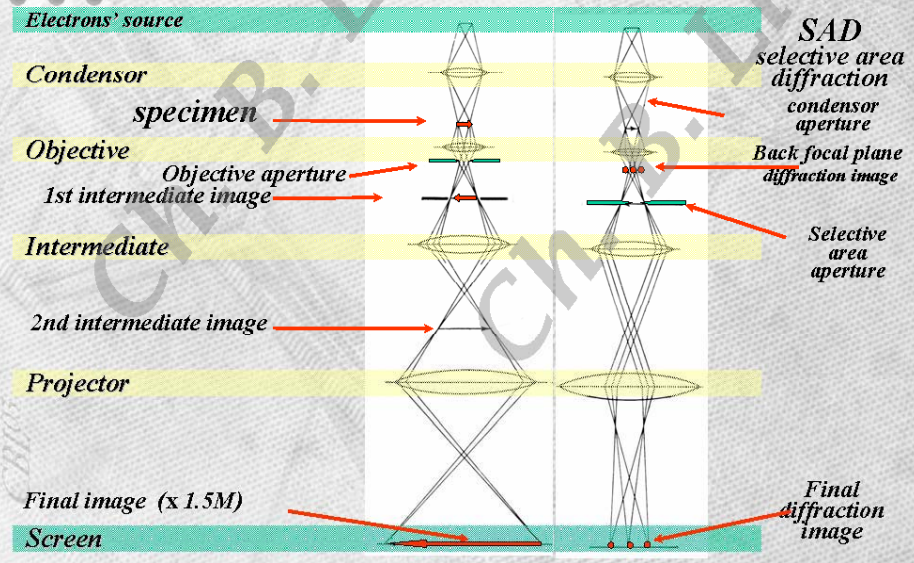

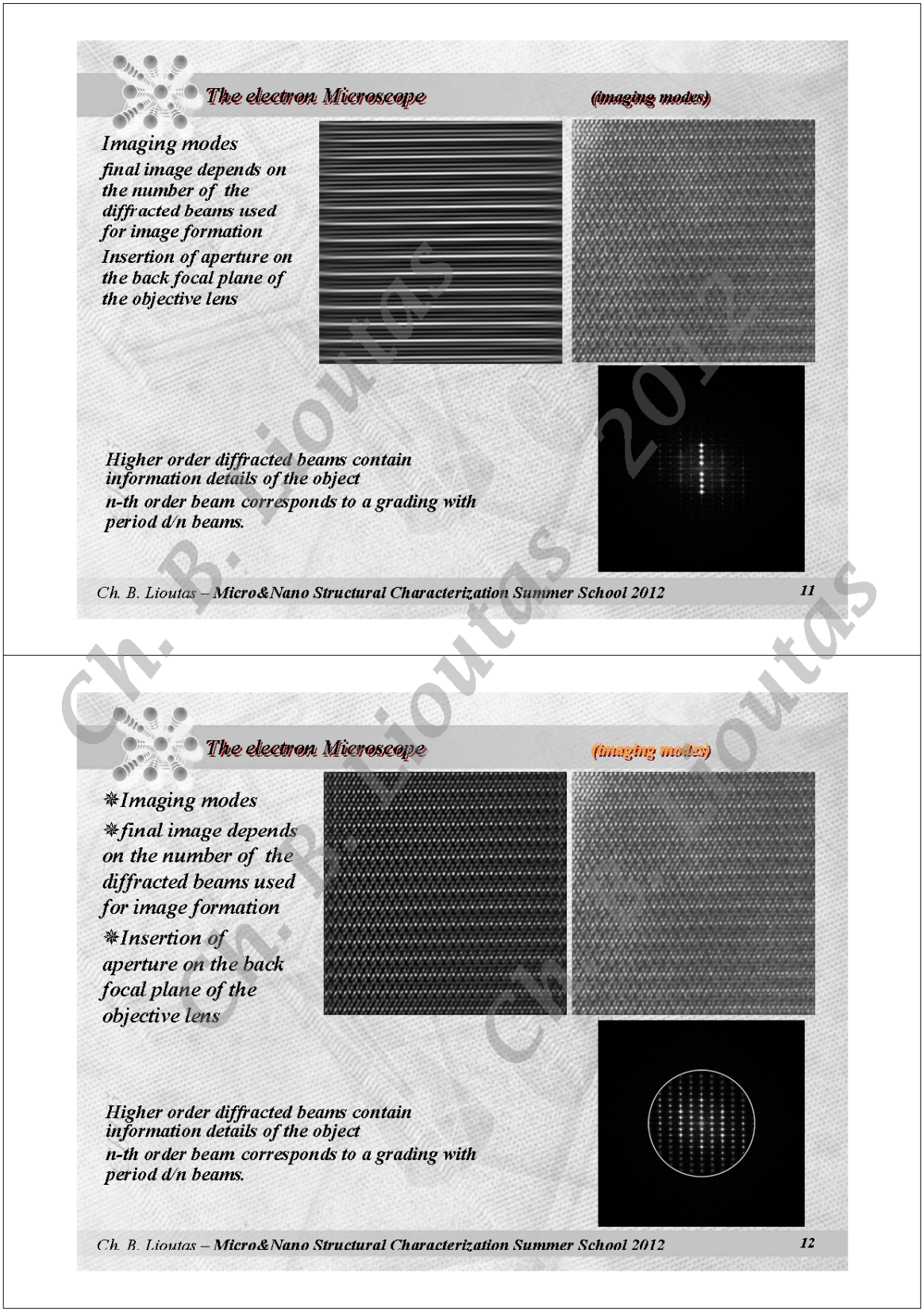
The electron Microscope
(imaging modes)
Imaging modes
final image depends on the number of the diffracted beams used for image formation
Insertion of aperture on the back focal plane of the objective lens
Higher order diffracted beams contain information details of the object
n-th order beam corresponds to a grading with period d/n beams.
Ch. B. Lioutas – Micro&Nano Structural Characterization Summer School 2012
11
The electron Microscope
(imaging modes)
Imaging modes
final image depends on the number of the diffracted beams used for image formation
Insertion of aperture on the back focal plane of the objective lens
Higher order diffracted beams contain information details of the object
n-th order beam corresponds to a grading with period d/n beams.
Ch. B. Lioutas – Micro&Nano Structural Characterization Summer School 2012
12

Imaging Theory & Diffraction I

Ernst Abbe's Imaging Theory, 1872 *first step*

- *In every single case the interaction of the light beam (or incident wave) with the object can be described by the diffraction of the light's wavelet.*
- *A Fraunhofer diffraction image appears on the back focal plane of the objective lens.*

Mathematical analysis of the Fraunhofer diffraction proves that the diffraction image represents the Fourier Transform of the object's transparence function

$$Q(u,v)=\mathcal{F}[q(x,y)]$$

The spatial frequencies correspond to the diffracted beams with intensities

$$F_{uv} = |Q(u,v)|^2$$

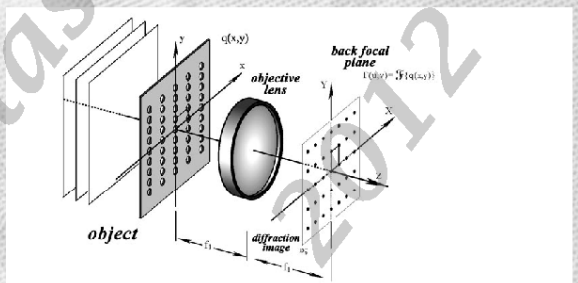

- *Periodic object's diffraction image consists of sharp spots*
- *Continuous object gives rise to continuous diffraction pattern*

Imaging Theory & Diffraction II

Ernst Abbe's Imaging Theory, 1872 *second step*

- *The back focal plane acts as a set of Huyghens sources*
- *The final image is produced from the interference of the diffracted beams on the back focal plane of the eyepiece lens.*

Image formation represents the inverse Fourier Transform of the diffraction image

$$\Psi(x,y)= \mathcal{F}^{-1}[Q(u,v)]$$

The intensity of the observed image is

$$I_{uv} \sim |\Psi(x,y)|^2$$

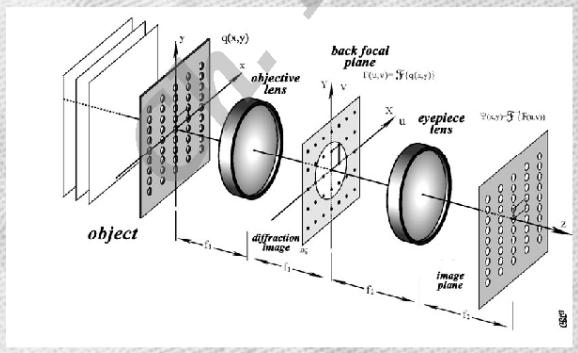

Imaging in TEM (imaging modes)

Bright Field (BF)
image formation only from the undiffracted beam

Dark Field (DF)
image formation only from one of the diffracteed beams

High Resolution (HRTEM)
image formation from the undiffracted as well from a number of diffracted beams.

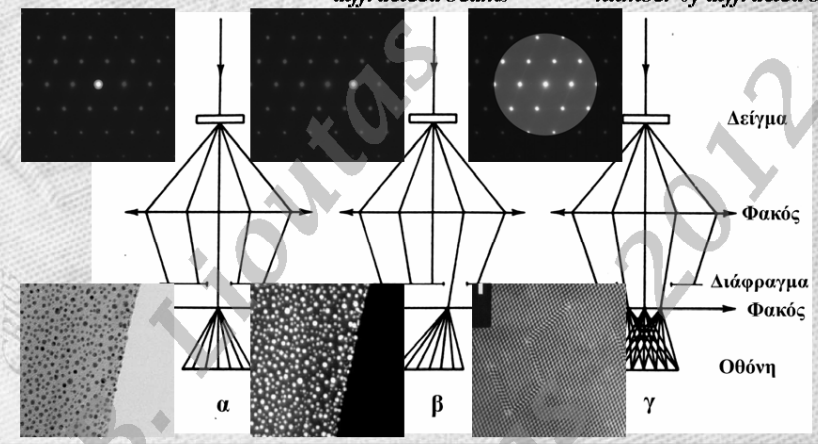

The Resolving Power of the Microscope

Magnification of an "optic" instrument is related with to the resolution limit.
The minimum distance to distinguish two points of the observed object

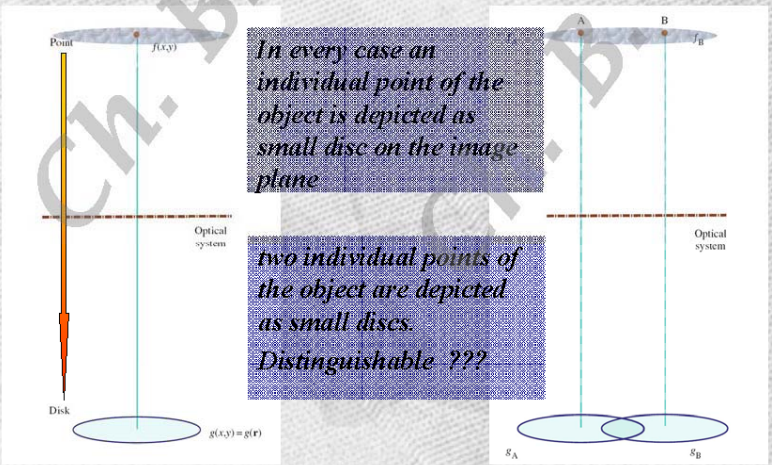

In every case an individual point of the object is depicted as small disc on the image plane

two individual points of the object are depicted as small discs. Distinguishable ???

Electrons versus Light

Magnification of an optic instrument is related with to the resolution limit.
The minimum distance to distinguish two points of the observed object

$$\delta = 0.61\lambda / A \qquad \text{(Rayleigh 19th century)}$$

λ wavelength, A an instrument's parameter A~1

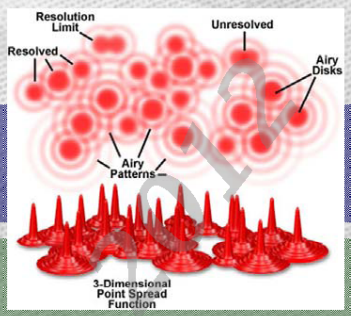

Optical microscope
λ ~ 492nm
300 nm

Electron microscope
E=100keV
λ=0.0037nm
2.3 10⁻³ nm *lenses aberrations* *0.1 nm*

Ch. B. Lioutas – Micro&Nano Structural Characterization Summer School 2012 17

II PHASE MICROSCOPY

Ch. B. Lioutas – Micro&Nano Structural Characterization Summer School 2012 18

Phase Contrast Microscopy

A lot of objects change the phase rather than the intensity of the incident beam

In the simple case of an one dimensional object the wave function at the exit surface of the specimen is

$q(x)=exp[i\varphi(x)]$

$\varphi(x)$ the phase change at the point x

$q(x)=exp[i\varphi(x)]$

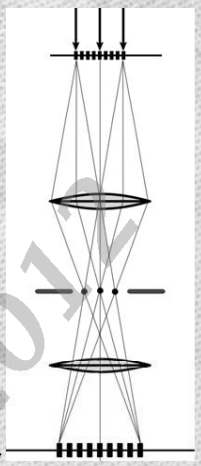

The ideal Microscope produces an image performing two Fourier Transforms

$Q(u)=\mathcal{F}[q(x)]$

The intensity distribution on the image plane

$|q(x)|^2=|exp[i\varphi(x)]|^2=1$

$\Psi(x)=\mathcal{F}^{-1}[Q(u)]$

$\Psi(x)=exp[i\varphi(x)]$

There is NO CONTRAST

CONTRAST is the difference in intensity (ΔI) between two adjacent areas C=ΔI / Io

Phase Contrast Microscopy (WPO)

In the case of a Weak Phase Object (WPO)

$\varphi(x) << 1$

$q(x)=exp[i\varphi(x)]$

$\sim 1+i\varphi(x)$

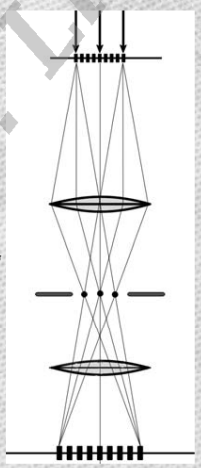

$Q(u)=\mathcal{F}[q(x)]$

$\mathcal{F}[1+i\varphi(x)]=$

$\delta(x)+i\mathcal{F}[\varphi(x)]$

The intensity on the image plane

$|\Psi(x)|^2=(1+i\varphi(x))(1-i\varphi(x))=1-\varphi(x)^2\sim 1$

$\varphi(x) << 1, \varphi(x)^2 \sim 0$

$\Psi(x)=\mathcal{F}^{-1}[Q(u)]$

$\Psi(x)\sim 1+i\varphi(x)$

There is NO CONTRAST

Phase Contrast Microscopy

In the case of a Weak Phase Object (WPO)

$\varphi(x) << 1$

$q(x)=\exp[i\varphi(x)]$

$\sim 1+i\varphi(x)$

$Q(u)=\mathcal{F}[q(x)]$

$\mathcal{F}[1+i\varphi(x)]=$

$\delta(x)+i\mathcal{F}[\varphi(x)]$

It is possible to induce a phase shift of $\pi/2$ in diffracted beams only

(in the optical microscope by inserting a glass plate)

$Q_1(u)=$

$\delta(x)+i\mathcal{F}[\varphi(x)]e^{in\pi/2}=$

$\delta(x)-\mathcal{F}[\varphi(x)]$

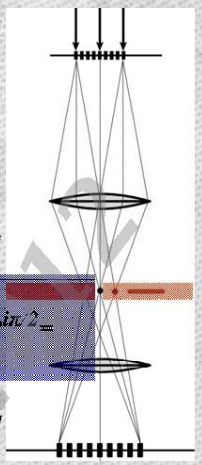

The intensity on the image plane

$|\Psi(x)|^2=[1-\varphi(x)]^2=1-2\varphi(x)+\varphi(x)^2\sim 1-2\varphi(x)$

$\varphi(x) << 1,\ \varphi(x)^2 \sim 0$

$\Psi(x)=\mathcal{F}^{-1}[Q_1(u)]$

$\Psi(x)\sim 1-\varphi(x)$

The CONTRAST on the image plane is a PERFECT REPRESENTATION of the object's phase

Extension in two dimensions without any difference

The specimen as Phase Object

Any specimen is characterized by a three-dimensional potential V(x,y,z) that induces a phase shift dx(z) along the propagation of the electrons' wave in a distance dz (relative to the propagation in the vacuum)

$$\lambda'(r)=\frac{h}{\{2me[E+V(r)]\}^{1/2}}$$

$$dx(z)=2\pi\left(\frac{1}{\lambda'}-\frac{1}{\lambda}\right)dz=\frac{2\pi}{\lambda}\left(\frac{\lambda}{\lambda'}-1\right)dz$$

$$dx(z)=\frac{2\pi}{\lambda}\left[\frac{(E+V)^{1/2}}{E^{1/2}}-1\right]dz=\frac{2\pi}{\lambda}\left[\left(1+\frac{V}{E}\right)^{1/2}-1\right]$$

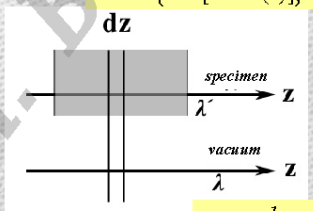

$$\lambda=\frac{h}{(2meE)^{1/2}}$$

$V << E$ *(energy of the incident electrons)*

$$dx(z)\cong\frac{2\pi}{\lambda}\cdot\left(\frac{1}{2}\frac{V}{E}\right)dz=\sigma V dz \qquad \sigma=\pi/\lambda E$$

The specimen as Phase Object

The total phase shift in any point at the exit surface of the specimen is calculated by integration over all the thickness of the specimen

$$X(x,y) = \sigma \int_0^z V(x,y,z)dz = \sigma\, \varphi(x,y)$$

φ(x,y) yields the potential's projection along electron beam, direction Oz

The specimen interacts as pure phase object with two dimensional transparency function $q(x,y)=\exp[i\,\sigma\varphi(x,y)]$

We can take account of electrons' absorption by including a function μ(x,y) $q(x,y)=\exp[i\,\sigma\varphi(x,y) - \mu(x,y)]$

The absorption term does not affect the result in the final image contrast in the first order approximation

φ(x,y) varies from point to point on the unit cell projection
For a very large number of materials $\varphi(x,y) << 1$ *when* $z \leq 10$ *nm*
$q(x,y) \cong 1 + i\,\sigma\varphi(x,y)]$ *the specimen acts as Weak Phase Object*

Electron Microscope - Optical System

Imaging → *The transfer of the information from the object (exit face of the specimen) to the image plane*

It can be represented with a function H(u) including three factors
(in reciprocal space) $u=\sin(\theta)/\lambda \cong \theta/\lambda$ *(θ the diffraction angle)*

Apertures	→ *The aperture function A(u)*
Attenuation of the wave	→ *The envelope function E(u)*
Aberrations of the lens	→ *The aberration function B(u)*

$$H(u) = A(u)\,E(u)\,B(u)$$

Describe the cut off all values of u greater than some selected value
A(u) imposed by objective diaphragm (radius of the aperture)
E(u) property of the lens itself (may be either more or less restricting than A(u))

B(u) is usually expressed as:
$B(u)= \exp[i\,\chi(u)]$
χ(u) the phase sift induced by the electron microscope

The Electron Microscope as phase contrast microscope

The phase sift induced by the electron microscope is a function of the diffraction angle θ mainly affected by:

Spherical aberration

$$\chi(\theta) = \frac{\pi}{2} C_s \frac{\theta^4}{\lambda} + \pi \varepsilon \frac{\theta^2}{\lambda}$$

Defocus

- C_s — *spherical aberration coefficient given instrument's manufacturer*
- λ — *electrons' wavelength Accelerating voltage*
- ε — *defocus value selected during observation*

For an optimum defocus ε value (Scherzer defocus) χ(θ) takes the value of $-\pi/2$ or equivalent $\sin[\chi(\theta)] = -1$ for a large range of θ values

Electron Microscope ⇔ Phase Contrast Microscope

Ch. B. Lioutas – Micro&Nano Structural Characterization Summer School 2012 25

High Resolution Electron Microscopy

The specimen acts as pure phase object with transparency function proportional to the projection of the structure's potential

$$q(x,y)=\exp[i\,\sigma\varphi(x,y)]$$

$$X(x,y)= \sigma \int_0^z V(x,y)dz = \sigma\,\varphi(x,y)$$

phase sift of $-\pi/2$
Induced by spherical aberration & defocus

Intensity on the image plane
$|\Psi(x,y)|^2=[1-\sigma\varphi(x,y)]^2 \sim 1-2\sigma\varphi(x,y)$

HRTEM image Contrast
- *exact representation of the object's phase*
- *proportional to the projection of specimen's potential*
- *Direct illustration of structural characteristics of the specimen*

$q(x)=\exp[i\varphi(x)] \sim 1+i\varphi(x)$

$Q(u)=\mathcal{F}[q(x)]= \mathcal{F}[1+i\varphi(x)]= \delta(x)+i\,\mathcal{F}[\varphi(x)]$

$Q_1(u)= \delta(x)+i\,\mathcal{F}[\varphi(x)]e^{i\pi/2} = \delta(x) - \mathcal{F}[\varphi(x)]$

$\Psi(x)=\mathcal{F}^{-1}[Q_1(u)]$

$\Psi(x)\sim 1 - \varphi(x)$

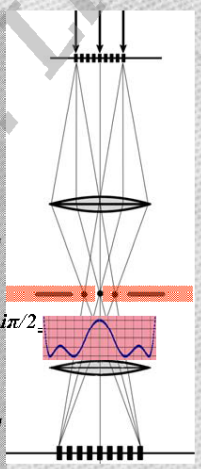

Ch. B. Lioutas – Micro&Nano Structural Characterization Summer School 2012 26

The Resolving Power of the Microscope

Point or structural resolution ρ_s

the minimum distance between to points of the object

in order to be resolved in the image plane

→ *projection of a crystal's structure*

- *electron diffraction*
- *diffracting object (crystal)*
- *the instrument's parameters*

$$\rho_s \cong 0.66\, C_s^{1/4}\, \lambda^{3/4}$$

V=200 kV ρ_s*=0.19 – 0.3 nm*

V > 200kV ρ_s*=0.12 nm*

Line resolution

the minimum distance between two parallel lines on the object

in order to be resolved in the image plane.

→ *atomic planes*

V=200 kV ρ_s*=0.14 – 0.2 nm*

Ch. B. Lioutas – Micro&Nano Structural Characterization Summer School 2012 27

III
IMAGE SIMULATION & PROCESSING

CBL05

Ch. B. Lioutas – Micro&Nano Structural Characterization Summer School 2012 28

Structural Analysis

interpretation of HRTEM micrographs

The contrast on the HRTEM micrograph has lost the phase of the electrons wavefunction that holds the projection of the 3D potential of the specimen

How is possible to have interpretable structural details ?

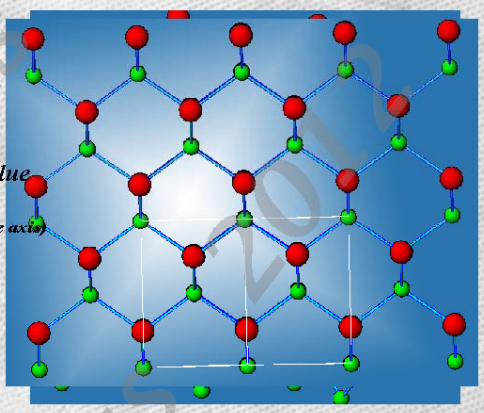

Experimental requirements

- *Very thin specimen*
- *Defocus close to that of Scherzer value*
- *Appropriate projection*
  (electron beam aligned along a low-index zone axis)

Ch. B. Lioutas – Micro&Nano Structural Characterization Summer School 2012 29

HRTEM micrographs Simulation

Mathematical relations (analytical or numerical) accurately reproducing

- *Interaction Electron Beam - specimen (Diffraction)*
- *Interaction Electron Beam – Lenses , Apertures (Imaging)*

COMPUTER CALCULATION

HRTEM IMAGE SIMULATION SOFTWARE

Cerius2 *by Accerlys*
Runs on UNIX

EMS & jEMS *by Pierre Stadleman (Very widely used and user-friendly)*
Multi-platform: Mac, Unix, Windows. The 'j' denotes the java version

Kirkland *by Earl Kirkland. Well described in his book on the subject*

MacTEMPAS *by Roar Kilaas* *Runs on a Mac (so it's very user-friendly)*

WinHREM & MacHREM
by HREM Research Inc. (Kazuo Ishizuka)

Ch. B. Lioutas – Micro&Nano Structural Characterization Summer School 2012 30

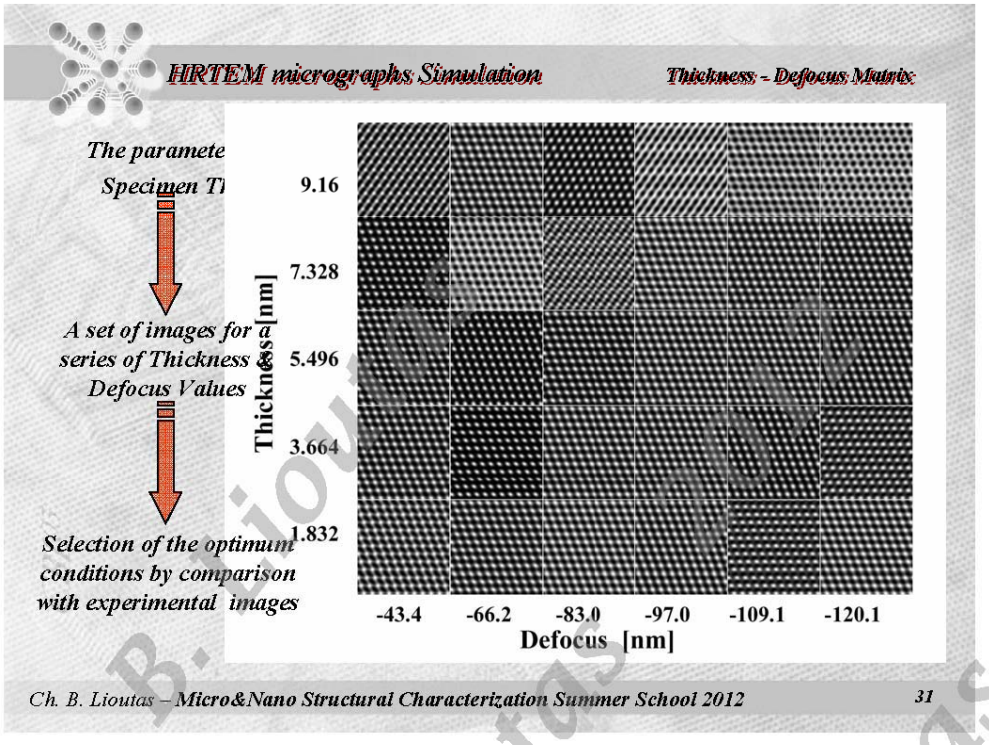
HRTEM micrographs Simulation
Thickness - Defocus Matrix
The paramete
Specimen Ti
A set of images for a series of Thickness & Defocus Values
Selection of the optimum conditions by comparison with experimental images
Thickness [nm]
9.16
7.328
5.496
3.664
1.832
-43.4
-66.2
-83.0
-97.0
-109.1
-120.1
Defocus [nm]
Ch. B. Lioutas – Micro&Nano Structural Characterization Summer School 2012
31

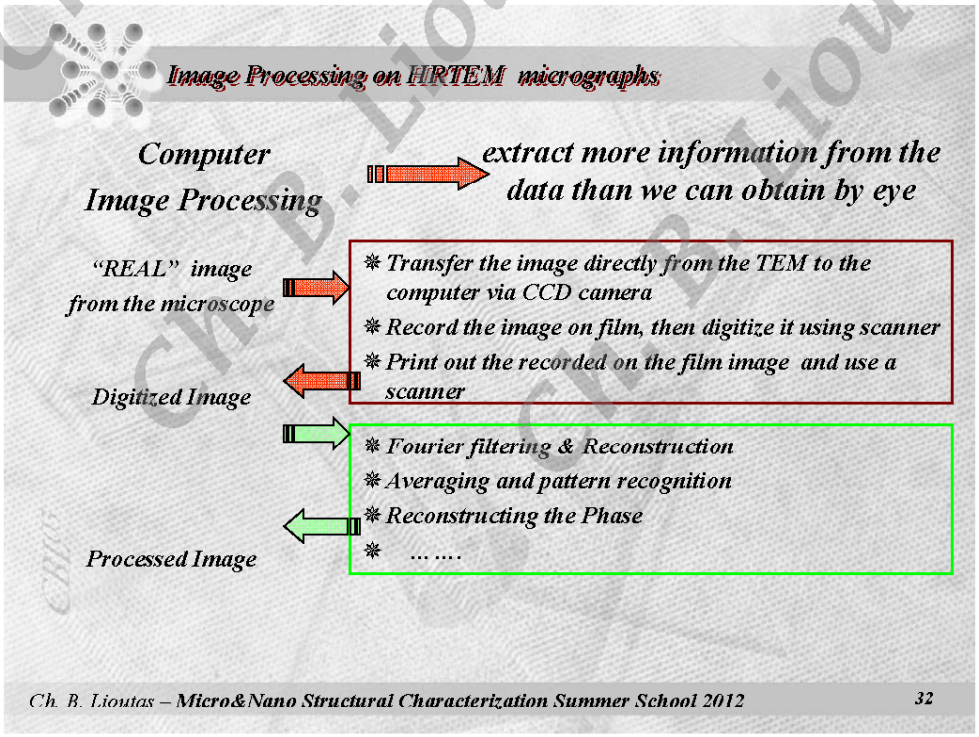
Image Processing on HRTEM micrographs
Computer Image Processing
extract more information from the data than we can obtain by eye
"REAL" image from the microscope
Digitized Image
Transfer the image directly from the TEM to the computer via CCD camera
Record the image on film, then digitize it using scanner
Print out the recorded on the film image and use a scanner
Processed Image
Fourier filtering & Reconstruction
Averaging and pattern recognition
Reconstructing the Phase
… ….
Ch. B. Lioutas – Micro&Nano Structural Characterization Summer School 2012
32

IV
EXAMPLES
& CASE STYDIES

CBL05

Ch. B. Lioutas – Micro&Nano Structural Characterization Summer School 2012 33

HRTEM examples I

$FeSi_2$ along [012]

projection of the crystal' structure

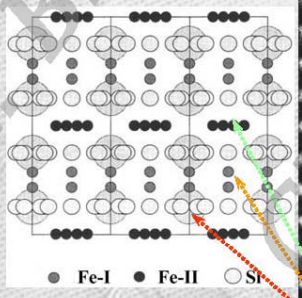

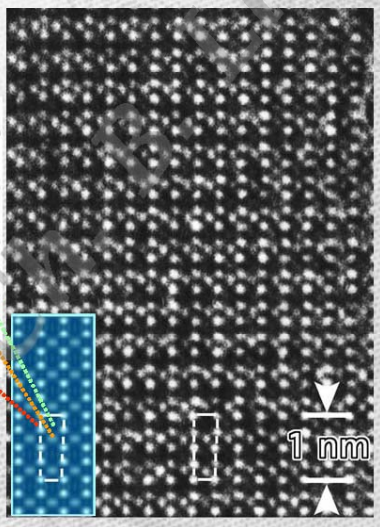

HRTEM image simulation
intense dots Si complex
less intense dots Fe-I
very weak dots Fe-II

Ch. B. Lioutas – Micro&Nano Structural Characterization Summer School 2012 34

HRTEM examples II

HRTEM micrograph dislocation in SiGe

Burgers' vector determination

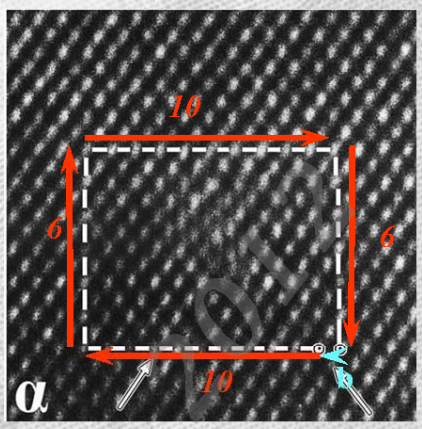

Ch. B. Lioutas – Micro&Nano Structural Characterization Summer School 2012 35

HRTEM examples III

HRTEM images from stacking faults in CdTe

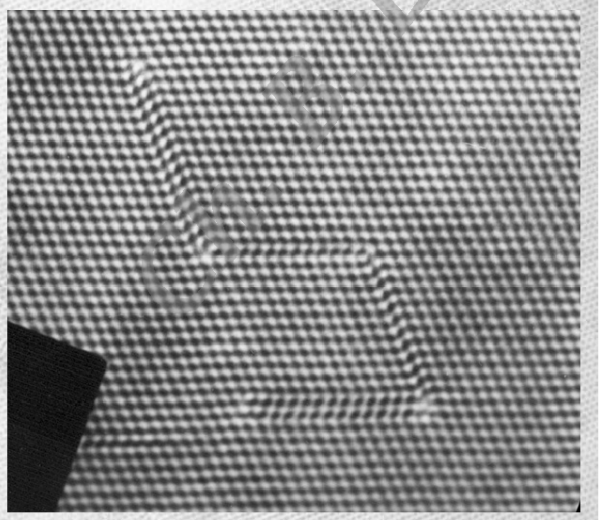

Ch. B. Lioutas – Micro&Nano Structural Characterization Summer School 2012 36

HRTEM examples IV

Grain boundaries

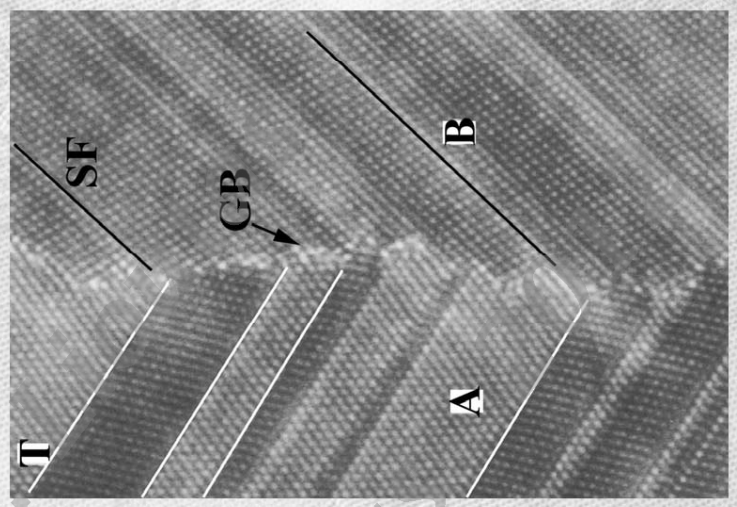

Ch. B. Lioutas – Micro&Nano Structural Characterization Summer School 2012 37

HRTEM examples IV

Polycrystalline Si in amorphous SiO_2 matrix

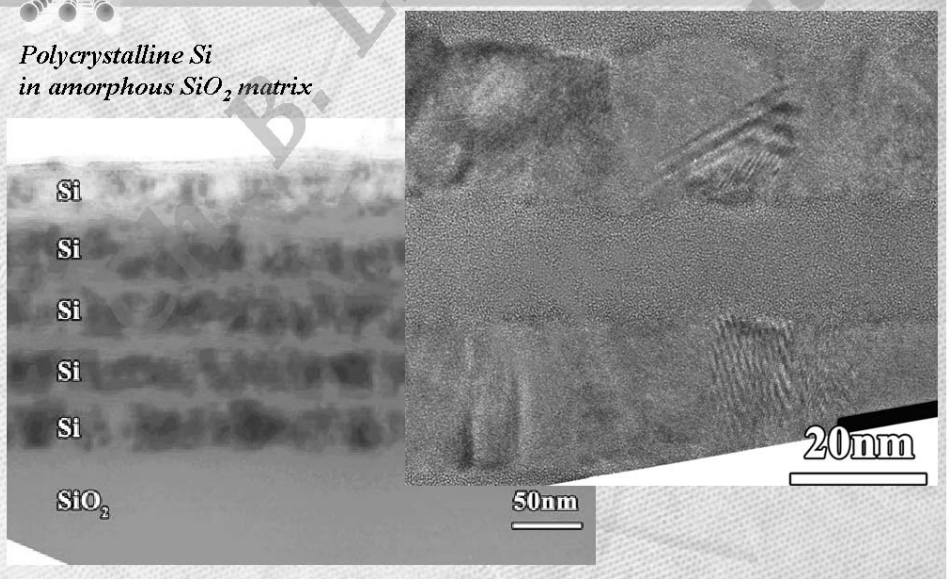

Ch. B. Lioutas – Micro&Nano Structural Characterization Summer School 2012 38

Application of transmission electron microscopy in solving some problems of shape memory alloys

Danuta Stróż
University of Silesia

Summer School on Micro- and Nanostructural Charaterisation of Materials,
July 11-15,2012, Thessaloniki, Greece

Outline

I – Introduction

II – Transmission electron microscopy

III – Shape memory alloys

IV – Problems solved by TEM

Summer School on Micro- and Nanostructural Charaterisation of Materials,
July 11-15,2012, Thessaloniki, Greece

Outline

I – Introduction

II – Transmission electron microscopy

III – Shape memory alloys

IV – Problems solved by TEM

Summer School on Micro- and Nanostructural Charaterisation of Materials,
July 11-15,2012, Thessaloniki, Greece

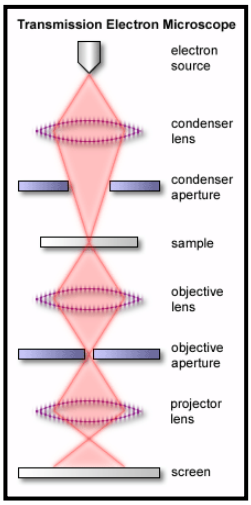

A simplified ray diagram of a TEM consists of an electron source, condenser lens with aperture, specimen, objective lens with aperture, projector lens and fluorescent screen.

Summer School on Micro- and Nanostructural Charaterisation of Materials,
July 11-15,2012, Thessaloniki, Greece

Ray path in TEM under microscopy (A) and diffraction (B) conditions

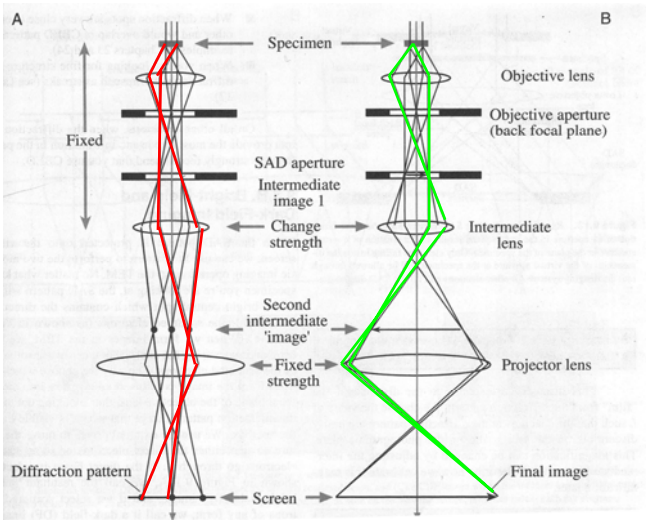

Summer School on Micro- and Nanostructural Charaterisation of Materials, July 11-15,2012, Thessaloniki, Greece

Two types of images:
1. a microscope image

TEM presents 2D images of 3D specimens viewed in transmission

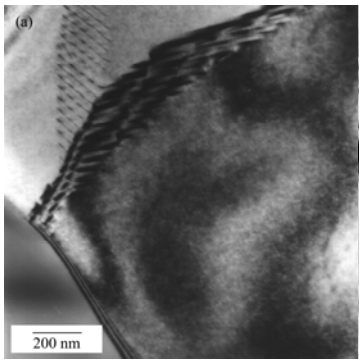

Hayes (1980): „When we see this image we laugh, but when we see equivalnet image in TEM, we publish."

D.B. Williams, C.B.Carter, Transmission Electron Microscopy, A Text book for Materials Science, Springer 2009

Summer School on Micro- and Nanostructural Charaterisation of Materials, July 11-15,2012, Thessaloniki, Greece

Two types of images:
2. a diffraction pattern

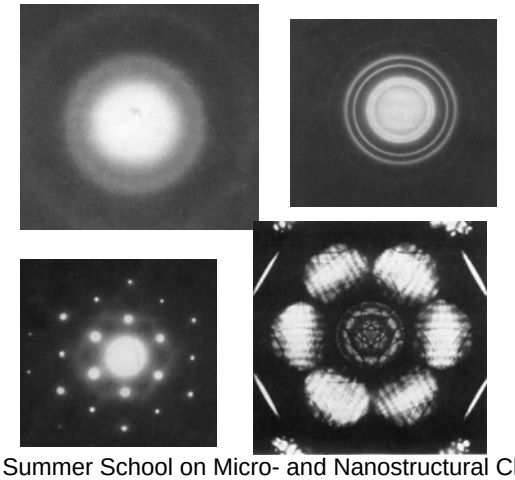

D.B. Williams, C.B.Carter, Transmission Electron Microscopy, A Text book for Materials Science, Springer 2009

Summer School on Micro- and Nanostructural Charaterisation of Materials, July 11-15,2012, Thessaloniki, Greece

Microscope image – contrast in TEM
a) Amplitude contrast

Absorption contrast

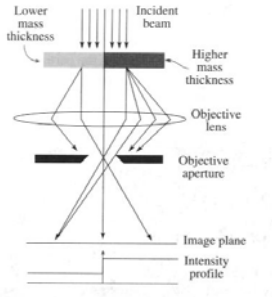

Diffraction contrast

crystalline materials, Bragg diffraction controls the type of contrast .

Two beams conditions

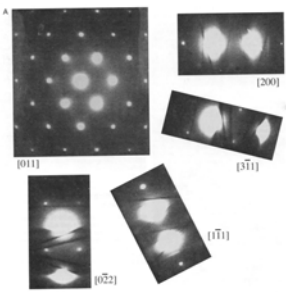

D.B. Williams, C.B.Carter, Transmission Electron Microscopy, A Text book for Materials Science, Springer 2009

Summer School on Micro- and Nanostructural Charaterisation of Materials, July 11-15,2012, Thessaloniki, Greece

a) Amplitude contrast

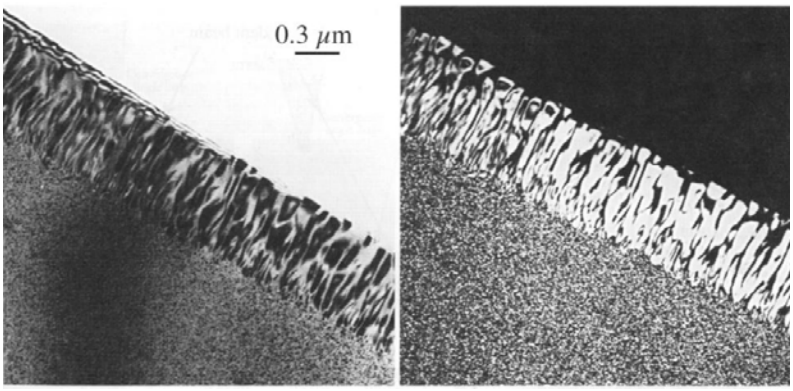

D.B. Williams, C.B.Carter, Transmission Electron Microscopy, A Text book for Materials Science, Springer 2009

Summer School on Micro- and Nanostructural Charaterisation of Materials, July 11-15,2012, Thessaloniki, Greece

b) phase contrast

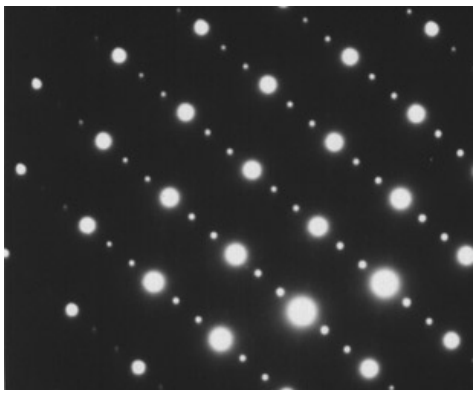

Summer School on Micro- and Nanostructural Charaterisation of Materials, July 11-15,2012, Thessaloniki, Greece

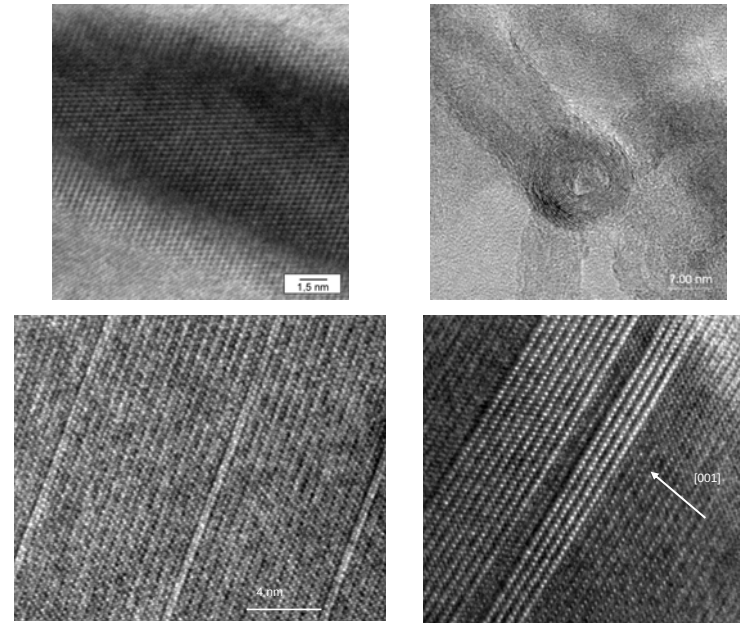

Summer School on Micro- and Nanostructural Charaterisation of Materials,
July 11-15,2012, Thessaloniki, Greece

Outline

I – Introduction

II – Transmission electron microscopy

III – Shape memory alloys

IV – Problems solved by TEM

Summer School on Micro- and Nanostructural Charaterisation of Materials,
July 11-15,2012, Thessaloniki, Greece

Shape memory effects:

- one-way shape memory effect
- Two-way shape memory effect
- Pseudo-elasticity

↓

Thermoelastic martensitic transformation

Martensitic transformation

↓

a lattice transformation involving shearing deformation resulting from cooperative atomic movement

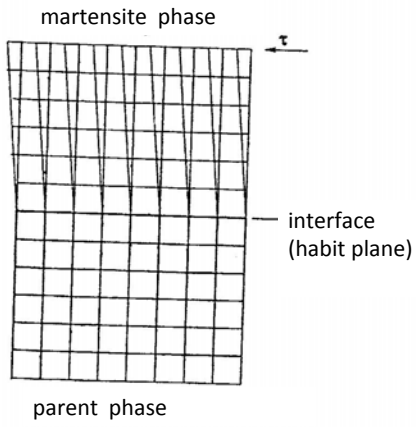

- diffusionless
- accompanied by the shape changes (or surface relief)
- M crystal has a specific „habit plane”
- definite orientation relationship between the P and M

Transformation thermodynamics

Assume a lens-shape M of r-radius and 2t (r>>t) has nucleated

$$\Delta G = \pi r^3 t \Delta g_c + 2\,\pi r^2 \sigma + \pi r t^2 A + \pi r t^2 B$$

chemical free energy

interface energy

Plastic deformation term

elastic strain energy

$$\Delta G = \pi r^3 t \Delta g_c + 2\,\pi r^2 \sigma + \pi r t^2 A + \pi r t^2 B$$

Thus, the transformation is characterised by thermal and elastic terms, so it's thermoelastic.

The thermal equilibrium between the two terms can be disrupted by the change of temperature or application of external stress

One-way shape memory effect

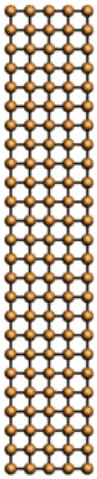

One-way shape memory effect

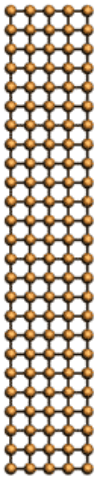

T ↓

$T<M_f$

One-way shape memory effect

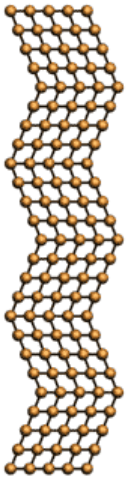

T ↓

$T<M_f$

ε ↑

One-way shape memory effect

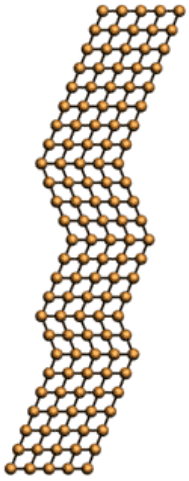

T ↓

$T<M_f$

ε ↑↑

One-way shape memory effect

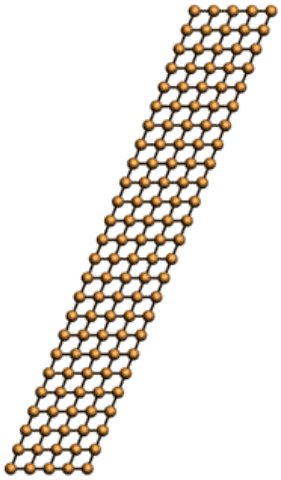

T ↓

$T<M_f$

ε ↑↑

T ↑

One-way shape memory effect

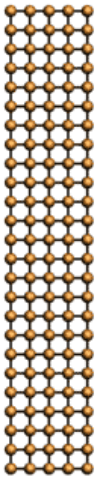

T ↓

$T<M_f$

ε ↑↑

T ↑

$T > A_f$

Two-way shape memory effect

- plastic deformation in the martensitic state
- constraint ageing
- thermal cycling
- utilisation of precipitates

Pseudo-elasticity

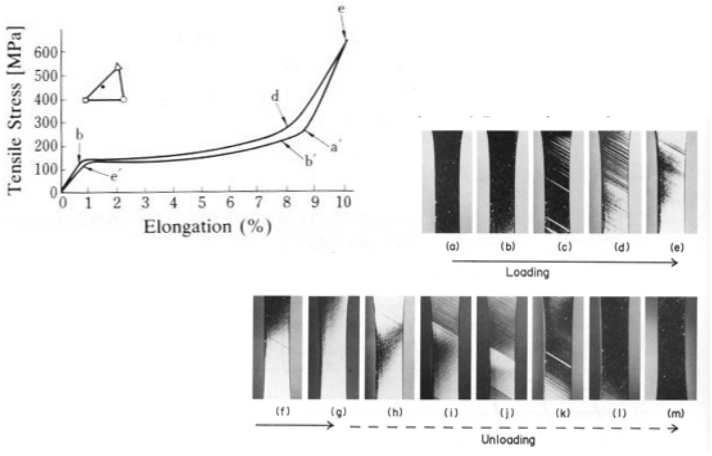

Shape memory materials

1. NiTi – based alloys
2. Cu- based alloys (Cu-Zn-Al, Cu-Al-Ni, Cu-Al-Nb)
3. Ferromagnetic shape memory alloys (NiMnGa, NiMnIn)

Applications

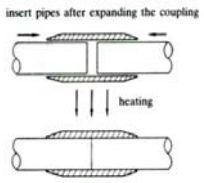

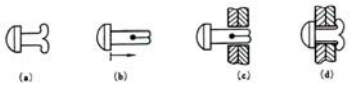

Applications

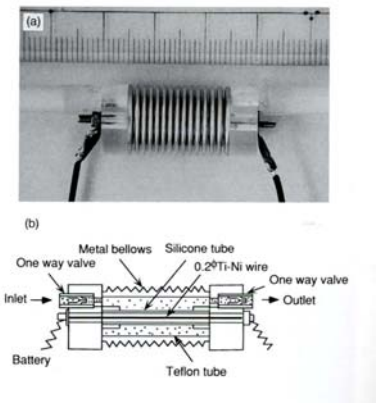

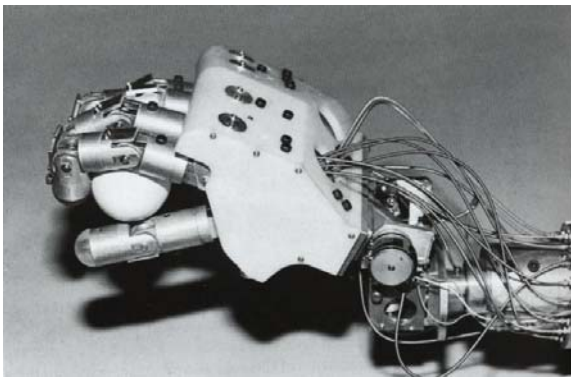

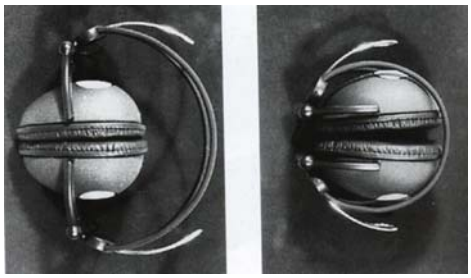

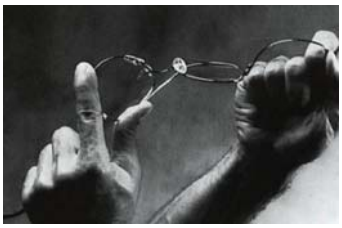

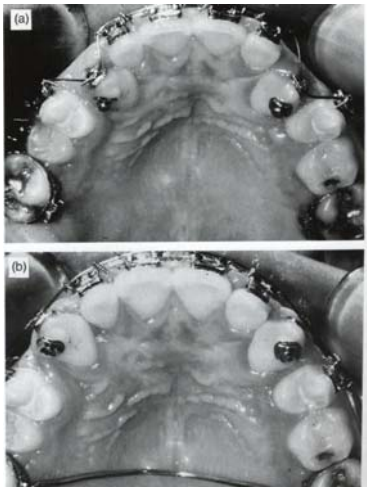

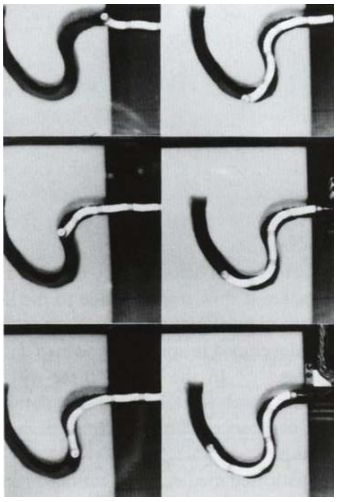

Outline

I – Introduction

II – Transmission electron microscopy

III – Shape memory alloys

IV – Problems solved by TEM

Summer School on Micro- and Nanostructural Charaterisation of Materials,
July 11-15,2012, Thessaloniki, Greece

NiTi-based alloys

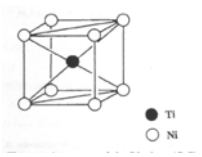

B2 ⟶⟵ B19’

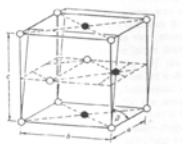

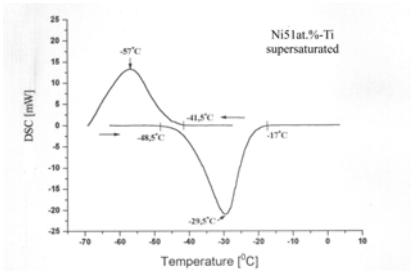

1.

R-phase transformation precedes the B19’ martensite in:

- thermomechanically treated near-equiatomic Ni-Ti alloys
- nickel-rich Ni-Ti alloys aged at an appropriate low temperature
- in some ternary alloys such as Ti-Ni-Fe, Ni-Ti-Co, Ni-Ti-Al alloys

R-phase transformation is also martensitic and thermoelastic, thus it gives rise to shape memory effects.
It yields a small shape change (about 0.8%) - the associated recoverable strain is small.
The temperature hysteresis is very small (e.g. 1.5 ^{0}C).

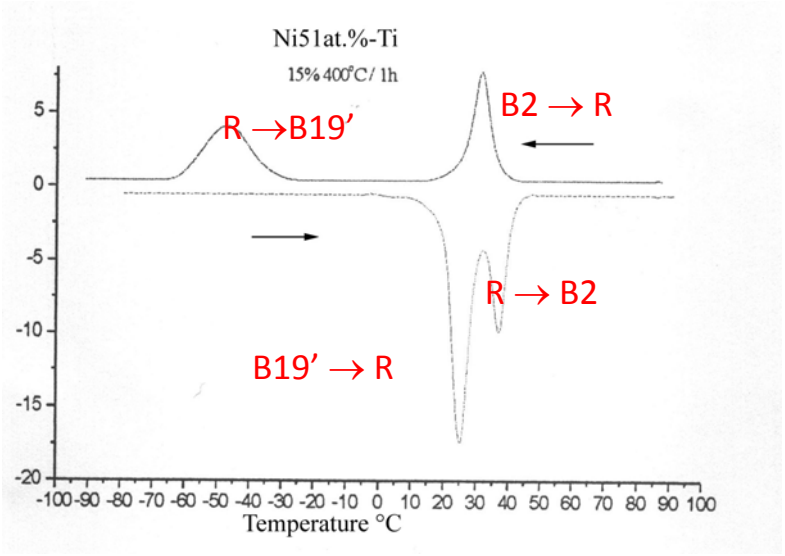

„R phase" - „Rhombohedral distortion" of the cubic cell of B2

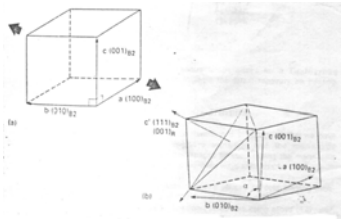

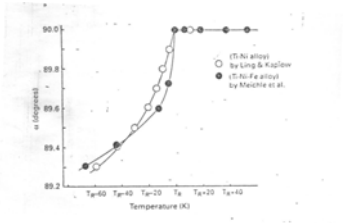

Experiments for Ni-Ti-Fe alloys using neutron, X-ray diffraction, electron microscopy, electrical resistivity, magnetic suceptibility [C.M. Hwang *et al.*, Phil.Mag. A47 (1983),9; M.B. Salamon *et al.*, Phys.Rev. B31 (1985), 7306] - revealed incommensurate state prior to the R-phase and anomalies in some physical properties.

These are:
- increase in electrical resistivity
- change in magnetic susceptibility
- softening of the TA_2 phonon branch near (1/3,1/3,0)
- others e.g. internal friction, elastic modulus

The transformation sequence:

$$B2 \rightarrow I \rightarrow R \rightarrow B19'$$

Ni51-Ti, 850^{0}C/1h + 5% + 300^{0}C/1h

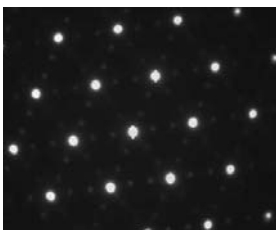

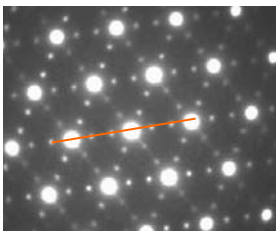

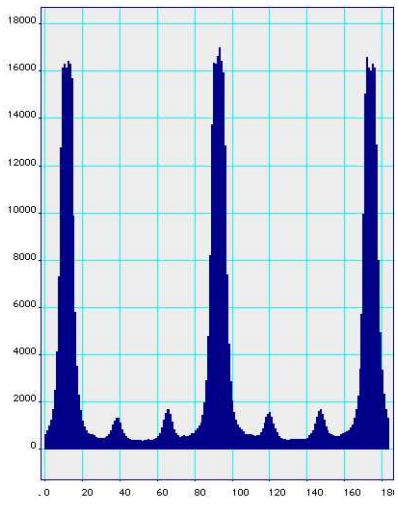

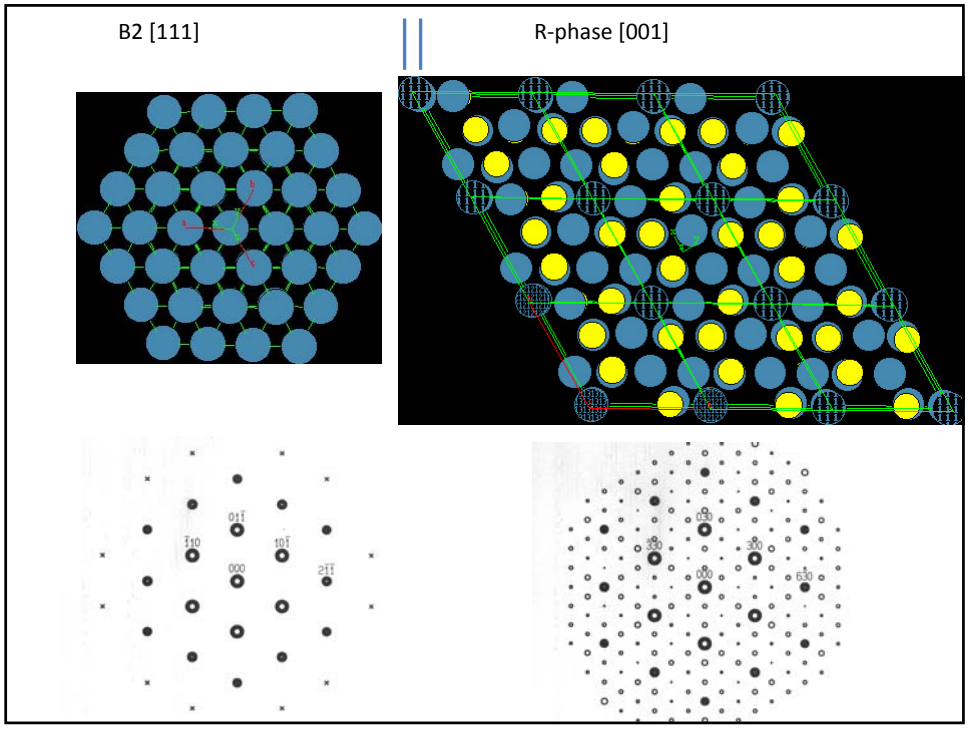
B2 [111]
R-phase [001]

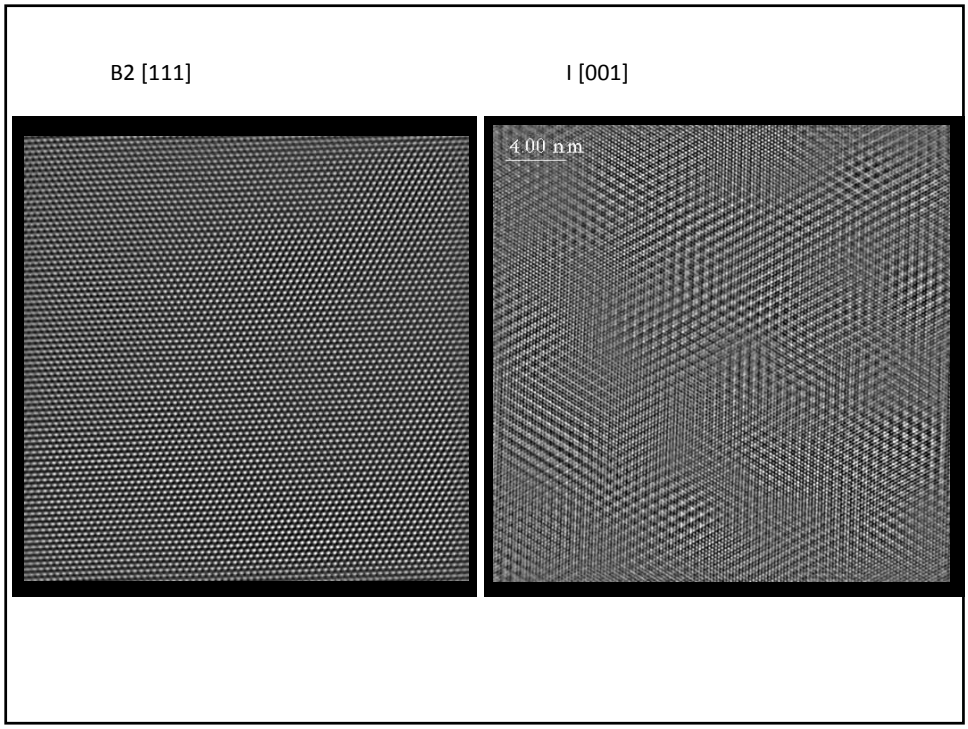
B2 [111]
I [001]
4.00 nm

2. Multistage martensitic transformation in NiTi alloys

Ni51%-Ti
aged at 500^{0}C

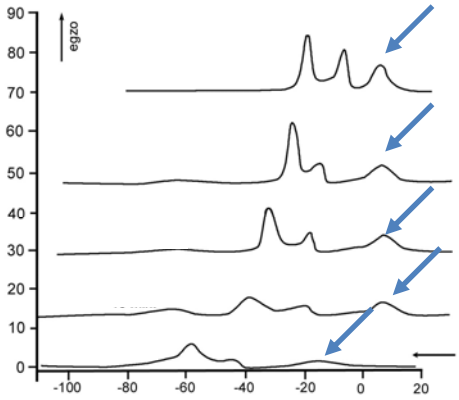

R

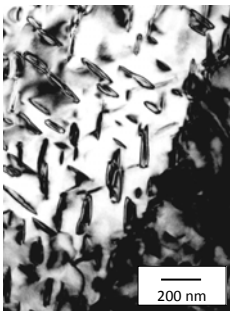

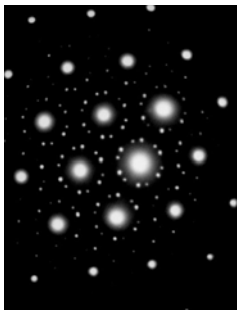

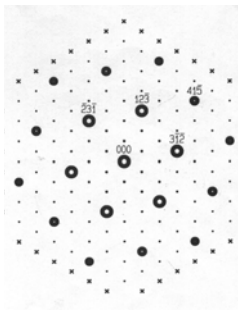

$B2_0 \rightarrow B2_1 + Ni_4Ti_3 \rightarrow B2_2 + Ni_3Ti_2 \rightarrow B2_3 + Ni_3Ti$

Precipitate habit plane - {111}

Crystallographic relationship

$(001)_p \,||\, (111)_m \quad [010]_w \,||\, [2\bar{1}\bar{3}]_m$

Ni51%-Ti, 400^{0}C/1h

Dark-field image in two-beam conditions

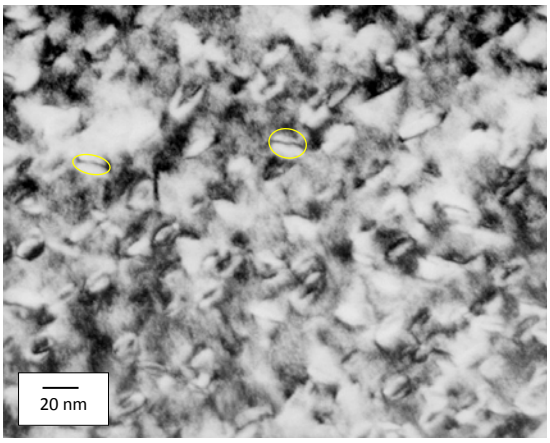

In-situ cooling TEM

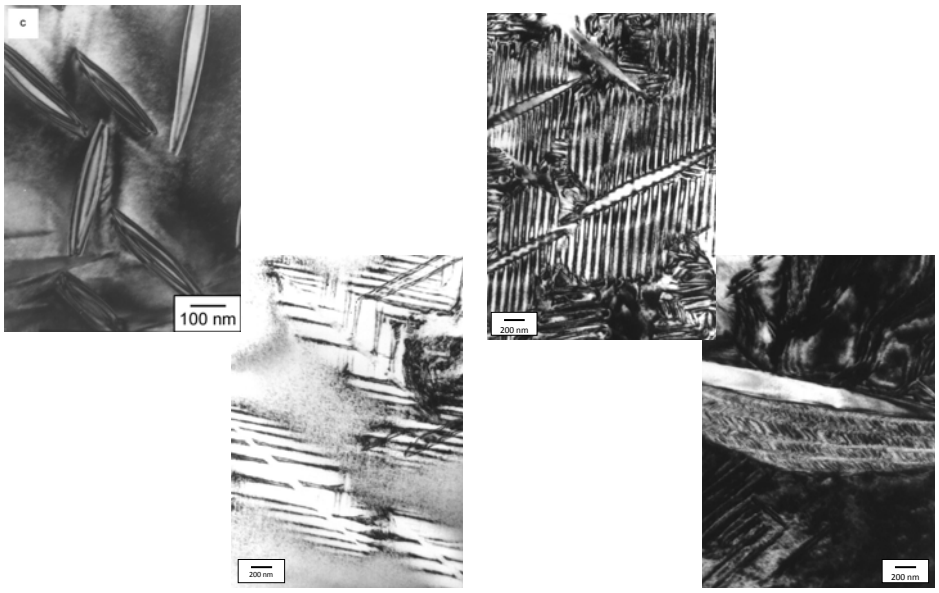

3. Ni_4Ti_3 precipitates

quantitative strain field determination

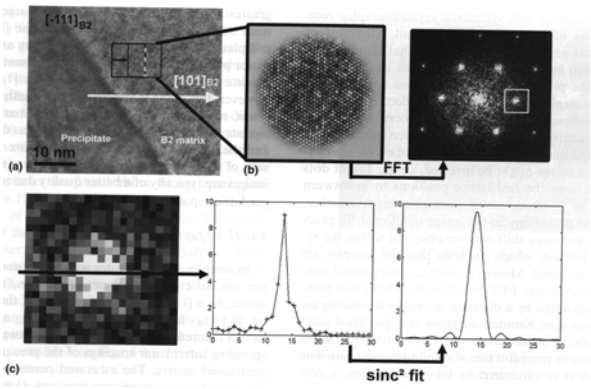

W. Tirry, D. Schryvers, Acta Materialia, **53** (2005) 1041

Ni_4Ti_3 precipitates

quantitative strain field determination

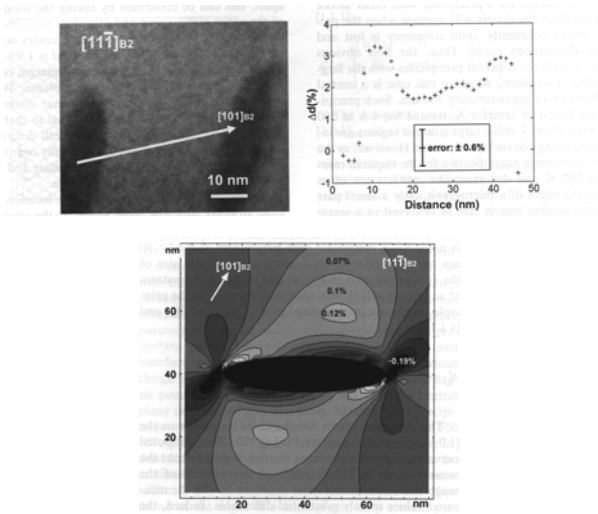

W. Tirry, D. Schryvers, Acta Materialia, **53** (2005) 1041

4. NiTi – nanocrystalline alloys

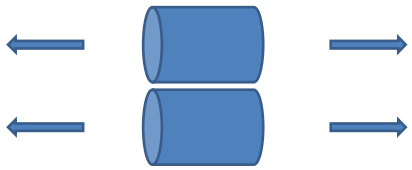

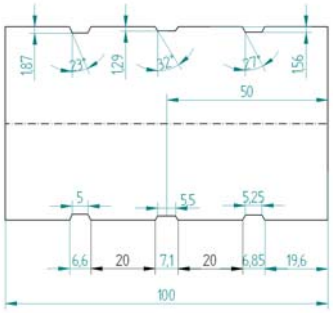

Roll shape with passes fitted to the sample dimensions

Results: TEM as-deformed

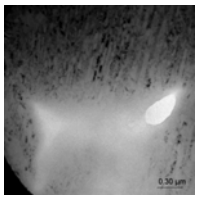

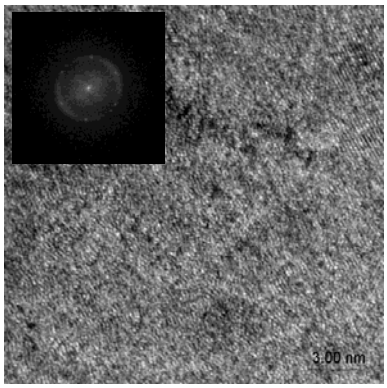

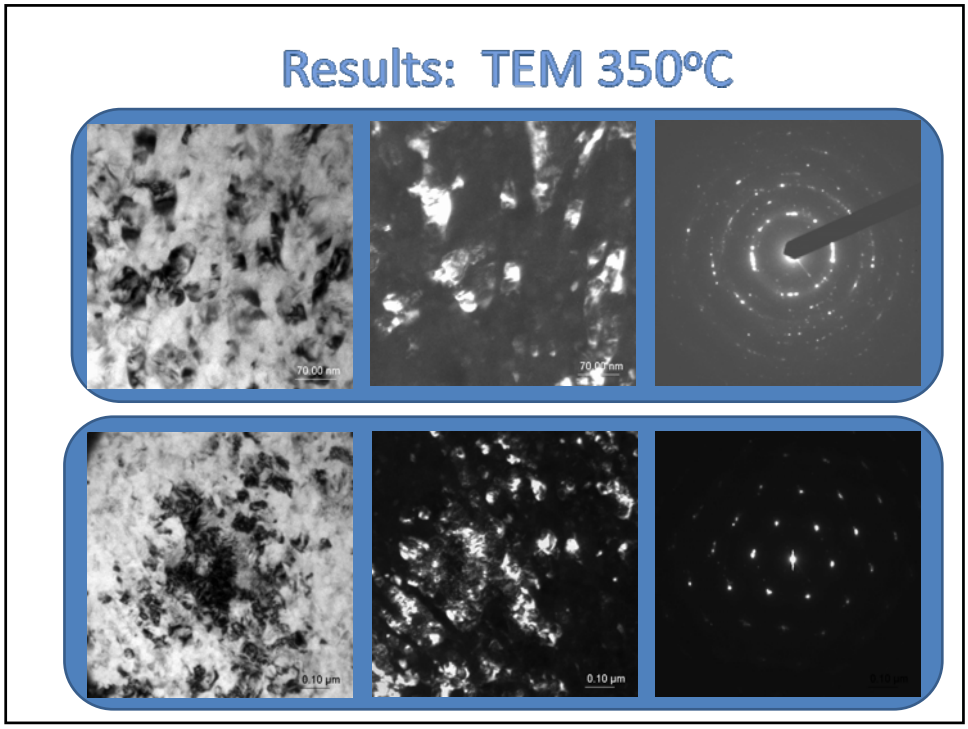
Results: TEM 350°C
70.00 nm
70.00 nm
0.10 µm
0.10 µm

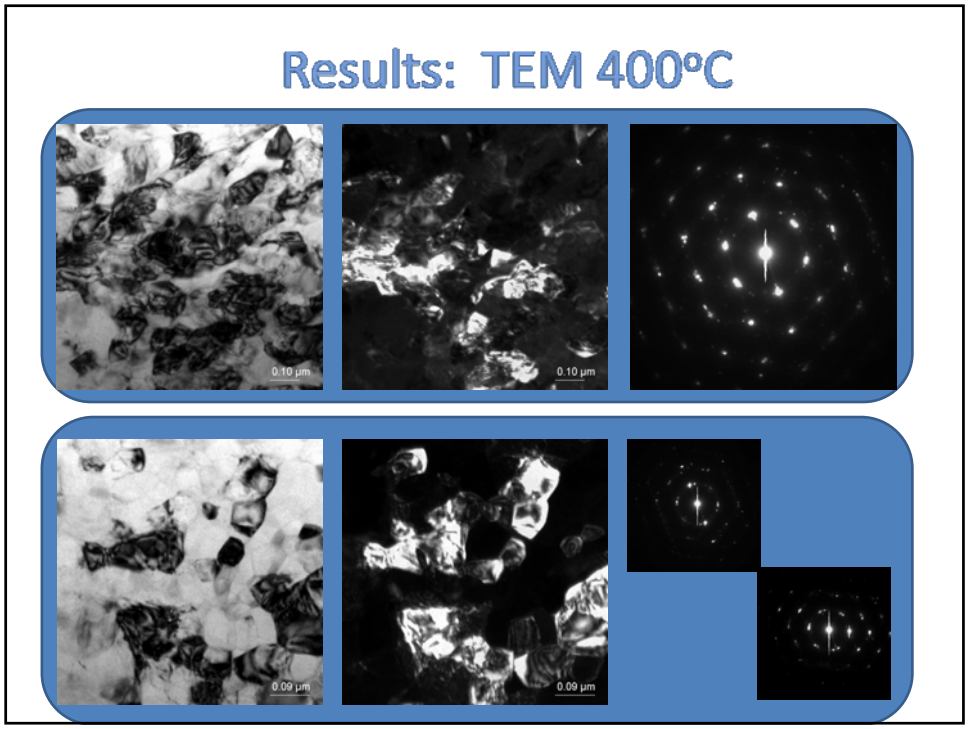
Results: TEM 400°C
0.10 µm
0.10 µm
0.09 µm
0.09 µm

The ASTAR attachment (Nanomegas) for the JEM 3010 (JEOL) TEM was used to scan the sample and acquire the diffraction patterns (DP).

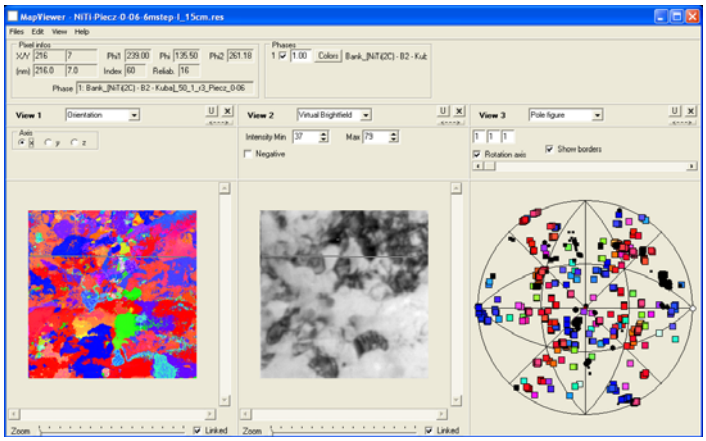

Screenshot from the software showing the grain orientation distribution (the left hand image), the virtual bright field (image in the centre) and the pole figure along the line shown in the previous images and indication the distribution of the {111} type planes .

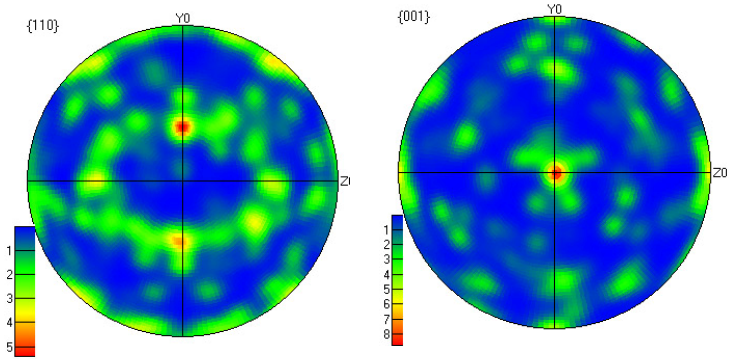

The pole figures for two different orientations obtained from the data imported to the HKL Channel 5 program. The obtained results prove that the alloy shows a full texture of {100}<001>

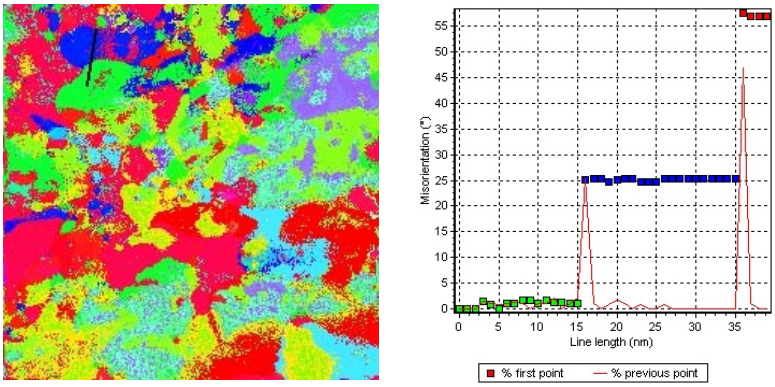

High angle boundaries in the studied NiTi alloy, the angle between the grains is about 25-30°

5. Cu-Al-Nb high temperature alloys

a). Two –phase alloys
b). Chracteristic temperatures increase up to about 600°C

Significant amount of primary precipitates of intermetalic Nb-based phases. Their presence in the martensite matrix causes specific conditions for the alloy behaviour during plasic deformation and also during inducing shape memory effects.

Primary precipitates of intermetalic Nb-base phases play main role in simultaneous increase of strength and plasticity of the shape memory Cu-Al-Nb-X alloys.

J. Lalatko, Habilitation thesis, University of Silesia,Katowice, 2005

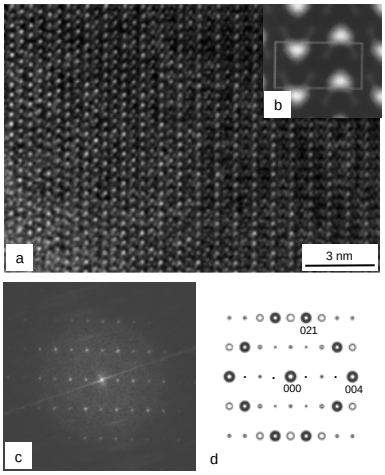

High resolution image of $Nb(Cu,Al)_2$ phase (a), potential map for thhe chosen symetry (a unit cell is marked) (b), Fourier transform FFT of the image (c) and electron difraction diagram, zone axis [100] (d)

J. Lalatko, Habilitation thesis, University of Silesia,Katowice, 2005

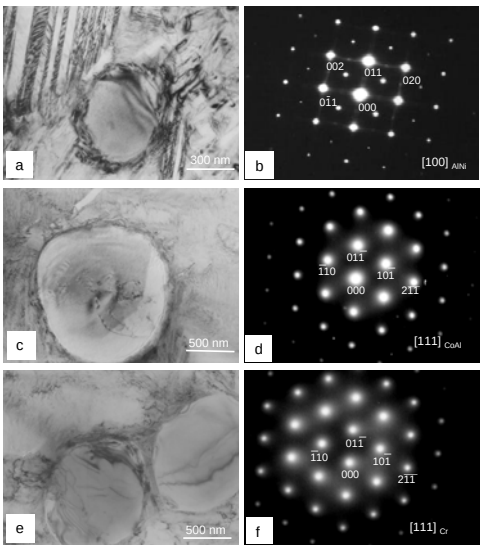

Precipitates of NiAl phase (a), AlCo phase (b) and Cr (c) in alloys of different chemical composition

J. Lalatko, Habilitation thesis, University of Silesia,Katowice, 2005

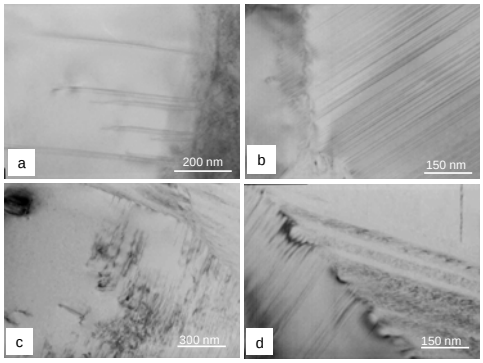

Microstructure of precipitates in the alloys deformed above A_f

Stacking faults and dislocation tangle can be seen.

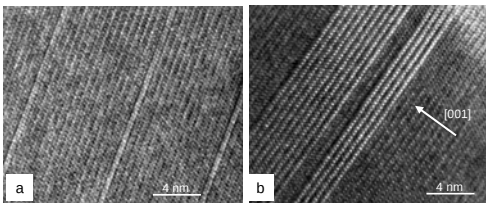

Microtwins were also observed.

J. Lalatko, Habilitation thesis, University of Silesia,Katowice, 2005

6. Ferromagnetic shape memory alloys

Co_2NiGa → Co49-Ni21.2-Ga29.8

Parent phase structures (a,b,c) Transformation into martensite $L1_o$ (d), BCT (e) and L1 (f)

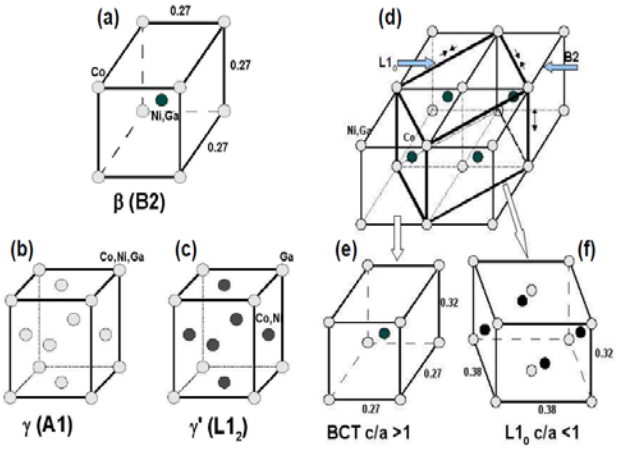

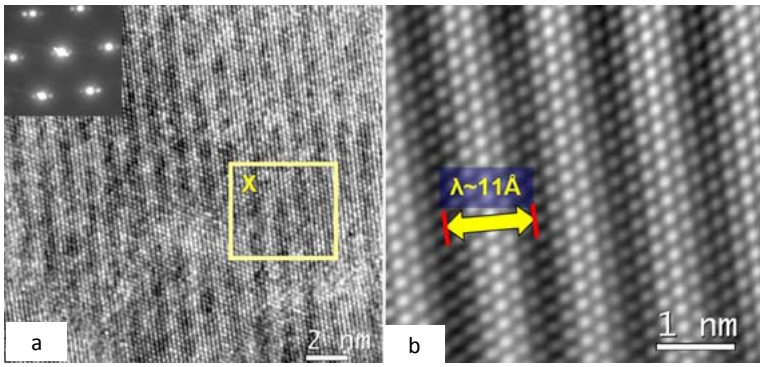

Modulation in martensite in [111] zone axis direction (a), enlarged X area (b)

K. Prusik, Ph.D thesis, University of Silesia, Katowice 2008

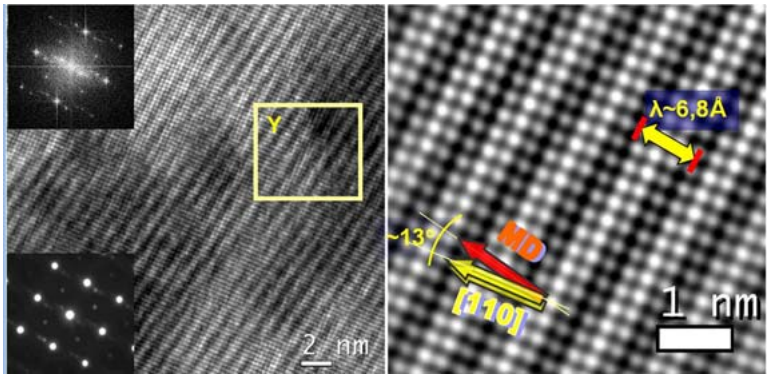

Modulation in martensite in [001] zone axis direction (a), enlarged X area (b)

K. Prusik, Ph.D thesis, University of Silesia, Katowice 2008

Thank you for your attention

First Electron Microscope with Resolving Power Higher than that of a Light Microscope
Author: J Brew, uploaded on the English-speaking Wikipedia by en:User:Hat'nCoat

Surface chemical analysis by electron spectroscopy techniques: XPS/AES, SAM/Topographic XPS

Panos A. Patsalas
University of Ioannina
Department of Materials Science and Engineering, GR-45110, Ioannina, Greece
ppats@cc.uoi.gr

Spectroscopic Techniques for Chemical Analysis

•The chemical analysis of solid surfaces and thin films are studied through the electronic structure (binding energies of electrons) of the constituent elements.

•In order to study the electronic structure (i.e. to identify the binding energies of the electrons in the solid) electronic transitions should be provoked.

•This is achieved by an initial electron excitation/ionization of the solid's electrons by an electron or X-ray beam, which colloquially known as the 'primary beam'.

•After the occurred electronic transitions electrons or X-ray photons are emitted from the solid.

•The various spectroscopic techniques are discriminated based on the nature of the primary beam and the emitted (particles (electrons or X-Ray photons).

University of Ioannina
Department of Materials Science and Engineering

Spectroscopic Techniques for Chemical Analysis

Classification of spectroscopic techniques for chemical analysis

	X-Rays	Electrons
X-Rays	XRF, EXAFS, NEXAFS	XPS/ESCA, XAES
Electrons	EDX/EPMA	AES, EELS

AES: Auger Electron Spectroscopy
EELS: Electron Energy Loss Spectroscopy
ESCA: electron Spectroscopy for Chemical
EXAFS: Extended X-ray Absorption Fine Structure
NEXAFS: Near-Edge X-Ray Absorption Fine Structure
XAES: X-Ray Excited Auger Electron Spectroscopy
XRF: X-ray fluorescence
XPS: X-ray Photoelectron Spectroscopy

University of Ioannina
Department of Materials Science and Engineering

Spectroscopic Techniques for Chemical Analysis

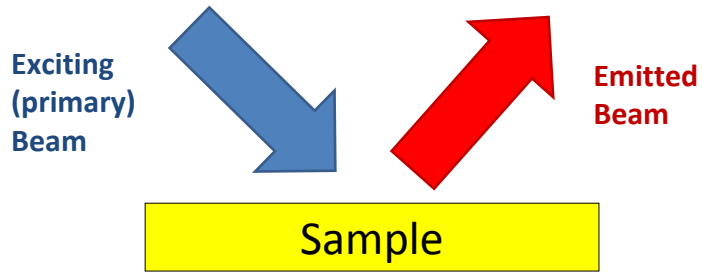

University of Ioannina
Department of Materials Science and Engineering

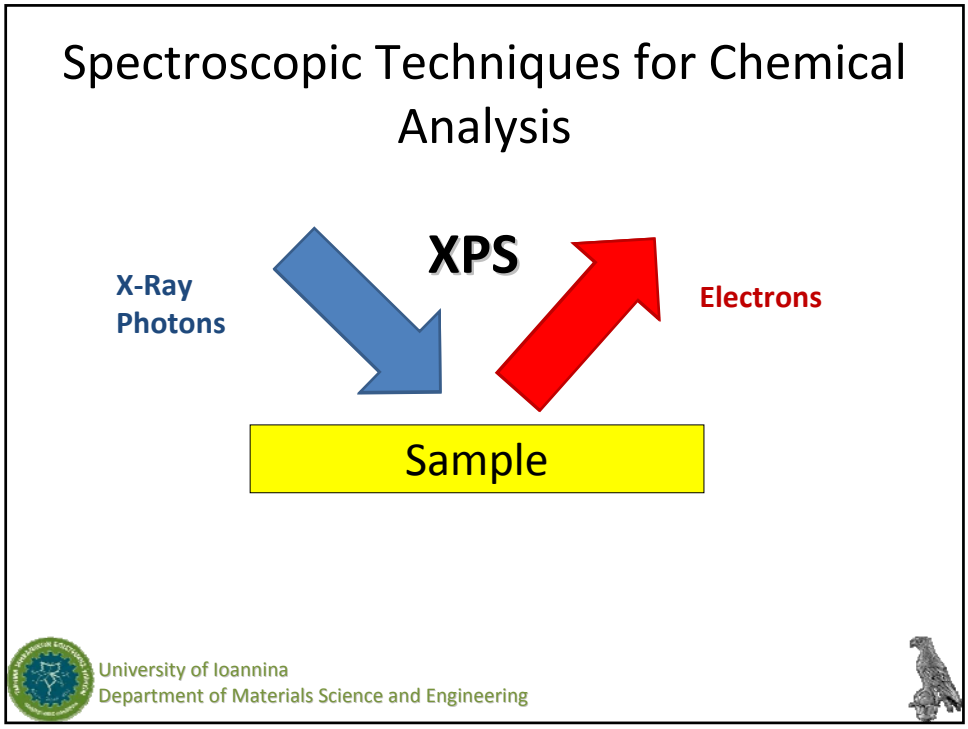
Spectroscopic Techniques for Chemical Analysis
XPS
X-Ray Photons
Electrons
Sample
University of Ioannina
Department of Materials Science and Engineering

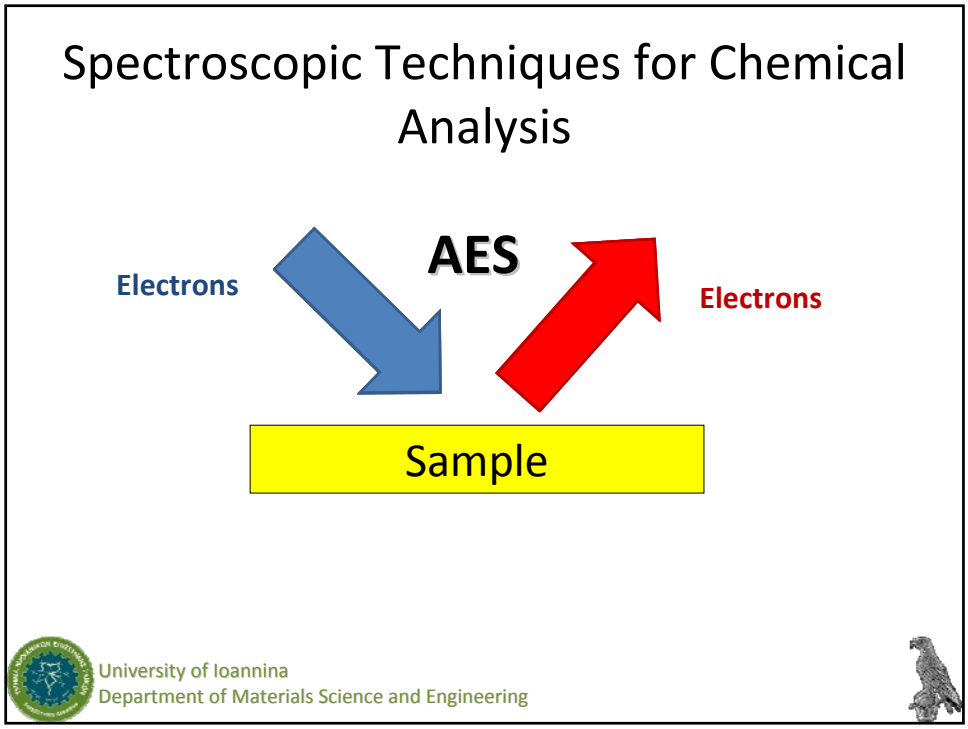
Spectroscopic Techniques for Chemical Analysis
AES
Electrons
Electrons
Sample
University of Ioannina
Department of Materials Science and Engineering

Spectroscopic Techniques for Chemical Analysis

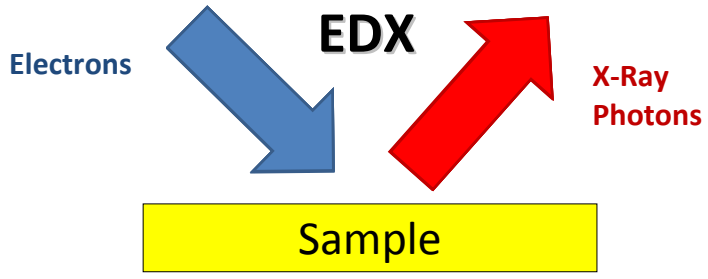

University of Ioannina
Department of Materials Science and Engineering

Spectroscopic Techniques for Chemical Analysis

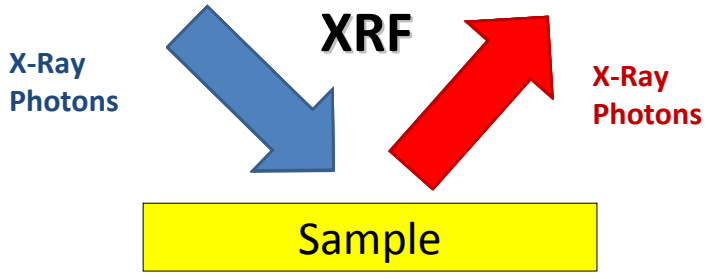

University of Ioannina
Department of Materials Science and Engineering

Electron and X-Ray Spectroscopy

Study of electronic structure

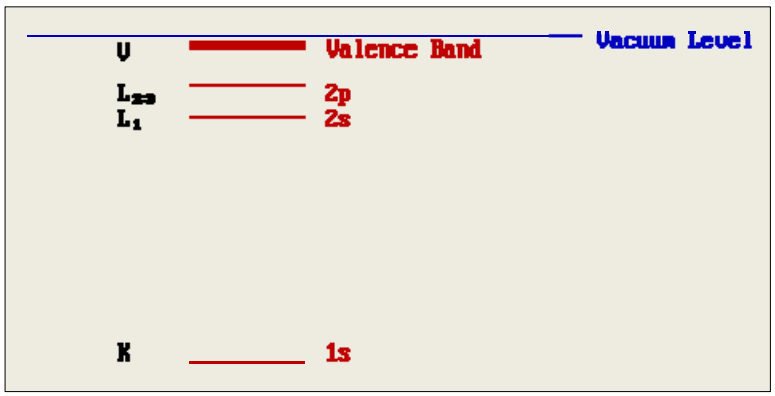

University of Ioannina
Department of Materials Science and Engineering

Electron and X-Ray Spectroscopy

Step 1: Ionization process

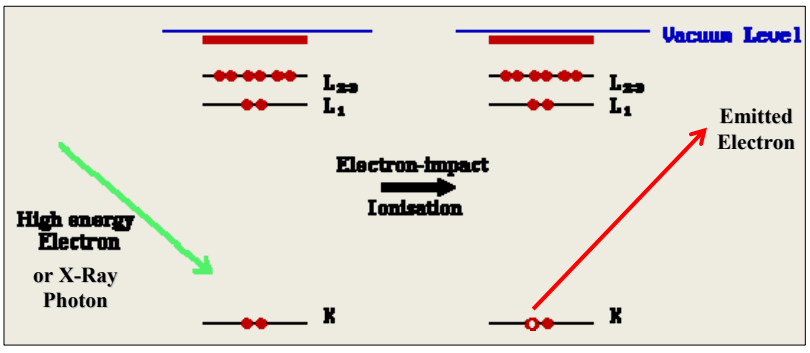

XPS!

University of Ioannina
Department of Materials Science and Engineering

Electron and X-Ray Spectroscopy

Step 2: electronic transition to fill the hole and minimize the energy of the atom.
The energy difference is emitted as:

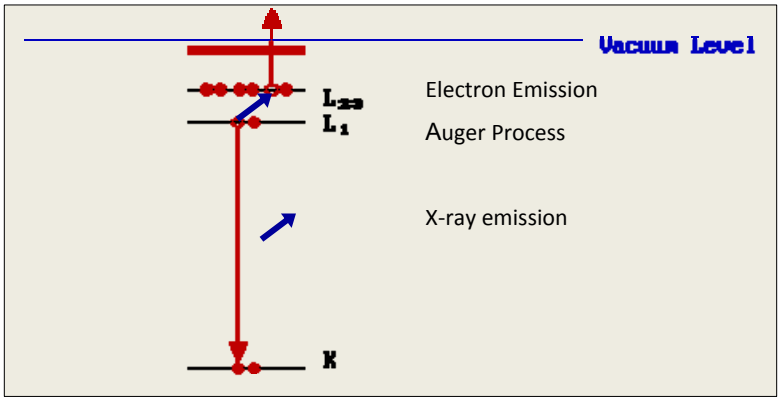

AES!

EDX!

University of Ioannina
Department of Materials Science and Engineering

Efficiency of AES and Electron Emission for Light Elements used in Coatings

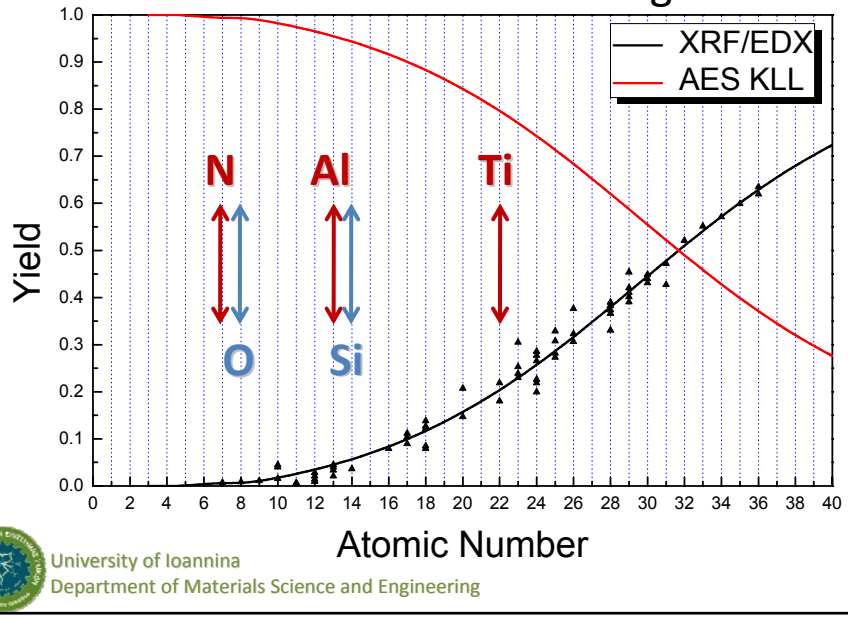

University of Ioannina
Department of Materials Science and Engineering

Surface sensitivity of electron based techniques

Analysis (escape) depth:

$\lambda = h/p = h/(2mE)^{1/2}$ (1)

$\lambda(Å) = [150/E(eV)]^{1/2}$ (2)

This surface sensitivity dictates the use of ULTRA HIGH VACUUM conditions (¬10^{-10} mbar)

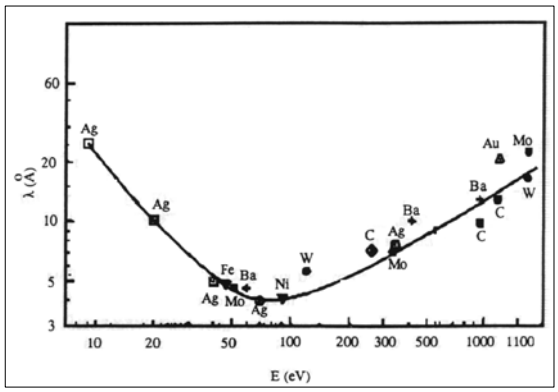

University of Ioannina
Department of Materials Science and Engineering

Instrumentation of electron spectrometers

Primary Beam:

Electron sources:

- Thermionic W-filament
- Thermionic LaB_6 filament
- Field Emission Gun (FEG)

X-Ray sources:

- Twin anode Mg/Al (full beam Ka1/Ka2/Kb)
- Monochromated Al (Ka1
- Synchrotron

Electron Analyzers:

- Cylindrical Mirror Analyzer (CMA), has been used for AES
- Hemispherical Sector Analyzer (HSA), the current standard for XPS/AES
- Spherical Mirror Analyzer (SMA), used for topographic XPS and SAM

University of Ioannina
Department of Materials Science and Engineering

Instrumentation of electron spectrometers

CMA

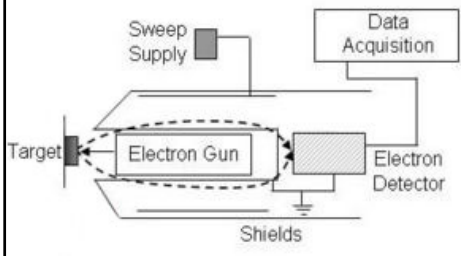

SMA

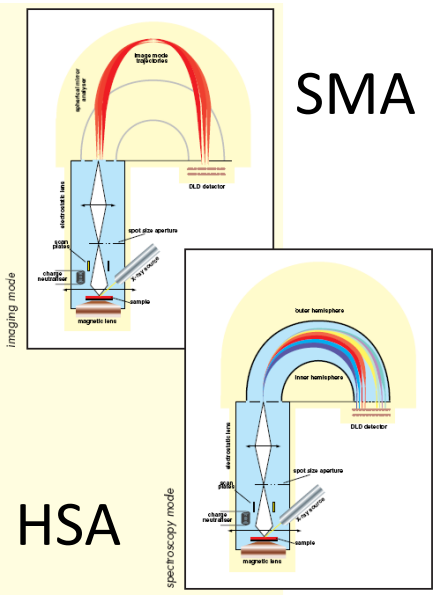

HSA

University of Ioannina
Department of Materials Science and Engineering

Instrumentation of electron spectrometers: Combined Electron- and X-Ray-excited Processes (Combined XPS and AES)

If the electron source is upgraded to be a FEG in a SEM column, then microscopy scans using only electrons of specific energy; this is the Scanning Auger Microscope (SAM).

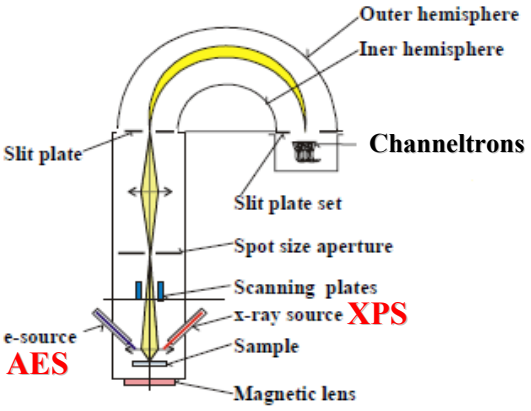

University of Ioannina
Department of Materials Science and Engineering

Basic AES System

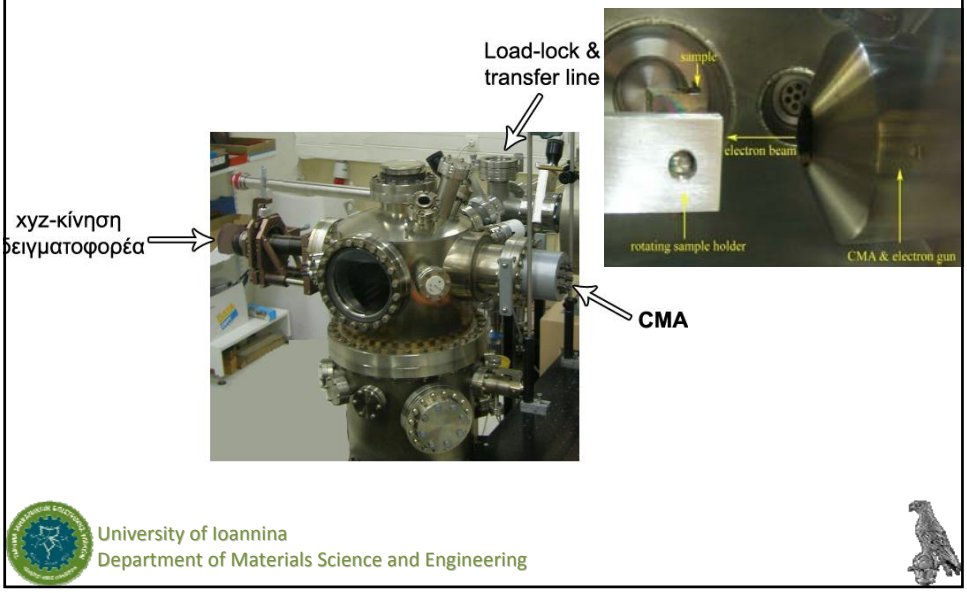

University of Ioannina
Department of Materials Science and Engineering

Basic XPS System

Twin Anode X-ray Source

University of Ioannina
Department of Materials Science and Engineering

Combined Topographic XPS, AES/SAM/SEM System (AUTh)

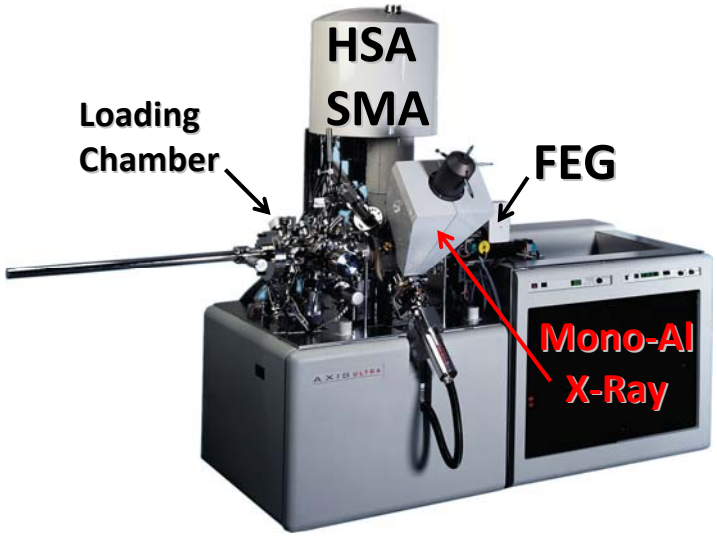

University of Ioannina
Department of Materials Science and Engineering

UHV clusters

- The requirements of UHV conditions and clean surfaces result in combining electron spectroscopy systems with thin film growth systems:

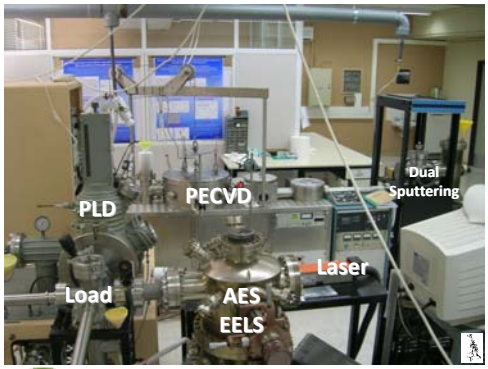

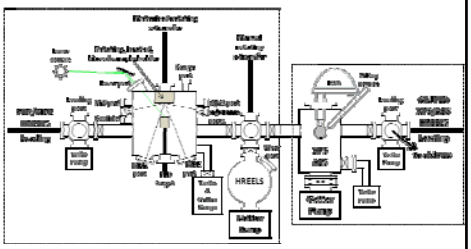

University of Ioannina
Department of Materials Science and Engineering

Combined Topographic XPS, AES/SAM/SEM System: Potential

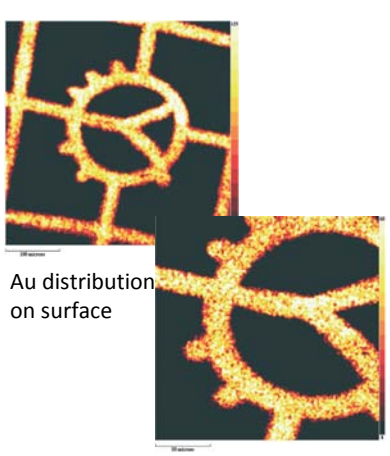

Au distribution on surface

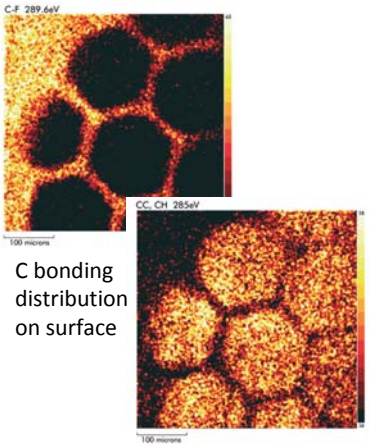

C bonding distribution on surface

University of Ioannina
Department of Materials Science and Engineering

Combined Topographic XPS, AES/SAM/SEM System: Potential

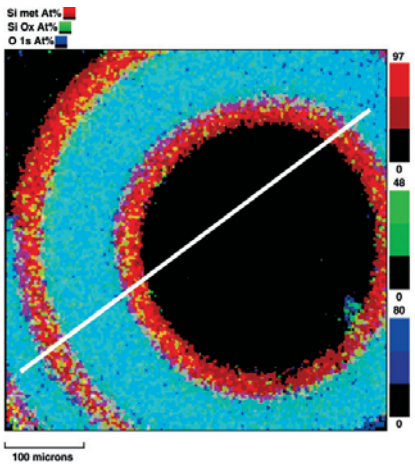

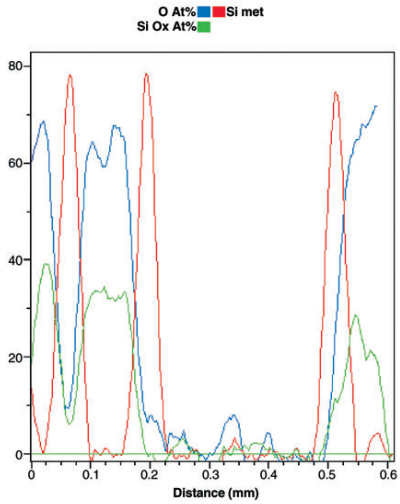

Patterned SiO_2/Si rings

University of Ioannina
Department of Materials Science and Engineering

Auger Electron Spectroscopy (AES)

The Auger process

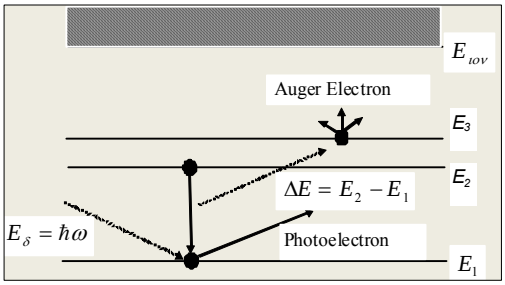

$KE = (E_1 - E_2) - E_3$

$KE = E_1 - (E_2 + E_3)$

University of Ioannina
Department of Materials Science and Engineering

Auger Electron Spectroscopy (AES)

Normal spectrum

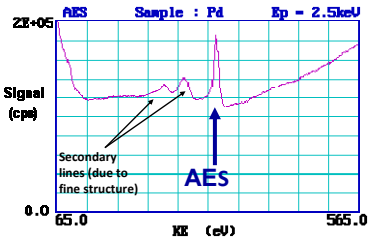

Differential spectrum

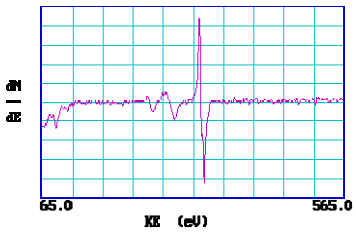

University of Ioannina
Department of Materials Science and Engineering

Auger Electron Spectroscopy (AES)

Normal spectrum

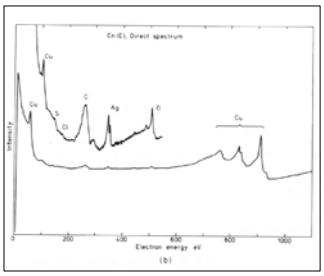

Differential spectrum

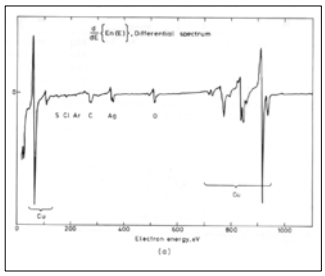

The elemental analysis is based upon measuring the peak to peak heights of the relative Auger lines in the differential spectrum, taking into account the corresponding sensitivity factors.

University of Ioannina
Department of Materials Science and Engineering

Auger Electron Spectroscopy (AES)

Depth profile

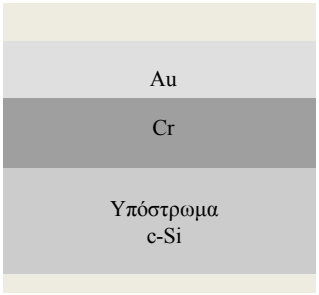

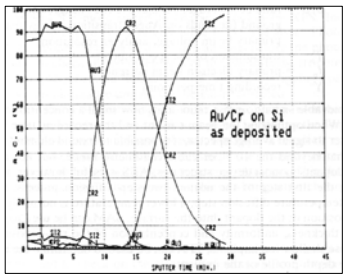

University of Ioannina
Department of Materials Science and Engineering

X-Ray Photoelectron Spectroscopy (XPS)

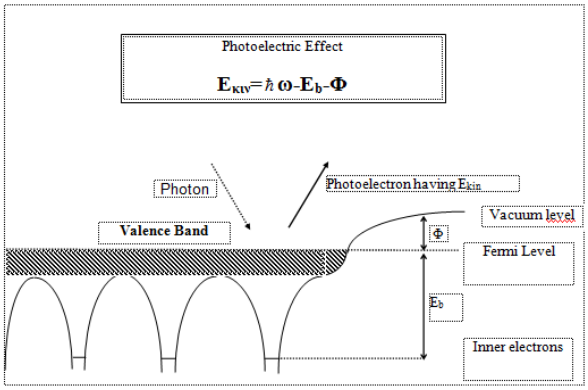

$$E_{\kappa\iota\nu}=\hbar\omega-E_b-\Phi$$

University of Ioannina
Department of Materials Science and Engineering

X-Ray Photoelectron Spectroscopy (XPS)

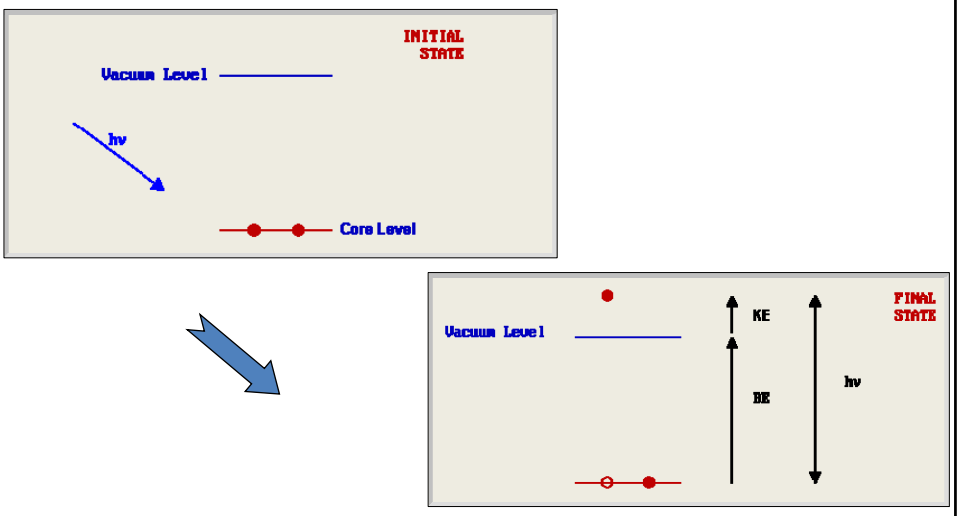

University of Ioannina
Department of Materials Science and Engineering

X-Ray Photoelectron Spectroscopy (XPS)

Survey-scan spectra: elemental analysis

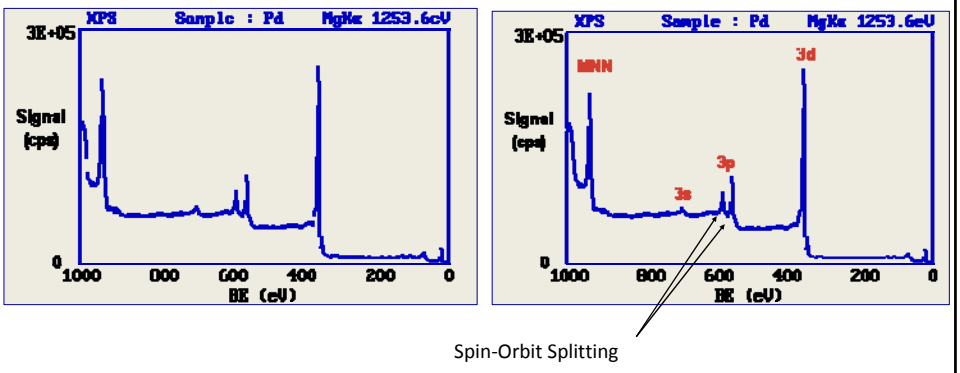

Spin-Orbit Splitting

University of Ioannina
Department of Materials Science and Engineering

X-Ray Photoelectron Spectroscopy (XPS)

Survey-scan spectra: elemental analysis

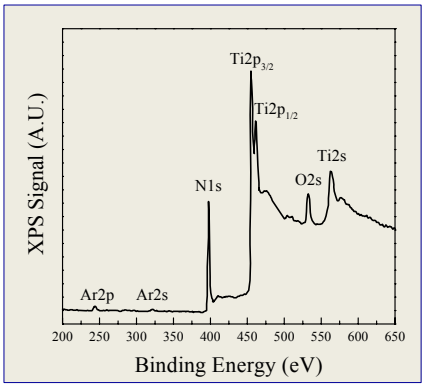

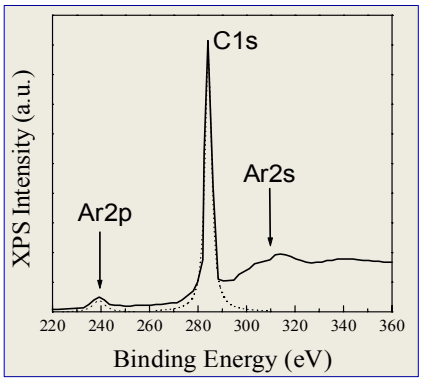

University of Ioannina
Department of Materials Science and Engineering

X-Ray Photoelectron Spectroscopy (XPS)

High-resolution spectra: chemical bonding

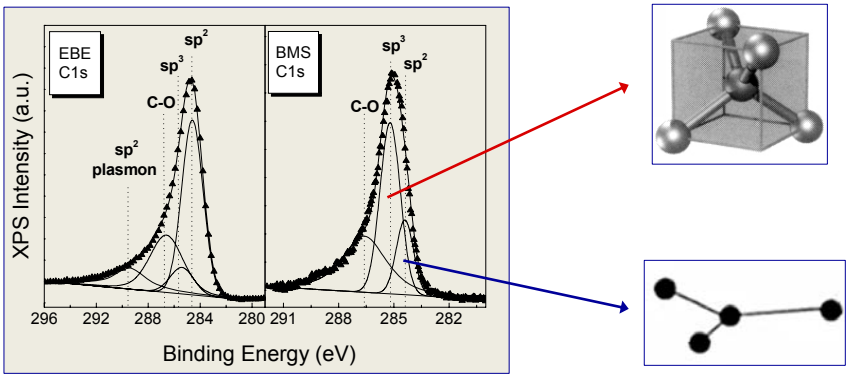

University of Ioannina
Department of Materials Science and Engineering

X-Ray Photoelectron Spectroscopy (XPS)

Angle Resolved XPS: Increasing the surface sensitivity

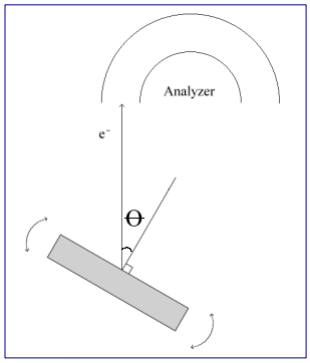

Effective escape depth:

$$D_{eff}=D\sin\theta$$

University of Ioannina
Department of Materials Science and Engineering

X-Ray Photoelectron Spectroscopy (XPS)

Angle Resolved XPS: Increasing the surface sensitivity

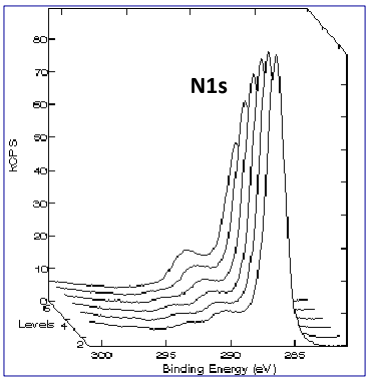

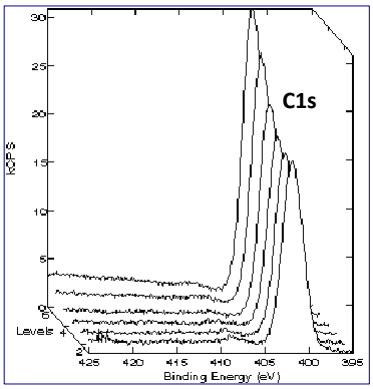

University of Ioannina
Department of Materials Science and Engineering

Case study: Amorphous Carbon and Carbon Nanotubes

University of Ioannina
Department of Materials Science and Engineering

a-C Classification

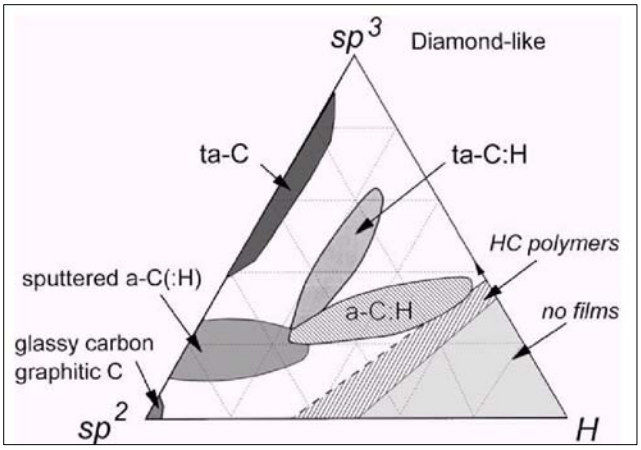

After Robertson, Mater. Sci. Eng. R37, 129 (2002).

University of Ioannina
Department of Materials Science and Engineering

Motivation

Why studying the surface properties of a-C, ta-C and related materials?

- Surface topography and electroic structure are crucial for applications such as:
  - tribology
  - biomedical
  - recording media
- The surface topography is closely associated to the growth mechanism of films (e.g. PLD-FCVA differences)
- The surface electronic structure determines the interactions of the film with the outer environment
- sp^3/sp^2 determination from inner state electronic transitions

University of Ioannina
Department of Materials Science and Engineering

Electronic Structure of amorphous Carbon and Electron Spectroscopy Techniques

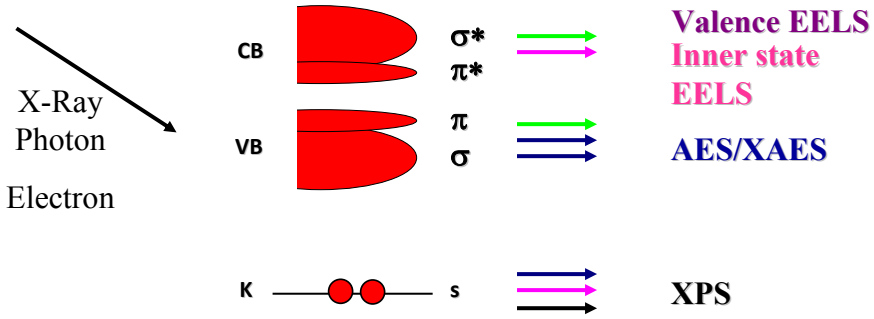

University of Ioannina
Department of Materials Science and Engineering

Electron Spectra of a-C using CMA

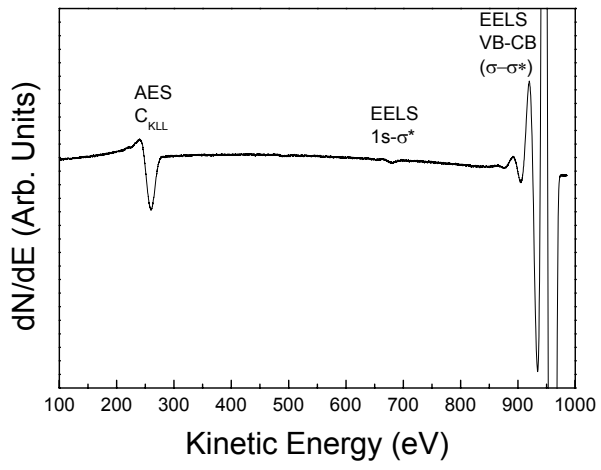

University of Ioannina
Department of Materials Science and Engineering

Electron Spectra of a-C using CMA

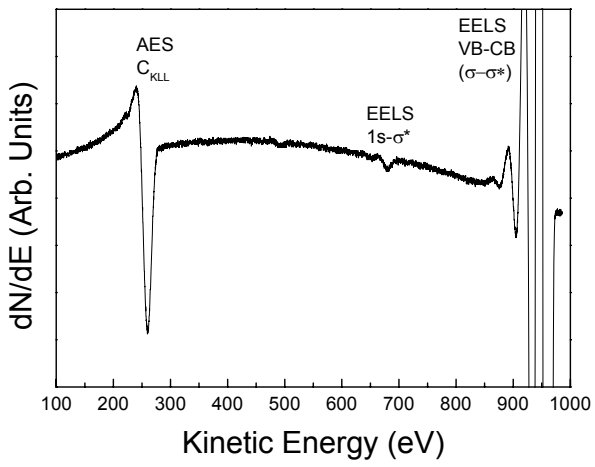

University of Ioannina
Department of Materials Science and Engineering

Electromagnetic dispersion in a-C

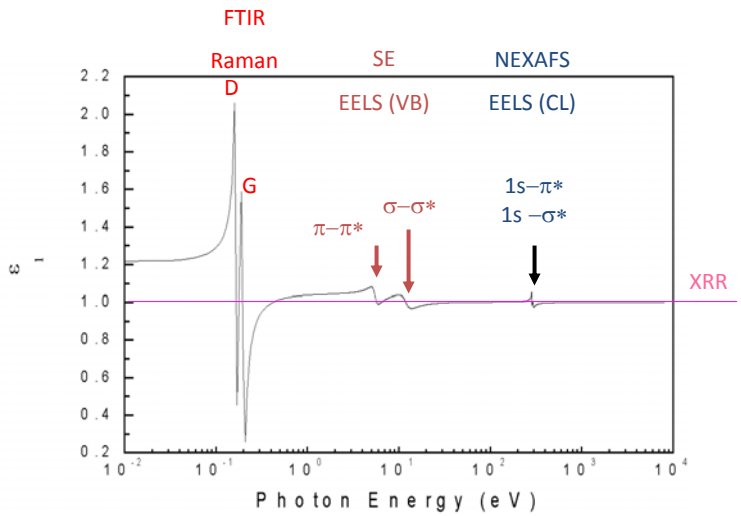

University of Ioannina
Department of Materials Science and Engineering

Auger Electron Spectroscopy (AES) of Graphite, Diamond and a-C

Electronic Structure of sp^2-bonded Carbon

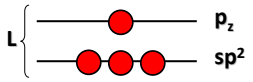

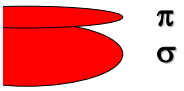

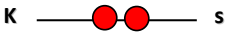

KLL Auger Transition

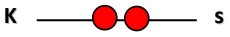

KVV Auger Transition

University of Ioannina
Department of Materials Science and Engineering

Auger Electron Spectroscopy (AES) of Graphite, Diamond and a-C

Electronic Structure of sp^3-bonded Carbon

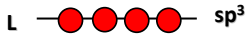

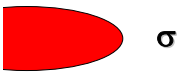

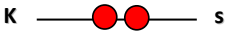

KLL Auger Transition

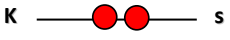

KVV Auger Transition

University of Ioannina
Department of Materials Science and Engineering

Auger Electron Spectroscopy (AES) of Graphite and Diamond*

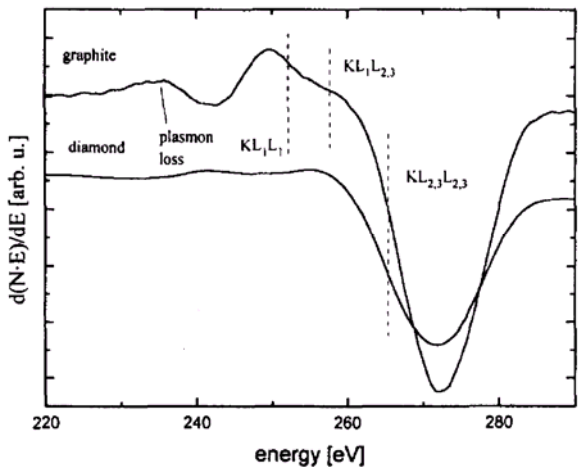

* After A. Fuchs et al, Thin Solid Films 232, 51 (1993)

University of Ioannina
Department of Materials Science and Engineering

Auger Electron Spectroscopy (AES) of ta-C

sp^2-bonded Carbon

Complex C_{KLL}

sp^3-bonded Carbon

Featureless C_{KLL}

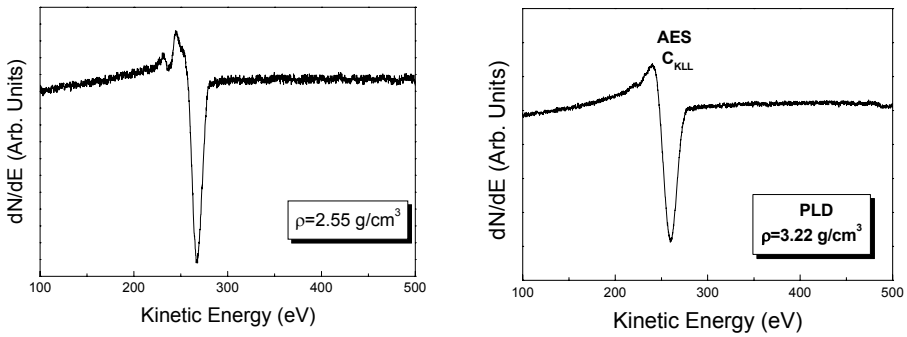

University of Ioannina
Department of Materials Science and Engineering

Auger Electron Spectroscopy (AES): Charging Effects

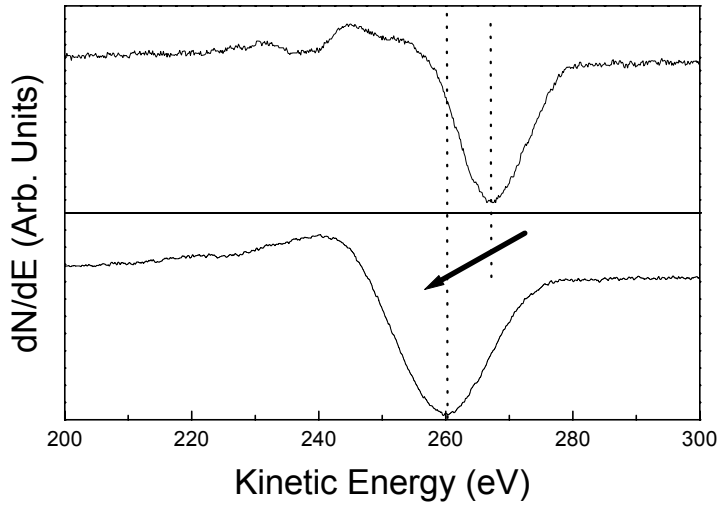

University of Ioannina
Department of Materials Science and Engineering

Auger Electron Spectroscopy (AES): Determination of sp^3/sp^2 *

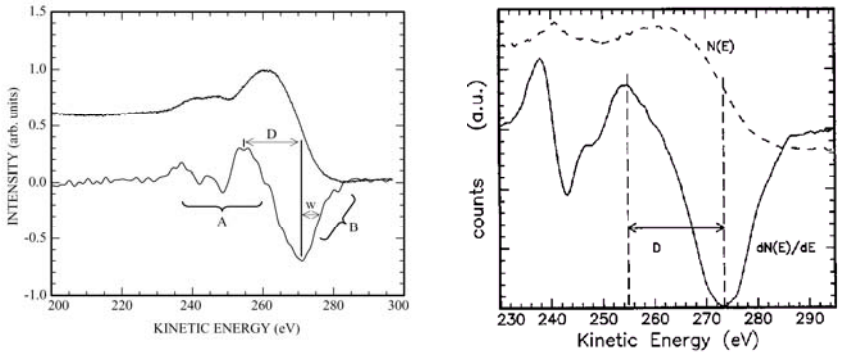

* After

L. Calliarri, Diam. Relat. Mater.14, 1232 (2005)

J.C. Lascovich, S. Scaglione, Applied Surface Science 78, 17 (1994)

University of Ioannina
Department of Materials Science and Engineering

Auger Electron Spectroscopy (AES): Technical Limitations

The AES spectra depend on:

- Excitation Particle

usually X-Ray excited AES gives sharper peaks and if we use calibration for electron-excited AES the sp^3 content is severely overestimated

- Charging Effects

the more sp^3 the film, the more shift of C_{KLL}/C_{KVV} to lower kinetic energy

University of Ioannina
Department of Materials Science and Engineering

Determination of sp^2 and sp^3 content from photoemmision experiments

The sp^3/sp^2 content of ta-C has been long determined by XPS using a simple deconvolusion of the C1s peak to components corresponding to the two phases.

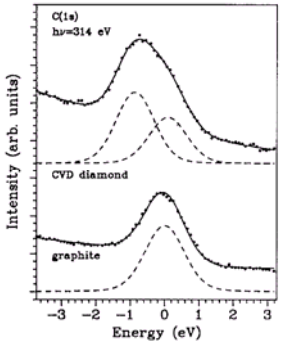

J.K. Simmons et al, J. Appl. Phys. 76, 5481 (1994)

University of Ioannina
Department of Materials Science and Engineering

Determination of sp^2 and sp^3 content from photoemmision experiments

However, in ex-situ experiments the situation is more complicated:

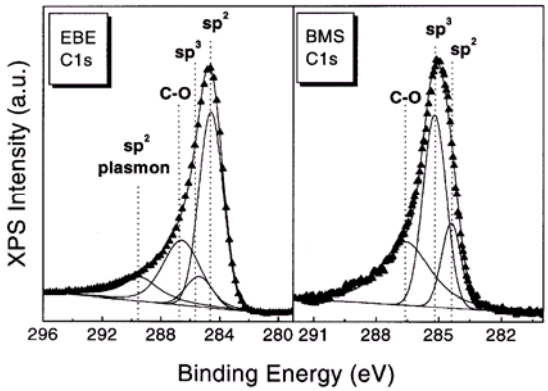

P. Patsalas et al, Diam. Relat. Mater. 10, 960 (2001); Thin Solid Films 428, 211 (2003)

University of Ioannina
Department of Materials Science and Engineering

Application I: a-C:Ag Films

a-C:Ag nanocomposites are very intersting for biomedical applications (denstistry and orthopaedics)

Their structure and stability as well as the correlation of the features of the a-C matrix and the embedded metall Ag grains are essential for engineering such materials

University of Ioannina
Department of Materials Science and Engineering

Electron Spectrum of a-C:Ag grown by PLD

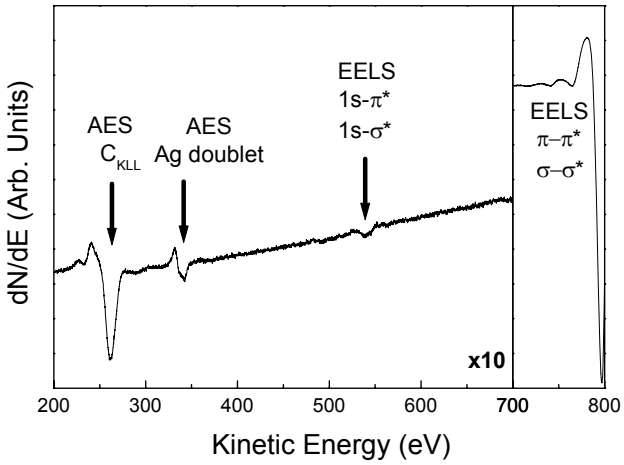

G.M. Matenoglou et al, Appl. Surf. Science, submitted (2006)

University of Ioannina
Department of Materials Science and Engineering

Variations of Electron Spectra of a-C:Ag

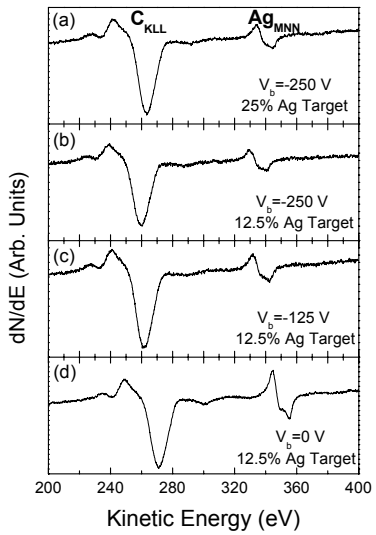

University of Ioannina
Department of Materials Science and Engineering

Correlation between [Ag] and [sp^3] implementing *in-situ* AES

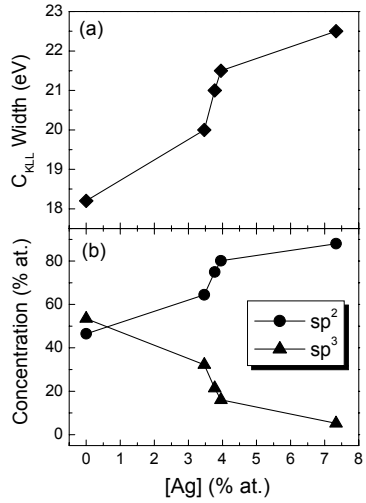

University of Ioannina
Department of Materials Science and Engineering

Highly performing semiconductor quantum dots, towards commercialization in optoelectronics and photovoltaics

Alexandros Stavrinadis, D.Phil.

Semiconductor quantum dots (QDs) are intensively investigated today as photoactive nanomaterials for a variety of optoelectronic applications like photovoltaics, photodetectors and displays. Much of this research is motivated by the fact that the optoelectronic properties of QDs, like their electronic band structure, bandgap and excitonic photoresponce can be tuned as a function of the QDs´ size and shape due to the quantum confinement. Quantum confinement is also associated with the increased multiple exciton generation effect in QDs materials compared to respective bulk semiconductors, a phenomenon which if utilized in photovoltaics could result to solar cells with >100% external quantum efficiencies[1].

QDs can be synthesized via physical vapor deposition or via colloidal chemistry methods with the second one considered to be a low financial cost approach. A wide variety of colloidal QDs (CQDs) materials like III-V, II-VI etc materials can be synthesized using colloidal chemistry, moreover their size and shape can be finely controlled by optimizing the methods´ growth parameters, typically these parameters are the temperature, the growth time, the ion precursor concentrations, the species and concentrations of the organic moieties (ligands) used to control the growth and colloidal stability of the QDs, the atmospheric environment in which QD synthesis takes place [2]. The shape of QDs and semiconductor nanoparticles in general can be controlled via different mechanisms, e.g. PbSe nanocubes, nanosperes, straight or zigzag nanowires, nanostars, nanorings [3. 4] etc. can be synthesized by utilizing individually or in combination the different growth rates of certain crystallographic planes, the selective adsorption of ligands on specific planes, the self-assembly and necking of individual nanoparticles. Other complex nanoparticles like CdSe tetrapods can be synthesized in a two-stage growth scheme: at first quasispherical zinc blend CdSe QDs are grown at low <170oC temperatures, afterwards the temperature is raised and CdSe wurtzide arms epitxially grow onto the facets of the zinc blend particles forming the final tetrapod-shaped nanoparticles [5].

The colloidal chemistry approach also allows for fine control of the stoichiometry and structure of semiconductor nanocrystals towards making ternary, quaternary etc. CQDs as well as heterostructured nanoparticles. This can be done by using more than one anion (or cation) elements [6, 7] in the CQD synthesis reaction, or post-synthetically by inducing ion exchange reactions [8-10]. A different aspect of stoichiometric control

concerns control of the nature and amount of organic moieties attached to the surface of CQDs. Usually CQDs are originally capped with fatty carboxylic acids (e.g. oleic acid), amines, thiols etc. used in the synthesis of the CQDs. For CQD-based optoelectronics though it is often required to exchange these ligands with shorter ones or even remove them because the nature and length of the ligands affect the optoelectronic properties of the CQDs and their thin film solids [11-15]. For example as synthesized PbS CQDs which are widely studied today as a photoactive material for photovoltaics and photodetectors are commonly passivated with oleic acid which needs to be replaced with much shorted moieties like ethanedithiol (EDT) or mercaptopropionic aci (MPA) when using the CQDs in photovoltaic devices. Due to their small length the shorter molecules allow for efficient dot-to-dot charge transfer. At the same time their functional groups (thiols) affect the doping density of the CQDs by passivating elelctronic trap states and control the oxidation rate and oxide species on the surface of the dots [11-15]. Control over the surface chemistry of CQDs has led to the development of photodetectors with detectivity values in the IR comparable to bulk InGaAs technology [23]. The ligand exchange process can take place in solution or in solid state (CQD thin film solids). A very successful approach is to perform ligand exchange on QD thin films formed in a layer-by-layer fashion using spin casting or dip-coating techniques [11-15].

The use of EDT, MPA and other short organic and inorganic ligands has played a major role in the development of quantum dot based optoelectronics, particularly PbS and PbSe CQD all-inorganic photodetectors and photovoltaics. Schottky junction solar cells were among the first to studied [16] and their electronic characteristics are valuable tools in studying QD thin films properties as a function of CQD size, stoichiometry and surface chemistry control; Schottky cells with efficiencies up to 3.5% have been achieved using $PbSe_xS_{1-x}$ ternary quantum dots passivated with EDT [7]. Higher efficiencies in the order of 5-6% can be achieved by utilizing MPA or EDT passivated CQD PbS in TiO2/PbS [17, 18] or PbS/ZnO [19] respectively depleted heterojunction solar cells. Various other device architectures, like tandem cells, quantum funnel cells [17], polymer/QD [20] and QD/QD bulk heterojunction cells [21], and QD materials, like Bi_2S_3 [21] and CdSe [20], are also under development. Two recent works, one a Bi_2S_3/PbS nanoparticle based and 4.9% efficient bulk heterojunction solar cell [21], and the second on a grapheme/PbS phototransistor with ultra high gain which outperforms conventional inGaAs technology [22], are examples of how CQD optoelectronics are currently being improved through advancements in new nanomaterials and device concepts.

The advancements made during the last 10 years in the synthesis, properties and optoelectronic application of CQDs set a positive outlook on their potential commercialization and the industrial sector is active to that direction. For example *IBM* develops PbS QD based solar cells [24], *Samsung* develops QD based displays [25] and *Siemens* develops QD based imaging photodetectors [26]. The materials industry is also active in this field, *Nanoco* and *Evident Technologies* are examples of companies working towards large scale (Kg) synthesis of CQDs to supply the growing CQD optoelectronics R/D community.

[1] A. Nozik, Chem. Phys. Lett., 457, 3-11, (2008)
[2] A. L. Rogach, et al., 3, 536-537, (2007)
[3] J. Xu, et al., J. Phys. Chem. B, 110, 2497-2501, (2006)
[4] K. S. Cho, et al., J. Am. Chem. Soc., 127, 7140-7147, (2005)
[5] S. Jumar, et al., Small, 2, 316-329, (2006)
[6] M. D. Regulacio, et al., J. Am. Chem. Soc., 133, 2052-2055, (2011)
[7]) W. Ma, et al., Nano Lett., 9, 1699-1703, (2009)
[8] D. H., Son, et al., 306, 1009, (2004)
[9] J. Park, et al., J. Mater. Chem., 21, 3745-3750, (2011)
[10] B. Sadtler, et al., J. Am. Chem. Soc., 131, 5285-5293, (2009)
[11] A. T. Fafarman, et al., 133, 15753-15761, (2011)
[12] G. Konstantatos, et al., Nature Photon., 1, 531-534, (2007)
[13] G. Konstantatos, et al., 8, 1446-1450, (2008)
[14] M. Law, et al., J. Am. Chem. Soc., 130, 5947-5985, (2008)
[15] J. M. Luther, et al., ACS Nano, 2, 271-280, (2008)
[16] R. Debnath, et al., J. Am. Chem. Soc., 132, 5952-5953, (2010)
[17] R. Debnath, et a., En. Env. Scien., 4, 4870-4881, (2011)
[18] J. Kramer, E. Sargent., ACS Nano, 5, 8506-8514, (2011)
[19] J. M. Luther., et al., Adv. Mater., 22, 3704-3707, (2010)
[20] I. Gur, et al., Nano Lett., 7, 409-414, (2007)
[21] A. Rath, et al., Nature Photon., 6, 529-534, (2012)
[22] G. Konstantatos, et al., Nature. Naotech., 7, 363-368, (2012)
[23] G. Konstantatos, E. Sargent, Proc. IEEE., 97, 10, 1666-1683, (2009)
[24] I. J., Kramer, et al., Adv. Mater., 24, 2315-2319, (2012)
[25] TH Kim, et al., Nature Photon., 5, 176-182, (2011)
[26] T. Rauch, et al., Nature Photonics, 3, 332-336, (2009)

Micro- and Nano-structural study of SiC, Polytypes and Stacking Faults

M. Marinova,

Electron Microscopy Group, Physics Department,
Aristotle University of Thessaloniki

Outline

- Motivation
  - General Aspects
  - SiC Advantages
  - 3C-SiC Advantages
- Common Defects In SiC
  - Classification of Defects in SiC;
  - Influence of the growth conditions on the appearance of defects;
- Summary

The SiC polytypes

- **Polytypism** - one-dimensional polymorphism (> 200 polytypes)

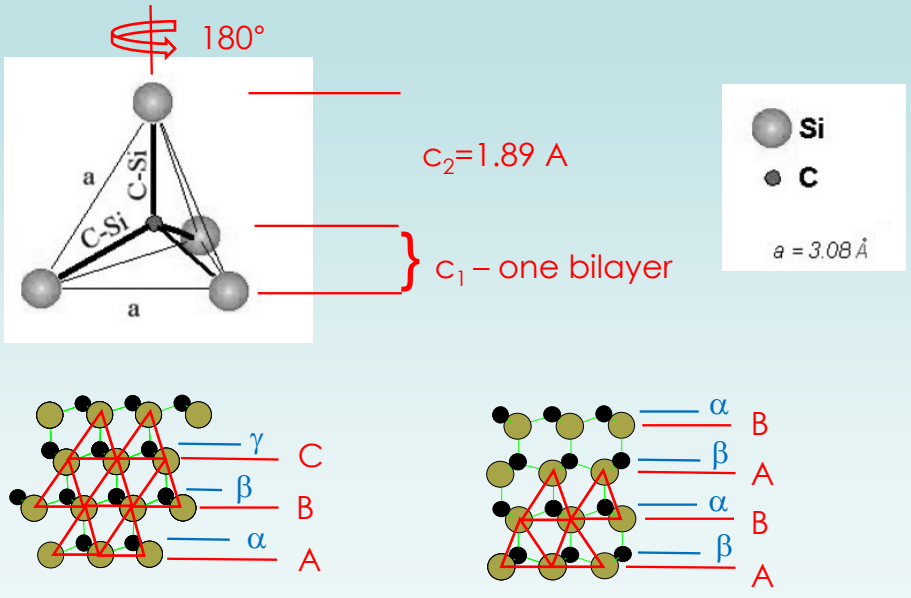

The SiC polytypes

- **Important example**: 3C-SiC (with zinc-blende structure); 2H-SiC (pure wurzite strucutre). The other polytypes (4H-SiC; 6H-SiC; 15R-SiC) - combination of hexagonal and cubic symmetry

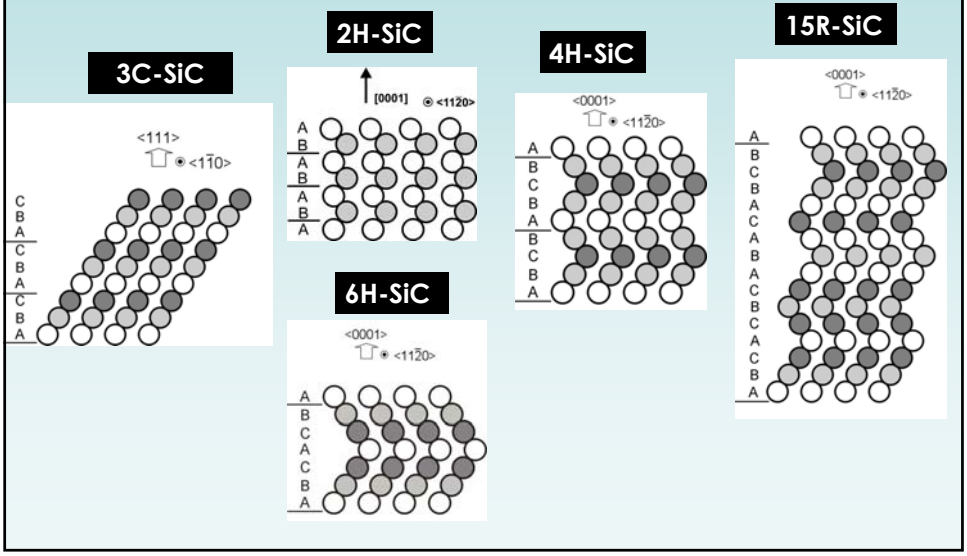

The SiC properties

- ***Structural symmetry changes*** → affect *the polytypes properties properties.*
- The Choyke-Hamilton-Patrick rule: a linear relationship between the band gap and the degree of hexagonality. Band gap energies: 2.4 (3C) - 3.3 eV (2H).
- Possibility for development of **heterostructure devices**, as for III-V compounds. **Advantages:** no difference in the chemical constituents; defect-free, lattice-matched and coherent heterointerface

Hexagonality: 0 | 0,33 | 0,5 | 0,4 | 1

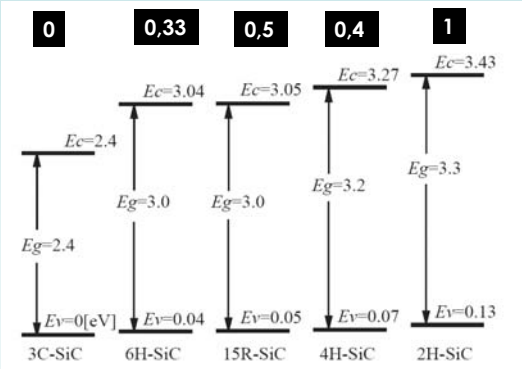

Energy band gaps of the most important polytypes - Iwata *et al* Physica B 340 (2003) 165

Why Silicon Carbide?

- high-temperature operation of the SiC electronic devices compared to Si
- high radiation and chemical resistance
- high thermal conductivity (better than Cu)
- high hardness and Young's modulus (typically 450 GPa compared with 130 GPa for Si)

	Si	GaAs	3C-SiC	6H-SiC	4H-SiC	Diamond
Lattice α [Å]	5.43	5.65	4.36	3.08	3.08	3.567
Lattice *C* [Å]	n.a.	n.a.	n.a.	10.05	15.12	n.a.
Bond length [Å]	2.35	2.45	1.89	1.89	1.89	1.54
Ther.cond.[W/cmK]	1.5	0.5	5	5	5	20
Elect. Mob. [cm^2/Vs]	1350	8500	1000	a=720 c=650	a=370 c=50	1900
Breakdown electric field [10^6 V/cm]	0.3	0.4	4.0	2.0	2.4	5.6
Saturated electron drift velocity [10^7 cm/s]	1.0	2.0	2.7	2.0	2.0	2.7
Maximum operation T [°C]	300	460	1240	1240	1240	1100

N.G. Wright *et al*, Materials Today 11 (2008) 16

The Cubic SiC polytype

- Isotropic properties
- The highest electron mobility, breakdown electric field, saturated electron drift velocity;
- Lowest density of traps at the SiC/SiO_2 interface.

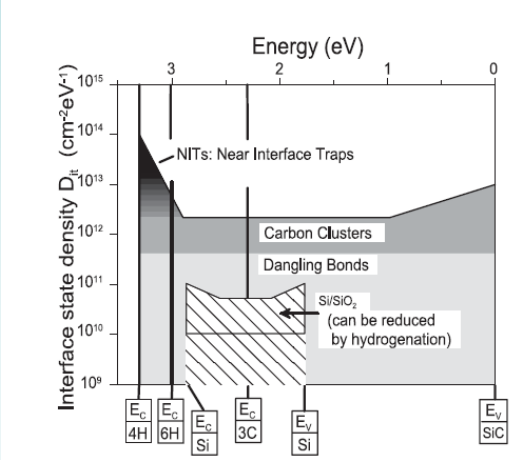

Schöner et al , CVD 2006, 12, 523–530

Problems

- Usually the growing crystal undergoes **polytypic transition** and **spontaneous generation** of defects;
- Adapted growth method;
- Reproducibility;
- Control of the doping;
- Lack of appropriate substrates for growth
  on Si (20% lattice mismatch) → high density of defects and (8% thermal coefficient mismatch) → wafer bowing

  Growth on a-SiC or by homoepitaxy on 3C-SiC - a solution

Growth methods

From liquid phase

- Vapour-Liquid-Solid (VLS) mechanism
- Liquid Phase Epitaxy (LPE)

From vapour phase

- Chemical Vapour Deposition (CVD)
- Sublimation Epitaxy (SE)
- Continuous Feed Physical Vapour Transport (CF-PVT)

The studied samples

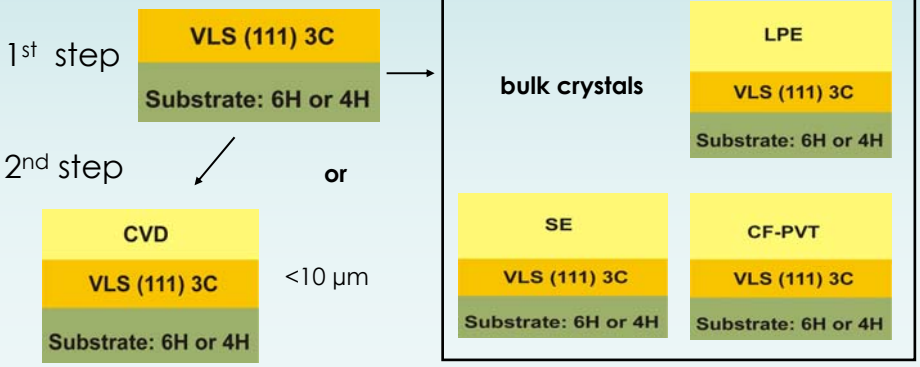

Classification Of Defects In SiC

- Dislocations (*linear defects*);
- SFs In Different Polytypes (*planar defects*);
- Polytypic Inclusions And Polytypes (*3D*);
- Inversion Domain Boundaries (IDBs) (*planar defects*);
- Low Angle Boundaries (LABs) (*planar defects*);
- Twin Boundaries In 3C (*planar defects*);
- Incorporation And Precipitation Of Dopants And Impurities (*planar and 3D*);

Classification Of Defects – Planar Defects/Interfaces

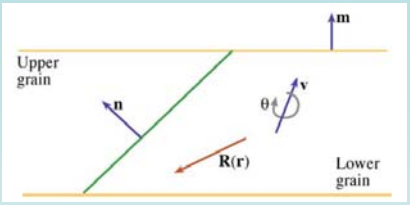

n – direction parallel to the defect plane;
θ – rotation angle between the two grains along a vector ***v***;
R(r) – translation vector between the two grains

- Translation boundary – only translation is allowed R(r) – ***SFs and anti-phase boundaries***;
- Grain boundary - Any values of R(r), n, and θ are allowed, but the chemistry and structure of the two grains must be the same;

  Low Angle Boundaries – they involve rotation only at small angles θ usually accommodated by arrays of dislocations;

  High Angle Boundaries – *they can adopt specific values for* ***n and θ*** – different twin boundaries and the IDBs.
- Phase boundary, PB. As for a GB, but the chemistry and/or structure of the two regions can differ.

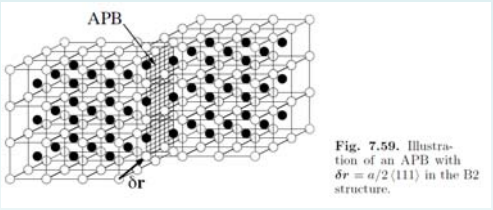

Fig. 7.59. Illustration of an APB with $\delta r = a/2\langle 111\rangle$ in the B2 structure.

Stacking Faults

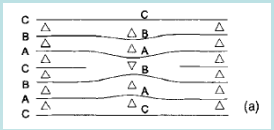

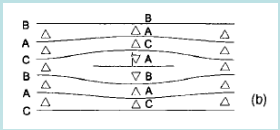

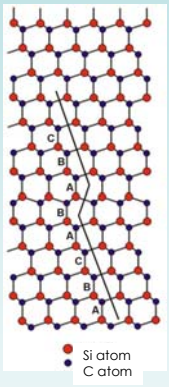

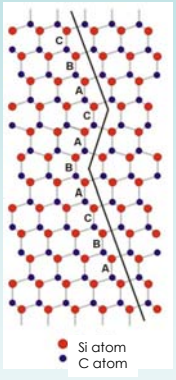

Intrinsic SF
removal of a layer – a break in the stacking sequence

Extrinsic SF
introduction of a layer – two breaks in the stacking sequence

Courtesy of Dr. A. Mantzari, PhD thesis

Stacking Faults - formation

Dissociation of a perfect dislocation into ***Shockley partials***: 1/2 <110> -> 1/6<211>+1/6<12$\underline{1}$>

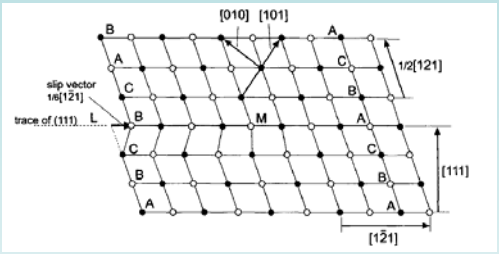

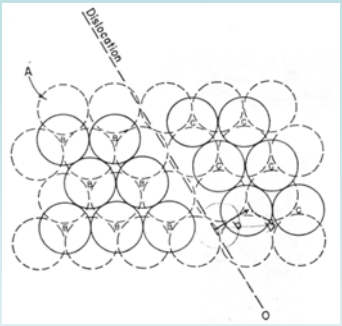

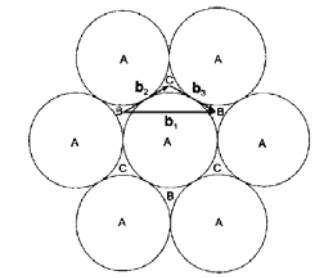

Stacking Faults - formation

Dissociation of a perfect dislocation into ***Frank partials***: 1/2 <110> -> 1/6<211>+1/3<111>

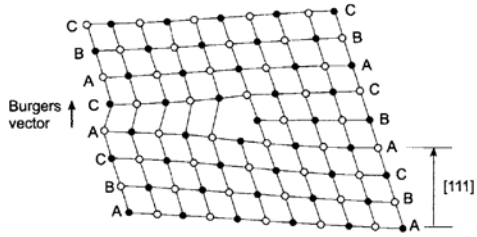

Inserting (extrinsic SF) or removing (intrinsic SF) one close-packed {111} layer of atoms.

$$d = \frac{G.b^2}{4\pi\gamma^2}$$

d - width of a SF;
b – Burgers vector
G – shear modulus
γ – SF energy

Common in-grown defects in 3C-SiC

Stacking faults (SFs) are inevitably present in 3C-SiC due to the very low energy:

SF energies (mJ/m²)		3C-SiC	4H-SiC	6H-SiC
Supercell method	SF I	-1.71	17.7	3.10
	SF II		18.1	40.10
	SF III			3.35
Supercell method	SF I	-2.70	18.4	1.35
	SF II		18.7	38.4
	SF III			1.63
ANNI model	SF I	-6.27	18.3	3.14
	SF II		18.3	36.6
	SF III			3.14

Theoretically predicted SF energies calculated by different methods
Lindefelt et al PRB 67 (2003) 155204

Comparison:

280 mJ/m² in diamond
55 mJ/m² in Si
45 mJ/m² in GaAs

SFs strongly increase the leakage current in devices.
Required density is $<10^3$ cm^{-1}.
For most of the growth methods used: **~2x10⁴ cm⁻¹ or higher.**

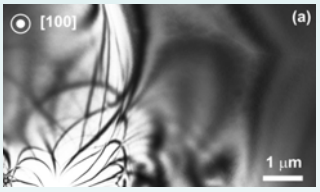

Unseeded 3C-SiC crystals grown by CF-PVT method:
< 10³ cm⁻¹

Problem with the sizes

Common in-grown defects in 3C-SiC

(011) 3C-SiC

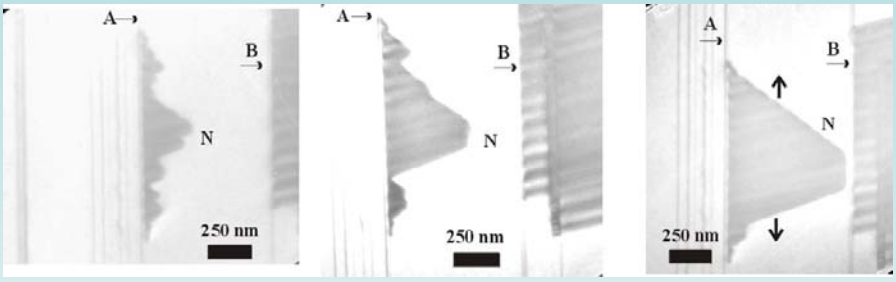

- The length of a SF in 3C-SiC can be limited by the size of the crystal or the presence of other defects that act as obstacles
- Converging the electron beam in an area for 15s was sufficient to develop stress due to thermal gradient ⇒ generation of a new SF of (111) type denoted by letter (N), in contact with another SF denoted by letter (A)
- SF (B) acts as an obstacle for (N), which was extended laterally

E.K. Polychroniadis et.al.: Materials Science Forum Vols. 483-485 (2005) pp. 319-322

Courtesy of Dr. A. Mantzari, PhD thesis

Common in-grown defects in 3C-SiC

• For the 3C (fcc) polytype SFs exist in four {111} planes – depending orientation and diffraction conditions we see the SF differently

(111) 3C-SiC

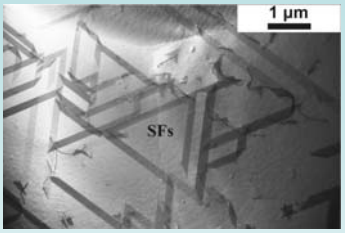

(011) 3C-SiC

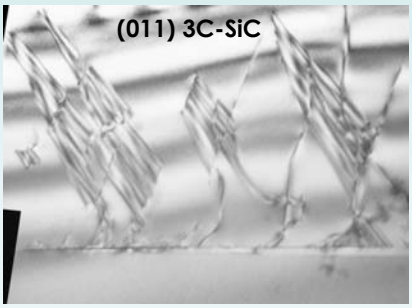

(100) 3C-SiC

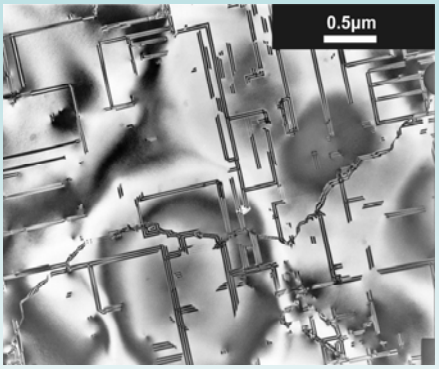

PVTEM micrographs of 3C-SiC having an (a) (111) orientation and (b) (001) orientation.

When SF (and other coherent interface) are present the displacements introduces additional phase factor 2□g.R(r) into the main and diffracted beam amplitudes.

BF of a SFs in a fcc material viewed with strong diffraction (000) and (002) beams within the [013] zone section and the corresponding stereographic projection

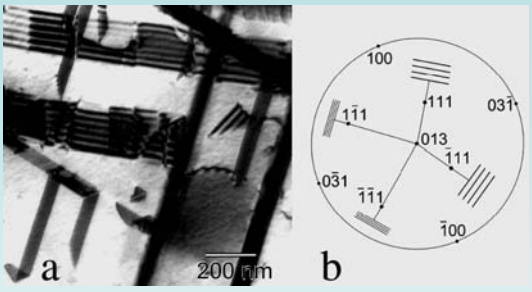

(011) 3C-SiC

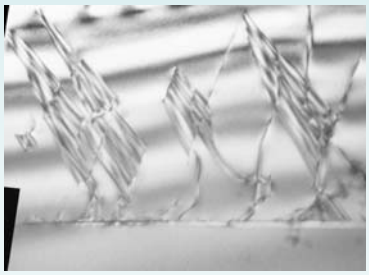

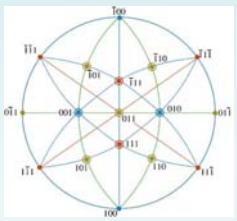

($\underline{1}\underline{1}1$) and ($\underline{1}\underline{1}\underline{1}$) are observed edge on within (011) section

"TEM and Diffractometry of Materials" Fultz and Howe
Williams and Carter "Transmission Electron Microscopy"

Using two-beam diffraction condition the type of SF can be determined

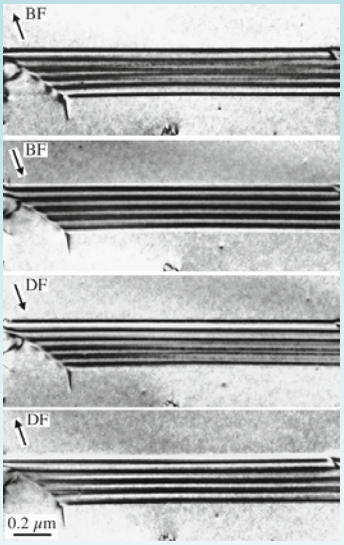

Intrinsic SF

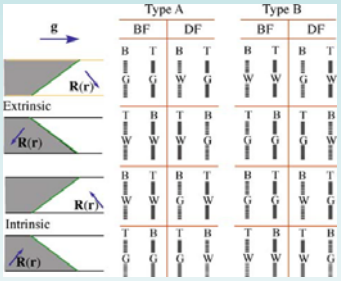

Williams and Carter, "Transmission Electron Microscopy" p. 425

HRTEM image of SFs in 3C-SiC

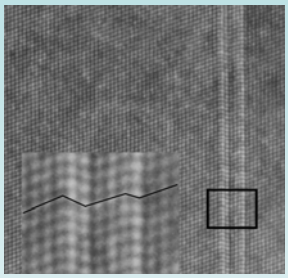

Extrinsic **Intrinsic**

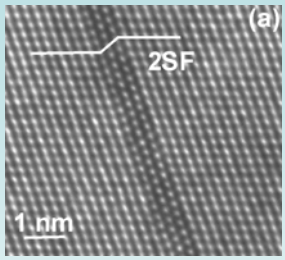

Extrinsic

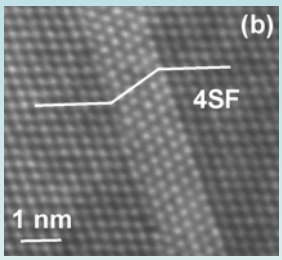

Multiple SF or a nano-twin lamella

Intrinsic and Extrinsic SF in 3C

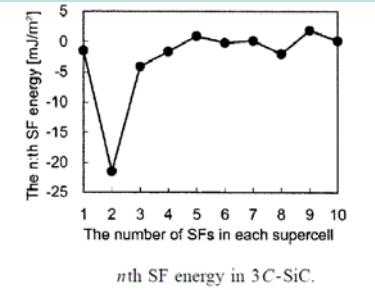

*n*th SF energy in 3*C*-SiC.

Iwata et al PRB **68**, 113202 (2003)

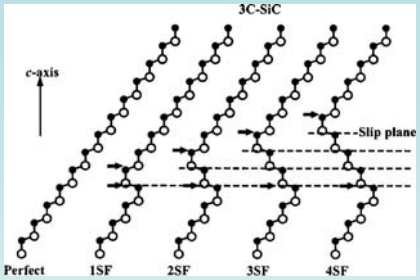

By the introduction and propagation of several adjacent partial dislocation multiple SF (micro-twins) can form

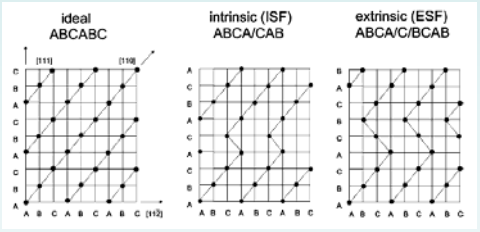

ISF -3.4 mJ/m^2
ESF -28 mJ/m^2

Käckell *et al*, PRB 58 (1998) 1326

Formation of extrinsic SF in CF-PVT grown layers

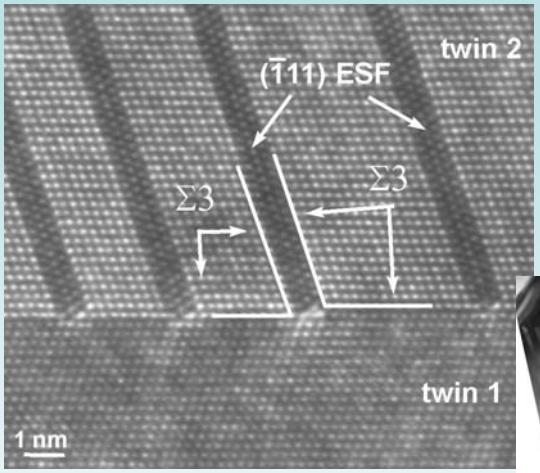

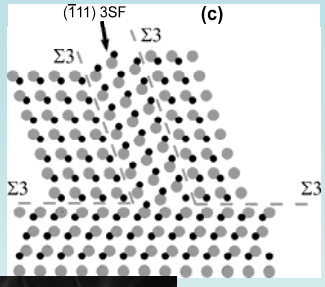

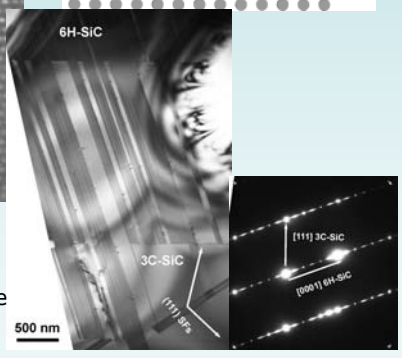

- (0001)6H-SiC II (-111) 3C-SiC
- 6H-SiC inclusions reach the surface
- And since we have (111)3C||(1-102)6H orientation there are meany regions where the hexagonal symmetry of the (111) surface is destroyed.

Reduction of the SF density in 3C

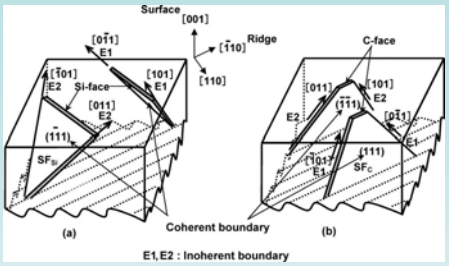

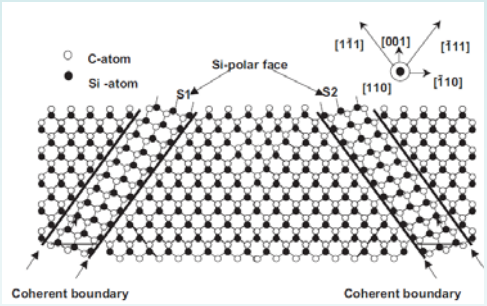

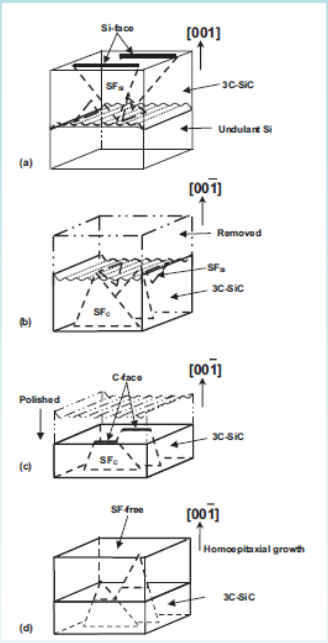

H. Nagasawa et al Chem. Vap. Deposition **2006**, *12*, 502–508

6H-SiC – Schockley SFs

SF(4,2)

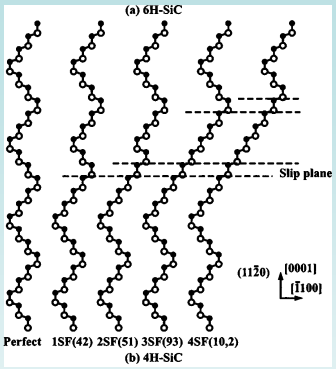

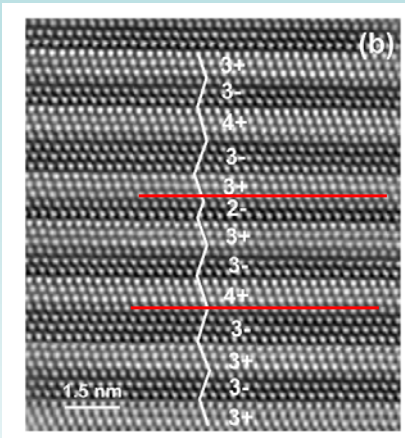

Polytype	SF (initial)→SF (final)	Supercell	ANNNI
6*H*-SiC	γ_1 [perfect→1SF(42)]	3.6	3.1
	γ_2 [1SF(42)→2SF(51)]	21.0	21.4
	γ_3 [2SF(51)→3SF(93)]	6.4	6.3
	γ_4 [3SF(93)→4SF(10,2)]	3.8	3.1

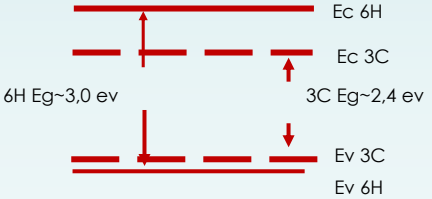

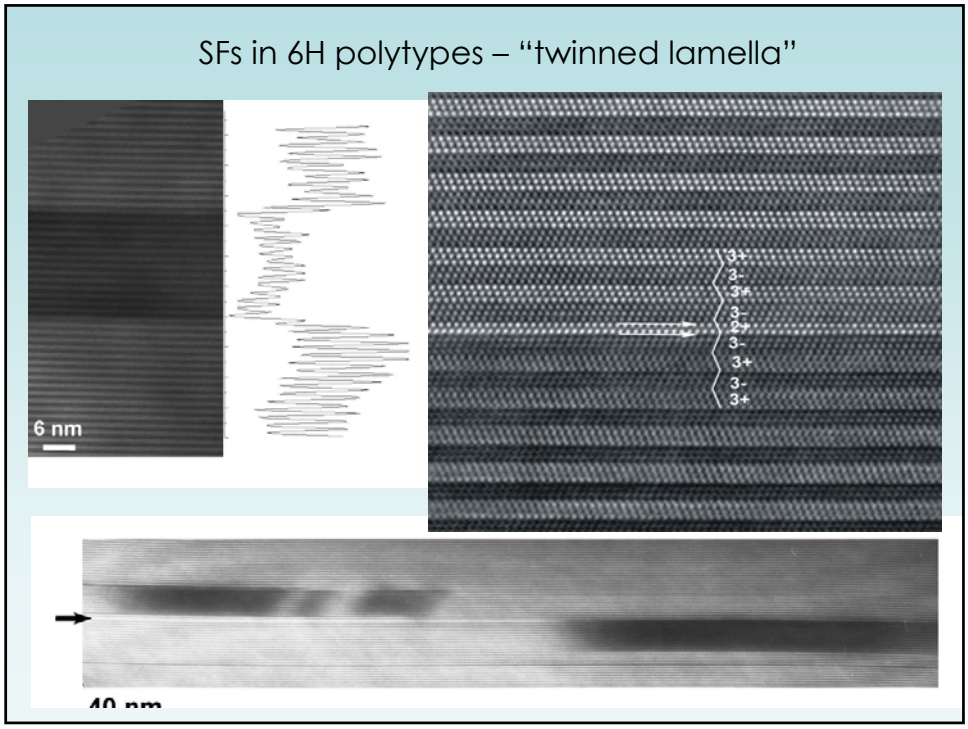

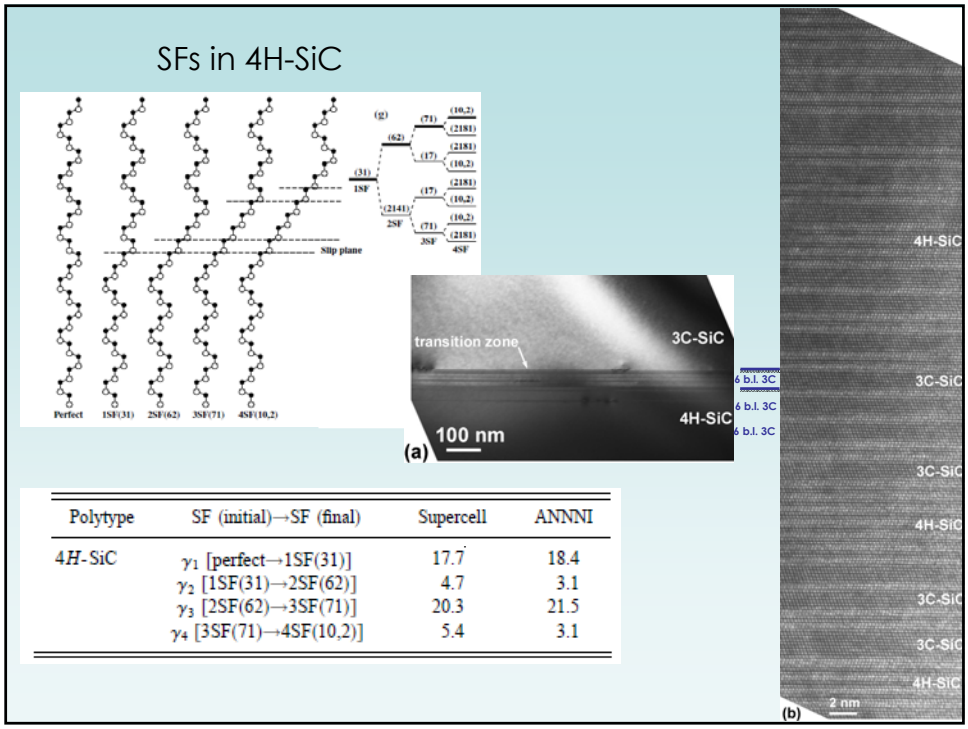

Polytype	SF (initial)→SF (final)	Supercell	ANNNI
4*H*-SiC	γ_1 [perfect→1SF(31)]	17.7	18.4
	γ_2 [1SF(31)→2SF(62)]	4.7	3.1
	γ_3 [2SF(62)→3SF(71)]	20.3	21.5
	γ_4 [3SF(71)→4SF(10,2)]	5.4	3.1

SFs in the 4H

4H-SiC – Schockley SFs

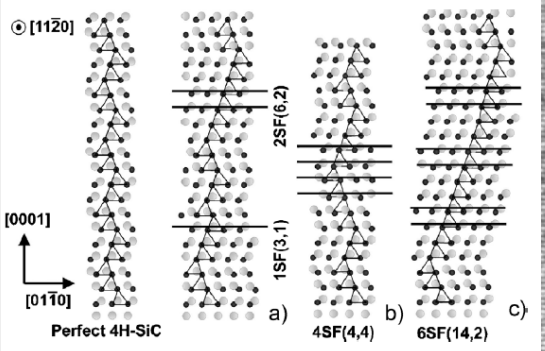

4 SF(4,4)

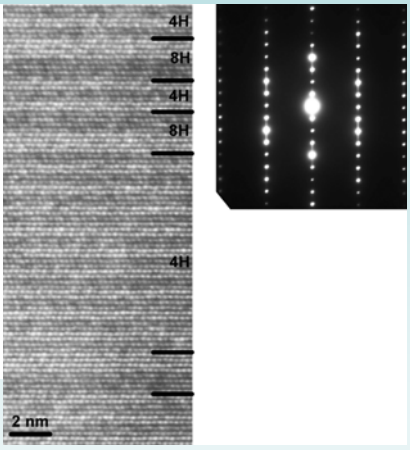

4H-SiC – Schockley SFs – increased SF density – more complex structures

8 SF(4,6,4,2)

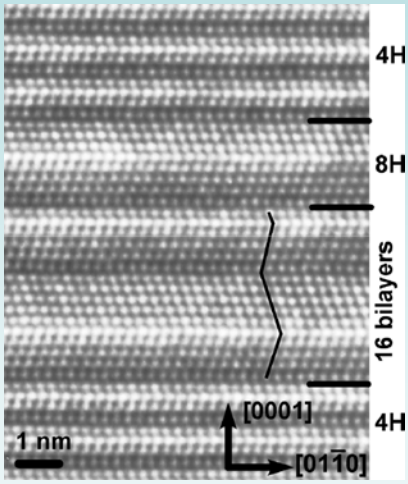

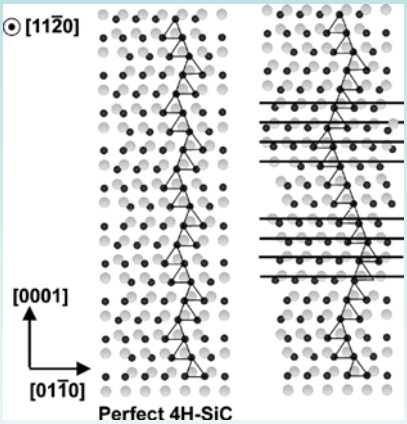

4H-SiC – Schockley SFs – incommensurate modulated structures:

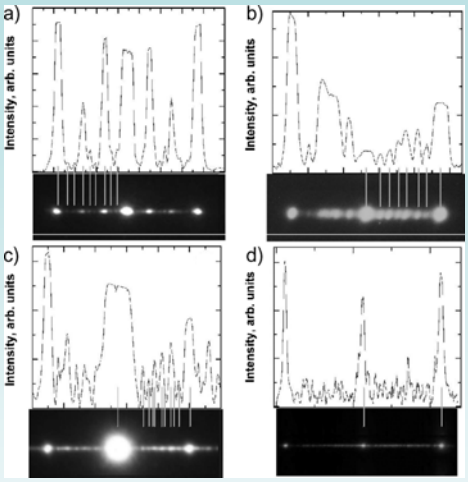

Incommensurate structure of 36 bilayers a): 1x8H+1x4H

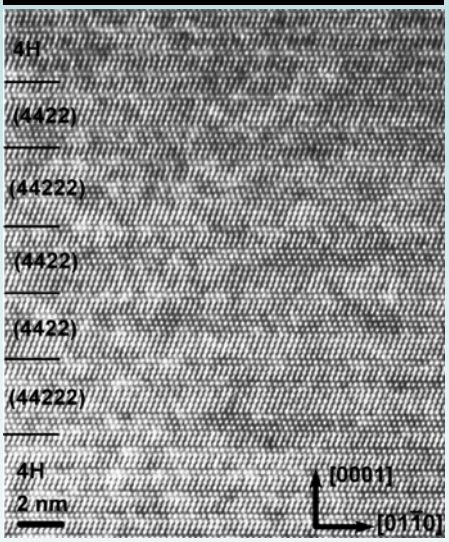

4H-SiC – Schockley SFs – incommensurate modulated structures:

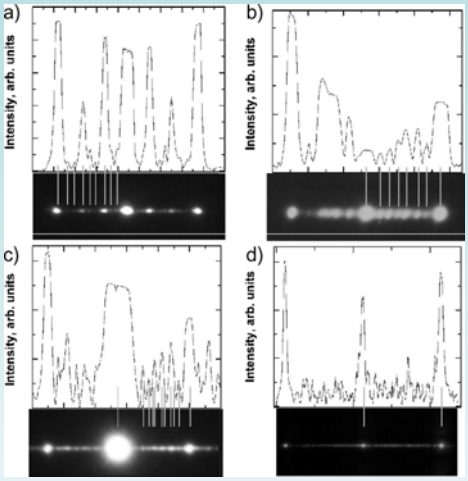

Incommensurate structure of 28 bilayers b): 1x8H+<5>x4H

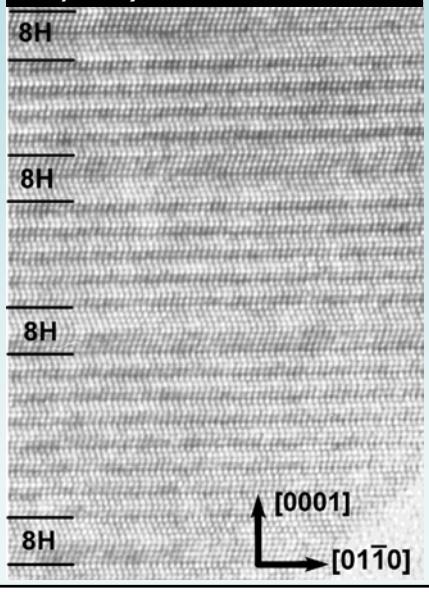

4H-SiC – Schockley SFs – incommensurate modulated structures:

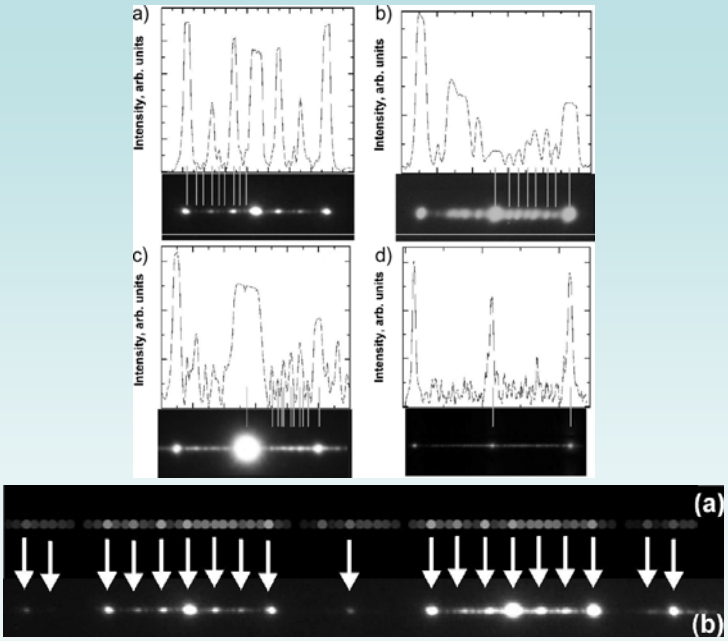

4H-SiC – Schockley SFs – incommensurate modulated structures:

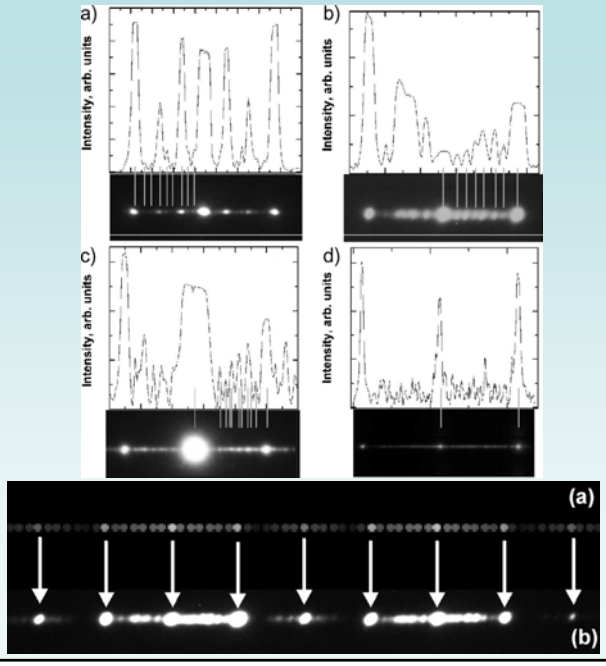

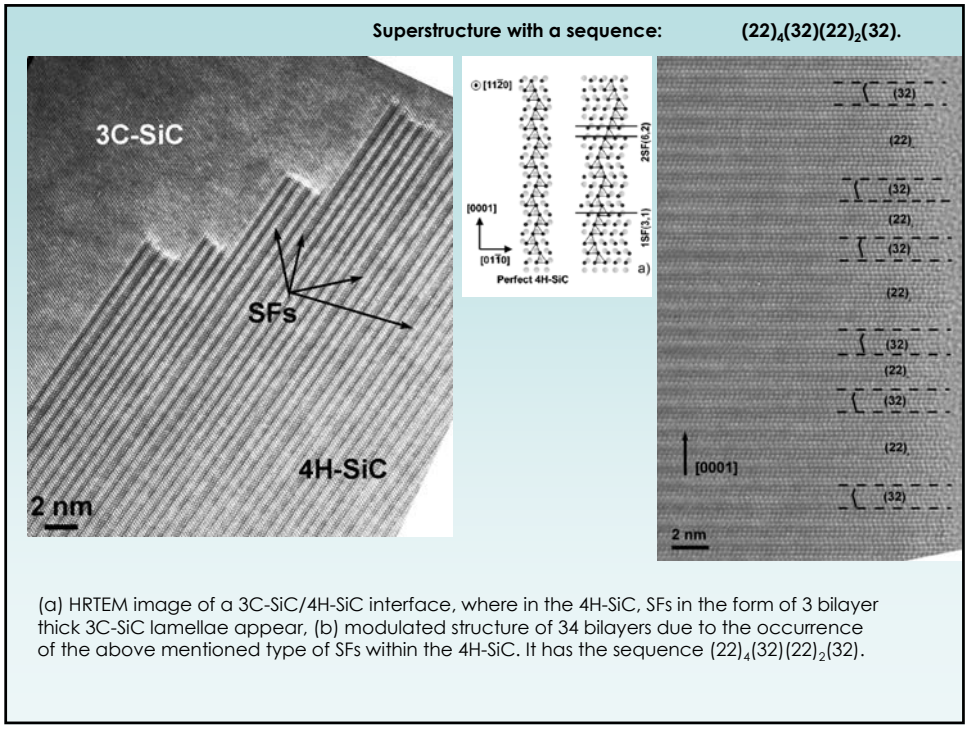

(a) HRTEM image of a 3C-SiC/4H-SiC interface, where in the 4H-SiC, SFs in the form of 3 bilayer thick 3C-SiC lamellae appear, (b) modulated structure of 34 bilayers due to the occurrence of the above mentioned type of SFs within the 4H-SiC. It has the sequence $(22)_4(32)(22)_2(32)$.

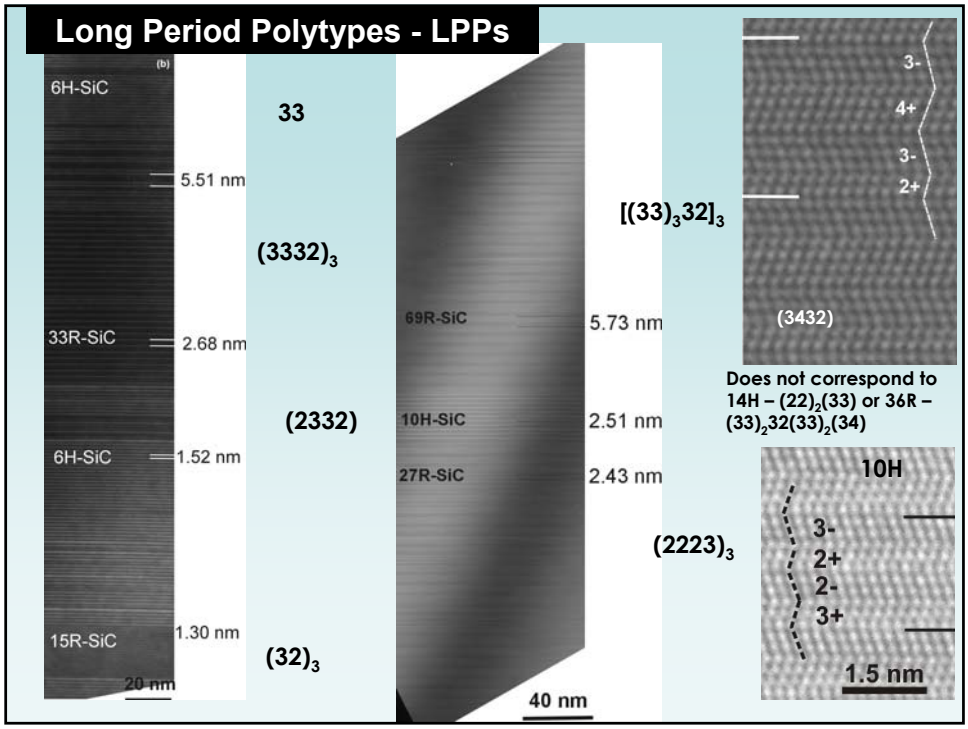

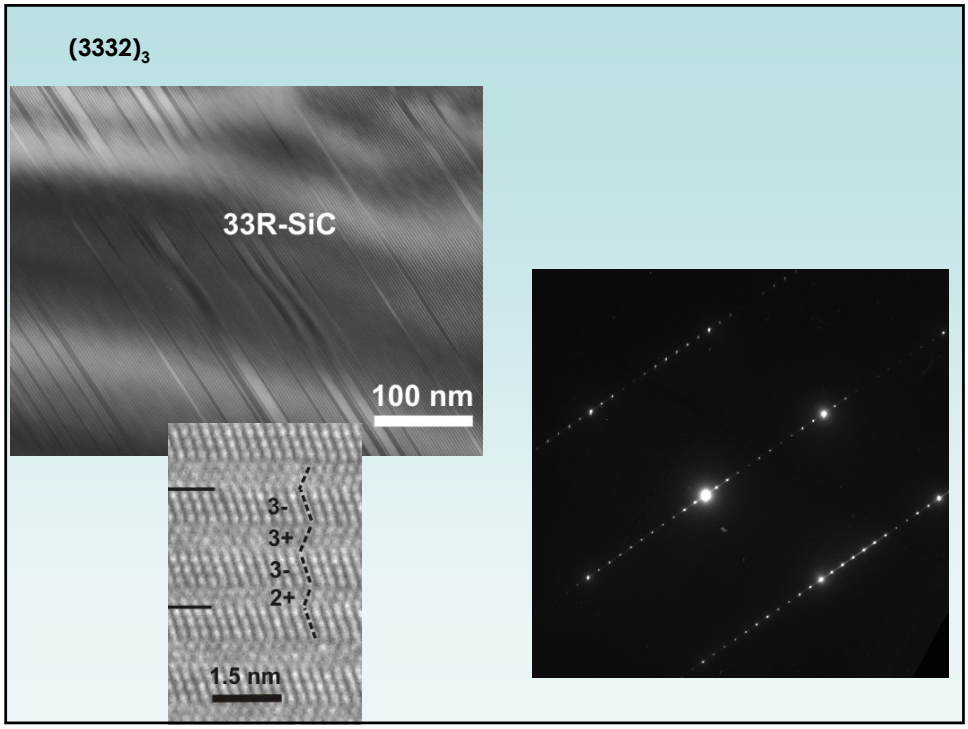
$(3332)_3$
33R-SiC
100 nm
3-
3+
3-
2+
1.5 nm

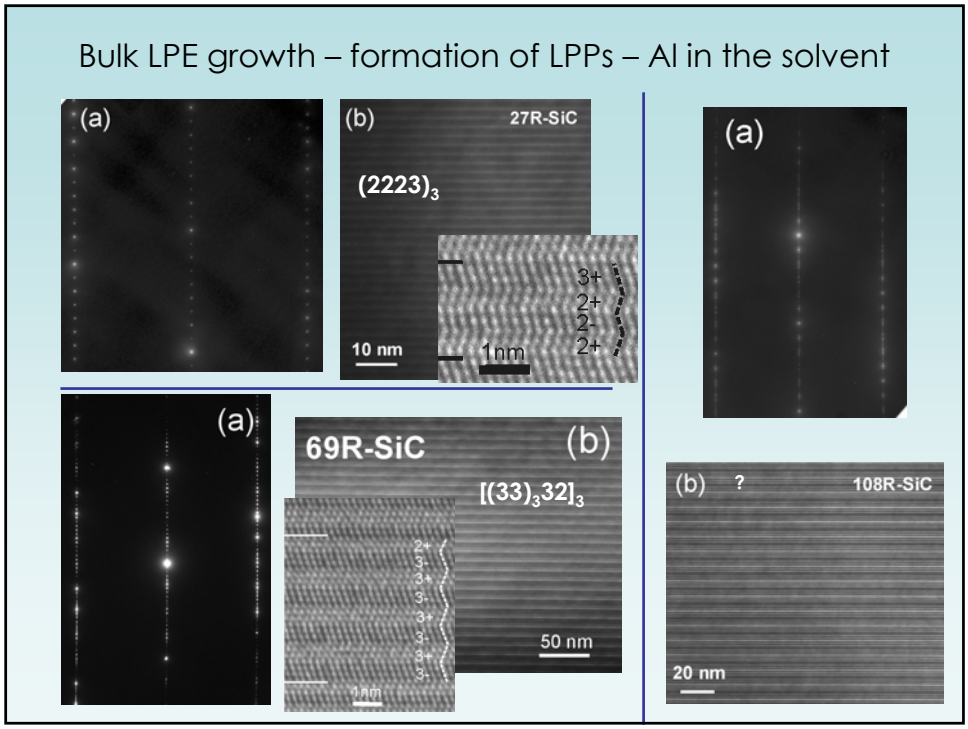
Bulk LPE growth – formation of LPPs – Al in the solvent
(a)
(b)
27R-SiC
$(2223)_3$
10 nm
1nm
3+
2+
2-
2+
(a)
(a)
69R-SiC
(b)
$[(33)_3 32]_3$
50 nm
(b) ?
108R-SiC
20 nm

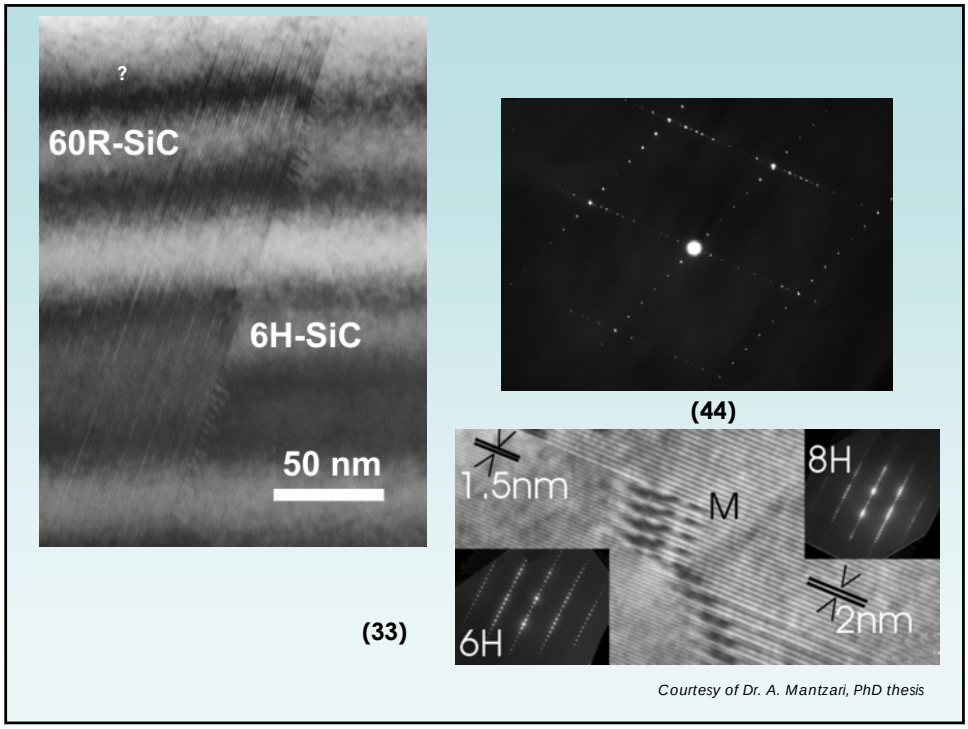
?
60R-SiC
6H-SiC
50 nm
(44)
1.5nm
M
8H
2nm
6H
(33)
Courtesy of Dr. A. Mantzari, PhD thesis

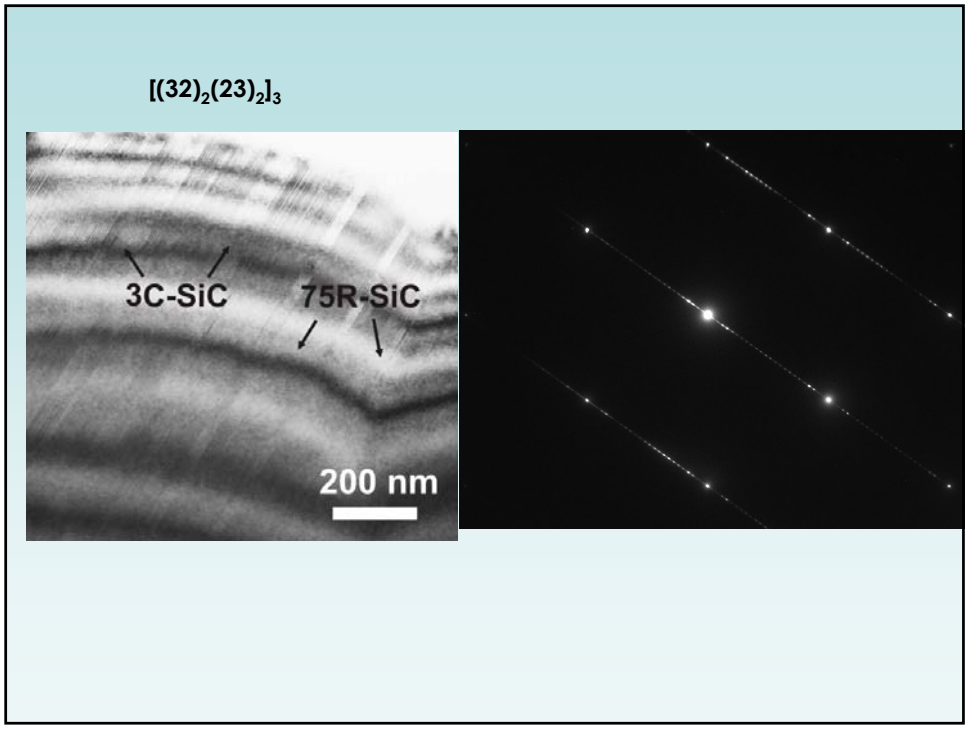
$[(32)_2(23)_2]_3$
3C-SiC
75R-SiC
200 nm

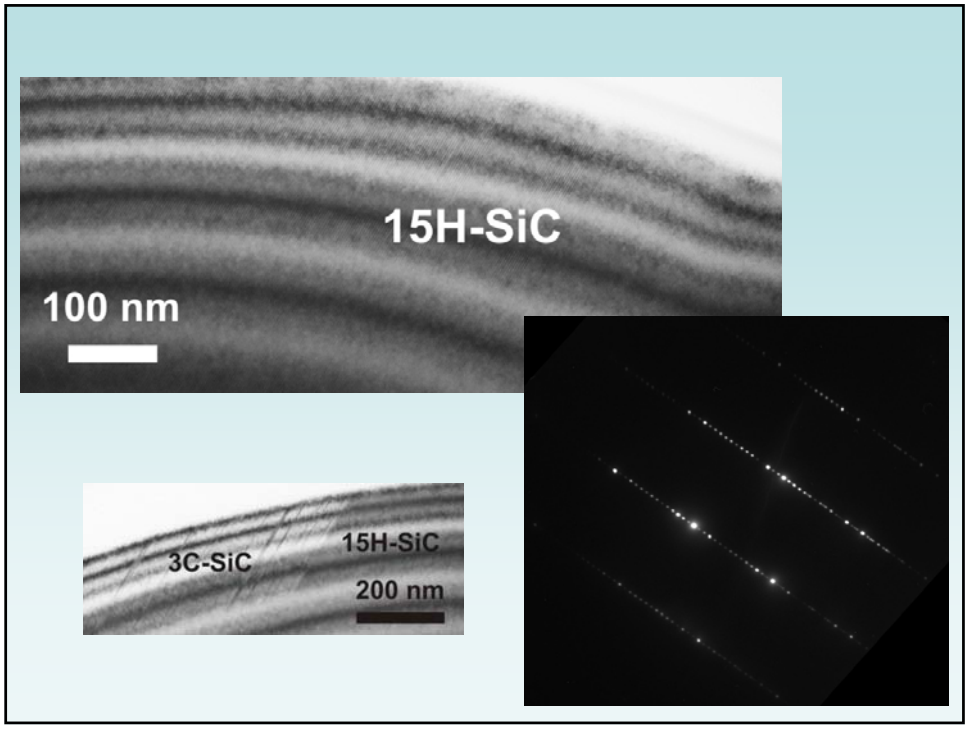
15H-SiC
100 nm
3C-SiC
15H-SiC
200 nm

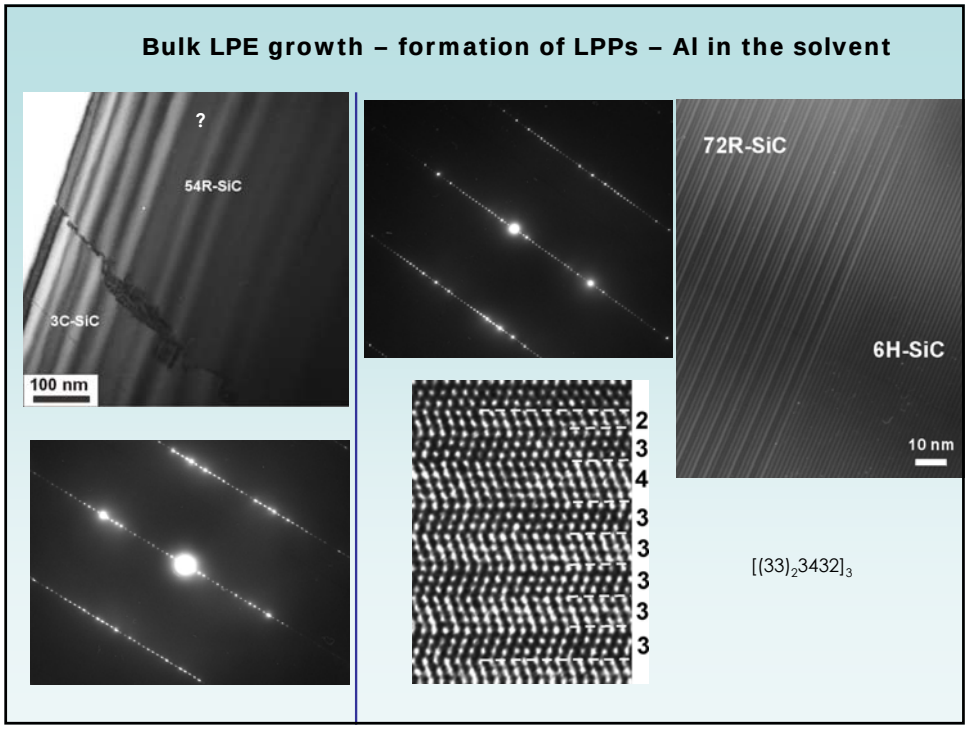
Bulk LPE growth – formation of LPPs – Al in the solvent
?
54R-SiC
3C-SiC
100 nm
72R-SiC
6H-SiC
10 nm
2
3
4
3
3
3
3
3
[(33)23432]3

Formation of long period polytypes (LPPs)

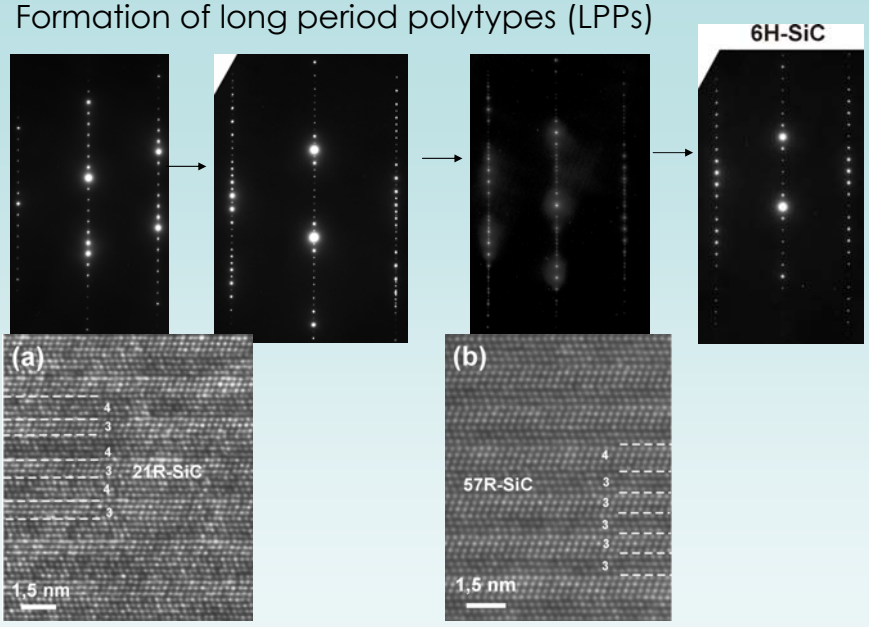

21R-SiC $(34)_3$ → 39R-SiC $(3334)_3$ → 57R-SiC $[(33)_2(34)]_3$ → 6H-SiC (33)

Bulk LPE growth – formation of LPPs

The VLS seed

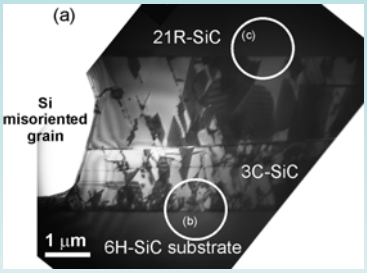

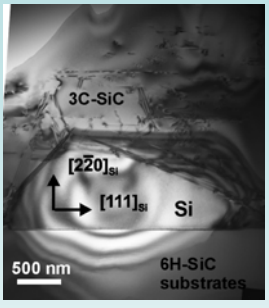

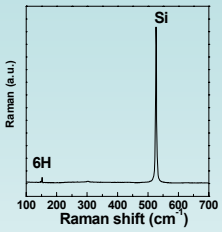

(i) along the **growth direction**, i.e. [111]3C-SiC | | [2-20]Si the mismatch is **ε=+34.25 %;**
(ii) and **in the (111) plane**: along [2-20]3C-SiC | | [111]Si the mismatch is **ε=+1.38 %;**
along the perpendicular [11-2]3C-SiC | | [11-2]Si it is **ε=+19.60%.**

The Si inclusions are formed during initial dissolution step of the LPE process
They induce heterogeneously distributed strain within the layers

Inversion Domain Boundaries (IDBs) – usually formed when one grows a polar material on a non polar substrate like 3C-SiC/Si

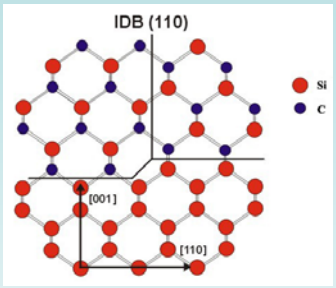

Geometrical consideration for formation of an (110) IDB when there is a step at the surface of the substrate with a height of $a_{Si}/4[001]$

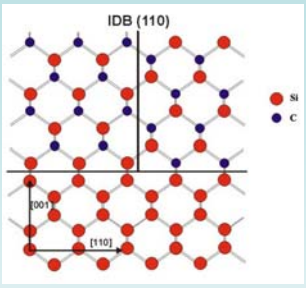

Geometrical consideration for formation of an (110) IDB when two nuclei are in contact, one of which has Si atoms in the first layer and the other C atoms

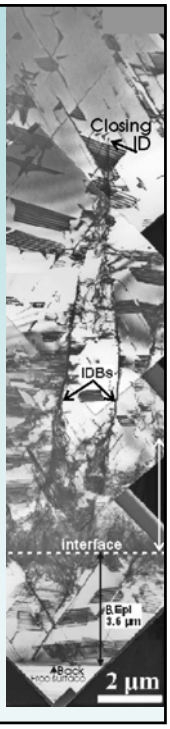

A. Mantzari, C.B. Lioutas and E.K. Polychroniadis: Materials Science Forum Vols. 600-603 (2009) pp. 67-70

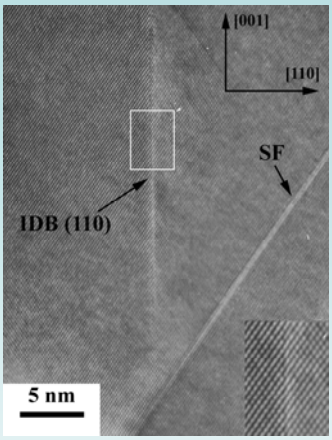

HRTEM micrograph of an area with an (110) IDB and a SF. A magnified image of the IDB area is inserted as inset. It is clear that the appearance of the IDB produces only a slight modification on the contrast.

Structural model for the (110) IDB where the number of Si-Si bonds is equal to the number of C-C bonds across the interface.

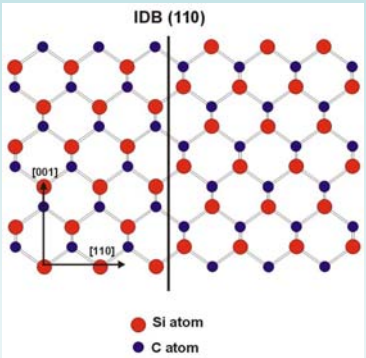

A. Mantzari, C.B. Lioutas and E.K. Polychroniadis: Materials Science Forum Vols. 600-603 (2009) pp. 67-70

Common in-grown defects in 3C-SiC III

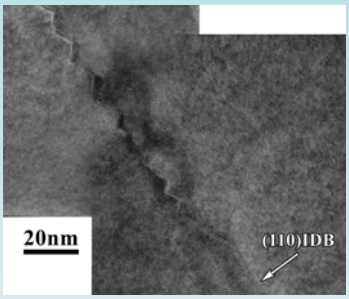

HRTEM micrograph where it is obvious that the initial (110) IDB alternatively lies on {111} planes which results in a zig-zag propagation

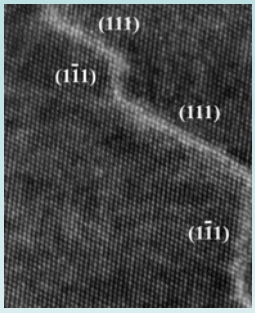

HRTEM high magnification image of a thinner area of the specimen

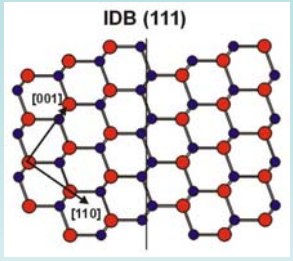

A structural model for the (111) IDB where only C-C bonds are present across the interface

A simulated image based on the above model which is calculated for a thickness of 8.32 nm and a defocus value of -43.4 nm. It is obvious that it represents in very good approximation the packing sequence and the contrast modification of the experimental image.

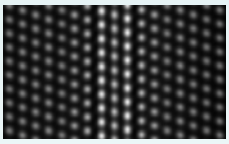

A. Mantzari, C.B. Lioutas and E.K. Polychroniadis: Materials Science Forum Vols. 600-603 (2009) pp. 67-70

Low angle boundaries (LABs)

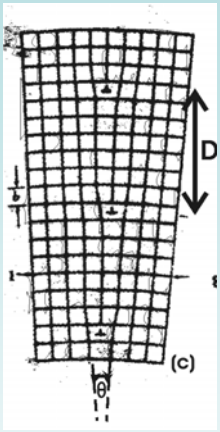

□=b/D

δ~2,5 □

□= □ /δ

□ – angle measured from the Moiré patterns

δ - mismatch between the lattices

Courtesy of Dr. A. Andreadou, PhD thesis

Common in-grown defects in 3C-SiC: Twins or Double Positioning Boundaries (DPBs)

VLS growth in $Si_{50}Ge_{50}$ melt on 6H-SiC substrates

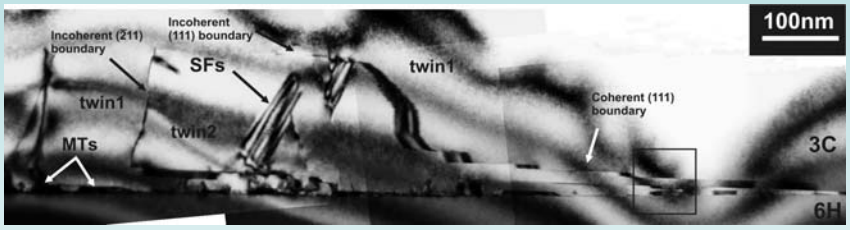

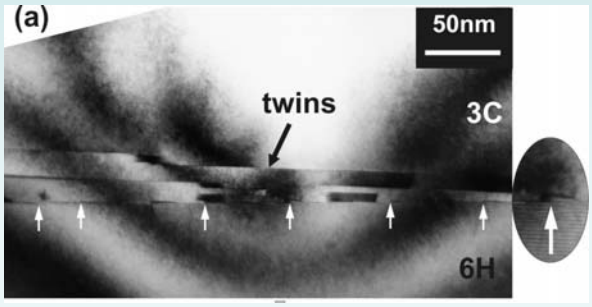

Common in-grown defects in 3C-SiC: Twins or Double Positioning Boundaries (DPBs) Twin

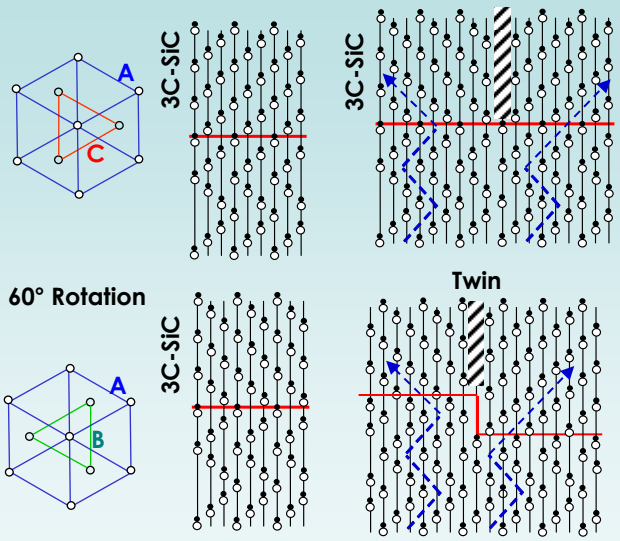

Courtesy of Dr. G. Ferro,

Common in-grown defects in 3C-SiC: Twins or Double Positioning Boundaries (DPBs) Twin

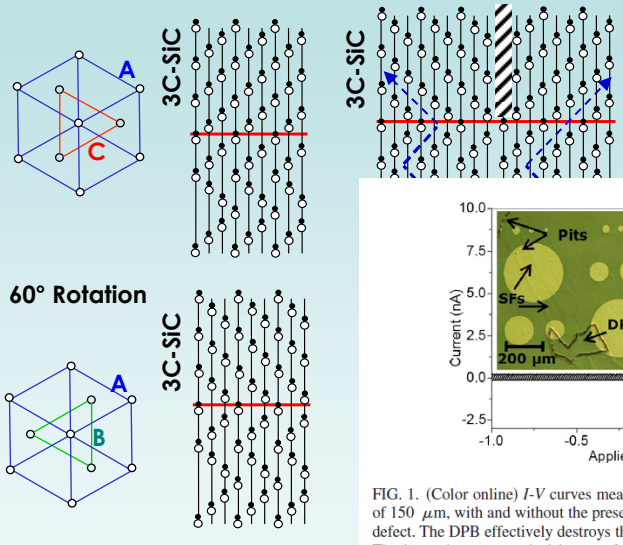

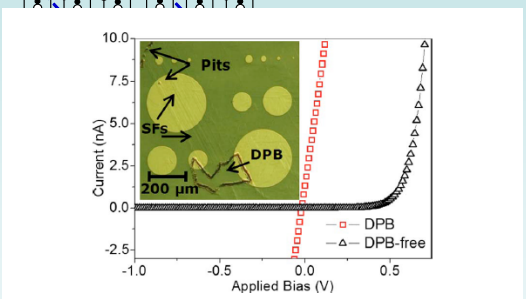

FIG. 1. (Color online) *I-V* curves measured on diodes with a contact radius of 150 μm, with and without the presence of a double positioning boundary defect. The DPB effectively destroys the rectifying properties of the contact. The inset shows an optical image of the surface of the 3*C*-SiC, with patterned Au contacts. The visible defects include DPBs, SFs, and triangular pits.

Courtesy of Dr. G. Ferro,

Table 1. [011] Coincidence Site Lattices up to $\Sigma=107$.

Σ	θ (°)	First Diffraction Twin Plane	Second Diffraction Twin Planes
3	70.529	{1̄ 1̄ 1}	{2 1̄ 1}
9	38.942	{1̄ 2 2}	{4 1̄ 1}
11	50.479	{2̄ 3̄ 3}	{3 1̄ 1}
17	86.628	{4 3̄ 3}	{3 2̄ 2}
19	26.525	{1̄ 3̄ 3}	{6 1̄ 1}
27	31.586	{2̄ 5̄ 5}	{5 1̄ 1}
33a	20.050	{1̄ 4̄ 4}	{8 1̄ 1}
33b	58.992	{4̄ 5̄ 5}	{5 2̄ 2}
41	55.877	{3̄ 4̄ 4}	{8 3̄ 3}
43	80.631	{6̄ 5̄ 5}	{5 3̄ 3}
51a	16.099	{1̄ 5̄ 5}	{10 1̄ 1}
51b	22.844	{2̄ 7̄ 7}	{7 1̄ 1}
57	82.946	{5̄ 4̄ 4}	{8 5̄ 5}
59	45.980	{3̄ 5̄ 5}	{10 3̄ 3}
67	62.439	{6̄ 7̄ 7}	{7 3̄ 3}
73	13.443	{1̄ 6̄ 6}	{12 1̄ 1}
81a	38.942	{1̄ 2̄ 2}	{4 1̄ 1}
81b	77.885	{8̄ 7̄ 7}	{7 4̄ 4}
83	17.860	{2̄ 9̄ 9}	{9 1̄ 1}
89	34.893	{4̄ 9̄ 9}	{9 2̄ 2}
97	61.018	{5̄ 6̄ 6}	{12 5̄ 5}
99a	11.536	{1̄ 7̄ 7}	{14 1̄ 1}
99b	89.421	{7̄ 5̄ 5}	{10 7̄ 7}
107	33.718	{3̄ 7̄ 7}	{14 3̄ 3}

Twins and coincidence site lattice notation

- High angle boundaries which have special values of contact plains and rotation angles:
- Σ- is the inverse of the fraction of the number of common lattice site between the two grains

Common in-grown defects in 3C-SiC: Propagation of twins boundaries

Three types of twin configurations

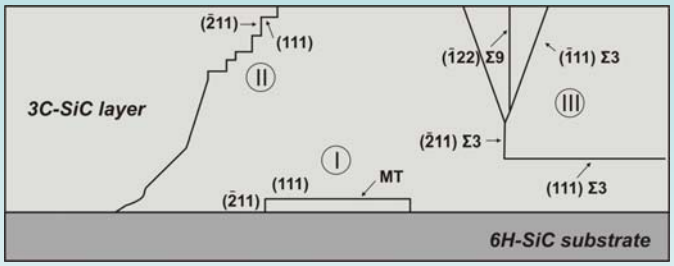

I) and II) appear in VLS layers mainly

III) appears in layers grown by vapour phase methods

I) Formation of microtwins in the vicinity of the interface
II) A step-like interface occurs with facets along the {111} and the (-211) planes:
III) Formation of a fourfold twin

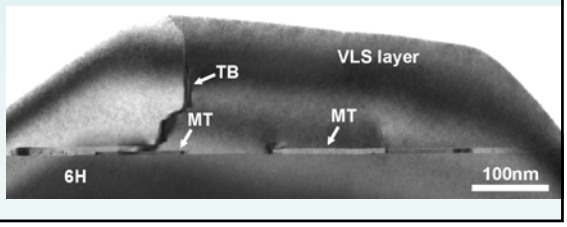

Common in-grown defects in 3C-SiC: Propagation of twins boundaries

Three types of twin configurations

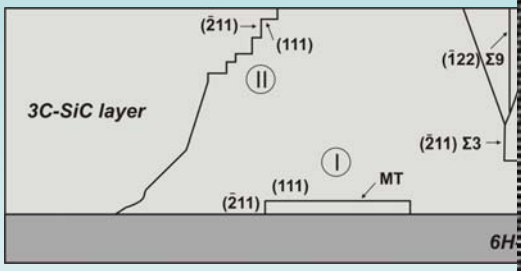

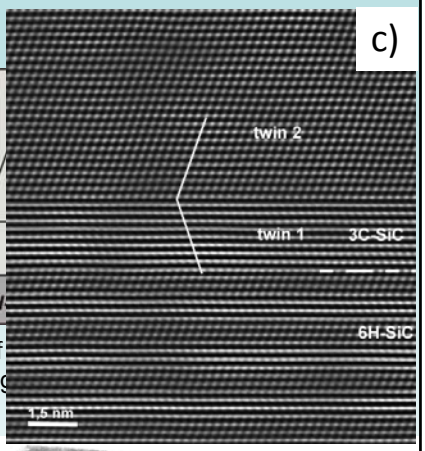

I) Formation of microtwins in the vicinity of
II) A step-like interface occurs with facets along
the (-211) planes:
III) Formation of a fourfold twin

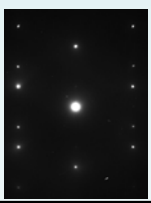

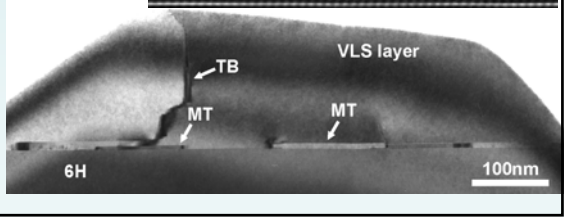

Common in-grown defects in 3C-SiC: Propagation of twins boundaries: **case II) step like propagation**

Annihilation of twin boundaries and formation of twinned islands

VLS growth

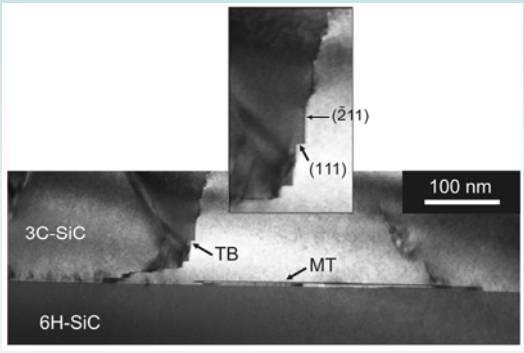

CVD growth

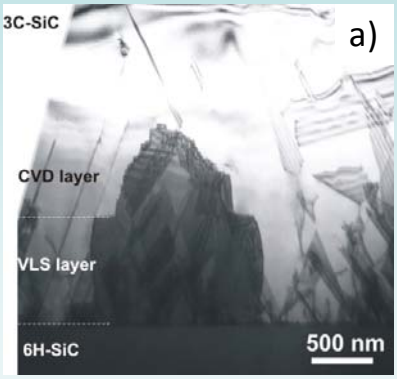

Step like propagation

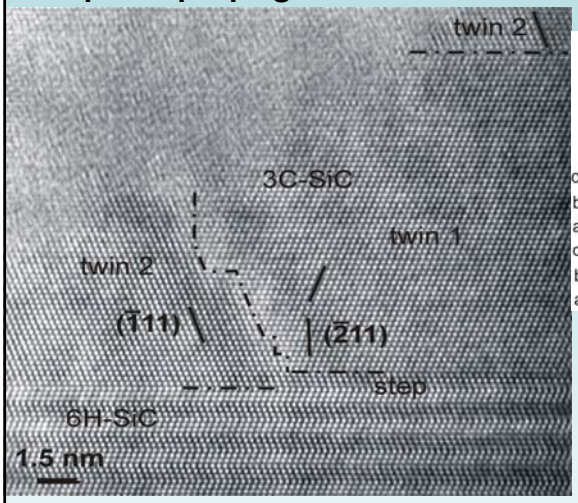

CSL model

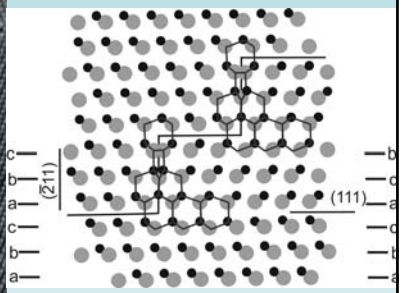

3C-6H transformation

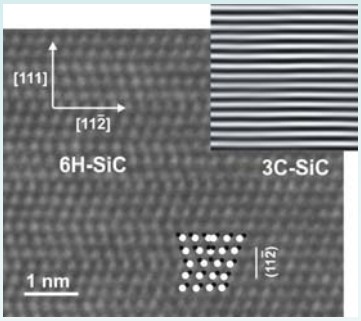

The CSL model: - no displacement (rigid body translation), but dangling and wrong bond – unstable and thus pinned to (111) interfaces.

Formation of fourfold twins (case III):

During CVD and SE growth processes

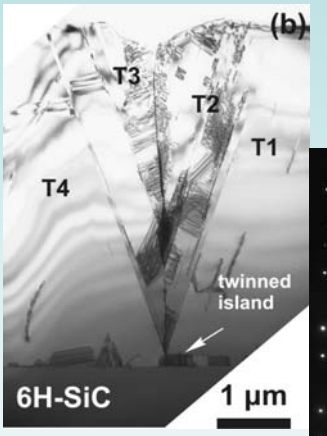

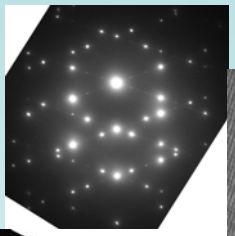

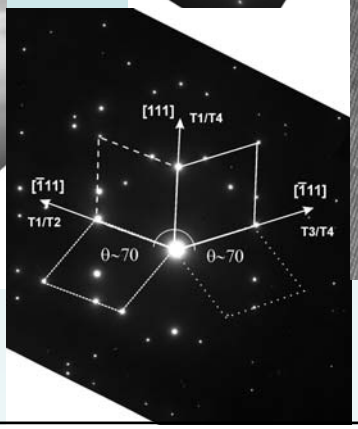

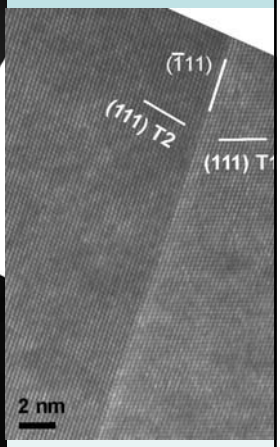

Formation of fourfold twins (case III) on 6H:

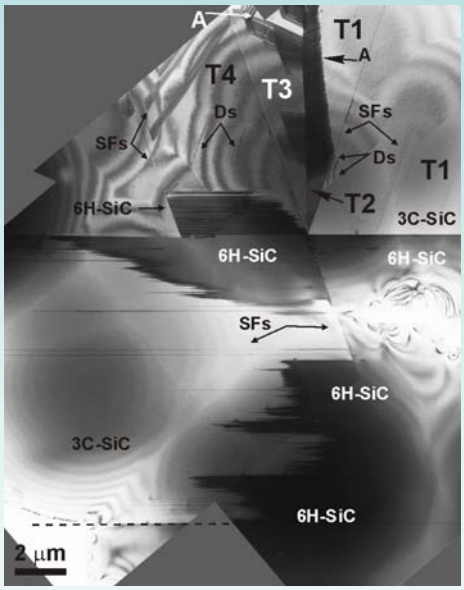

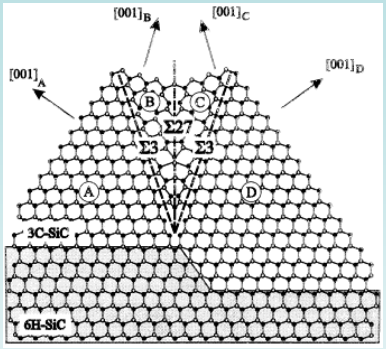

V. Papaioannou et. al., Journal of Crystal Growth 194 (1998) 342-352

The fourfold twin complex

This twin complex is strongly dependent on the growth conditions:

- Its density increases when high C/Si ratios;
- low growth temperature.

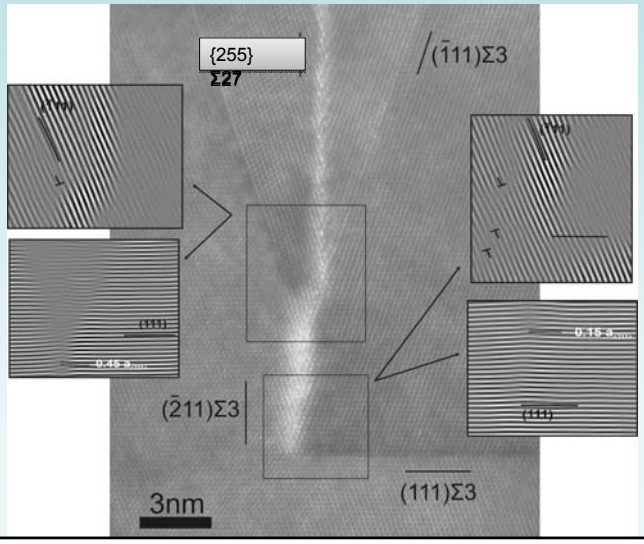

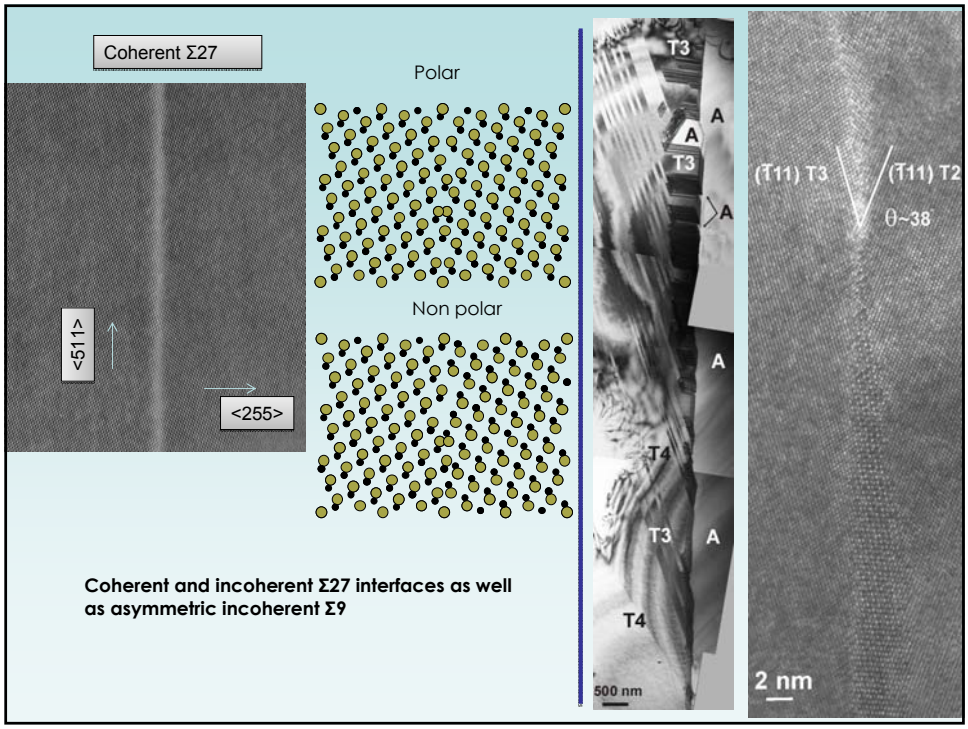

Vapour-Liquid-Solid (VLS) mechanism

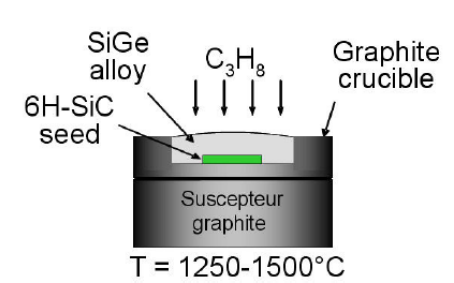

- **VLS is essentially a LPE process**
- **In classical LPE the C is supplied by the graphite container;**
- **In VLS the growth proceeds by reaction of C containing gaseous phase with a Si-Metal liquid**
- **The metal can be Sn, Ge (isoelectric) or Al, In, Ga for p type doping**

VLS layers – incorporation of the metal

Clustering of **Ge** atomes has not been observed for lower **Ge concentrations**

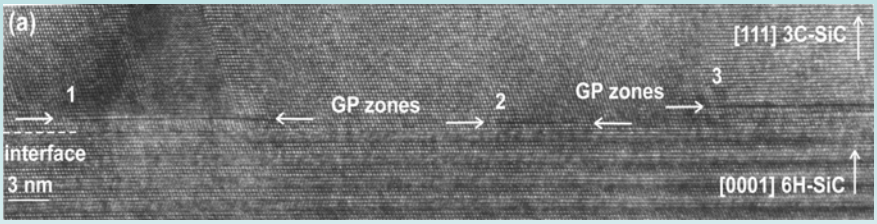

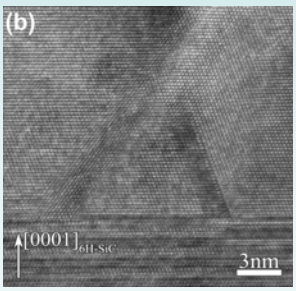

Planar defect along the four {111} planes without changing the stacking sequence

Marinova *at al* MSF 2008

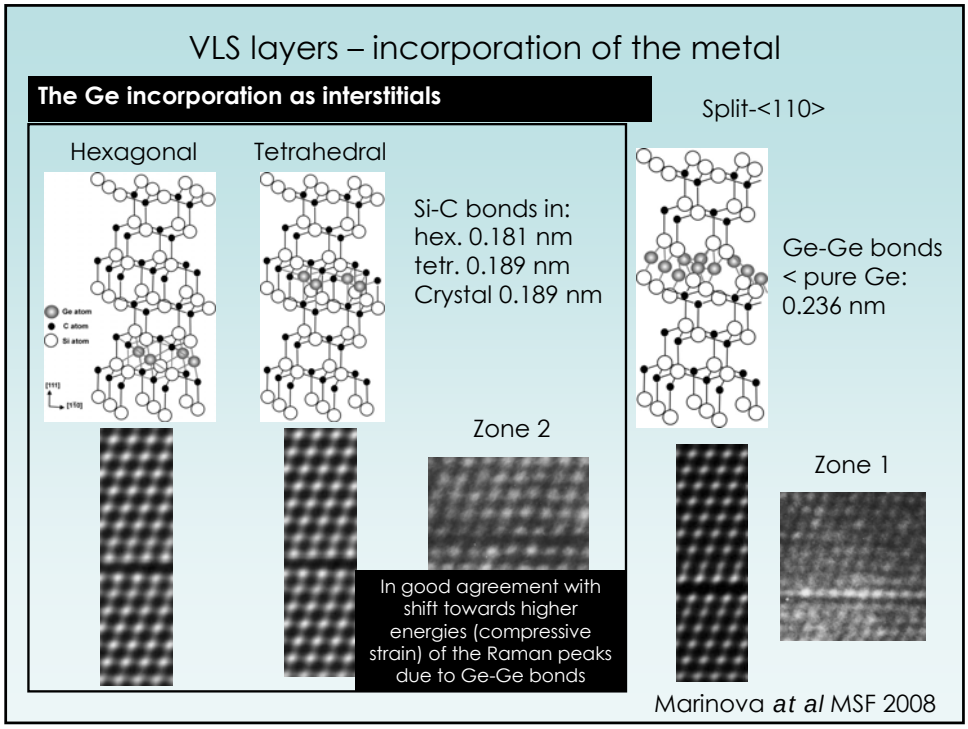
VLS layers – incorporation of the metal
The Ge incorporation as interstitials
Hexagonal
Tetrahedral
Si-C bonds in:
hex. 0.181 nm
tetr. 0.189 nm
Crystal 0.189 nm
Split-<110>
Ge-Ge bonds
< pure Ge:
0.236 nm
Zone 2
Zone 1
In good agreement with shift towards higher energies (compressive strain) of the Raman peaks due to Ge-Ge bonds
Marinova at al MSF 2008

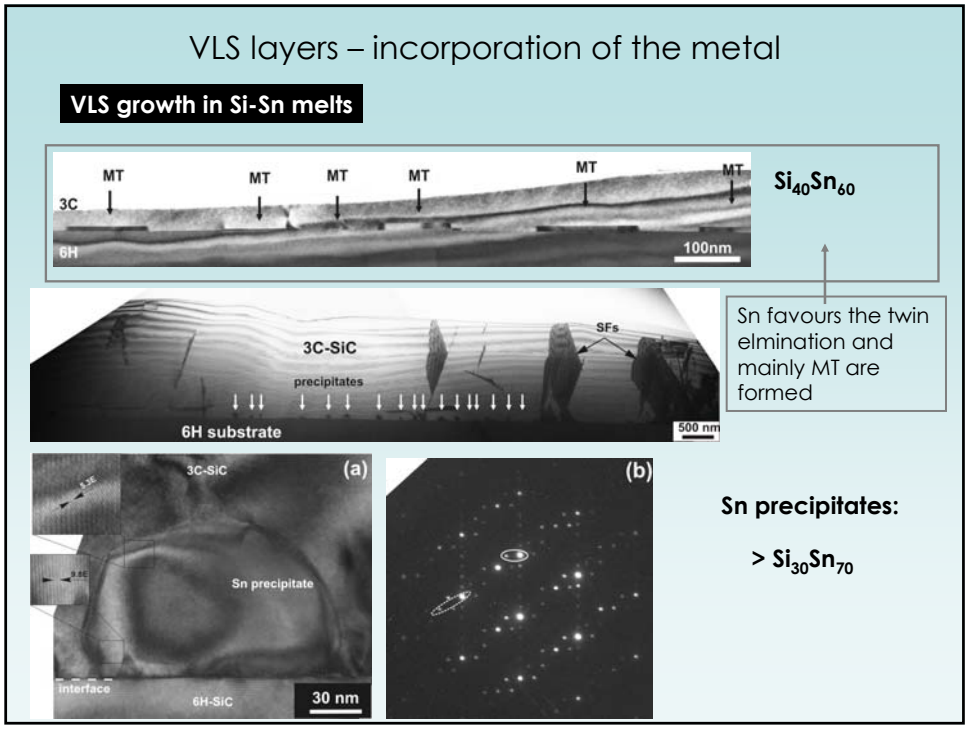
VLS layers – incorporation of the metal
VLS growth in Si-Sn melts
MT
3C
6H
100nm
Si40Sn60
Sn favours the twin elmination and mainly MT are formed
3C-SiC
SFs
precipitates
6H substrate
500 nm
(a)
Sn precipitate
interface
6H-SiC
30 nm
(b)
Sn precipitates:
> Si30Sn70

VLS layers – incorporation of the metal

Growth in Si-Ga melts for p-type doping

Ga –particles: the lowest Si-Ga melt composition

$Si_{50}Ga_{50}$ T=1300 °C

4H-SiC

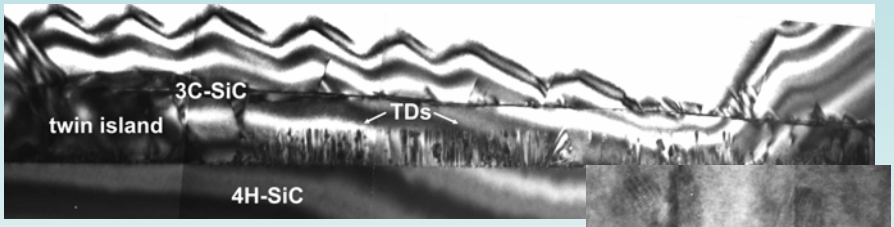

EDX spectra

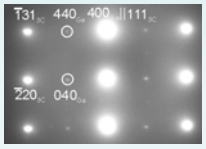

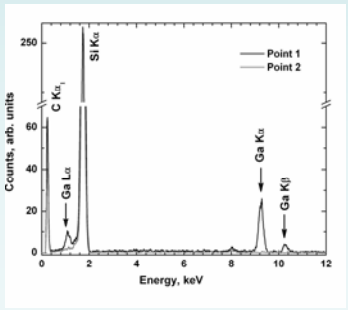

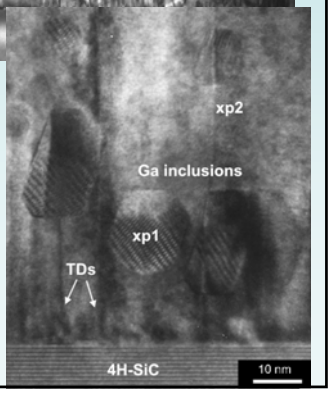

VLS layers – incorporation of the metal

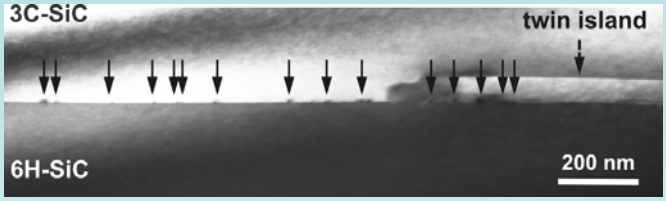

$Si_{50}Ga_{50}$ T=1300 °C

6H-SiC

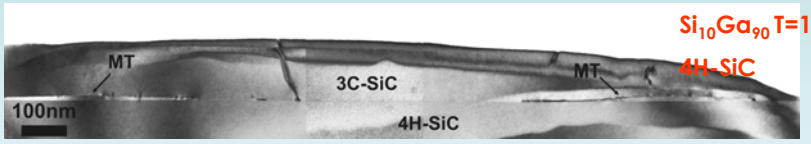

$Si_{10}Ga_{90}$ T=1050 °C

4H-SiC

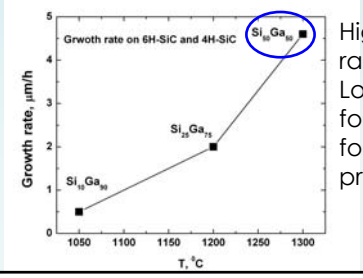

Highest growth rate for $Si_{50}Ga_{50}$

Low solubility of Ga for this melt => formation of precipitates

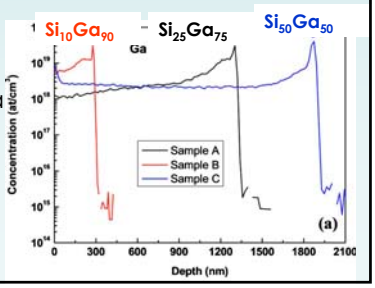

VLS layers – incorporation of the metal

SFs in the 3C-SiC layers grown in Ga melts on 6H-SiC substrates

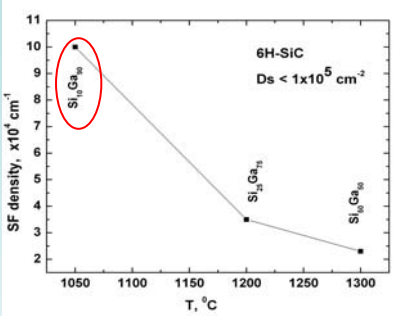

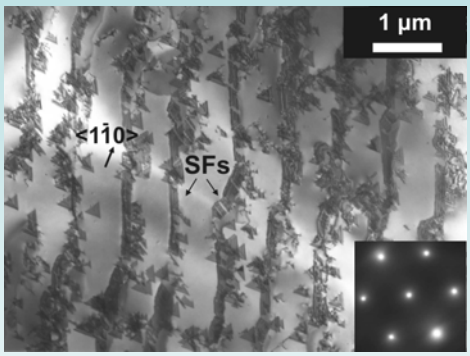

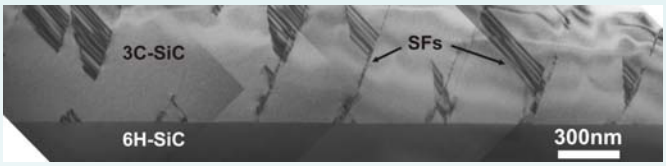

High density and periodical arrangement of SFs in $Si_{10}Ga_{90}$

VLS layers – incorporation of the metal

SFs and Ds in the 3C-SiC layers grown in Ga melts on 4H-SiC seeds

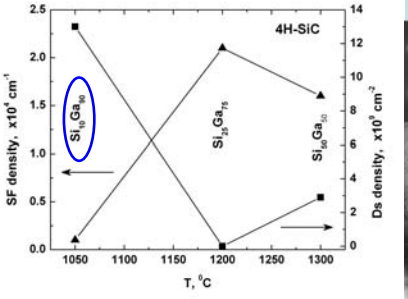

Low density of SFs is accompanied with enhanced Ds density. Periodical bands of dislocations

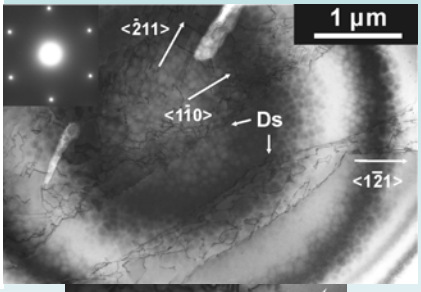

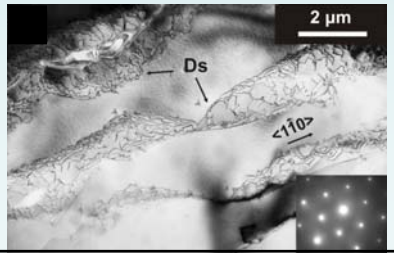

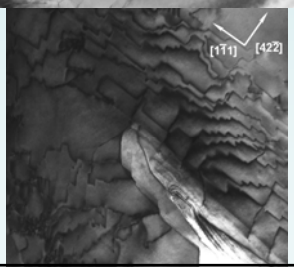

Summary

1. SFs and twin boundaries are the main defects in 3C-SiC and control over their introduction is very difficult during the growth process (except for the triangular defects).
2. The incorporation of impurities and dopants strongly affects the structural quality within the layers;
3. Formation of many different polytypes is possible during LPE.

Acknowledgements

MANSiC project (MRTN-CT-2006-035735) financially supported from the EU wit FP

Dr. A. Mantzari, Dr. A. Andreadou, Prof. E.K.Polychroniadis, Prof. Ch. Lioutas, Prof. N. Frangis (AUTH)

Dr. G. Ferro UCBL Lyon
Dr. D. Chaussende INPG Grenoble
Dr. R. Yakimova LiU Linkoping
Prof. Jean Camassel , Dr. Sandrine Juillaguet (UM2)

Irina, Frederic, Remis, Milena, Teddy, Nikoletta, Jean, Georgios, Lia (MANSiC colleagues)

Thank you for your attention!

SEM, basics and applications

Dr. Lori Nalbandian
Centre for Research and Technology Hellas

Summer School on Micro- and nano-structural characterization of materials, focused on electron microscopy, July 11-15, 2012, Thessaloniki, Greece

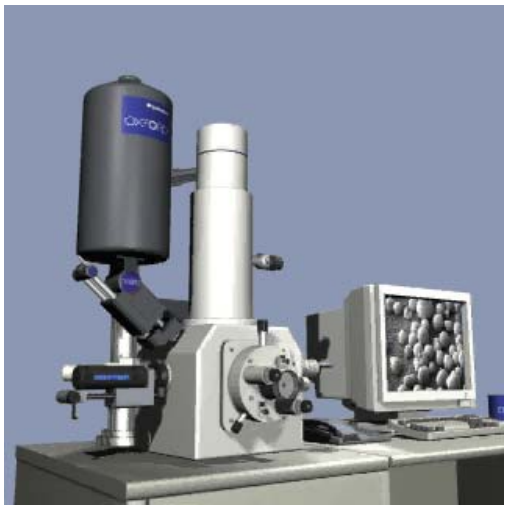

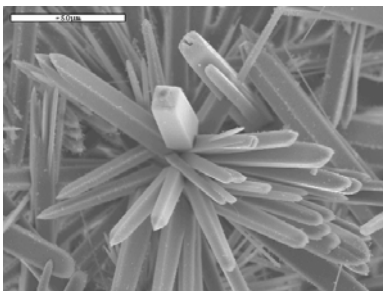

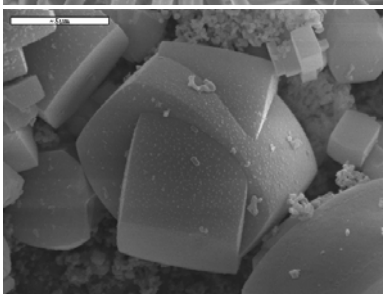

Summer School on Micro- and nano- structural characterization of materials, focused on electron microscopy, July 11-15, 2012, Thessaloniki, Greece

History

- It is not completely clear who first proposed the principle of scanning the surface of a specimen with a finely focused electron beam to produce an image.
- The first published description appeared in 1935 in a paper by the German physicist Max Knoll.
- Although another German physicist, Manfred von Ardenne, performed some experiments with what could be called a scanning electron microscope (SEM) in 1937.
- It was not until 1942 that three Americans, Zworykin, Hillier, and Snijder, first described a true SEM with a resolving power of 50 nm.
- The first commercial Scanning Electron Microscope (SEM) debuted around 1965.
- Its late development was due to the electronics involved in "scanning" the beam of electrons across the sample.
- Modern SEMs can have resolving power better than 1 nm.

Summer School on Micro- and nano- structural characterization of materials, focused on electron microscopy, July 11-15, 2012, Thessaloniki, Greece

Comparing Microscopes

Summer School on Micro- and nano- structural characterization of materials, focused on electron microscopy, July 11-15, 2012, Thessaloniki, Greece

Comparing Microscopes

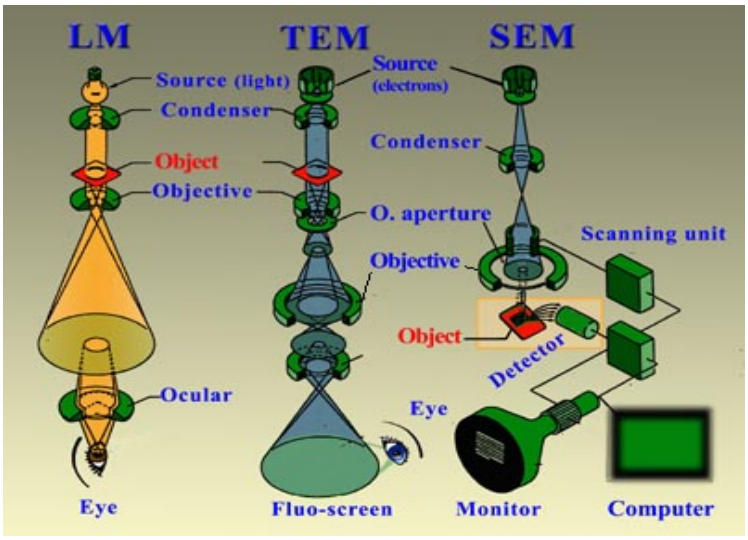

Summer School on Micro- and nano- structural characterization of materials, focused on electron microscopy, July 11-15, 2012, Thessaloniki, Greece

Comparing Microscopes: OM vs EM

	OPTICAL MICROSCOPE	ELECTRON MICROSCOPE
The source of illumination	The ambient light source is light for the microscope	Electrons are used to "see" – light is replaced by an electron gun built into the column
The lens type	Glass lenses	Electromagnetic lenses
Magnification method	Magnification is changed by moving the lens	Focal length is changed by changing the current through the lens coil
Viewing the sample	Eyepiece	Fluorescent screen or digital camera
Use of vacuum	No vacuum	Entire electron path from gun to camera must be under vacuum

Summer School on Micro- and nano- structural characterization of materials, focused on electron microscopy, July 11-15, 2012, Thessaloniki, Greece

Advantages of Using SEM over OM

	Magnification	Depth of Field	Resolution
OM	4x – 1400x	0.5mm	~ 0.2mm
SEM	10x – 500Kx	30mm	1.5nm

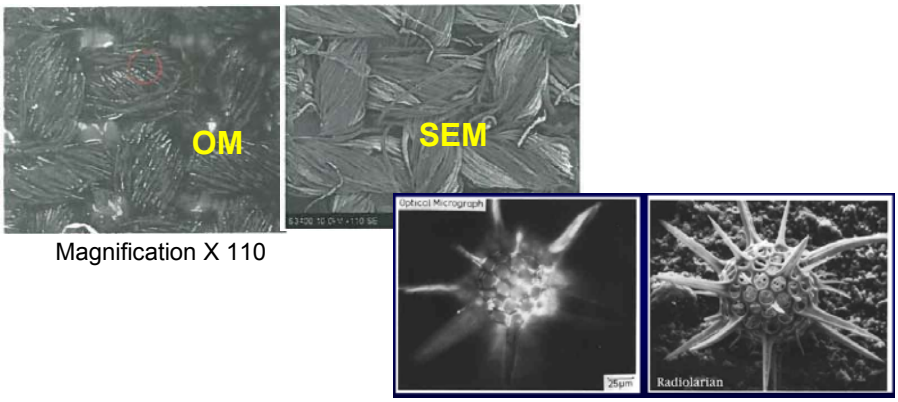

Magnification X 110

Summer School on Micro- and nano- structural characterization of materials, focused on electron microscopy, July 11-15, 2012, Thessaloniki, Greece

Depth of field is the height of a specimen that appears in focus in an image. More than 300 times the depth of field compared to the LM. This means that great topographical detail can be obtained. Specimen images with three dimensional (3D) appearance, can provide, even at low magnifications, much more information about a specimen than is available using the LM .

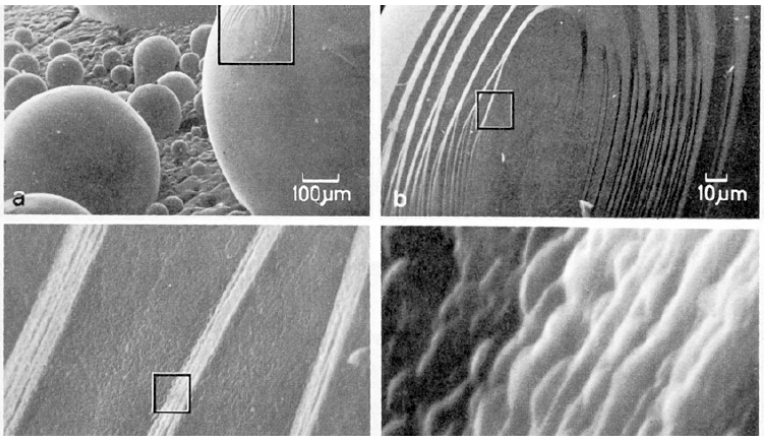

Summer School on Micro- and nano- structural characterization of materials, focused on electron microscopy, July 11-15, 2012, Thessaloniki, Greece

Comparing Microscopes

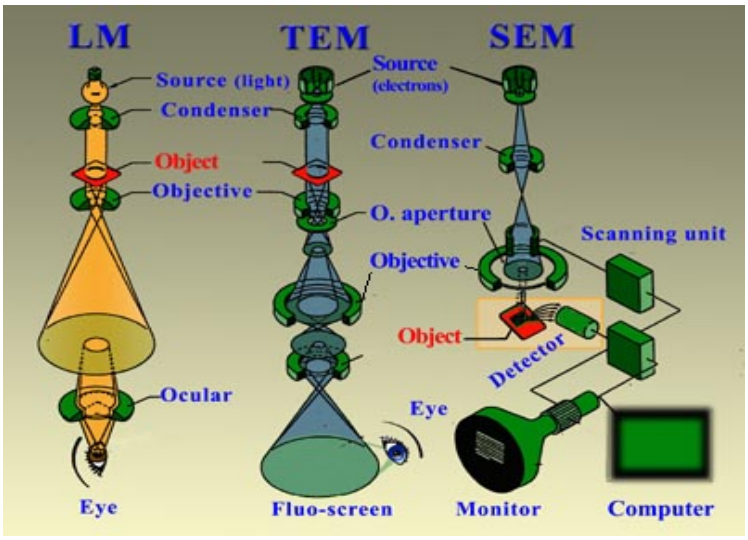

Summer School on Micro- and nano- structural characterization of materials, focused on electron microscopy, July 11-15, 2012, Thessaloniki, Greece

Comparing Microscopes: TEM vs SEM

	TEM	SEM
Specimen	Specimen must be very thin	Wide range of specimens allowed; simplifies sample preparation
Imaging	Electrons must pass through and be transmitted by the specimen	Information needed is collected near the surface of the specimen
Electron Beam	Broad static beams	Beam focused to fine point; sample is scanned line by line
Image recording	Transmitted electrons are collectively focused by the objective lens and magnified to create a real image	Beam is scanned along the surface of the sample to built up the image
Magnification - Resolution	50 million – 0.5 angstroms	2 million – 0.4 nanometers
Voltages needed	TEM voltage ranges from 60-300000 volts	Accelerating voltage much lower; not necessary to penetrate the specimen (50 to 30,000 volts)

Summer School on Micro- and nano- structural characterization of materials, focused on electron microscopy, July 11-15, 2012, Thessaloniki, Greece

Comparing Microscopes: TEM vs SEM

- A scanning electron microscope, like a TEM, consists of an electron optical column, a vacuum system, electronics, and software.
- The column is considerably shorter because the only lenses needed are those above the specimen used to focus the electrons into a fine spot on the specimen surface. There are no lenses below the specimen.
- The specimen chamber, on the other hand, is larger because the SEM technique does not impose any restriction on specimen size other than that set by the size of the specimen chamber.

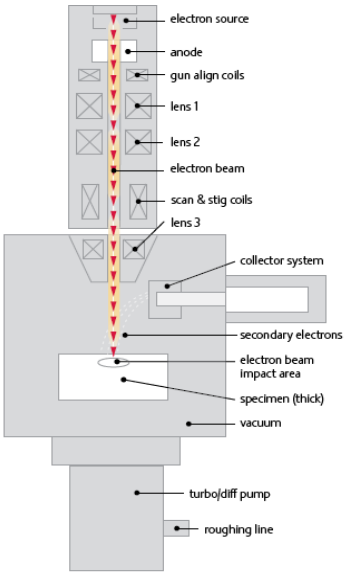

Summer School on Micro- and nano- structural characterization of n
15, 2012, Thessaloniki, G

Scanning Electron Microscope

Summer School on Micro- and nano- structural characterization of materials, focused on electron microscopy, July 11-15, 2012, Thessaloniki, Greece

Scanning Electron Microscopy

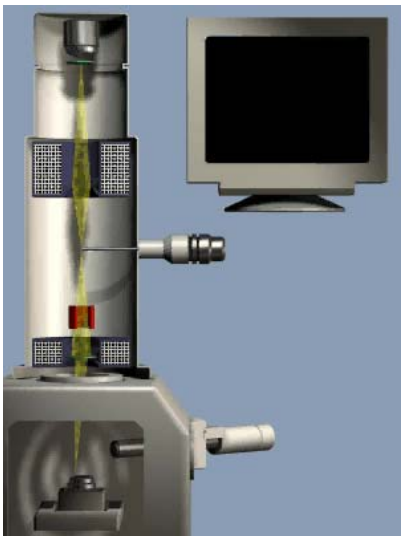

- ✓A stream of electrons is formed in high vacuum (by electron guns).
- ✓This stream is accelerated towards the specimen (with a positive electrical potential) while is confined and focused using metal apertures and magnetic lenses into a thin, focused, monochromatic beam.
- ✓The electron beam is focused into a fine spot as small as 1 nm in diameter on the specimen surface.
- ✓This beam is scanned in a rectangular raster over the specimen and the intensities of various signals created by interactions between the beam electrons and the specimen are measured and stored in computer memory.
- ✓The stored values are then mapped as variations in brightness on the image display.

Summer School on Micro- and nano- structural characterization of materials, focused on electron microscopy, July 11-15, 2012, Thessaloniki, Greece

Scanning Electron Microscopy

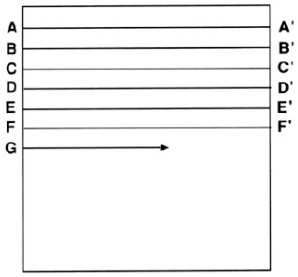

The ratio of the size of the displayed image to the size of the area scanned on the specimen gives the magnification. Increasing the magnification is achieved by reducing the size of the area scanned on the specimen

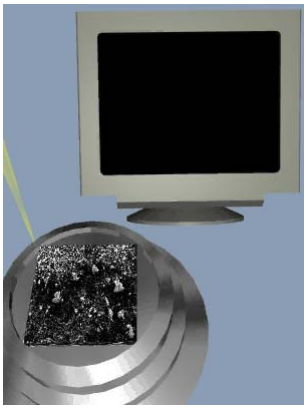

Summer School on Micro- and nano- structural characterization of materials, focused on electron microscopy, July 11-15, 2012, Thessaloniki, Greece

How it works

1) The electron gun produces a stream of monochromatic electrons.
2) The stream is condensed by the first condenser lens (usually controlled by the "coarse probe current knob"). This lens is used to both form the beam and limit the amount of current in the beam. It works in conjunction with the condenser aperture to eliminate the high-angle electrons from the beam.
3) The beam is then constricted by the condenser aperture (usually not user selectable), eliminating some high-angle electrons
4) The second condenser lens forms the electrons into a thin, tight, coherent beam and is usually controlled by the "fine probe current knob".
5) A user selectable objective aperture further eliminates high-angle electrons from the beam.

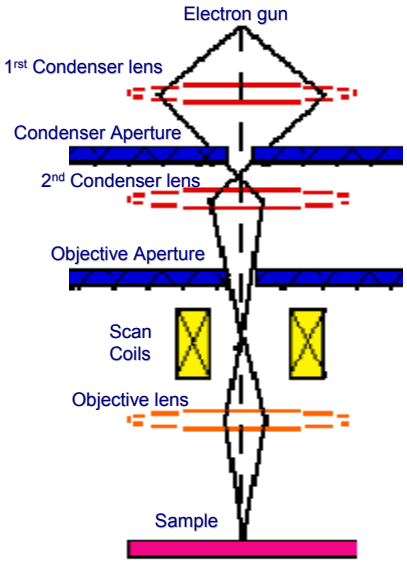

Summer School on Micro- and nano- structural characterization of materials, focused on electron microscopy, July 11-15, 2012, Thessaloniki, Greece

6) A user selectable objective aperture further eliminates high-angle electrons from the beam.
7) A set of coils then "scan" or "sweep" the beam in a grid fashion (like a television), dwelling on points for a period of time determined by the scan speed (usually in the microsecond range).
8) The final lens, the objective, focuses the scanning beam onto the part of the specimen desired.
9) When the beam strikes the sample (and dwells for a few microseconds) interactions occur inside the sample and are detected with various instruments.
10) Before the beam moves to its next dwell point these instruments count the number of e- interactions and display a pixel on a CRT whose intensity is determined by this number (the more reactions the brighter the pixel).
11) This process is repeated until the grid scan is finished and then repeated, the entire pattern can be scanned 30 times/sec.

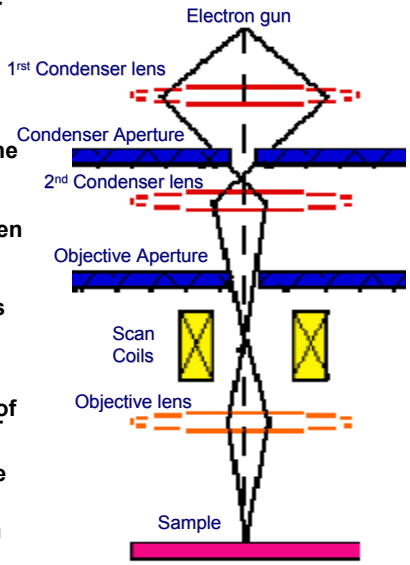

Summer School on Micro- and nano- structural characterization of materials, focused on electron microscopy, July 11-15, 2012, Thessaloniki, Greece

Electron gun

Thermionic Gun - W

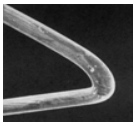

Thermionic Gun-LaB_6

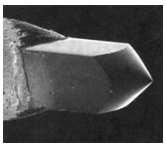

Field Emission Gun – single crystal W

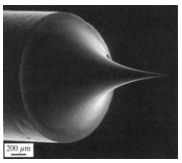

A **thermionic electron gun** consists essentially of a heated wire or compound from which electrons are given enough thermal energy to overcome the work function of the source, combined with an electric potential to give the newly free electrons a direction and velocity

- ✓ Tungsten has a very high melting temperature, so more thermal energy can be made available
- ✓ LaB_6 has a low work function and a high melting temperature.

A **field emission gun** consists of a sharply pointed tungsten tip held at several kilovolts negative potential relative to a nearby electrode, so that there is a very high potential gradient at the surface of the tungsten tip.

Summer School on Micro- and nano- structural characterization of materials, focused on electron microscopy, July 11-15, 2012, Thessaloniki, Greece

Comparison of Electron Guns

Kind of gun	Tungsten hairpin	LaB_6	Field emission
Cathode material	Tungsten	Lanthanum hexaboride single (multi) crystal	Tungsten
Cathode temperature (K)	2,600	1,800	Room temp.
Cathode work function (eV)	4.4	2.6 to 2.7	4.1
Electron source diam.	30 μm	10 μm	5 nm
Brightness ($A/cm^2 \cdot sr$)	10^6	10^7	10^9
Energy width (eV)	2.0	1.5	0.2
Max. probe current (A)	10^{-7}	10^{-7}	10^{-9}
Working pressure (Pa)	10^{-4}	10^{-5}	10^{-8}
Cathode lifetime	~50 hr	~1000 hr	1 year or more

Summer School on Micro- and nano- structural characterization of materials, focused on electron microscopy, July 11-15, 2012, Thessaloniki, Greece

Interactions between the beam electrons and sample atoms

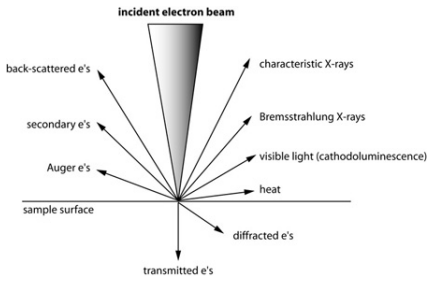

Depending on the incident energy of the electron beam, a variety of

- electrons (secondary, backscattered and auger)
- X-rays (characteristic and Bremsstrahlung),
- light (cathodoluminescence) and
- heat (phonons)

are emitted. Several of these interactions are used for imaging, semi-quantitative analysis and/or quantitation analysis.

Summer School on Micro- and nano- structural characterization of materials, focused on electron microscopy, July 11-15, 2012, Thessaloniki, Greece

Interactions between the beam electrons and sample atoms
1. Secondary Electrons

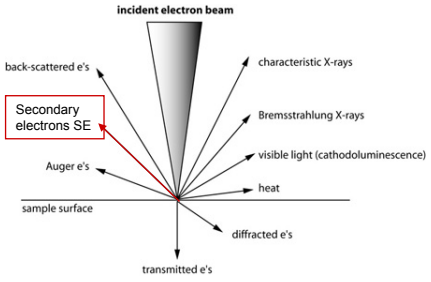

The impinging electrons can knock electrons from sample atoms. The most frequent result is the ejection of an electron from the atom with relatively low energy, a few eV. If this occurs near the sample surface, the liberated electron may escape and be detected as a secondary electron.

Summer School on Micro- and nano- structural characterization of materials, focused on electron microscopy, July 11-15, 2012, Thessaloniki, Greece

Interactions between the beam electrons and sample atoms
2. Backscattered Electrons

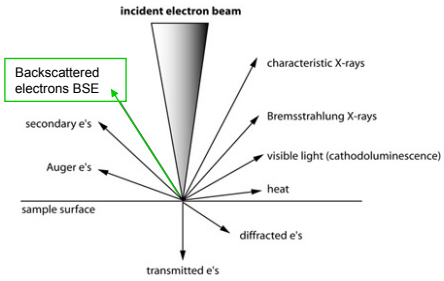

The incoming beam electron can interact with the nucleus and be backscattered with virtually undiminished energy (just as a space probe is deviated by the gravity of a planet during a fly-by). Some of the impinging electrons are deflected through large angles or reflected (backscattered) by sample nuclei (backscattered electrons, BSE). These backscattered electrons can also cause the emission of secondary electrons as they travel through the sample and exit the sample surface.

Summer School on Micro- and nano- structural characterization of materials, focused on electron microscopy, July 11-15, 2012, Thessaloniki, Greece

Interactions between the beam electrons and sample atoms
3. Characteristic X-rays

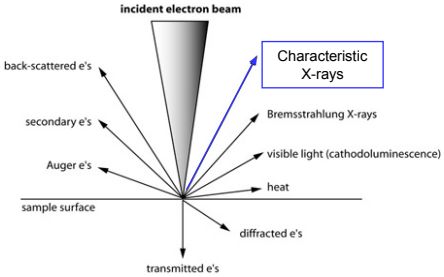

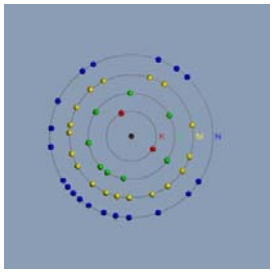

The impinging electrons may cause specimen atoms to emit X-rays whose energy and wavelength are related to the specimen's elemental composition; these are called characteristic X-rays.

Summer School on Micro- and nano- structural characterization of materials, focused on electron microscopy, July 11-15, 2012, Thessaloniki, Greece

4. Auger Electrons

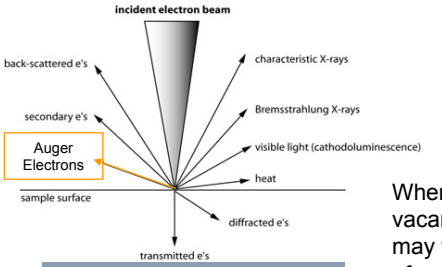

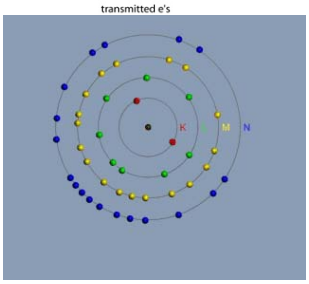

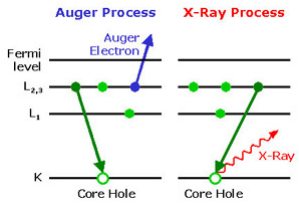

When a core electron is removed, leaving a vacancy, an electron from a higher energy level may fall into the vacancy, resulting in a release of energy. Although most of the times this energy is released in the form of an emitted photon, the energy can also be transferred to another electron, which is ejected from the atom. This second ejected electron is called an **Auger electron**

Auger electrons are characteristic of the fine structure of the atom.

Light elements are more susceptible to the formation of Auger electrons

Summer School on Micro- and nano- structural characterization of materials, focused on electron microscopy, July 11-15, 2012, Thessaloniki, Greece

Energy distribution of the Secondary and Backscattered Electrons emitted when a specimen is irradiated with the incident electron beam

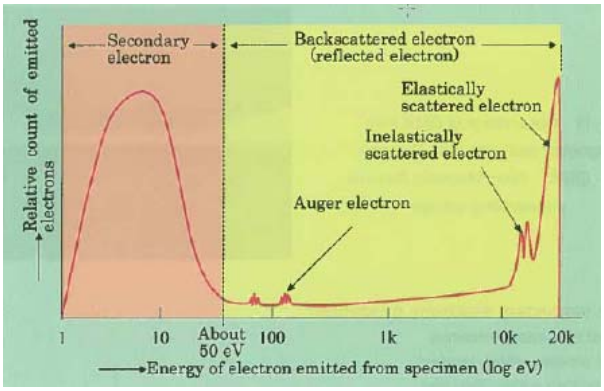

Summer School on Micro- and nano- structural characterization of materials, focused on electron microscopy, July 11-15, 2012, Thessaloniki, Greece

Specimen Interaction Volume

The volume inside the specimen in which interactions occur while interacting with an electron beam.

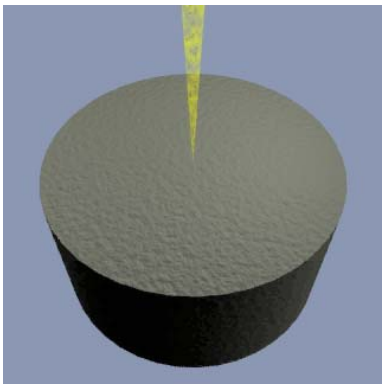

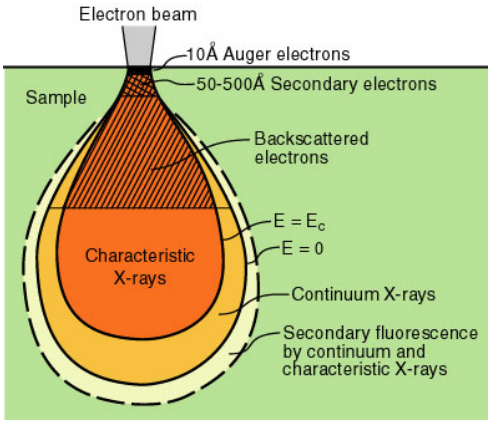

Summer School on Micro- and nano- structural characterization of materials, focused on electron microscopy, July 11-15, 2012, Thessaloniki, Greece

Effect on the interaction volume of the acceleration voltage and sample atomic number.

Electron Scattering inside Specimen as visualized by Monte Carlo Simulation

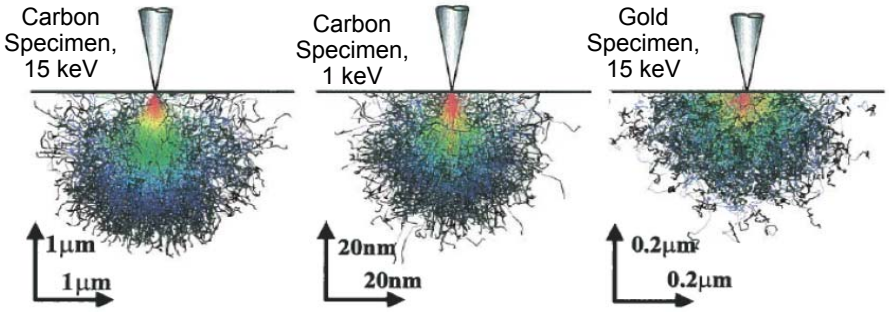

Higher accelerating voltages penetrate farther into the sample and generate a larger interaction volume

Higher atomic number materials absorb or stop more electrons , smaller interaction volume

Summer School on Micro- and nano- structural characterization of materials, focused on electron microscopy, July 11-15, 2012, Thessaloniki, Greece

Specimen Interaction Volume

- specimen atomic number 28,
- accelerating voltage 20 kV
- incident beam tilt 0° degrees, (normal to specimen surface)

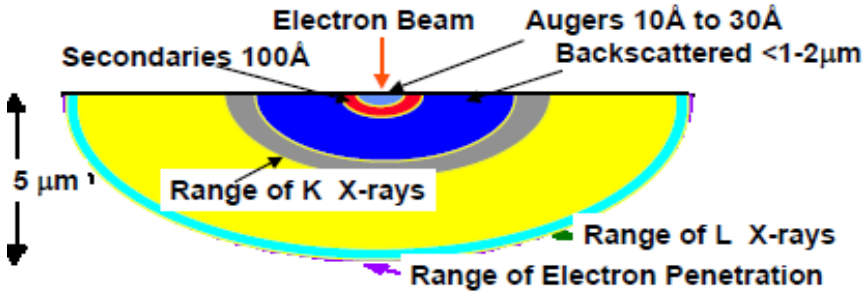

Summer School on Micro- and nano- structural characterization of materials, focused on electron microscopy, July 11-15, 2012, Thessaloniki, Greece

Secondary Electron (SE) Image

The secondary electron (SE) signal is the most frequently used signal. It varies with the topography of the sample surface much like an aerial photograph: edges are bright, recesses are dark.

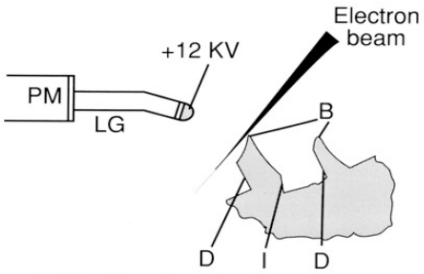

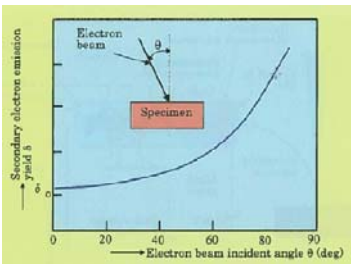

Three dimensionality and contrast are due to the yield of secondary electrons from various parts of the specimen. Areas marked B face the beam and are in line of sight with the detector, so that they will appear bright. I (intermediate brightness) faces the beam but fewer secondary electrons reach the detector since it is not in line of sight. D is dark in appearance since the beam does not strike this area and no secondary electrons are generated.

Summer School on Micro- and nano- structural characterization of materials, focused on electron microscopy, July 11-15, 2012, Thessaloniki, Greece

BackScattered Electron (BSE) Image

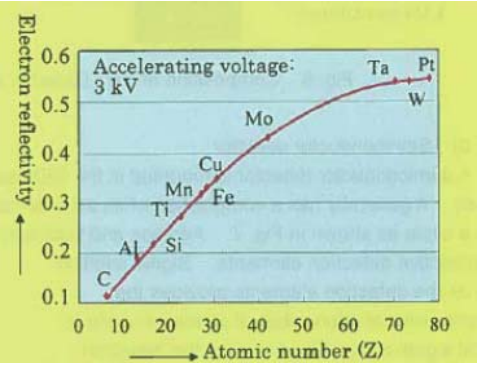

The count ratio of backscattered electrons to electrons incident on specimen surface is called "electron reflectivity".

A change in this reflectivity renders a contrast to backscattered electron image.

The Figure shows the differences in electron reflectivity among some specimens. The reflectivity value becomes larger as the mean atomic number (or density) of specimen increases.

Parameters affecting SEM image quality

Summer School on Micro- and nano- structural characterization of materials, focused on electron microscopy, July 11-15, 2012, Thessaloniki, Greece

Effect of Accelerating Voltage

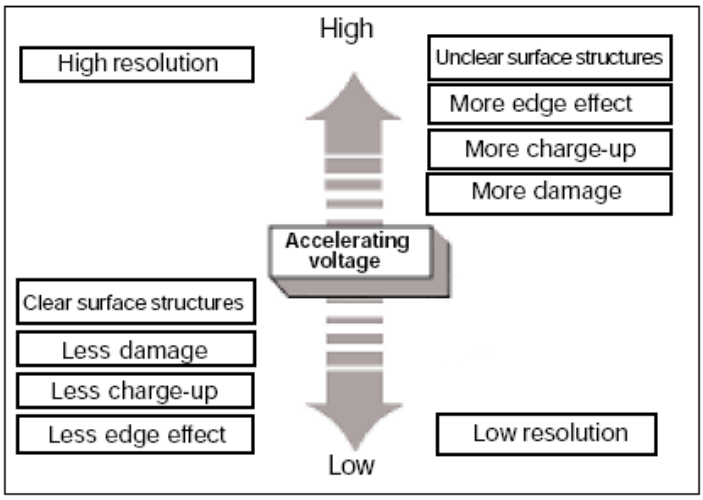

Summer School on Micro- and nano- structural characterization of materials, focused on electron microscopy, July 11-15, 2012, Thessaloniki, Greece

Effect of Accelerating Voltage

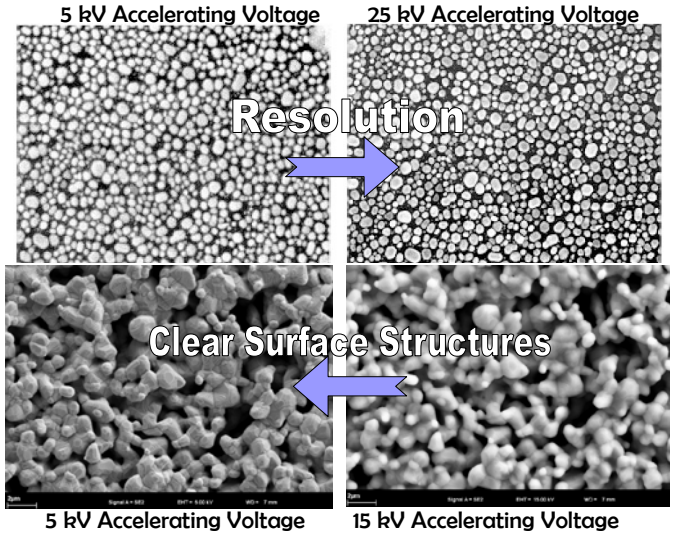

Summer School on Micro- and nano- structural characterization of materials, focused on electron microscopy, July 11-15, 2012, Thessaloniki, Greece

Effect of Working Distance

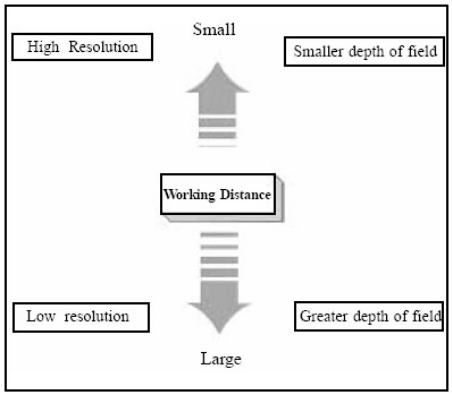

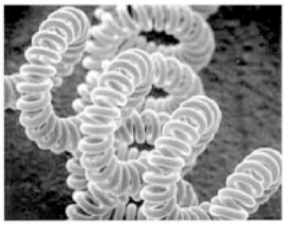

10 mm Working Distance

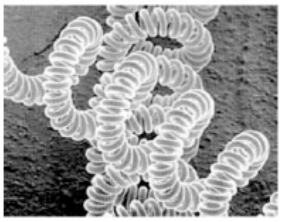

38 mm Working Distance

Summer School on Micro- and nano- structural characterization of materials, focused on electron microscopy, July 11-15, 2012, Thessaloniki, Greece

Effect of Spot Size

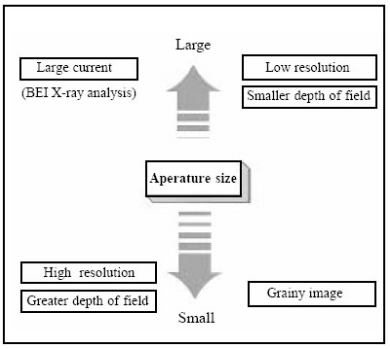

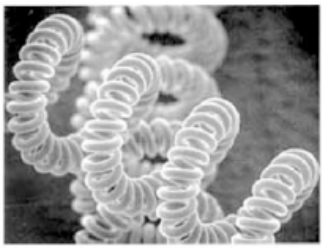

600 micron spot size

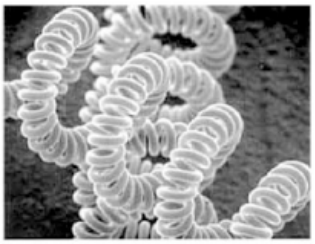

200 micron spot size

Summer School on Micro- and nano- structural characterization of materials, focused on electron microscopy, July 11-15, 2012, Thessaloniki, Greece

SEM Image distortions

Charge-up Problem

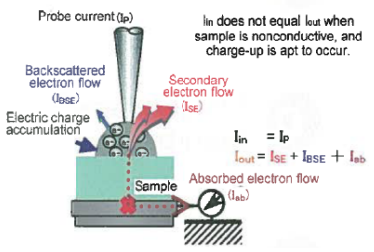

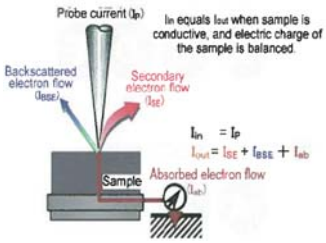

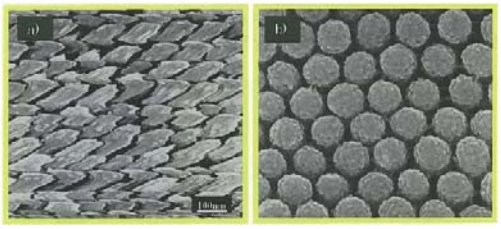

- Reduce accelerating voltage
- Reduce sample irradiating current
- Apply a thicker conductive coating
- Integrate the image
- Observe image in a low-vacuum mode

Contamination Problem

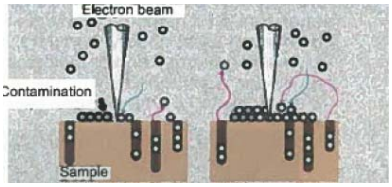

The phenomenon by which gas molecules of hydrocarbons existing around the sample collect on the sample due to electron beam irradiation, then bond together and adhere to the sample surface. The clarity of the image at that area decreases and becomes darker. The reason for the darkness is thought to be that the matter accumulated on the sample surface suppresses the discharge of Secondary Electrons from the sample.

Measures

- Use of minimum amount of conductive paste or tape when mounting the sample in the instrument
- Thoroughly dry the conductive paste prior to inserting the sample into the instrument
- Heat and degas the sample in a vacuum device
- Avoid observing the same location for a long time, especially at high magnification
- Observe samples while cooling the sample surroundings with a cold trap

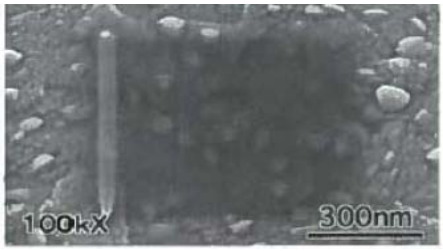

Summer School on Micro- and nano- structural characterization of materials, focused on electron microscopy, July 11-15, 2012, Thessaloniki, Greece

Beam Damage by Irradiation

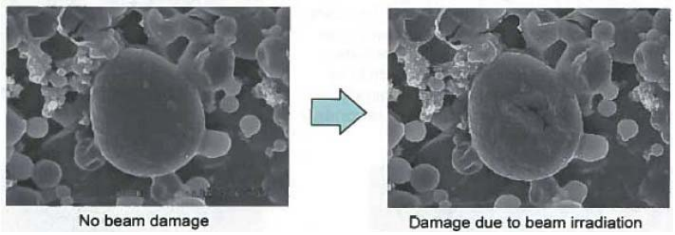

✓ Thermal or Chemical damage of the sample.

✓ Especially often in biological samples & polymers

Measures to avoid it

- Reduce the sample irradiation current
- Lower the accelerating voltage
- Apply metal coating (to improve heat conductivity)
- Observe the sample while cooling it (special instruments required)

Summer School on Micro- and nano- structural characterization of materials, focused on electron microscopy, July 11-15, 2012, Thessaloniki, Greece

Vibration

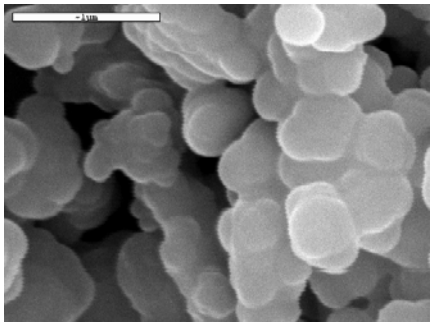

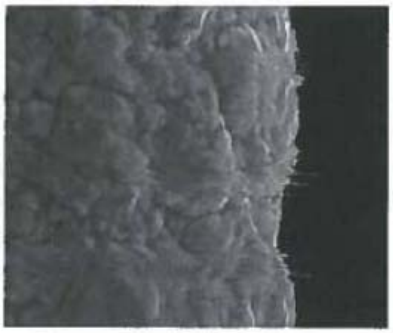

Countermeasures for image disturbance due to vibration include:

- Keep the instrument well away fromvibration sources such as air-conditioner or pumps (or elevators)
- Do not let high voltage cables from the column come in contact with the walls or other installation items
- Do not let the draft from an air-conditioner outlet contact the column directly.

Summer School on Micro- and nano- structural characterization of materials, focused on electron microscopy, July 11-15, 2012, Thessaloniki, Greece

Magnetic field disturbance

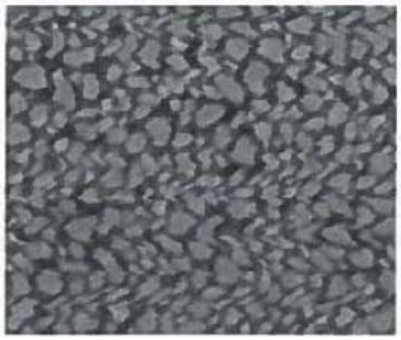

Countermeasures for image disturbance due to a stray magnetic field

- Keep the instrument well away from magnetic field sources such as transformer or large capacity power cables
- Shorten the working distance and apply strong excitation to the condenser lens to counter the effect of the magnetic field
- Use a magnetic field canceller (e.g. Faraday cage)

Summer School on Micro- and nano- structural characterization of materials, focused on electron microscopy, July 11-15, 2012, Thessaloniki, Greece

X-ray Spectroscopy in SEM

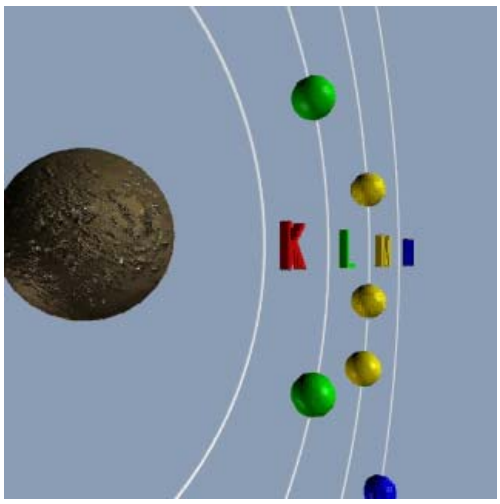

Summer School on Micro- and nano- structural characterization of materials, focused on electron microscopy, July 11-15, 2012, Thessaloniki, Greece

Characteristic X-rays

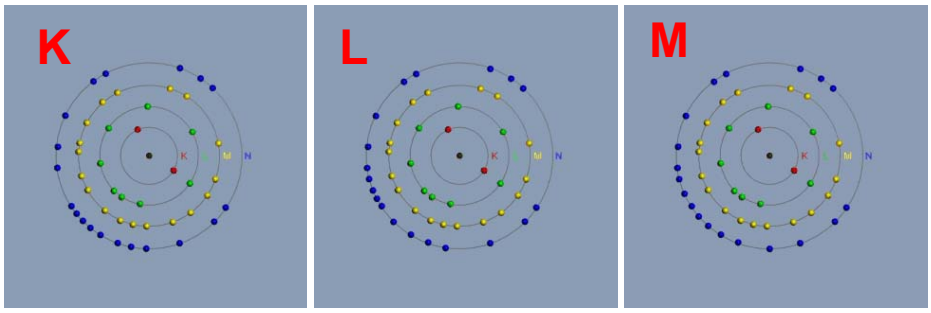

Summer School on Micro- and nano- structural characterization of materials, focused on electron microscopy, July 11-15, 2012, Thessaloniki, Greece

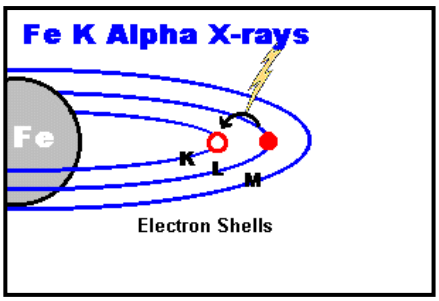

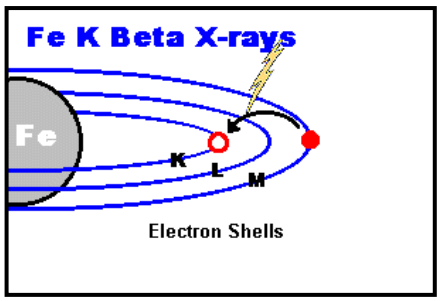

Kα Kβ

When an electron from a K-shell is replaced by one from the closest shell (L), it is designated as a Kα event

When an electron from a K-shell is replaced by one from the second closest shell (M), it is designated as a Kβ event

Summer School on Micro- and nano- structural characterization of materials, focused on electron microscopy, July 11-15, 2012, Thessaloniki, Greece

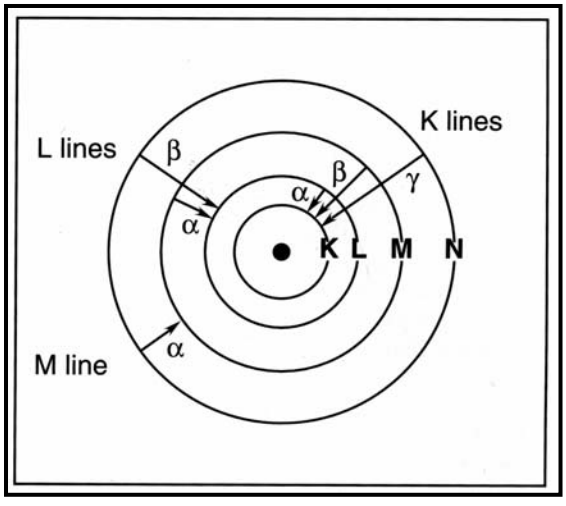

Certain transitions as Mα, Lβ, and Kγ are possible only in atoms of sufficient atomic weight

Summer School on Micro- and nano- structural characterization of materials, focused on electron microscopy, July 11-15, 2012, Thessaloniki, Greece

The Complete Range of Possible Electron Transitions that Give Rise to K, L and M Characteristic X-Rays

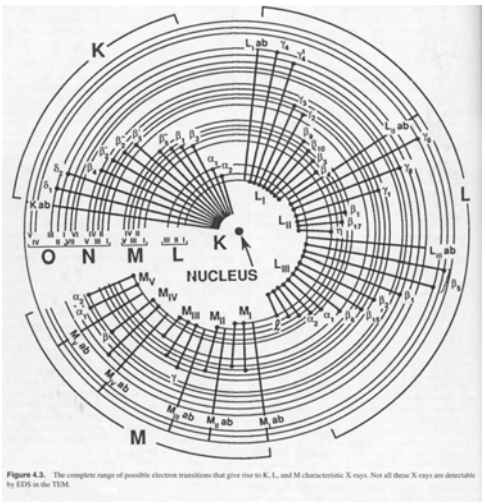

Summer School on Micro- and nano- structural characterization of materials, focused on electron microscopy, July 11-15, 2012, Thessaloniki, Greece

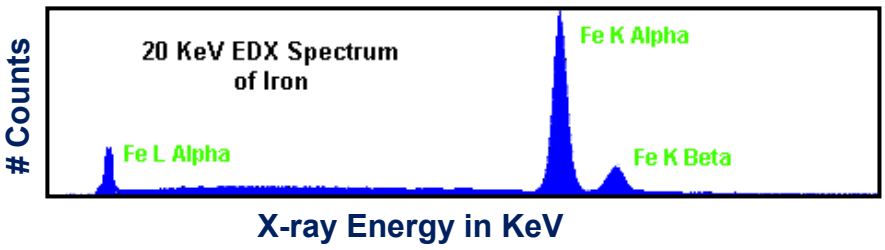

An X-ray spectrum for a sample is composed of all the possible signals for that given set of elements.

These will differ in terms of energies (KeV) and probabilities (likelihood) scored as number of such signals collected over a given period of time.

Summer School on Micro- and nano- structural characterization of materials, focused on electron microscopy, July 11-15, 2012, Thessaloniki, Greece

Table of X-ray Emission and Absorption Edge Energies (keV)

atomic number	Kα	Kβ	$K_{(ab)}$	Lα	$L_{\beta 1}$	$L_{\beta 2}$	$L_{\gamma 1}$	$L_{III(ab)}$	$L_{II(ab)}$	$M_{V(ab)}$	Mα
1 H			0.014								
2 He			0.025								
3 Li			0.055					0.003	0.003		
4 Be			0.112					0.002	0.002		
5 B			0.186					0.003	0.003		
6 C	0.277		0.282					0.002	0.002		
7 N	0.392		0.400					0.008	0.008		
8 O	0.525		0.531					0.009	0.009		
9 F	0.677		0.692								
10 Ne	0.848		0.874					0.019	0.019		
11 Na	1.041	1.067	1.070					0.031	0.031		
12 Mg	1.253	1.295	1.303					0.050	0.050		
13 Al	1.486	1.553	1.559					0.073	0.073		
14 Si	1.739	1.829	1.842					0.102	0.103		
15 P	2.013	2.136	2.142					0.128	0.129		
16 S	2.307	2.464	2.470					0.163	0.164		
17 Cl	2.621	2.815	2.820					0.197	0.199		
18 Ar	2.957	3.190	3.200					0.224	0.246		
19 K	3.312	3.589	3.609					0.295	0.298		
20 Ca	3.690	4.012	4.038	0.341	0.345		0.350	0.346	0.350		
21 Sc	4.088	4.460	4.496	0.395	0.400		0.407	0.403	0.411		
22 Ti	4.508	4.931	4.964	0.452	0.458		0.460	0.454	0.460		
23 V	4.949	5.426	5.464	0.511	0.519		0.520	0.513	0.519		
24 Cr	5.411	5.924	5.987	0.573	0.583		0.583	0.574	0.581		
25 Mn	5.894	6.489	6.537	0.637	0.649		0.652	0.641	0.650		
26 Fe	6.398	7.057	7.111	0.705	0.718		0.721	0.709	0.720		
27 Co	6.924	7.648	7.709	0.776	0.791		0.794	0.779	0.794		
28 Ni	7.471	8.263	8.331	0.851	0.869			0.854	0.871		
29 Cu	8.040	8.904	8.981	0.930	0.950			0.933	0.953		
30 Zn	8.630	9.570	9.661	1.012	1.034			1.022	1.045		

Each element has a family of characteristic X-rays associated with it

Summer School on Micro- and nano- structural characterization of materials, focused on electron microscopy, July 11-15, 2012, Thessaloniki, Greece

Production of "continuum" X-rays

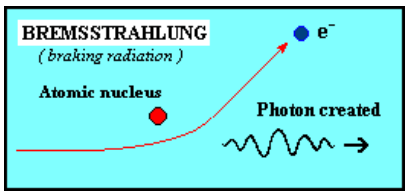

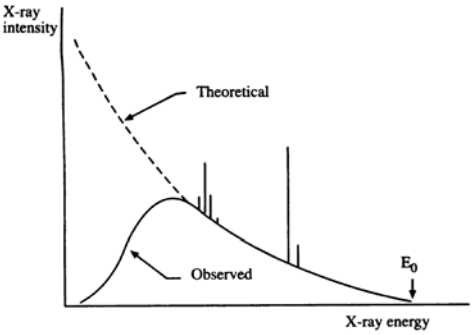

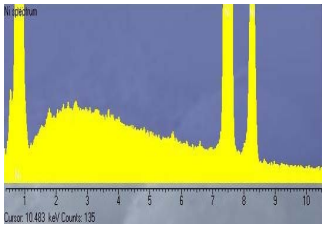

"Bremsstrahlung" means "braking radiation" and comes from the original German to describe the radiation which is emitted when electrons are decelerated or "braked" when they interact with the specimen.

Summer School on Micro- and nano- structural characterization of materials, focused on electron microscopy, July 11-15, 2012, Thessaloniki, Greece

X-ray Microanalysis – Qualitative analysis

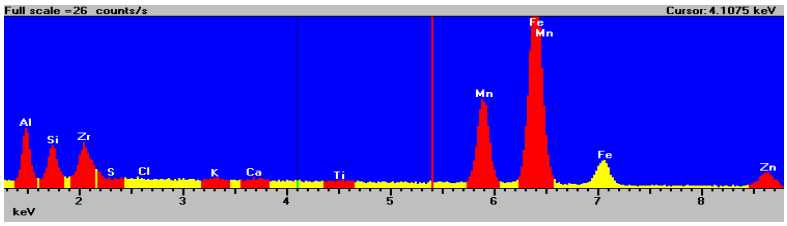

In microanalysis we only use the most intense lines, usually the α lines (or, if we can't resolve them, we use the α and β line).

There are energy peak overlaps among different elements, particularly those corresponding to x-rays generated by emission from different energy-level shells (K, L and M) in different elements.

For example, there are close overlaps of Mn-Kα and Cr-Kβ, or Ti-Kα and various L lines in Ba. Particularly at higher energies, individual peaks may correspond to several different elements; in this case, the user can apply deconvolution methods to try peak separation, or look at a series of minor peaks if they are present, or simply consider which elements make "most sense" given the known context of the sample.

Summer School on Micro- and nano- structural characterization of materials, focused on electron microscopy, July 11-15, 2012, Thessaloniki, Greece

X-ray Microanalysis – Quantitative analysis

In order to determine the concentration C_A of element A in an unknown specimen, the following effects need to be taken into account;

<1> "Z" effect meaning that the occurrence of characteristic x-rays varies with the mean atomic number (Z) of a specimen,

<2> "A" effect, i.e., a characteristic x-ray generated in the specimen receives a self-absorption by the specimen until it escapes into vacuum and

<3> "F" effect, i.e. a certain characteristic x-ray is subjected to fluorescence excitation by other x-ray.

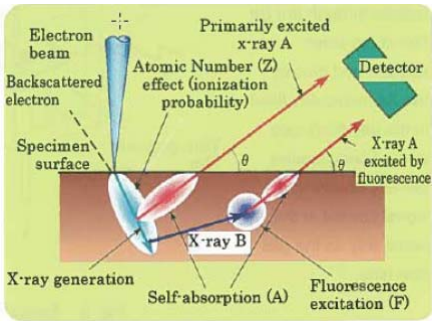

Therefore, the concentration C_A in element A in an unknown specimen is obtainable by taking each correction of the Z, A and F effects into account.

$$C_A = I_{AU}/I_{AS} \bullet Z \bullet A \bullet F$$

I_{AU}: sample x-ray intensity
I_{AS}: x-ray intensity of standard specimen (100% concentration)

Summer School on Micro- and nano- structural characterization of materials, focused on electron microscopy, July 11-15, 2012, Thessaloniki, Greece

The EDS Detector

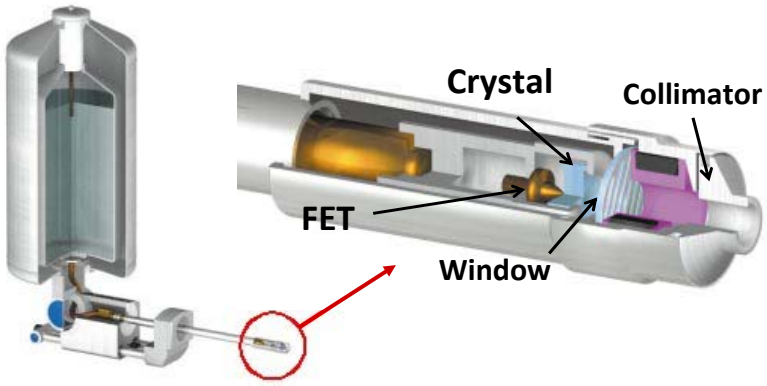

Summer School on Micro- and nano- structural characterization of materials, focused on electron microscopy, July 11-15, 2012, Thessaloniki, Greece

Conversion of X-ray signals into a voltage 'ramp' by the EDS detector

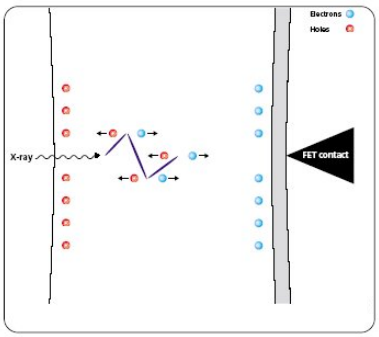

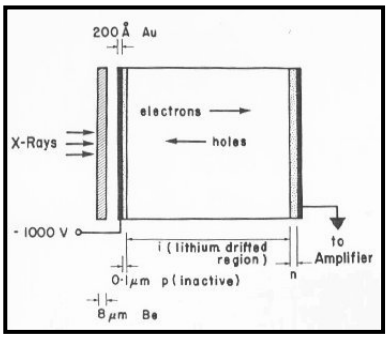

Generation and measurement of electron-hole pairs in the crystal

Each ionized atom of silicon absorbs 3.8 eV of energy, so an X-ray of 3.8 KeV (e.g. Ca Ka 3.7 KeV) will ionize approximately 1000 silicon atoms.

The output voltage is proportional to the X-ray energy.

Summer School on Micro- and nano- structural characterization of materials, focused on electron microscopy, July 11-15, 2012, Thessaloniki, Greece

Sample Preparation for SEM

Summer School on Micro- and nano- structural characterization of materials, focused on electron microscopy, July 11-15, 2012, Thessaloniki, Greece

Carbon Coating

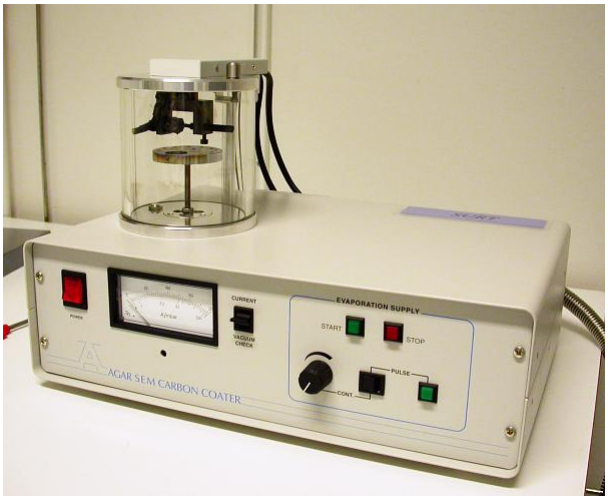

Two carbon tips are making electrical contact and a current is running through them, heating them to a red/white glow.

Carbon molecules are emitted in all directions inside the vacuum chamber.

Summer School on Micro- and nano- structural characterization of materials, focused on electron microscopy, July 11-15, 2012, Thessaloniki, Greece

Gold Sputtering

A gold (gold-palladium, or platinum) target is bombarded with heavy gas atoms (usually argon).

Metal atoms ejected from the target by the ionised gas cross the plasma to deposit onto the any surface within the coating unit including the specimen.

A low vacuum environment is used (0.1 to 0.05 mbar), which with one of the modern low voltage sputter coaters, enables metal to be deposited at up to 1nm/s1

Summer School on Micro- and nano- structural characterization of materials, focused on electron microscopy, July 11-15, 2012, Thessaloniki, Greece

SEM & X-ray Microanalysis Applications

Summer School on Micro- and nano- structural characterization of materials, focused on electron microscopy, July 11-15, 2012, Thessaloniki, Greece

SEM Imaging

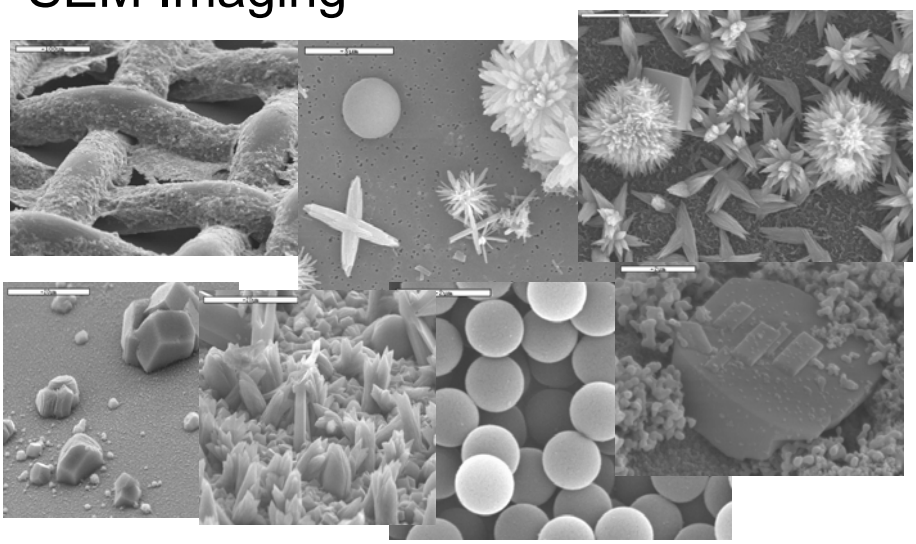

Summer School on Micro- and nano- structural characterization of materials, focused on electron microscopy, July 11-15, 2012, Thessaloniki, Greece

Impurity detection and Identification

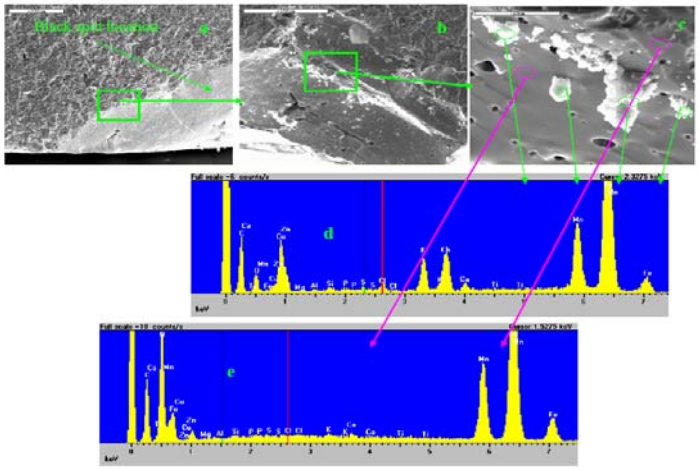

Summer School on Micro- and nano- structural characterization of materials, focused on electron microscopy, July 11-15, 2012, Thessaloniki, Greece

Distribution of metal poisons Ni and V in FCC catalysts

SE Images and LINESCANs for Al, Si, V and Ni, from FCC catalyst particle, embedded in epoxy resin

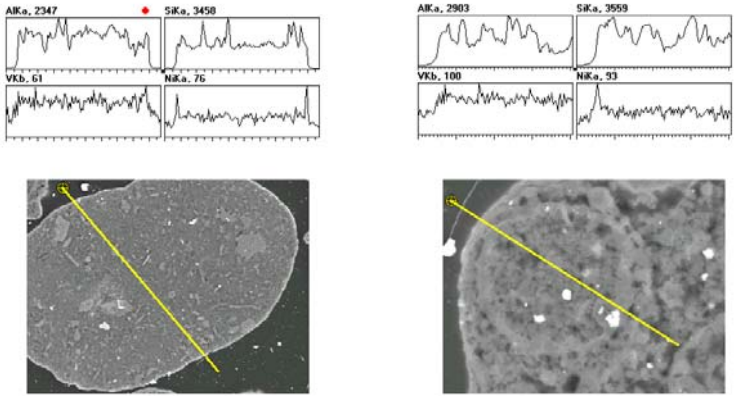

Summer School on Micro- and nano- structural characterization of materials, focused on electron microscopy, July 11-15, 2012, Thessaloniki, Greece

SE Image and Al, Si, V KAl Ni elemental mapping in FCC catalyst particle

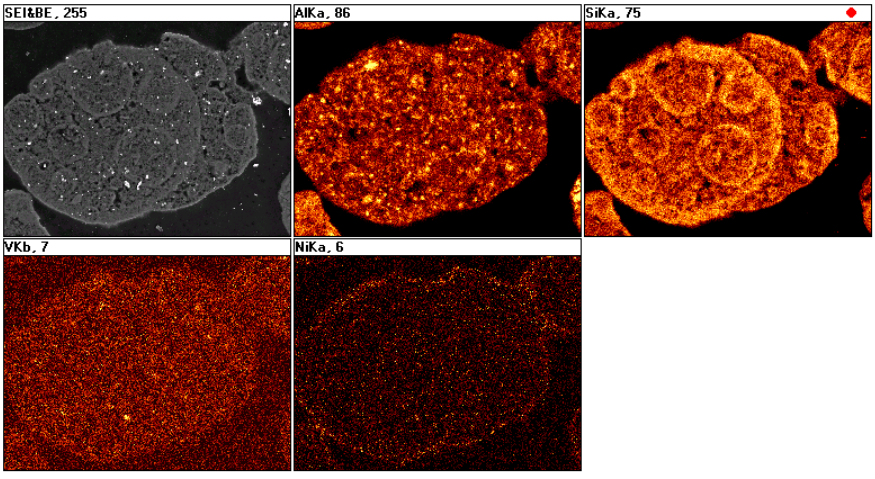

Summer School on Micro- and nano- structural characterization of materials, focused on electron microscopy, July 11-15, 2012, Thessaloniki, Greece

Distribution of Ni and V across FCC catalyst particles. Point analysis technique.

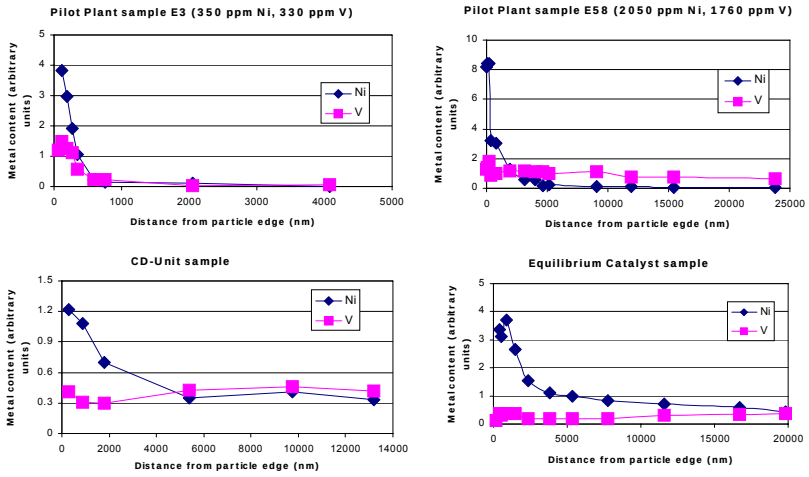

Summer School on Micro- and nano- structural characterization of materials, focused on electron microscopy, July 11-15, 2012, Thessaloniki, Greece

Monitoring of coverage of γ-alumina particles with thin ZSM-5 zeolite layers.

SEI image

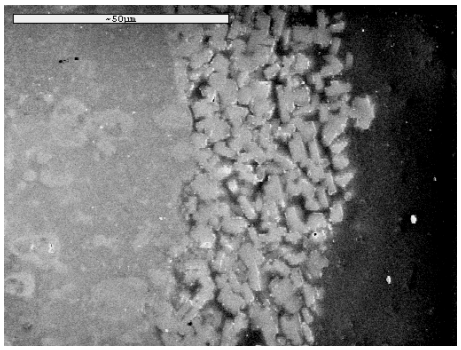

Si map

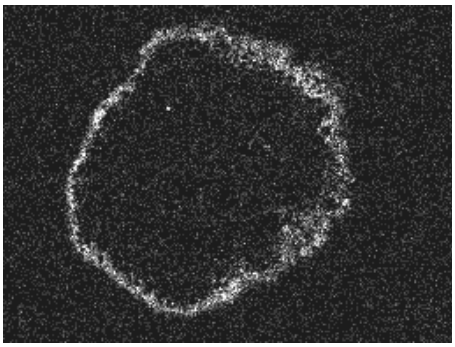

Summer School on Micro- and nano- structural characterization of materials, focused on electron microscopy, July 11-15, 2012, Thessaloniki, Greece

Preparation of Silicalite Membranes by in-situ Crystallization on Porous Alumina Supports

Silicalite membrane around a g-Al2O3 particle

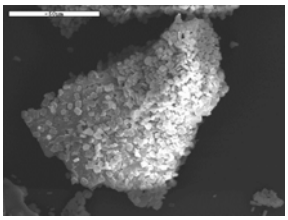

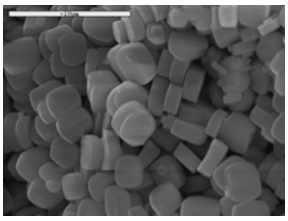

detail from the outer surface

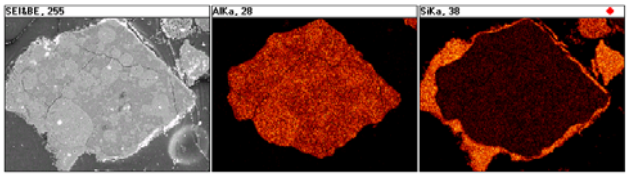

Al- and Si- maps on a particle cross-section, showing full coverage with silicalite layer

Summer School on Micro- and nano- structural characterization of materials, focused on electron microscopy, July 11-15, 2012, Thessaloniki, Greece

Conjugation of magnetic nanoparticles to cancer cells through antibody-antigen bonds

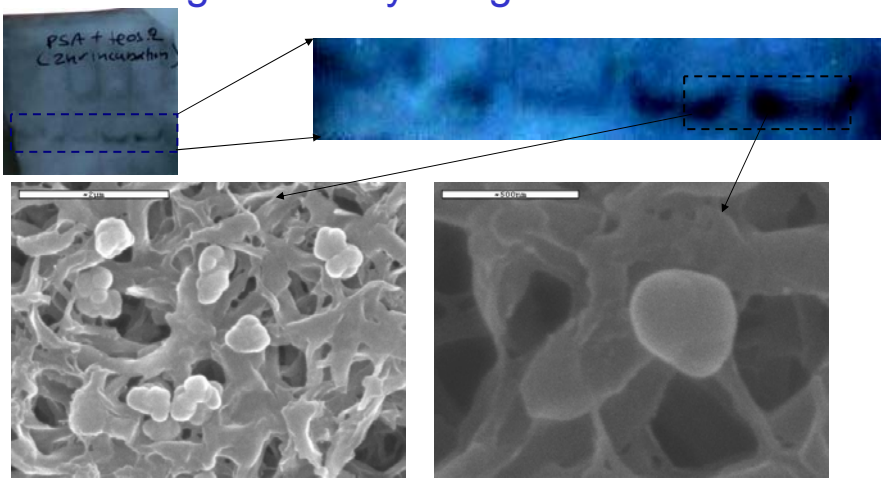

SEM images of the nanoparticles present on the membrane

Summer School on Micro- and nano- structural characterization of materials, focused on electron microscopy, July 11-15, 2012, Thessaloniki, Greece

Pt particles overgrowth in γ-alumina carrier, leading to reduced catalyst activity.

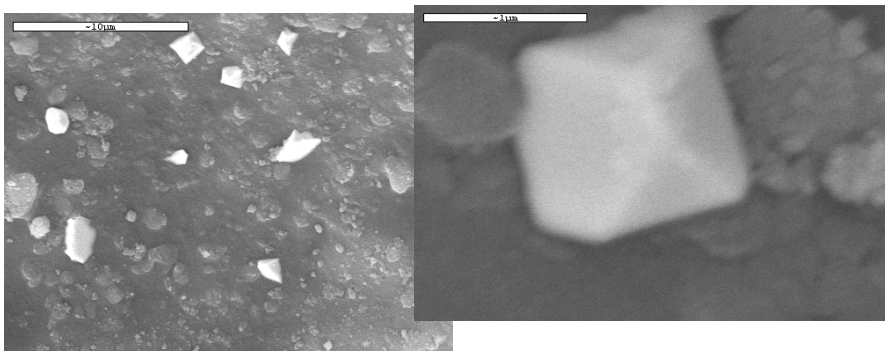

Summer School on Micro- and nano- structural characterization of materials, focused on electron microscopy, July 11-15, 2012, Thessaloniki, Greece

Forensic Applications

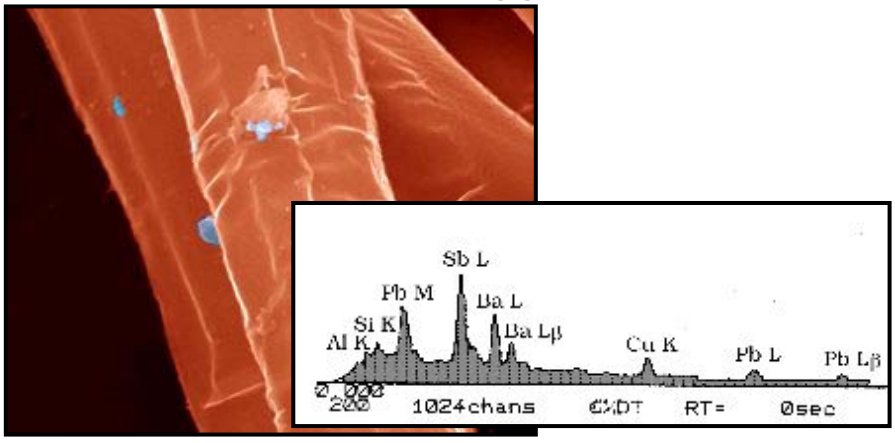

Bullet fragments (blue) can be identified on cloth fibers and distinguished from other metal pieces by their elemental composition

Summer School on Micro- and nano- structural characterization of materials, focused on electron microscopy, July 11-15, 2012, Thessaloniki, Greece

Gunshot Residue (GSR) Analysis

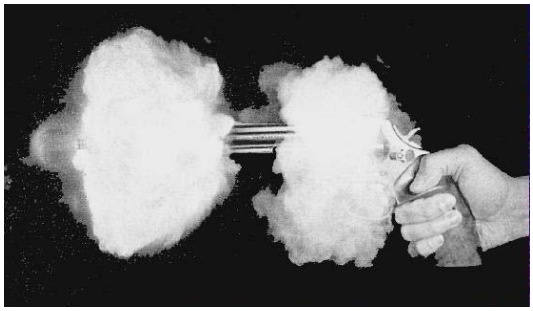

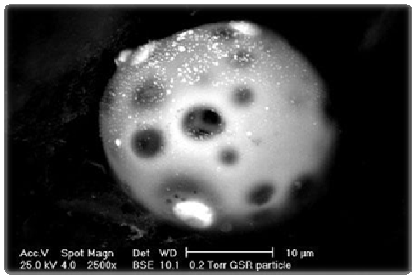

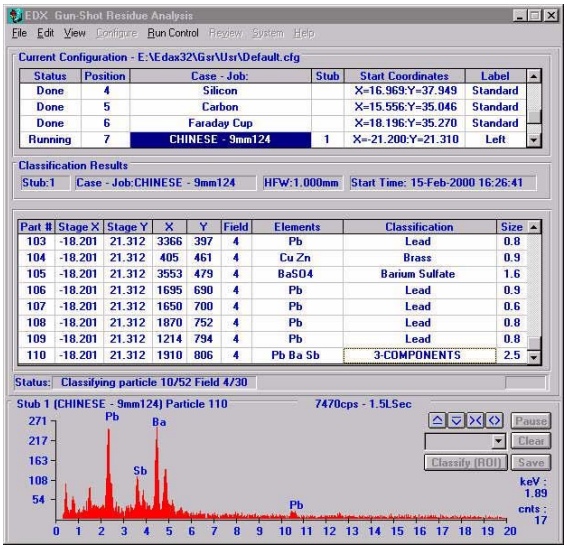

The proportion of elements present in GSR differ slightly and databases of GSR from different manufacturers can be used to identify what ammunition was used in a crime.
GSR is often found on criminals and also on victims if shot at close range.

Summer School on Micro- and nano- structural characterization of materials, focused on electron microscopy, July 11-15, 2012, Thessaloniki, Greece

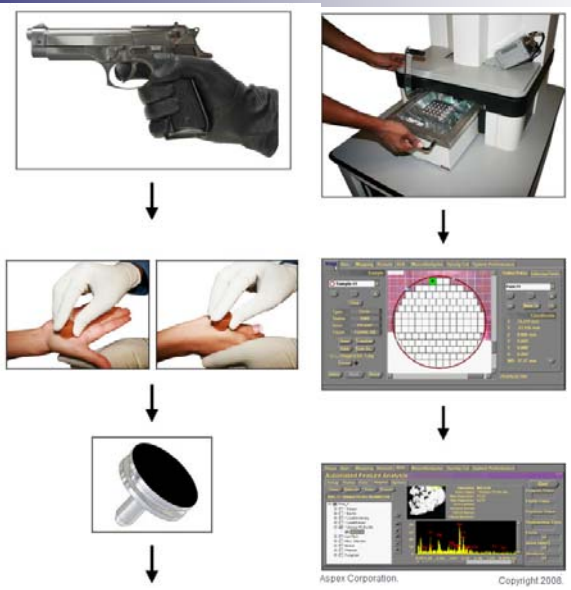

Gun-shot residual (GSR) analysis for forensics

Summer School on Micro- and nano- structural characterization of materials, focused on electron microscopy, July 11-15, 2012, Thessaloniki, Greece

SEM Image Processing Applications

Summer School on Micro- and nano- structural characterization of materials, focused on electron microscopy, July 11-15, 2012, Thessaloniki, Greece

Macropore Size Determination in catalytic materials

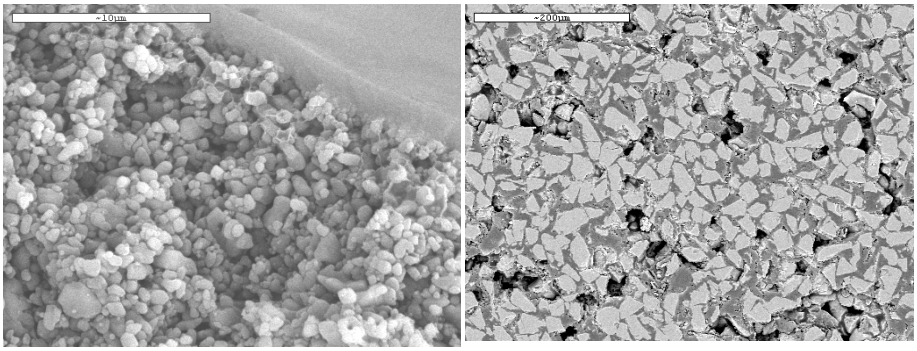

Summer School on Micro- and nano- structural characterization of materials, focused on electron microscopy, July 11-15, 2012, Thessaloniki, Greece

Study of the morphology of polycrystalline ceramics
Pore Size Distribution Determination

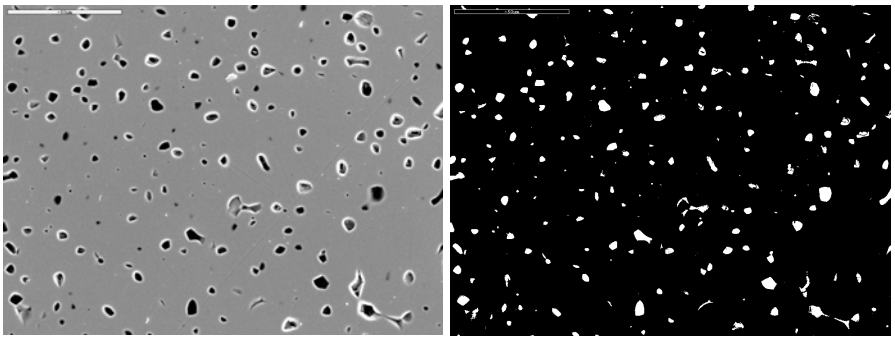

Original Image Processed image

Summer School on Micro- and nano- structural characterization of materials, focused on electron microscopy, July 11-15, 2012, Thessaloniki, Greece

Classification of pores according to their size

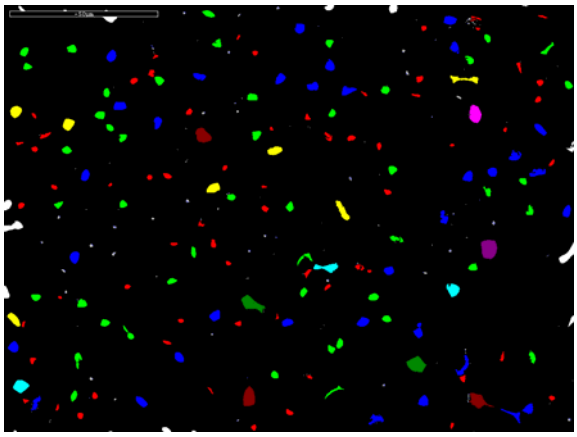

Class ID	From μm^2	To μm^2
1	1.0	4.1
2	4.1	7.2
3	7.2	10.3
4	10.3	13.4
5	13.4	16.5
6	16.5	19.6
7	19.6	22.7
8	22.7	25.8
9	25.8	28.9
10	28.9	32.0

Summer School on Micro- and nano- structural characterization of materials, focused on electron microscopy, July 11-15, 2012, Thessaloniki, Greece

Pore Size Distribution Results

Label ROI	ID Class	From μm^2	To μm^2	Particle Count #	Mean Area μm^2	Area Class μm^2	Area Fraction %	Mean Convex Perimeter μm	Mean Perimeter μm	Mean Shape Factor
Frame_Region				76	0.361	27.447	0.098	1.715	2.129	0.988
Frame_Region	1	1.0	4.1	66	2.430	160.41	0.573	6.069	6.577	0.730
Frame_Region	2	4.1	7.2	47	5.592	262.83	0.939	9.580	10.212	0.744
Frame_Region	3	7.2	10.3	34	8.872	301.64	1.077	12.247	13.244	0.709
Frame_Region	4	10.3	13.4	7	11.631	81.417	0.291	15.125	15.710	0.700
Frame_Region	5	13.4	16.5	3	14.703	44.108	0.158	16.699	18.031	0.622
Frame_Region	6	16.5	19.6	1	19.153	19.153	0.068	16.905	17.726	0.766
Frame_Region	7	19.6	22.7	3	20.731	62.193	0.222	19.298	19.895	0.712
Frame_Region	8	22.7	25.8	2	23.852	47.704	0.170	20.954	21.241	0.698
Frame_Region	9	25.8	28.9	0	0	0	0	0	0	0
Frame_Region	10	28.9	32.0	1	29.37	29.37	0.105	20.523	20.638	0.867

Summer School on Micro- and nano- structural characterization of materials, focused on electron microscopy, July 11-15, 2012, Thessaloniki, Greece

Pore Size Distribution Graphs

Number of pores vs class ID

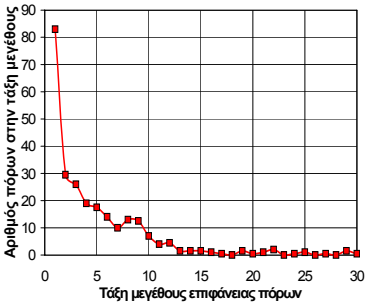

% of total pore surface vs class ID

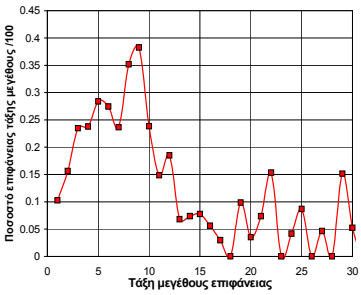

Summer School on Micro- and nano- structural characterization of materials, focused on electron microscopy, July 11-15, 2012, Thessaloniki, Greece

Study of the morphology of polycrystalline ceramics

Grain Size Distribution Determination

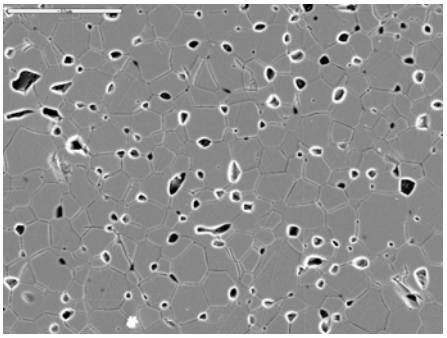

Original Image

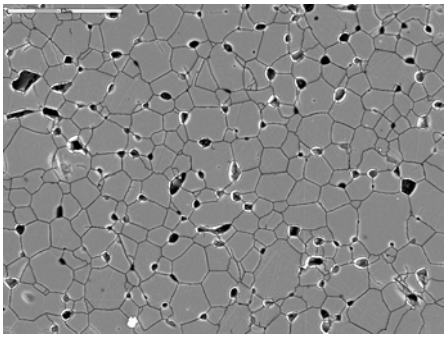

Processed image

Summer School on Micro- and nano- structural characterization of materials, focused on electron microscopy, July 11-15, 2012, Thessaloniki, Greece

Classification of grains according to their size

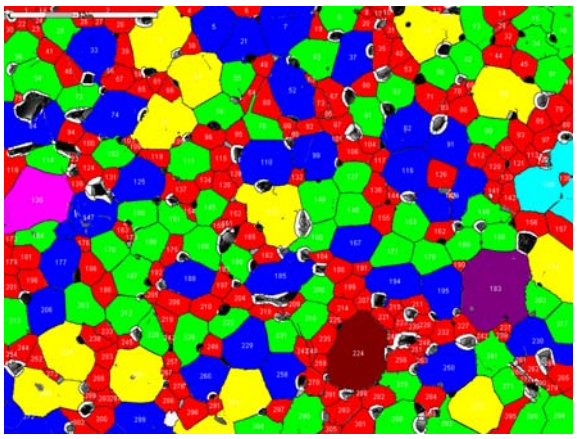

Class ID	From μm^2	To μm^2
1	1.0	40.9
2	40.9	80.9
3	80.9	120.8
4	120.8	160.7
5	160.7	200.7
6	200.7	240.6
7	240.6	280.5
8	280.5	320.5
9	320.5	360.4
10	360.4	400.3
11	400.3	440.3
12	440.3	480.2
13	480.2	520.1
14	520.1	560.1

Summer School on Micro- and nano- structural characterization of materials, focused on electron microscopy, July 11-15, 2012, Thessaloniki, Greece

Grain Size Distribution Results

Label ROI	ID Class	From μm^2	To μm^2	Particle Count	Mean Area μm^2	Area Class μm^2	Area Fraction %	Mean Convex Perimeter µm	Mean Perimeter µm	Mean Shape Factor
Frame_Region				0	0.00	0.0	0.00	0.00	0.00	0.00
Frame_Region	1	1.0	40.9	116	19.41	2251.5	8.04	18.53	20.59	0.55
Frame_Region	2	40.9	80.9	82	57.60	4723.2	16.87	32.44	35.95	0.60
Frame_Region	3	80.9	120.8	46	101.28	4658.8	16.64	42.51	49.06	0.56
Frame_Region	4	120.8	160.7	15	138.83	2082.5	7.44	49.17	57.12	0.56
Frame_Region	5	160.7	200.7	18	178.59	3214.6	11.48	56.40	64.45	0.59
Frame_Region	6	200.7	240.6	12	220.61	2647.3	9.46	62.82	84.51	0.46
Frame_Region	7	240.6	280.5	8	259.95	2079.6	7.43	66.47	80.00	0.53
Frame_Region	8	280.5	320.5	4	305.53	1222.1	4.37	77.90	100.60	0.41
Frame_Region	9	320.5	360.4	1	330.97	331.0	1.18	85.15	139.90	0.21
Frame_Region	10	360.4	400.3	1	372.55	372.6	1.33	81.00	107.59	0.40
Frame_Region	11	400.3	440.3	1	413.92	413.9	1.48	81.29	94.91	0.58
Frame_Region	12	440.3	480.2	0	0.00	0.0	0.00	0.00	0.00	0.00
Frame_Region	13	480.2	520.1	0	0.00	0.0	0.00	0.00	0.00	0.00
Frame_Region	14	520.1	560.1	1	523.75	523.7	1.87	90.29	111.36	0.53
Frame_Region	15	560.1	600.0	0	0.00	0.0	0.00	0.00	0.00	0.00

Summer School on Micro- and nano- structural characterization of materials, focused on electron microscopy, July 11-15, 2012, Thessaloniki, Greece

Grain Size Distribution Graphs

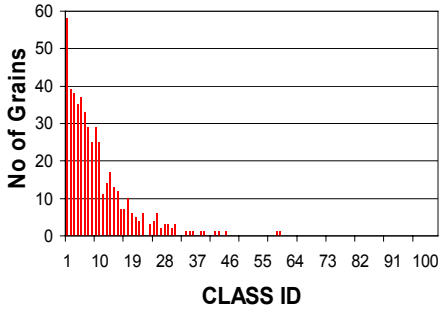

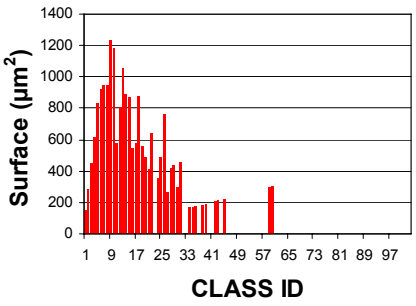

Summer School on Micro- and nano- structural characterization of materials, focused on electron microscopy, July 11-15, 2012, Thessaloniki, Greece

Magnetic Losses as a function of the mean grain size of the material, derided by SEM

Summer School on Micro- and nano- structural characterization of materials, focused on electron microscopy, July 11-15, 2012, Thessaloniki, Greece

Particle Size Distribution of catalytically active metal supported on γ-alumina carrier

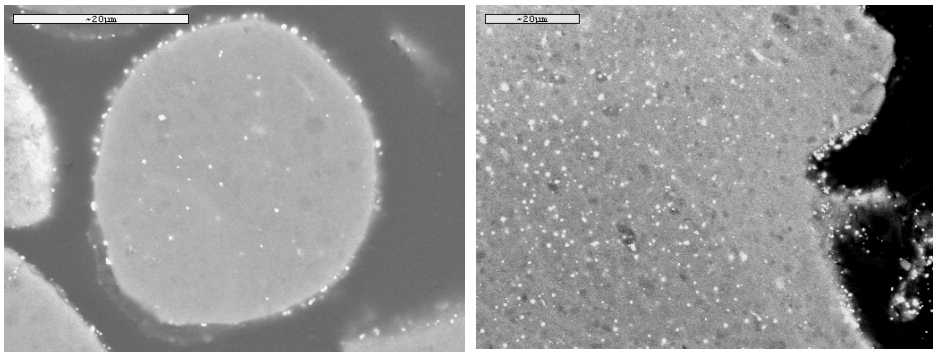

Summer School on Micro- and nano- structural characterization of materials, focused on electron microscopy, July 11-15, 2012, Thessaloniki, Greece

SE Image Processing with special software for the determination of the particle size distribution

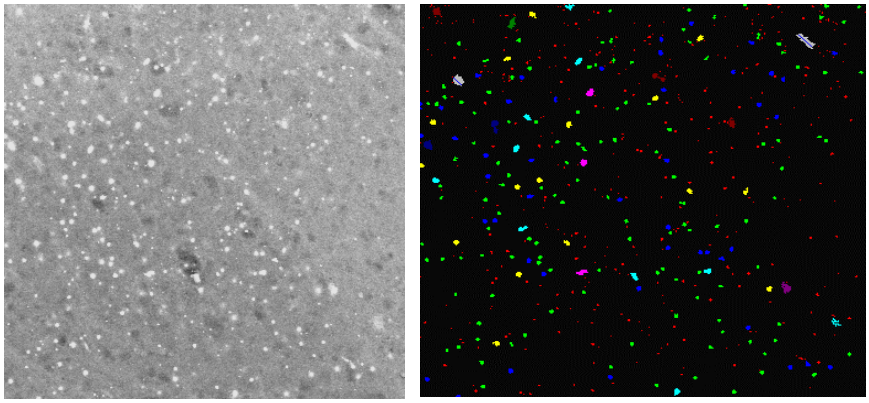

Summer School on Micro- and nano- structural characterization of materials, focused on electron microscopy, July 11-15, 2012, Thessaloniki, Greece

Particle Size Distribution of active metal, as determined by SEM Image processing

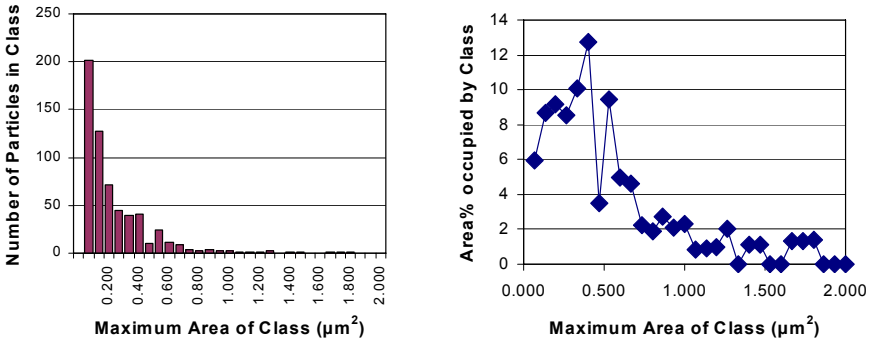

Summer School on Micro- and nano- structural characterization of materials, focused on electron microscopy, July 11-15, 2012, Thessaloniki, Greece

PORE STRUCTURE CHARACTERIZATION AND PHYSICAL PROPERTIES ESTIMATION OF POROUS MATERIALS WITH STOCHASTIC RECONSTRACTION OF SCANNING ELECTRON MICROSCOPE IMAGES

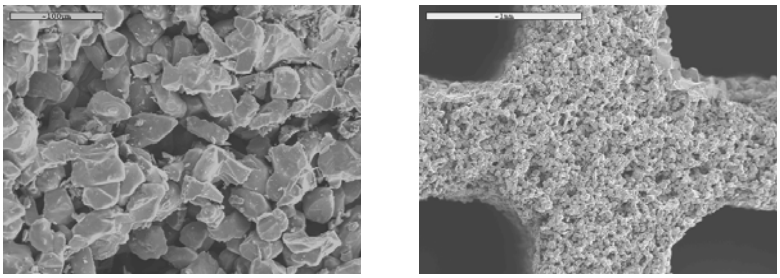

Summer School on Micro- and nano- structural characterization of materials, focused on electron microscopy, July 11-15, 2012, Thessaloniki, Greece

In order to obtain suitable SEM images the samples are embedded in epoxy resin and treated under conditions that allow for the resin to penetrate into the pores.
After grinding and polishing the surface of the samples becomes flat and smooth.

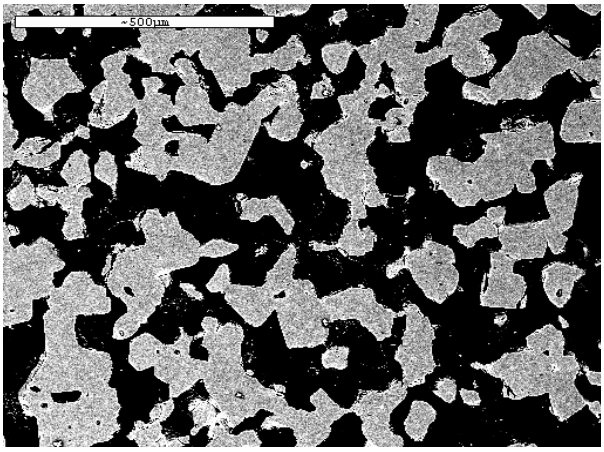

Backscattered electron images are obtained where the dark areas represent the pores while the light areas represent the solid particles

Summer School on Micro- and nano- structural characterization of materials, focused on electron microscopy, July 11-15, 2012, Thessaloniki, Greece

Accordingly, a thresholding technique is applied on the grayscale images to obtain digitized binary images with values 1,0, representing the void and solid phase of the material, respectively.

Black is SiC – White is void (pore)

SEM Image after thresholding and binary transformation

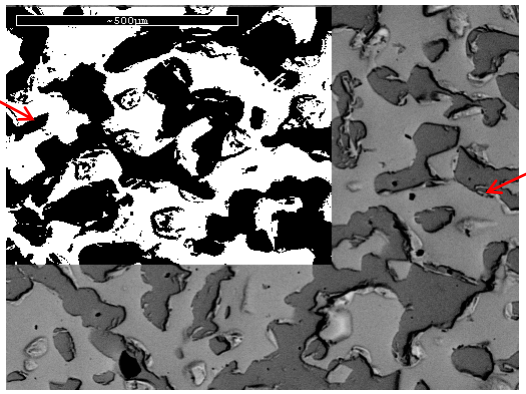

Raw SEM Image

Summer School on Micro- and nano- structural characterization of materials, focused on electron microscopy, July 11-15, 2012, Thessaloniki, Greece

The porosity and the autocorrelation function of the material are then calculated on the digitized domains and these properties are averaged over 5-10 images.

✓Porosity Determination

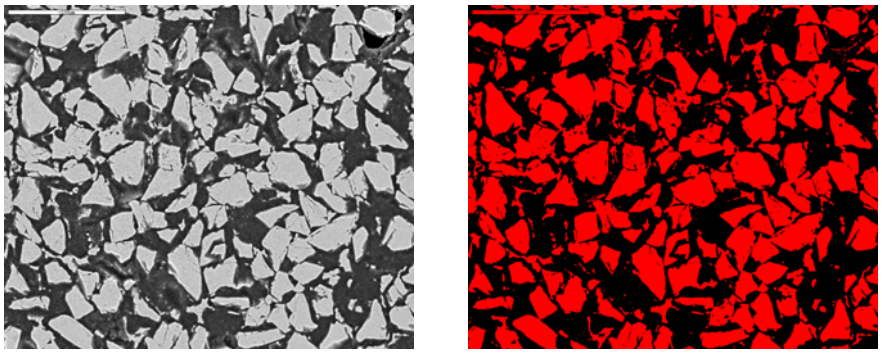

Area Phase 1 : 49.27%

Summer School on Micro- and nano- structural characterization of materials, focused on electron microscopy, July 11-15, 2012, Thessaloniki, Greece

Autocorrelation function determination

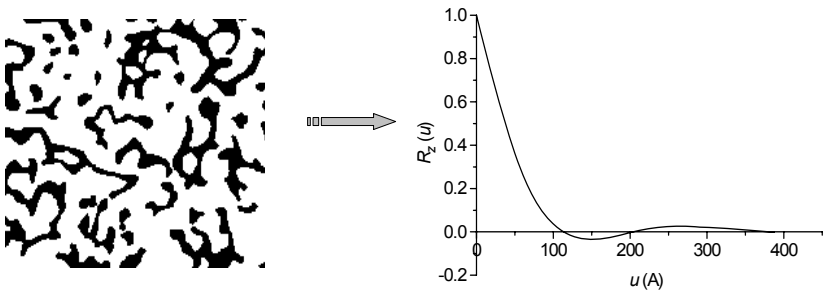

The 2-point autocorrelation function expresses the relative probability that 2 different points with distance r belong to the same phase of the material (solid or void). It is calculated based on image processed SEM data.

Summer School on Micro- and nano- structural characterization of materials, focused on electron microscopy, July 11-15, 2012, Thessaloniki, Greece

Stochastic Reconstruction

3-dimensional reconstruction processes are employed to match the structural properties obtained on the SEM images assuming structural homogeneity and isotropy.

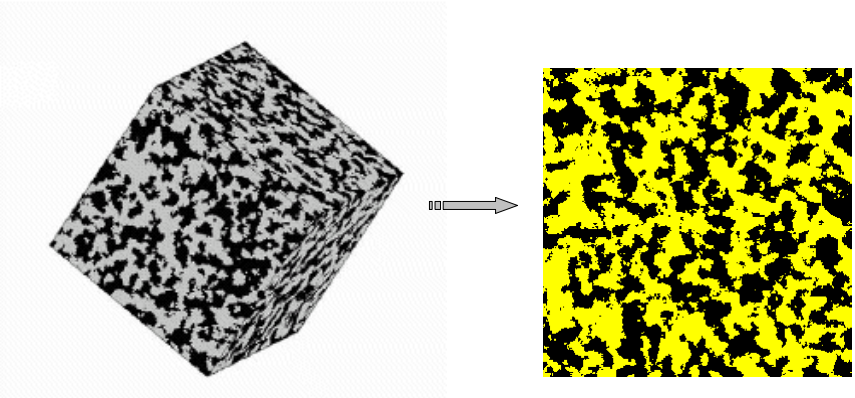

Summer School on Micro- and nano- structural characterization of materials, focused on electron microscopy, July 11-15, 2012, Thessaloniki, Greece

Stochastic reconstruction

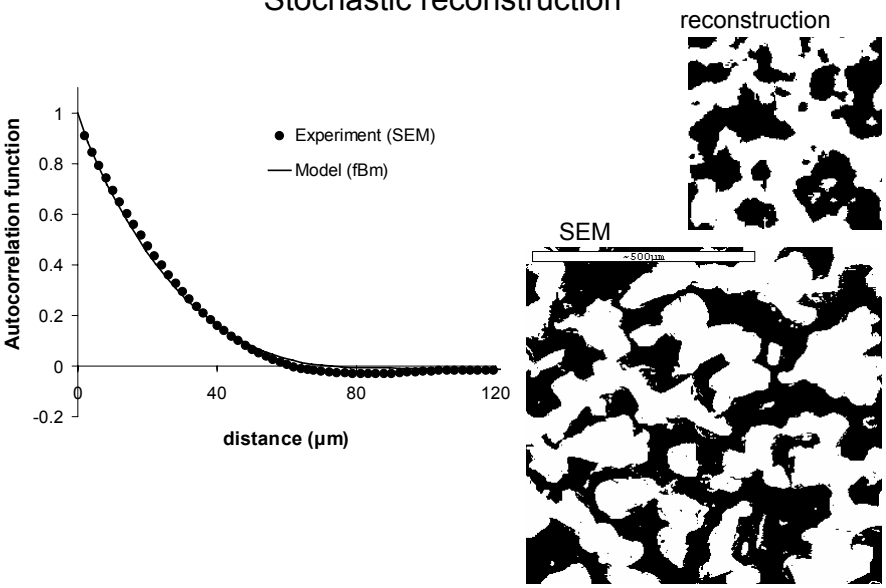

Summer School on Micro- and nano- structural characterization of materials, focused on electron microscopy, July 11-15, 2012, Thessaloniki, Greece


Thank you for your attention
Summer School on Micro- and nano- structural characterization of materials, focused on electron microscopy, July 11-15, 2012, Thessaloniki, Greece

SCANNING TUNNELING MICROSCOPY (STM), ATOMIC FORCE MICROSCOPY (AFM) : PRINCIPLES AND APPLICATIONS

N. Frangis

Solid State Physics Section,
Department of Physics, Aristotle University of Thessaloniki,
GR-54124 Thessaloniki, Greece

Summer School on Micro- and Nano-structural characterization of materials
July 11-15, 2012, Thessaloniki, Greece

HISTORY

1982: Scanning Tunneling Microscope (STM) with atomic resolution, by Binning and Rohrer.

1986: Atomic Force Microscope (AFM) or Scanning Force Microscope (SFM) with atomic resolution, by Binning, Quate and Gerber.

Advantage of AFM: it can work for both conductive and non-conductive samples.

Today: A few decades modifications of STM and AFM, under the name Scanning Probe Microscopy (SPM)

Ernst Ruska

Gerd Binnig

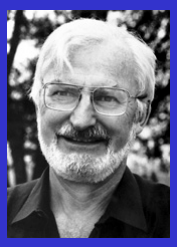

Heinrich Rohrer

The Nobel Prize in Physics 1986 was divided, one half awarded to Ernst Ruska *"for his fundamental work in electron optics, and for the design of the first electron microscope"*, the other half jointly to Gerd Binnig and Heinrich Rohrer *"for their design of the scanning tunneling microscope"*.

SPM: tip–sample interaction

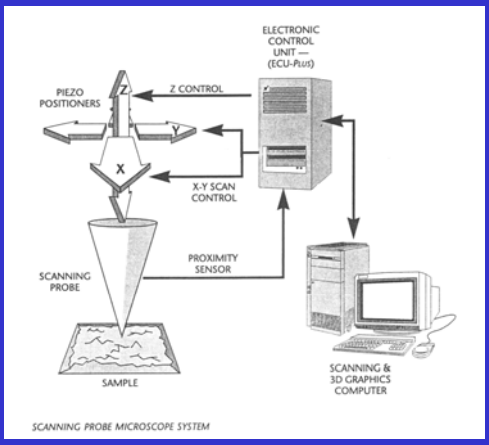

In each "point", measure of a "local" physical quantity related with the interaction: in STM the tunneling current, in AFM the cantilever deflection, due to attractive or repulsive force.

All the data are transferred to a PC, where, with the use of the appropriate software, an image of the surface is created.
Image: from simple topography and roughness down to atomic resolution

STM

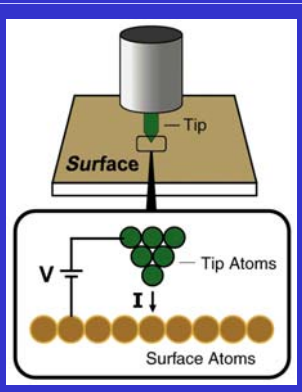

$I \sim (V/d)\exp(-A\Phi^{1/2}d)$

AFM

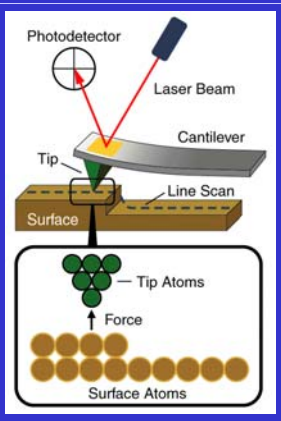

Hooke's law connects the applied force with the cantilever deflection : F= -kd

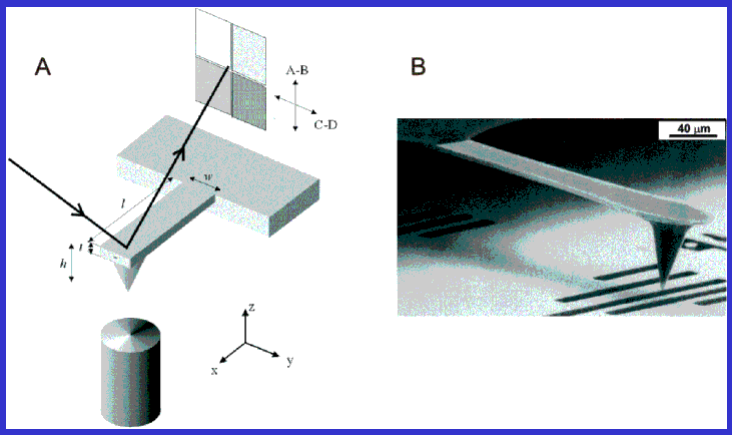

The scanner

Piezocrystals: expand or contract in the presence of voltage gradient and create a voltage gradient when forced to expand or contract

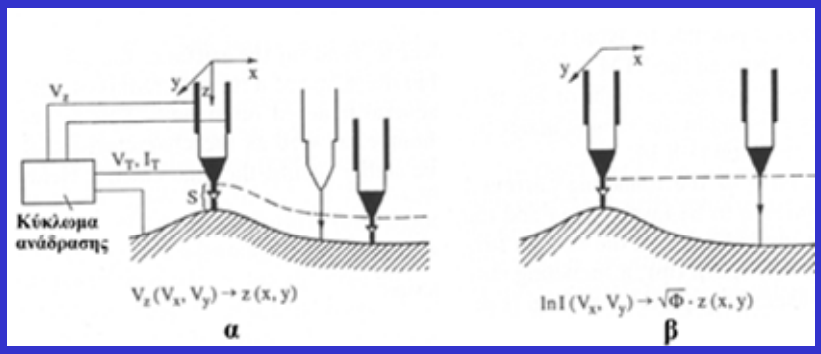

SPMs work in air or under high vacuum

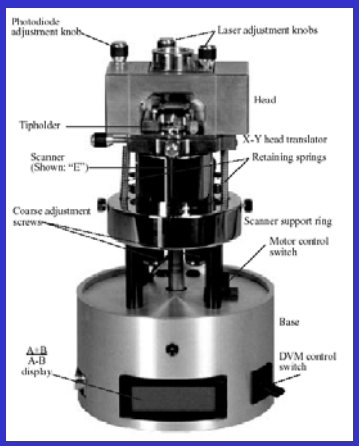

The tip of the STM is used:

- for imaging
- as a nanoscale tool, i.e. for atom manipulation, for bending, cutting and extracting soft materials at the submicron scale under high-resolution image control

Si (111) 7X7 surface as seen by STM

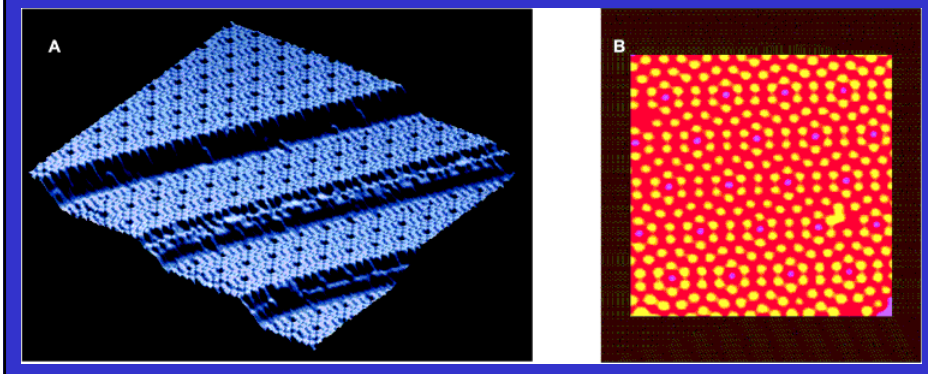

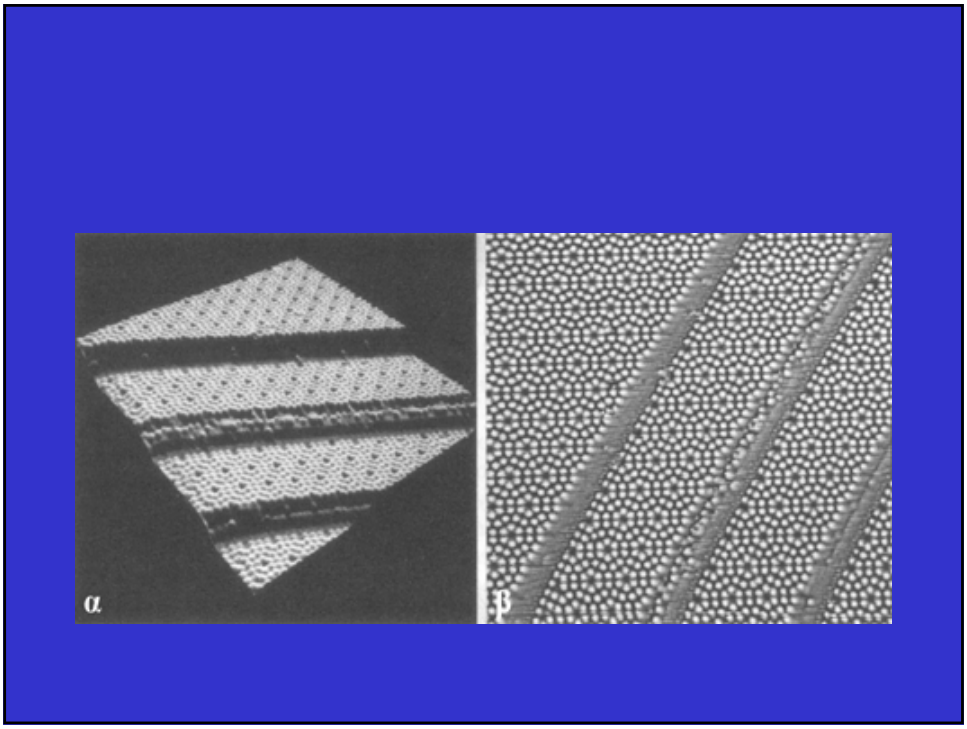

Atom manipulation by STM

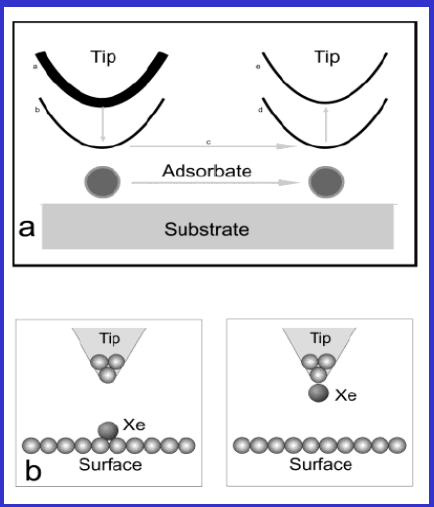

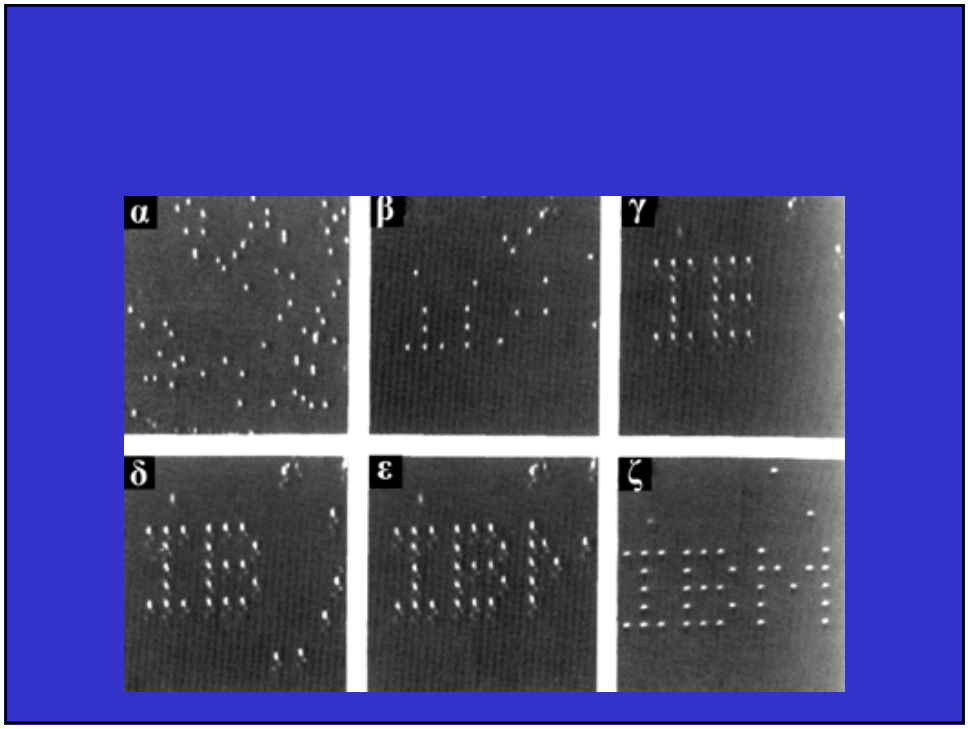
α
β
γ
δ
ε
ζ

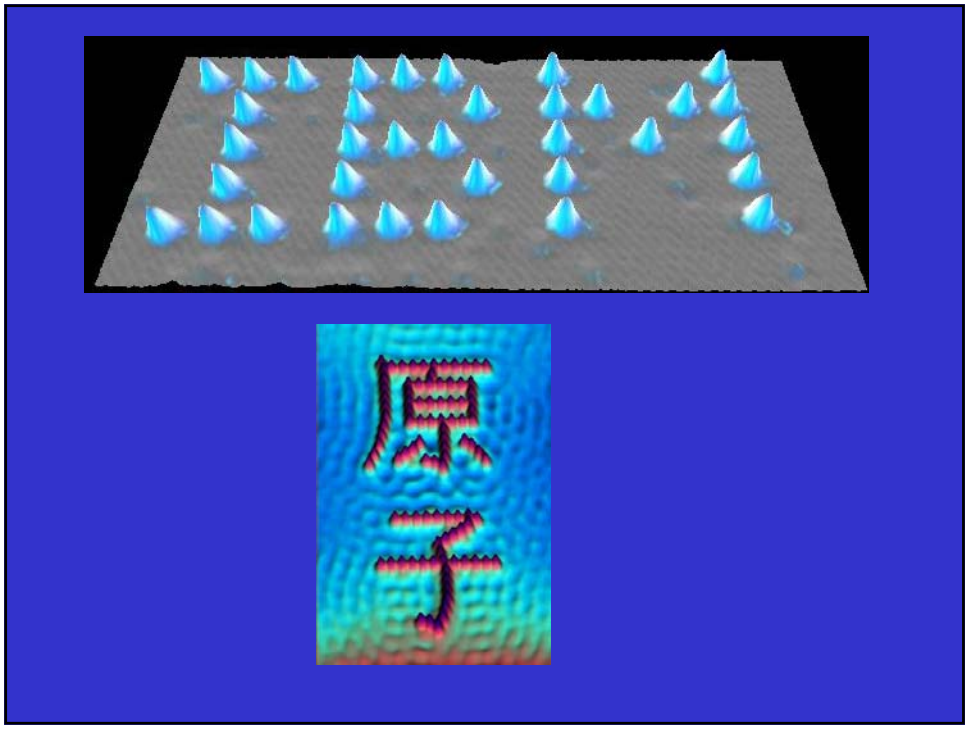


Quantum
Corrals
Fe/Cu(111)
M.F. Crommie, C.P. Lutz, D.M. Eigler
Science 262 (1993) 218

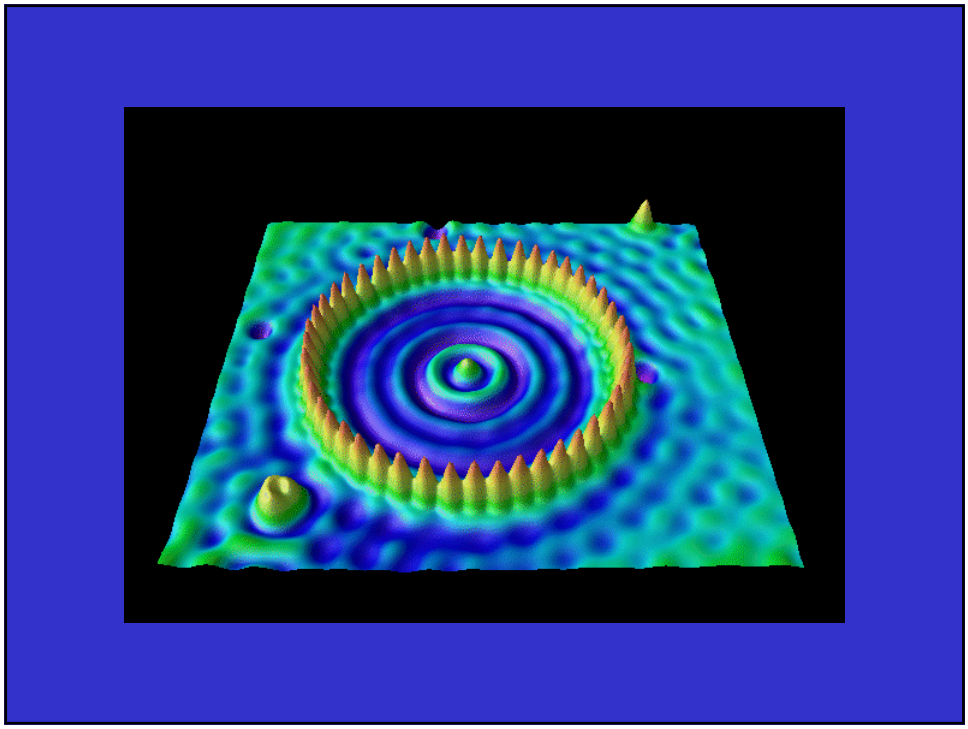

Atomic Scale Bond Breaking & Nanochemistry

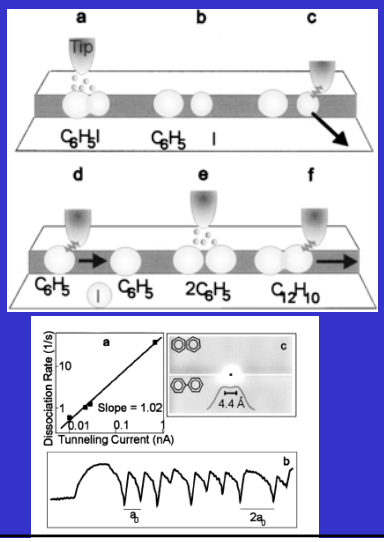

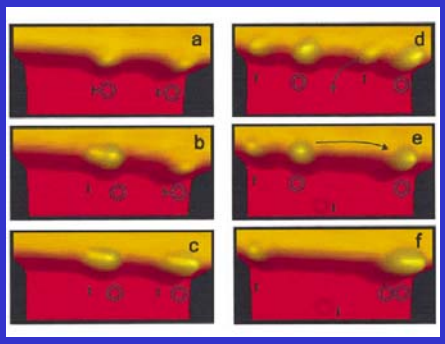

(a →e) $C_6H_5I \rightarrow C_6H_5 + I$,

(f) $2C_6H_5 \rightarrow C_{12}H_{10}$

S.-W. Hla, L. Bartels, G. Meyer, &
Karl-Heinz Rieder, PRL 85(2000)2777

SCANNING TUNNELING SPECTROSCOPY-STS

Al on Si

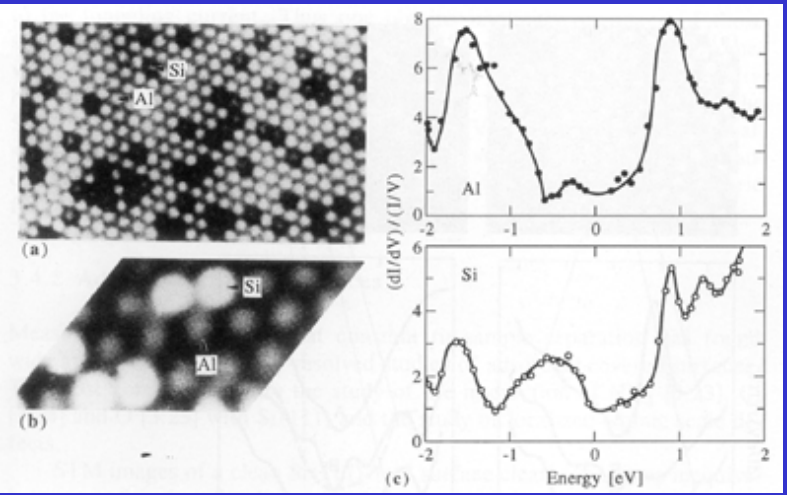

AFM

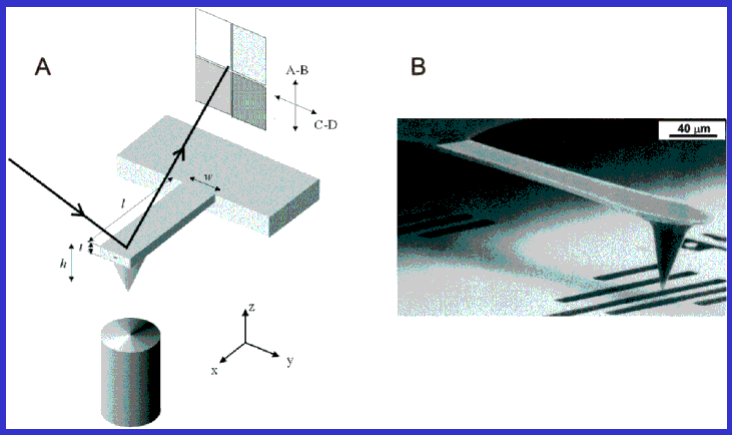

The scanner

Piezocrystals: expand or contract in the presence of voltage gradient and create a voltage gradient when forced to expand or contract

The scanned cantilever/tip system

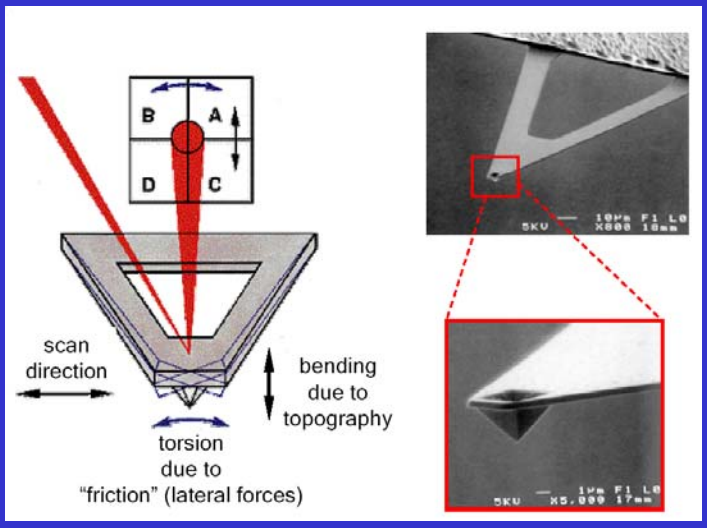

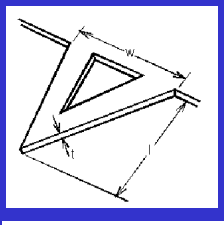

Cantilevers sizes range:
from 100 to 200µm in length (l),
10 to 40 µm in width (w), and
0.3 to 2µm in thickness (t)

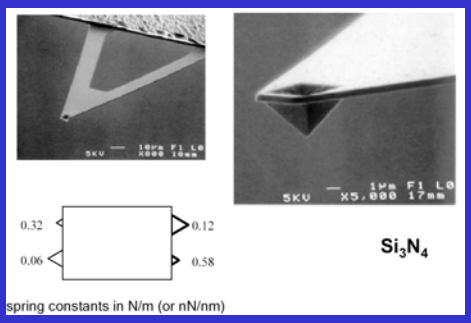

Integrated cantilevers are usually made from silicon or silicon nitride.
Carbon nanotubes are also used.

Forces

Pauli exclusion principle forces.
Van der Waals forces.

The Lenard-Jones potential: $V(r)=(C_{12}/r)^{12}- (C_6/r)^6$

The potential is attractive when they are far apart (non-contact), but it will become strongly repulsive when they are close together (contact).

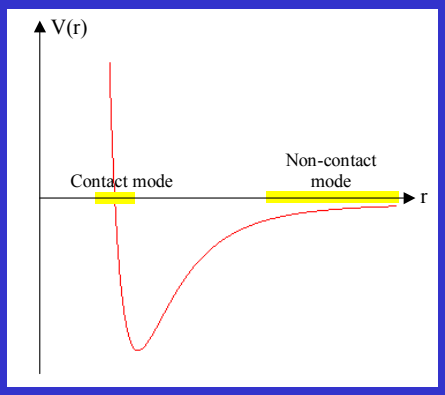

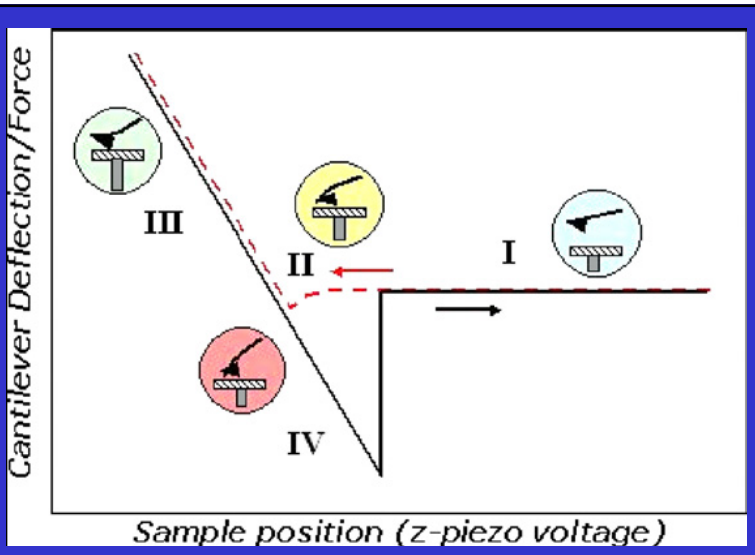

Scheme of a force curve with the different regions of the approach and withdrawal portions highlighted.

$$F = -kd$$

The tip of the AFM is used:

- for imaging
- for measuring forces (and mechanical properties) at the nanoscale
- as a nanoscale tool, i.e. for bending, cutting and extracting soft materials (such as polymers, DNA, and nanotubes), at the submicron scale under high-resolution image control

Imaging modes:
Contact mode
Non contact mode
Tapping mode (intermittent contact mode)

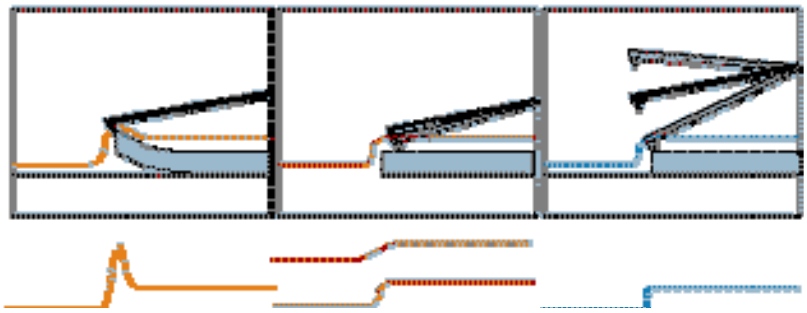

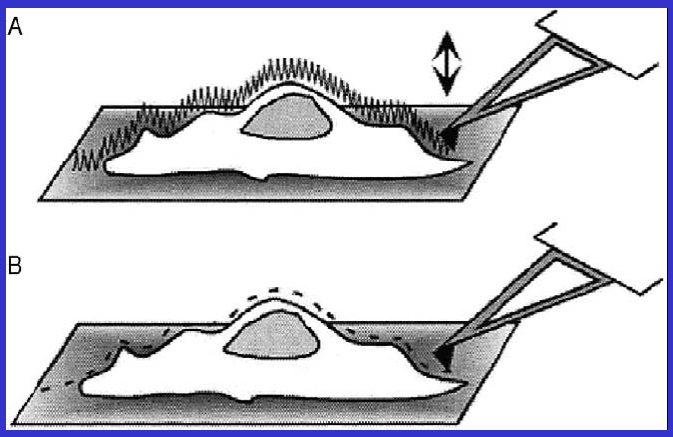

AFM imaging modes.
(A) Intermittent contact mode. The tip oscillates at each "point" of the sample.
(B) Contact mode

Imaging environment:
Air
Vacuum
Liquid

operation mode	Contact mode	Non-contact mode	Tapping mode
tip loading force	low → high	low	low
contact with sample surface	yes	no	periodical
manipulation of sample	yes	no	yes
contamination of AFM tip	yes	no	yes
microdissection	yes	no	no

x,y resolution:
0.1 nm for hard and flat surfaces
0.7-5 nm for soft materials (polymers and biological samples)

z resolution: 0.01 nm

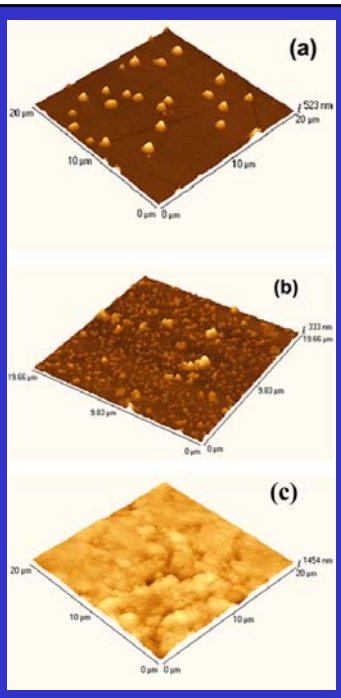

Three-dimensional AFM images from three different types of Pd samples, grown on 6H-SiC.

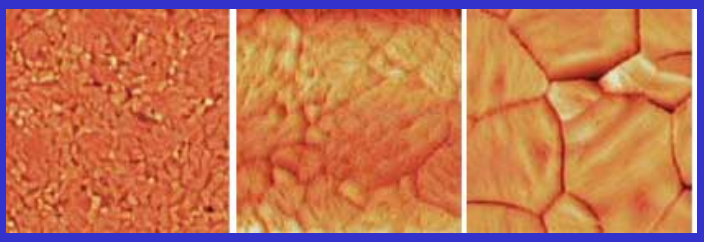

Tapping Mode AFM of Aluminum grains.

Field of view 5 µm x 5 µm
Images of aluminum grains grown at different temperatures.
TappingMode allows to use the same probe for each sample without tip damage that would introduce artifacts

From Veeco site

Field of view 10µm & 5µm

Non contact AFM images of titanium nitride grains

From Veeco site

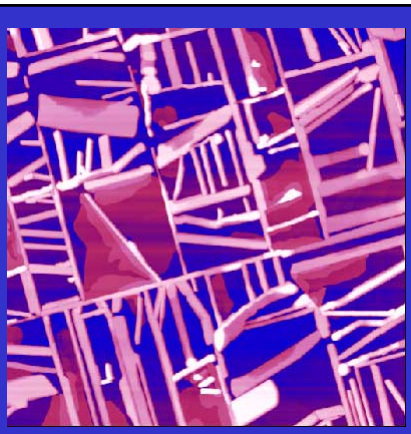

AFM topography image of highly ordered thin film of organic semiconductor para-sexiphenyl grown by Hot Wall Epitaxy on crystalline KCl substrate. 5μm scan imaged in TappingMode

From Veeco site

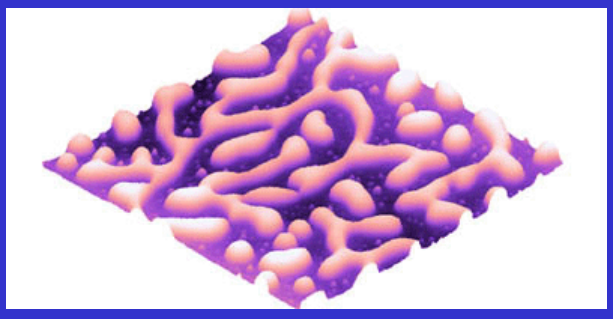

TappingMode AFM image of poly(styrene) and poly(methyl methacrylate) blend polymer film. The surface structure is resulted from the spinodal decomposition.

From Veeco site

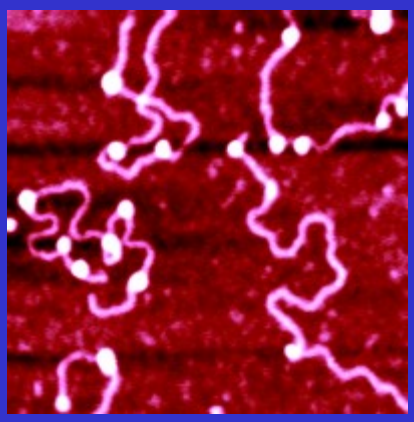

TappingMode image of nucleosomal DNA

From Veeco site

Atomic resolution AFM images of graphite

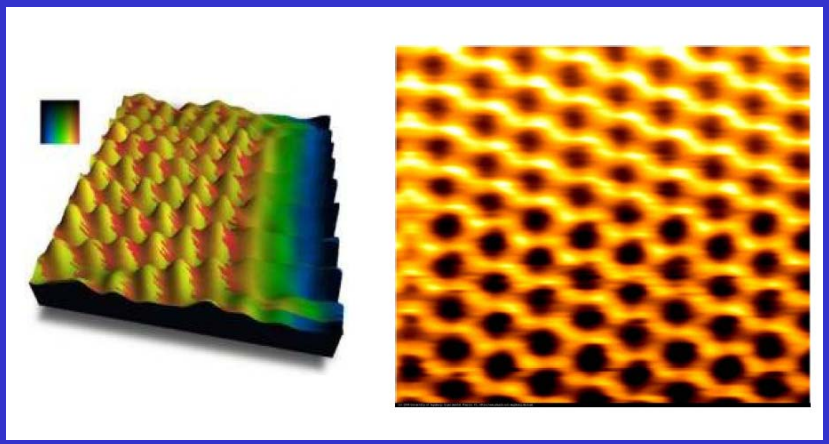

NC-AFM images of **Sn**/**Si**(111)-(√3×√3) surfaces

Sn:50% Si:50% **Sn:75% Si:25%** **Sn:99% Si:1%**

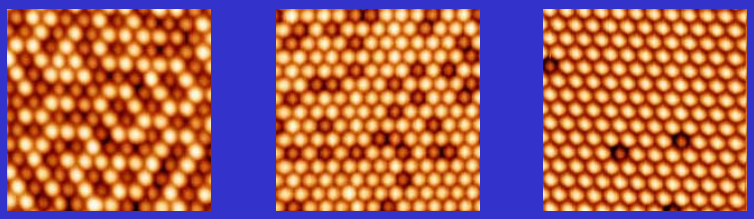

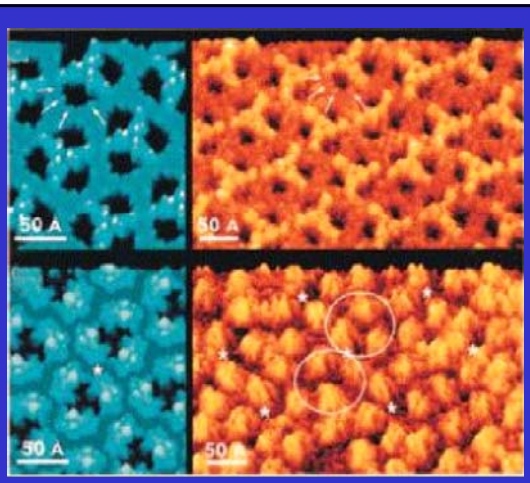

Conformational changes of porin OmpF. (*a*) The atomic model of the periplasmic surface rendered at 0.3 nm resolution (left) exhibits features which are recognized in the topograph (right). (*b*) The extracellular surface of OmpF. Atomic model (left), and topograph (right).

Nanomanipulation

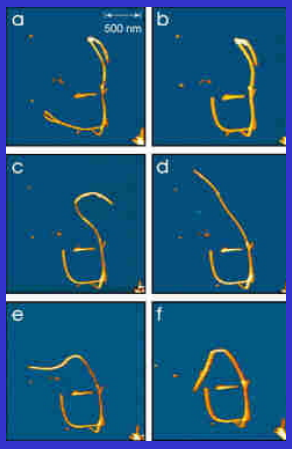

A nanotube can be manipulated to form complex shapes: the 6 frames are a series of AFM images of a nanotube on a silicon substrate.The AFM tip is used to create the Greek letter "theta" from a 2.5 micron long nanotube.

From IBM research site

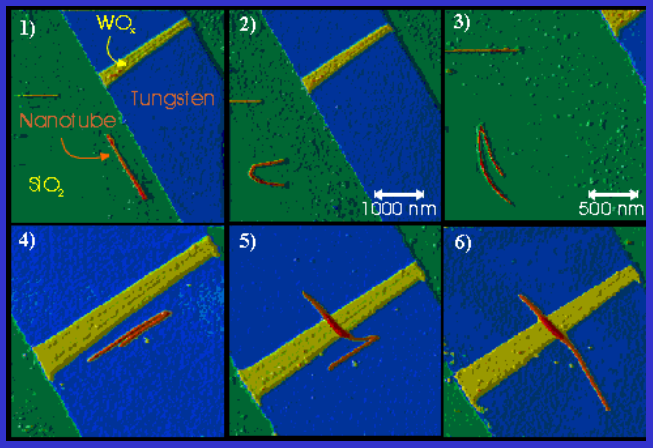

A single nanotube (in red) originally on an insulating substrate (SiO_2, shown in green) is manipulated in a number of steps onto a tungsten film thin wire (in blue), and finally is streched across an insulating tungsten oxide barrier (in yellow).

From IBM research site


Thank you for your attention!

New techniques for nanocrystal structure determination by precession electron diffraction

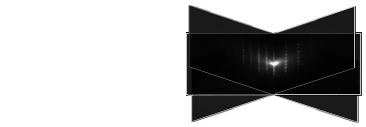

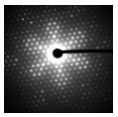

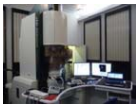

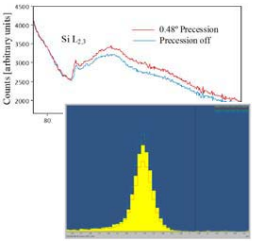

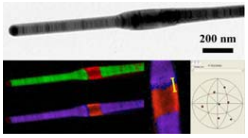

Dr. Stavros Nicolopoulos
Consultant IUCr Electron Crystallography Comission

NanoMEGAS
Advanced Tools for electron diffraction

www.nanomegas.com

X-ray Crystallography

X-ray crystallography is the science of determining the arrangement of atoms within a crystal from the manner in which a beam of X-rays is scattered from the electrons within the crystal. The method produces a three-dimensional picture of the density of electrons within the crystal, from which the mean atomic positions, their chemical bonds, their disorder and sundry other information can be derived.

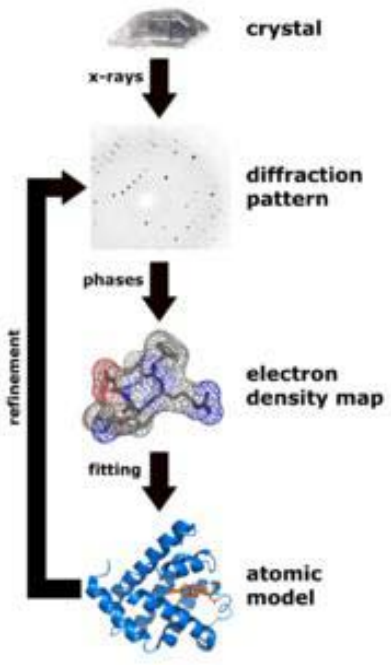

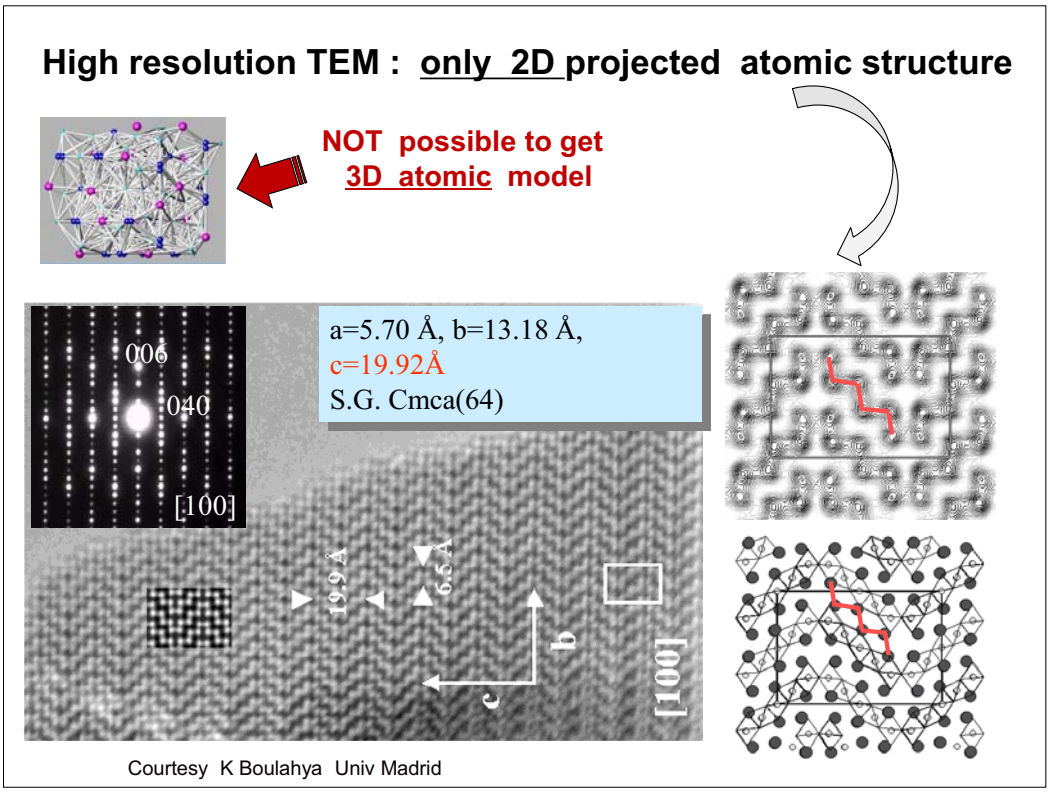
High resolution TEM : only 2D projected atomic structure
NOT possible to get
3D atomic model
006
040
[100]
a=5.70 Å, b=13.18 Å,
c=19.92Å
S.G. Cmca(64)
19.9 Å
6.5 Å
b
c
[001]
Courtesy K Boulahya Univ Madrid

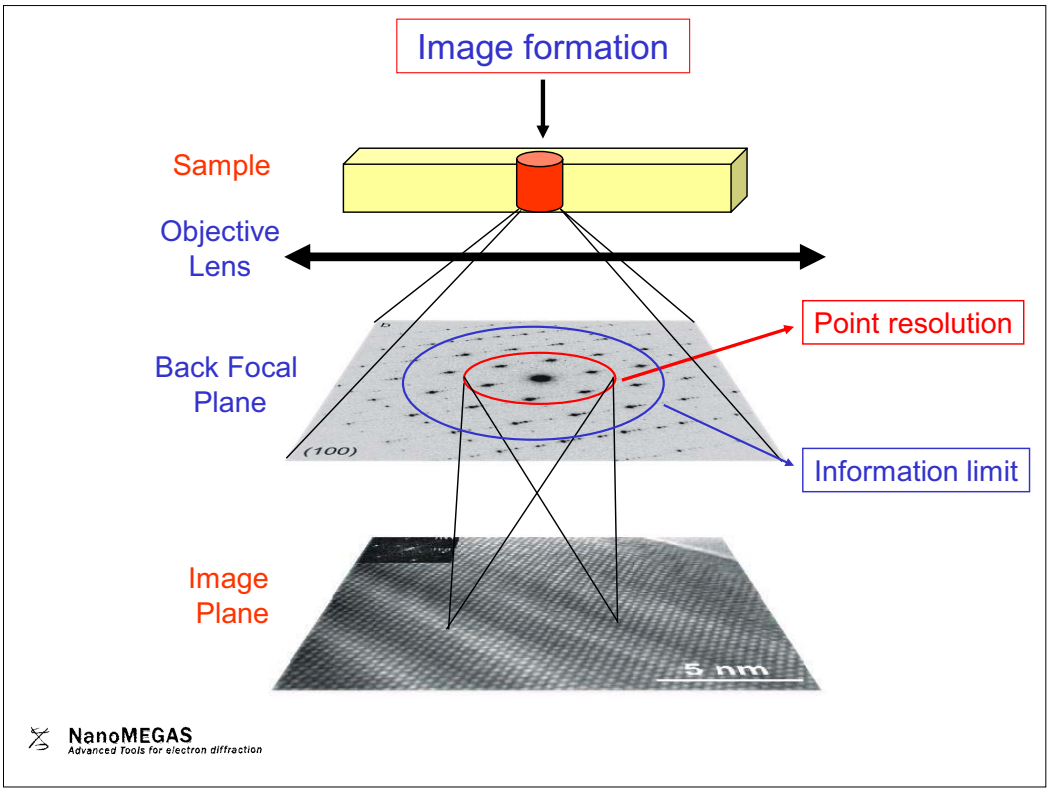
Image formation
Sample
Objective
Lens
Back Focal
Plane
Point resolution
(100)
Information limit
Image
Plane
5 nm
NanoMEGAS
Advanced Tools for electron diffraction

Characterization

for new unknown compound

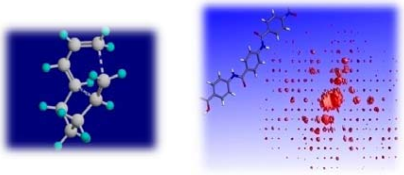

Find crystal cell parameters

Find crystal symmetry and atomic structure

NanoMEGAS
Advanced Tools for electron diffraction

Find crystal cell parameters

TEM : manual tilt series acquisition

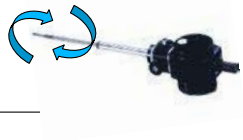

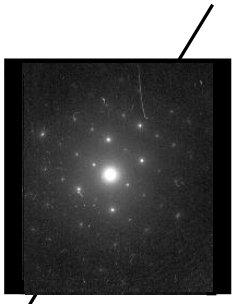

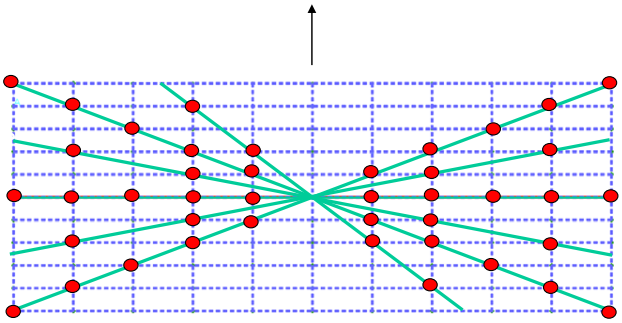

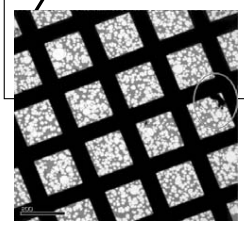

Problem : "missing cone" = lost data

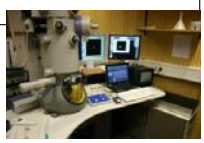

Courtesy : Prof. U Kolb UMainz

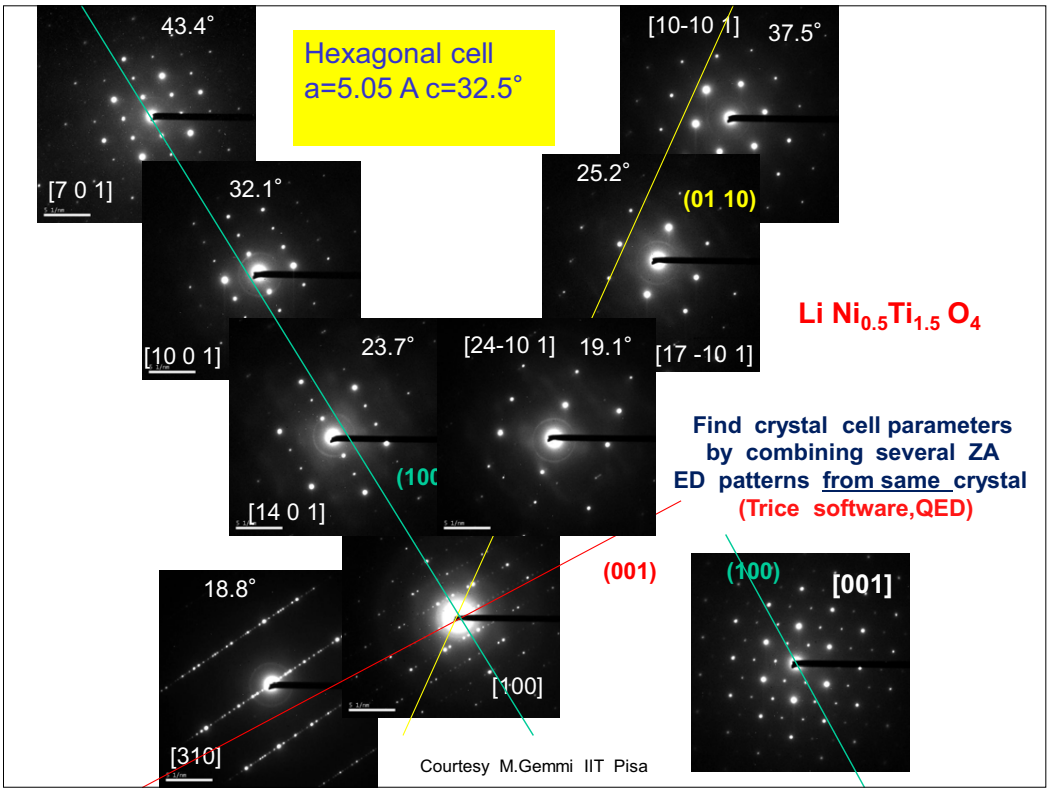
43.4°
Hexagonal cell
a=5.05 A c=32.5°
[10-10 1]
37.5°
[7 0 1]
32.1°
25.2°
(01 10)
Li Ni0.5Ti1.5 O4
[10 0 1]
23.7°
[24-10 1]
19.1°
[17 -10 1]
Find crystal cell parameters
by combining several ZA
ED patterns from same crystal
(Trice software,QED)
[14 0 1]
(001)
(100)
[001]
18.8°
[100]
[310]
Courtesy M.Gemmi IIT Pisa

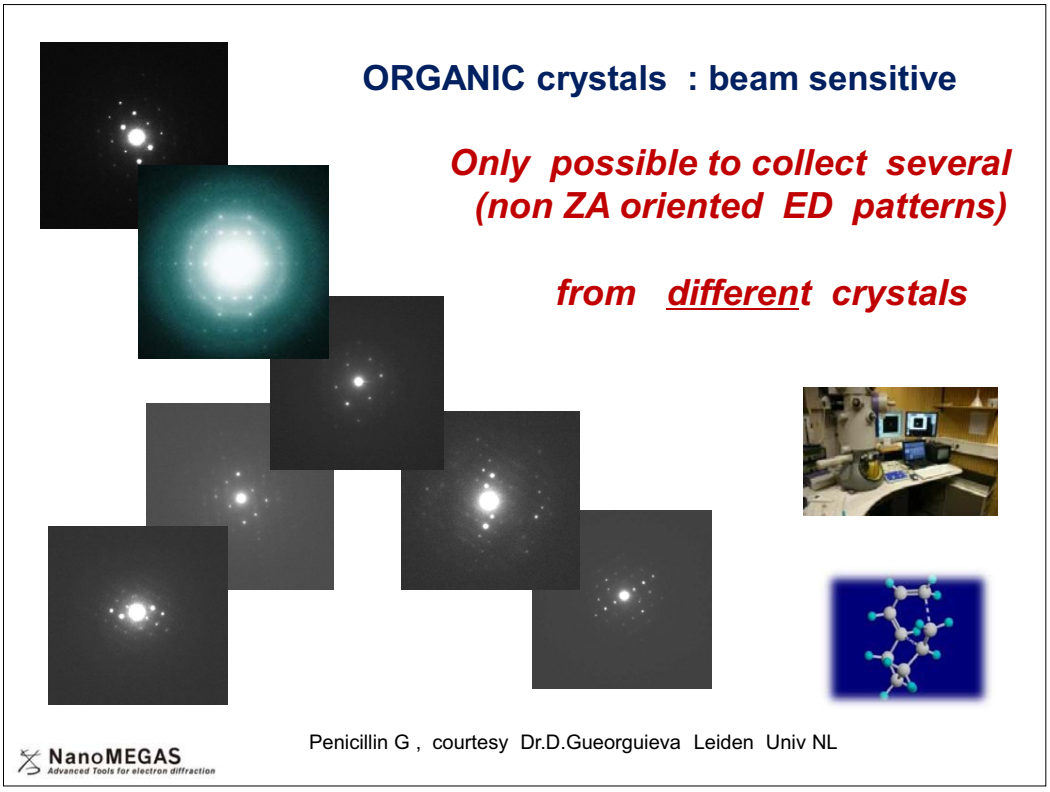
ORGANIC crystals : beam sensitive
Only possible to collect several
(non ZA oriented ED patterns)
from different crystals
Penicillin G , courtesy Dr.D.Gueorguieva Leiden Univ NL
NanoMEGAS
Advanced Tools for electron diffraction

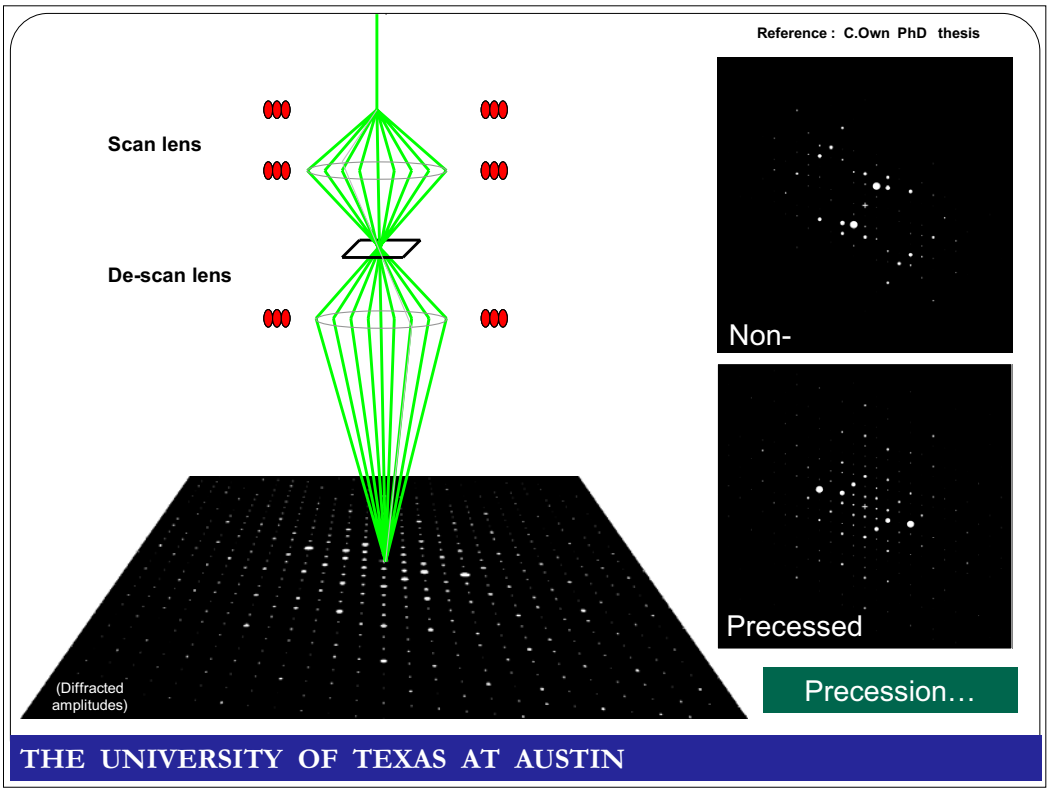
Reference : C.Own PhD thesis
Scan lens
De-scan lens
(Diffracted amplitudes)
Non-
Precessed
Precession…
THE UNIVERSITY OF TEXAS AT AUSTIN

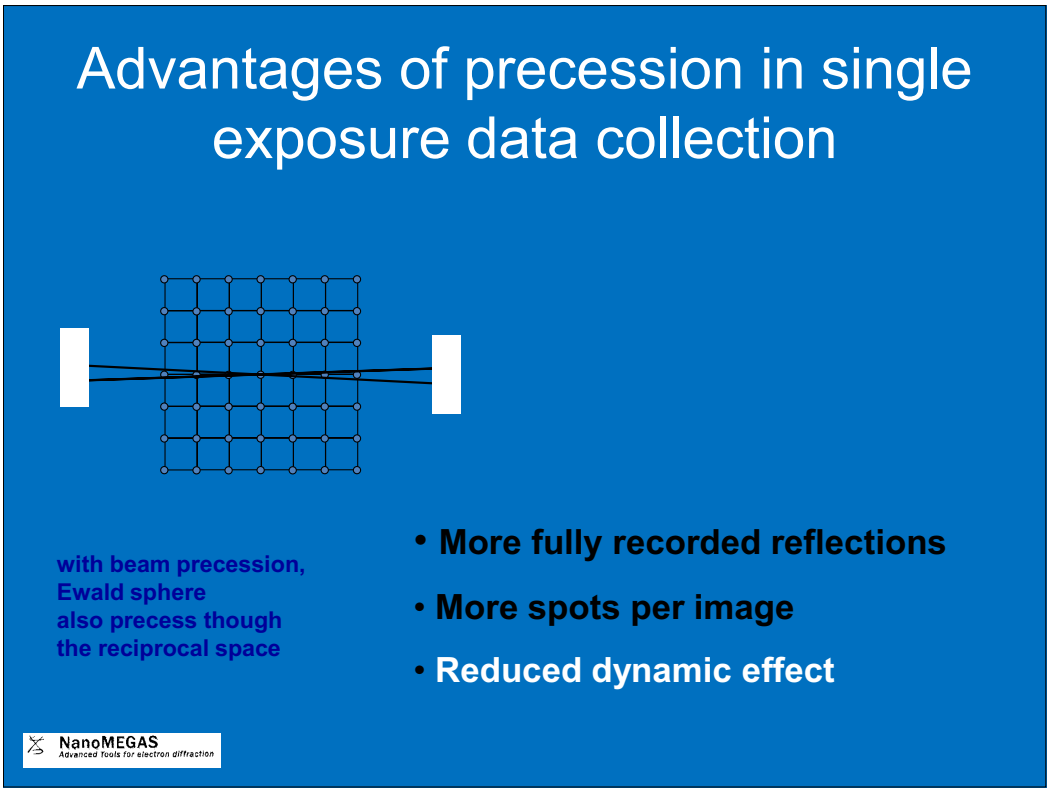
Advantages of precession in single exposure data collection
with beam precession, Ewald sphere also precess though the reciprocal space
• More fully recorded reflections
• More spots per image
• Reduced dynamic effect
NanoMEGAS
Advanced Tools for electron diffraction

DigiStar Digital precession unit

With "DigiSTAR" is possible to visualize directly and rapidly modify precession angle using (memory saved) TEM alignements

NanoMEGAS
Advanced Tools for electron diffraction

DigiSTAR : Precession Microscopy for advanced TEM

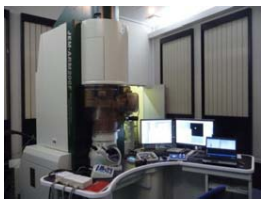

JEOL microscopes

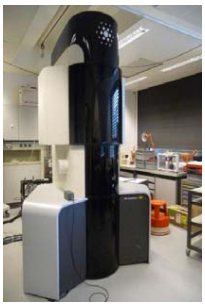

Zeiss microscopes

FEI microscopes

NanoMEGAS
Advanced Tools for electron diffraction

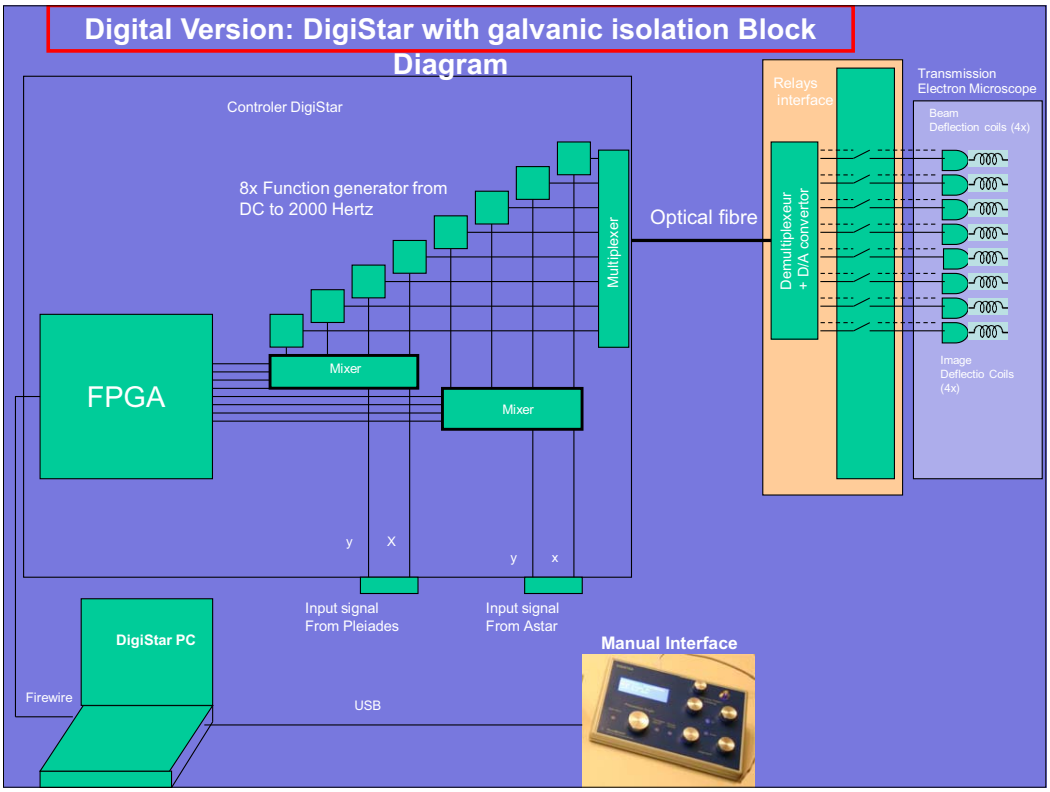
Digital Version: DigiStar with galvanic isolation Block Diagram
Controler DigiStar
8x Function generator from DC to 2000 Hertz
Multiplexer
Optical fibre
Relays interface
Demultiplexeur + D/A convertor
Transmission Electron Microscope
Beam Deflection coils (4x)
Image Deflectio Coils (4x)
FPGA
Mixer
Mixer
y
X
y
x
Input signal From Pleiades
Input signal From Astar
DigiStar PC
Firewire
USB
Manual Interface

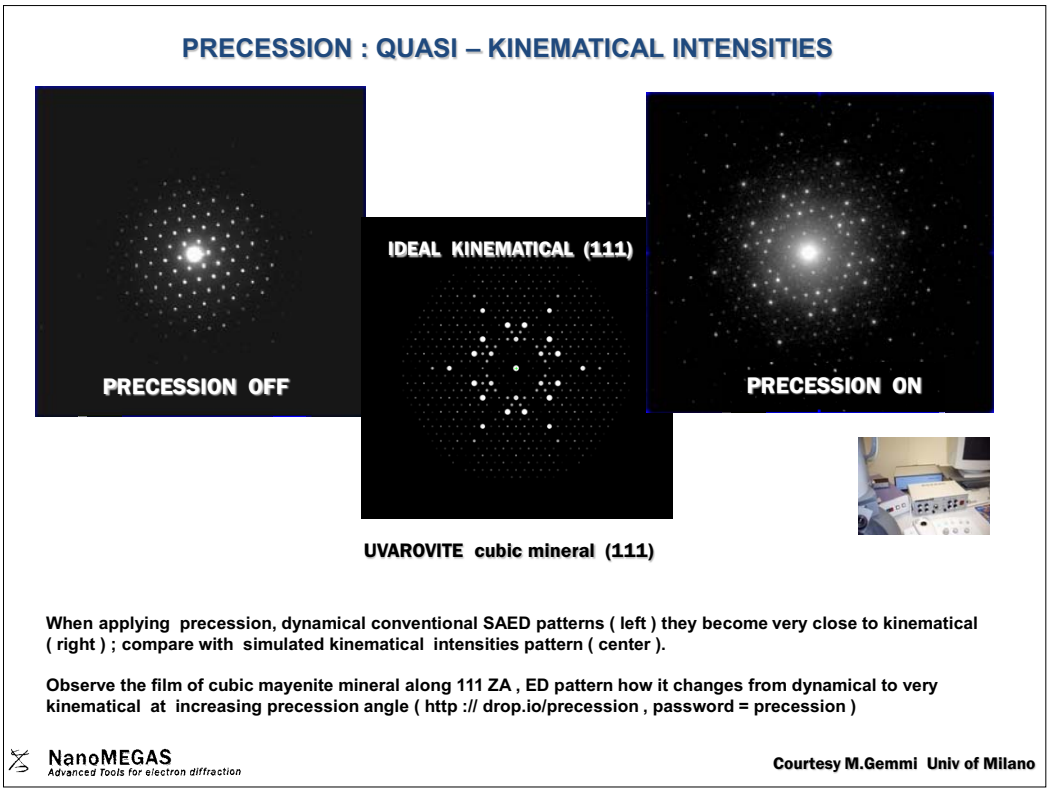
PRECESSION : QUASI – KINEMATICAL INTENSITIES
PRECESSION OFF
IDEAL KINEMATICAL (111)
PRECESSION ON
UVAROVITE cubic mineral (111)
When applying precession, dynamical conventional SAED patterns (left) they become very close to kinematical (right) ; compare with simulated kinematical intensities pattern (center).
Observe the film of cubic mayenite mineral along 111 ZA , ED pattern how it changes from dynamical to very kinematical at increasing precession angle (http :// drop.io/precession , password = precession)
NanoMEGAS
Advanced Tools for electron diffraction
Courtesy M.Gemmi Univ of Milano

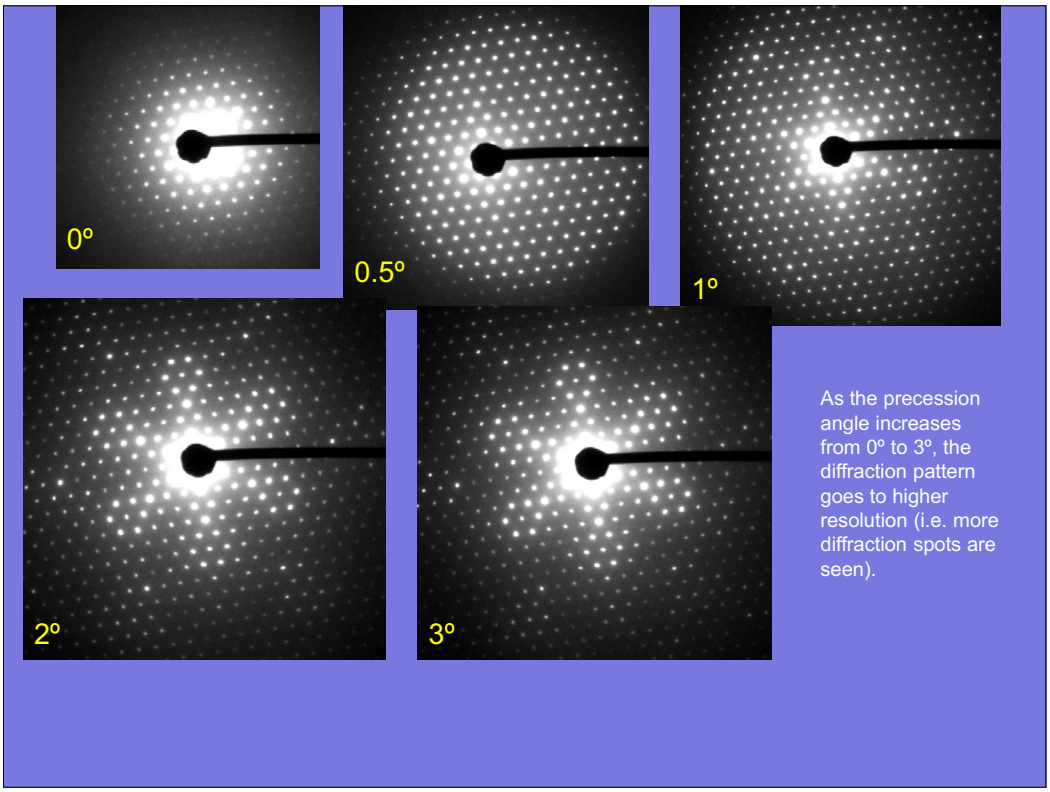
0º
0.5º
1º
2º
3º
As the precession angle increases from 0º to 3º, the diffraction pattern goes to higher resolution (i.e. more diffraction spots are seen).

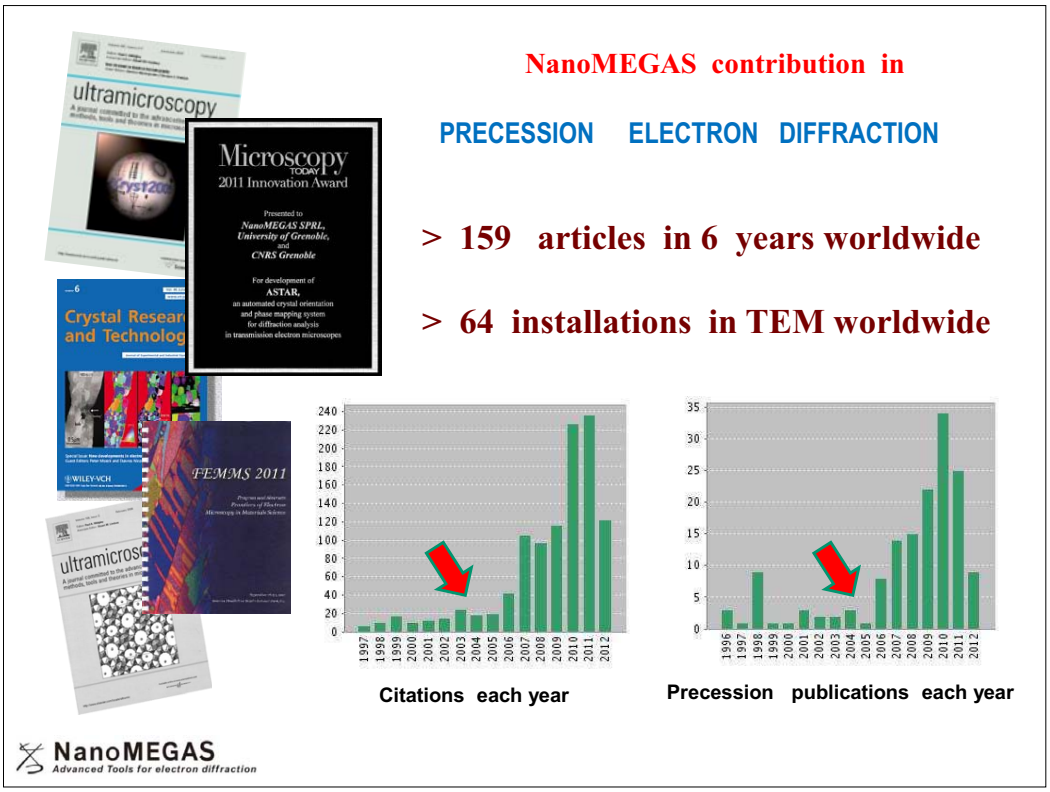
NanoMEGAS contribution in
PRECESSION ELECTRON DIFFRACTION
> 159 articles in 6 years worldwide
> 64 installations in TEM worldwide
ultramicroscopy
Microscopy TODAY
2011 Innovation Award
Presented to
NanoMEGAS SPRL,
University of Grenoble,
and
CNRS Grenoble
For development of
ASTAR,
an automated crystal orientation and phase mapping system for diffraction analysis in transmission electron microscopes
Crystal Research and Technology
WILEY-VCH
FEMMS 2011
ultramicros
Citations each year
Precession publications each year
NanoMEGAS
Advanced Tools for electron diffraction

Characterization

for new unknown compound

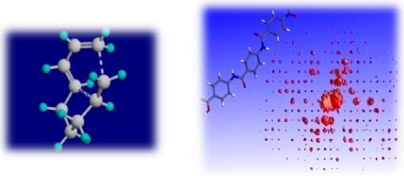

Find crystal cell parameters

Find crystal symmetry and atomic structure

NanoMEGAS
Advanced Tools for electron diffraction

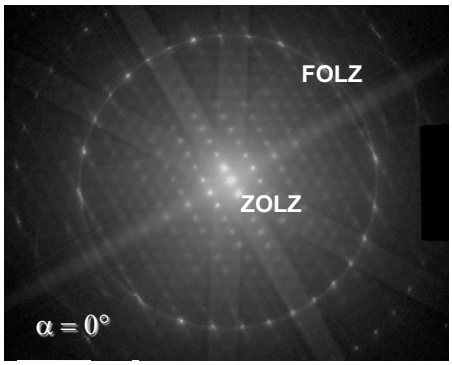

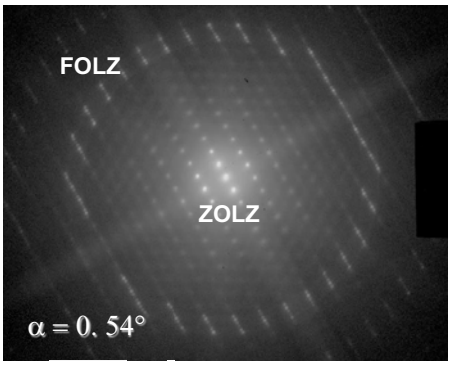

SiC

Space group deterrmination by

PRECESSION ELECTRON DIFFRACTION

SiC 4H hexagonal $P6_3mc$

Courtesy JP Mornirolli Univ of Lille France

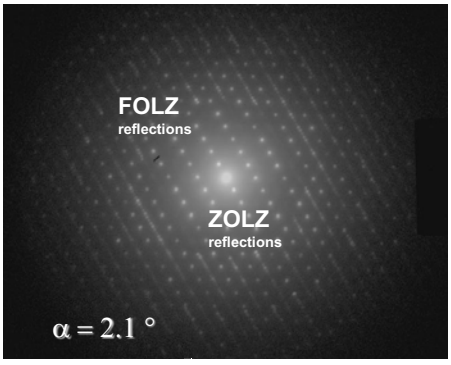

How to find crystal symmetry

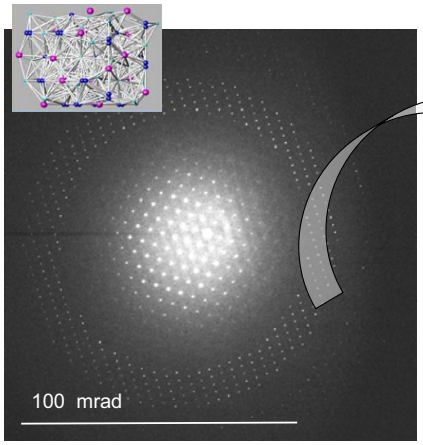

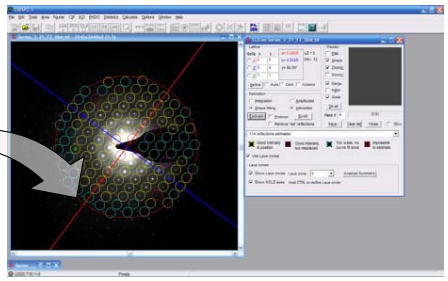

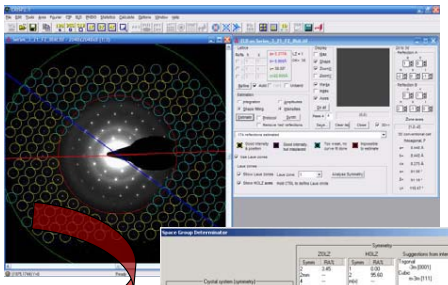

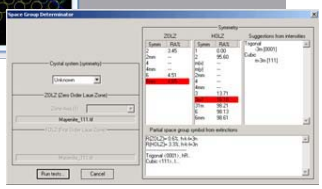

Space Group Determinator Calidris

PRECESSION DIFFRACTION + FILTER

High visibility FOLZ reflections : Find Point and Space group symmetry

PED 'ideal' symmetries
They are connected with the 11 Laue Classes

Crystal system	Laue class	<111>	<001>	<110>	<uv0>	<uuw>	<uvw>	
Cubic	*m3m*	(6mm) 3m	(4mm) 4mm	(2mm) 2mm	(2mm) m	(2mm) m	(2) 1	
	m3	(6) 3	(2mm) 2mm		(2mm) m		(2) 1	
Hexagonal	*6/mmm*	[0001] (6mm1) 6mm	<11$\bar{2}$0> (2mm) 2mm	<1$\bar{1}$00> (2mm) 2mm	<uvt0> (2mm) m	<uutw> (2mm) m	<uū0w> (2mm) m	<uvtw> (2) 1
	6/m	(6) 6			(2mm) m			(2) 1
Trigonal		[0001]	<11$\bar{2}$0>	<1$\bar{1}$00>	<uvt0>	<uutw>	<uū0w>	<uvtw>
	3m	(6mm) 3m	(2) 2				(2mm) m	(2) 1
	$\bar{3}$	(6) 3						(2) 1
Tetragonal	*4/mmm*	[001] (4mm) 4mm	<100> (2mm) 2mm	<110> (2mm) 2mm	<u0w> (2mm) m	<uv0> (2mm) m	<uuw> (2mm) m	<uvw> (2) 1
	4/m	(4) 4				(2mm) 2		(2) 1
Orthorhombic	*mmm*	[100] (2mm) 2mm	[010] (2mm) 2mm	[001] (2mm) 2mm	[uv0] (2mm) m	[u0w] (2mm) m	[0vw] (2mm) m	[uvw] (1) 1
Monoclinic	*2/m*	[010] (2) 2	[u0w] (2mm) m	<uvw> (2) 1				
Triclinic	$\bar{1}$	<uvw> (2) 1						

Reference : JP Morniroli ATLAS of Electron Zone Axis Patterns

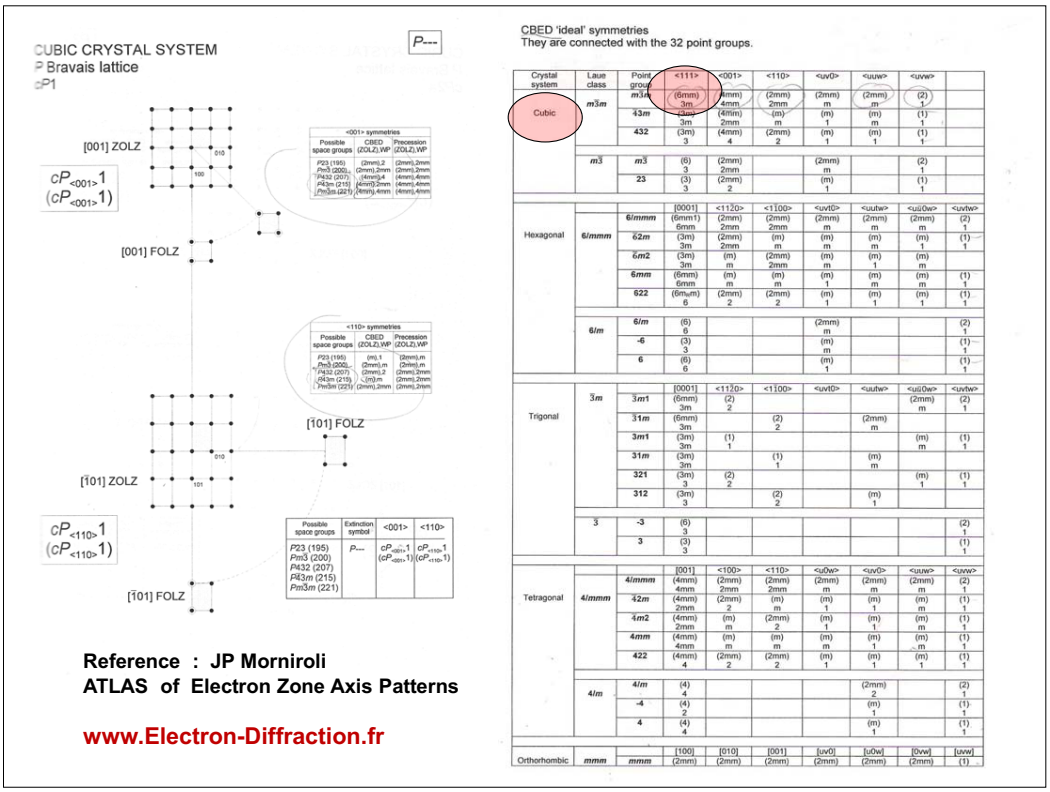
CUBIC CRYSTAL SYSTEM
P Bravais lattice
cP1
P---
[001] ZOLZ
[001] FOLZ
[101] FOLZ
[$\bar{1}$01] ZOLZ
[$\bar{1}$01] FOLZ
Reference : JP Morniroli
ATLAS of Electron Zone Axis Patterns
www.Electron-Diffraction.fr
CBED 'ideal' symmetries
They are connected with the 32 point groups.

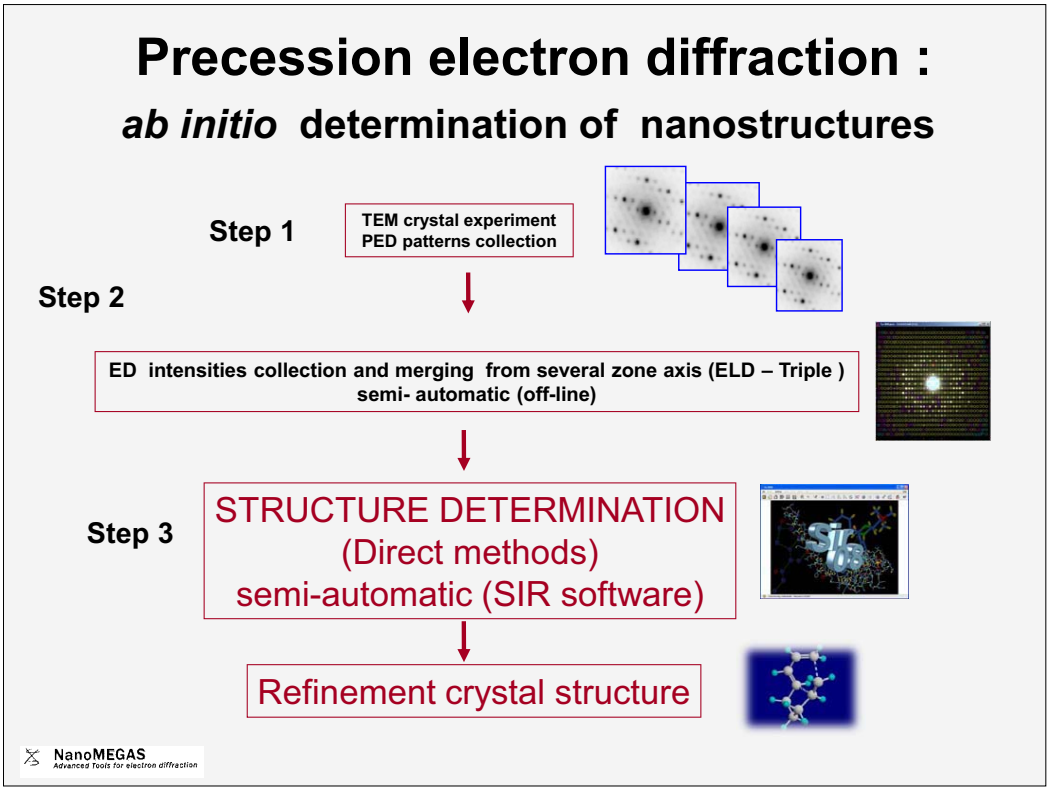
Precession electron diffraction :
ab initio determination of nanostructures
Step 1
TEM crystal experiment
PED patterns collection
Step 2
ED intensities collection and merging from several zone axis (ELD – Triple)
semi- automatic (off-line)
Step 3
STRUCTURE DETERMINATION
(Direct methods)
semi-automatic (SIR software)
Refinement crystal structure
NanoMEGAS
Advanced Tools for electron diffraction

Electron diffraction intensities are measured automatically

FROM

Image plates
Photo film

OR

CCD camera
1k x 1k
2k x 2k
4k x 4k

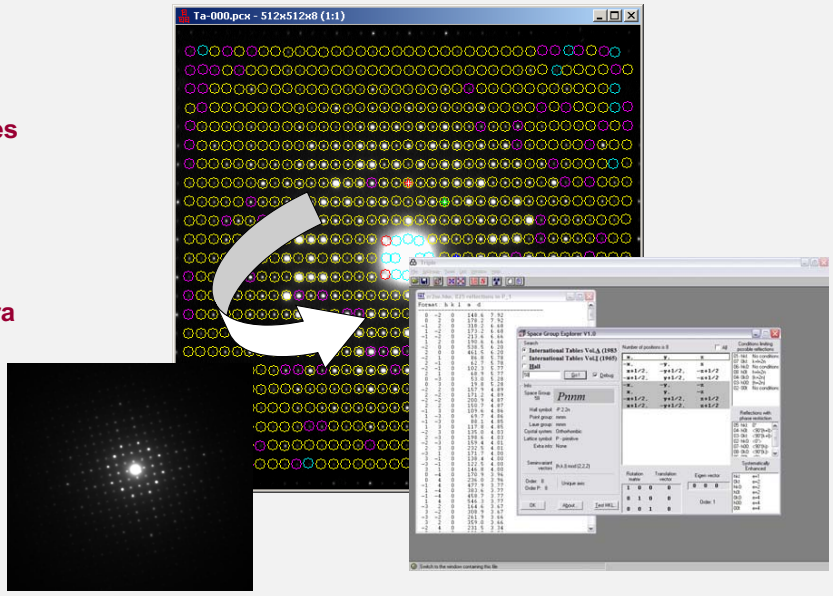

NanoMEGAS
Advanced Tools for electron diffraction

TVIPS

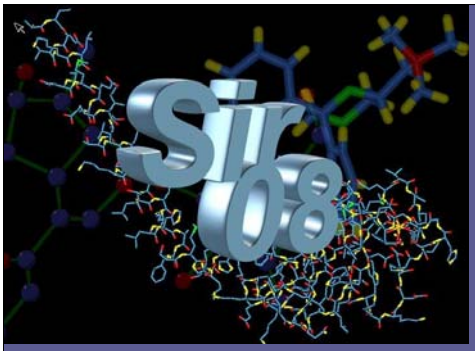

DIRECT METHODS (electron scattering)

SIR 96, SIR 2007, SIR 2008, FOX ,....

Structure solution with direct methods: SIR2008

http://www.ic.cnr.it/registration_form.php

FullProf suite : http://www.ill.eu/sites/fullprof/

Use precession diffraction intensities to solve crystal structures

In this example PED intensities from 5 zone axis (ZA) from **Mg_5Pd_2 nanocrystal** have been collected with a 100 kV TEM. Use of **SIR2008** direct methods software allowed direct calculation of all the (Mg,Pd) atomic positions.

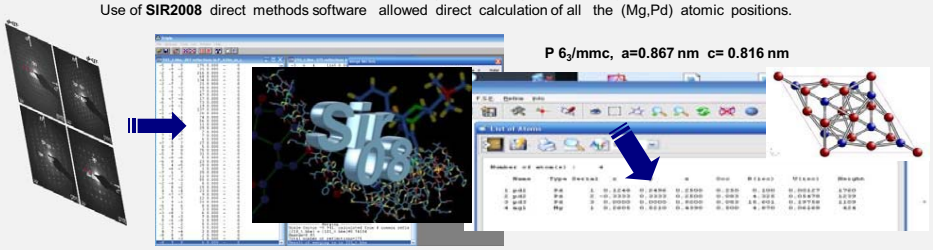

Collection of **3 ZA ([0 0 1], [1 0 1] ,[1 0 2]) PED intensities** with a 200KV TEM from **uvarovite mineral $Ca_3Cr_2(SiO_4)_3$ cubic Ia-3d a=1.2nm** and the use of SIR2008 revealed precise atomic structure (see table) ***calculated atomic positions are very close to X-Ray*** 3D refined atomic model

h	k	l	F (hkl)
0	6	0	6031
2	5	0	5981
3	1	0	5220
3	4	0	4751
1	7	0	4262
4	0	0	4189
1	6	0	3782
2	3	0	3705
5	4	0	3315
2	6	0	3285
3	4	0	2958
4	5	0	2763
4	3	0	2657
6	0	0	2578
1	8	0	2111
4	4	0	1868
4	2	0	1607
3	2	0	1512

Atom	X(Six)	Y(Six)	Z(Six)	X(Pub)	Y(Pub)	Z(Pub)	Distance
Cr	0.000	0.000	0.500	0.500	0.000	0.500	0.00000
Ca	0.000	0.750	0.375	0.750	0.125	0.500	0.00000
Si	0.000	0.750	0.625	0.750	-0.125	0.500	0.00000
O	0.654	0.963	0.455	0.039	0.047	0.653	0.02687

Using set of simulated PED intensities from 2 ZA of complex commensurate structure of **antigorite mineral ~$Mg_3Si_2O_5(OH)_4$** and solving with direct methods (SIR2008), **most of the atomic positions are revealed**

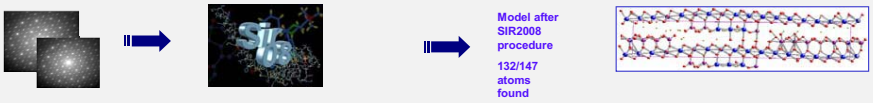

Combining precession electron diffraction - powder X-Ray diffraction to solve complex structures

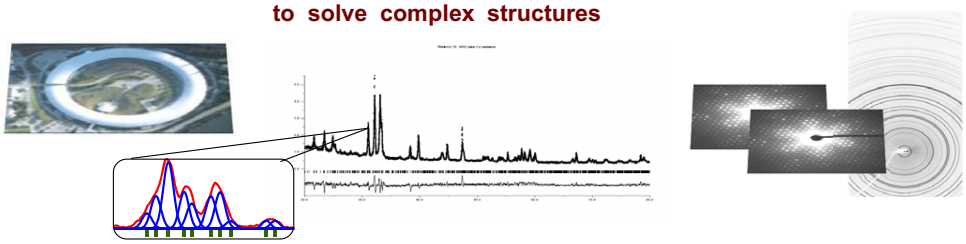

Information from PED can be combined with *hkl reflections from X-Ray* powder diffraction to accurately solve and refine *ab-initio* structures using either *charge-flipping* algorithms or direct methods.

- **technique is useful for poorly crystallized / nm size pollycrystalline materials**
- **useful for solving structures of complex organic and inorganic materials**
- **useful in presence of unknown phases in X-Ray powder pattern**

one of the **most complex known zeolites TNU-9 ($Si_{19}O_{234}$) has been solved** [6] **by combining Synchrotron X-Ray powder results and data from 5 ZA PED patterns from 300 kV TEM**

$Li_4Ti_8Ni_3O_{21}$ has been solved [7] using X-Ray Synchrotron powder results and PED data from 300 kV TEM.

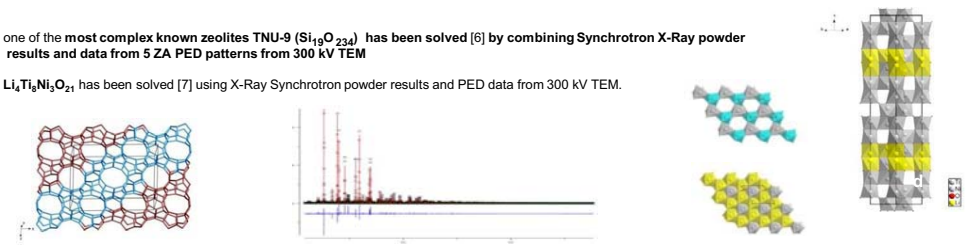

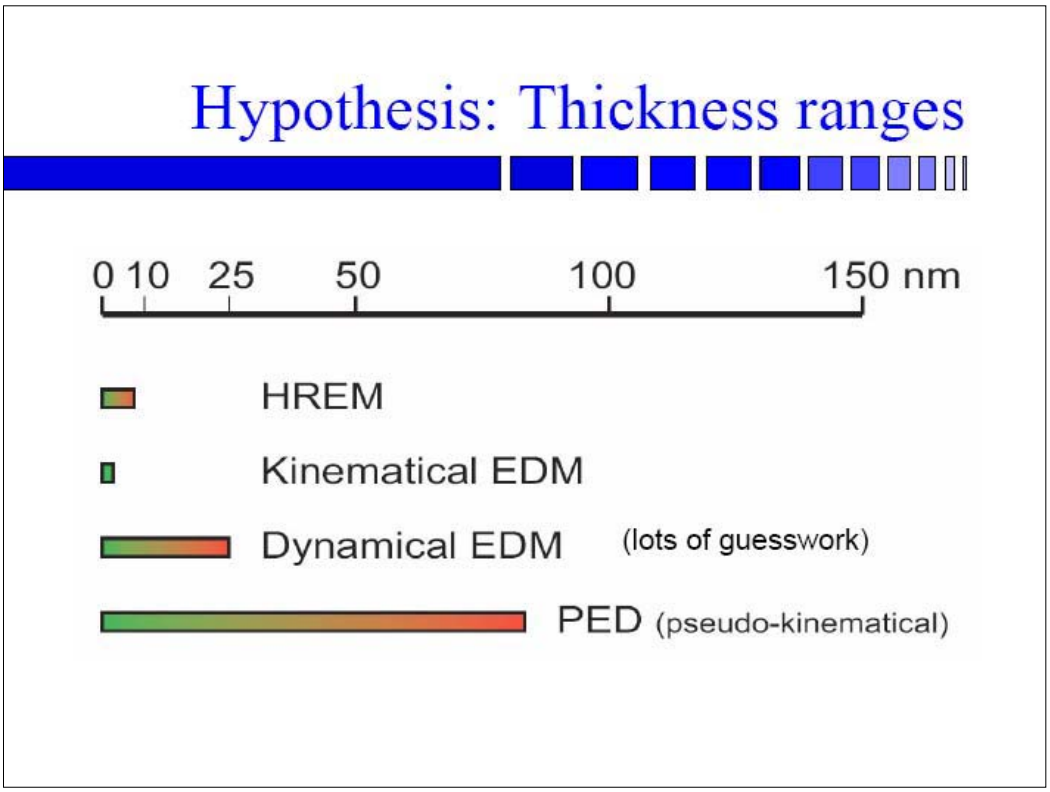
Hypothesis: Thickness ranges
0 10 25 50 100 150 nm
HREM
Kinematical EDM
Dynamical EDM
(lots of guesswork)
PED (pseudo-kinematical)

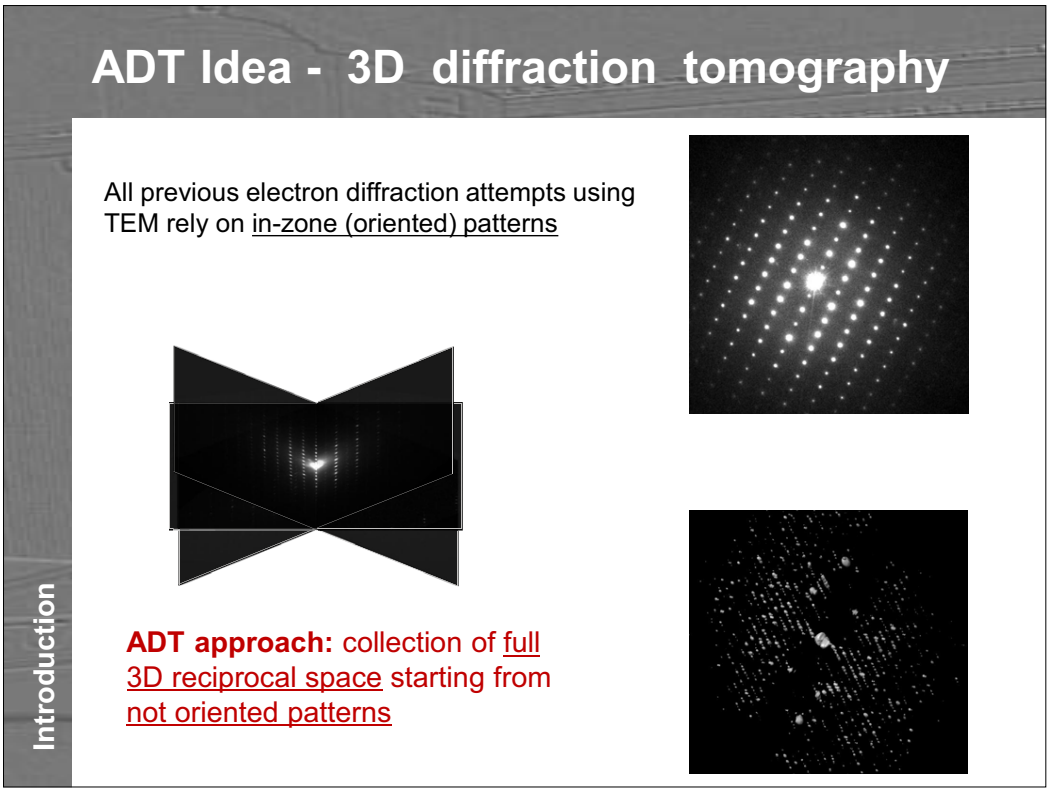
ADT Idea - 3D diffraction tomography
All previous electron diffraction attempts using TEM rely on in-zone (oriented) patterns
ADT approach: collection of full 3D reciprocal space starting from not oriented patterns
Introduction

TEM :zone axis tilt series acquisition

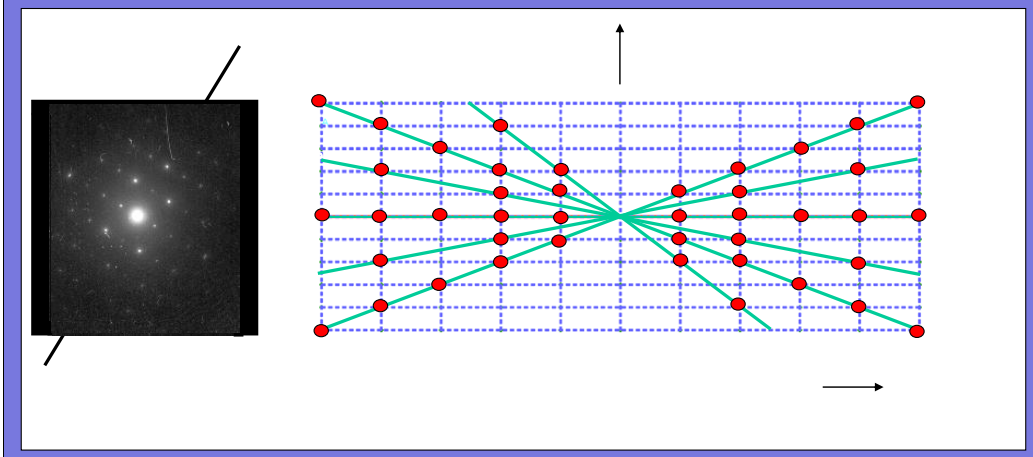

Courtesy : Prof. U Kolb UMainz

Problems of zone axis tilt series

- intensive training to get good tilts
- data collection is slow and tedious
- you miss most of high indexed reflections, especially in the peripheral areas of the reciprocal space

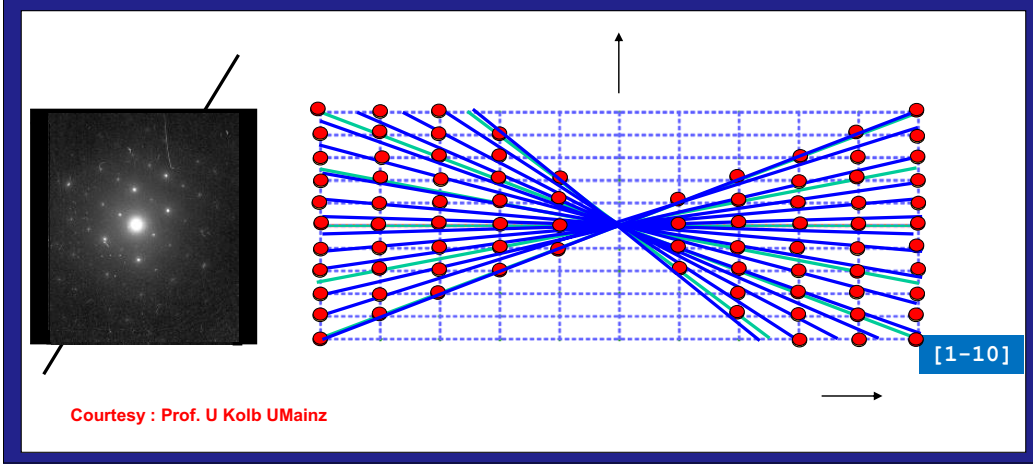

Courtesy : Prof. U Kolb UMainz

Data analysis – ADT3D

Technique

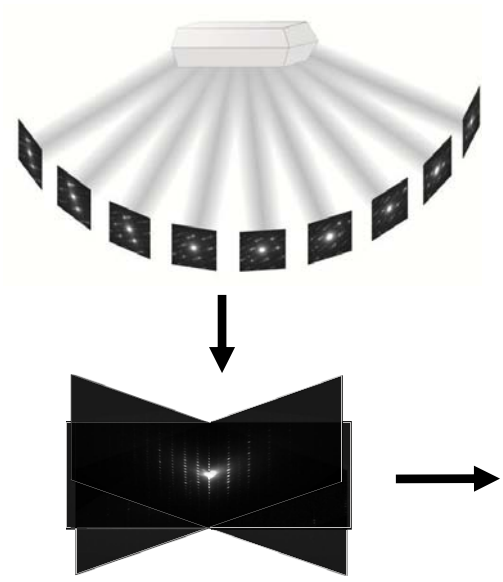

Data analysis by ADT3D
3D reconstrucution of diffraction space

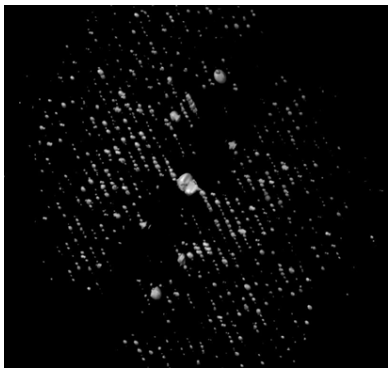

diffraction tomography. Part II – Cell parameter determination. U. Kolb, T. Gorelik and M.T. Otten, *Ultramicroscopy*, **108**, 763-772 (2008).

3D sampling of reciprocal space

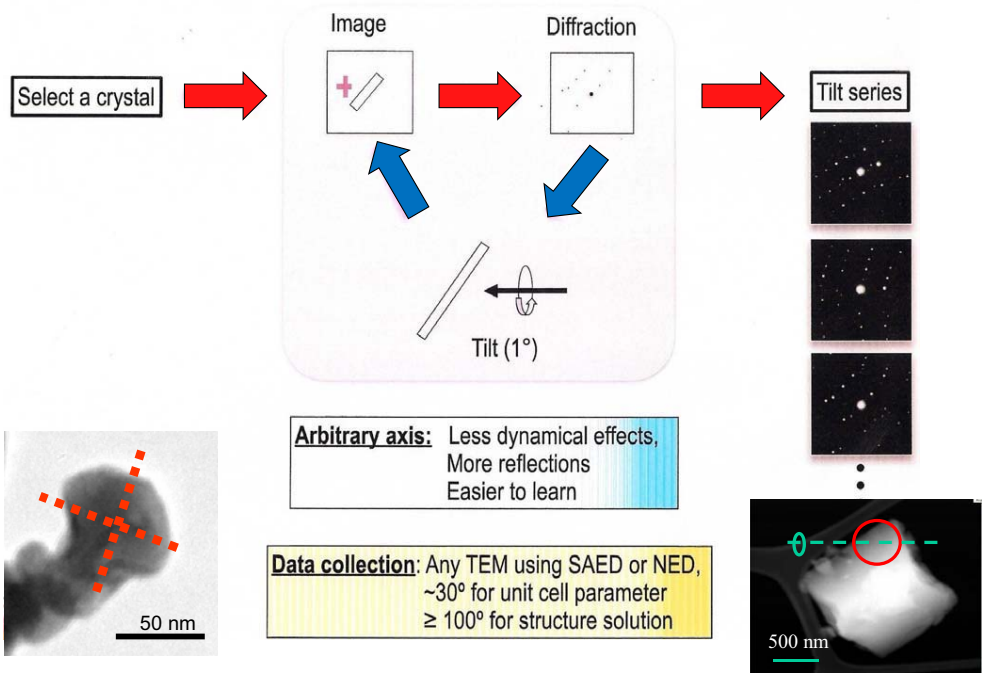

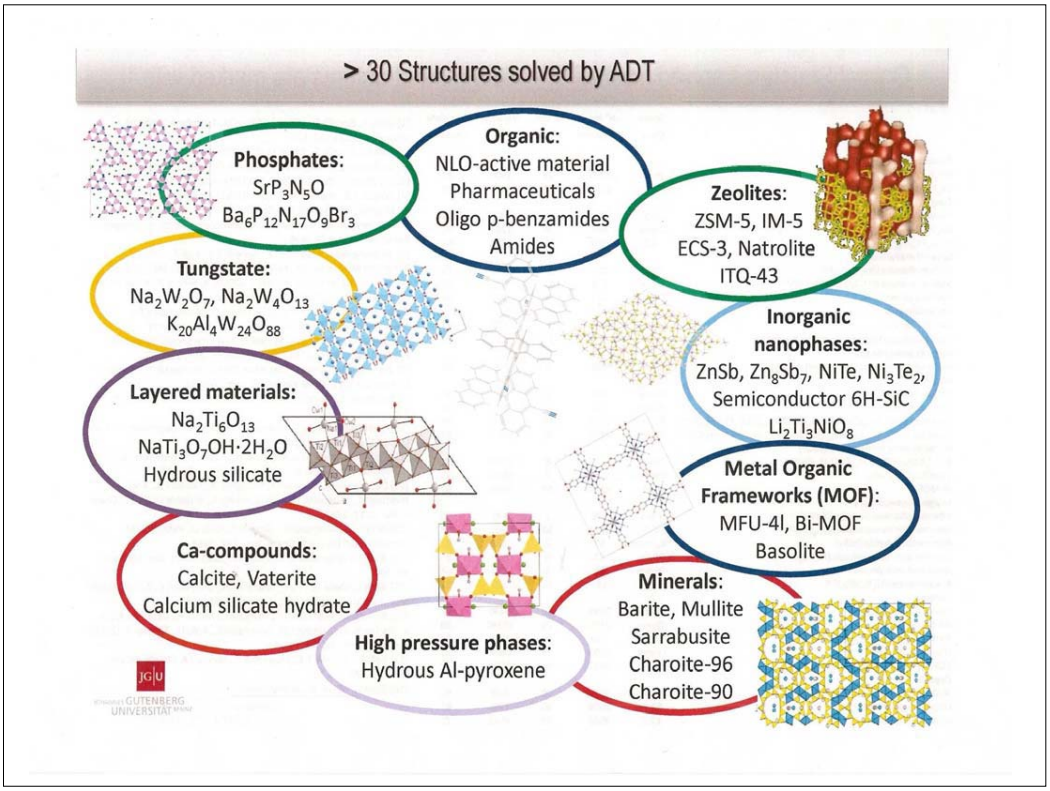

Precession enhances EELS signal

(EPO Patent filed)

Better element quantification (specially at ZA orientations)

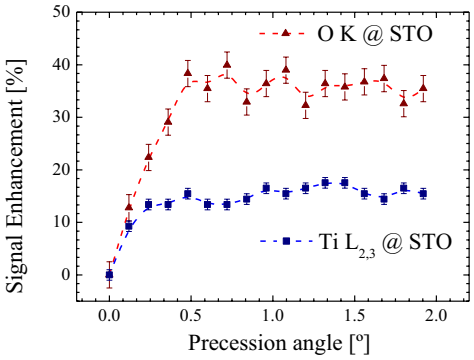

EELS Signal increase a lot with precession

NanoMEGAS
Advanced Tools for electron diffraction

EELS –EDS signal improvement with precession diffraction

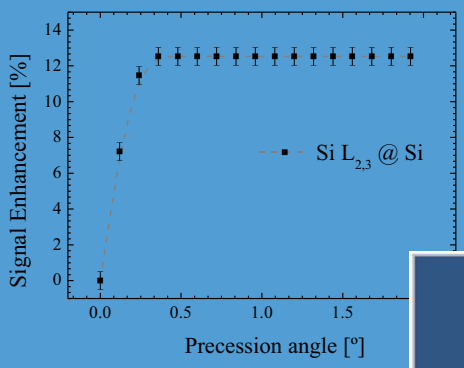

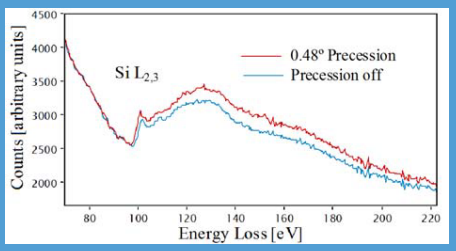

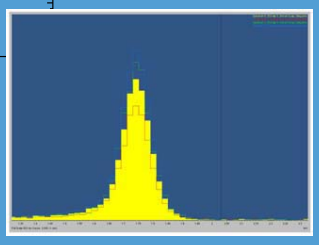

NanoMEGAS
Advanced Tools for electron diffraction

Innovation in instrumentation
ASTAR : texture materials characterization at nm scale

from 50 nm

EBSD-SEM

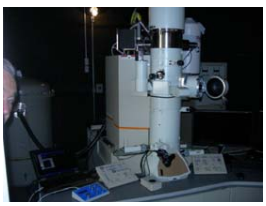

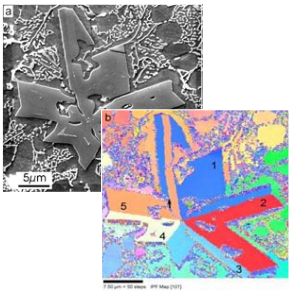

to 1 nm

EBSD -like TEM

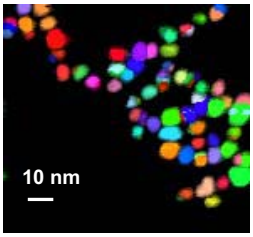

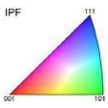

NanoMEGAS
Advanced Tools for electron diffraction

Grenoble INP

ASTAR : combine scanning with precession

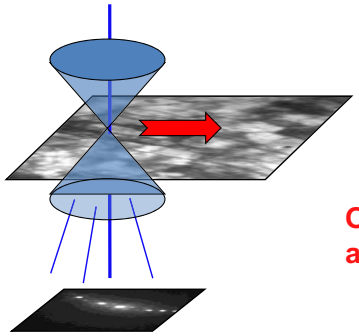

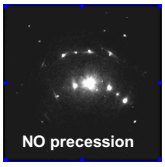

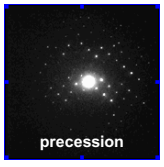

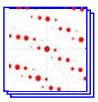

Orientation - Phase maps are obtained at 1 nm resolution in TEM

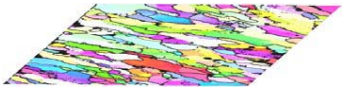

Orientation map

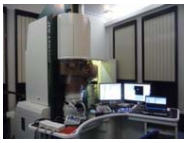

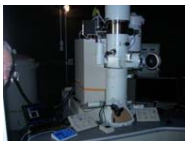

NanoMEGAS
Advanced Tools for electron diffraction

DiffGen : Template generator

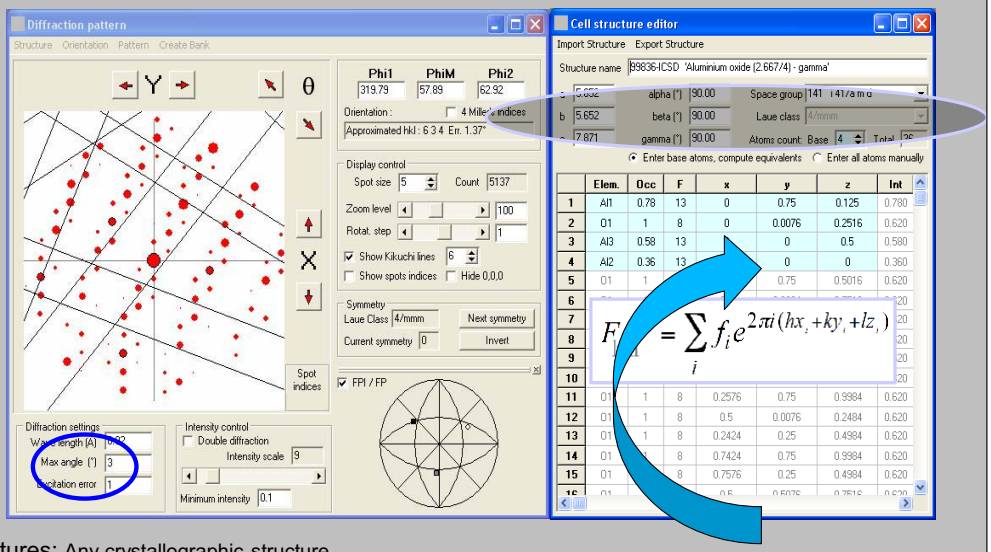

Features: Any crystallographic structure
Laue class adapted to the space group
Structure generator (space group, structure factor equ.)

input from ICDD, FIZ, COD database

NanoMEGAS
Advanced Tools for electron diffraction

ASTAR : crystallographic orientation identification

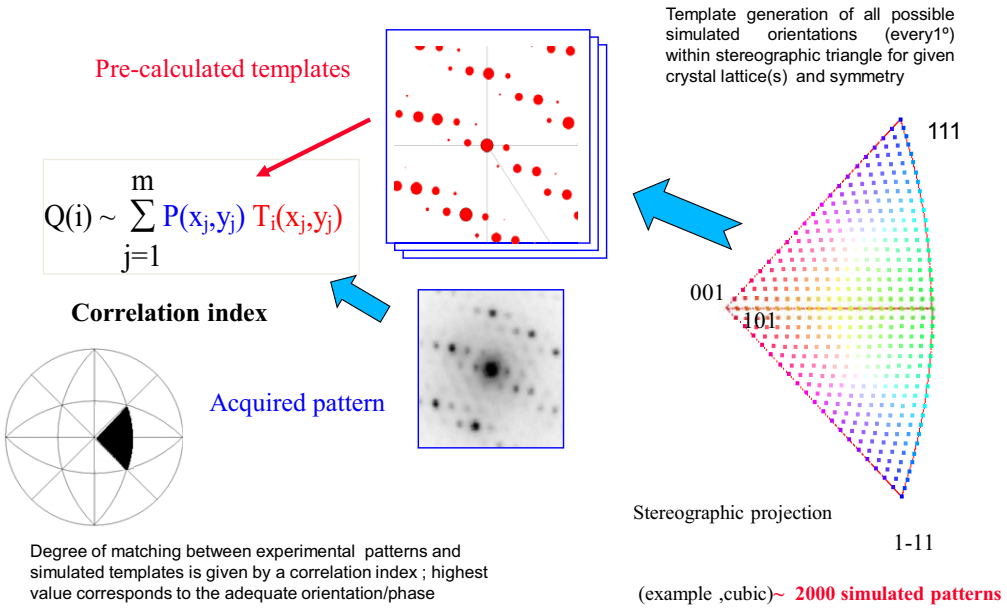

Degree of matching between experimental patterns and simulated templates is given by a correlation index ; highest value corresponds to the adequate orientation/phase

(example ,cubic)~ **2000 simulated patterns**

NanoMEGAS Advanced Tools for electron diffraction

ASTAR identification example : nanocrystalline Cu

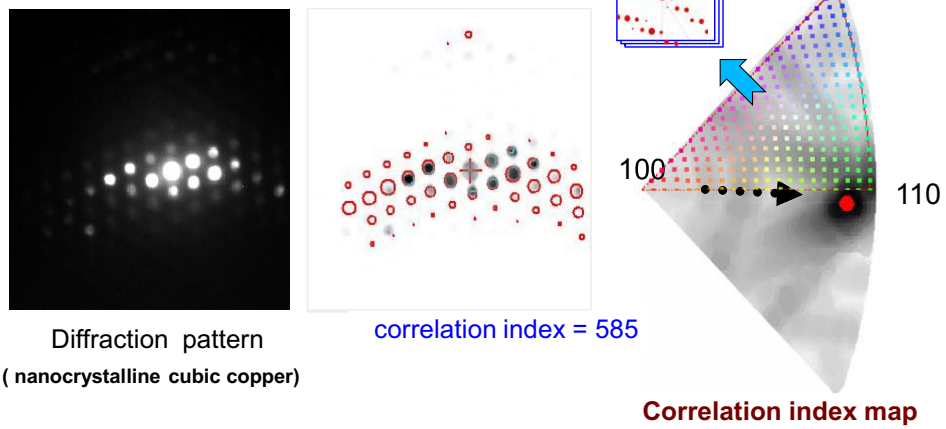

Diffraction pattern

(nanocrystalline cubic copper)

Correlation index map

For a given ED pattern, the correlation index map is calculated for all possible template orientations and plotted on a map that represents a portion of the stereographic projection (reduced to a double standard triangle). That resulting map reveals the most probable orientation for every experimental spot ED pattern (in this case ED pattern is found to be close to 110 ZA orientation)

ASTAR : ultra-fast TEM orientation map

Sample : severely deformed copper

Orientation map

250 x 200 pixel data adquisition

5-10 min

Typical software data analysis time (for cubic)

5-15 min

(hexagonal , tetragonal)

x 3- 4 more time

Map resolution equals beam size resolution

NBD step 20 nm (LaB6)

NanoMEGAS
Advanced Tools for electron diffraction

ASTAR: Orientation Microscopy for advanced TEM

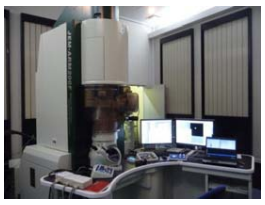

JEOL microscopes

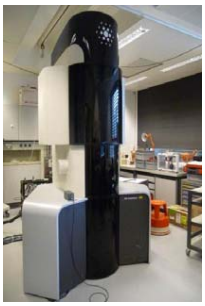

Zeiss microscopes

FEI microscopes

NanoMEGAS
Advanced Tools for electron diffraction

ASTAR combination for JEOL - FEI - Zeiss TEMs

ASTAR-Digistar

…some examples

Jeol 2100 - Jeol 2010 FE
UB Barcelona

Same ASTAR- DigiSTAR can work between different TEMs .

ASTAR-Digistar

Jeol 3010 - Jeol 2010 FF
CEA Grenoble

NanoMEGAS
Advanced Tools for electron diffraction

EBSD-TEM like applications

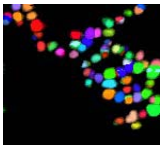

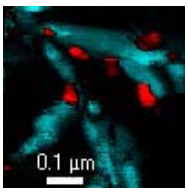

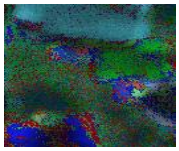

TEM nm orientation mapping

TEM nm phase mapping

orientation /phase maps with precession

NanoMEGAS
Advanced Tools for electron diffraction

0.5µm

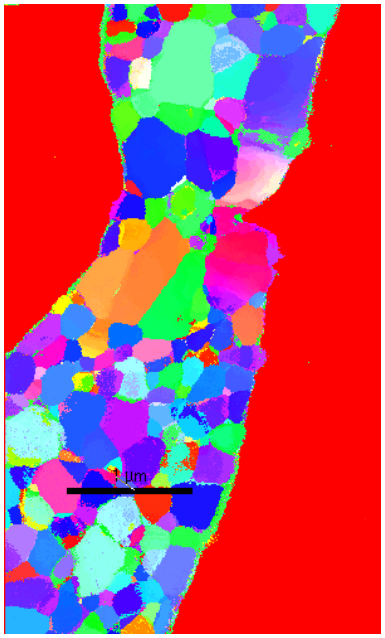

- Comparison of TEM image, and ASTAR results **8 nm resolution**
- CM20 UTwin LaB6 courtresy Prof . S.Godet ULB Brussels ,Aluminium deformed sample

Power of the ASTAR Technique : nanoparticles

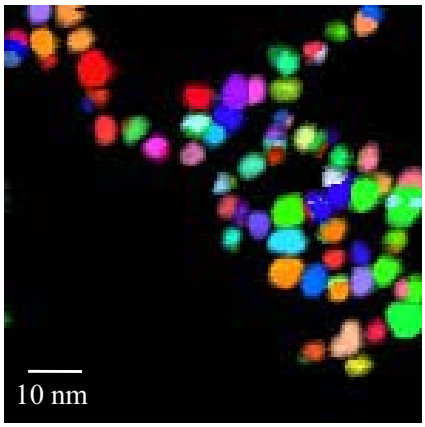

ASTAR : Orientation analysis from Pt ~100 particles ~ 6 nm in size

1 nm resolution for orientation map

Data courtesy Prof. P.Ferreira, J.Ganesh Univ Texas at Austin USA **JEOL 2010 FEG**

THE UNIVERSITY OF TEXAS AT AUSTIN

ASTAR - Thin films analysis

W on Si and Encapsulated with SiO_2

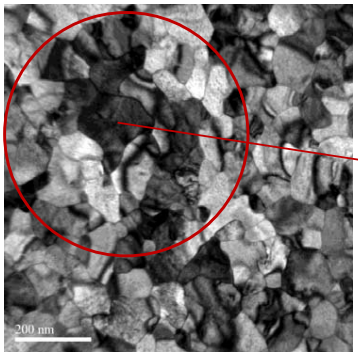

Bright Field TEM image. Circular area indicated in red approximately depicts the area mapped for orientation analysis

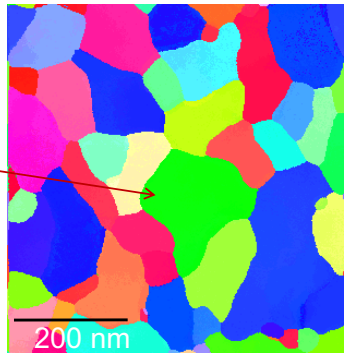

Orientation Map of the selected area on the bright field TEM image

Sample: 40 nm thick W Film sputter deposited on Si and encapsulated with 20 nm of amorphous SiO_2 followed by annealing :Data courtesy ***Prof. C.Barmak Carneggie Mellon University USA***

EBSD-TEM like applications

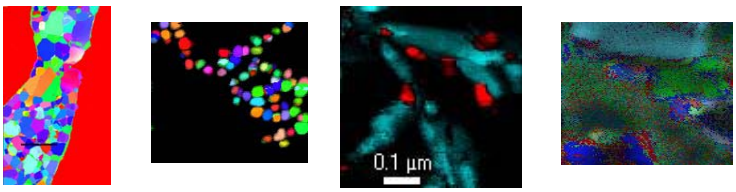

TEM nm orientation mapping

TEM nm phase mapping

orientation /phase maps with precession

NanoMEGAS
Advanced Tools for electron diffraction

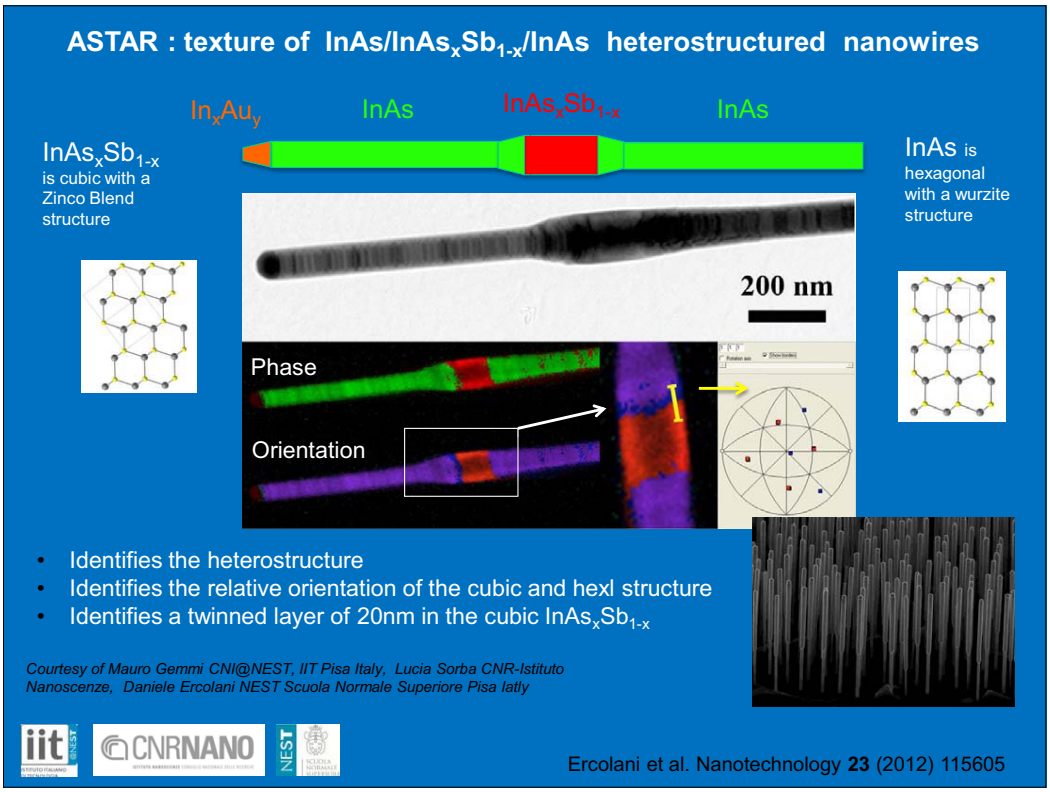
ASTAR : texture of InAs/InAsxSb1-x/InAs heterostructured nanowires
InxAuy
InAs
InAsxSb1-x
InAs
InAsxSb1-x is cubic with a Zinco Blend structure
InAs is hexagonal with a wurzite structure
200 nm
Phase
Orientation
Identifies the heterostructure
Identifies the relative orientation of the cubic and hexl structure
Identifies a twinned layer of 20nm in the cubic InAsxSb1-x
Courtesy of Mauro Gemmi CNI@NEST, IIT Pisa Italy, Lucia Sorba CNR-Istituto Nanoscenze, Daniele Ercolani NEST Scuola Normale Superiore Pisa Italy
Ercolani et al. Nanotechnology 23 (2012) 115605

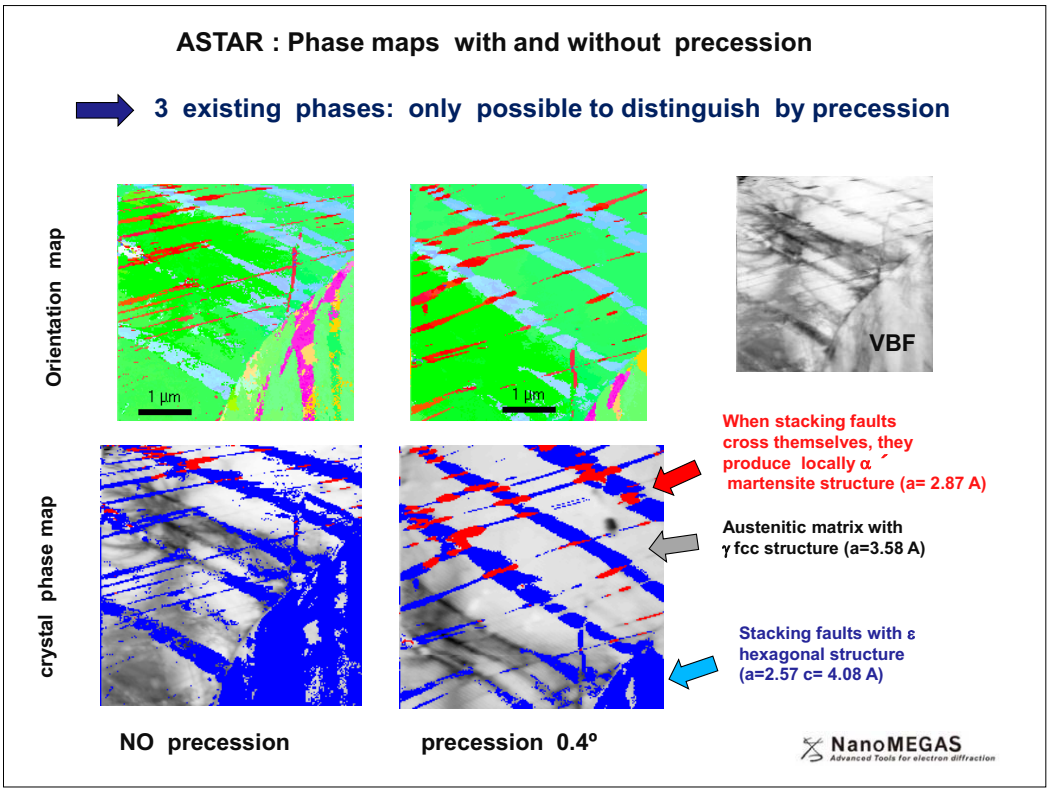
ASTAR : Phase maps with and without precession
3 existing phases: only possible to distinguish by precession
Orientation map
crystal phase map
1 µm
1 µm
VBF
When stacking faults cross themselves, they produce locally α´ martensite structure (a= 2.87 A)
Austenitic matrix with γ fcc structure (a=3.58 A)
Stacking faults with ε hexagonal structure (a=2.57 c= 4.08 A)
NO precession
precession 0.4°
NanoMEGAS

PROBLEM : distinguish between goethite (alpha-FeO(OH)) 300x40x10nm and brookite (TiO_2) platelets of 48nm diameter

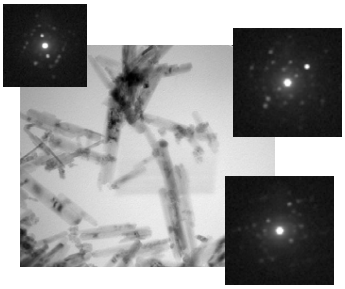

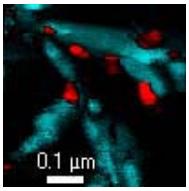

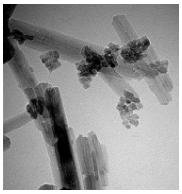

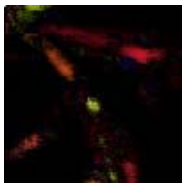

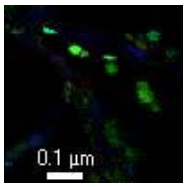

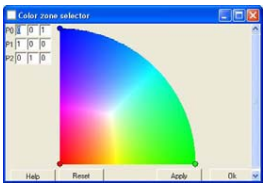

Orientations (alpha-FeO(OH)) *BrookiteTiO2* *Code de couleur*

NanoMEGAS Advanced Tools for electron diffraction

(Mn ,Ga) As clusters in GaAs matrix

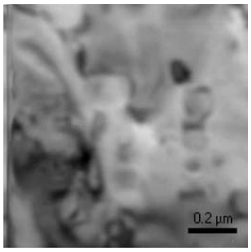

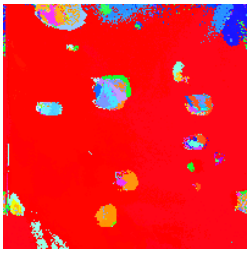

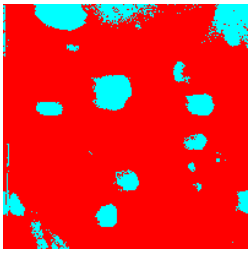

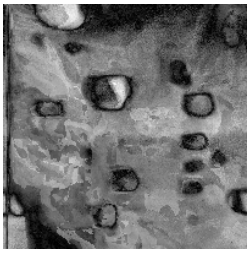

Virtual bright field map Orientation map Phase map Reliability map

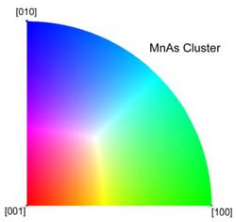

GaAs cubic F-43m (216) a= 0.56533 nm

MnAs β phase orthorhombic $P2_1/n2_1/m2_1/a$ (ζ^2)
a= 0.5704 nm, b= 0.3655 nm, c= 0.6365 nm

MnAs α phase hexagonal $P6_3/mmc$

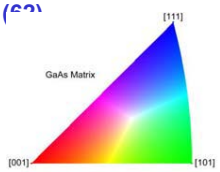

Courtesy Dr. Ines Haeusler Berlin Humboldt University, Germany

NanoMEGAS Advanced Tools for electron diffraction

RIST Steel (S.Korea) : Study martensite – ferrite interfaces

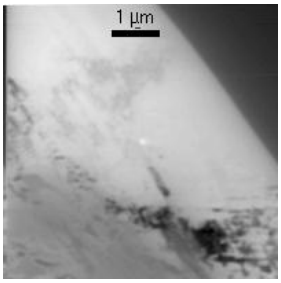

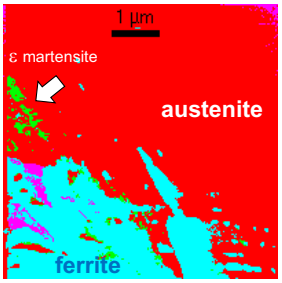

Astar Virtual brightfield : this map is reconstructed with the intensity of the central transmitted dot.	ASTAR Phase reliability Map : Dark lines indicates that we are at grain or phases boundary	**Phase Map : red= austenite, green = epsilon martensite, blue=ferrite, purple = quadratic martensite**

NanoMEGAS
Advanced Tools for electron diffraction

RIST Steel (S.Korea) : Study martensite – ferrite interfaces

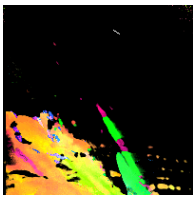

Ferrite orientation vs X axis

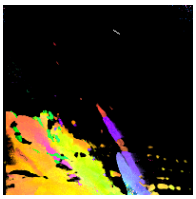

Ferrite orientation vs Y axis

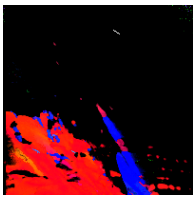

Ferrite orientation vs Z axis

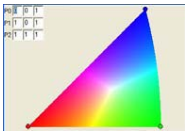

ferrite

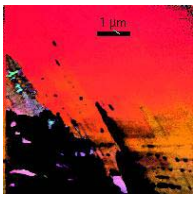

Austenite orientation vs X axis

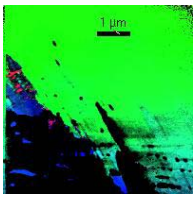

Austenite orientation vs Y axis

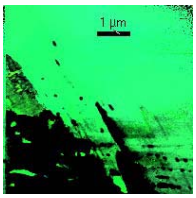

Austenite orientation vs Z axis

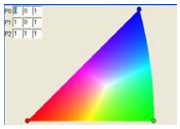

austenite

NanoMEGAS
Advanced Tools for electron diffraction

Study martensite – ferrite interfaces

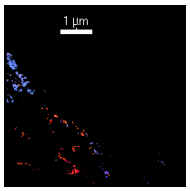

ε martensite orientation vs X axis

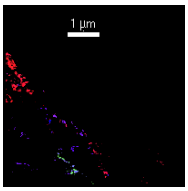

ε martensite orientation vs Y axis

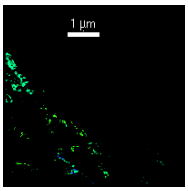

ε martensite orientation vs Z axis

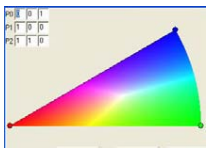

Hex martensite

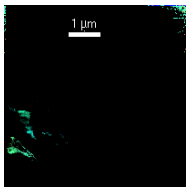

martensite orientation vs X axis

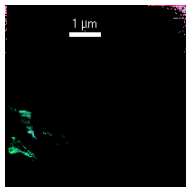

martensite orientation vs Y axis

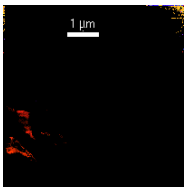

ε martensite orientation vs Z axis

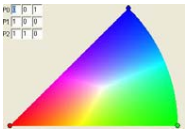

martensite

NanoMEGAS
Advanced Tools for electron diffraction

Problem : distinguish nanoparticles rutile - anatase (TiO_2) texture

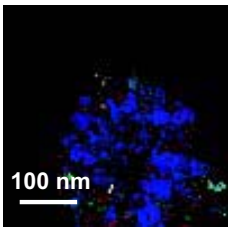

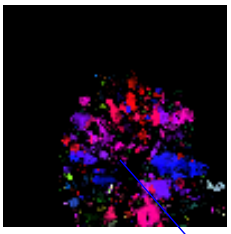

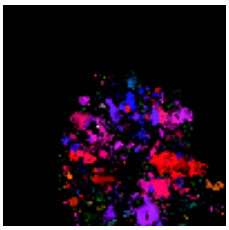

Rutile $P4_2/mnm$ a = 4.59 A , c = 2.95 A

Courtesy Dr. Bakardieva REZ Prague

Jeol 3010 – ASTAR

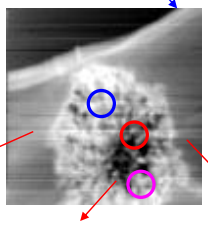

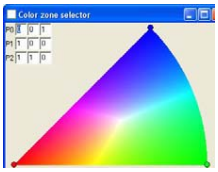

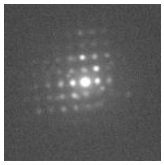

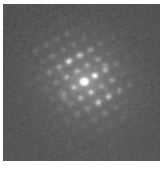

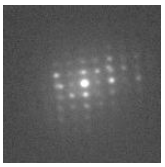

NanoMEGAS
Advanced Tools for electron diffraction

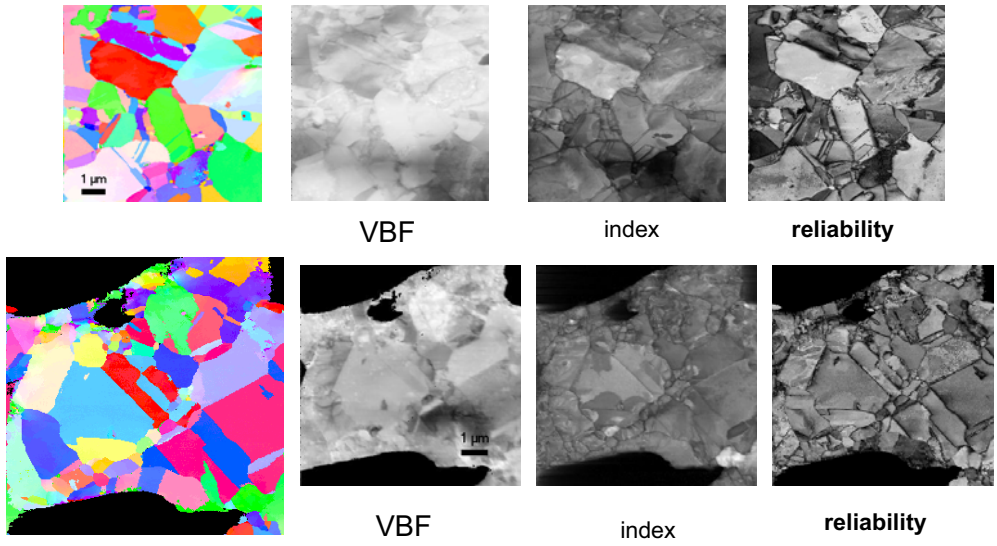

ASTAR (EBSD -TEM) orientation maps : Nanotwins in Cu

CBD mode Jeol 3010 microscope

NanoMEGAS
Advanced Tools for electron diffraction

TEMdpa : Virtual Bright Field on-line construction

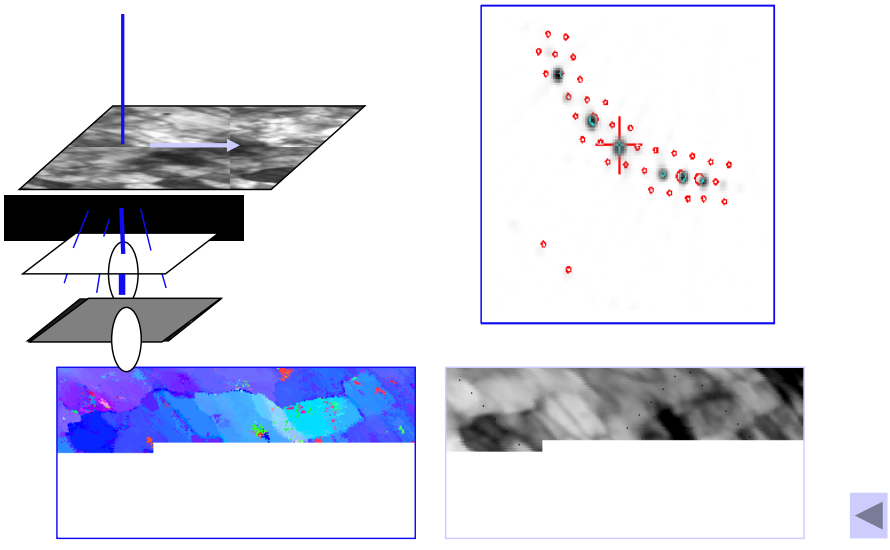

Orientation map Bright field

NanoMEGAS
Advanced Tools for electron diffraction

ASTAR : Reliability

Stereographic projection

Templates for copper

Superimposed diffraction patterns at a grain bounday

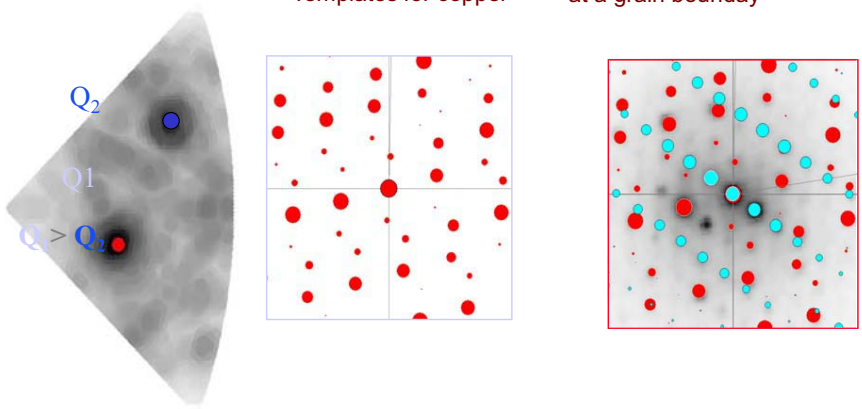

$$R = 100\ (1 - Q_2/Q_1)$$

Reliability

NanoMEGAS Advanced Tools for electron diffraction

Deconvolution of superimposed Diffraction patterns

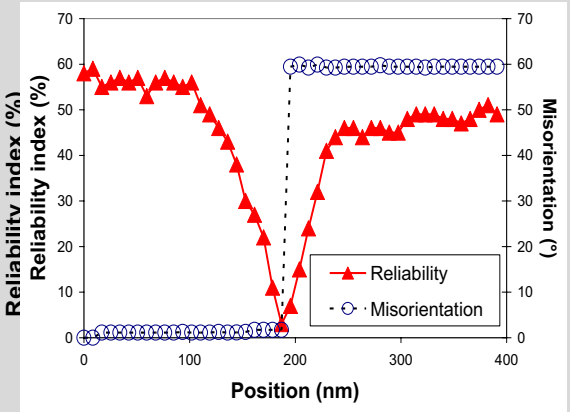

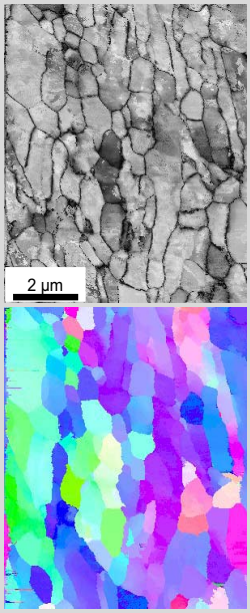

Position (nm)

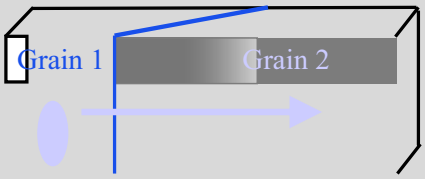

NanoMEGAS Advanced Tools for electron diffraction

Reliability : Super-deformed copper (ε=12)

Crystallographic orientations

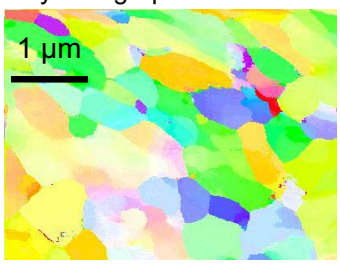

z

Reliability 0 < R < 64

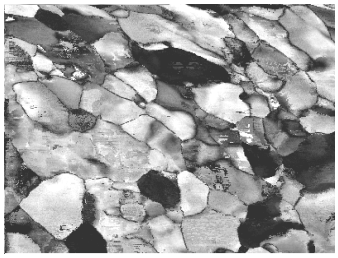

400x278, 11 nm step

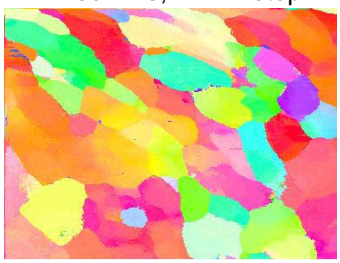

y

TEM image

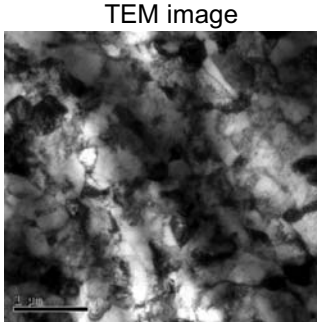

NanoMEGAS
Advanced Tools for electron diffraction

Reliability : Dark areas show overlapping crystals

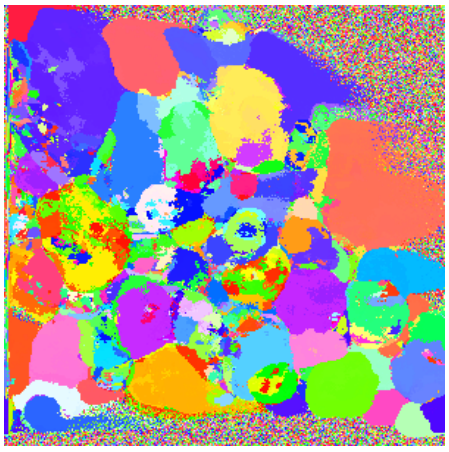

Orientation map

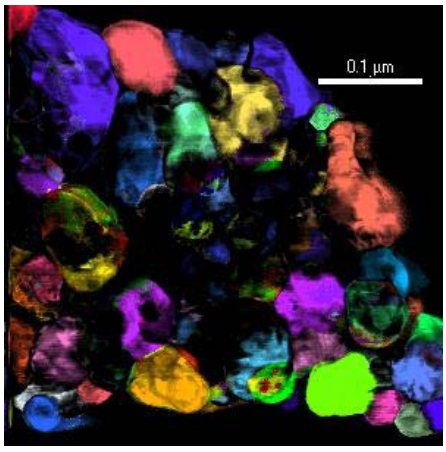

Orientation map + reliability

Pd nanoparticles , Jeol 2200 FS, 1 nm resolution

Courtesy Dr. Holm Kirmse Humboldt Univ Berlin

NanoMEGAS
Advanced Tools for electron diffraction

INDEX and create virtual dark and bright field maps

Diffraction Pattern viewer with virtual aperure

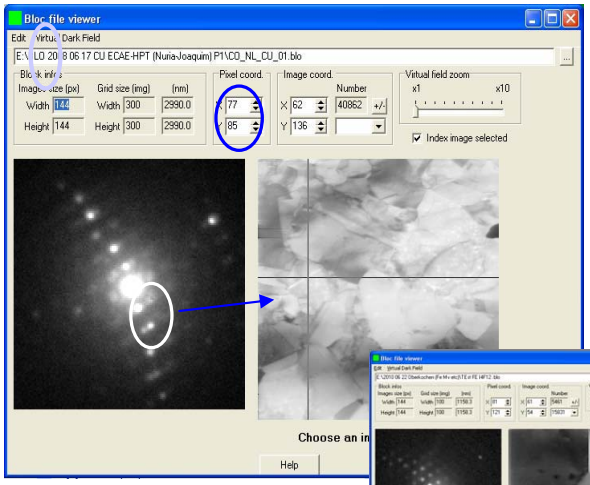

Virtual dark field image

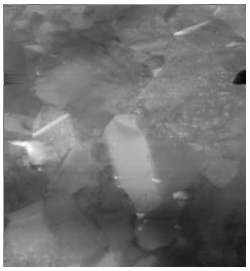

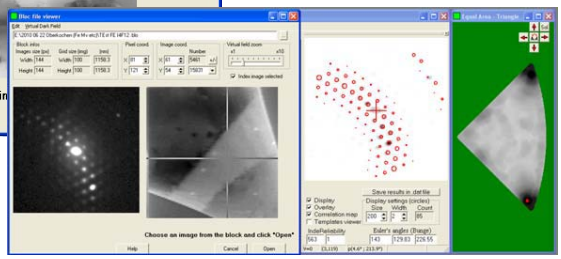

NanoMEGAS
Advanced Tools for electron diffraction

Polycrystalline Electron diffraction

" X-Ray amorphous" OR nanocrystalline ?

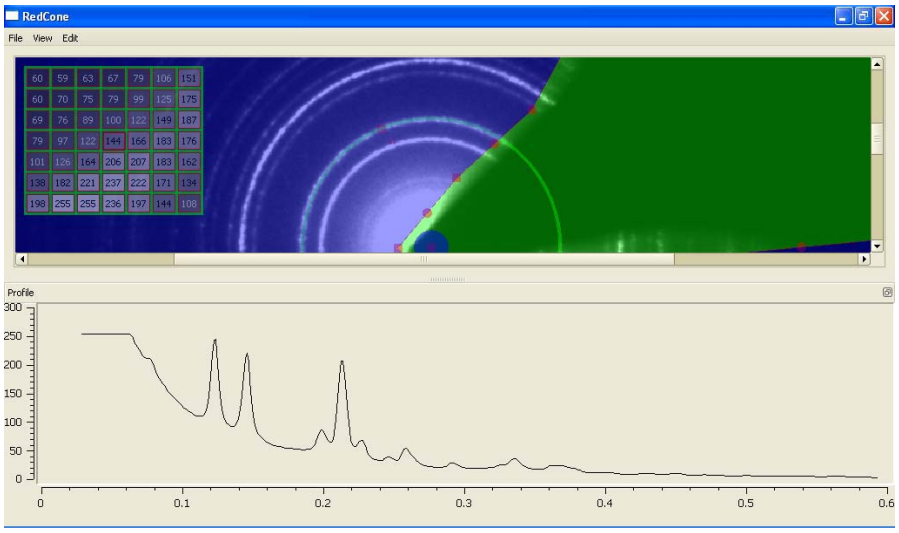

NanoMEGAS
Advanced Tools for electron diffraction

Orientation mapping on
Nanocrystallized polycrystalline Ni-Fe sample

Pollycrystalline thin film of Ni-Fe nanocrystals (average size 5-20 nm)

Data taken with JEOL JEM 2200F operating at 200 kV spot size 1-8 nm

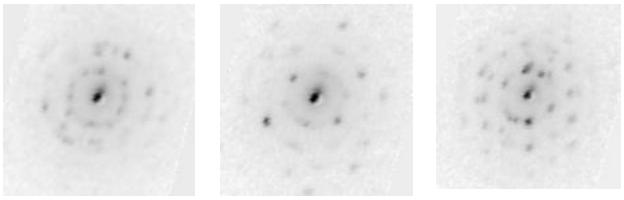

ASTAR can index even overlapping diffraction patterns from polycrystalline sample

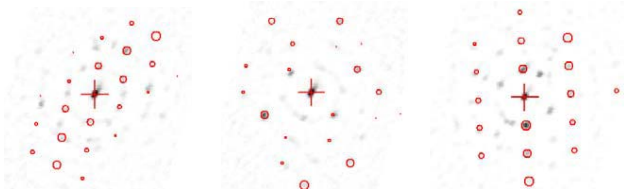

NanoMEGAS Advanced Tools for electron diffraction

Results courtesy Prof. Dr. E.Rauch CNRS Grenoble

Crystallographic orientation map

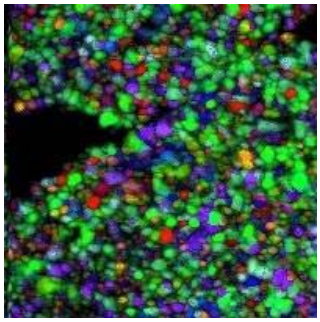

Orientation map (z)
+ index

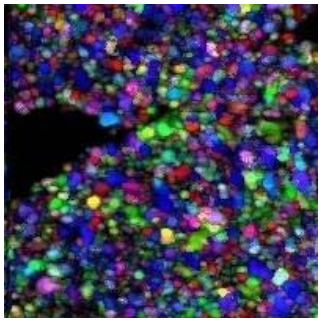

Orientation map (x)
+ index

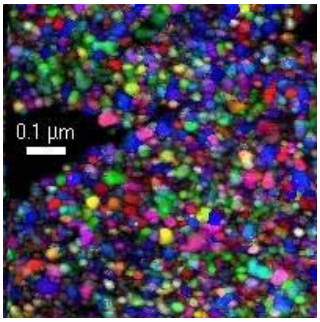

Orientation map (y)
+ index

As for EBSD equipments, the orientation of one particular axis (usually the z axis) is given through a colour code. This enables the individual crystals to be recognized and/or their size to be estimated (step size 4 nm)

NanoMEGAS Advanced Tools for electron diffraction

JEOL 2200 FS 200 KV, Humboldt Univ Berlin

Nanoparticle (50 nm) phase identification

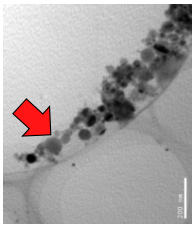

cubic 8.32 A

$Fd\bar{3}m$

Magnetite or maghemite ??

$P4_132$ **γ-Fe_2O_3**

Fe_3O_4

cubic 8.32 A

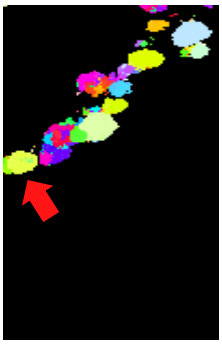

ALL Nanoparticles

REVEALED AS

magnetite (RED)

Orientation map precession 0.3º

PHASE map precession 0.3º

NanoMEGAS Advanced Tools for electron diffraction

Phase identification

Al–TiN multilayers

Credits: D. Bhattacharyya, LANL, Los Alamos NM

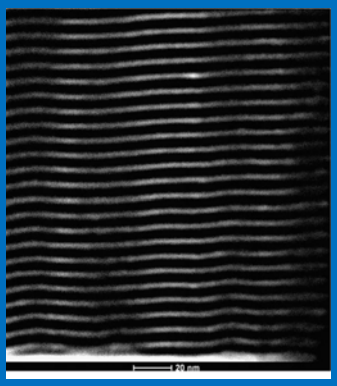

HAADF-STEM image
(D. Bhattacharyya et al, Acta Mater. 59 (2011) 3804–3816
Appl. Phys. Lett. 96, 093113)

Data acquired at Deakin Univ. - JEOL 2100 FEG
(spot size and step size: 0.5 nm)

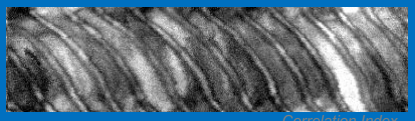

Correlation Index

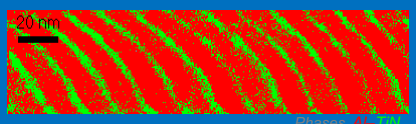

Phases Al–TiN

Two cubic phases with lattice parameters 4% apart

Orientation

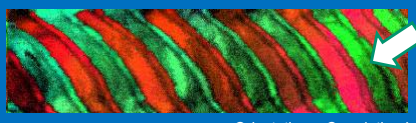

1 nm TiN layer

Orientation + Correlation Index

NanoMEGAS Advanced Tools for electron diffraction

ASTAR : reveal Li insertion in nanomaterials

- $LiFePO_4/FePO_4$ (LFP/FP) powder for lithium-ion batteries

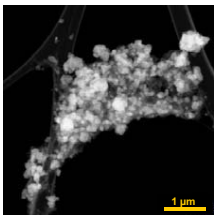

Particle size: 30-200 nm

Understanding the Li insertion/extraction mechanisms

- **Are the particles fully lithiated /delithiated or mixed ?**

$LiFePO_4$ $FePO_4$

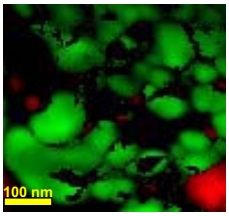

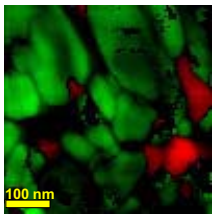

CONCLUSION
The particles are either fully lithiated or fully delithiated

leti liten

New application : ASTAR on organic structures

TRIS structure $C_{16}H_{48}N_4O_{12}$

$Pna2_1$ cell 0.7768 X 0.8725 X 0.8855 nm

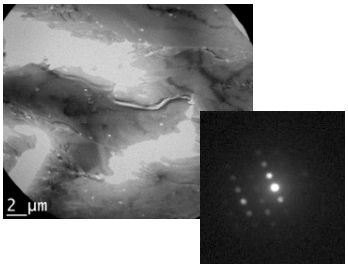

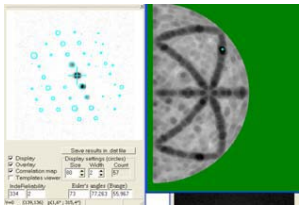

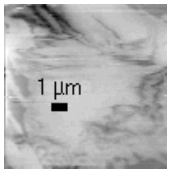

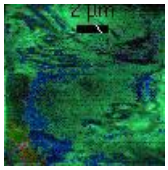

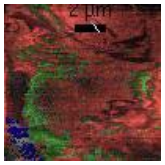

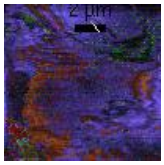

NanoMEGAS Advanced Tools for electron diffraction

Grenoble INP

Local stress simulations

Orientation Information → *Local Stress Analysis*

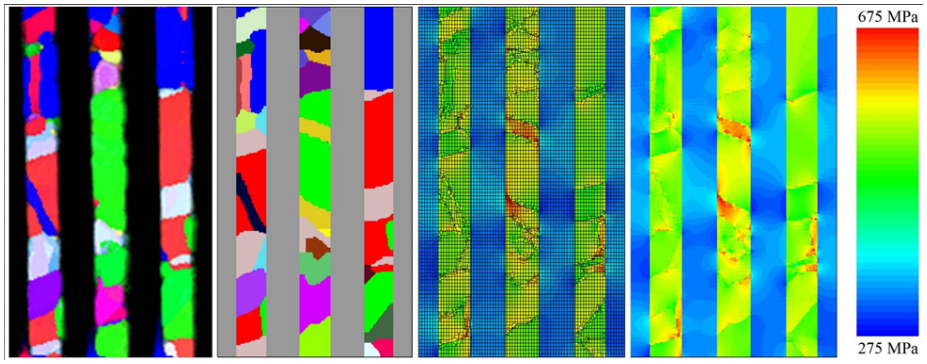

Orientation map Color coded Stress Contours

- x and y strain inputs from X-ray diffraction[1]
- Force Balance equations

Courtesy Dr. Ganesh , P.Ferreira Texas –Austin Univ USA

$$c_{ijkl} = \sum_{m=1}^{6}\sum_{n=1}^{6}\sum_{0=1}^{6}\sum_{p=1}^{6}\alpha_{im}\alpha_{jn}\alpha_{ko}\alpha_{lp}c_{mnop}$$

*Rhee, Y. Du, P. S. Ho, Journal of Applied Physics, **93** (2003) 3926*

THE UNIVERSITY OF TEXAS AT AUSTIN

Indexing high resolution image of anatase - TiO2

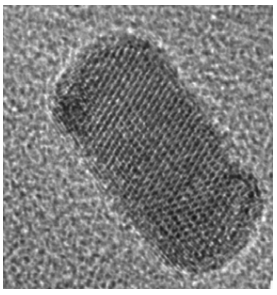

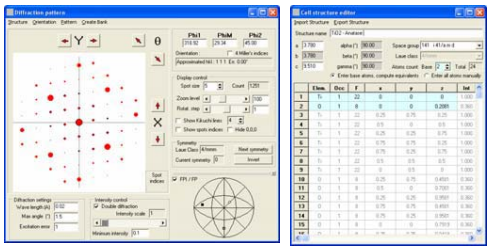

it is possible to detect automatically the nanoparticle orientation: close to [100]

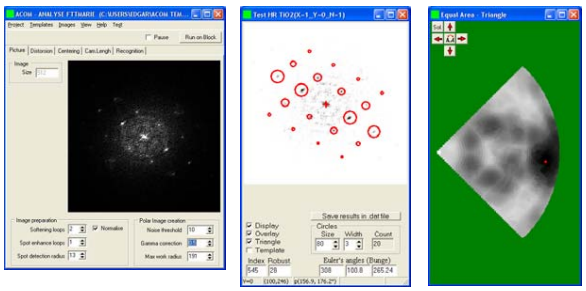

NanoMEGAS
Advanced Tools for electron diffraction

Grenoble INP

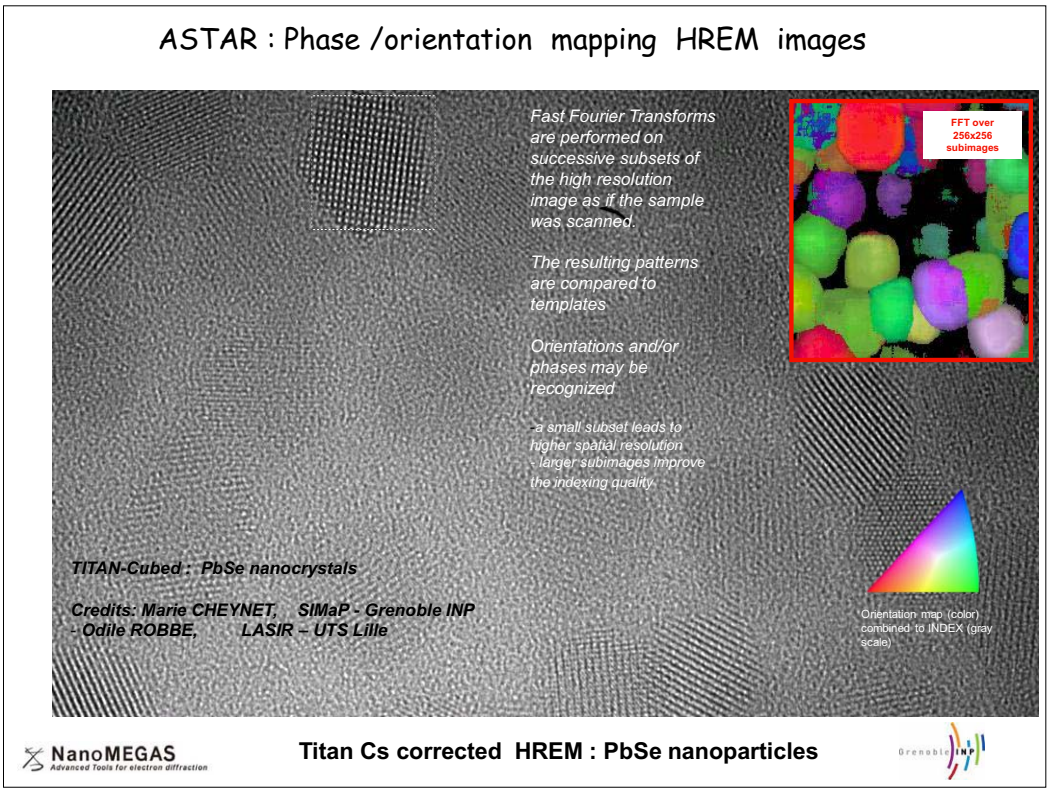
ASTAR : Phase /orientation mapping HREM images
Fast Fourier Transforms are performed on successive subsets of the high resolution image as if the sample was scanned.
The resulting patterns are compared to templates
Orientations and/or phases may be recognized
- a small subset leads to higher spatial resolution
- larger subimages improve the indexing quality.
FFT over 256x256 subimages
TITAN-Cubed : PbSe nanocrystals
Credits: Marie CHEYNET, SIMaP - Grenoble INP
- Odile ROBBE, LASIR – UTS Lille
Orientation map (color) combined to INDEX (gray scale)
NanoMEGAS
Advanced Tools for electron diffraction
Titan Cs corrected HREM : PbSe nanoparticles

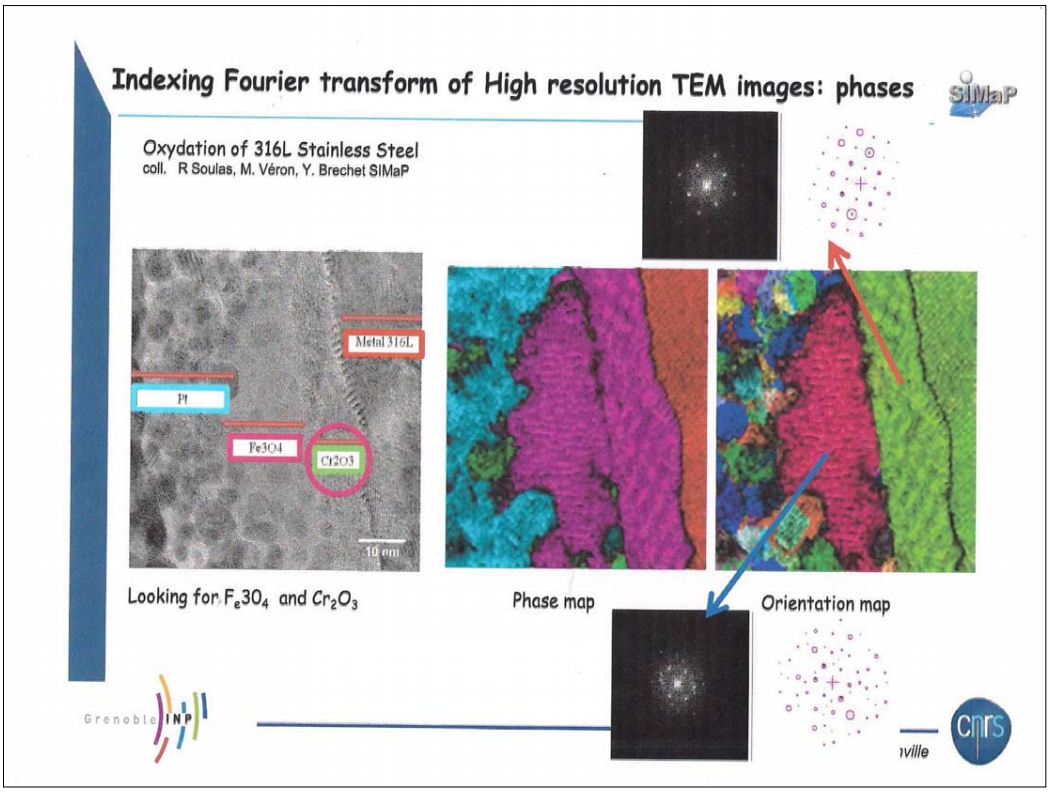
Indexing Fourier transform of High resolution TEM images: phases
SIMaP
Oxydation of 316L Stainless Steel
coll. R Soulas, M. Véron, Y. Brechet SIMaP
Metal 316L
Pt
Fe3O4
Cr2O3
10 nm
Looking for Fe_3O_4 and Cr_2O_3
Phase map
Orientation map
Grenoble INP
cnrs

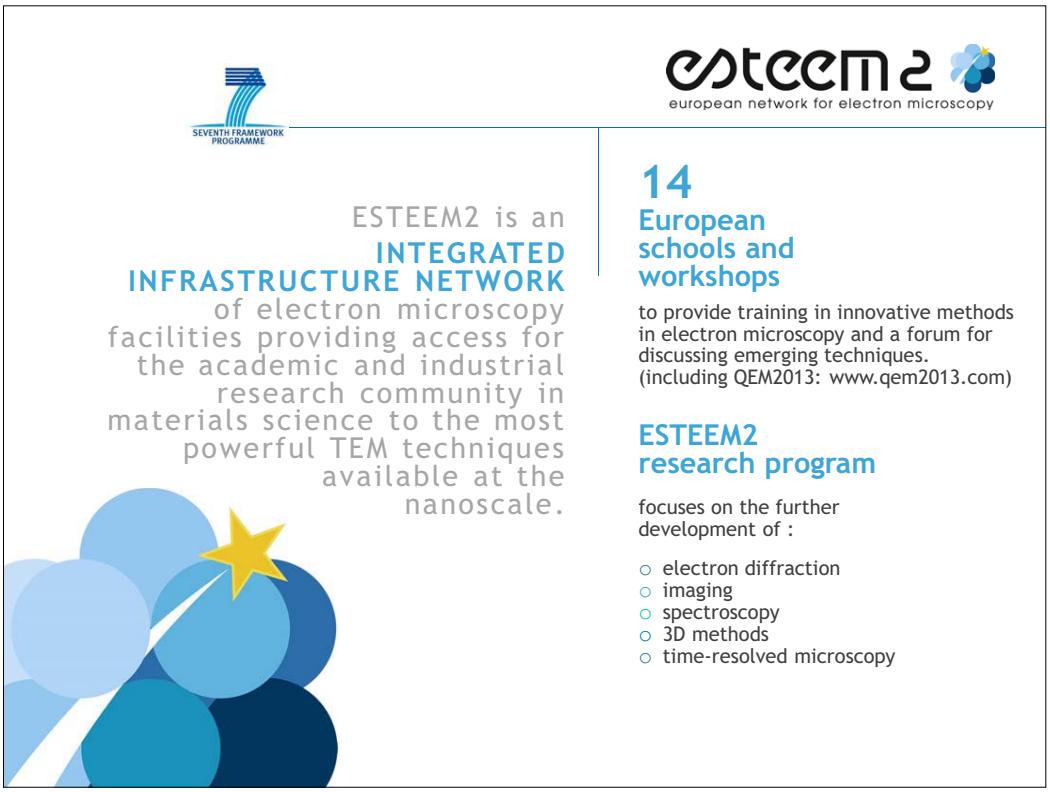
SEVENTH FRAMEWORK PROGRAMME
esteem2
european network for electron microscopy
ESTEEM2 is an
INTEGRATED INFRASTRUCTURE NETWORK
of electron microscopy facilities providing access for the academic and industrial research community in materials science to the most powerful TEM techniques available at the nanoscale.
14
European schools and workshops
to provide training in innovative methods in electron microscopy and a forum for discussing emerging techniques.
(including QEM2013: www.qem2013.com)
ESTEEM2 research program
focuses on the further development of :
electron diffraction
imaging
spectroscopy
3D methods
time-resolved microscopy

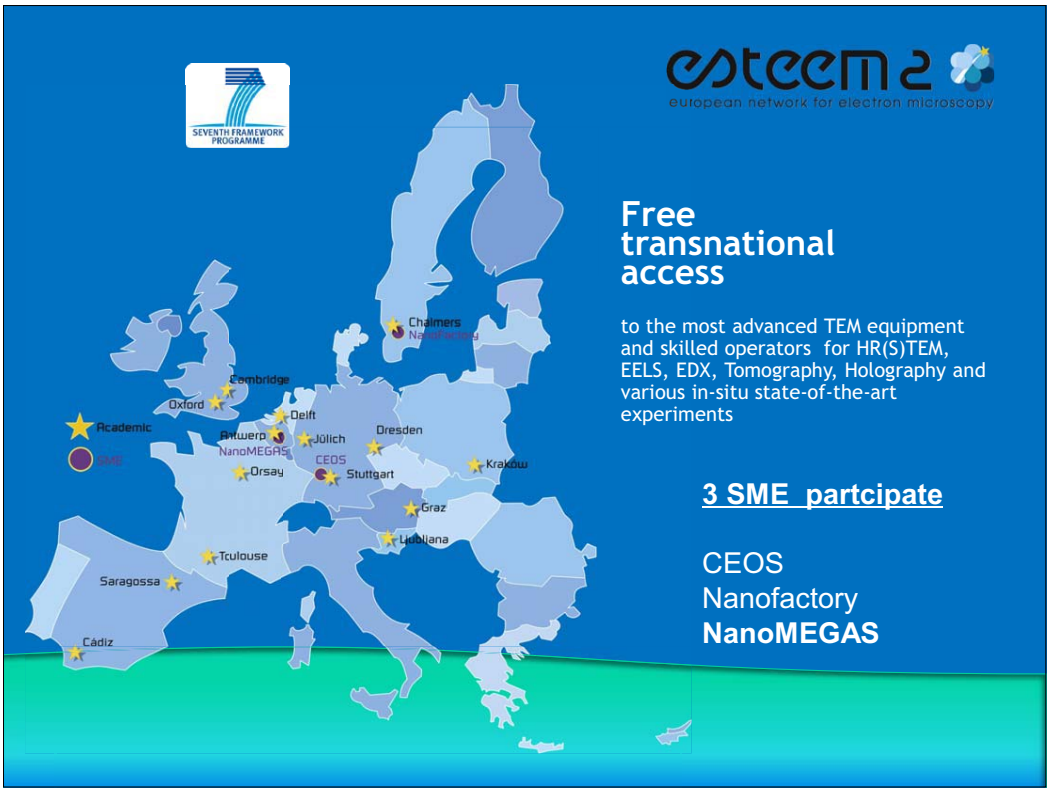
SEVENTH FRAMEWORK PROGRAMME
esteem2
european network for electron microscopy
Chalmers
Cambridge
Oxford
Delft
Academic
Antwerp
NanoMEGAS
Jülich
Dresden
CEOS
Orsay
Stuttgart
Kraków
Graz
Ljubljana
Tculouse
Saragossa
Cádiz
Free transnational access
to the most advanced TEM equipment and skilled operators for HR(S)TEM, EELS, EDX, Tomography, Holography and various in-situ state-of-the-art experiments
3 SME partcipate
CEOS
Nanofactory
NanoMEGAS

Thanks for your attention !!

COLLABORATORS

Daniel Bultreys (Brussels) Joaquim Portillo (Barcelona)
Spiros Panaretos (Athens) T. Galanis (Patras)

Edgar Rauch (CNRS Grenoble), Muriel Veron (CNRS Grenoble)

Robert Stroud (Nanomegas USA) , A. Darbal (Tempe Arizona)
Bruno Jansens (AppFive USA) , JK Weiss (AppFive USA)

info@nanomegas.com www.nanomegas.com

XRD for structural determination of materials – basics and applications

Tomasz Goryczka

Insitute of Materials Science University of Silesia

Outline

- Introduction
- Nature of X-rays and their properties
- Basic methods for materials characterization and examples
- Advanced method - structure solution, crystal size determination – examples and problems

On 8 November 1895…

Properties of X-rays – Roentgen present day

- A lot of materials are transparent for X-ray
- They make negatives and films dark
- They cause fluorescence of materials
- They don't reflect and interfere

What the X-rays are?

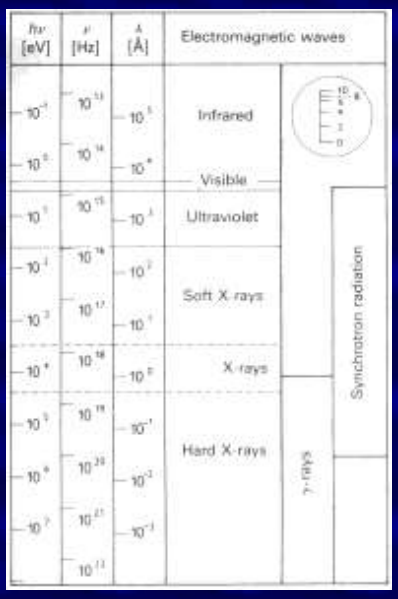

Electromagnetic radiation with wavelength from

0.01 nm to 50 nm (12 MeV – 25 eV)

For structure studies

0.2 – 2.5 Å

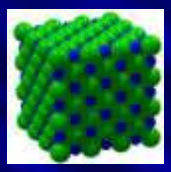

NaCl

Sources of X-rays

NATURAL

- Radioactive elements

„ARTIFICIAL"

- X-ray tube
- Synchrotron
- particle bombardment
  - protons
  - a particles
  - ion of heavy elements

Types of X-ray spectrum

- Continuous (white) spectrum
  branch of wavelength
  λ_1 ..... λ
- Characteristic spectrum
  one λ

Mechanism of continuous (white) spectrum formation

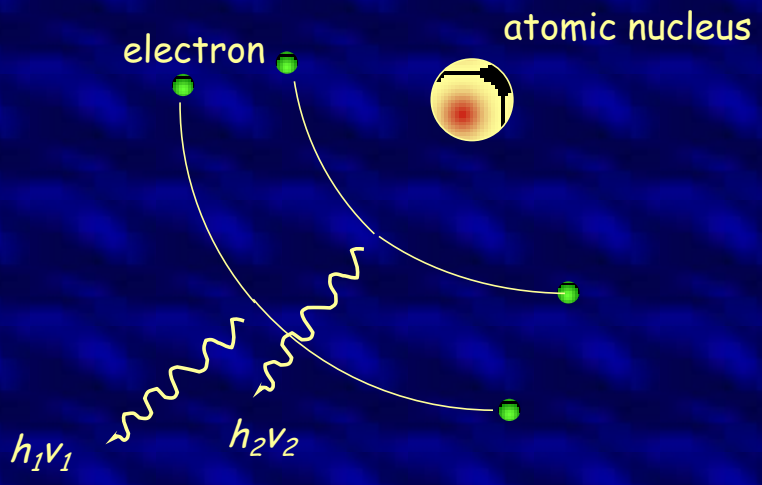

Continuous (white) spectrum

$$E = h\nu$$
$$E = eU$$

$$h\nu = eU$$
$$\nu = \frac{c}{\lambda}$$

$$\lambda = \frac{hc}{e} \cdot \frac{1}{U}$$

$$\lambda = \frac{12.39}{U}$$

Continuous spectrum vs voltage

$$\lambda = \frac{12.39}{U}$$

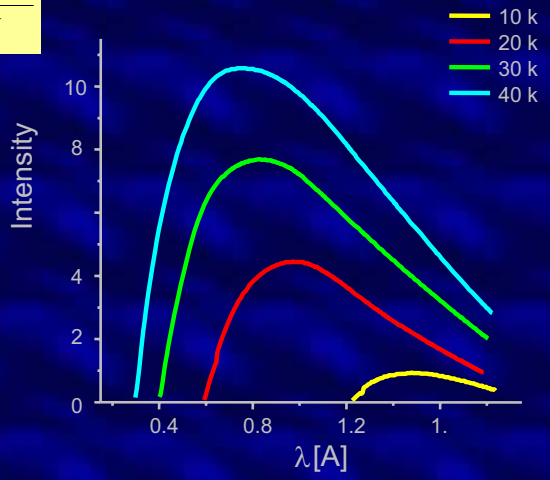

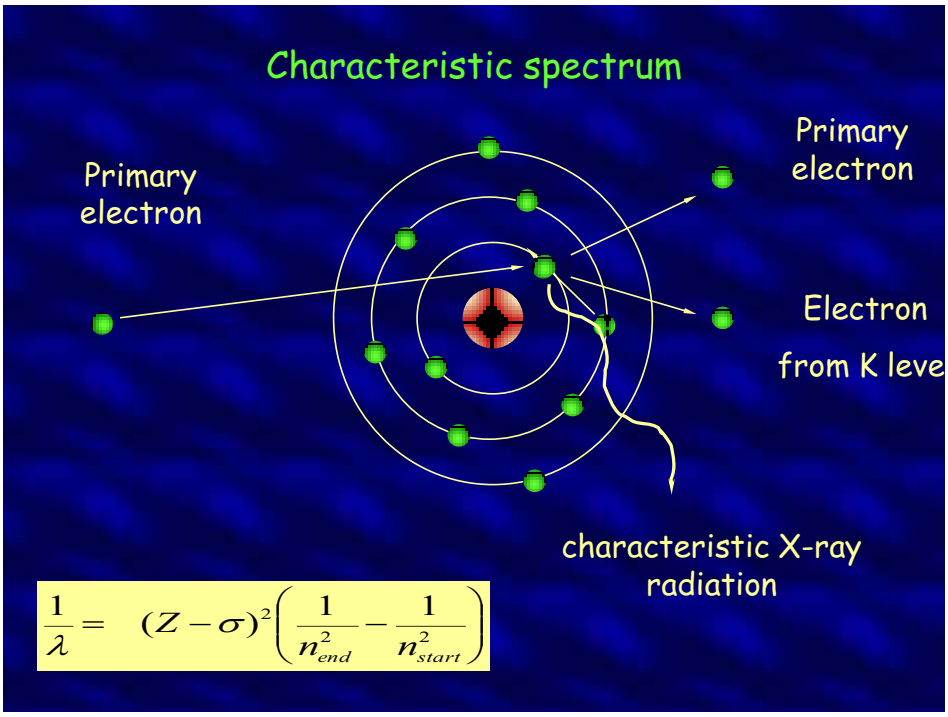
Characteristic spectrum
Primary electron
Primary electron
Electron
from K leve
characteristic X-ray radiation
$\frac{1}{\lambda} = (Z-\sigma)^2\left(\frac{1}{n_{end}^2} - \frac{1}{n_{start}^2}\right)$

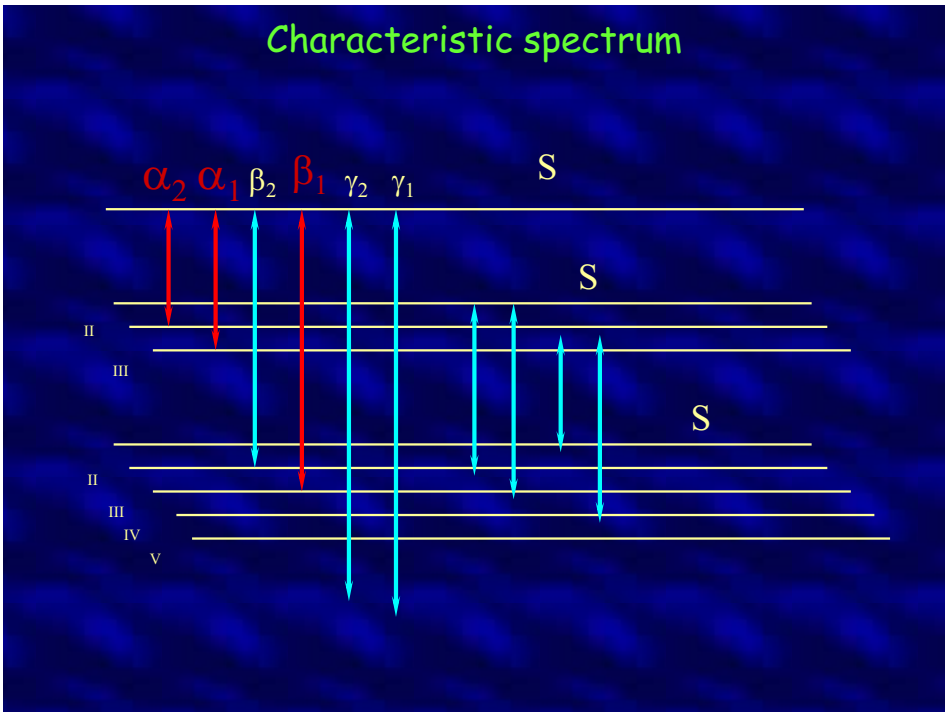
Characteristic spectrum
α_2 α_1 β_2 β_1 γ_2 γ_1
S
S
S
II
III
II
III
IV
V

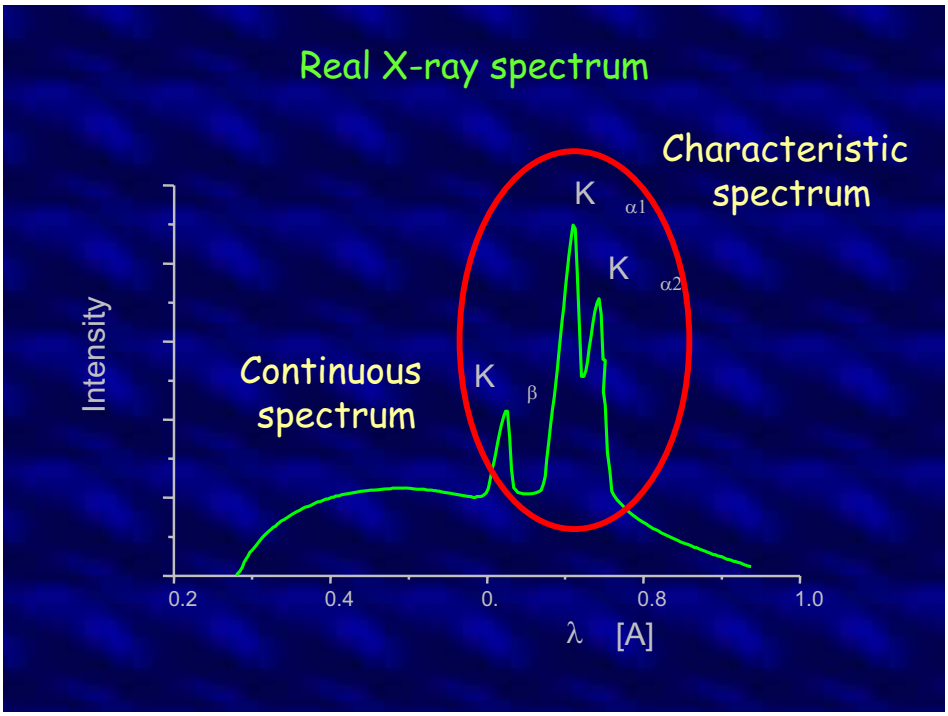
Real X-ray spectrum
Characteristic spectrum
K α1
K α2
K β
Continuous spectrum
Intensity
0.2
0.4
0.
0.8
1.0
λ [A]

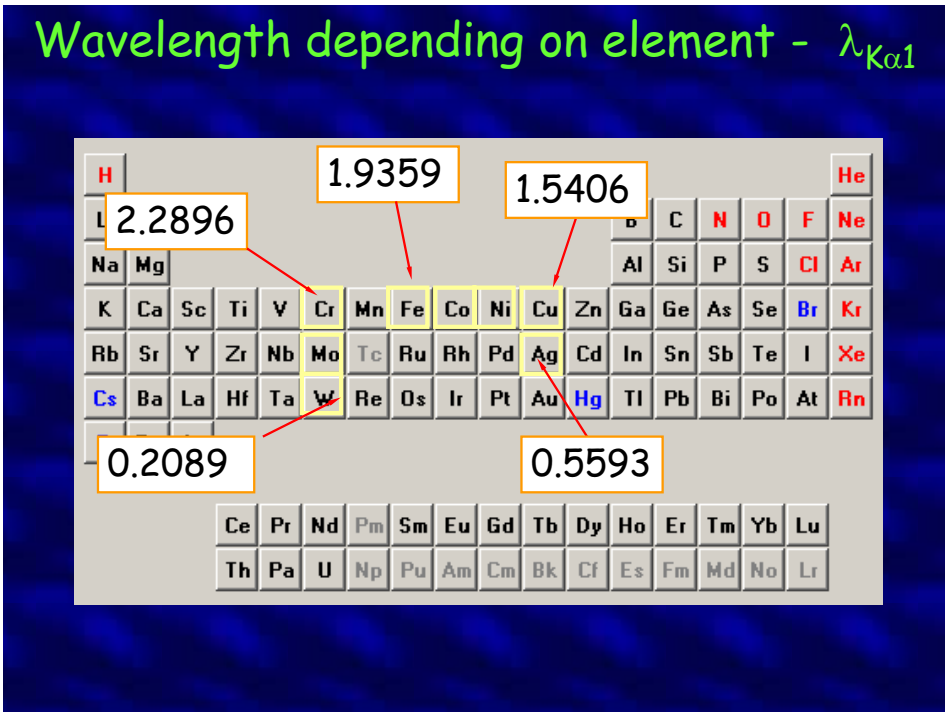
Wavelength depending on element - λKα1
1.9359
1.5406
2.2896
0.2089
0.5593

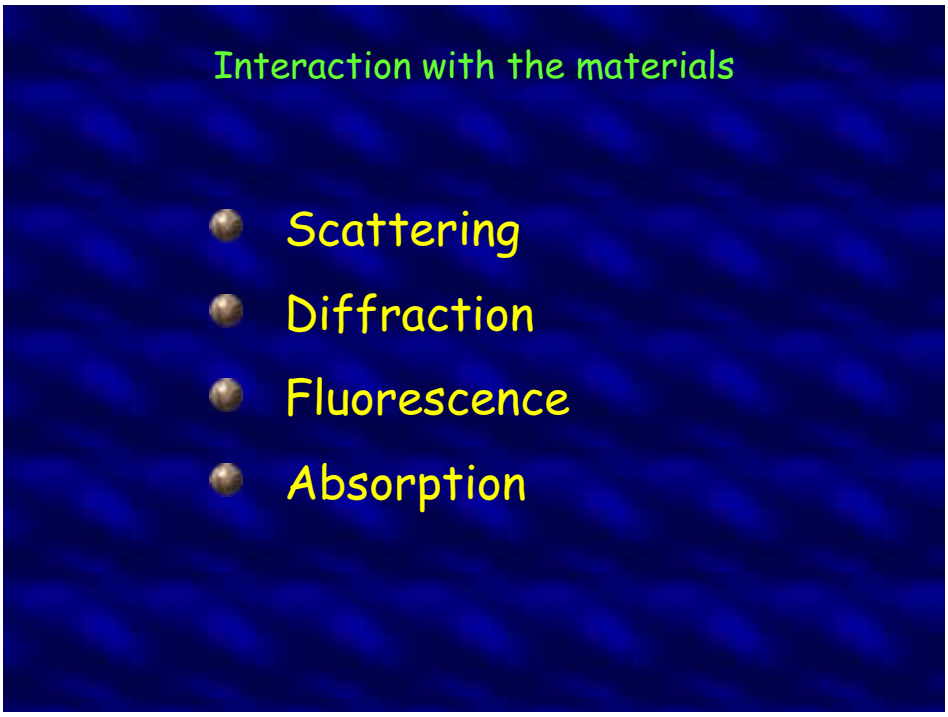
Interaction with the materials
Scattering
Diffraction
Fluorescence
Absorption

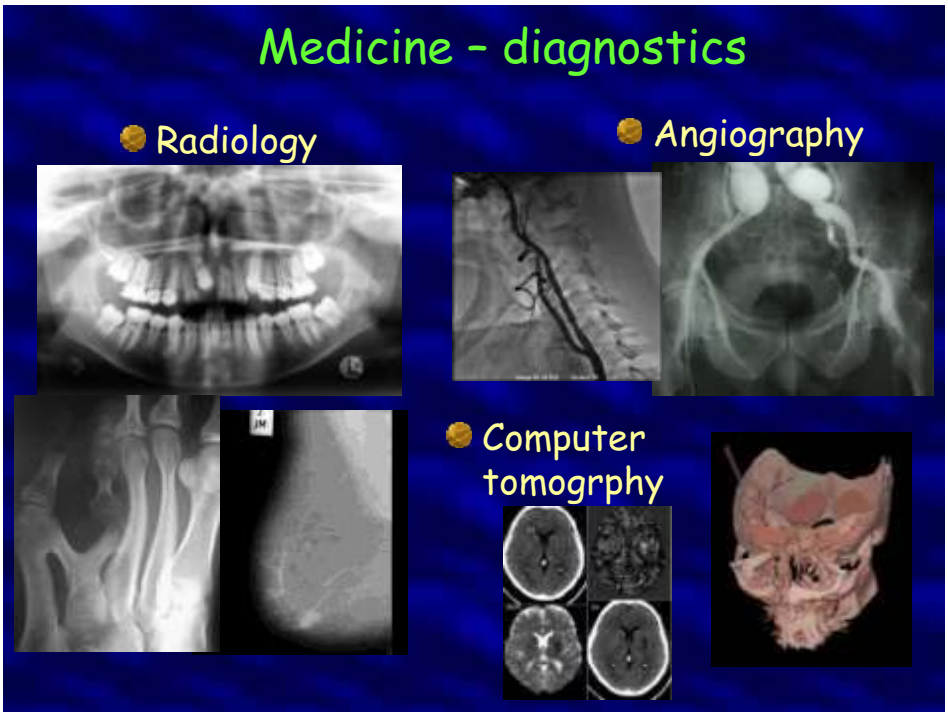
Medicine - diagnostics
Radiology
Angiography
Computer tomogrphy

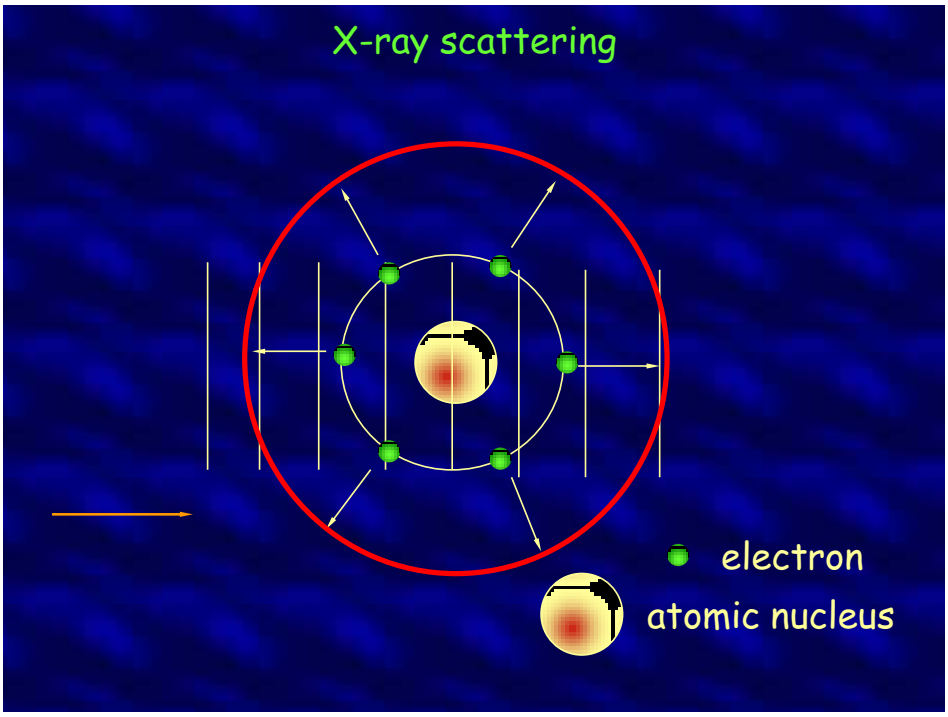
X-ray scattering
electron
atomic nucleus

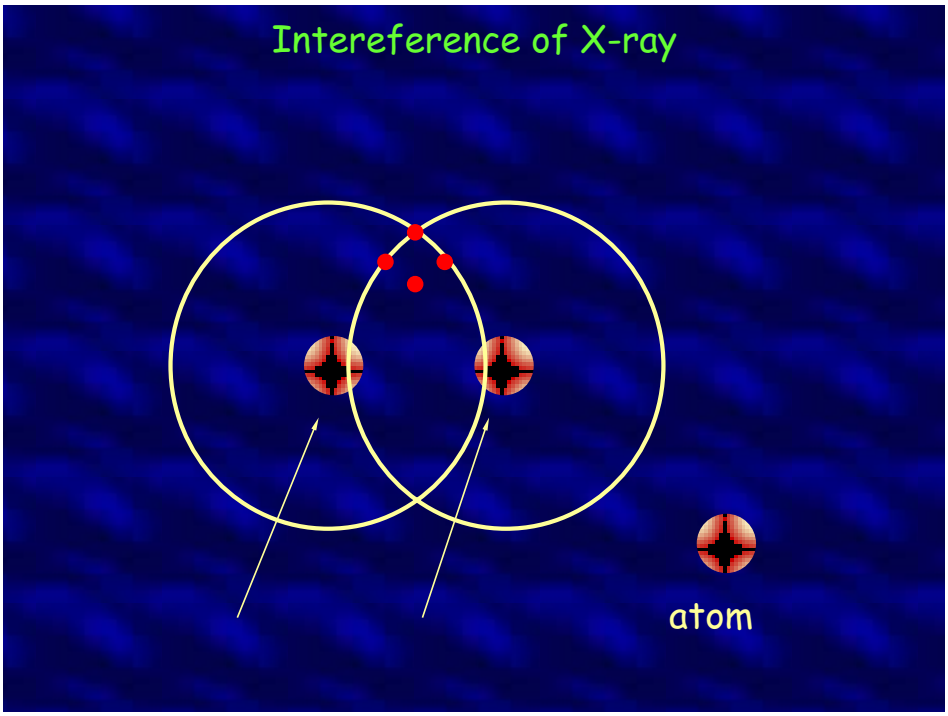
Intereference of X-ray
atom

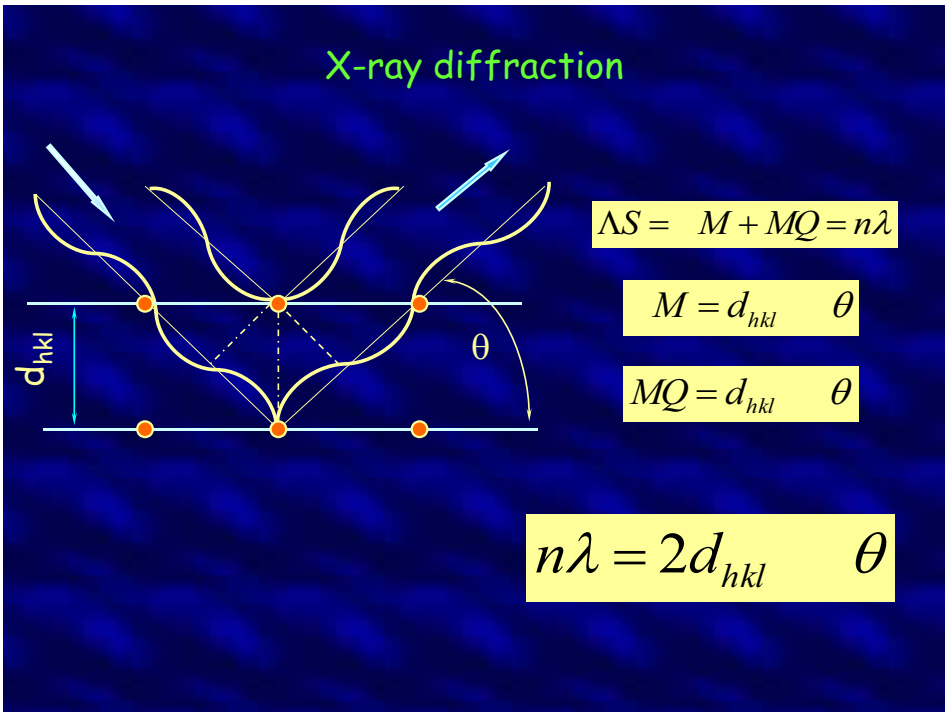
X-ray diffraction
$\Lambda S = M + MQ = n\lambda$
$M = d_{hkl} \quad \theta$
$MQ = d_{hkl} \quad \theta$
d_{hkl}
θ
$n\lambda = 2d_{hkl} \quad \theta$

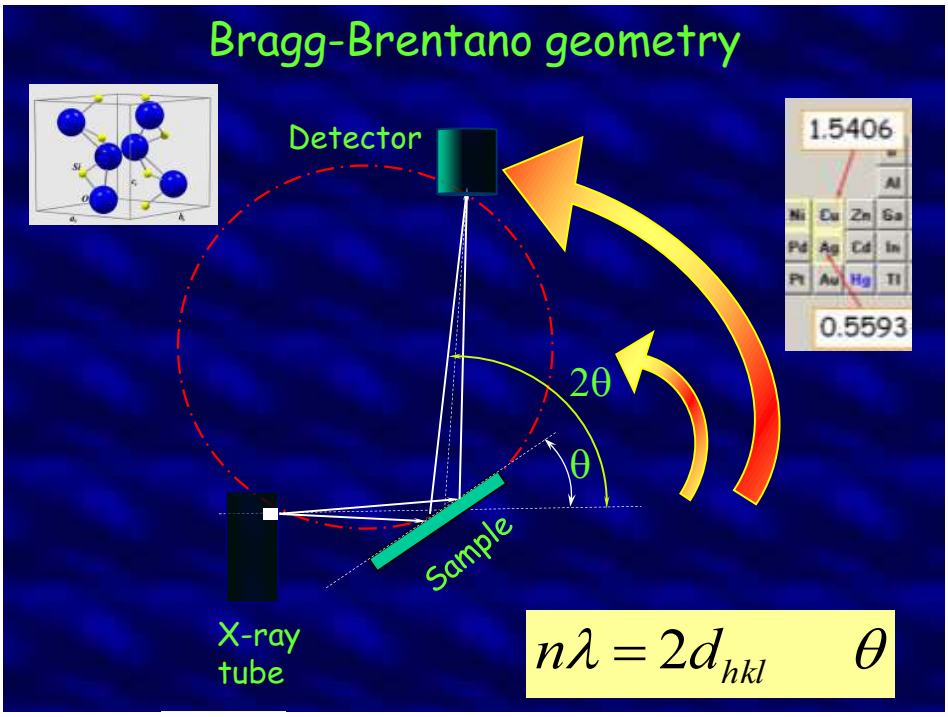
Bragg-Brentano geometry
Detector
1.5406
0.5593
2θ
θ
Sample
X-ray tube
$n\lambda = 2d_{hkl} \quad \theta$

Result of X-ray diffraction on crystal lattice

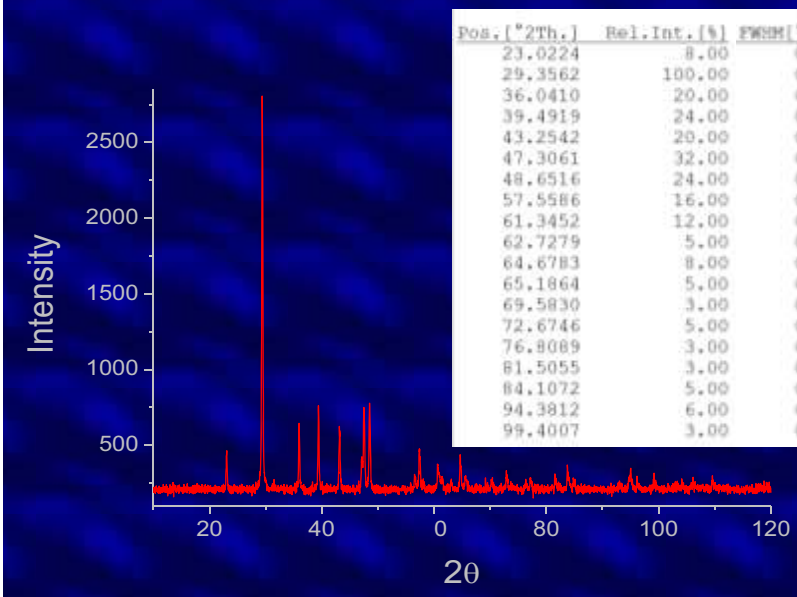

Pos.[°2Th.]	Rel.Int.[%]	FWHM[°2Th.]
23.0224	8.00	0.0694
29.3562	100.00	0.0694
36.0410	20.00	0.0694
39.4919	24.00	0.0694
43.2542	20.00	0.0694
47.3061	32.00	0.0694
48.6516	24.00	0.0694
57.5586	16.00	0.0694
61.3452	12.00	0.0694
62.7279	5.00	0.0694
64.6783	8.00	0.0694
65.1864	5.00	0.0694
69.5830	3.00	0.0694
72.6746	5.00	0.0694
76.8089	3.00	0.0694
81.5055	3.00	0.0694
84.1072	5.00	0.0694
94.3812	6.00	0.0694
99.4007	3.00	0.0694

Principals of the X-ray diffraction analysis

- each phase gives X-ray diffraction pattern characteristic only for itself;
- in a mixture, phase behaves just like it was alone;
- intensity of diffraction pattern is proportional to the phase amount;
- amount of the phase must exceed limit of detection.

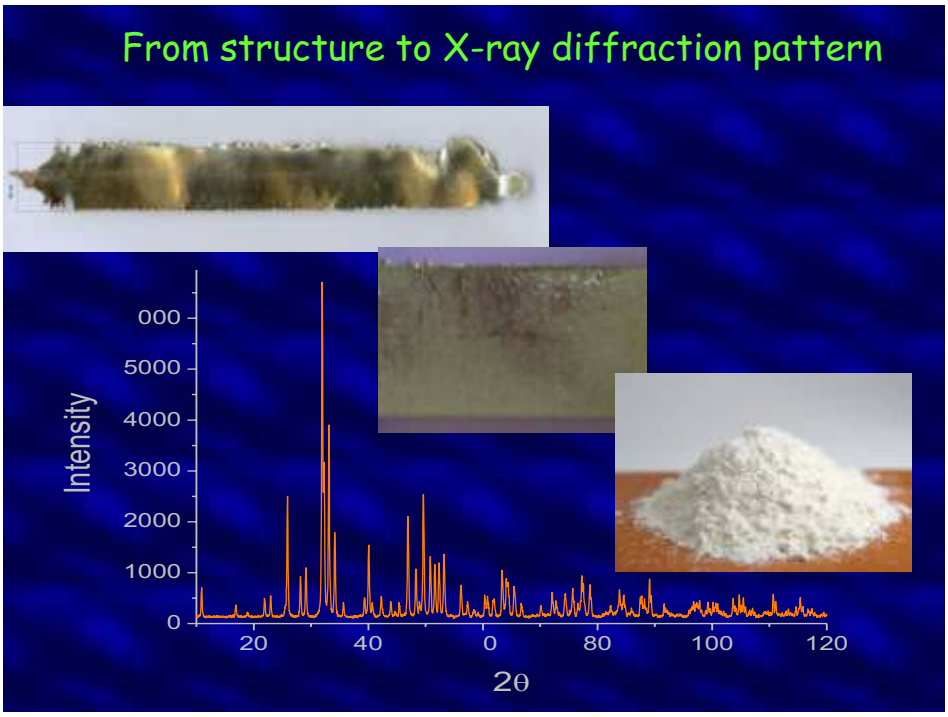
From structure to X-ray diffraction pattern
Intensity
000
5000
4000
3000
2000
1000
0
20
40
0
80
100
120
2θ

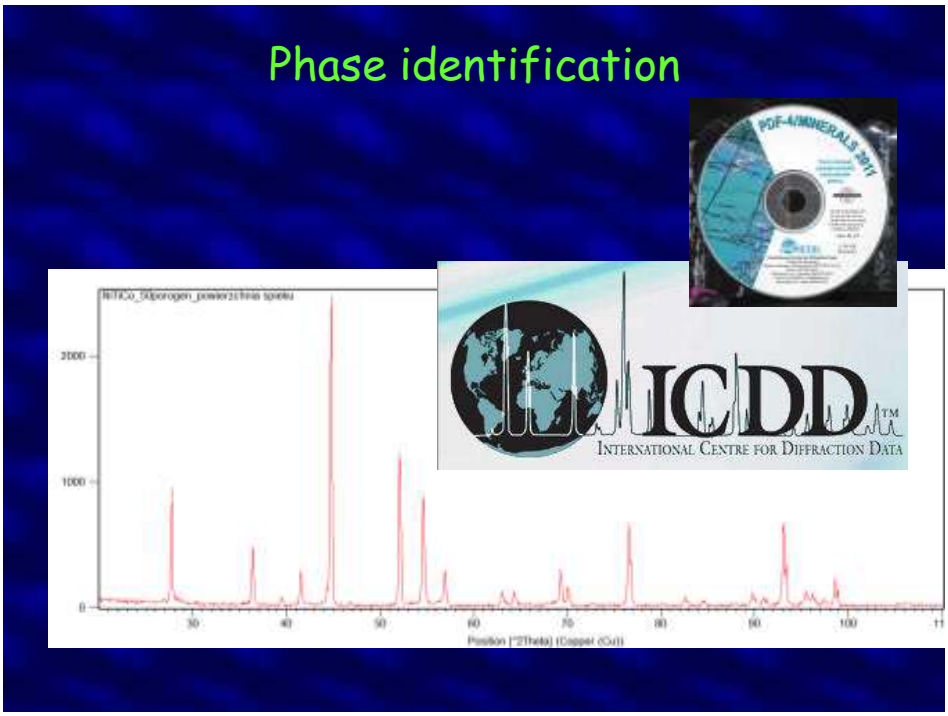
Phase identification
PDF-4/MINERALS 2011
ICDD
INTERNATIONAL CENTRE FOR DIFFRACTION DATA

It has been done

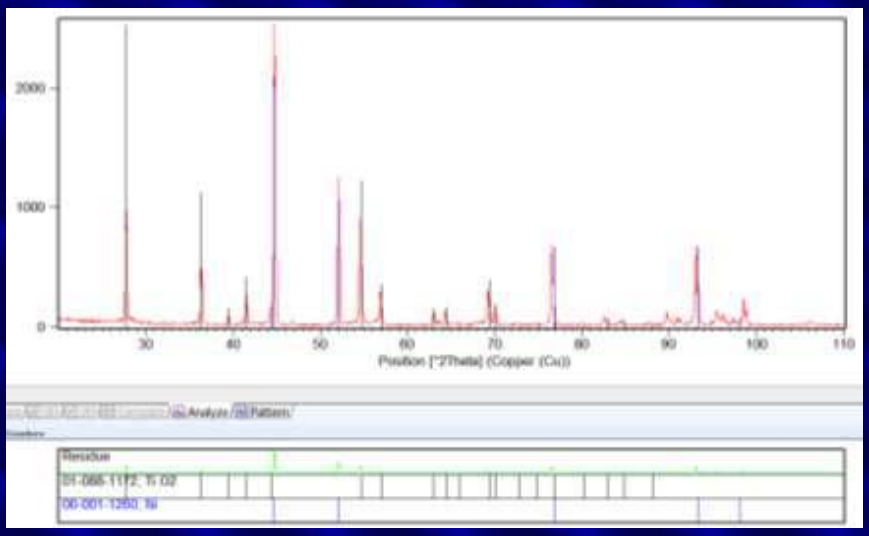

Application

(simple example)

van Gogh or no van Gogh ?

Pictures of Arles

- anatase (TiO_2)
- rutile (TiO_2)

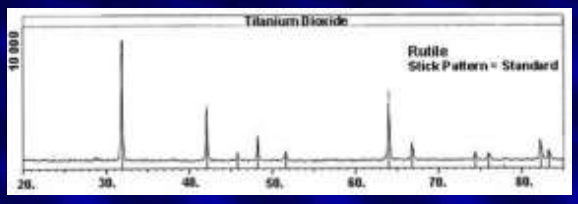

1938 – commertial production

(1853 – 1890)

Outline

- Introduction
- Nature of X-rays and their properties
- Basic methods for materials characterization and examples
- Advanced method - structure solution, crystal size determination – examples and problems

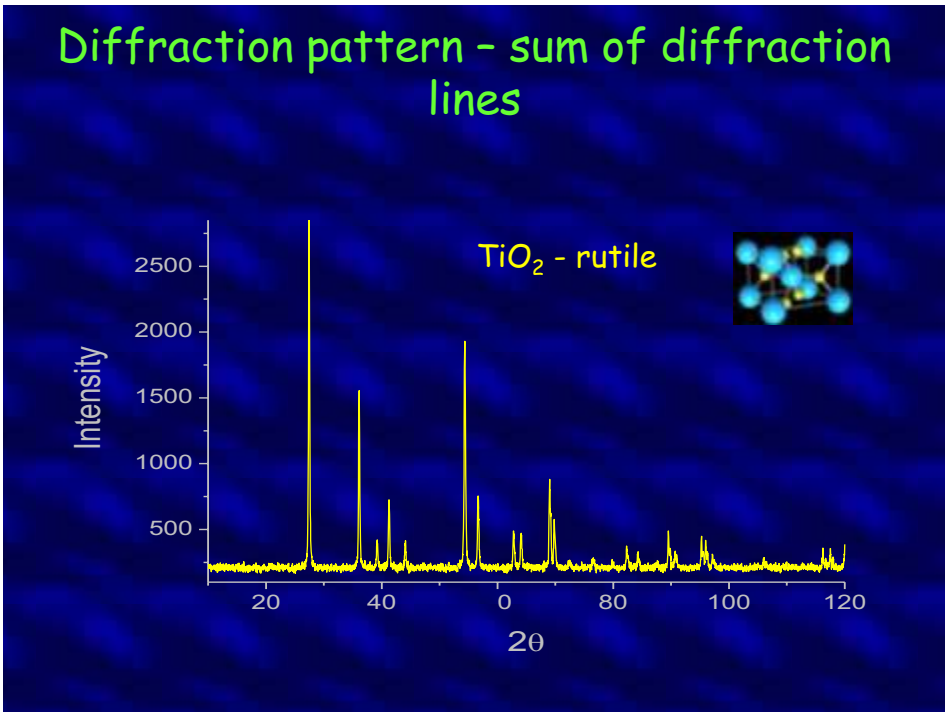
Diffraction pattern – sum of diffraction lines
TiO_2 - rutile
Intensity
2500
2000
1500
1000
500
20
40
0
80
100
120
2θ

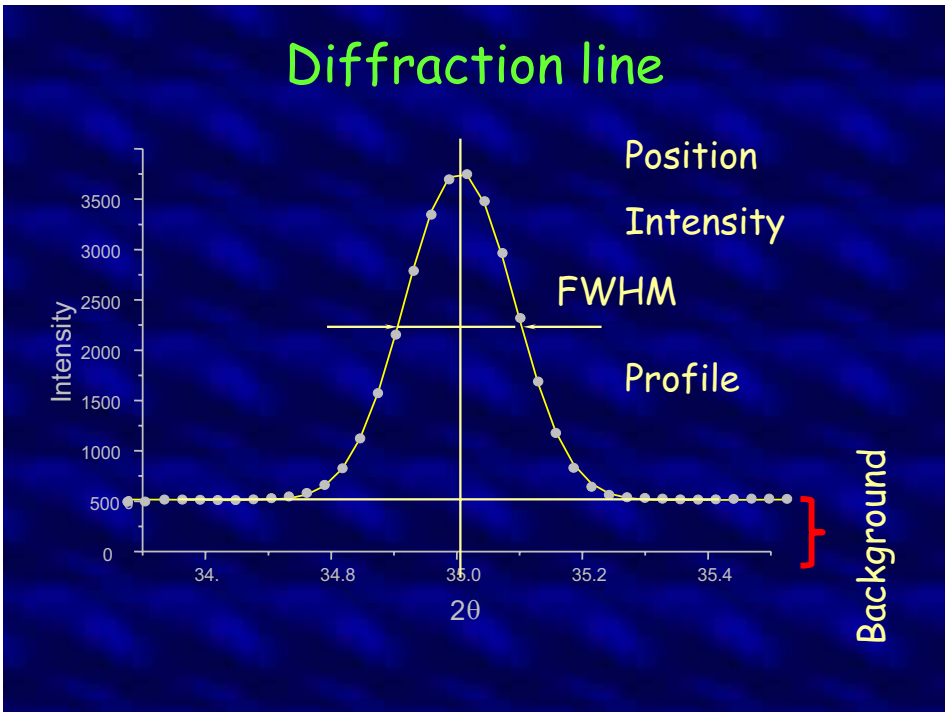
Diffraction line
Position
Intensity
FWHM
Profile
Background
Intensity
3500
3000
2500
2000
1500
1000
500
0
34.
34.8
35.0
35.2
35.4
2θ

Intensity of diffraction line
(kinematical theory)

Intensity of diffraction line

$$y_{ci} = \sum_z s_z \left(\sum_K {}_K p \left| F_K \right|^2 \Phi \ 2\theta_i) \ {}_K \ {}_K \ {}_K \right) + y_{bi}$$

K –Miller indexes – *h, k, l*

z - number of phase

Background

$$y_{ci} = \sum_z s_z \left(\sum_K {}_K p |F_K|^2 \Phi \ 2\theta_i) \ {}_K \ {}_K \ {}_K \right) + y_{bi}$$

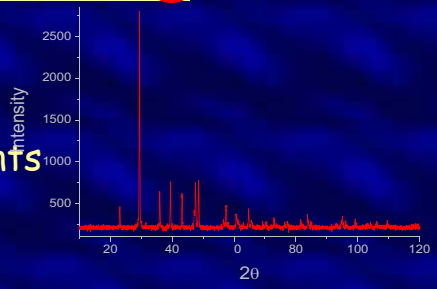

- Measured
- Interpolation of n-points
- Furrier's filtration
- Fitted with 6-th degree polynomial

$$y_{bi} = B_0 + B_1 \left[\frac{2\theta_i}{bkpos - 1} \right] + \ldots + B_6 \left[\frac{2\theta_i}{bkpos - 1} \right]^6$$

Scale factor

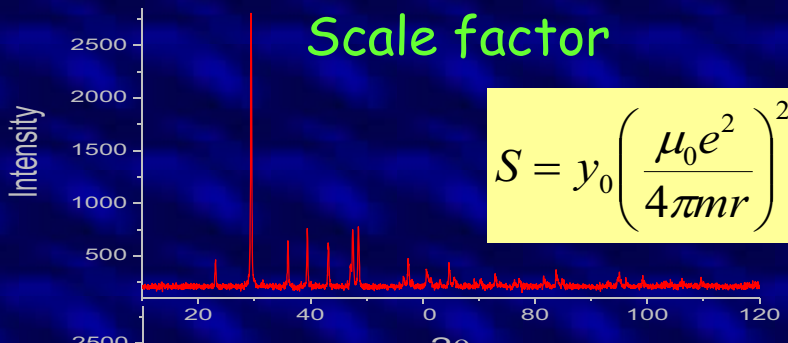

$$S = y_0 \left(\frac{\mu_0 e^2}{4\pi m r} \right)^2 \lambda^3 N^2$$

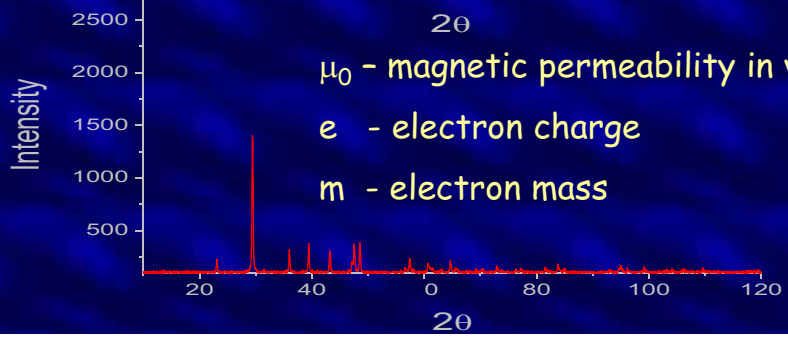

μ_0 – magnetic permeability in vacume

e – electron charge

m – electron mass

Quantitative phase analysis

$$W_p = \frac{S_p (ZMV)_p}{\sum_{i=1}^{N} S_i (ZMV)_i}$$

Z - number of molecules or atoms in the unit cell
M -mass of molecules or atoms
V - volume of the unit cell

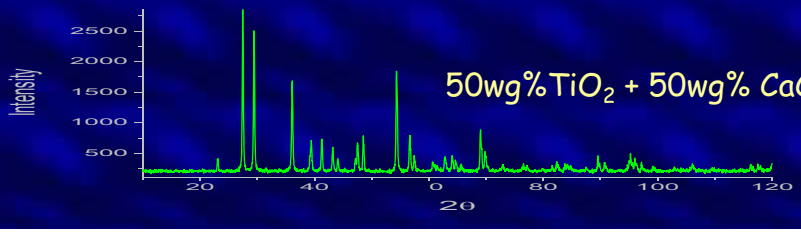

Polarisation factor, Lorentz factor and multiplicity of the plane

$$y_{ci} = \sum_z s_z \left(\sum_K {}_K |F_K|^2 \Phi \ (2\theta_i - 2\theta_K) \ {}_K \ {}_K \ {}_K \right) + y_{bi}$$

$$polarisation = \frac{(1 + \cos^2 2\theta)}{2}$$

Structure factor

$$F_K = \sum_j f_j \cdot \quad [2\pi i(hx_j + ky_j + lz_j)] \cdot N_j \cdot \quad [-M_j]$$

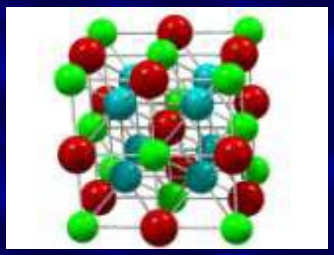

Theoretical structure

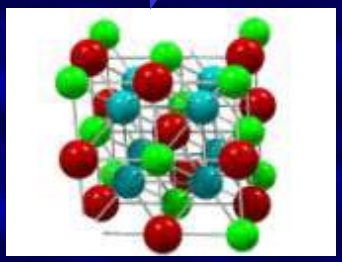

Real structure

Atomic scattering factor

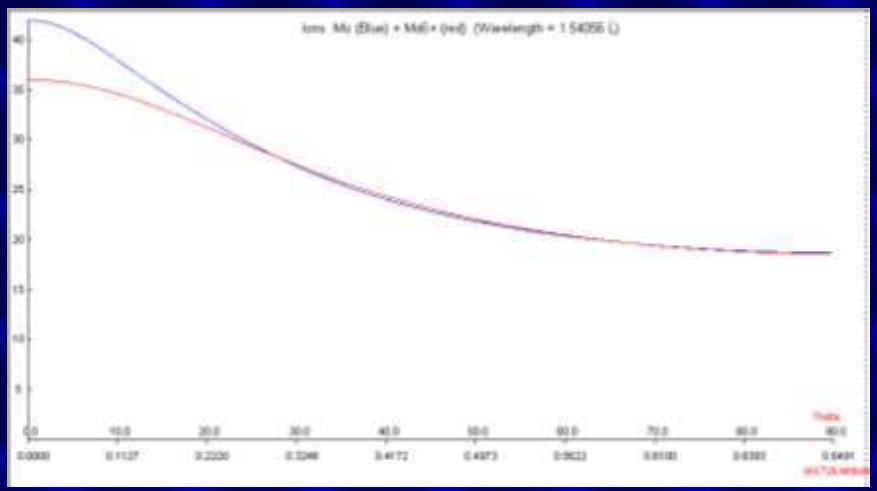

Temperature factors

$$M_j = 8\pi^2 \left\langle Biso_s^2 \right\rangle \quad {}^2\theta / \lambda$$

$$M_j = h^2 B_{11} + k^2 B_{22} + l^2 B_{33} + 2hkB_{12} + 2hlB_{13} + 2klB_{23}$$

Problem !!!!!

$$y_{ci} = \sum_z s_z \left(\sum_K {}_K \left| F_K \right|^2 \Phi \ 2\theta_i - 2\theta_K) \ {}_K \ {}_K \ {}_K \right) + y_{bi}$$

$$y_{ci} \approx \left| F_K \right|^2$$

$$F_K = \sum_j f_j \cdot \quad \left[2\pi i (hx_j + ky_j + lz_j) \right] \cdot N_j \cdot \quad [-M_j]$$

X-rays does not recognize the presence of symmetry center

Profile function

$$y_{ci} = \sum_z s_z \left(\sum_K {}_K |F_K|^2 \Phi \ 2\theta_i - 2\theta_{ic}) \ {}_K \ {}_K \ {}_K \right) + y_{bi}$$

Example of profile function

- Gaussa

$$G = \frac{\sqrt{C_0}}{{}_k\sqrt{\pi}} \cdot \left(-C_0 \frac{\Delta\theta_{i,k}^2}{{}_k^2} \right)$$

- Lorentza

$$= \frac{\sqrt{C_1}}{{}_k\pi} \cdot 1 / \left[1 + C_1 \frac{\Delta\theta_{i,k}^2}{{}_k^2} \right]$$

- Pearson VII

$$= \frac{C_5}{{}_k} \left[1 + 4\left(2^{1/m} - 1\right) \frac{\Delta\theta_{i,k}^2}{{}_k^2} \right]$$

- Splitt Pearson

$$S \ V \ - \ = C_4 \left[1 + \left(\frac{1+}{} \right)^2 \left(2^{1/m} - 1\right) \left(\Delta\theta_{i,k}^2\right) \right]^{-m}$$

$$S \ V \ - \ = C_4 \left[1 + (1+ \ )^2 \left(2^{1/m} - 1\right) \left(\Delta\theta_{i,k}^2\right) \right]^{-m}$$

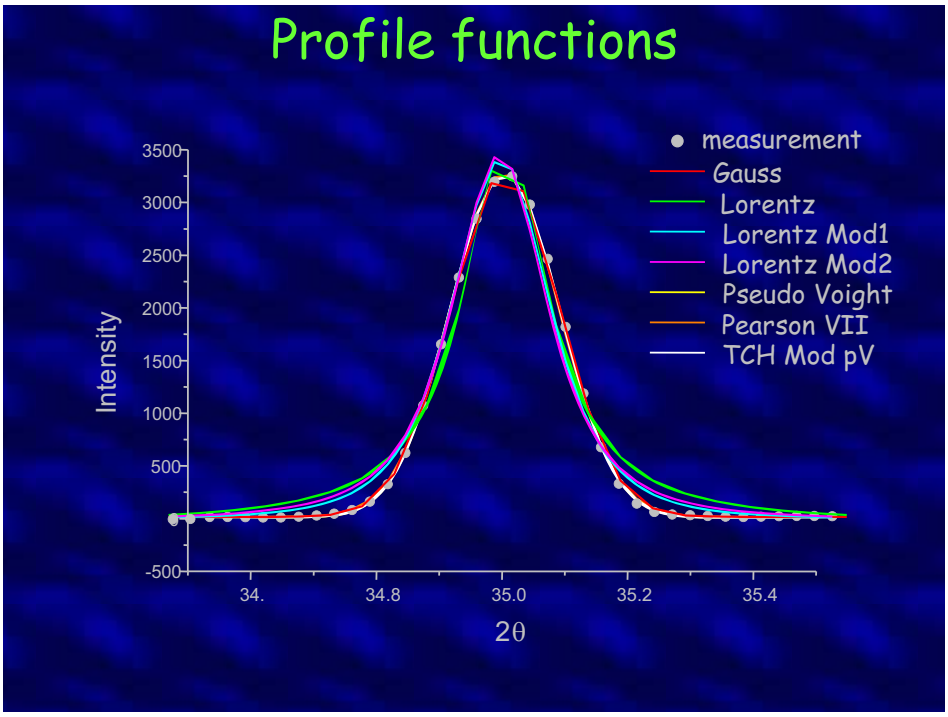
Profile functions
measurement
Gauss
Lorentz
Lorentz Mod1
Lorentz Mod2
Pseudo Voight
Pearson VII
TCH Mod pV
Intensity
3500
3000
2500
2000
1500
1000
500
-500
34.
34.8
35.0
35.2
35.4
2θ

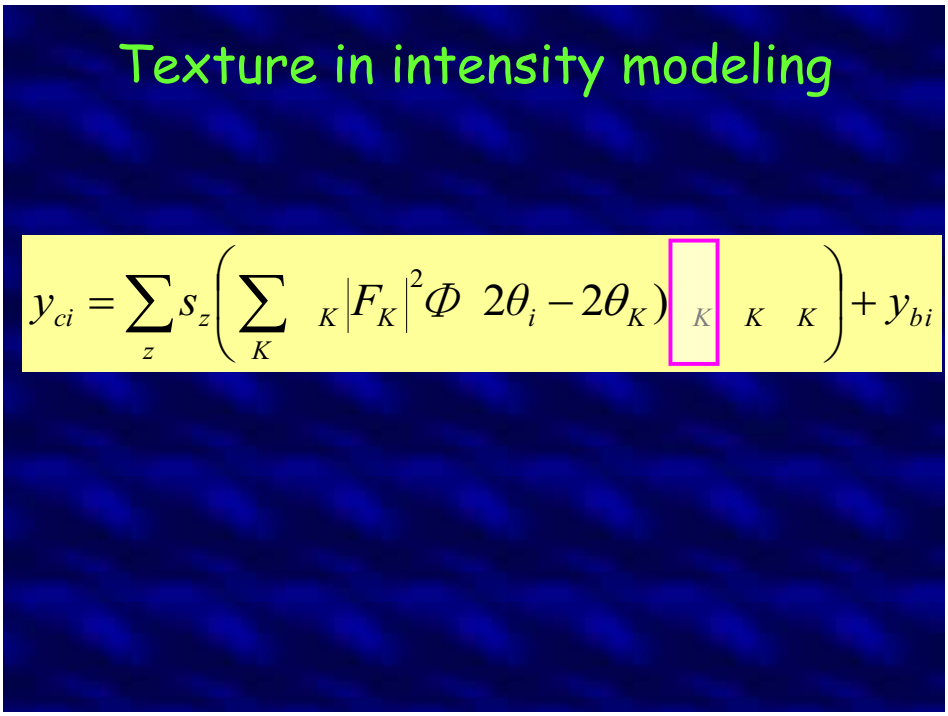
Texture in intensity modeling
$y_{ci} = \sum_z s_z \left(\sum_K {}_K \left| F_K \right|^2 \Phi \ (2\theta_i - 2\theta_K) \right) {}_K \ {}_K \ {}_K + y_{bi}$

Preffered orientation

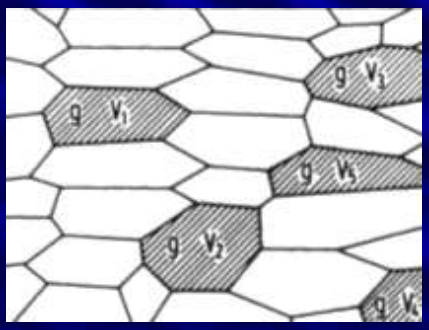

Distinguishable Direction

Transverse Direction

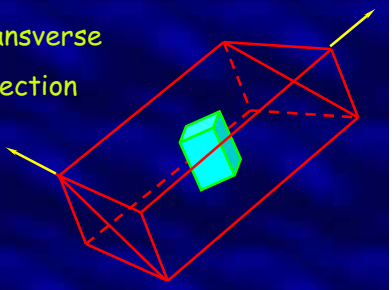

Texture is a part of the volume characterized by the same orientation.

Randomly oriented vs textured

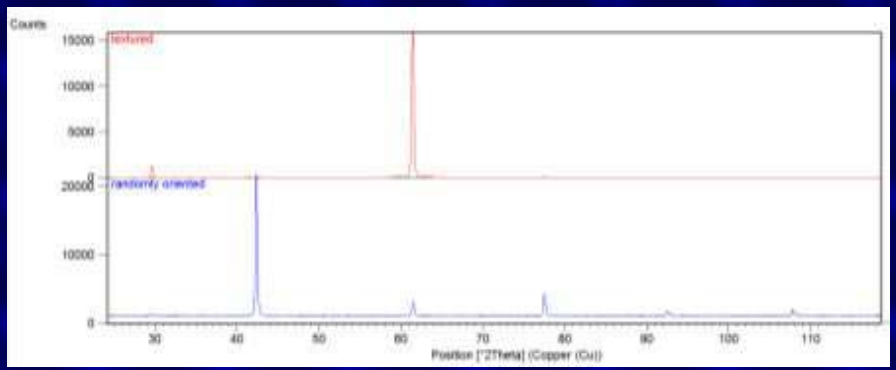

Absorption

$$y_{ci} = \sum_z s_z \left(\sum_K {}_K \left| F_K \right|^2 \Phi \ 2\theta_i - 2\theta_K) \ {}_K \ {}_K \ {}_K \right) + y_{bi}$$

Reduction of intensity:

$I / I0 = e^{-\mu x}$

μ- linear absorption coefficient

Application in structure determination

(advanced examples)

To solve a structure means

- crystallographic system — Tetragonal
- lattice parameters — a_0 = 4.9156 [Å], c_0 = 5.4081 [Å]
- space group — 3_121
- atom coordinations — Si: 0.470, 0.470, 0.000; O: 0.152, 0.412, 0.126

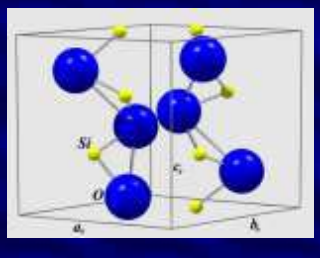

Problem !!!!

S c a c a

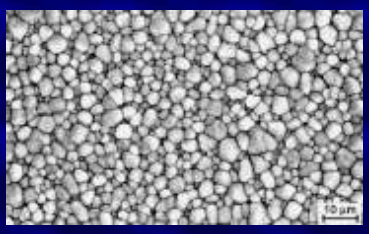

3 ma m 1 m a m

Step in structure solution

- crystal system determination
- X-ray diffraction pattern indexing
- lattice parameter determination
- choosing space group
- atom coordinates determination
- structure refinement and verification

Automatic indexing

- crystal system determination
- X-ray diffraction pattern indexing

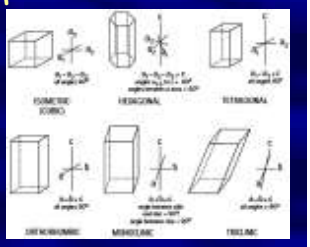

- lattice parameter determination

Automatic indexing

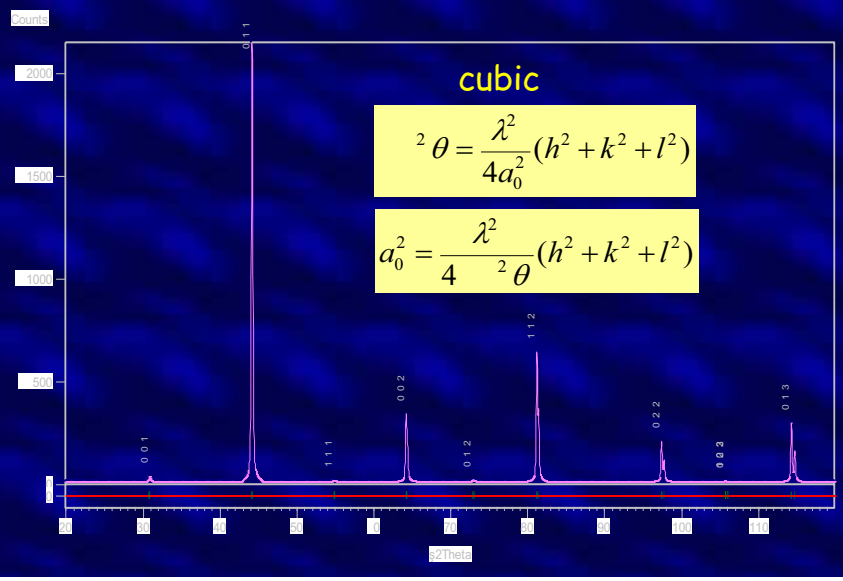

cubic

$$\sin^2\theta = \frac{\lambda^2}{4a_0^2}(h^2+k^2+l^2)$$

$$a_0^2 = \frac{\lambda^2}{4\sin^2\theta}(h^2+k^2+l^2)$$

How many atoms in unit cell?

$$m = \rho V$$

m – mass of one unit cell, ρ - density, V – volume of the unit cell

$$Z = \frac{m}{M} = \frac{\rho V}{M}$$

Z – number of atoms in unit cell

M – molecular weight

Space group determination

- X-ray diffraction pattern
- Suport form electron microsopy
  - CBED
  - Mikrodiffraction
  - MD + Beam precesion

Space group – from XRD

- model building together with atom position
- kinematically forbidden reflection

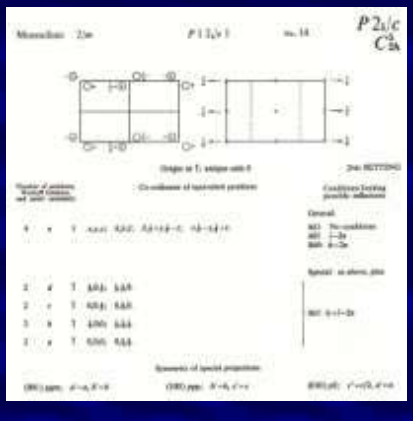

Position of atoms

(difficult)

Trialas and errors

- simple structures:
  diamond, graphite, iron
  1917 – difractometer

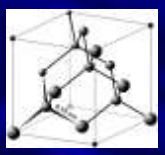

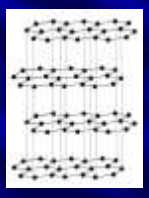

Adrenalina

Insuline

- systematic approach
  1940 – Zachariasen – UCl_3 - $P6_3/m$
  - heavy atoms U – permanent position in the crystal lattice
  - changing position for Cl

How to chose position?

- isostructural similarity
  - data base searching

Space group $P2_1/a$

$C_2(\quad_4)_3$ $\quad_2(\quad_4)_3$ $\quad_2(\quad_4)_3$ $\quad_2(\quad_4)_3$

$_{1.8}C_{0.2}(\quad_4)_3$

a ( ):	15.5690	a ( ):	15.7370
b ( ):	9.1707	b ( ):	9.2310
c ( ):	18.1410	c ( ):	18.2240
a (°):	125.3900	a (°):	125.4600

J Solid State Chem. 58 (1985) 452

$a = 15.3803$Å
$b = 9.0443$ Å
$c = 17.888$ Å
β = 125.4°

J Solid State Chem. 76 (1988) 328 333

$a = 7.697$ Å
$b = 11.535$ Å
$c = 11.944$ Å
β = 115.19°

S S a C m. 52 (1984) 313 319

Deduction from chemical formula

- c m ca c m

Z

G. . a , S. . aw , . H. & w. . ,

Nature 7 , 437 438 (30 a c 1978)

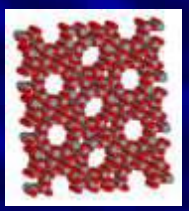

a ( ):	20.1080
b ( ):	19.9180
c ( ):	13.3920
a (°):	90
a (°):	90
Gamma (°):	90

G a a: ma

$^{+}_{/}$ [($_2$) (S $_2$)].mH$_2$

From X-ray diffraction patterns

$$y_{ci} \approx |F_K|^2$$

LeBail method or Powley method

$$S = \sum_i \frac{1}{F_o(i)} \left(F_o(i) - F_c(i)\right)^2$$

$F_c(i)$ = calculated square of structure factor for *i-th* step,

$F_o(i)$ = „measured" square of structure factor for *i-th* step,

Determination of atom position

- Direct methods

$$|E_{hkl}|^2 = \frac{|F_{hkl}|^2}{\langle |E_{hkl}|^2 \rangle}$$

- Patterson synthesis

$$P(uvw) = \frac{1}{v^2} \sum_h \sum_k \sum_l |F(hkl)|^2 exp - i2\pi(hx + ky + lz)$$

interatomic vectors

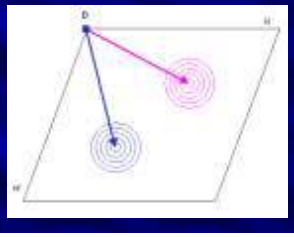

Determination of atom position

- Distribution of electron density

$$\rho(xyz) = \frac{1}{v}\sum_h\sum_k\sum_l |F(hkl)| \exp i\varphi(hkl) exp - i2\pi(hx + ky + lz)$$

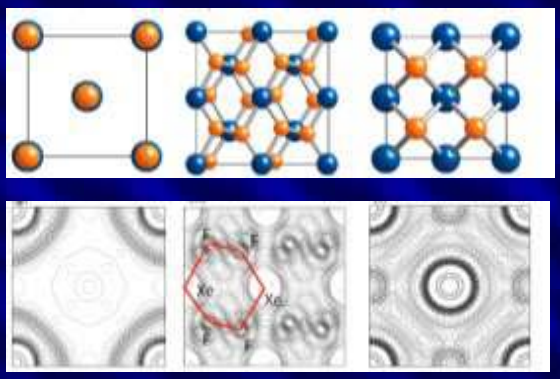

Model verification

65

J. Appl. Cryst. (1969). **2**, 65

A Profile Refinement Method for Nuclear and Magnetic Structures

BY H. M. RIETVELD

Reactor Centrum Nederland, Petten (N.H.), The Netherlands

(*Received* 29 *November* 1968)

$$S_y = \sum_i w_i (y_i - y_{ci})^2$$

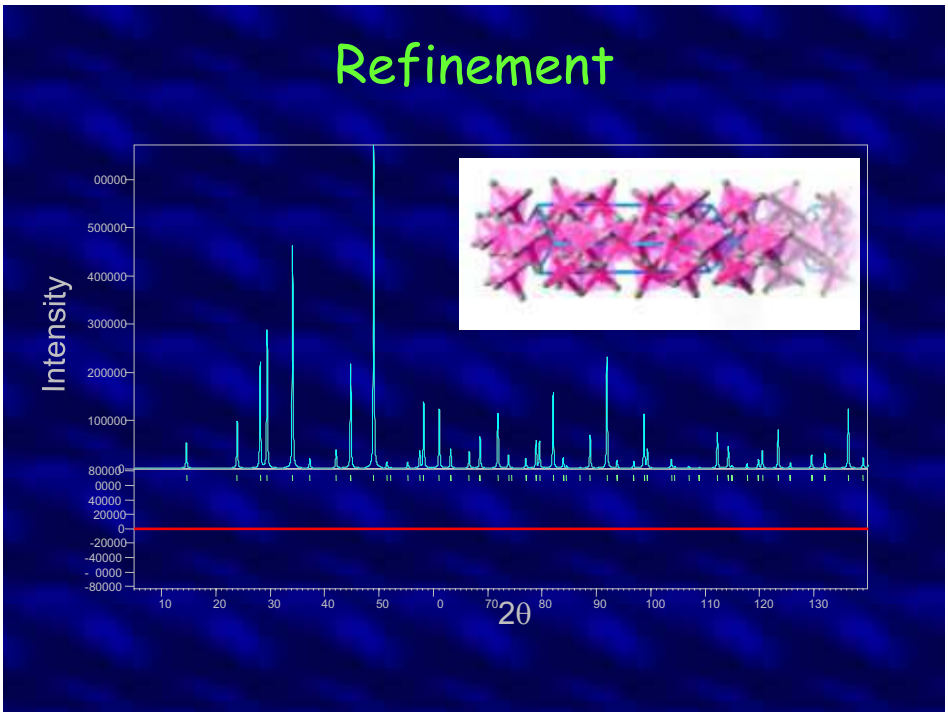
Refinement
Intensity
2θ

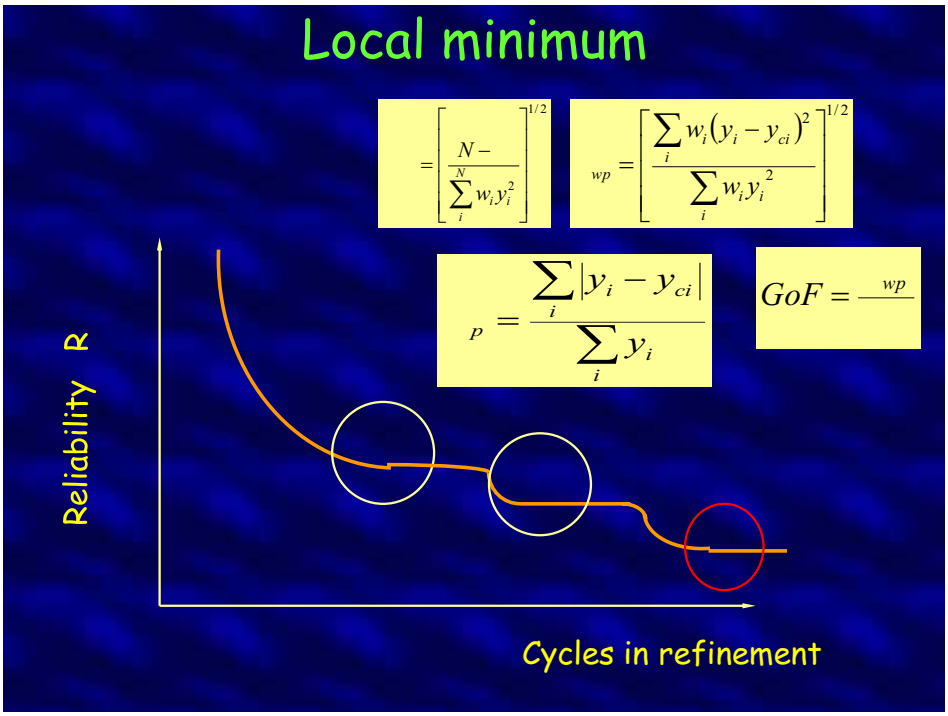
Local minimum
Reliability R
Cycles in refinement
GoF = wp

Example

Transformation in NiTi-based alloys

- One step transformation
  - B2 ⇔ B19
  - B2 ⇔ B19'
- Two steps transformation
  - B2 ⇔ R ⇔ B19'
  - B2 ⇔ B19 ⇔ B19'

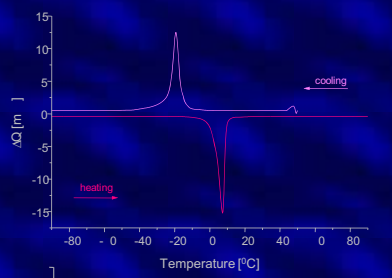

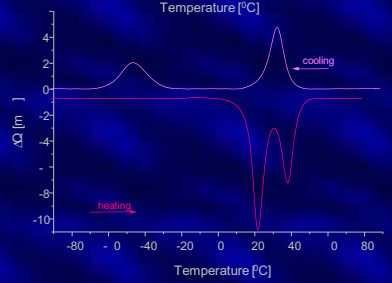

Known phases – B2

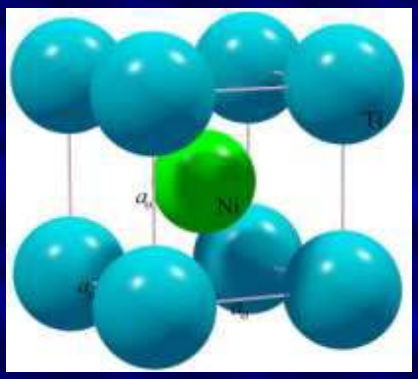

$P\,m\bar{3}m$

$a_0 = 2.8 \div 3.02$ [Å]

Interpretation of the R-phase creation

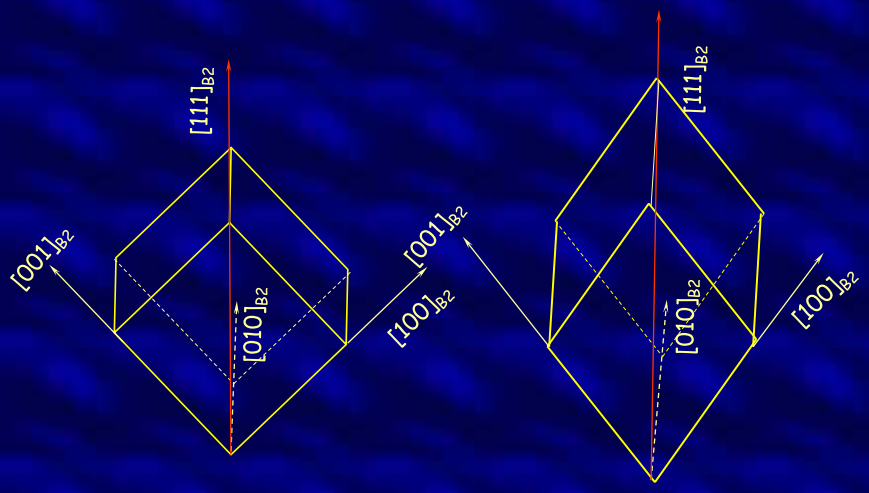

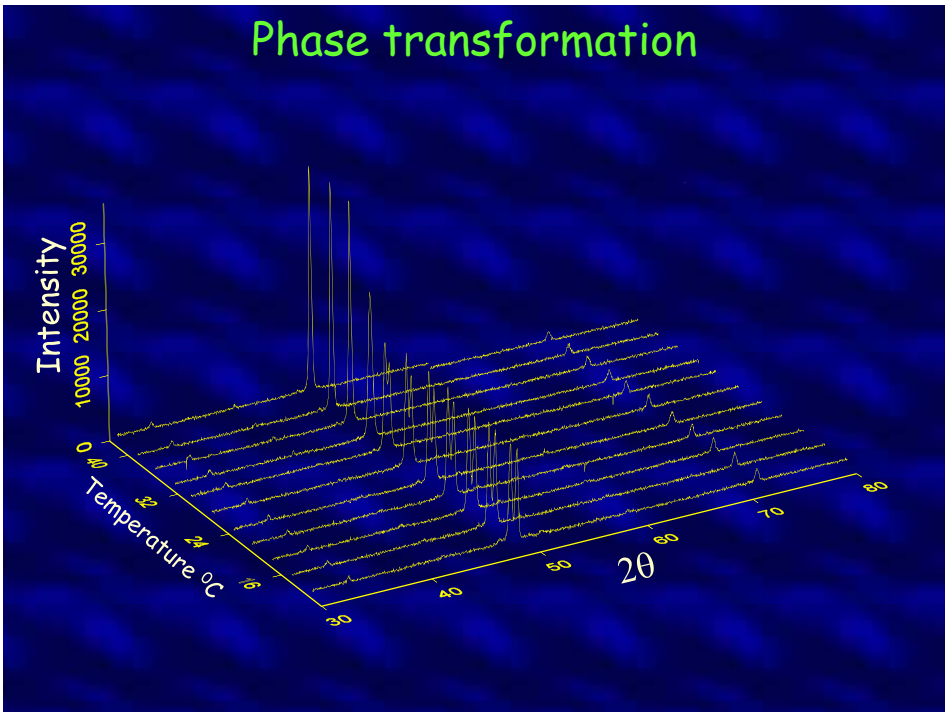
Phase transformation
Intensity
10000
20000
30000
Temperature °C
0
8
16
24
32
40
30
40
50
60
70
80
2θ

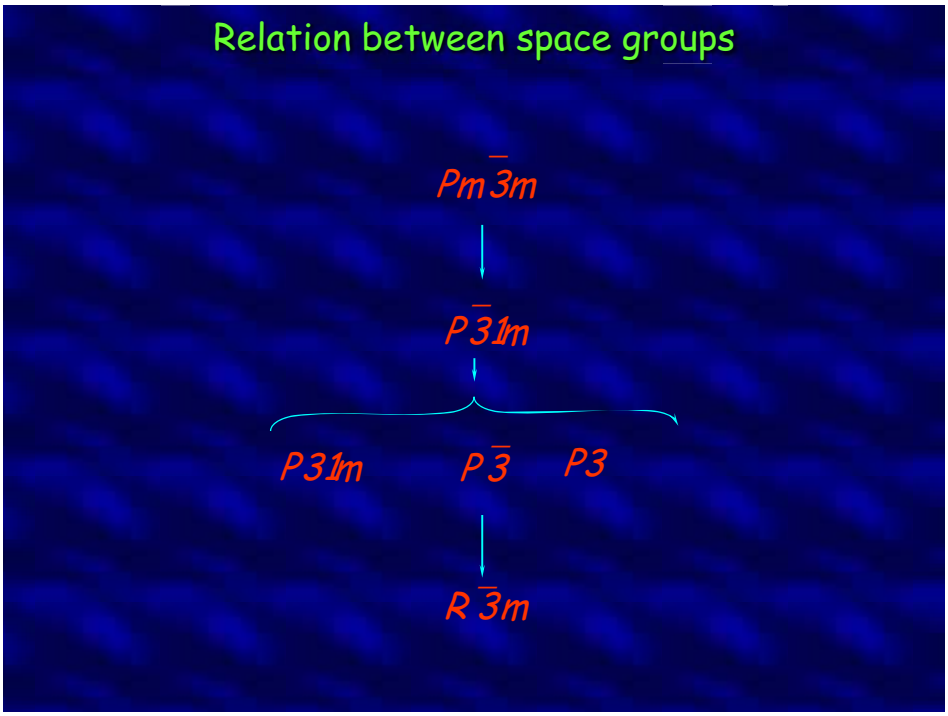
Relation between space groups
Pm3̄m
P3̄1m
P31m
P3̄
P3
R3̄m

Atom positions for model P-3

No. 147 $P\bar{3}$

enerators selected (1); $t(1,0,0)$; $t(0,1,0)$; $t(0,0,1)$; (2); (4)

sitions

Coordinates

Reflection conditions

General:

g	1	(1) x,y,z (4) $\bar{x},\bar{y},z$	(2) $\bar{y},x-y,z$ (5) $y,\bar{x}+y,z$	(3) $\bar{x}+y,\bar{x},z$ (6) $x-y,x,\bar{z}$	no conditions

Ti4 Ni4

Special:

f	$\bar{1}$	$\frac{1}{3},\frac{2}{3},z$	$\frac{2}{3},\frac{1}{3},\bar{z}$		no extra conditions
e	$\bar{1}$	$\frac{1}{3},\frac{2}{3},0$	$\frac{2}{3},\frac{1}{3},0$		
d	3..	$\frac{1}{3},\frac{2}{3},z$	$\frac{2}{3},\frac{1}{3},z$		
c	3..	$0,0,z$	$0,0,\bar{z}$		
b	$\bar{3}$..	$0,0,\frac{1}{2}$			
a	$\bar{3}$..	$0,0,0$			

Ti2 Ni2

Ni1

Ti1

Patterson maps

(001)

1/2[001]

2/3[001]

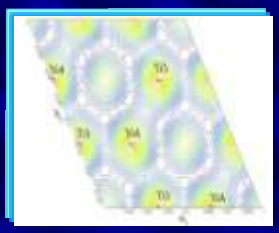

1/3[001]

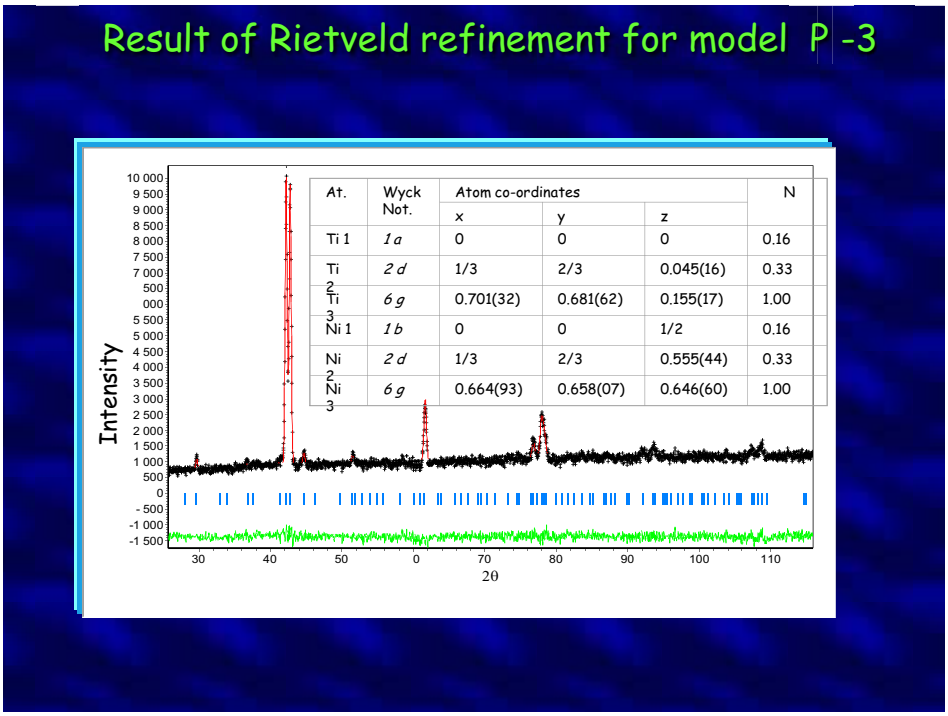

At.	Wyck Not.	Atom co-ordinates			N
		x	y	z	
Ti 1	*1 a*	0	0	0	0.16
Ti 2	*2 d*	1/3	2/3	0.045(16)	0.33
Ti 3	*6 g*	0.701(32)	0.681(62)	0.155(17)	1.00
Ni 1	*1 b*	0	0	1/2	0.16
Ni 2	*2 d*	1/3	2/3	0.555(44)	0.33
Ni 3	*6 g*	0.664(93)	0.658(07)	0.646(60)	1.00

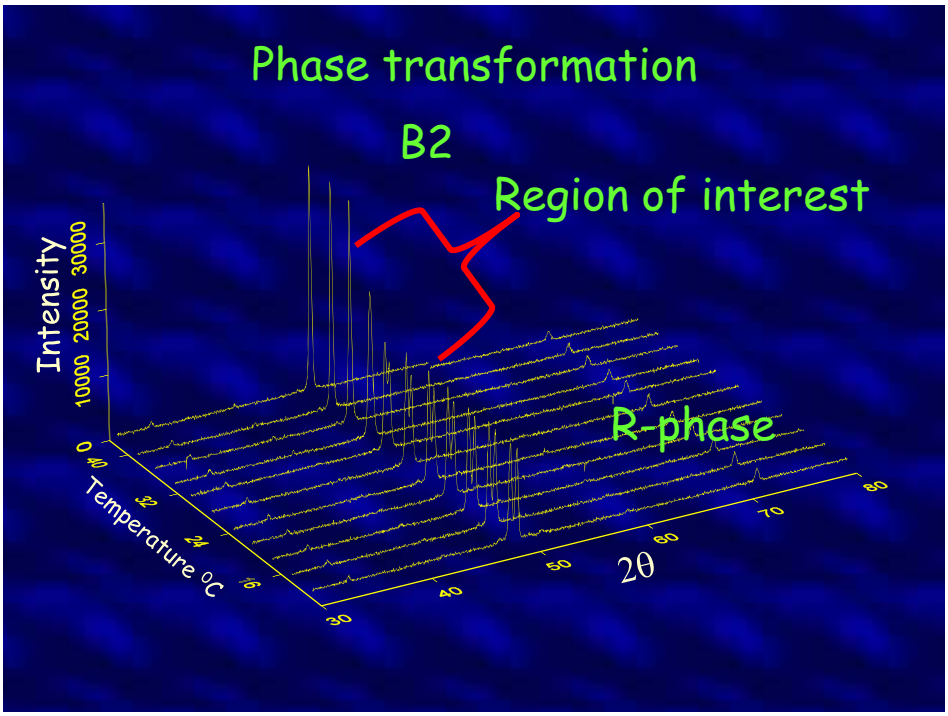

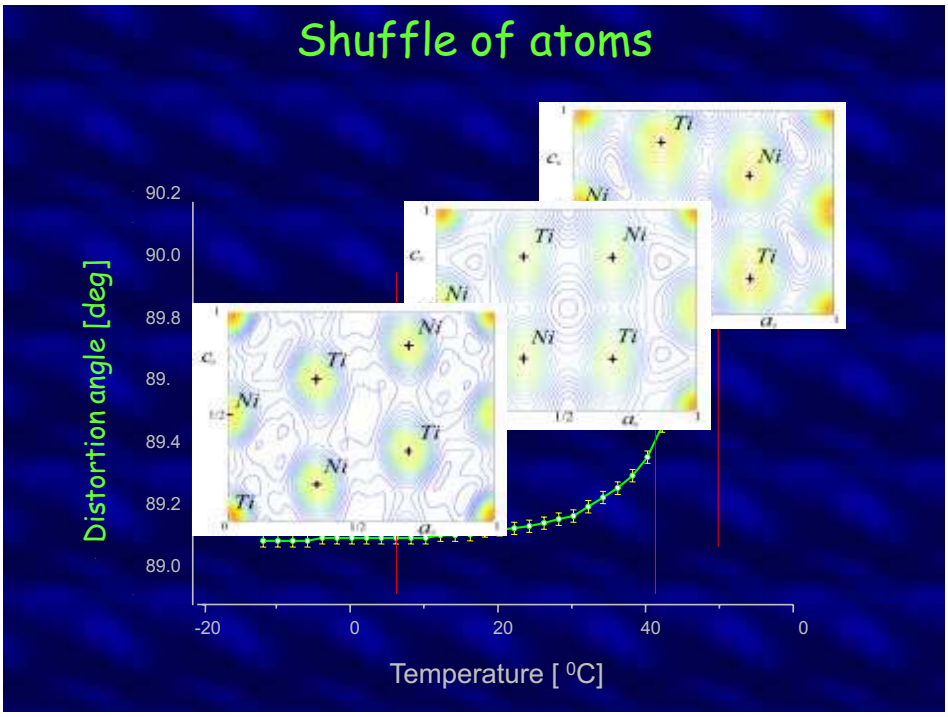
Shuffle of atoms
Distortion angle [deg]
90.2
90.0
89.8
89.
89.4
89.2
89.0
-20
0
20
40
0
Temperature [0C]
Ti
Ni
c
a

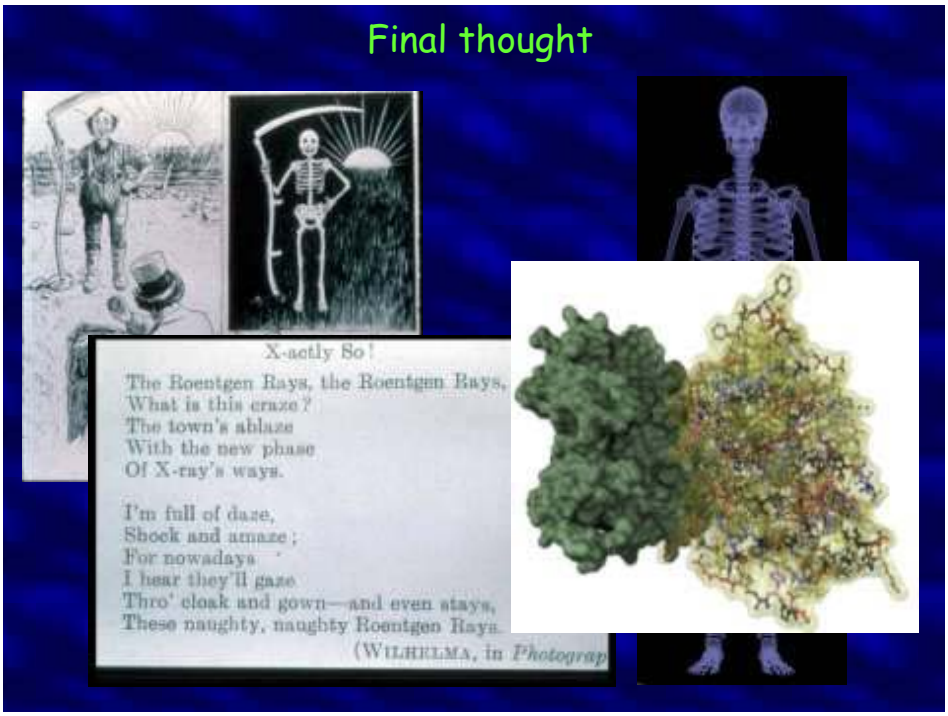
Final thought
X-actly So!
The Roentgen Rays, the Roentgen Rays,
What is this craze?
The town's ablaze
With the new phase
Of X-ray's ways.
I'm full of daze,
Shock and amaze;
For nowadays
I hear they'll gaze
Thro' cloak and gown—and even stays,
These naughty, naughty Roentgen Rays.
(WILHELMA, in Photograp

Electron Microscopy for High-Tech Materials and Structures: Examples of work

Kostas Giannakopoulos

Demokritos
National Centre for Scientific Research

Me...

Aristotle University of Thessaloniki, Degree in **Physics** (1995)
Silicides
The University of **Liverpool** UK, **PhD** (1998), Marie Curie Fellow
InGaAs on vicinal GaAs

STMicroelectronics Grenoble, France (2000-2001), Marie Curie Fellow
SiGe, Ta_2O_5 on Si
NCSR Demokritos, Athens, 2002 - today, Invited Researcher (ENTER)
Oxides, Nanodots etc
European Commission, Expert Evaluator (2003)
National Technical University of Athens, Lecturer:
Optics, High Technology Materials and Devices
TEI of Piraeus, 2003 - today, Lecturer in Electronics, Sensors
Mantis Deposition, UK (2008), Marie Curie Fellow
Nanoparticle Deposition
The **University of Cyprus**, Nicosia, (2007, 2009), Marie Curie Fellow
Hard Coatings, Nanoheaters

Demokritos
National Centre for Scientific Research

Outline

- Materials for the MOSFET
- Materials for non-volatile memories
- Materials for magnetic recording media
- ZnO nanostructures
- Core-shell nanoparticles for medical applications

Demokritos
National Centre for Scientific Research

Materials for the MOSFET

Demokritos
National Centre for Scientific Research

The Sector…

- Semiconductor market turnover, 2011: 313 *billion $, annually: +15%*
- The developments are mainly driven by innovation
- The investment cost can be very low
- Starting point for a variety of exciting applications in almost every other field (e.g. biosensors)

Demokritos
National Centre for Scientific Research

Materials for the MOSFET

The operation of the Metal–oxide–semiconductor field-effect transistor MOSFET:

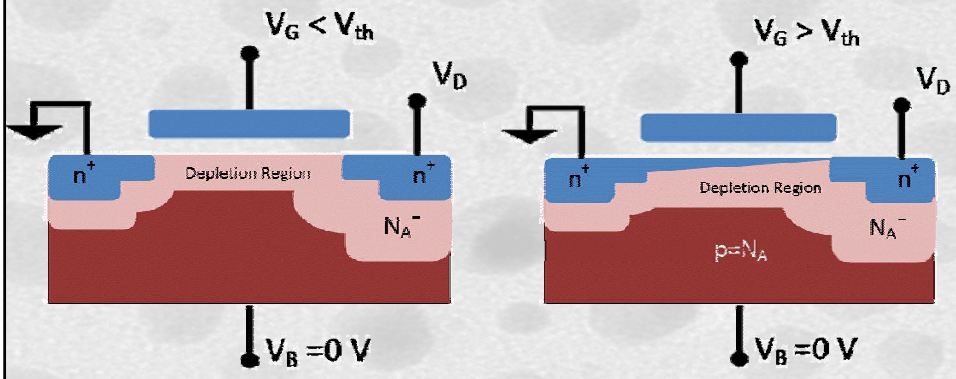

Blue areas: free charge carriers (conductivity)

Demokritos
National Centre for Scientific Research

Materials for the MOSFET

The MOSFET:

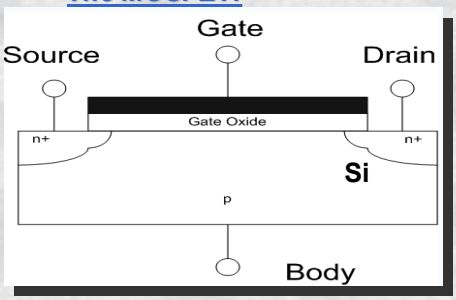

Semiconductor Roadmap Requirements:

- Si wafers diameter: 450mm
- Channel length: 13 nm
- Equivalent Oxide Thickness (EOT): ~ 1 nm
- Ultra shallow junctions

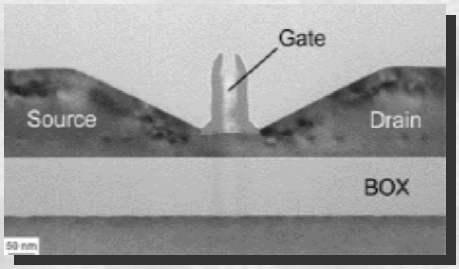

New materials for:

- Gate oxide (high-k dielectrics)
- Gate
- Alternative substrates (Ge, SOI, SON)
- Low-k dielectrics

Demokritos
National Centre for Scientific Research

Materials for the MOSFET

$$C = \frac{k\varepsilon_o S}{t_{ox}}$$

C: Capacitance,

k: Dielectric constant

ε_o: Vacuum permittivity

S: Surface area

t_{ox}: Oxide thickness

Demokritos
National Centre for Scientific Research

Materials for the MOSFET

Capacitance-Voltage Curve:

Simulation from

nanohub.org

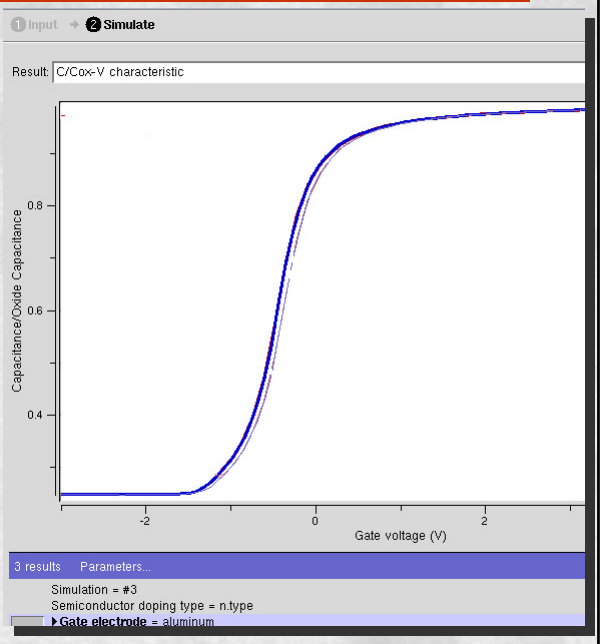

Demokritos
National Centre for Scientific Research

Materials for the MOSFET

HfO_2:
- k ~20-25
- Relatively large band gap
- Compatibility with silicon technology

***Liquid Pulsed* Metal-Organic Chemical Vapour Deposition (MOCVD):**
- Industrial method (300 mm wafers)
- Injector system: accurate flow

Targeted EOT : 1 nm and less → Physical thickness of HfO_2 < 5 nm

Information needed on:
- k value
- Layer Thickness
- Crystallinity (incl. phase structure)
- Stoichiometry

Demokritos
National Centre for Scientific Research

Materials for the MOSFET

Structural Characterisation Techniques:

- X-ray Diffraction (XRD)
- X-ray Photoelectron Spectroscopy (XPS)
- Spectroscopic Ellipsometry
- Secondary Ion Mass Spectroscopy (SIMS)
- Grazing Incidence XRD
- Grazing Incidence Small Angle X-ray Scattering
- TEM (Electron Diffraction, EDX, EELS)

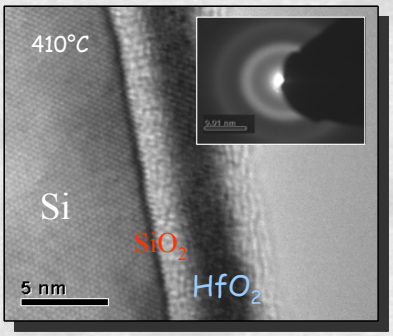

HRTEM image of HfO_2 grown at 410°C

Material identity:

- At 550°C : monoclinic phase. k: 20 to 22
- At lower T:
  - layers < 7 nm : amorphous-like films
  - layers > 7 nm : orthorhombic and monoclinic phase. k: 25 to 30
- Annealing improves stoichiometry, there is no change in crystallization or k

Demokritos National Centre for Scientific Research

Materials for the MOSFET

HfO_2 is already in production for the CMOS

Other Materials:

- High-k ($Hf_xTi_yO_z$, Y_2O_3 etc)
- Silicides / Gate metals
- SiGe or Ge channels
- Silicon on insulator + structures
- Laser annealing for shallow junctions
- Si and Ge dots
- Porous Alumina

Demokritos National Centre for Scientific Research

Materials for the MOSFET

More Info:

- Microfocus X-Ray Study of Selective Area Epitaxy of SiGe on Si, *K.P. Giannakopoulos, S. Roth, C. Fellous, D. Richard and D. Dutartre,* 2003, **Journal of Applied Physics** 93 (1), 259-264.
- Low Frequency Noise and Reliability Properties of 0.12 μm CMOS Devices with Ta2O5 as Gate Dielectric, *M. Fadlallah, A. Szewczyk, C. Giannakopoulos, B. Cretu, F. Monsieur, T. Devoivre, J. Jomaah and G. Ghibaudo,* 2001, **Microelectronics Reliability** 41 (9-10), 1361-1366 .
- EELS Study of Oxygen Superstructure in Epitaxial Y2O3 Layers, *A. Travlos, N. Boukos, G. Apostolopoulos, A. Dimoulas, C. Giannakopoulos*, 2004, **Materials Science and Engineering: B** 109, 52-55.
- Laser annealing of Plasma implanted Boron for Ultra-shallow Junctions in Silicon, *A. Florakis, D. Tsoukalas, I. Zergioti, K. Giannakopoulos, P. Dimitrakis, D.G. Papazoglou, G. Bennassayag, H. Bourdon, A. Halimaoui*, 2006, **Nuclear Instruments and Methods in Physics Research B,** 253, 13-17
- Laser annealing of Al implanted Silicon Carbide: Structural and optical Characterisation, *C. Boutopoulos, P. Terzis, I. Zergioti, A.G. Kontos, K. Zekentes, K. Giannakopoulos, Y.S. Raptis*, **Appl. Surf. Sc.** 253 7912–7916
- Growth and characterization of high density stoichiometric SiO2 dot arrays on Si through anodic porous alumina template, *M. Kokonou, A. G. Nassiopoulou, K.P. Giannakopoulos, A. Travlos, T. Stoica and S. Kennou,* **Nanotechnology**, 2006, 17 (9), pp. 2146-2151
- Sequential grafting of dielectric phosphates onto silicon oxide, *G. Freiman, P. Barboux, J. Perrière, K. Giannakopoulos*, **Chemistry of Materials**, 2007, *19,* 5862–5867
- Layer by layer deposition of zirconium oxide onto silicon, *G. Freiman, P. Barboux, J. Perrière, K. Giannakopoulos*, **Thin Solid Films** (2008), 517 (8), pp. 2670-2674
- Structural and Electrical Properties of HfO2 / Dy2O3 Gate Stacks on Ge Substrate, *E.K. Evangelou, M.S. Rahman, I.I. Androulidakis, A. Dimoulas, G. Mavrou, K. P. Giannakopoulos, D.F. Anagnostopoulos, R. Valicu, G.L. Borchert*, **Thin Solid Films**, in press.

Demokritos
National Centre for Scientific Research

Materials for non-volatile memories

Demokritos
National Centre for Scientific Research

Materials for non volatile memories

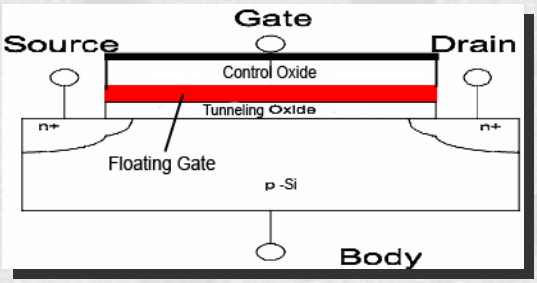

Demokritos
National Centre for Scientific Research

Materials for non volatile memories

Floating-gate memory devices:

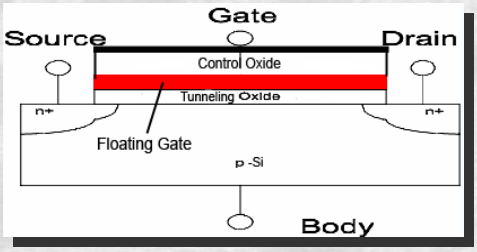

Tunneling oxides: very thin, easily damaged

Flash Memories with nanoparticles:

No charge transfer between dots → Thinner tunneling oxide

- Smaller operating voltages
- Better endurance
- Enhanced write/erase speeds
- Very high memory density

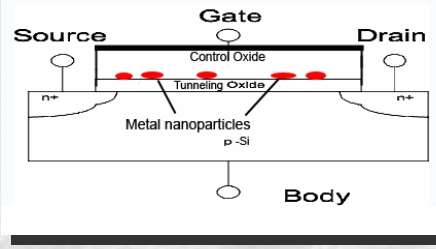

Demokritos
National Centre for Scientific Research

Materials for non volatile memories

Process flow

1) Dry oxidation of Si (for the tunneling oxide)
2) Nanoparticle deposition (evaporation of Pt, Pd, Ag, Au, W…)
3) Control oxide deposition (evaporation of HfO_2 pellet, T_{sub}=200 ºC, O_2 ambient)
4) Contact deposition (evaporation of Al, mask)

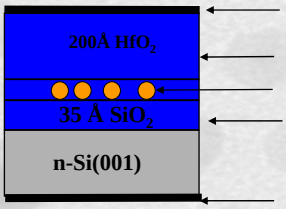

Gate metal (Al)
Control oxide
Nanoparticles
Tunneling oxide
Al contact

Electron gun evaporator

- High vacuum chamber
- 2 e-guns
- 2 piezoelectric crystal monitors

Analysis

Structure: TEM (EELS, EDX), XRD
Electrical: C-V

Demokritos
National Centre for Scientific Research

Materials for non volatile memories

The e-gun evaporator:

Demokritos
National Centre for Scientific Research

Materials for non volatile memories

Effect of thickness

Flux & Diffusion

Nucleation

Stable nuclei

Island growth

Growing islands

Coalescence

Effect of temperature

Low T_s

High T_s

Demokritos
National Centre for Scientific Research

Materials for non volatile memories

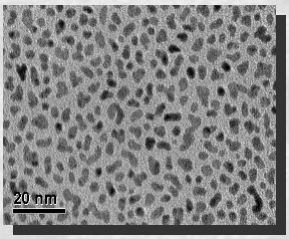

Plan view TEM image of Pt dots on SiO_2

Typical nanoparticles:

- ✓ Surface density: $3{,}2 \times 10^{12}$ ncs/cm^2
- ✓ Average diameter: 49 Å
- ✓ Good size uniformity

- **Dot size depends on:**
  - Element chosen
  - Evaporation rate
  - Wafer temperature
- **There is not material diffusion (EELS)**
- **Dots are surrounded by HfO_2**

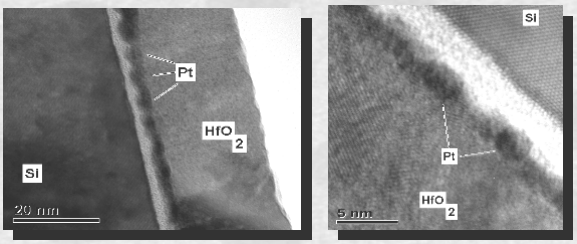

Demokritos
National Centre for Scientific Research

Cross-sectional TEM images of Pt dots on SiO_2

***Applied Physics Letters**, 88, 073106*

Materials for non volatile memories

C-V:
- We observe a clear memory effect
- 1 or 2 electrons stored per dot

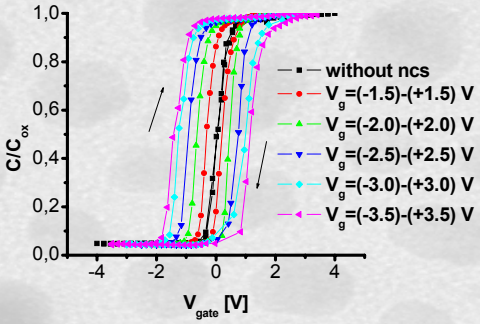

More Results with:
- Nanodots: Au, Pd, Pt, W, Si, Ni
- Tunneling oxide: SiO_2(+HfO_2)
- Control Oxide: SiO_2

Exploitation of various work functions → Possibility to tune:
speed of write-erase process / retention time

Demokritos
National Centre for Scientific Research

Materials for non volatile memories

Nanoparticle Source (Mantis Deposition, UK)

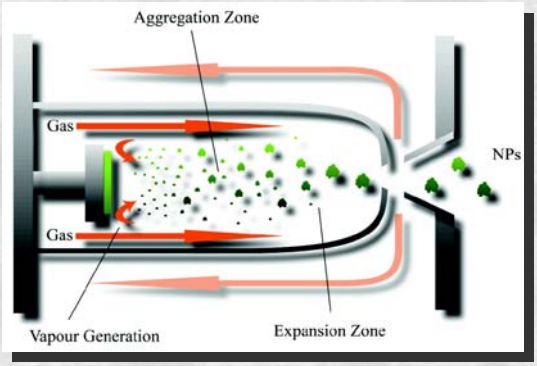

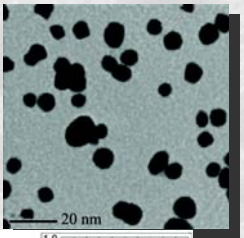

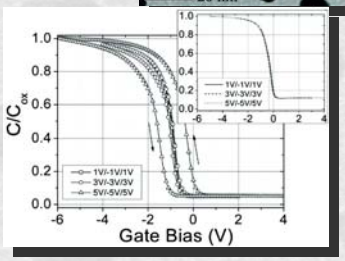

- ✓ Hard landing option
- ✓ Nitride and oxide particles possible
- ✓ 2% size resolution!

Demokritos
National Centre for Scientific Research

Journal of Materials Research 26 (2), pp. 209-214

Materials for non volatile memories

- ✓ **Ability to fabricate easily advanced memory cells**
- ✓ **Metal nanoparticles can be used for memories**
- ✓ **Compatibility with existing Si technology**

Demokritos
National Centre for Scientific Research

Materials for non volatile memories

More Info:

- A simple method for the fabrication of a high-k MOS capacitor embedded with Pt nanoparticles, *Ch. Sargentis, K. Giannakopoulos, A. Travlos, N. Boukos and D. Tsamakis*, 2006, **Applied Physics Letters** 88, 1.
- Growth of Two-Dimensional Arrays of Silicon Nanocrystals ın Thin SiO2 Layers By Low Pressure Chemical Vapour Deposition and High Temperature Annealing/Oxidation. Investigation of Their Charging Properties *A. Salonidou, A G Nassiopoulou, K Giannakopoulos, A Travlos, V Ioannou-Sougleridis and E Tsoi*, 2004, **Nanotechnology** 15, 1233–1239
- Fabrication and electrical characterization of a memory device containing self assembled metallic nanoparticles, *Ch. Sargentis, K. Giannakopoulos, A. Travlos, D. Tsamakis*, **Physica E**, 38 (2007) 85–88
- Electrical characterization of MOS memory devices containing metallic nanoparticles and a high-k control oxide layer, *Ch. Sargentis, K. Giannakopoulos, A. Travlos, D. Tsamakis*, **Surface Science**, 601 (13), p.2859, 2007
- Nickel nanoparticle deposition at room temperature for memory applications, *E. Verrelli, D. Tsoukalas, K. Giannakopoulos, D. Kouvatsos, P. Normand, D. E. Ioannou*, **Microelectronic Engineering**, 84 (9-10), p. 1994
- Synthesis and Electrical Characterisation of a MOS Memory Containing Pt Nanoparticles Deposited at a SiO2/ HfO2 Interface, *Ch. Sargentis, K. Giannakopoulos, A. Travlos, D. Tsamakis*, 2005, **Materials Research Society Symp. Proc.** 830, D6.4.1
- Fabrication and Characterization of a Metal Nanocrystal Memory using Molecular Beam Epitaxy, *Ch. Sargentis, K. Giannakopoulos, A. Travlos, D. Tsamakis*, 2005, **Journal of Physics: Conference Series**, 10, 53-56.
- Silicon Nanocrystal Memories by LPCVD of Amorphous Silicon Followed by Solid Phase Crystallisation and Thermal. Oxidation, *E. Tsoi, P. Normand, A.G Nassiopoulou, V. Ioannou-Sougleridis, A. Salonidou, K. Giannakopoulos*, 2005, **Journal of Physics: Conference Series**, 10, 31–34.

Demokritos
National Centre for Scientific Research

Materials for non volatile memories

- Dynamic Behavior of Charge in MOS Devices Embedded with Pt and Au Nanoparticles, *Ch. Sargentis, K. Giannakopoulos, A. Travlos, D. Tsamakis,* **Mat Sci Semicond Process**, Volume 12, Issues 1-2, February-April 2009, Pages 57-63
- Study of charge storage characteristics of memory devices embedded with metallic nanoparticles, *Ch. Sargentis, K. Giannakopoulos, A. Travlos, P. Normand, D. Tsamakis*, **Superlattices and Microstructures**, (2008),
- Deposition of uniform size metallic nanoparticles for use in non volatile memories, Verrelli E., Tsoukalas D., Giannakopoulos K., Ioannou D. **Materials Research Society Symposium Proceedings**, Volume 997, 2007, Pages 115-120
- A comparative study of MOS memory structures that contain platinum or gold nanoparticles, *Ch. Sargentis, K. Giannakopoulos, A. Travlos and D. Tsamakis,* **International Semiconductor Device Research Symposium**, Volume 2007
- Semiconductor nanocrystals in thin SiO2 layers for non-volatile memories, Nassiopoulou A.G., Salonidou A., Olzierski A., Kokonou M., Tsoi E., Normand P., Giannakopoulos K., **Semiconductor Nanocrystals**, (2005) *Proc. First Int. Workshop on Semiconductor Nanocrystals SEMINANO2005*, 2, p. 405., Budapest, Hungary
- Synthesis and Electrical Characterisation of a MOS Memory Containing Pt Nanoparticles Deposited at a SiO2/ HfO2 Interface, *Ch. Sargentis, K. Giannakopoulos, A. Travlos, D. Tsamakis*, **Materials Research Society Symp. Proc**. 2005, 830, 275-280
- Deposition and Electrical Characterisation of a MOS Memory Structure Containing Au Nanoparticles in a High-K Dielectric Layer, Ch. Sargentis, K. Giannakopoulos, A. Travlos, D. Tsamakis, G. Krokidis, **International Semiconductor Device Research Symposium**, Volume 2005, Article number 1596126, Pages 342-343
- Process and Device Characteristics of a Pd Nanocrystal MOS Memory, *Ch. Sargentis, K. Giannakopoulos, A. Travlos, D. Tsamakis,* **Proceedings of the International Semiconductor Device Research Symposium (ISDRS**), 2003, 218-219

Demokritos
National Centre for Scientific Research

Materials for magnetic recording media

Demokritos
National Centre for Scientific Research

Materials for magnetic recording media

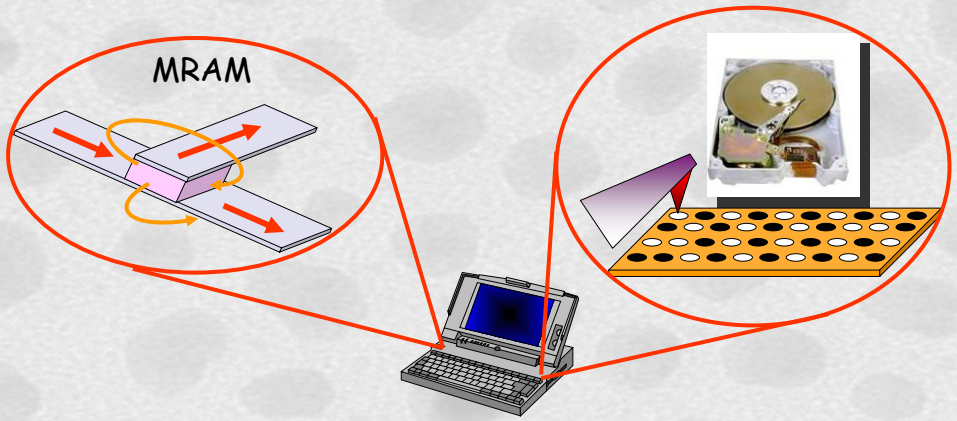

Hard Disk market turnover (2010): 27,7 b $

Demokritos
National Centre for Scientific Research

Materials for magnetic recording media

CoPt

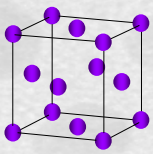

Co, Pt

a = 3.766 Å c = 3.766 Å

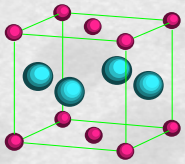

Pt
Co

a = 3.803 Å c = 3.701 Å

K_u ~ 0.5 MJ/m³

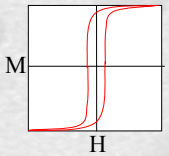

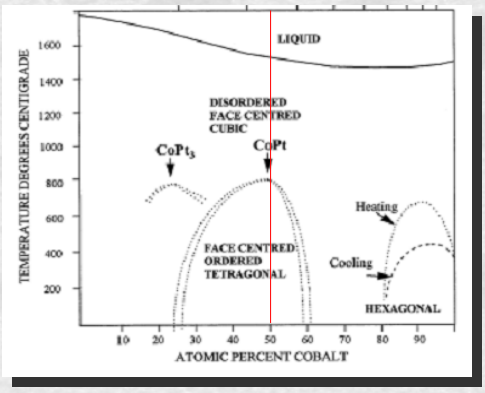

K_u ~ 5 MJ/m³

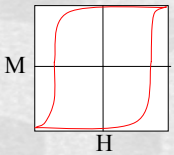

Demokritos
National Centre for Scientific Research

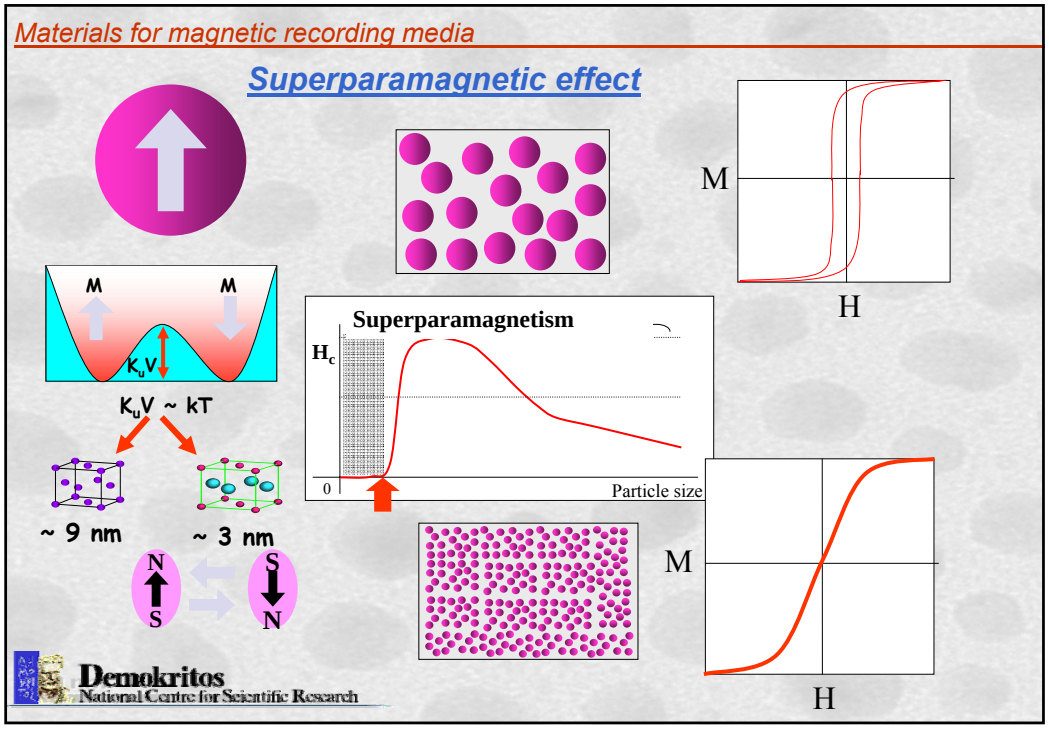
Materials for magnetic recording media
Superparamagnetic effect
M
H
M
M
K_uV
K_uV ~ kT
~ 9 nm
~ 3 nm
N
S
S
N
Superparamagnetism
H_c
0
Particle size
M
H
Demokritos
National Centre for Scientific Research

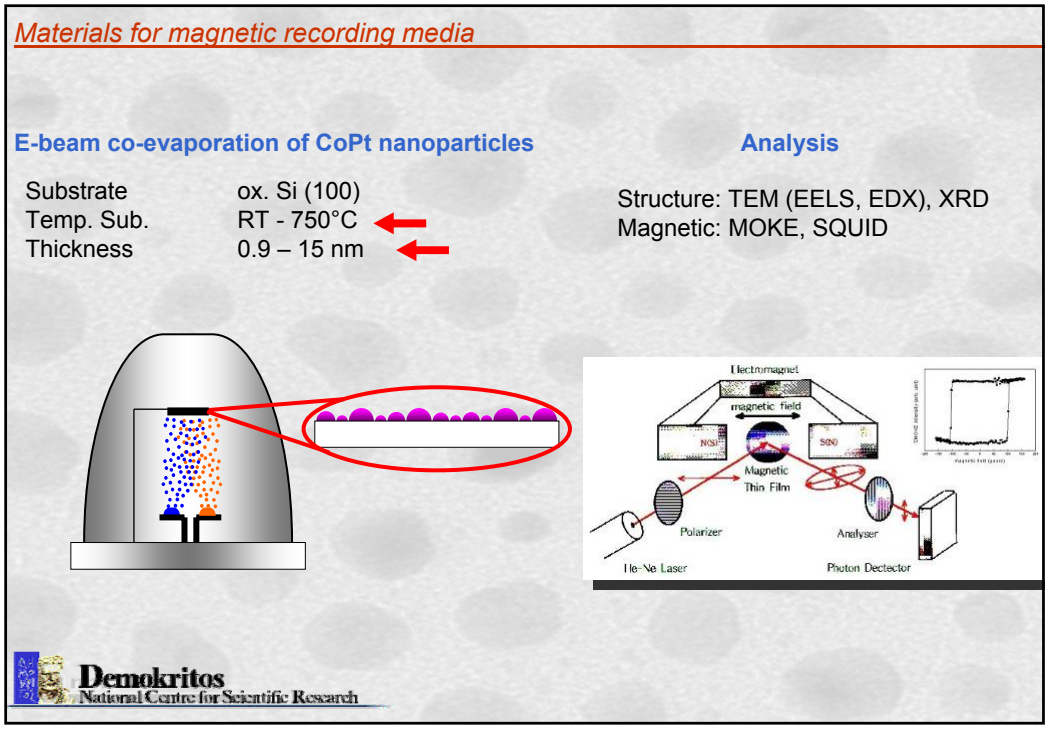
Materials for magnetic recording media
E-beam co-evaporation of CoPt nanoparticles
Substrate ox. Si (100)
Temp. Sub. RT - 750°C
Thickness 0.9 – 15 nm
Analysis
Structure: TEM (EELS, EDX), XRD
Magnetic: MOKE, SQUID
Electromagnet
magnetic field
Magnetic Thin Film
Polarizer
Analyser
He-Ne Laser
Photon Dectector
Demokritos
National Centre for Scientific Research

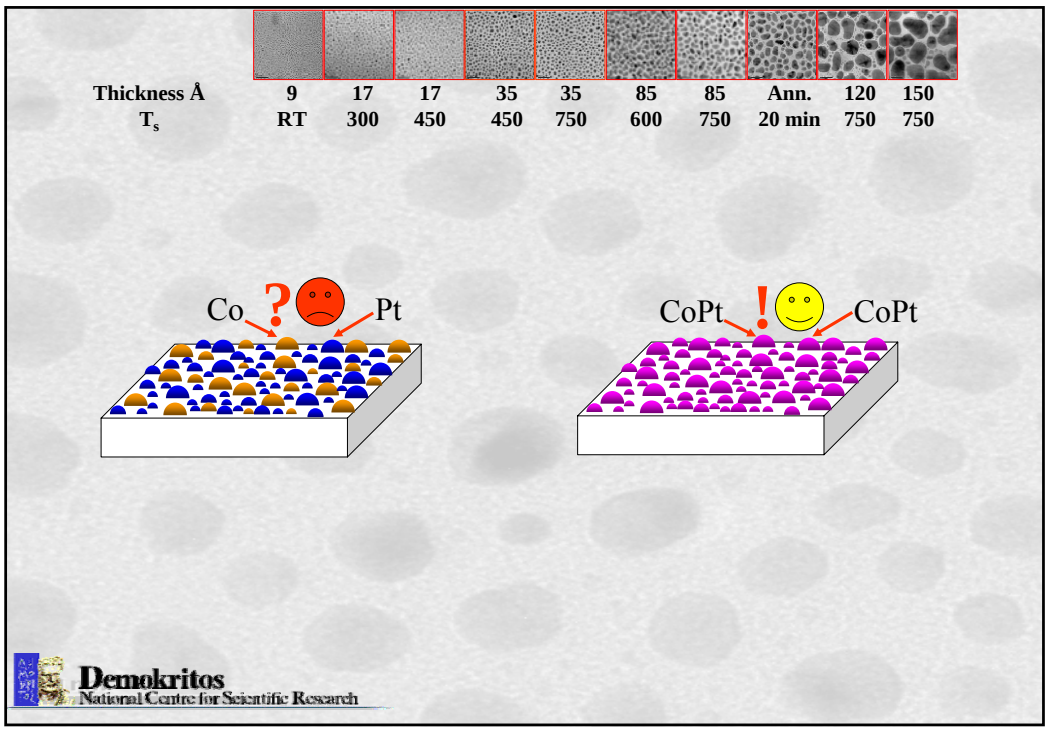
Thickness Å
T_s
9 RT
17 300
17 450
35 450
35 750
85 600
85 750
Ann. 20 min 750
120 750
150 750
Co
?
Pt
CoPt
!
CoPt
Demokritos
National Centre for Scientific Research

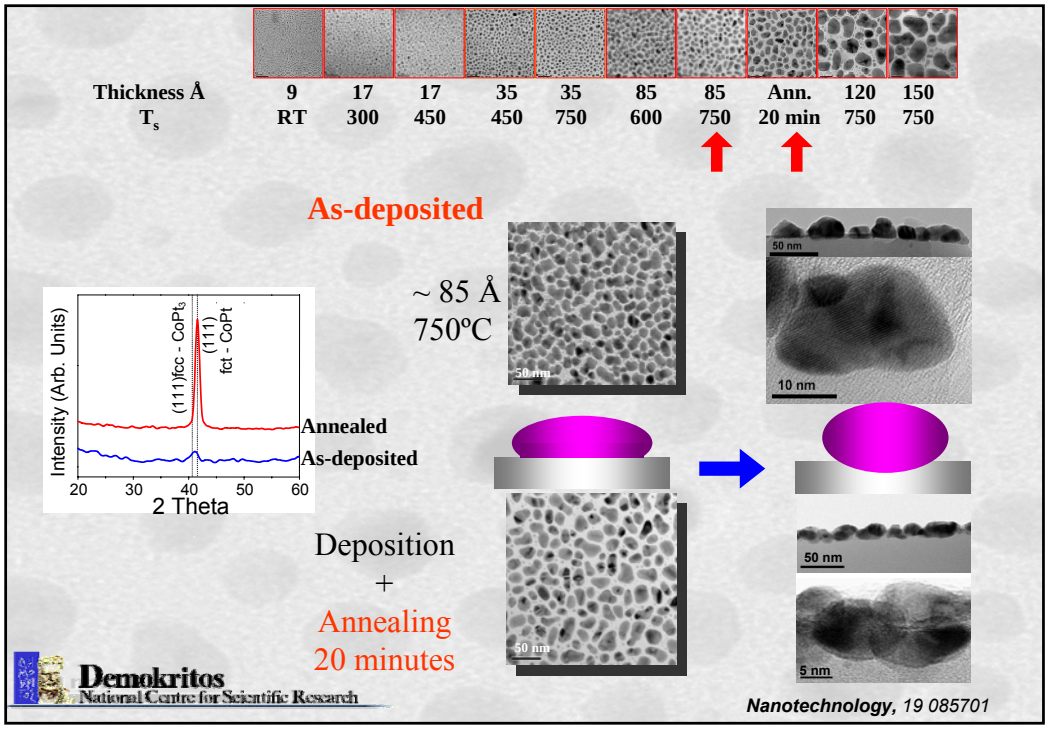
Thickness Å
T_s
9 RT
17 300
17 450
35 450
35 750
85 600
85 750
Ann. 20 min 750
120 750
150 750
As-deposited
~ 85 Å
750ºC
50 nm
50 nm
10 nm
Intensity (Arb. Units)
(111)fcc - $CoPt_3$
(111) fct - CoPt
20 30 40 50 60
2 Theta
Annealed
As-deposited
Deposition
+
Annealing
20 minutes
50 nm
50 nm
5 nm
Demokritos
National Centre for Scientific Research
Nanotechnology, 19 085701

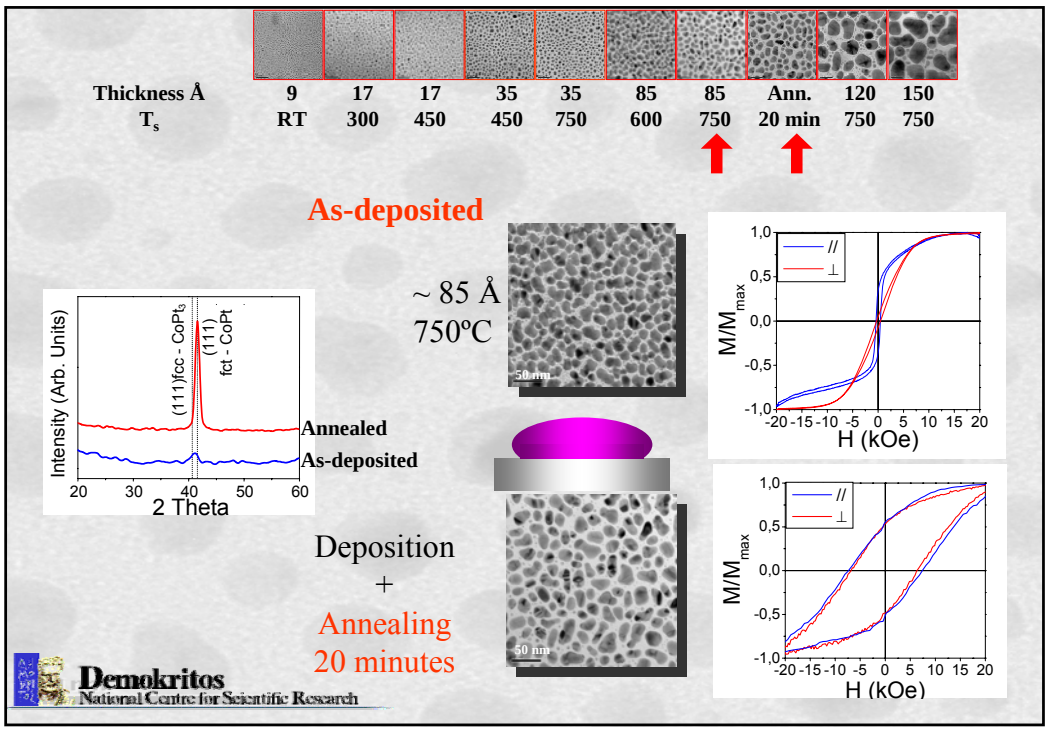
Thickness Å
T_s
9 RT
17 300
17 450
35 450
35 750
85 600
85 750
Ann. 20 min
120 750
150 750
As-deposited
~ 85 Å
750ºC
Intensity (Arb. Units)
(111)fcc - $CoPt_3$
(111) fct - CoPt
2 Theta
Annealed
As-deposited
Deposition
+
Annealing
20 minutes
50 nm
M/M$_{max}$
H (kOe)
Demokritos
National Centre for Scientific Research

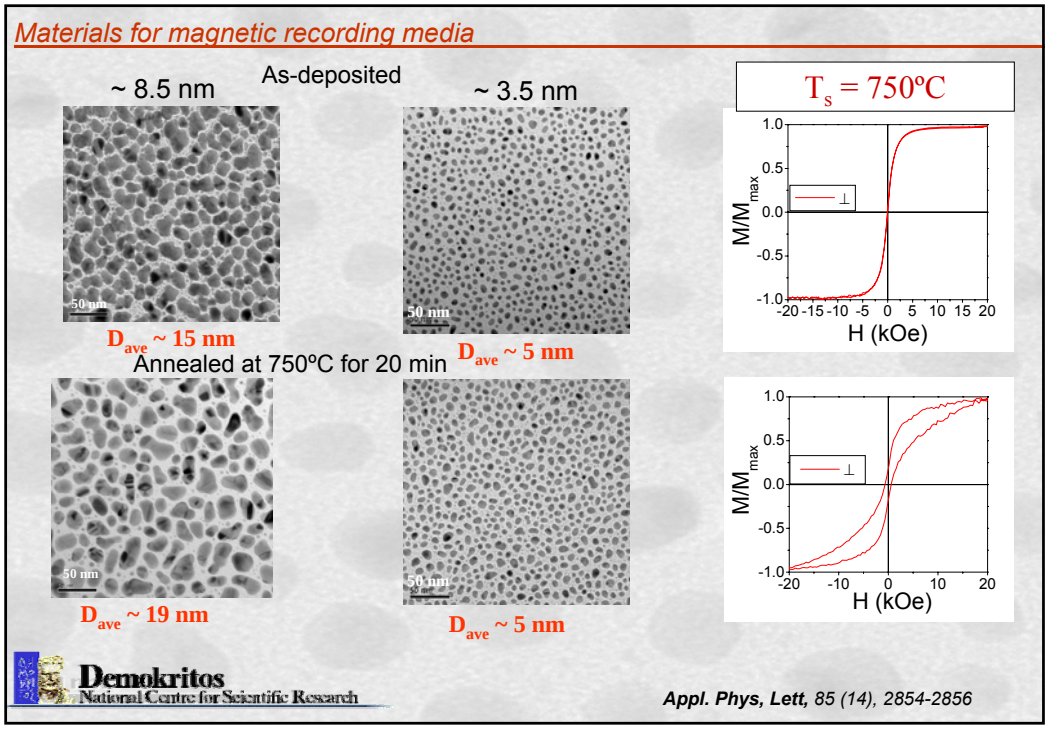
Materials for magnetic recording media
~ 8.5 nm
As-deposited
~ 3.5 nm
T_s = 750ºC
50 nm
D_{ave} ~ 15 nm
D_{ave} ~ 5 nm
Annealed at 750ºC for 20 min
D_{ave} ~ 19 nm
D_{ave} ~ 5 nm
M/M$_{max}$
H (kOe)
Demokritos
National Centre for Scientific Research
Appl. Phys, Lett, 85 (14), 2854-2856

Materials for magnetic recording media

Energy Filtering TEM on Ag/FePt nanoparticles

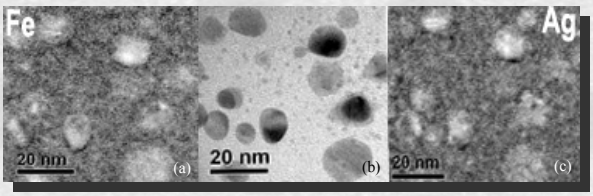

Fe map Ag map

Demokritos National Centre for Scientific Research

Journal of Applied Physics, *105 093914*

Materials for magnetic recording media

More Results:

- CoPt nanoparticle coercivity reaches 7,4 kOe
- FePt nanoparticle coercivity reaches 10,5 kOe
- Deposition of FePt on Ag particles improves the magnetic hardening

✓ Materials suitable for hard disk density of 11,43 Tbit/inch^2
(current record: 1Tbit/inch^2)

✓ Possible integration in Si technology

Demokritos National Centre for Scientific Research

Materials for magnetic recording media

More Info:

- Enhanced magnetic properties of FePt nanoparticles co-deposited on Ag nanoislands, *Lorenzo Castaldi, Konstantinos Giannakopoulos , A. Travlos , Nikos Boukos , D. Niarchos , Samy Boukari , Eric Beaurepaire* , **Journal of Applied Physics**, 105 093914 (2009)
- Structure and magnetic properties of the Sm(Co0.74Fe0.1Cu0.12Zr0.04)8 melt-spun nanostructured alloys, *M. Gjoka, D. Niarchos, K. Giannakopoulos, C. Sarafidis, O. Kalogirou, M. Grigoras, N. Lupu and H. Chiriac*, **Materials Science and Engineering B**, (2008),
- FePt and CoPt nanoparticles co-deposited on silicon dioxide: a comparative study, *L. Castaldi, K. Giannakopoulos, A. Travlos, S. Boukari, E. Beaurepaire, D. Niarchos,* **Nanotechnology**, 19 (2008) 085701.
- Engineering of FePt nanoparticles by co-deposition *L. Castaldi K. Giannakopoulos, A. Travlos, N. Boukos, D. Niarchos, S. Boukari and E. Beaurepaire*, **Nanotechnology**, 19 (2008) 135702.
- Coevaporation of CoPt nanoparticles, *L. Castaldi, K. Giannakopoulos, A. Travlos, D. Niarchos*, 2004, **Appl. Phys, Lett**, 85 (14), 2854-2856. Selected for the **Virtual Journal of Nanoscale Science & Technology** (http://www.vjnano.org)
- CoPt nanoparticles deposited by electron beam evaporation *L. Castaldi, K. Giannakopoulos, A. Travlos, D. Niarchos, S. Boukari, E. Beaurepaire,* 2005, **Journal of Magnetism and Magnetic Materials** 290-291, 544-546.
- Superparamagnetic and ferromagnetic CoPt nanoparticles deposited on silicon dioxide *L. Castaldi, K. Giannakopoulos, A. Travlos, D. Niarchos, S. Boukari, E. Beaurepaire*, 2005, **Journal of Physics: Conference Series**, 10, 155-158
- Co-deposition of FePt and CoPt nanoparticles on silicon dioxide, *Castaldi, L., Giannakopoulos, K. , Travlos, A. , Niarchos, D. , Boukari, S. , Beaurepaire, E.,* **INTERMAG ASIA 2005: Digests of the IEEE International Magnetics Conference**, 2005, 92

Demokritos
National Centre for Scientific Research

ZnO nanostructures

I. *ZnO dots*
II. *ZnO nanorods*
III. *EELS on ZnCoO nanorods*

Demokritos
National Centre for Scientific Research

ZnO nanostructures

Why ZnO?

Main Disadvantage:
p-type doping…

- Wide band gap (3,36 eV @ RT)
- CdO-ZnO-MgO: large band gap range (2.2 to 7.9 eV) with a smaller variation of the lattice parameter than in nitrides
- Ferromagnetic semiconductor (+Mn)
- Piezoelectric
- Large exciton binding energy (60 meV)
- Very large shear modulus of 45.5 GPa
- Existing ZnO substrates (still expensive)
- Resistant to radiation
- Non-toxic (used in sun-blocking creams)
- Cheap: 1600 euros/ton (GaN 540 euros for 5 g)

Demokritos
National Centre for Scientific Research

ZnO nanostructures

Applications:

- UV optoelectronics:
  - Short wavelength LED (+Mg, for UV)
  - Displays
  - Optical Storage
  - Transparent electronics
  - Solar blind UV detectors
- Light Bulbs (85% less consumption)
- High-T electronics
- Surface acoustic wave devices (>5GHz) for cellular phones
- Gas sensors
- Spintronics (quantum computers?)

Demokritos
National Centre for Scientific Research

ZnO nanostructures

Nanodots

Process flow:

1) Electron beam evaporation of pure Zn metal on SiO_2
2) Annealing in O_2 atmosphere for 1h at 570K -700K

Zn dot growth conditions:

- Substrate temperature: 190 to 300 K
- Vacuum $4x10^{-8}$ Torr
- Evaporation rate: 0.05 to 0.6 nm/s
- Equivalent thickness: 0.5 to 5 nm

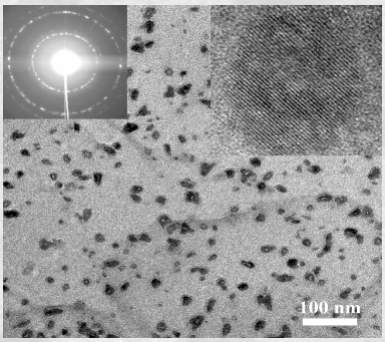

Plan view image of ZnO nanodots
Insets:
a) Electron Diffraction with ZnO rings
b) HRTEM of one dot

Demokritos
National Centre for Scientific Research

ZnO nanostructures

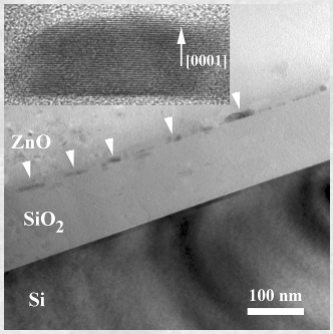

Cross-section TEM image of ZnO nanodots
Inset: HRTEM of one dot

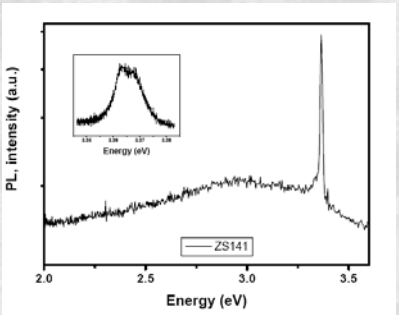

Photoluminescence spectra, at 10 K
Excitation source: He-Cd laser (325 nm)

Demokritos
National Centre for Scientific Research

ZnO nanostructures

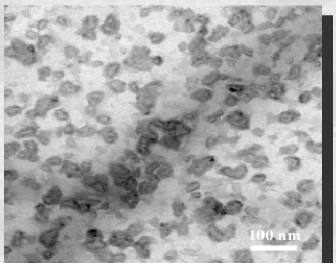

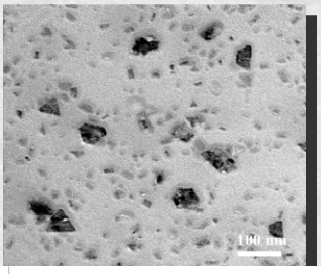

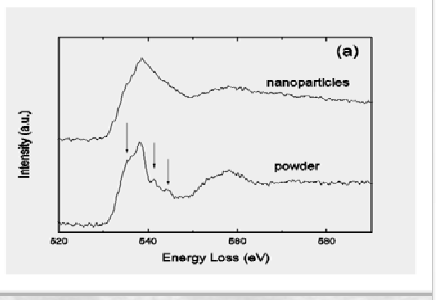

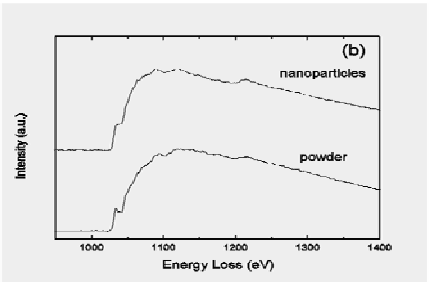

Demokritos National Centre for Scientific Research

PL spectra of sample and reference

ZnO nanostructures

- ✓ Dot diameters: 3 - 50 nm
- ✓ C axis vertical to the substrate
- ✓ Only near band edge photoluminescence (3.36eV)
- ✓ Compatible with Si technology

Demokritos National Centre for Scientific Research

ZnO nanostructures

I. ZnO dots
II. **ZnO nanorods**
III. EELS on ZnCoO nanorods

Demokritos
National Centre for Scientific Research

ZnO nanostructures - Nanorods

Nanorods

Chemical process by: H. Yu et. al.: J. Am. Chem. Soc. 127, 2378 (2005)

- Formamide solution in water
- Zn Source: Zn foil
- Substrates: Si (111), glass, Zn foil and ZnO on Si (111), glass
- Deposition time: 1 to 24 hours
- Solution Temperature: 40-80 ºC

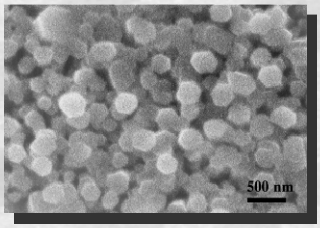

Top view SEM image of ZnO nanorods

Demokritos
National Centre for Scientific Research

***Superlattices and Microstructures**, 39, 115-123*

ZnO nanostructures - Nanorods

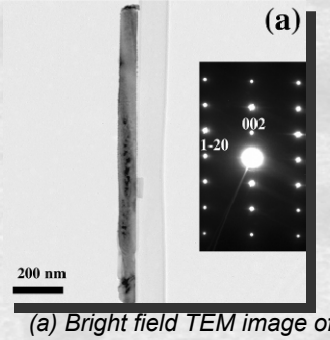

(a) Bright field TEM image of a ZnO nanorod grown on ZnO thin film/glass substrate
Inset: selected area electron diffraction pattern

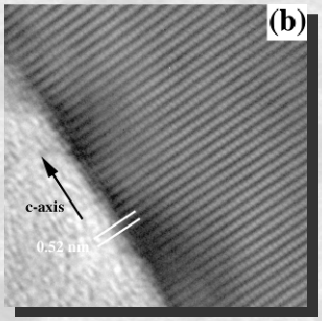

(b) High resolution TEM image of the same ZnO nanorod

Demokritos National Centre for Scientific Research

***Nanotechnology**, 18, No 27, 275601*

ZnO nanostructures - Nanorods

SEM images

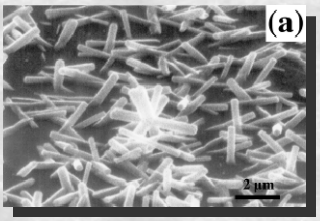

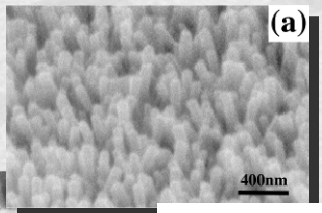

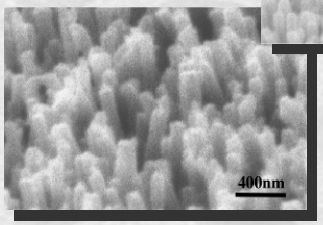

XRD data

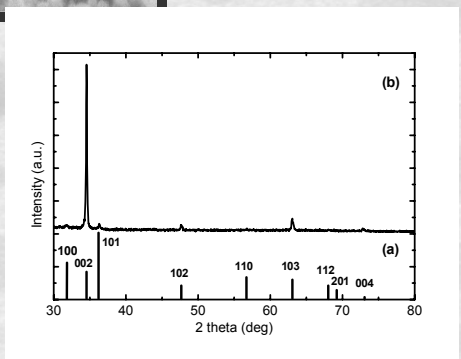

Demokritos National Centre for Scientific Research

ZnO nanostructures - Nanorods

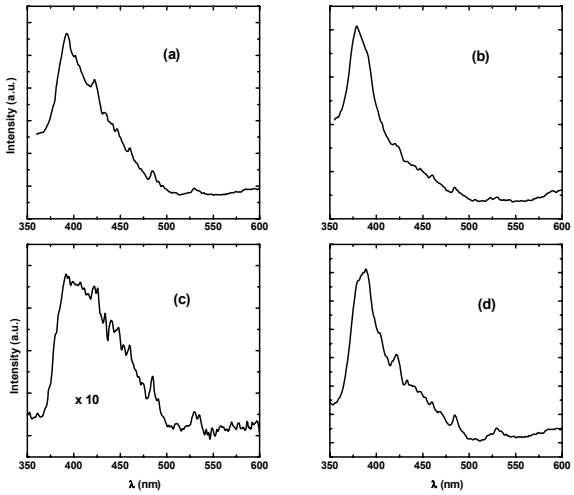

Room temperature PL spectra of ZnO nanorods grown on (a) Zn foil, bare (111) Si substrate at (b) 65 oC and (c) 80 oC (c) and (d) ZnO thin film/glass substrate.

ZnO nanostructures

✓ Nanorod size and morphology can be tuned with deposition conditions and substrate choice

- **Fabrication of self-assembled ZnO nanostructures**
- **Compatible with existing Si technology**

Demokritos
National Centre for Scientific Research

ZnO nanostructures

I. ZnO dots
II. ZnO nanorods
III. EELS on ZnCoO nanorods

Demokritos
National Centre for Scientific Research

ZnO nanostructures - EELS on ZnCoO nanorods

EELS:

a way to exploit the inelastically scattered electrons

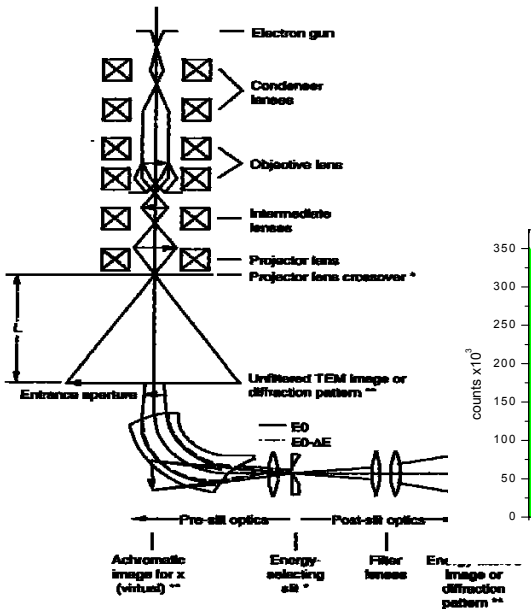

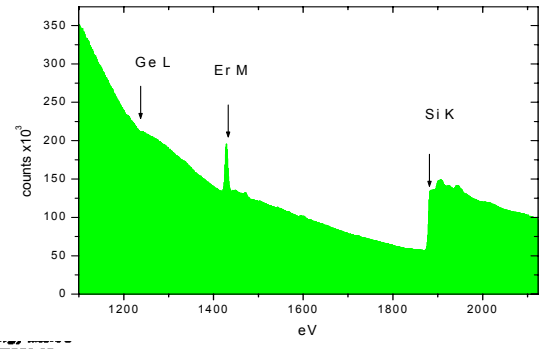

ZnO nanostructures - EELS on ZnCoO nanorods

Electron Energy Loss Spectroscopy (EELS)

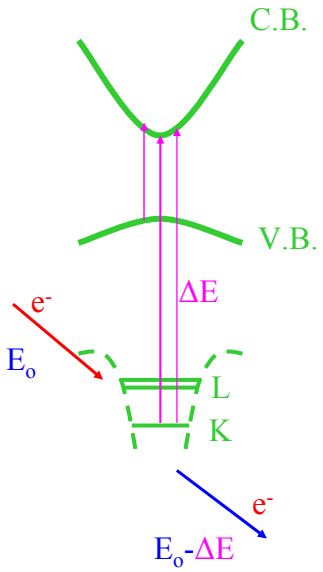

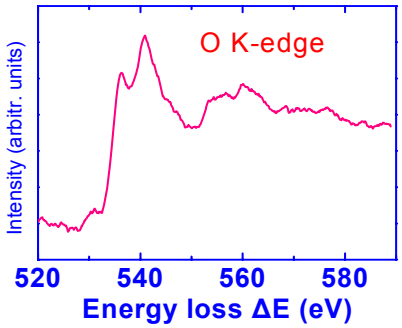

ZnO nanostructures - EELS on ZnCoO nanorods

ZnCoO nanorods

Magnetic Semiconductors ⟶ Spintronics

Questions:
- Are there ZnCoO nanorods?
- Is Co present in the ZnO lattice?

PLD at the University of Leipzig:

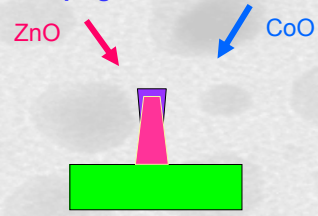

Demokritos
National Centre for Scientific Research

ZnO nanostructures - EELS on ZnCoO nanorods

EELS mapping of Co and O ZnCoO nanorods

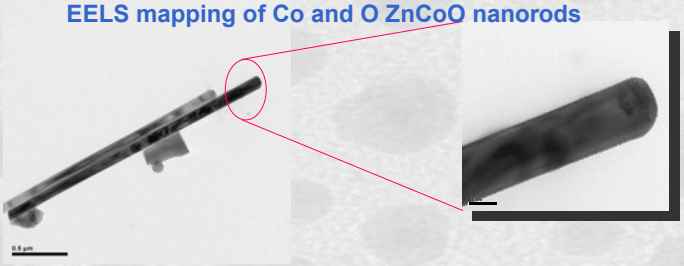

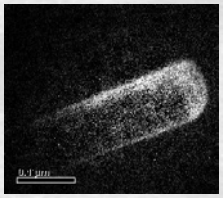

Co map

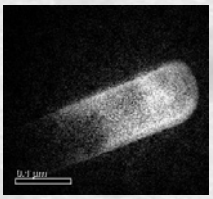

O map

ZnCoO creates a shell around the ZnO nanorod

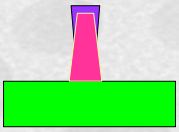

Demokritos
National Centre for Scientific Research

ZnO nanostructures - EELS on ZnCoO nanorods

Valence of Co at ZnCoO nanorods

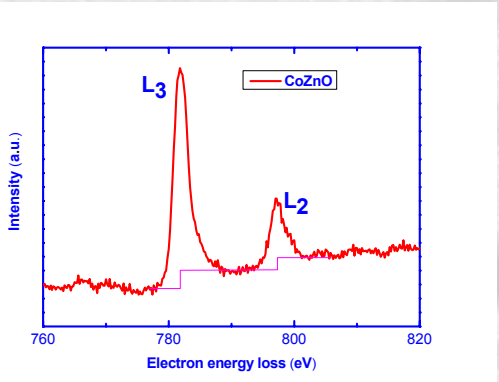

The L_2 and L_3 peaks of Co correspond to the electronic transitions:

From atomic levels $2p^{3/2}$ and $2p^{1/2}$ to 3d

L3/L2 → Co oxidation state

Demokritos
National Centre for Scientific Research

ZnO nanostructures - EELS on ZnCoO nanorods

L3/L2 comparison with reference materials:

Cobalt acetate $Co(CH_3COO)_2$ (Co^{+2})

Co_2O_3 (Co^{+3})

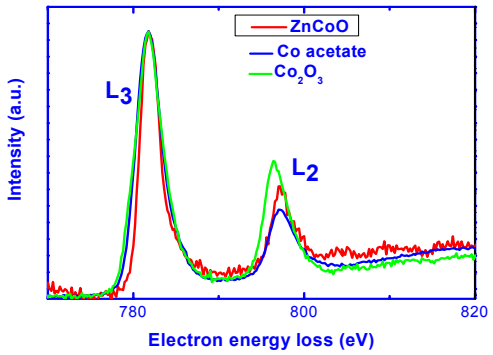

$Co(CH_3COO)_2$: L3/L2 = 4.4
Co_2O_3: L3/L2 =3.3
ZnCoO: L3/L2 = 4.1

Co has a valence near +2

⇩

Co substitutes Zn in the lattice

Demokritos
National Centre for Scientific Research

ZnO nanostructures - EELS on ZnCoO nanorods

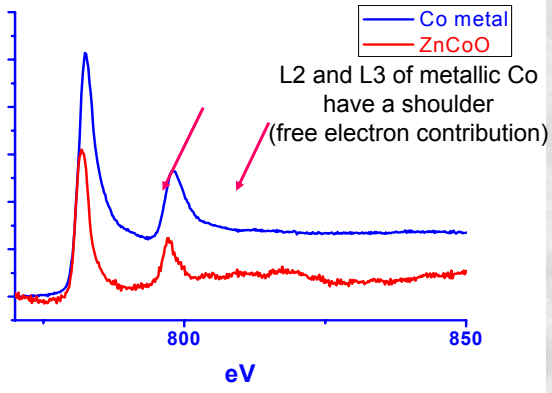

There is no free electron contribution in ZnCoO

⇩

ZnO is not in a metallic state

Demokritos
National Centre for Scientific Research

ZnO nanostructures

More Info:

- Low temperature growth of single crystal ZnO nanorods, *N Boukos, C Chandrinou, C Stogios, K. Giannakopoulos and A Travlos*, Nanotechnology, 18, No 27 (11 July 2007), 275601.
- Zinc oxide nanoparticles on silicon, *K Giannakopoulos, N Boukos and A Travlos*, 2006, Superlattices and Microstructures 39, 115-123.
- Structural and Photoluminescence Properties of ZnO Nanoparticles on Silicon Oxide, *K. Giannakopoulos, N. Boukos, A. Travlos, T. Monteiro, M.J. Soares, M. Peres, A. Neves and M.C. Carmo,* Applied Physics A, Materials Science & Processing, 88(1), 2007, 41-44
- Growth of ZnO Nanorods By A Simple Chemical Method, *N. Boukos, C. Chandrinou, K. Giannakopoulos, G. Pistolis, A. Travlos*, Applied Physics A, Materials Science & Processing, 88(1), 2007, 35-39
- Growth and optical study of ZnO nanorods, C. Chandrinou, N. Boukos, K. Giannakopoulos, A. Lusson, A. Travlos, Superlattices and Microstructures 42 (1), p.431-437, Jul 2007.
- Self-assembled zinc oxide nanodots on silicon oxide, *K Giannakopoulos, N Boukos and A. Travlos*, 2005, Journal of Physics: Conference Series, 10, 121-124.

Demokritos
National Centre for Scientific Research

Core-shell nanoparticles for medical applications

I. ***Silica core/mesoporous silica shell***
II. *Ferrite core/Silica shell*
III. *Silica core/nano-ferrite shell*

Demokritos
National Centre for Scientific Research

Core-shell nanoparticles for medical applications

Applications:
- Drug Delivery
- Magnetic hyperthermia
- Magnetic resonance imaging

Particle requirements for biomedicial applications:
- Size accuracy (membranes)
- Porosity accuracy (e.g. attachment of drugs in drug delivery)
- Surface chemistry (biocompatibility)
- No agglomeration esp. in magnetic particles
  (Superparamagnetic particles respond to magnetic fields)

Too much for one material! ⟹ Coating !

Demokritos National Centre for Scientific Research

Core-shell nanoparticles for medical applications

Silica (SiO_2):
- Biocompatible
- Stable against degradation
- Easy for surface modification
- Non-toxic

✓Template for the synthesis of various materials
✓Enzyme immobilization
✓Controlled drug delivery
✓Biocatalysis
✓Bioseparation
✓Biosensors

Magnetic nanoparticle applications:
✓Cell separation
✓Immobilization of enzymes
✓Isolation and purifications of proteins
✓Magnetic drug targeting
✓Antibody immobilization
✓Magnetic Resonance Imaging
✓Magnetic hyperthermia

Demokritos National Centre for Scientific Research

Core-shell nanoparticles for medical applications – Silica core/mesoporous silica shell

Electrostatic assembly (No pore swelling agents)

Silica nanoparticles
highly basic
sodium silicate solution

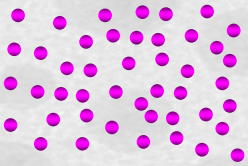

Silica core –Silica Shell

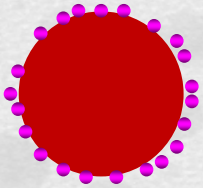

Silica core particles

Stoeber process:
hydrolysis and condensation of
tetraethylorthosilicate,
TEOS ($Si(OC_4H_9)_4$

+

Functionalisation :
3-aminopropyltriethoxysilane (**APTES**)
or
poly diallyldimethylammonium chloride (**PDDA**)

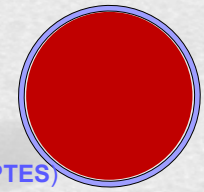

• Centrifugation
• Drying

Demokritos
National Centre for Scientific Research

Core-shell nanoparticles for medical applications – Silica core/mesoporous silica shell

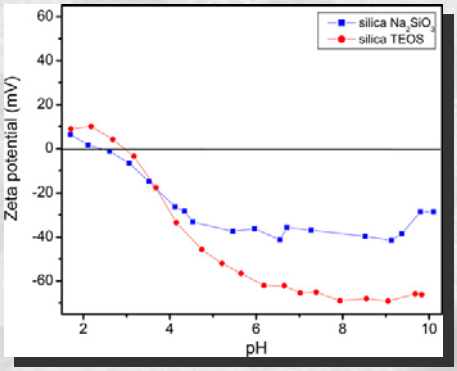

Core and layer particles have the same sign for the Zeta potential

No assembly is possible!

Synthesis Parameters:
•Functionalization agent
•Core/shell material concentrations
•pH
•Temperature
•Reaction Time

Demokritos
National Centre for Scientific Research

Core-shell nanoparticles for medical applications – Silica core/mesoporous silica shell

The effect of the surface functionalization on the zeta potential

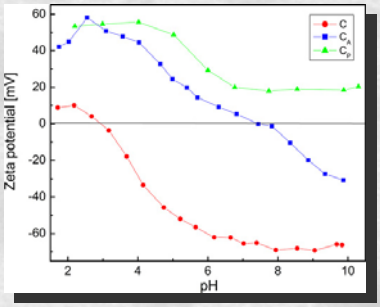

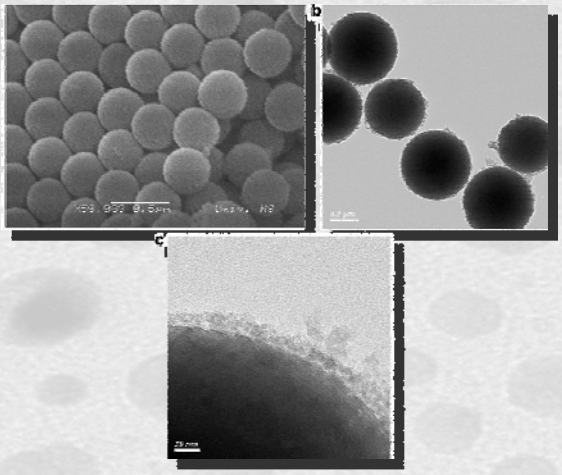

Core particle Zeta potential
pure silica (C)
APTES-modified (CA)
PDDA-modified (CP)

Demokritos National Centre for Scientific Research

Microporous and Mesoporous Materials 155 (2012) 8–13

Core-shell nanoparticles for medical applications – Silica core/mesoporous silica shell

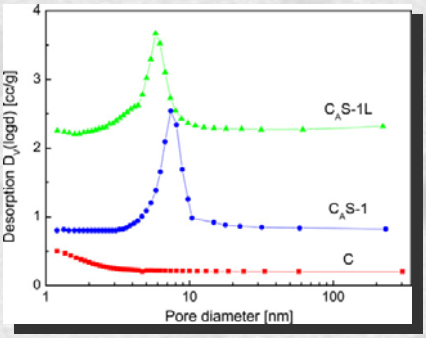

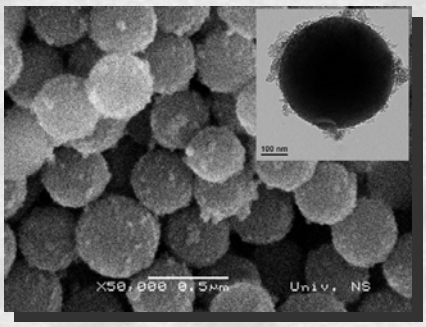

Mesoporous structure with relatively narrow size distribution

⇩

Immobilization of enzymes

Demokritos National Centre for Scientific Research

Microporous and Mesoporous Materials 155 (2012) 8–13

Core-shell nanoparticles for medical applications

I. *Silica core/mesoporous silica shell*
II. ***Ferrite core/Silica shell***
III. *Silica core/nano-ferrite shell*

Demokritos
National Centre for Scientific Research

Core-shell nanoparticles for medical applications – Ferrite core/Silica shell

Silica Coated Ferrites
(SiO_2 core/ Magnetite **- Fe_3O_4** or Nickel ferrite **- $NiFe_2O_4$shell)**

Ferrite applications in biotechnology:
•Magnetically assisted drug delivery
•Immobilization of proteins and enzymes

Silica shell advantages:
•Biocompatible
•Prevents agglomeration of magnetic nanoparticles

Demokritos
National Centre for Scientific Research

Core-shell nanoparticles for medical applications – Ferrite core/Silica shell

Ferrite core particles:
Magnetite (Fe_3O_4)
or
Nickel ferrite($NiFe_2O_4$)

+

Functionalisation:
Citric acid (biocompatible)

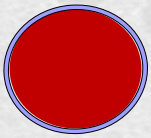

Stoeber process (sol gel) –
TEOS

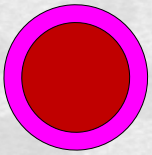

Ferrite core –Silica Shell

- Centrifugation
- Drying

Demokritos
National Centre for Scientific Research

Core-shell nanoparticles for medical applications – Ferrite core/Silica shell

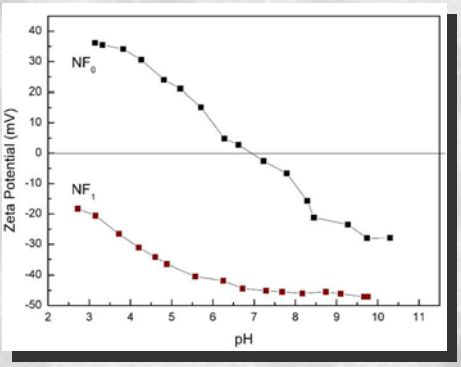

Influence of Citric Acid on the Zeta Potential of $NiFe_2O_4$

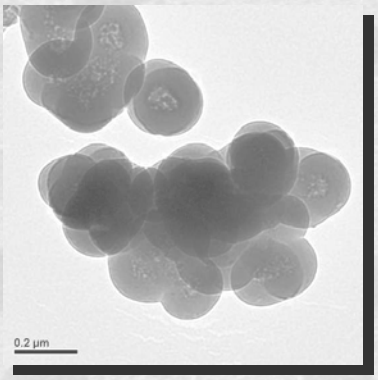

$NiFe_2O_4$ core /Silica shell

Demokritos
National Centre for Scientific Research

Ceramics International http://dx.doi.org/10.1016/j.ceramint.2012.05.050

Core-shell nanoparticles for medical applications – Ferrite core/Silica shell

$NiFe_2O_4$ core / SiO_2 shell

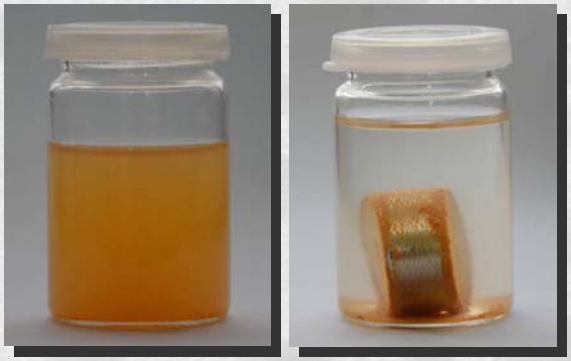

Near a 0.3 T magnet

Demokritos National Centre for Scientific Research

Ceramics International http://dx.doi.org/10.1016/j.ceramint.2012.05.050

Core-shell nanoparticles for medical applications

I. Silica core/mesoporous silica shell

II. Ferrite core/Silica shell

III. Silica core/nano-ferrite shell

Demokritos National Centre for Scientific Research

Core-shell nanoparticles for medical applications - Silica core/nano-ferrite shell

Silica core/nano-ferrite shell (SiO_2 core/ Fe_3O_4)

Intermediate step for the formation of
a magnetic layer between silica and mesoporous silica

Silica Functionalisation:
APTES or PDDA

Ni-Ferrite Functionalisation:
Citric Acid

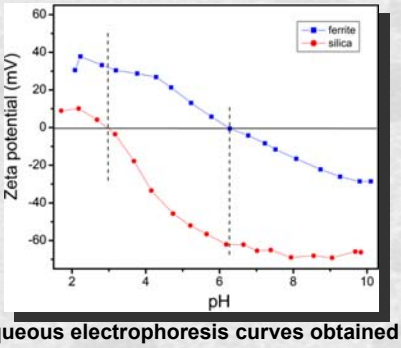

Aqueous electrophoresis curves obtained for silica and ferrite particles

Demokritos National Centre for Scientific Research

Materials Research Bulletin, 47, Issue 6, 2012, p. 1513–1519

Core-shell nanoparticles for medical applications - Silica core/nano-ferrite shell

Silica core/nano-ferrite shell particles (SiO_2/ Fe_3O_4)

Silica (Core)

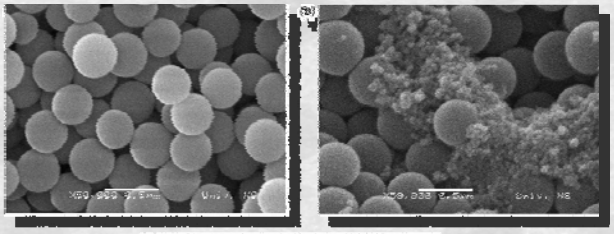

pH 7,5

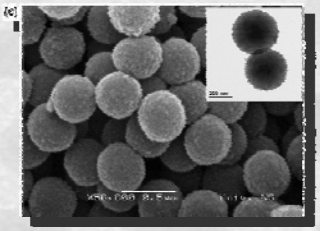

pH 5,4

Demokritos National Centre for Scientific Research

Materials Research Bulletin, 47, Issue 6, 2012, p. 1513–1519

Core-shell nanoparticles for medical applications - Silica core/nano-ferrite shell

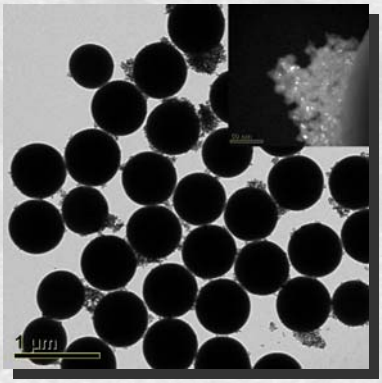

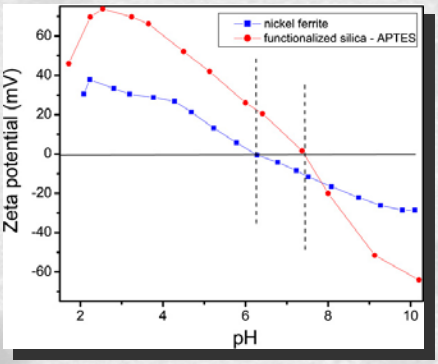

APTES-functionalized silica core/ $NiFe_2O_4$ shell: not full coverage

Demokritos National Centre for Scientific Research

Materials Research Bulletin, 47, Issue 6, 2012, p. 1513–1519

Core-shell nanoparticles for medical applications - Silica core/nano-ferrite shell

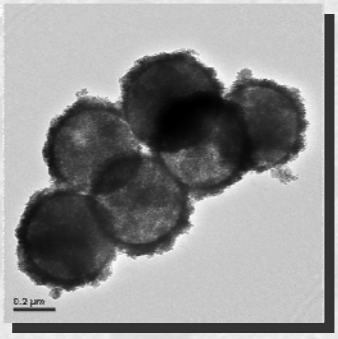

PDDA-functionalized silica and surface modified $NiFe_2O_4$ with citric acid

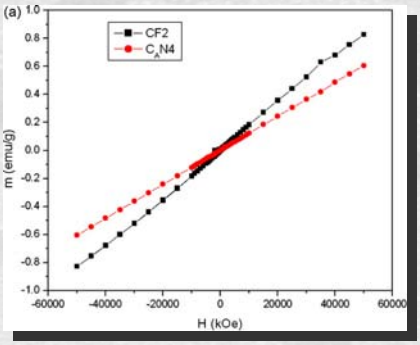

Magnetization measurements: no Hysteresis effects

Particles in the superparamagnetic regime

Demokritos National Centre for Scientific Research

Materials Research Bulletin, 47, Issue 6, 2012, p. 1513–1519

Acknowledgements

- L. Castaldi (Oerlikon)
- N. Boukos (NCSR Demokritos)
- D. Bensahel (STMicroelectronics)
- A. Travlos (NCSR Demokritos)
- V. Srdic (Un. of Novi Sad)
- C. Sargentis (NCSR Demokritos - NTUA)

- STMicroelectronics/Philips Semiconductors/Freescale Semiconductor
- Project ENTER (Greek Ministry of Development)

General Introduction to European Fundings

NetFISiC Training School
July 15th, 2012
Thessaloniki, Greece

Cécile LE DUC – Lyon Ingénierie Projets – cecile.leduc@lyoningenierie.fr

General Introduction to European Fundings

- I. History –in brief
- II. Short introduction
- III. General overview of the main tools
- IV. Targeted information on near-future calls and some advice to answer European calls in general

I. History –in brief

- **1951 ECSC Treaty** constituting the European Coal and Steel Community;
- **1957 Rome Treaty** encourages research in common agriculture policy + **Euratom Treaty** stands for the begin of a common research policy with the European Atomic Energy Community;
- **1974 Scientific and Technical Research Committee and Council** tries to coordinate national policies in scientific and technological field;

At this stage, research is still **no area of competence** for the European Union.

I. History –in brief

- **1980 Big specific programmes** are launched like ESPRIT to develop information technologies;
- **1984 the first Framework Programme for Research and Technological Development** is launched to support community activities by co-funding policies;
- **1985 the Single European Act** lays the first legal basis by giving the Union the competence in the research and development field;
- **1992 the Maastricht Treaty** sets the global strategy towards international competition, sustainable growth, employment and social security, etc.

I. History –in brief

- **2000 the Lisbon Strategy** makes of the European knowledge economy the « most dynamic competitive knowledge-based economy in the world » by investing 3% of its GDP in R&D;

We talk now about **the Knowledge Triangle**: Research, Education and Innovation;

The European Research Area is created, that the EU will use as a political platform for R&D, aiming at turning research in Europe into a kind of « common market ».

In this system, **the 7th Framework Programme** (**FP7**) plays a major role.

I. History –in brief

=> Nowadays, t**he European Research Funding System** is based on

strategic priorities of research

⇩

calls for proposals

⇩

« funding by projects »

This is what you are going to face,
and this is why you need to learn how to raise those funds!

II. Short Introduction

BUT

« Europe » does not mean one single provider of funds…

Indeed, it is split into a **multiplicity of departments, sections, agencies**, each of them
- **answering a strategic axis of research** (ex: lifelong learning, health)
- **lauching targeted calls for proposals** with each time their own rules (that can be changed for a same kind of project, even from one year to another, ex: ITNs)
- **distributing a specific budget** (ex: 50 521 million Euros for FP7 for the period 2007-2013) to the projects that were positively assessed against various rules of use of this money.

II. Short Introduction

This makes the whole system very **complex**, very **heavy**, not easily understandable and accessible for researchers despite the efforts of the EU.

=> Universities **adapt** themselves, with the aim of offering to their researchers some help in this fund raising (not only for the **budget** it brings to the University but also for the **image** of the University that it disseminates (prestige)):
- via **European departments or sections**, that are inside the University, dedicated to fund raising;
- or via **dedicated societies** like mine, subsidiary of the University of Lyon (France), specialized in the promotion of the University's research by the project engineering of all kinds.

=> Since its creation (2006) LIP has developed an expertise in:

II. Short Introduction

- **Strategic watch** all year long
- **Programm analysis** and **targeted promotion**
- **Technical set-up of the proposal:** assistance in the constitution of the partnership, strategic advices, intellectual property management, legal and financial expertise in order to optimize the budget and the « shape » of the proposal, translation, rewriting, corrections, negotiation with Europe when the project obtains a positive feedback from the EU
- **Project Management:** assistance to the scientific coordination, management of all administrative and financial aspects of the project, organisation and implementation of the reporting all project long, communication management and results dissemination
- **Organisation of scientific events**

III. General overview of MAIN European Funding Tools

Who?	What?	Why?	How?
DG Research			
DG Regio (regional)			
DG Education & European Agency EAC			
European Science Foundation			

III. General overview of MAIN European Funding Tools

Who?	What?	Why?	How?
DG Research	FP7	**Fundamental and applied research, researchers' mobility, research facilities**	Networks, collaborative and individual projects, mobility fellowships
DG Regio (regional)			
DG Education & European Agency EAC			
European Science Foundation			

III. General overview of MAIN European Funding Tools

Who?	What?	Why?	How?
DG Research	FP7	**Fundamental and applied research, researchers' mobility, research facilities**	Networks, collaborative and individual projects, mobility fellowships
DG Regio (regional)	regional development and cooperations (FEDER & Interreg)	**Sustainable development in the wider approach, social and regional cohesion**	Networks, collaborative projects
DG Education & European Agency EAC			
European Science Foundation			

III. General overview of MAIN European Funding Tools

Who?	What?	Why?	How?
DG Research	FP7	**Fundamental and applied research, researchers' mobility, research facilities**	Networks, collaborative and individual projects, mobility fellowships
DG Regio (regional)	regional development and cooperations (FEDER & Interreg)	**Sustainable development in the wider approach, social and regional cohesion**	Networks, collaborative projects
DG Education & European Agency EAC	Programme EFTLV, Erasmus Mundus, Tempus, Culture Program	**Education and Lifelong learning (higher education, continuing education)** **Promotion of the European Culture and Heritage**	Networks and collaborative projects (including masters and international PhDs)
European Science Foundation			

III. General overview of MAIN European Funding Tools

Qui ?	Quoi ?	Pour quoi ?	Comment ?
DG Research	FP7	**Fundamental and applied research, researchers' mobility, research facilities**	Networks, collaborative and individual projects, mobility fellowships
DG Regio (regional)	regional development and cooperations (FEDER & Interreg)	**Sustainable development in the wider approach, social and regional cohesion**	Networks, collaborative projects
DG Education & European Agency EAC	Programme EFTLV, Erasmus Mundus, Tempus, Culture Program	**Education and Lifelong learning (higher education, continuing education)** **Promotion of the European Culture and Heritage**	Networks and collaborative projects (including masters and international PhDs)
European Science Foundation	COST, Eurocores, exploratory workshops, etc.	**Scientific coordination, conferences, research**	Networks, individual projects

III. Targeted information on near-future calls

FP7 – Marie Curie Actions – 2013

- No specific topic, "open calls"
- Basic principle: **mobility**
- **Collaborative Projects (**min 3 partners of 3 different countries) and **individual fellowships (**PhD funding)
- **Marie Curie collaborative project**: Calls in **July 2012**, for a submission of the proposal to the EU between **Nov. 2012 to Jan. 2013**
- **Marie Curie individual fellowships 2013:** Call in **March 2013,** for a submission on **August 14th, 2013.**

III. Targeted information on near-future calls

FP7 – Individual Marie Curie fellowships

2012 Calls for proposals for individual fellowships,

with a submission on August 16th, 2012

- IEF= Intra **European** Fellowship
- IIF= **International Incoming** Fellowship
- IOF=**International Outgoing** Fellowship
- "Experimented" Researchers
- 100% of the flat-rate salary funded during 2 or 3 years + a monthly grant for the purchase of consumables
- Good percentage of success

III. Targeted information on near-future calls

FP7 Marie Curie Actions – ITNs like NetFISiC

- **"Initial Training Networks":** Network **for** and **by** research training = research programme + training programme
- Collaborative project of **4 years**, in which each partner recruit and "exchange" young researchers
- **Mobility** conditions
- Call in July 2012 – Submission in November 2012
- Collaborative project: at least 3 partners of 3 different countries
- **Funding of PhDs** and actions of training networks
- Funding: **100%** of the expenses – flat-rate amounts
- Requires the involvement of private partners (SMEs or big groups, compulsory)

III. Targeted information on near-future calls

Programme "Education and Lifelong Learning"

- **Erasmus/Tempus: higher education** (wide networks, innovative teaching tools, cursus, mobilities..)
- **Leonardo Da Vinci: professional training** (cursus, intersectorial dialogue, innovative teaching tools, exchanges..)
- **Jean Monnet:** training aroung the question of the **European construction and integration** (workshops, conferences, exchanges..)
- **Grundtvig:** training for **adults**
- **Publication of calls in October – submission bet. January-March**
- Collaborative projects of all scales, for 1 to 3 years
- Funding until 100 000 to 250 000 Euros/year
- Limited to 75% of the costs (Salaries, Consumables, travel, equipment)

General advices for answering a European Call for Proposal

1. Try to define the most appropriate tool

- What do I do and what do I want to do?
- What (and how much) do I need?
- With whom do I want to work?
- What are the time constraints that are beyond my control?

Why would my project need a European funding and a transnational partnership?

2. Answer the call requirements

- Collect all documents related to the call: for the FP7 it means the work programme and annexes, the guide for applicant, and the call fiche, all available under the cordis website once the call is published: http://cordis.europa.eu/
- Read them!
- Answer to ALL requirements of the call, taking into account the global context in which the call is launched
- **Strictly respect the limits or else your proposal might not even be evaluated :** pages, budget, required contribution, submission date and hour, partnership, etc.

3. Writing while thinking of your evaluator

- While writing your proposal, **keep an eye on the evaluation criteria and try to meet them**
- Keep in mind that your evaluator is a scientist or an industrial, generally from your field but **not necessarily expert in your specific topic**
- Keep in mind that he shall evaluates tens of proposals like yours: **be as much simple and concise as possible**
- Falicitate him the reading by integrating **visual elements** to the text (schemes, tables, illustrations, etc.)
- Your English must be correct but no Shakepeare's one is required!

4. How to « make the difference »?

➢ **When the scientific quality of both projects is equal,** the proposal that will be selected is the one who will demonstrate the best "impact":

- ➢ *Added value for **science***
- ➢ *Added value for **Europe** (politically, economically, position)*
- ➢ *Added value for the **society** in the wider meaning: dissemination is highly valuable for Europe, specifically for the public outreach (not for the experts only) and the exploitation*
- ➢ *Added value for **partnerships** (sustainable collaborations, joint results exploitation, etc).*

➢ Keep in mind that Europe **INVEST** in you by funding your project: the feedback is very important and expected!

5. Possible Supports in your countries

- ➢ ***European Departments** of your Universities (or subsidiaries like LIP)*
- ➢ ***National Contact Points** of the different Programmes, in order to get some explanations on calls and related rules and conditions*
- ➢ ***Your colleagues** may be good reviewers for a critical reading of your proposal*
- ➢ *…*

Example on a FP7 call

Set-Up - Description of the main tasks

"Shaping"and writing of the proposal
Scientific and technical parts of the proposal: objectives, workpackages, deliverables, risk evaluation, milestones calendar, partners' roles, etc
Data collection and integration of individual partner presentations
Project management and resources distribution
Corrective reading

Administrative aspects
Collection and validation of administrative information by all partners
Integration of those data in the EU templates (tables and locked files)

Financial aspects
Data collection by all partners, validation of the distribution of the expenses by activity type, calculation and correction of the budget
Validation of costs models of each partner (depending on the call's rules and the status of the partner)

Submission
Upload from data onto the European server, control of the file, electronic submission

Example on a FP7 call

Negotiation – Description of the main tasks

Scientific part
Study of the evaluation report
Advices on the changes to be brought to the proposal
Shaping your proposal into the technical annex of your future contract

Administrative aspects
Collection and validation of complementary administrative information by partners
Filling EU templates with administrative required data
Corrective reading of the contract, signature and sending of contractual documents

Financial aspects
Negotiation with the EU, validation by all partners of the budget, the dedicated manpower, and filling EU templates with financial information

Relations with EU
Participation to the kick off meeting with the Project Officer
Intermediary between the coordinator and the EU

Intellectual property
Writing and negotiation of the consortium agreement with all partners

Lyon Ingénierie

Thank you for your attention !

Dislocations in solids

Gabrielle Regula,
Associate Professor, habilitation

IM2NP, Aix-Marseille University

Main sources are lectures of F. Minari, B. Pichaud
Introduction to dislocations D.Hull and D. J. Bacon 3rd Edition
Theory of dislocations, John Price Hirth and Jens Lothe, 2nd Edition (1982)

Outline

0- Dislocations in casual life…

1- Some history: where does the concept of dislocation come from ?

2- Physics of dislocations

3- Dislocations in real structures: few applications to semiconductors

4- Observation of dislocations: methods, examples

5- Conclusion

0- Dislocations in casual life

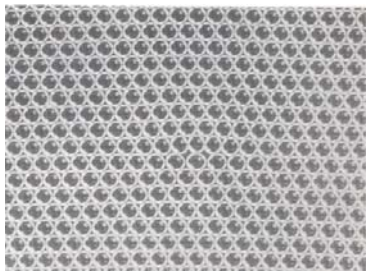
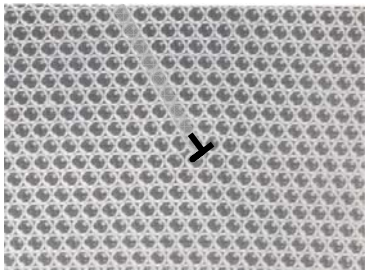
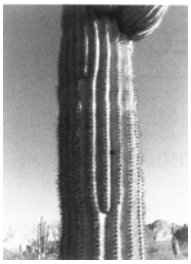
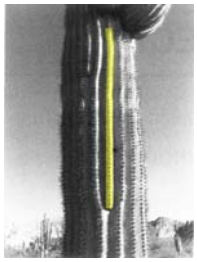

Thessaloniki, Summer School, 11th-15th July 2012 gabrielle.regula@univ-amu.fr

Institut Matériaux Microélectronique Nanosciences de Provence
UMR CNRS 7334, Universités Aix-Marseille et Sud Toulon-Var

1- Some history: where does the concept of dislocation come from ?

A dislocation is a 1D-defect in the periodic structure of crystals. To understand its role and how it was discovered we have to consider the mechanical properties of materials since they are mainly concerned with this defect

1.1 A few definitions

When a solid is deformed (stretched, compressed…), there are pressures (@ every points in the bulk) on local surfaces
→stresses (σ) which are expressed as forces per unit surface
$N.m^{-2}$ or Pa

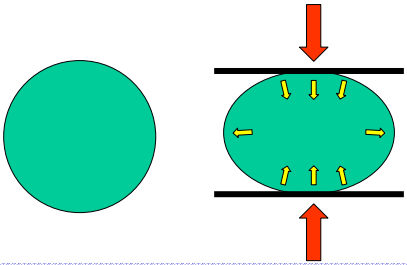

Thessaloniki, Summer School, 11th-15th July 2012 gabrielle.regula@univ-amu.fr

Institut Matériaux Microélectronique Nanosciences de Provence
UMR CNRS 7334, Universités Aix-Marseille et Sud Toulon-Var

There are two types of stresses:

- uniaxial stresses (forces normal to the surface)

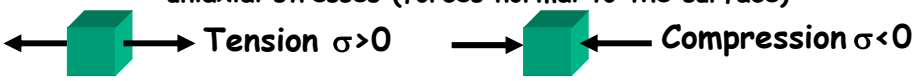

- shear stresses (forces tangent to the surface)

To describe the internal pressures in each points of the solid resulting from external actions, 6 stress components are needed: 3 uniaxial stresses and 3 shear stresses (σ_1 to σ_6)

As the solid is deformed the distance between two given points changes. The relative change of this distance is named Strain (ε)

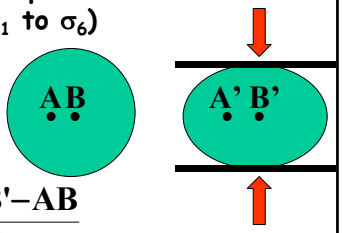

$$\varepsilon = \frac{A'B' - AB}{AB}$$

To describe the response of the solid to the stresses at each points resulting from external actions, 6 strain components are needed: 3 uniaxial strains and 3 shear strains (ε_{ij} i=direction; j=plane)

@ rest→elemental volume @ mechanical equilibrium→ $\varepsilon_{ij} = \varepsilon_{ji}$

1.2 Classical linear elasticity: Hooke's law

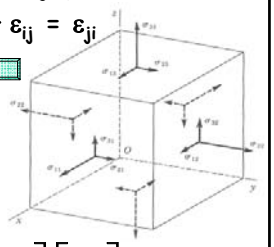

If the strains are small, there is a linear relationship between stresses (σ_i) and strains (ε_i). This can be expressed as a matrix product:

$$\begin{bmatrix} \varepsilon_{11} \\ \varepsilon_{22} \\ \varepsilon_{33} \\ \varepsilon_{23} \\ \varepsilon_{31} \\ \varepsilon_{12} \end{bmatrix} = \begin{bmatrix} \varepsilon_1 \\ \varepsilon_2 \\ \varepsilon_3 \\ \varepsilon_4 \\ \varepsilon_5 \\ \varepsilon_6 \end{bmatrix} = \begin{bmatrix} S_{11} & S_{12} & S_{13} & S_{14} & S_{15} & S_{16} \\ S_{12} & S_{22} & S_{23} & S_{24} & S_{25} & S_{26} \\ S_{13} & S_{23} & S_{33} & S_{34} & S_{35} & S_{36} \\ S_{14} & S_{24} & S_{34} & S_{44} & S_{45} & S_{46} \\ S_{15} & S_{25} & S_{35} & S_{45} & S_{55} & S_{56} \\ S_{16} & S_{26} & S_{36} & S_{46} & S_{56} & S_{66} \end{bmatrix} \cdot \begin{bmatrix} \sigma_1 \\ \sigma_2 \\ \sigma_3 \\ \sigma_4 \\ \sigma_5 \\ \sigma_6 \end{bmatrix}$$

normal strains / shear strains

It is a quite complicated operation. Fortunately when applying this law to real crystals the symmetries of the crystal reduce the number of independent components of σ (the higher the symmetry the smaller the number of independent components)

For example in the case of isotropy:

$$\begin{bmatrix}\varepsilon_1\\ \varepsilon_2\\ \varepsilon_3\\ \varepsilon_4\\ \varepsilon_5\\ \varepsilon_6\end{bmatrix} = \begin{bmatrix} 1/E & -\nu/E & -\nu/E & 0 & 0 & 0\\ -\nu/E & 1/E & -\nu/E & 0 & 0 & 0\\ -\nu/E & -\nu/E & 1/E & 0 & 0 & 0\\ 0 & 0 & 0 & 1/\mu & 0 & 0\\ 0 & 0 & 0 & 0 & 1/\mu & 0\\ 0 & 0 & 0 & 0 & 0 & 1/\mu \end{bmatrix} \cdot \begin{bmatrix}\sigma_1\\ \sigma_2\\ \sigma_3\\ \sigma_4\\ \sigma_5\\ \sigma_6\end{bmatrix}$$

With E, μ and ν respectively the Young's modulus, the shear modulus and the Poisson's ratio. These coefficients are usually tabulated for all the materials which could be considered as mechanically isotropic

For metals and ceramics, $40<E<600$ GNm^{-2} and $0.2<\nu<0.45$

Example: tension experiment

A cylindrical bar is stretched along its axis

If we consider the following reference system, there is only one stress component:

$$\sigma_3 = F/S > 0$$

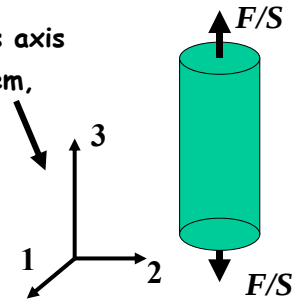

$$\begin{Bmatrix}\text{normal strains}\\ \text{shear strains}\end{Bmatrix} \begin{bmatrix}\varepsilon_1\\ \varepsilon_2\\ \varepsilon_3\\ \varepsilon_4\\ \varepsilon_5\\ \varepsilon_6\end{bmatrix} = \begin{bmatrix} 1/E & -\nu/E & -\nu/E & 0 & 0 & 0\\ -\nu/E & 1/E & -\nu/E & 0 & 0 & 0\\ -\nu/E & -\nu/E & 1/E & 0 & 0 & 0\\ 0 & 0 & 0 & 1/\mu & 0 & 0\\ 0 & 0 & 0 & 0 & 1/\mu & 0\\ 0 & 0 & 0 & 0 & 0 & 1/\mu \end{bmatrix} \cdot \begin{bmatrix}0\\ 0\\ F/S\\ 0\\ 0\\ 0\end{bmatrix}$$

which gives only three strain components, the bar is elongated along the axis $\varepsilon_3 = F/SE > 0$
but it is also compressed along the two transversal directions $\varepsilon_1 = -\nu F/SE < 0$ and $\varepsilon_2 = -\nu F/SE < 0$ → $\nu = -\varepsilon_1/\varepsilon_3$

1.3 Elasticity/plasticity of materials

Let us still consider the tension experiment. The length of the bar is increased by a special machine (with a constant strain velocity $\dot{\varepsilon}$=Cst). Suppose that we measure the stress during the experiment (with a force probe) and let us display the variations of that stress as the function of the strain, the obtained-curve is:

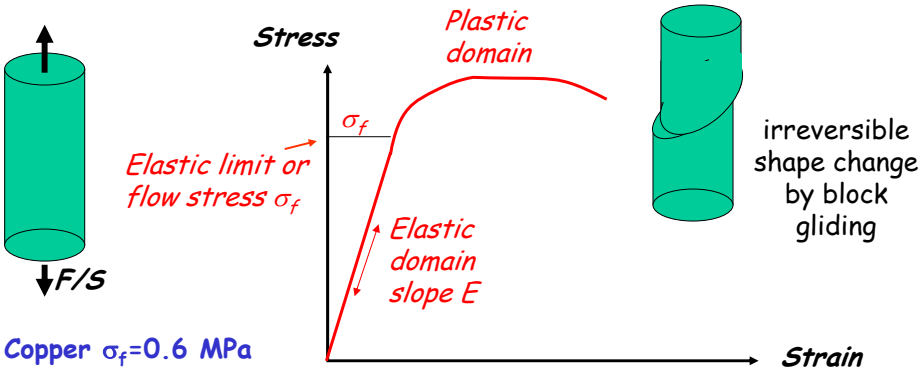

Copper σ_f=0.6 MPa

The flow stress can be taken as the threshold stress which allows the block gliding to be operative. How to estimate this stress?

Let us consider the gliding of one block on the other due to a shear stress applied parallel to the interface.

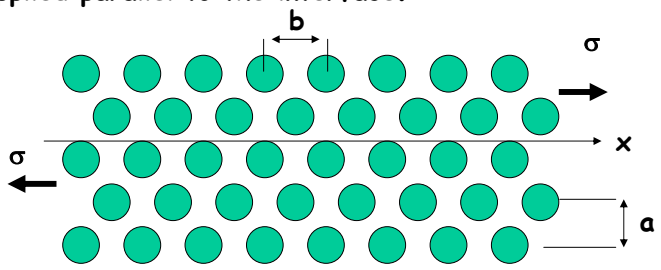

The shear stress along x is a periodic function of x, with a period b

$\sigma = A\sin(2\pi x/b)$ with A a constant [1] (1)

A small displacement x (x<b) of the upper block corresponds to a shear strain $\varepsilon = x/a$

[1] J. Frenkel, Z. Phys,37:572, 1926

Applying the Hooke's law gives a shear stress

$\sigma = \mu\varepsilon = \mu x/a$ (2)

since x is small one can re-write eq (1) as: $\sigma = A2\pi x/b$ (3)

equating both expressions (2 and 3) for σ gives:

$$A = \frac{\mu}{2\pi}\frac{b}{a}$$

$$\sigma_{max} = \frac{\mu}{2\pi}\frac{b}{a} \approx \frac{\mu}{10}$$

The maximun value of the shear stress should correspond to the measured flow stress σ_f

For copper, $\mu = 5.5\ 10^{11} N.m^{-2}$ → $\sigma_{max} = 5.5\ 10^{10}$ Pa = $5.5\ 10^4$ MPa is 10^5 too high as compared to σ_f = 0.6MPa. This discrepancy is so large that the mechanism of block gliding has to be questioned

Something which help the gliding of one block as respect to the other has to be found. The answer came from the idea proposed by Orowan, Taylor and Polanyi (in a humoristic way) of the existence of a defect helping to glide…

Analogy between the block gliding and the gliding of a very large carpet on a floor (1940)

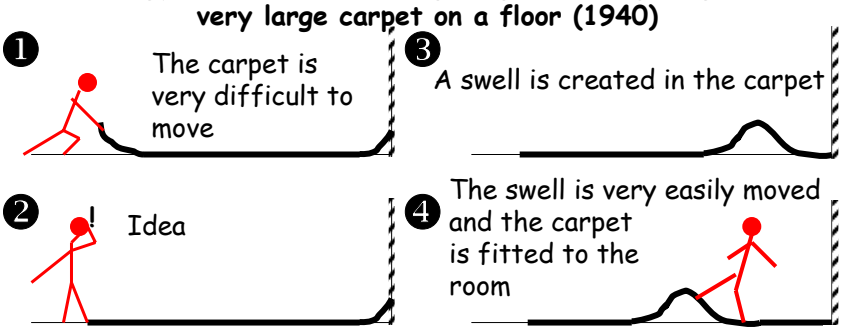

What is the defect which could play the role of the swell in crystals? In the 40s it was proposed a structural defect named dislocation, its theory was developed all along the 40s and the 50s and this defect was finally observed in the 60s and the 70s when the technique of transmission electron microscopy (TEM) had become easier to carry out

Vito Volterra (Italian mathematician & physicist)

original cut of a homogeneous isotropic cylinder

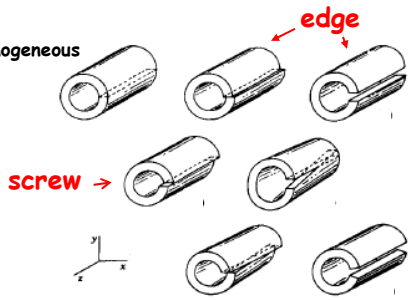

Fig. 2 — The types of dislocations as classified by Volterra.[9]

and other 3 types of disclinations ….

A Brief History of Dislocation Theory

J. P. HIRTH

Early developments leading to the concept of a dislocation are discussed. The discoveries of 1934 are described. The subsequent evolution of various aspects of dislocation theory is outlined.

Dislocation observations in 1950 Hedges & Mitchell

→ TEM in 1956 Hirsch

→ TEM in situ: dislocation motion: Louchet, Kubin 1976

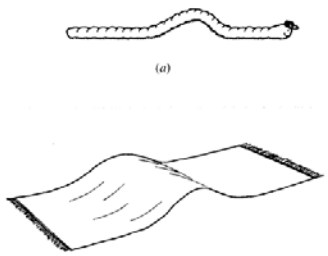

(a) (b)

Fig. 1 — Dislocation analogs used for pedagogical purposes: the caterpillar and the carpet.

METALLURGICAL TRANSACTIONS A VOLUME 16A, DECEMBER 1985 — 2085

This paper is based on a presentation made at the symposium "50th Anniversary of the Introduction of Dislocations" held at the fall meeting of the TMS-AIME in Detroit, Michigan in October 1984 under the TMS-AIME Mechanical Metallurgy and Physical Metallurgy Committees.

Thessaloniki, Summer School, 11th-15th July 2012 gabrielle.regula@univ-amu.fr
Institut Matériaux Microélectronique Nanosciences de Provence
UMR CNRS 7334, Universités Aix-Marseille et Sud Toulon-Var

Dislocation: line limiting the additional half lattice plane

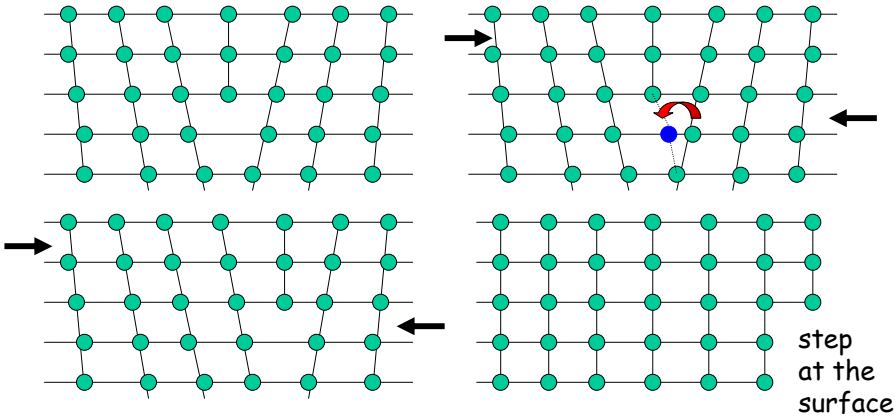

The dislocation movement is easy, it needs only bond exchange while gliding without dislocation needs the breaking of all the bonds @ the same time @ the interface

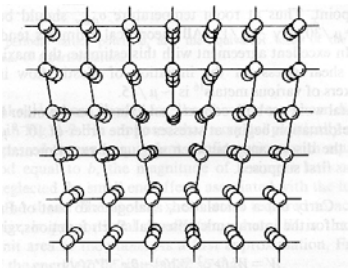

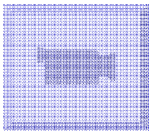

Thessaloniki, Summer School, 11th-15th July 2012 gabrielle.regula@univ-amu.fr
Institut Matériaux Microélectronique Nanosciences de Provence
UMR CNRS 7334, Universités Aix-Marseille et Sud Toulon-Var

2- Physics of dislocations

2.1 Geometrical description

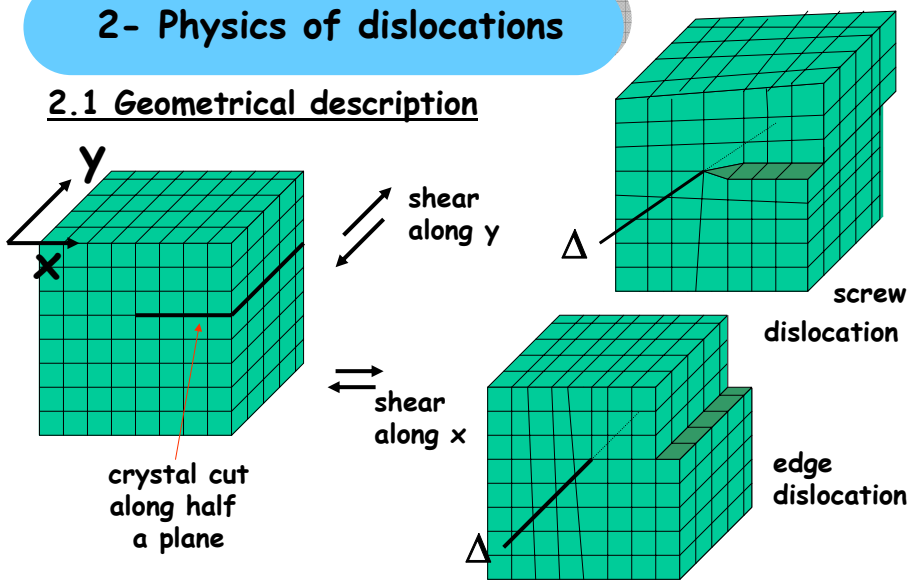

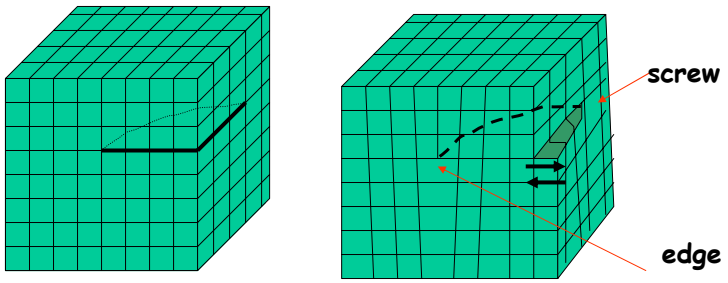

A dislocation can not stop in a crystal, it should be connected to the surface, another dislocation or itself. A dislocation line is a frontier between a sheared region and an un-sheared one

To describe a dislocation in a crystal we must precise:
- its position ($\vec{r}$)
- its character (screw, edge or mixed) in each point of the line

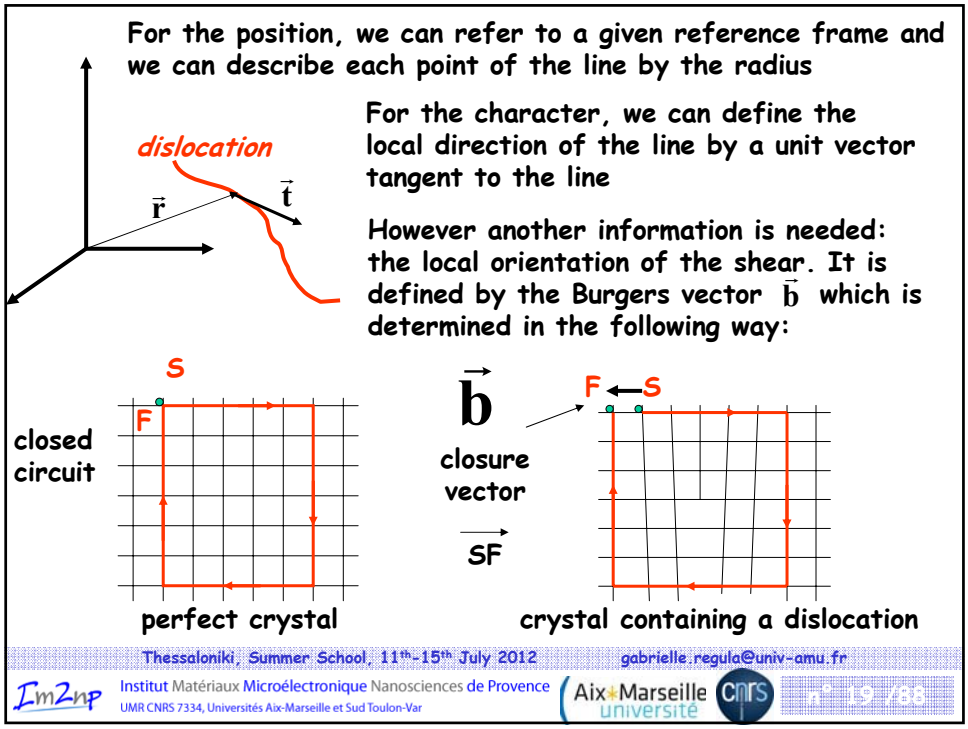
For the position, we can refer to a given reference frame and we can describe each point of the line by the radius
dislocation
$\vec{r}$
$\vec{t}$
For the character, we can define the local direction of the line by a unit vector tangent to the line
However another information is needed: the local orientation of the shear. It is defined by the Burgers vector $\vec{b}$ which is determined in the following way:
S
F
closed circuit
perfect crystal
$\vec{b}$
closure vector
$\overrightarrow{SF}$
F
S
crystal containing a dislocation
Thessaloniki, Summer School, 11th-15th July 2012
gabrielle.regula@univ-amu.fr
Institut Matériaux Microélectronique Nanosciences de Provence
UMR CNRS 7334, Universités Aix-Marseille et Sud Toulon-Var
Aix Marseille université
cnrs

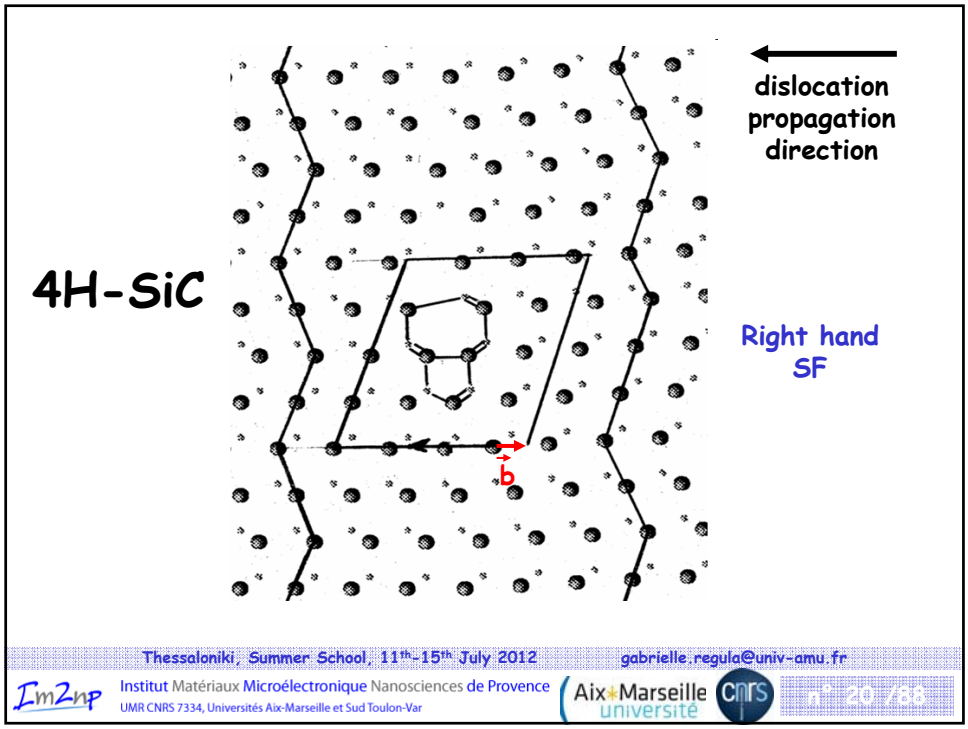
4H-SiC
dislocation propagation direction
Right hand SF
$\vec{b}$
Thessaloniki, Summer School, 11th-15th July 2012
gabrielle.regula@univ-amu.fr
Institut Matériaux Microélectronique Nanosciences de Provence
UMR CNRS 7334, Universités Aix-Marseille et Sud Toulon-Var
Aix Marseille université
cnrs

A Burgers vector is the same all along a dislocation line, the local character of a dislocation is thus determined by the pair $\vec{b}$,$\vec{t}$:

$\vec{b} \perp \vec{t}$ edge dislocation $\vec{b} \parallel \vec{T}$ screw dislocation

$(\vec{b}, \vec{t}) = \theta$ mixed dislocation

The character of a curved dislocation changes along its line

2.2 Dislocation movement

The movement of dislocations is at the basis of the plastic deformation. Thanks to it, materials can be formed (stamping, rolling…). There are two types of dislocation movement:

- the movement in the glide plane which is defined as the plane containing $\vec{b}$ and $\vec{t}$. This movement is relatively easy in materials, of course depending of the bond strength (the weaker the bonds, the easier)
- the movement out of (normal to) the glide plane named climb

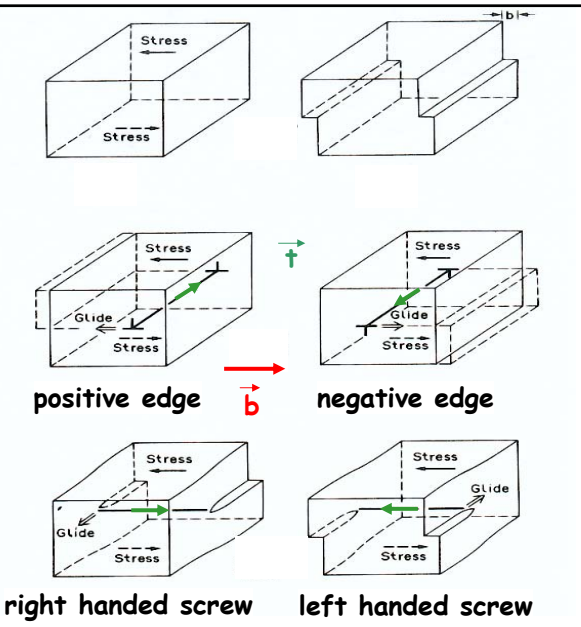

Glide

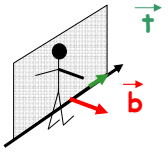

dislocations of opposite sign glide in opposite directions under the same stress

for dislocation glide, a shear stress must act on the slip plane in the direction of b irrespective of the direction of the dislocation line

Thessaloniki, Summer School, 11th-15th July 2012 gabrielle.regula@univ-amu.fr
Institut Matériaux Microélectronique Nanosciences de Provence
UMR CNRS 7334, Universités Aix-Marseille et Sud Toulon-Var

Cross slip

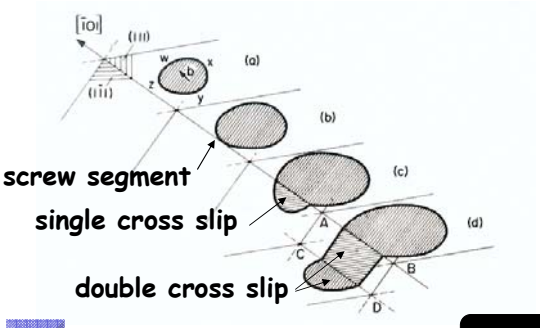

in CFC the screw dislocations move in {111} type plane but can switch from one to another

TEM

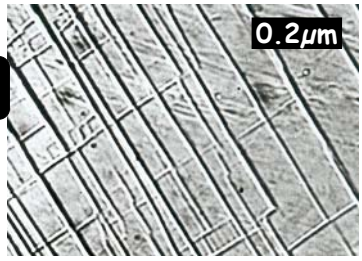

example of cross slip on the polished surface of a single crystal of 3.5% silicon iron

Thessaloniki, Summer School, 11th-15th July 2012 gabrielle.regula@univ-amu.fr

Institut Matériaux Microélectronique Nanosciences de Provence
UMR CNRS 7334, Universités Aix-Marseille et Sud Toulon-Var

FCC stereographic projection

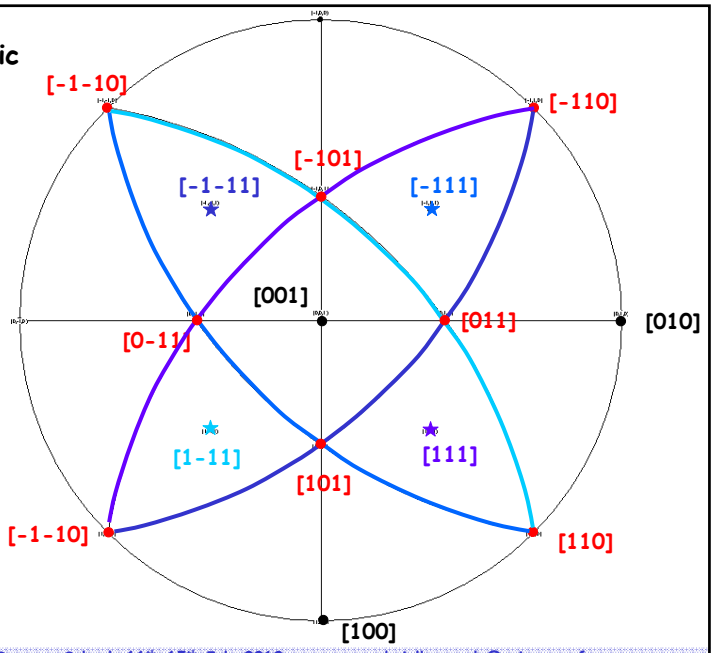

Thessaloniki, Summer School, 11th-15th July 2012 gabrielle.regula@univ-amu.fr

Institut Matériaux Microélectronique Nanosciences de Provence
UMR CNRS 7334, Universités Aix-Marseille et Sud Toulon-Var

Climb

To move the dislocation line normal to the glide plane the atom row at the edge of the additional half plane has to move down or upward. For that, atoms must be added to this atom row or must be eliminated. These operations need atomic transport, diffusion of atoms or point defects (V)

Type of materials	glide temp. (°C)	climb temp. (°C)
Copper T_m=1083°C	-200 to 800	>800
Silicon T_m=1412°C	600 to 1100	>1100

This climbing movement is thus quite difficult and is only possible @ high T

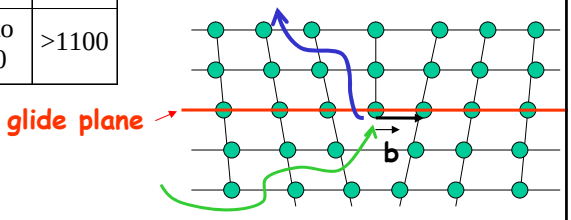

Climb

Requires thermal activation

Most common climb processes involve V diffusion either towards or away from the dislocation

So far, assumption that complete row of atoms is removed simultaneously, though in practice, V or clusters of V diffuse to the dislocation → creation of jogs, which are steps on the dislocation which move it from one atomic slip plane to another. Steps which displace the dislocation on the same slip plane are called kinks

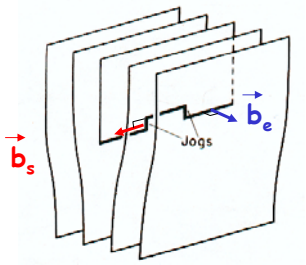

climb proceeds by nucleation and motion of jogs: conversely, jogs are sources and sinks for V

Kinks having the same slip plane as the dislocation line, do not impede dislocation motion

Similarly, jogs on edge dislocations do not affect glide

Jog on screw dislocation has an edge character → jog can only glide along the line; movements at right angles to b require climb → jogs impede glide of the screw dislocations and result in point defect production during slip

$E_f(I) >> E_f(V)$ in metals → V production dominates

climbing force per unit length $f = (bkT/\Omega) \ln(C/C_o)$ where Co is the equilibrium concentration of V in a stress free crystal and Ω is the volume per atom

A jog has a height of one lattice spacing and $E_j \sim 1eV$ due to the increase in dislocation length

$n_j = n_o \exp(-E_j/kT)$ number of jogs per unit length of dislocation @ thermodynamic equilibrium

n_o is the number of atom sites per unit length of dislocation

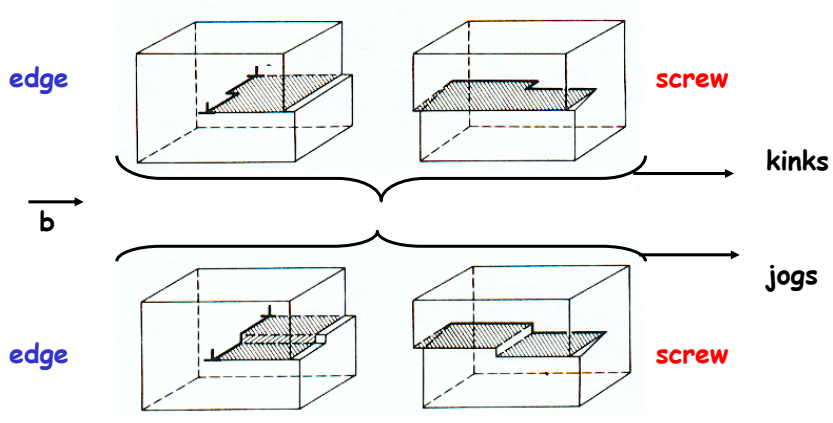

Image force

A dislocation near a surface experiences forces not encountered in the bulk: it is attracted towards a free surface because the material is effectively more compliant there and the dislocation energy is lower. Conversely, it is repelled by a rigid surface. Math treatment needs extra terms to be added to the infinite body stress components

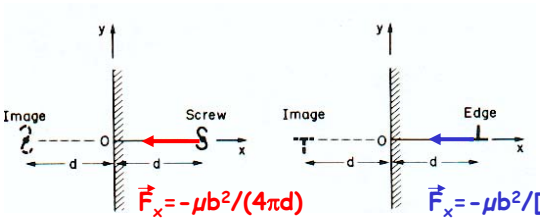

$\vec{F}_x = -\mu b^2/(4\pi d)$ $\vec{F}_x = -\mu b^2/[4\pi(1-\nu)d]$

The image forces decrease slowly with d and are capable of removing dislocations from near surface regions. They are important for instance in specimens for TEM when the slip planes are orientated @ large angles (≈90°) to the surface

2.3 Dislocation intersections: kinks and jogs

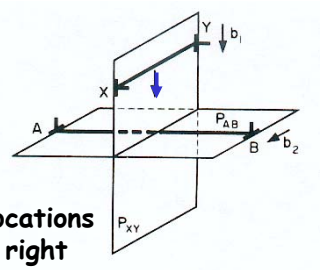

edge dislocations with b @ right angles to each other

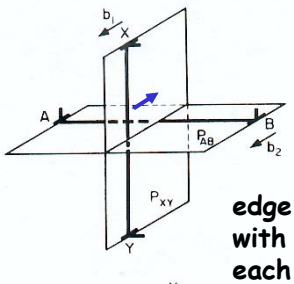

edge dislocations with $\vec{b}$ // to each other

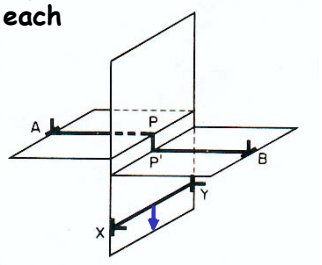

1 jog

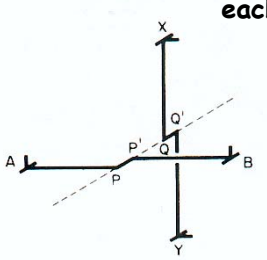

2 kinks

super jogs

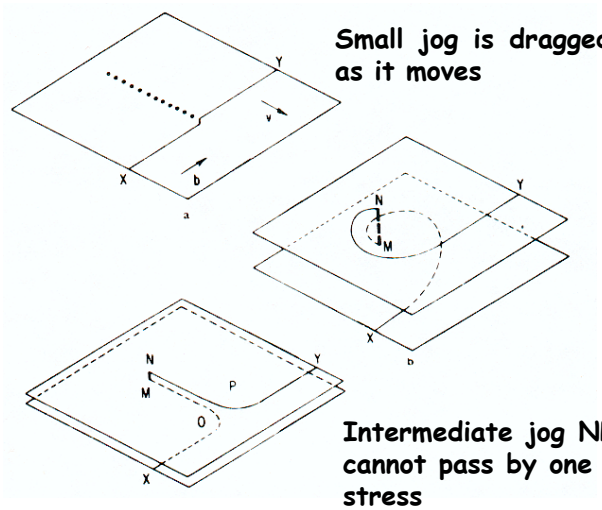

Small jog is dragged along, creating V as it moves

Very large jog, NY and XM move independently

Intermediate jog NP and MO interact and cannot pass by one another except @ high stress

« Forest » mechanism

Mobile dislocations in a glide plane may intersect other dislocations in another glide plane or elsewhere (sessile dislocations)

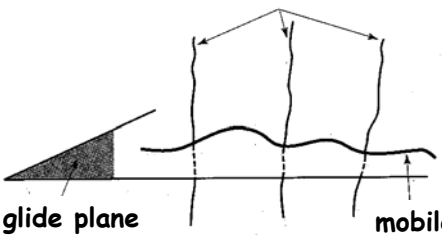

glide plane

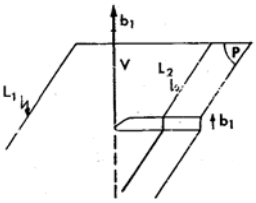

mobile dislocation

Creation of kinks or jogs which can decrease the dislocation mobility

→ hardening mechanism

single crystal

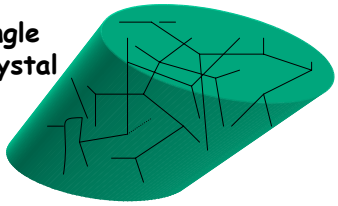

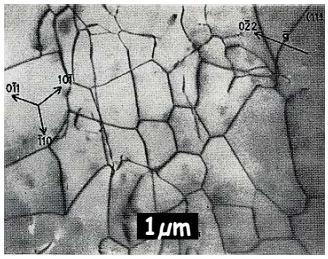

2.4 Dislocation distribution

The dislocations are generally very numerous in crystals. It is very difficult to eliminate them, except for Si, Ge some other semiconductors and very well annealed metals

The dislocations are arranged in a 3D network, named Frank network which was built during crystal growth. The dislocation density in a single crystal is defined as the total length of dislocation within a volume unit

Materials	elect. grade Si	GaAs	annealed metals	deformed metals	rock salt as grown
ρ(cm.cm^{-3})	0-10^2	10^4-10^5	10^2-10^5	10^9-10^{11}	10^5-10^6

2.5 Strain field and stress field associated with a dislocation

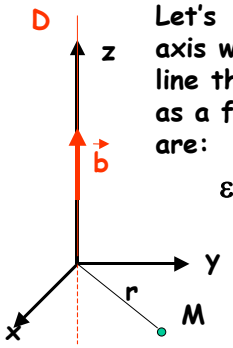

Let's consider an infinite dislocation parallel to the z axis with a Burgers vector along the z axis. Around this line there is a strain field the components of which vary as a function of the distance r from the line. The strain are:

$$\varepsilon_1=\varepsilon_2=\varepsilon_3=\varepsilon_6=0 \qquad \varepsilon_{23}=\varepsilon_4=-\frac{b}{2\pi}\frac{x}{r^2} \qquad \varepsilon_{31}=\varepsilon_5=\frac{b}{2\pi}\frac{y}{r^2}$$

These strains are small (except very close to the line) so the elasticity can be applied:

If the crystal is isotropic, around the line there is a stress field the components of which are:

$$\sigma_1=\sigma_2=\sigma_3=\sigma_6=0 \qquad \sigma_4=-\frac{\mu}{2\pi}\frac{b}{r^2}\frac{x}{r^2} \qquad \sigma_5=\frac{\mu}{2\pi}\frac{b}{r^2}\frac{y}{r^2}$$

Remarks:

➡ strains and stresses vary in 1/r → zero at infinite distance (very far from the dislocation).
→The dislocations produce long range stresses in crystals

➡ strains not small very close to the dislocation core + no tool to treat these high strains, the mechanics very close to the dislocation is not correct
→ Far from the dislocation the elasticity works

2.6 elastic energy associated with a dislocation

The law of elasticity gives the elastic energy per unit volume associated with an elastic deformation as: $dE_{el}=0.5\ dV\ \Sigma(\sigma_i\ \varepsilon_i)$

For a unit length of screw dislocation that gives:

$$E=\frac{\mu b^2}{4\pi}\int_{r_0}^{R}\frac{dr}{r}=\frac{\mu b^2}{4\pi}Ln\left(\frac{R}{r_0}\right)$$

The integration limits are r_0 a core radius (1 to 4b, <1nm in most cases) eliminated (inelasticity of the core) and R is the mean half distance between dislocations

Remarks:

·In fact the total energy per unit length of dislocation should include the contribution of the core. This contribution was calculated by non-linear atomistic simulation and was found below 10%. For simplicity this contribution is often neglected
·The mean half distance between dislocations R is involved in a logarithm so the energy is not very sensitive to this distance and therefore to the dislocation density. It is only for crystals with quite different dislocation densities that the energy of dislocations per unit length are different.

·$E \sim b^2$, so the more stable dislocations are those with the smallest Burgers vector allowed by the structure.

Order of magnitude:
for aluminum $b=2.9\ 10^{-10}$ m; $\mu=2.8\ 10^{10}$ N. $m^{-2}= 2.8\ 10^{10}$ Pa
taking $R=10^5 b$ for instance, gives $E=1.8\ 10^{-9}$ J.m^{-1}
for a length b → $E_L=5.2\ 10^{-19}$ J=3.3eV
3 times the energy of a vacancy

For an edge dislocation: $E = \frac{\mu b^2}{4\pi(1-\nu)} Ln\left(\frac{R}{r_0}\right)$

For a mixed dislocation: $E = \frac{\mu b^2}{4\pi K} Ln\left(\frac{R}{r_0}\right)$ with $\frac{1}{K} = \cos^2\theta + \frac{\sin^2\theta}{1-\nu}$ (screw component)

$\theta = (\vec{b}, \vec{t})$ (edge component)

E(elastic edge) = 1/(1-ν) E(elastic screw)

3/2

$E_{el} = \alpha \mu b^2$ where $\alpha \sim 0.5\text{-}1.0$

2.7 Force on a dislocation

Mutual forces, interaction forces

Study of the interactions between dislocations → energy arguments
2 dislocations close or far from one each other → the energy associated with the pair in each case can be calculated and compared: the lowest energy will determine the stable configuration.
For close dislocations one can use an unique Burgers circuit whereas two separated circuits have to be used in the other case.

1st case: same dislocations

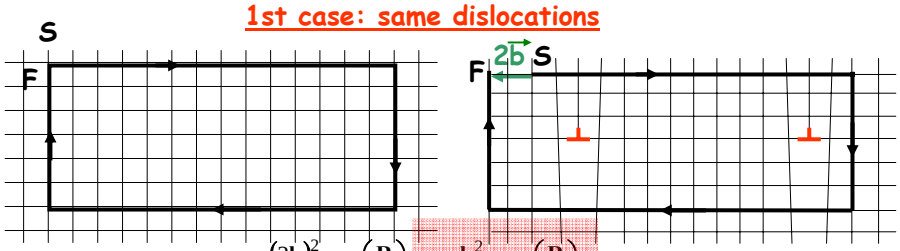

$E_c = \frac{\mu(2b)^2}{4\pi(1-\nu)} Ln\left(\frac{R}{r_0}\right) = \frac{\mu b^2}{\pi(1-\nu)} Ln\left(\frac{R}{r_0}\right)$

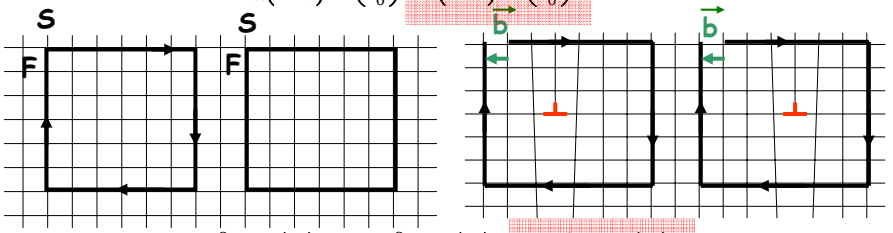

$E_\infty = \frac{\mu(b)^2}{4\pi(1-\nu)} Ln\left(\frac{R}{r_0}\right) + \frac{\mu(b)^2}{4\pi(1-\nu)} Ln\left(\frac{R}{r_0}\right) = \frac{\mu b^2}{2\pi(1-\nu)} Ln\left(\frac{R}{r_0}\right)$

Stable case repulsion

$E_\infty < E_c$

Thessaloniki, Summer School, 11th-15th July 2012 gabrielle.regula@univ-amu.fr
Institut Matériaux Microélectronique Nanosciences de Provence
UMR CNRS 7334, Universités Aix-Marseille et Sud Toulon-Var

2nd case: opposite dislocations

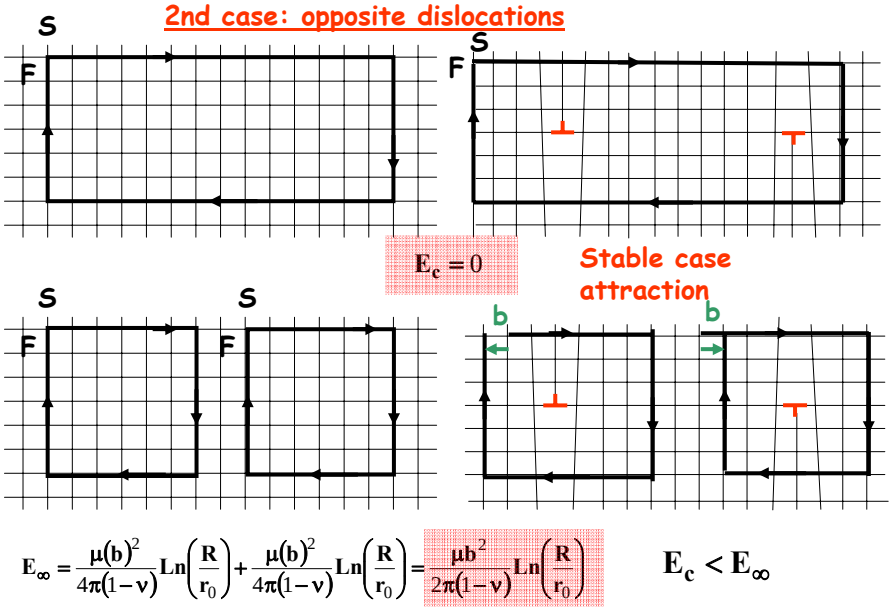

$E_c = 0$

Stable case attraction

$$E_\infty = \frac{\mu(b)^2}{4\pi(1-\nu)}\mathrm{Ln}\left(\frac{R}{r_0}\right) + \frac{\mu(b)^2}{4\pi(1-\nu)}\mathrm{Ln}\left(\frac{R}{r_0}\right) = \frac{\mu b^2}{2\pi(1-\nu)}\mathrm{Ln}\left(\frac{R}{r_0}\right)$$

$E_c < E_\infty$

Generalization: Frank's rule

For two parallel dislocations with the same vector $\vec{t}$, the interaction forces are determined by the following rule:

$\vec{b}_1$ and $\vec{b}_2$ are the Burgers vectors

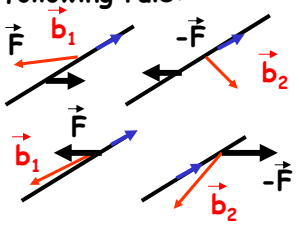

- if $(\vec{b}_1, \vec{b}_2) > \pi/2$ $\quad (\vec{b}_1+\vec{b}_2)^2 < \vec{b}_1^2+\vec{b}_2^2$
the forces are attractive
- if $(\vec{b}_1, \vec{b}_2) < \pi/2$ $\quad (\vec{b}_1+\vec{b}_2)^2 > \vec{b}_1^2+\vec{b}_2^2$
the forces are repulsive
- if $(\vec{b}_1, \vec{b}_2) = \pi/2$ $\quad (\vec{b}_1+\vec{b}_2)^2 = \vec{b}_1^2+\vec{b}_2^2$ no force is applied

Applied forces on dislocations

When a stress field is applied to a crystal, forces per unit length are applied to the dislocations in this crystal. These forces are normal to the line in the glide plane and can be calculated using tensorial mathematics…

It has been shown that a force due to a stress tensor [σ] on a dislocation of Burgers vector $\vec{b}$ and unit vector $\vec{t}$ is:

$$\vec{F}=[\sigma]\,\vec{b}\wedge\vec{t}$$ Peach-Koehler

This force is always normal to the line. In fact if the climb movements are neglected (low or medium temperature) the only component of the force on the dislocation is its projection in the glide plane

$\vec{F}_g$: glide force

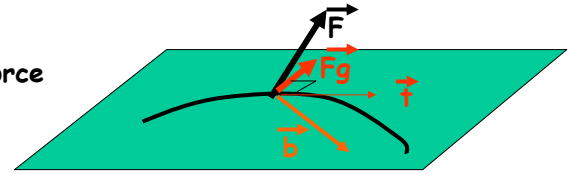

In the simple case of an uniaxial stress σ (tension experiment, axis Oz) the modulus of that force is given by:

$$F_g = m\,b\,\sigma$$

$F_g = m\,b\,\sigma$ b= Burgers vector modulus

Schmid factor $m=\cos\alpha\cos\beta$ where α and β are respectively the angle(b,F) and the angle(F,n) n normal to the glide plane

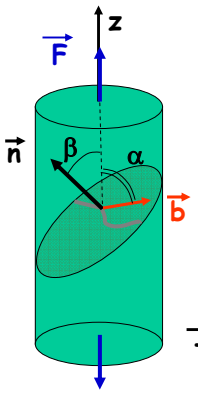

$m\,\sigma=\sigma_r$ is the resolved shear stress

In the general case, σ can be either a stress tensor due to the applied strain or the stress tensor due to dislocations in the neighborhood of the starting one

$$\vec{F}_1=[\sigma_2]\,\vec{b}_1\wedge\vec{t}_1$$
$$\vec{F}_2=[\sigma_1]\,\vec{b}_2\wedge\vec{t}_2$$

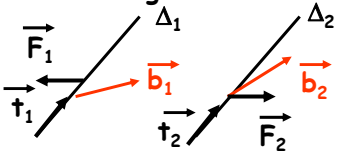

Mutual forces

NB: no forces act between a pair of parallel dislocations consisting of a pure edge and a pure screw as expected from the lack of mixing of their stress fields

Example of $\vec{F}$ calculation with external stress

Peach Köhler forces

$\vec{F} = [\sigma]\vec{b} \wedge \vec{u}$ $\quad \sigma = \begin{pmatrix} -k & 0 & 0 \\ 0 & 0 & 0 \\ 0 & 0 & 0 \end{pmatrix}$ uniaxial compressive stress, where $k = \frac{E\,t}{2R}$

$\vec{F}_{(90°)} = kb/\sqrt{2}$ | 0 | −1 | 0 — SFA grows

$\vec{F}_{(90°)} = kb/\sqrt{2}$ | 0 | −1 | 0 — SFC shrinks

$\vec{b}_A = a/3[1\text{-}100] = -\vec{b}_C$

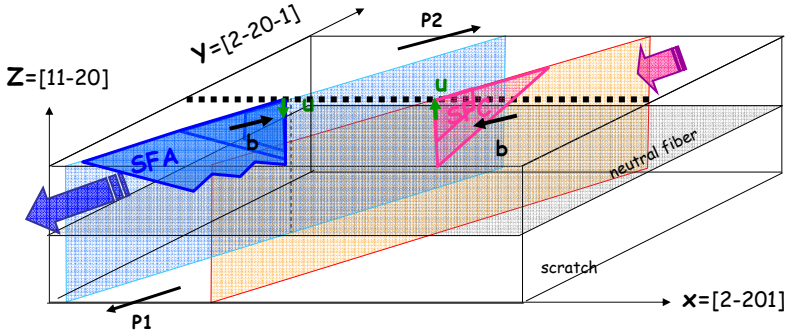

Line tension T

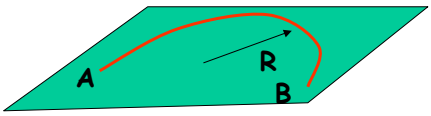

When a dislocation bows in its glide plane due to applied forces and anchored points A and B, its length increases so does its energy. There is a back force repelling the dislocation which was named line tension. At the equilibrium this line tension is exactly compensated by F_g the glide force (projection of the applied force in the glide plane)

The line tension is analogous to the surface tension of a soap bubble or a liquid. Its unit is energy per unit length.

T=increase in E per unit increase of L of a dislocation

$$T = \alpha\mu b^2 = \sigma_r b$$

If ν=0 (otherwise the circle → torque), the expression for the stress to bend a dislocation to a radius R is: $\alpha\mu b/R$ (R=AB/2 in the schema)

Application: Frank-Read source

the plastic deformation is due to the dislocation glide in planes up to their exit at the surface
→ very difficult to understand why the dislocation density increases during plastic deformation → concept of dislocation source

Frank-Read source in Si (Dash, Dislocations and Mechanical properties of Crystals, Wiley (1957))

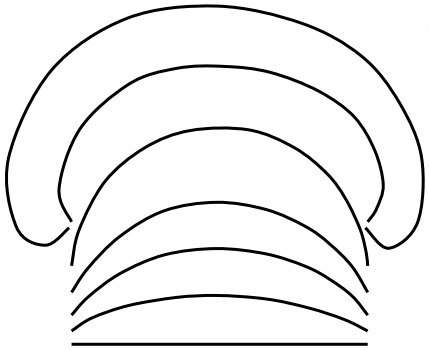

The anchors may be due to dislocation intersections, jogs, precipitates etc…

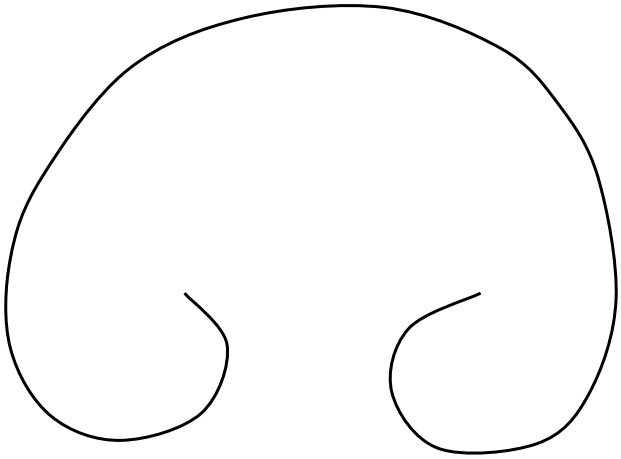

Thessaloniki, Summer School, 11th-15th July 2012 gabrielle.regula@univ-amu.fr
Institut Matériaux Microélectronique Nanosciences de Provence
UMR CNRS 7334, Universités Aix-Marseille et Sud Toulon-Var

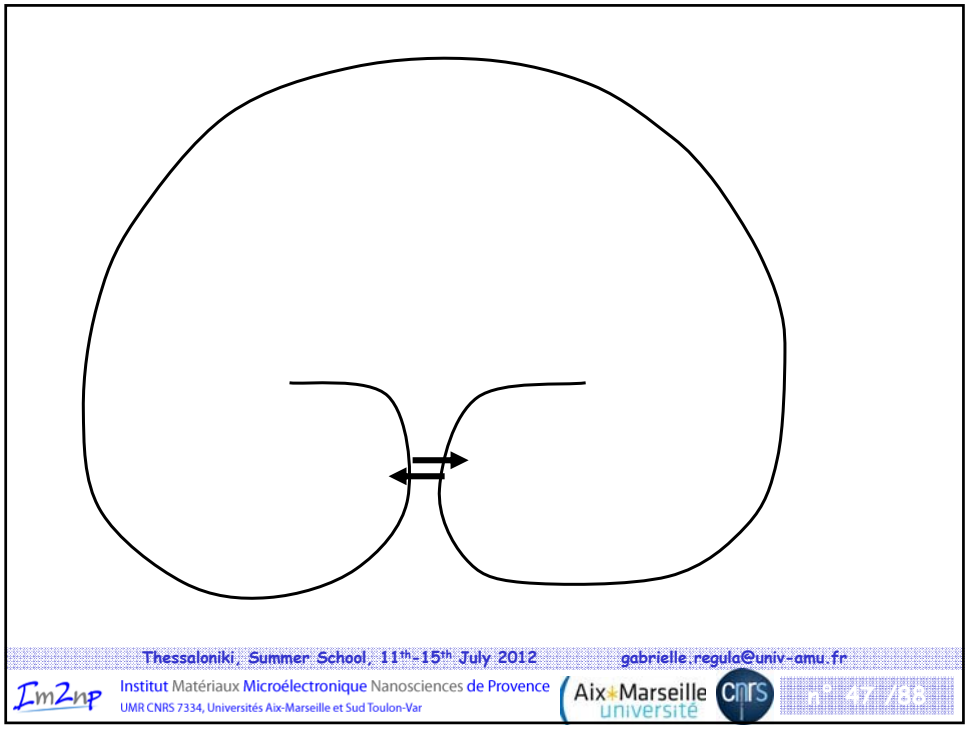
Thessaloniki, Summer School, 11th-15th July 2012
gabrielle.regula@univ-amu.fr
Institut Matériaux Microélectronique Nanosciences de Provence
UMR CNRS 7334, Universités Aix-Marseille et Sud Toulon-Var
Aix Marseille université
cnrs

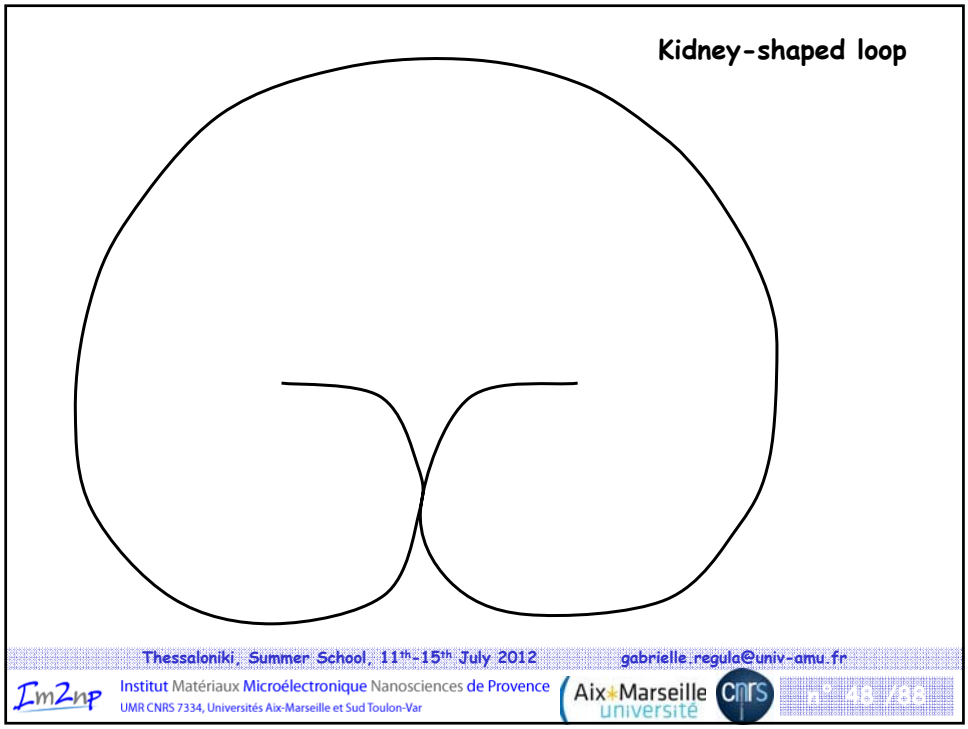
Kidney-shaped loop
Thessaloniki, Summer School, 11th-15th July 2012
gabrielle.regula@univ-amu.fr
Institut Matériaux Microélectronique Nanosciences de Provence
UMR CNRS 7334, Universités Aix-Marseille et Sud Toulon-Var
Aix Marseille université
cnrs

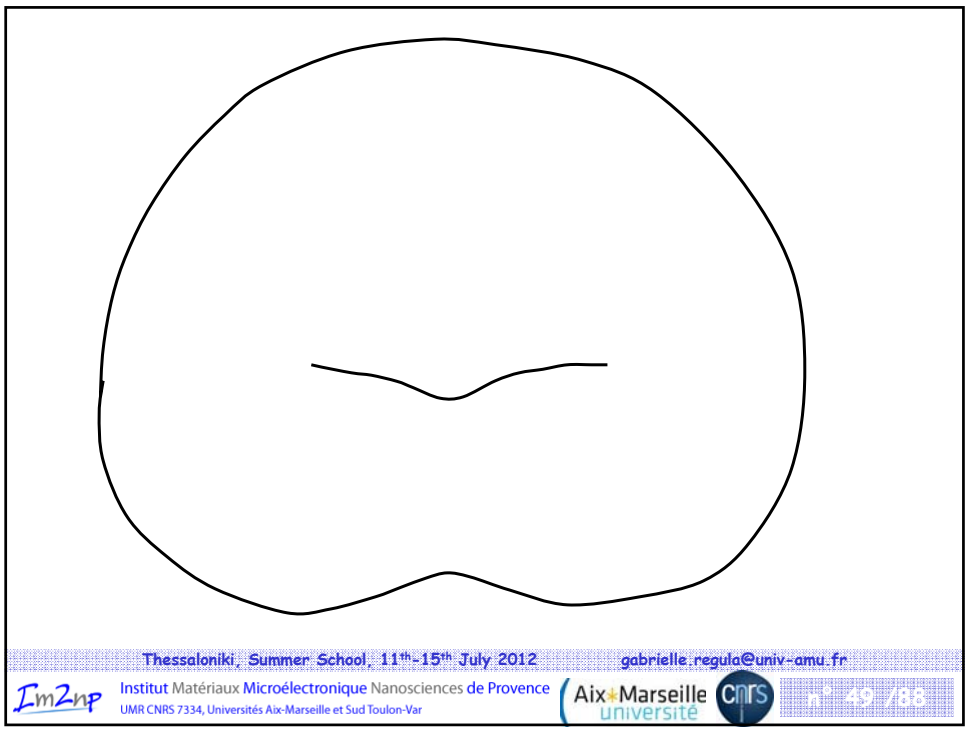

Regenerative multiplication mechanisms

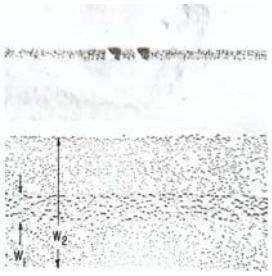

width growth of glide bands in lithium fluoride (succession of etching and deformation)

- Frank Read sources
- Multiple cross slip (more effective for more rapid multiplication) see p.23
- Climb
  *expansion of prismatic loop
  *spiraling of dislocation with predominantly screw character
  *Regeneretive→Bardeen-Herring source of length L

$$Ln(C/C_O)=2\alpha\mu b/(LkT)$$

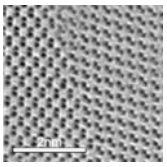

- Grain boundary sources

Thessaloniki, Summer School, 11th-15th July 2012
gabrielle.regula@univ-amu.fr
Institut Matériaux Microélectronique Nanosciences de Provence
UMR CNRS 7334, Universités Aix-Marseille et Sud Toulon-Var
Aix Marseille université
cnrs

3- Dislocations in real structures: a few applications to semiconductors

In a given crystallographic structure, Burgers vectors and glide planes are specific:

➡ the glide plane is the densest

➡ b corresponds to the shortest distance between atoms in the structure

A slip plane and a slip direction in the plane = slip system

in close packed hexagonal structure [(0001); <-12-10>]

CFC metals [{111};<110>]

Body centered metals [{112}&{110}(@lowTprefered);<111>]

slip results in a formation of steps on the crystal surface

FCC stereographic projection

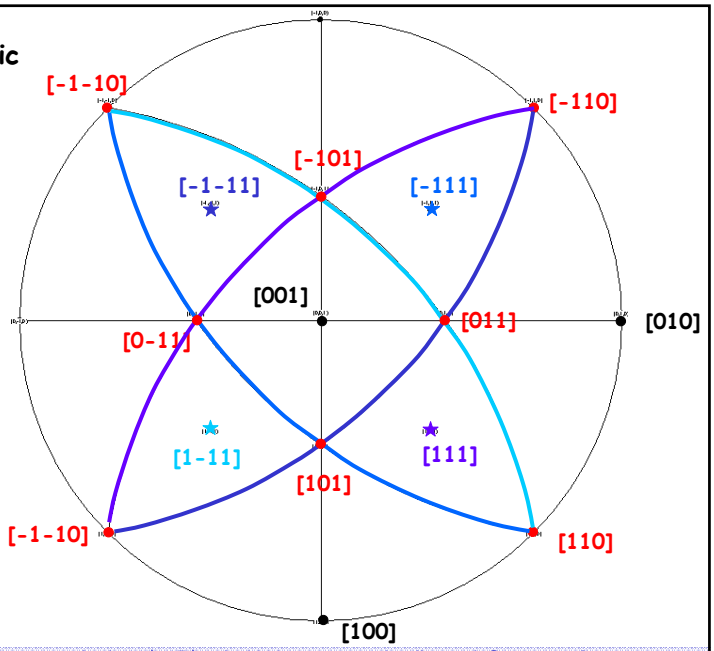

Thessaloniki, Summer School, 11th-15th July 2012 gabrielle.regula@univ-amu.fr
Institut Matériaux Microélectronique Nanosciences de Provence
UMR CNRS 7334, Universités Aix-Marseille et Sud Toulon-Var

3.1 three examples

1. Cubic structure

b=a<100>

glide plane {100}

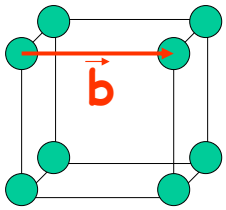

a[100](010)
a[100](001)
a[010](001)
a[010](100)
a[001](010)
a[001](100)

2. Cubic body centered

$\vec{b}$=a/2<111>

glide plane {110}

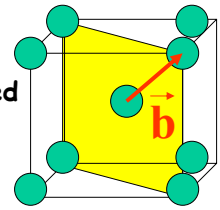

a[111](1$\bar{1}$0) a[$\bar{1}$11](110)
a[111](10$\bar{1}$) a[$\bar{1}$11](011)
a[111](01$\bar{1}$) a[$\bar{1}$11](10$\bar{1}$)
a[$\bar{1}$11](110) a[1$\bar{1}$1](1$\bar{1}$0)
a[$\bar{1}$11](101) a[1$\bar{1}$1](101)
a[$\bar{1}$11](01$\bar{1}$) a[1$\bar{1}$1](011)

Iron plastic deformation uses 12 types of dislocations
(only 1 or 2 are favored by the deformation geometry)

3. Cubic face centered

$\vec{b}$=a/2<110>

glide plane {111}

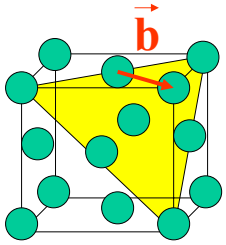

a[1$\bar{1}$0](111) a[110](1$\bar{1}$1)
a[101](111) a[101](111)
a[011](111) a[011](111)
a[110](111) a[110](111)
a[101](111) a[101](111)
a[011](111) a[011](111)

12 types of dislocations in Cu

3.2 Dissociation of dislocations (extended configurations)

In centered structures (faces, body…) the dislocation scheme is not as simple as in simple structures. To get an edge dislocation, they have to remove 2 half-planes → huge core deformation → high mechanical energy → the defect dissociates into 2 partial dislocations and a stacking fault

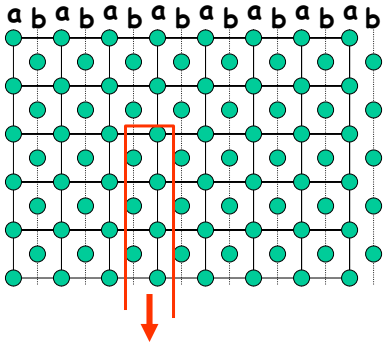

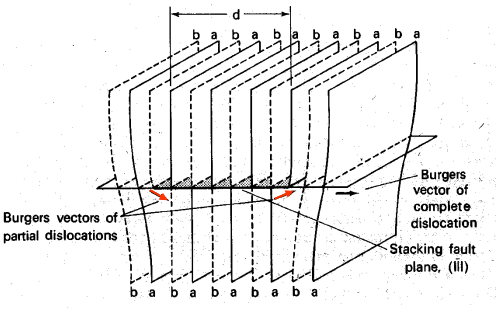

dissociated dislocation = stacking fault ribbon limited by 2 partial dislocations

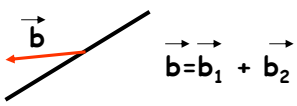

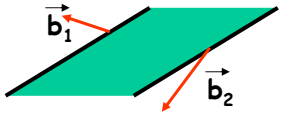

$$E = \frac{\mu b^2}{4\pi K} \mathrm{Ln}\left(\frac{R}{r_0}\right) \qquad E = \frac{\mu b_1^2}{4\pi K_1} \mathrm{Ln}\left(\frac{R}{r_0}\right) + \frac{\mu b_2^2}{4\pi K_2} \mathrm{Ln}\left(\frac{R}{r_0}\right) + \gamma d$$

If the partials are repulsive, even with an additional energetic term, the dissociation is energetically favorable

Far from the dislocation x>>d, effect of stress or strain field is the same as a perfect dislocation…

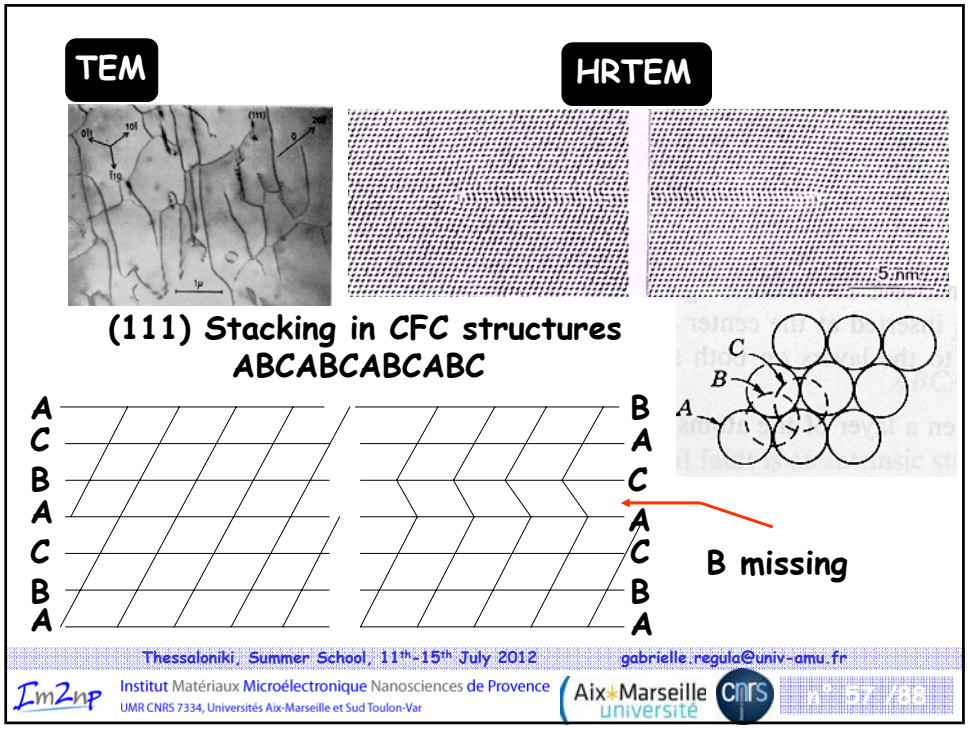
TEM
HRTEM
5 nm
(111) Stacking in CFC structures
ABCABCABCABC
A
C
B
A
C
B
A
B
A
C
A
C
B
A
B missing
Thessaloniki, Summer School, 11th-15th July 2012
gabrielle.regula@univ-amu.fr
Im2np
Institut Matériaux Microélectronique Nanosciences de Provence
UMR CNRS 7334, Universités Aix-Marseille et Sud Toulon-Var
Aix Marseille université
cnrs

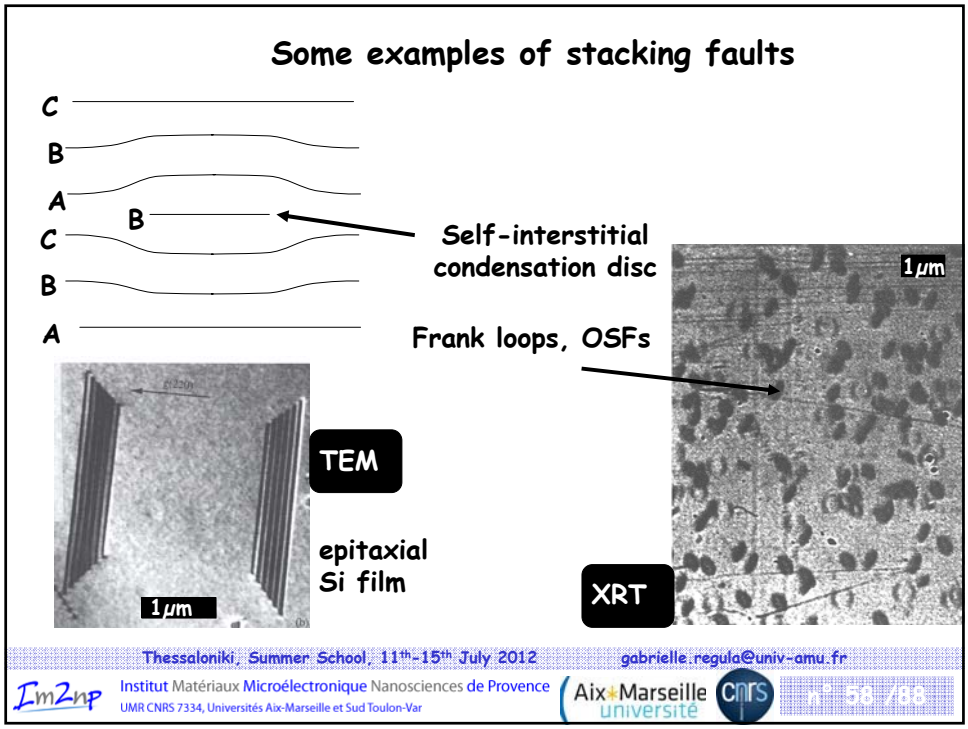
Some examples of stacking faults
C
B
A
B
C
B
A
Self-interstitial
condensation disc
Frank loops, OSFs
1 µm
TEM
epitaxial
Si film
1 µm
XRT
Thessaloniki, Summer School, 11th-15th July 2012
gabrielle.regula@univ-amu.fr
Im2np
Institut Matériaux Microélectronique Nanosciences de Provence
UMR CNRS 7334, Universités Aix-Marseille et Sud Toulon-Var
Aix Marseille université
cnrs

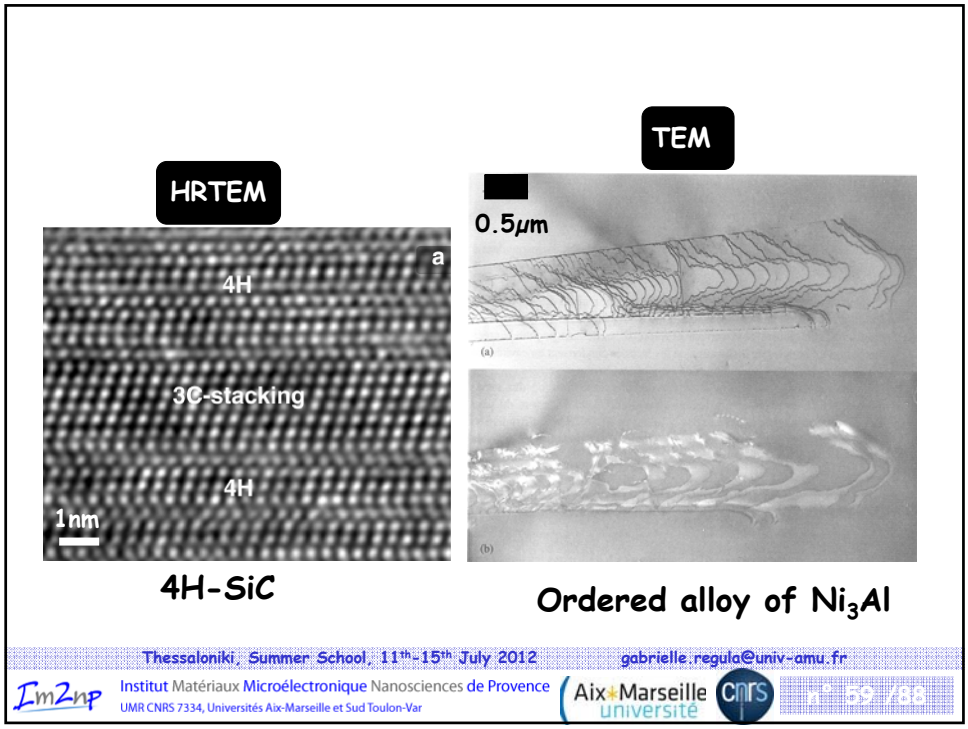
HRTEM
TEM
a
4H
3C-stacking
4H
1nm
0.5μm
4H-SiC
Ordered alloy of Ni_3Al
Thessaloniki, Summer School, 11th-15th July 2012
gabrielle.regula@univ-amu.fr
Institut Matériaux Microélectronique Nanosciences de Provence
UMR CNRS 7334, Universités Aix-Marseille et Sud Toulon-Var
Aix Marseille université
cnrs

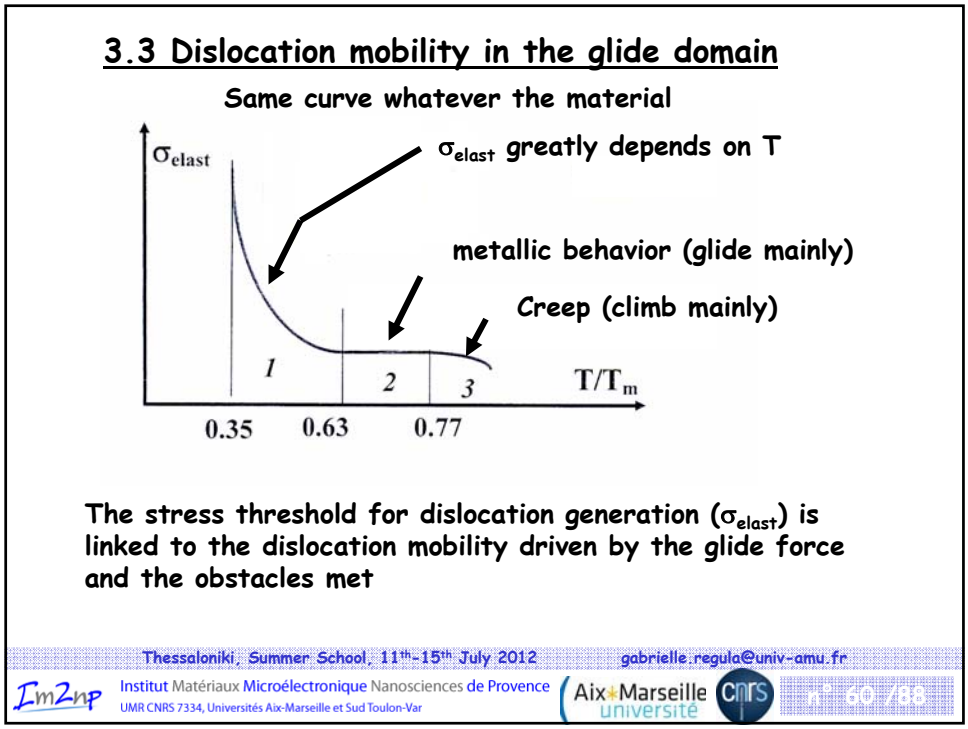
3.3 Dislocation mobility in the glide domain
Same curve whatever the material
σ_{elast}
σ_{elast} greatly depends on T
metallic behavior (glide mainly)
Creep (climb mainly)
1
2
3
T/T_m
0.35
0.63
0.77
The stress threshold for dislocation generation (σ_{elast}) is linked to the dislocation mobility driven by the glide force and the obstacles met
Thessaloniki, Summer School, 11th-15th July 2012
gabrielle.regula@univ-amu.fr
Institut Matériaux Microélectronique Nanosciences de Provence
UMR CNRS 7334, Universités Aix-Marseille et Sud Toulon-Var
Aix Marseille université
cnrs

Obstacles:

- Visquous friction force linked to thermal vibrations of the atoms
- Periodic anchor force linked to friction of the network of atoms
- Localized forces due to close interactions between dislocations
- Anchor force due to atoms in solid solution and to precipitates introduced on purpose in the alloys for hardenning

Let's consider only intrinsic effects (no impurity no precipitates etc..) → regimes 1 et 2 may appear

Regime 1 (thermally activated) lattice resistance to the dislocation motion → the stress required to overcome it is the **Peierls-Nabarro** force
Very important in covalent materials, very weak in CFC metals, 100 times bigger in CC metals. In CC for instance, Peierls force is 20 times bigger for screw dislocations→ observation of long lines in screw orientation in these metals

XRT

Potential valleys = Peierls valleys

Dislocation shape is highly influenced by these valleys → geometric shape

V(Disloc) = 10^{-8}-10 m.s^{-1}

Half hexagonal loop

Si deformed @ 600°C

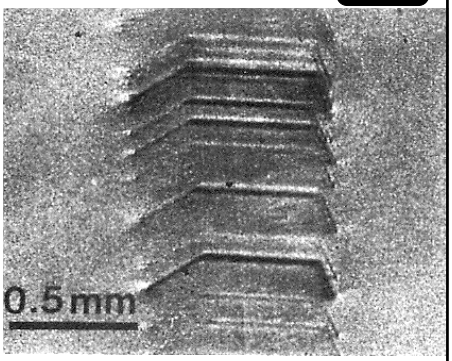

Thessaloniki, Summer School, 11th-15th July 2012 gabrielle.regula@univ-amu.fr
Institut Matériaux Microélectronique Nanosciences de Provence
UMR CNRS 7334, Universités Aix-Marseille et Sud Toulon-Var

With the existence of the Peierls valleys, movement of dislocations is difficult and takes place via double kink formation and collision:

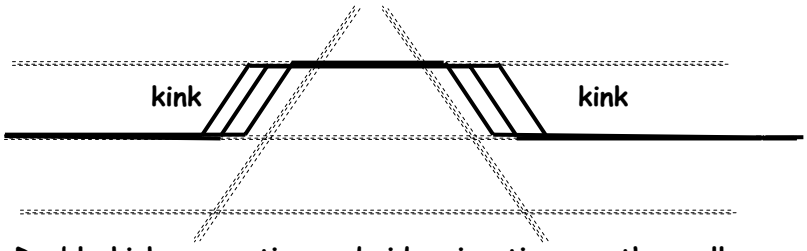

Double kink generation and side migration are thermally activated, which gives a dislocation mobility:

material constant

$$V = A\ \sigma^{m} \exp\left(-\frac{Q}{kT}\right)$$

m=1 @300K in pure crystals, increases up to 2-5 with alloying

kink migration energy

with $Q = F/2 + W_m$

double kink nucleation energy

4H-SiC

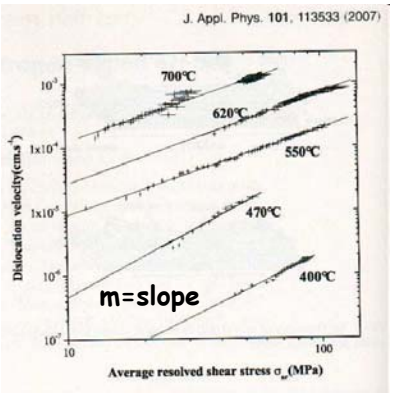

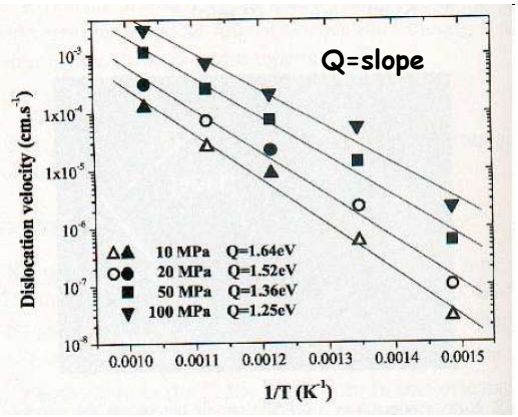

Q ↘ as σ ↗ (predicted by Hirth & Lothe theory)

Regime 2 corresponds to a dislocation motion without lattice resistance nor directional anisotropy
Dislocations have more rounded shapes
Their velocity hardly depends on T
V(disloc) ≈ V(sound) in solids (≈10^3m.s^{-1})

XRT

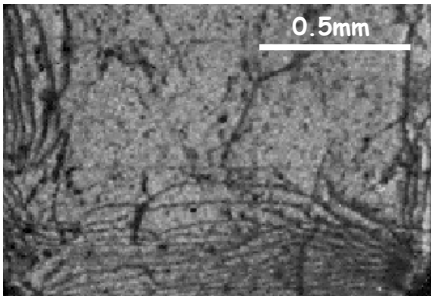

obstacles to dislocation motion:
* elastic stress field of other dislocations
* more local direct interactions like intersections

3.4 Elastic interaction: dislocation pile-up

obstacle= (grain boundary for instance) in a glide plane where loops are emitted from a Frank-Read source

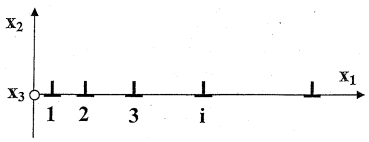

The dislocations are piling up against this barrier and elasticity theory allows to calculate the balance between forces under equilibrium conditions → on the obstacle, the resulting stress is $n\sigma_R$ with σ_R the resolved stress and n the number of piled up dislocations.
The pile up plays the role of a stress concentrator

Application: in metal polycrystals, this stress $n\sigma_R$ allows to trigger the glide of dislocations in the neighbor grain
→ Grain size is linked with the elastic limit of the material

4- Defect revelation by etch pits

Oldest method used to observe dislocations (developed by Johnston & Gilman in the 50s), and surely the cheapest. Not very powerful but very easy to perform and especially well adapted to semiconductor characterization. Can give the orientation of the studied surface

1.1 Principle of the revelation

Preferential chemical etch at the very emerging point of a dislocation at surface

The hole obtained or "pit" develops by displaying the crystallographic planes with the lowest surface energy i.e. those which are more stable and the dissolution of which is the slowest ({111} planes in silicon). They are also the planes with closest packed atoms

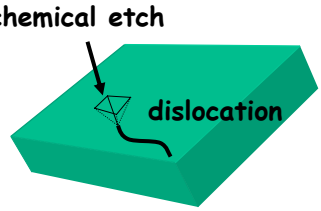

Pits of pyramidal shapes bottom up with

a square base on a {100} surface (4-fold symmetry)

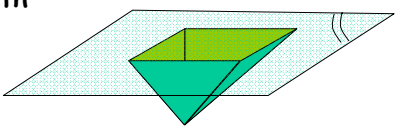

a triangular base on a {111} surface (3-fold symmetry)

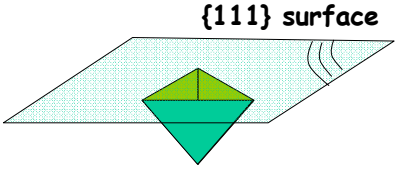

Some reagents give more or less "rounded-shape" pits especially in (100) planes
Flat bottom pits when the defect has moved during the etch or in between two successive etches → measurements of dislocation velocities

V=d/t
d moved distance during time t of the application of a stress at a given temperature 700<T<1300°C

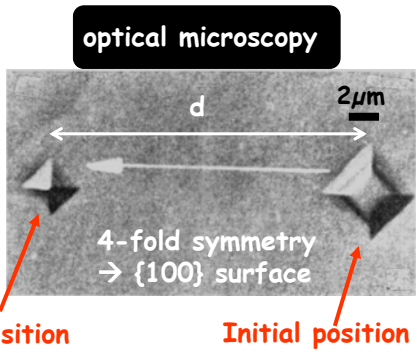

1.2 Defects revealed by etch pits

The defects revealed are the dislocations, the stacking faults and other micro defects

Dislocations and stacking faults cannot be separated in Si because they always coexist, one or the other aspect dominates depending on the origin of the defect.

Deformation (glide dislocation) Point defects condensation

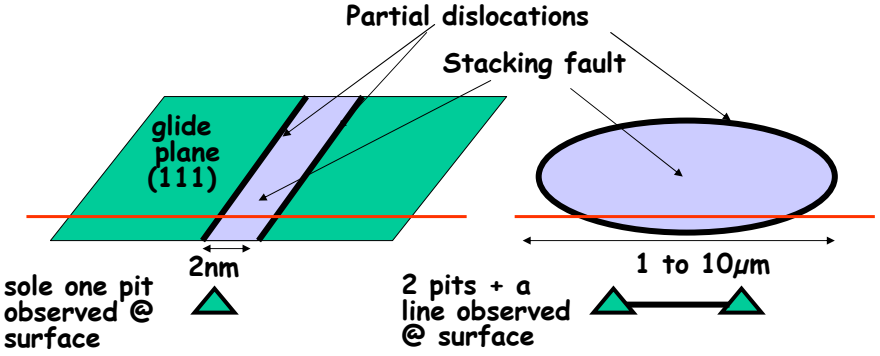

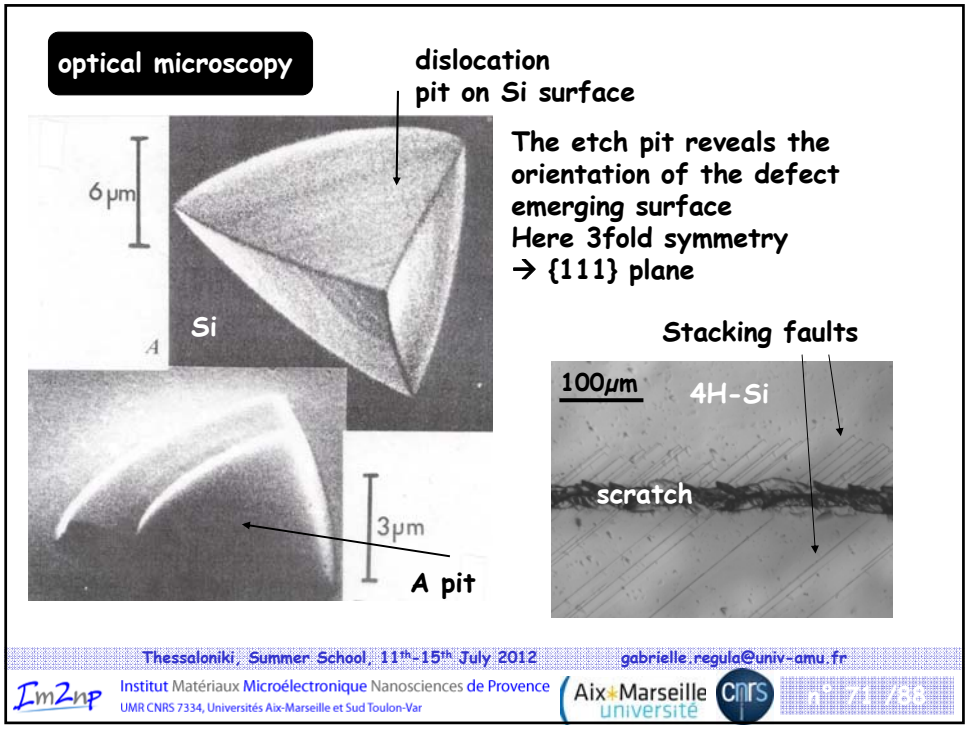
optical microscopy
dislocation
pit on Si surface
6 µm
Si
A
The etch pit reveals the orientation of the defect emerging surface
Here 3fold symmetry
→ {111} plane
Stacking faults
100µm
4H-Si
scratch
3µm
A pit
Thessaloniki, Summer School, 11th-15th July 2012
gabrielle.regula@univ-amu.fr
Institut Matériaux Microélectronique Nanosciences de Provence
UMR CNRS 7334, Universités Aix-Marseille et Sud Toulon-Var
Aix Marseille université
cnrs

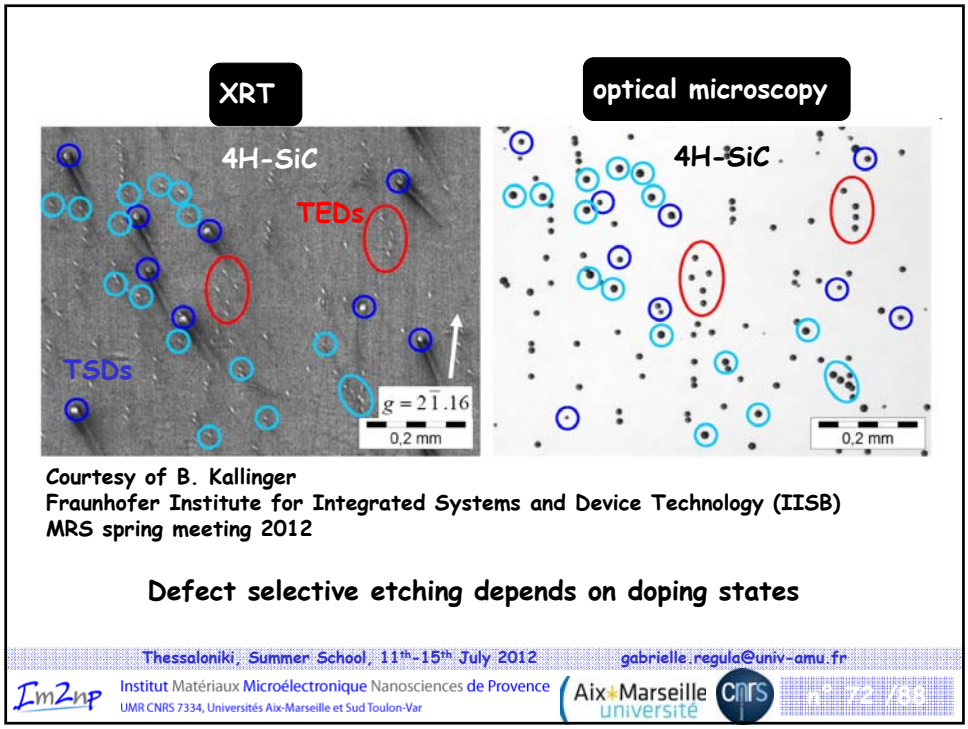
XRT
optical microscopy
4H-SiC
TEDs
TSDs
g = 2 1̄.16
0,2 mm
4H-SiC
0,2 mm
Courtesy of B. Kallinger
Fraunhofer Institute for Integrated Systems and Device Technology (IISB)
MRS spring meeting 2012
Defect selective etching depends on doping states
Thessaloniki, Summer School, 11th-15th July 2012
gabrielle.regula@univ-amu.fr
Institut Matériaux Microélectronique Nanosciences de Provence
UMR CNRS 7334, Universités Aix-Marseille et Sud Toulon-Var
Aix Marseille université
cnrs

optical microscopy

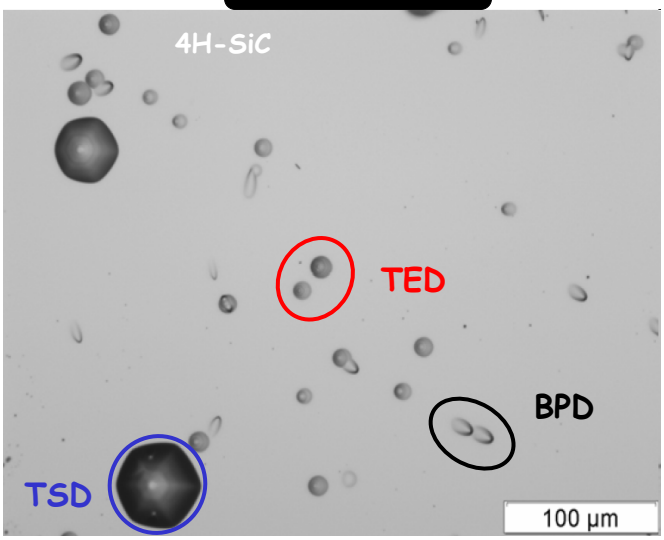

Courtesy of B. Kallinger, Fraunhofer Institute for Integrated Systems and Device Technology (IISB)

Thessaloniki, Summer School, 11th-15th July 2012 gabrielle.regula@univ-amu.fr

Institut Matériaux Microélectronique Nanosciences de Provence
UMR CNRS 7334, Universités Aix-Marseille et Sud Toulon-Var

optical microscopy

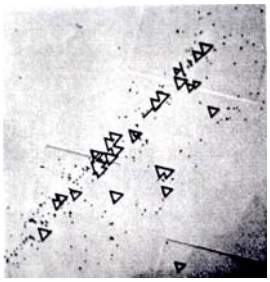

Dislocations & tetrahedral SFs

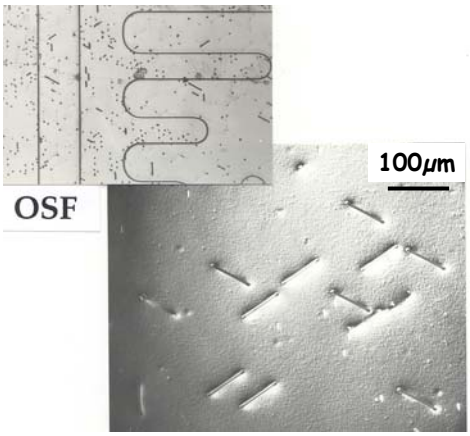

oxidation stacking faults (OSF)

Thessaloniki, Summer School, 11th-15th July 2012 gabrielle.regula@univ-amu.fr

Institut Matériaux Microélectronique Nanosciences de Provence
UMR CNRS 7334, Universités Aix-Marseille et Sud Toulon-Var

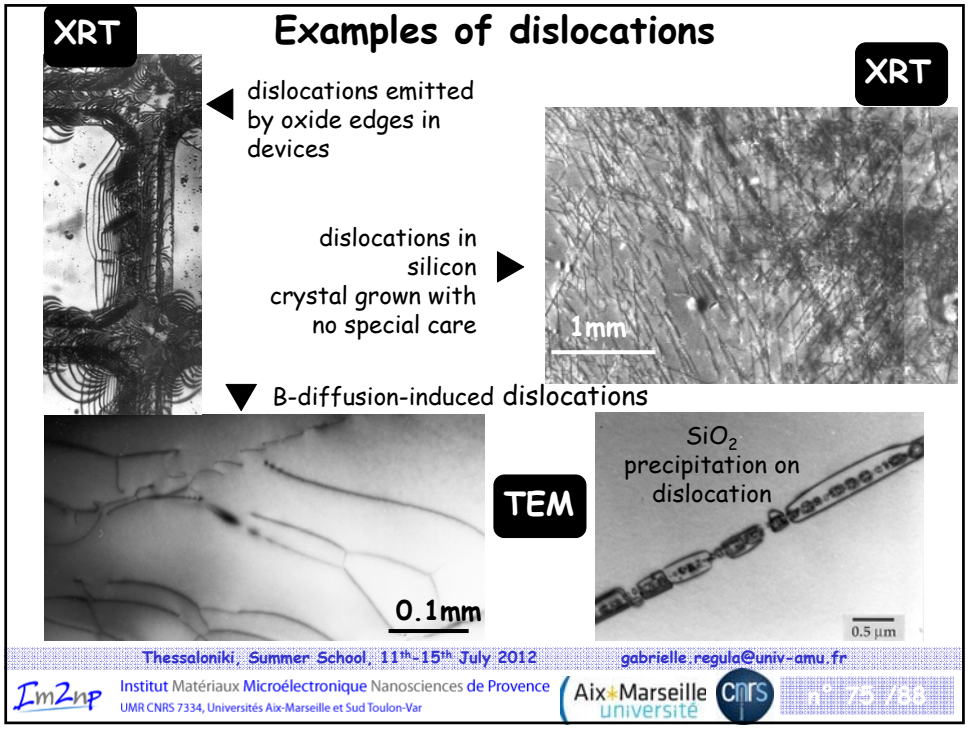
XRT
Examples of dislocations
XRT
dislocations emitted by oxide edges in devices
dislocations in silicon crystal grown with no special care
1mm
B-diffusion-induced dislocations
TEM
SiO_2 precipitation on dislocation
0.1mm
0.5 µm
Thessaloniki, Summer School, 11th-15th July 2012
gabrielle.regula@univ-amu.fr
Institut Matériaux Microélectronique Nanosciences de Provence
UMR CNRS 7334, Universités Aix-Marseille et Sud Toulon-Var
Aix Marseille université
cnrs

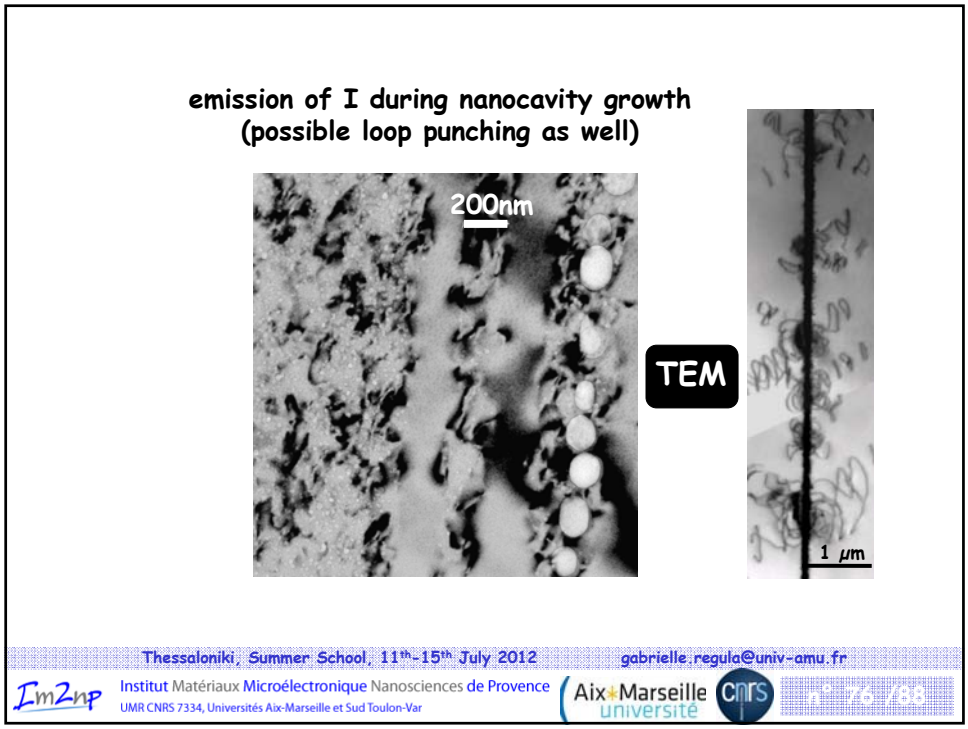
emission of I during nanocavity growth
(possible loop punching as well)
200nm
TEM
1 µm
Thessaloniki, Summer School, 11th-15th July 2012
gabrielle.regula@univ-amu.fr
Institut Matériaux Microélectronique Nanosciences de Provence
UMR CNRS 7334, Universités Aix-Marseille et Sud Toulon-Var
Aix Marseille université
cnrs

5- Conclusion

- Dislocation = boundary between the slipped and unslipped parts of the crystal
- Dislocation velocity depend on the applied shear stress on the purity of the crystal, on T and on their character
- @ low T, the movement of dislocations is restricted almost entirely to glide; @ higher T, an edge dislocation can climb
- Dislocations can be used for hardening in metallurgy, for pipe diffusion
- Dislocations must be avoided in semiconductors , they give leakage current, they modify dopant concentrations (gettering) etc… They are detrimental to device performances (whatever the device) → Combination of stress and temperature must be avoided

- Behavior and effects (on properties of crystalline solids) of point, line, surface, volume defects are intimately related

A prismatic loop is a result of I or V condensation, punching loops may occur during precipitation or bubble growth, some grain boundaries can be seen as a dislocation wall

In the case of small angle misorientation we have

$\theta = b/d$

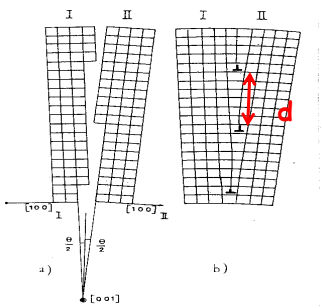

Tilt GB (symmetric) in hexagonal SiC

HRTEM

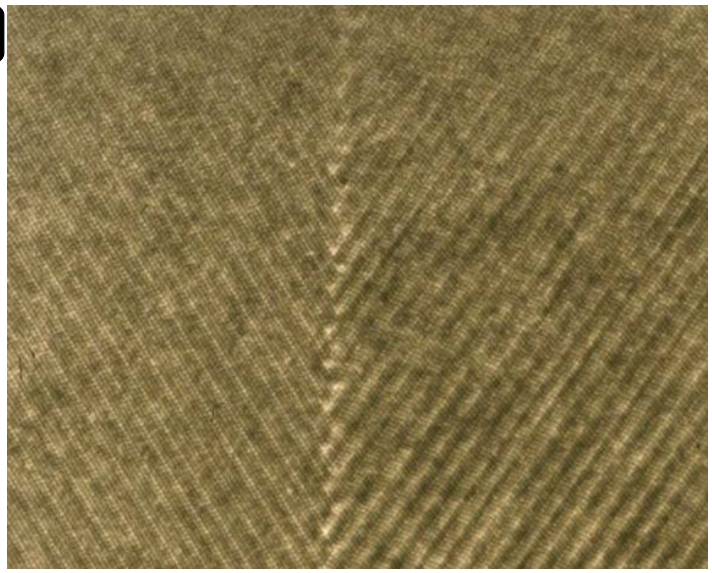

Description of GBs thanks to dislocations

- **Intrinsic dislocations**: fit the misorientation between 2 grains
  - primary dislocations

Bad orientation fit areas → relaxations → dislocation cores the b of which belong to those of the matrix

  - secondary dislocations

Both grains are not in coïncidence (no Σ)
→ Best fit coincidence accommodated by dislocations the b of which belong to the DSC

- **Extrinsic dislocations** :

formed by interaction between dislocation of the matrix and GB during the crystal growth, mechanical or thermal treatments

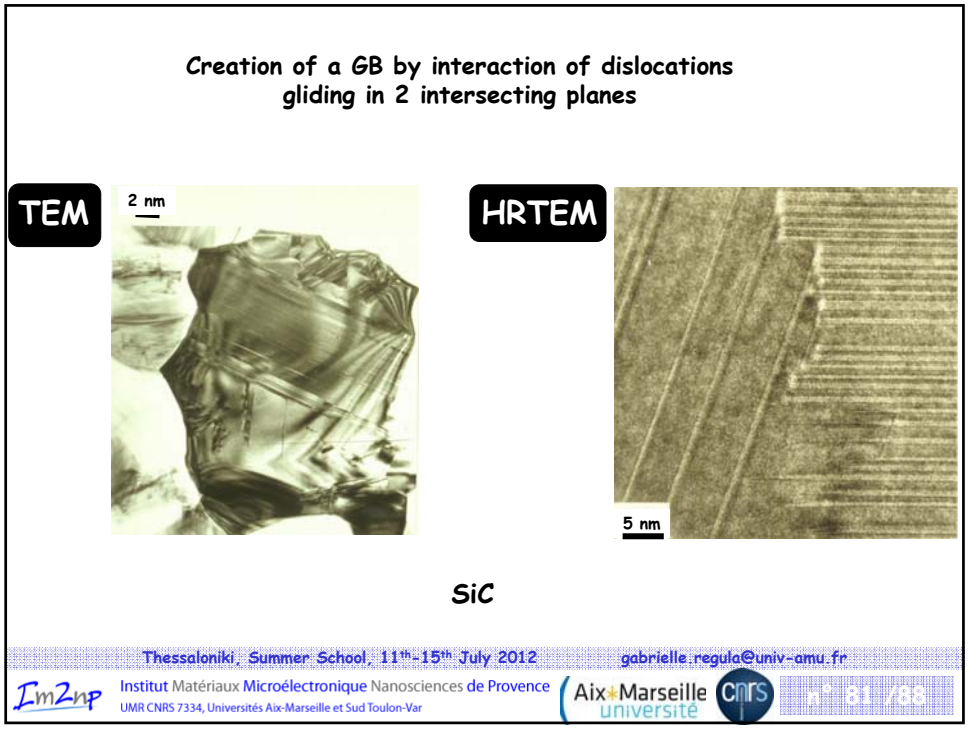
Creation of a GB by interaction of dislocations gliding in 2 intersecting planes
TEM
2 nm
HRTEM
5 nm
SiC
Thessaloniki, Summer School, 11th-15th July 2012
gabrielle.regula@univ-amu.fr
Institut Matériaux Microélectronique Nanosciences de Provence
UMR CNRS 7334, Universités Aix-Marseille et Sud Toulon-Var
Aix Marseille université
cnrs

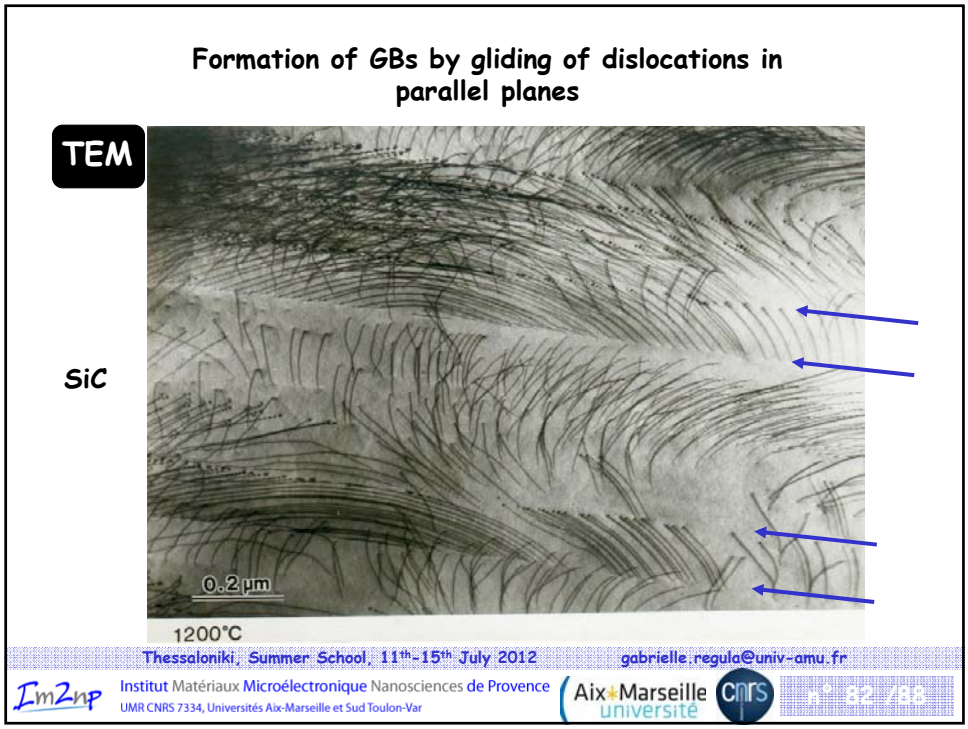
Formation of GBs by gliding of dislocations in parallel planes
TEM
SiC
0.2 µm
1200°C
Thessaloniki, Summer School, 11th-15th July 2012
gabrielle.regula@univ-amu.fr
Institut Matériaux Microélectronique Nanosciences de Provence
UMR CNRS 7334, Universités Aix-Marseille et Sud Toulon-Var
Aix Marseille université
cnrs

HRTEM

SiC

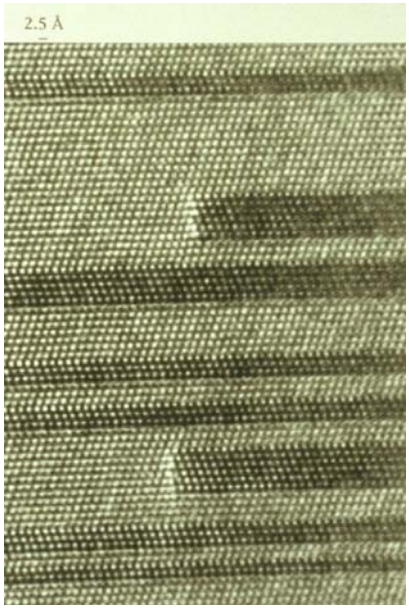

Thanks for your attention

Basic aspects of optical investigation methods

Jean Camassel

Collaboration: **Sandrine Juillaguet,**
Hervé Peyre,
Antoine Tiberj

Outline

- **Introduction**
- **Basic understanding**
- **Main applications**
  - **Réflectivity (visible, UV, IR)**
  - **Absorption, transmission**
  - **Photoluminescence**
  - **Raman spectroscopy**

Introduction (1)

- **Interest of optical techniques:**
  - **Non destructive;**
  - **Free of complicated surface (or contact) preparation;**
  - **Useful from as-grown material to final device inspection (including clean room facilities).**
- **Problem:**
  - **The world of semiconductors is a very large one.**
  - **It starts from carbon sp^2 and finish with carbon sp^3.**
  - **This may look very narrow but is not.**
  - **In between the ending carbon compounds are very big players. Let's consider in more details.**

Introduction (2)

Moving through the world of group IV elements and related compounds

Diamond (BG~5.5eV) «Ultimate SC»

SiC (and SiCOI) with BGEs from ~2.5 eV to ~3.5 eV

Nitrides (~3.5 eV)

Si (SOI, sSOI, etc…)

SiGe and Ge

Phosphides, Arsenides, Antimonides

Graphene (SM or Zero BG SC)

Introduction (3)

- **Taking into account the large difference in BG energy, very few techniques can cover the entire field with the same set-up.**
- **Most of them have a restricted application field and, from compound to compound, this means using:**
  - **A different excitation source;**
  - **A different detection technique;**
  - **A different set-up and,**
  - **Many often, a different language. (VERSATILITY?)**

Introduction (4)

Among the most versatile techniques are:

- X-ray diffraction: Lattice constants (lattice matching and strain).
- **Raman: Phonon spectrum (vibrational frequencies, stress, alloying effects and e-phonon coupling).**
- **Reflectivity: Dielectric function with (from the UV to IR) contributions of the electronic interband transitions and IR-active phonons.**
- XPS and UPS (X-ray and UV Photoelectron Spectroscopy): Band structure imaging
- **Absorption and Photoluminescence: Defects and impurities**

Introduction (5)

All of them use EM waves, with different λ.

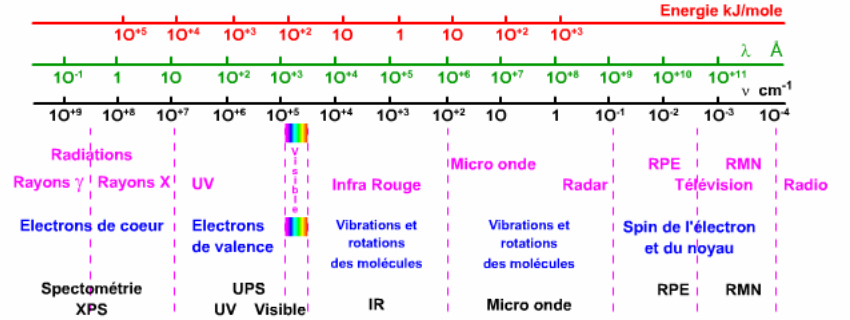

In this work, we will focus on Raman, Reflectivity, Absorption and PL

Basic understanding (1)

Let's consider a simple material system:

I_1 incident intensity

I_R reflected intensity

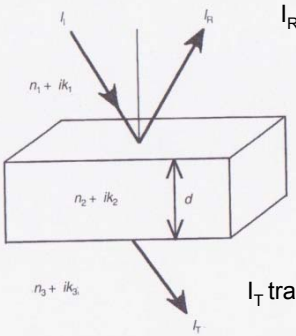

I_T transmited intensity

Fig. 2.1 A semiconductor sample of thickness d (medium 2) between media 1 and 3, showing incident, reflected, and transmitted intensities. Each medium is described by its complex refractive index $n_j + ik_j$ ($j = 1, 2, 3$). These determine the reflectance and transmittance of the sample.

Basic understanding (2)

Whatever the medium (1 to 3) the ligth propagation obeys:

$$\Delta \mathcal{E} - \mu\,\mu_0\,\sigma\frac{d\mathcal{E}}{dt} - \mu\,\mu_0\varepsilon\varepsilon_0\frac{d^2\mathcal{E}}{dt^2} = 0 \qquad (1)$$

- Plane waves, linearly polarized:

$$\mathcal{E} = \mathcal{E}_0 \exp\, j\omega\left(t - \frac{z}{v}\right) \qquad (2)$$

- v is a complex velocity:

$$\frac{1}{\tilde{v}^2} = \mu\,\mu_0\varepsilon\varepsilon_0 - j\frac{\sigma\mu\,\mu_0}{\omega} \qquad (3)$$

In vacuum:

$$\sigma = 0,\ \mu = \varepsilon = 1,\quad \frac{1}{c^2} = \mu_0\varepsilon_0 \qquad (4)$$

Basic understanding (3)

<u>In vacuum</u>: c = **300 000 km/s**

<u>In a solid</u>, the ligth interaction with the medium reduces the propagation velocity and one introduces a complex refractive index (*n*) such that:

$$\tilde{n} = \frac{c}{\tilde{v}} = n + jk \qquad (5)$$

(where n is the real part and k the extinction coefficient).

Combining equations 3, 4 and 5 gives:

$$\boxed{\tilde{n}^2 = \mu\varepsilon + j\frac{\sigma\mu}{\omega\varepsilon_0} \qquad (6)}$$

Basic understanding (4)

Note: in this expression,

$$\tilde{n}^2 = \mu\varepsilon + j\frac{\sigma\mu}{\omega\varepsilon_0} \quad (6)$$

μ=1 for a non magnetic medium while σ and ε are dispersive (i.e. wavelength interdependant) coefficients. As soon as σ is non nul (i.e. as soon as there is an interaction of the ligth with the medium) ε changes accordingly.

From Equations 5 and 6, one can also solve to get n and k versus σ and ε. This gives:

$$n^2 = \varepsilon/2 \{[1 + (4\pi\sigma/\omega\varepsilon)]^{1/2} + 1\}$$
$$k^2 = \varepsilon/2 \{[1 + (4\pi\sigma/\omega\varepsilon)]^{1/2} - 1\}$$

Basic understanding (5)

As already said, if $\sigma = 0$ (which is always the case in the low frequency limit):

$$n(\omega=0) = [\varepsilon(\omega=0)]^{1/2}.$$

Everywhere else, **n and k (or σ and ε) are interdependant** and obey the well-known Kramers-Kronig relationship:

$$n(\omega) = 1 + 2/\pi \int [\omega' k(\omega')] d(\omega')/[\omega'^2 - \omega^2]$$

From this expression, it appears clearly that the dispersion (wavelength dependence) of the refractive index $n(\omega)$ in a given medium is ruled by the intensity and energetic distancy of all the extinction processes encountered in the medium.

Not taken into account up to now is the effect of damping.

This is shown on the next slides.

Basic understanding (6)

Small interaction with a weak damping.

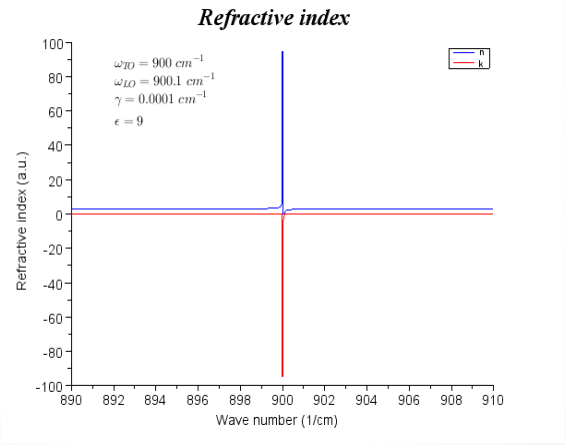

Basic understanding (7)

Same (small) interaction with a larger damping.

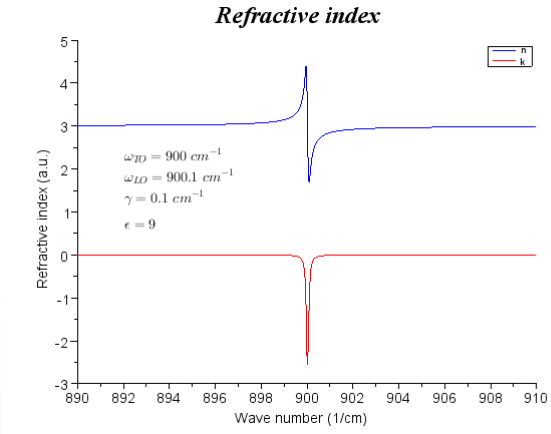

Basic understanding (8)

Idem with an extremely large damping.

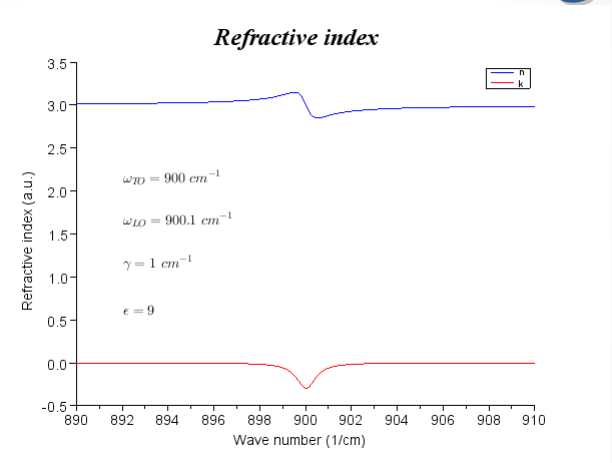

Basic understanding (9)

- For device people, the net conclusion is that one cannot get a high dielectric constant (high-k material) with lattice vibrational modes that couple only weakly with the EM field.
- One must look for the strongest possible interaction between ligth and phonons at the lowest possible energy.
- Let see what happens when increasing the coupling (oscillator strength) for different values of the broadening parameter.

Basic understanding (10)

Increasing the ligth-matter coupling but keeping a reasonable value of the oscillator strength.

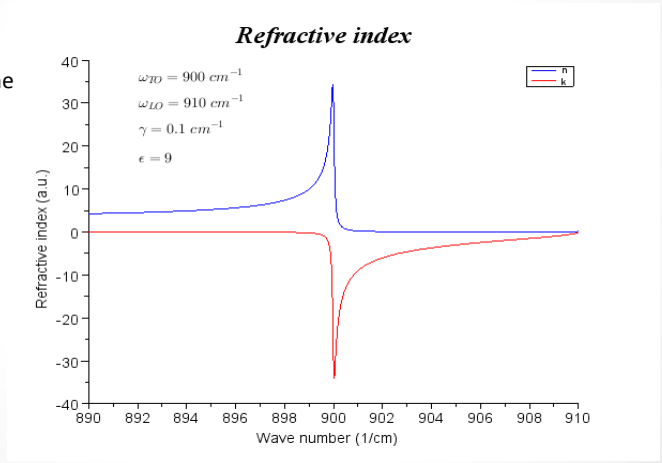

Basic understanding (11)

Increasing the ligth-matter coupling and the oscillator strength.

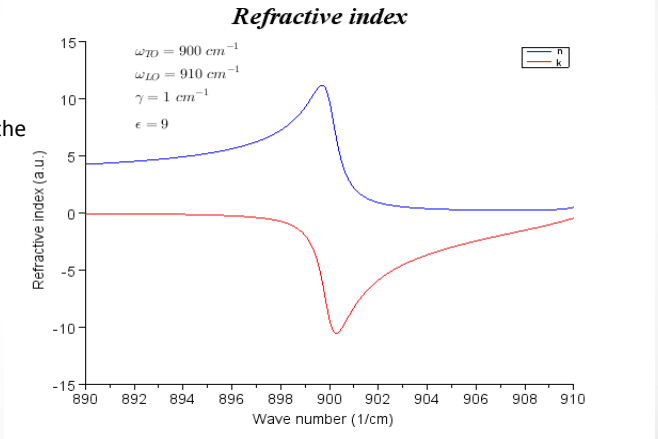

To summarize

- When travelling in the different media, the incident beam encounters linear response terms which come from the excitation (polarization) of internal dipoles such that: $P = \varepsilon(\omega_i) E$.
- P contains lattice vibration terms (phonons) at low frequency and electronic response terms (interband transitions) at high frequency.
- These linear response terms rule all the optical properties (R, α, T) from the far IR to the deep UV.

Reflectivity (1)

- Let us focus on the interface between two successive media (medium 1 and medium 2, for instance). Under normal incidence, the reflected and transmited intensities are given by:

$R = r\, r^*$ $T = t\, t^*$

in which r and t depend on both complex index values:

$$r = \frac{E_r}{E_i} = \frac{\tilde{n}_1 - \tilde{n}_2}{\tilde{n}_1 + \tilde{n}_2} \qquad t = \frac{E_r}{E_i} = \frac{2\tilde{n}_1}{\tilde{n}_1 + \tilde{n}_2}$$

Reflectivity (2)

Assume that medium 1 is air, with $n_1=1$ and $k_1=0$.

Assume that medium 2 is SiC, with $n_2=n+ik$.

$$R=r\,r^*=\frac{(n-1)^2+k^2}{(n+1)^2+k^2}$$

The in-depth transmitted light will be given by:

$$I_t=I_i\,e^{-\alpha d}$$

where α is the absorption coefficient.

From the experimental value of α, one can define a so-called «penetration depth» δ, which is given by:

$$\delta=1/\alpha.$$

Finally, just below the interface, the transmitted intensity (I_t) is given by:

$$I_t(d=0) = 4n^2/[(n+1)^2+k^2]$$

Basic set-up

- *Bruker IFS66V Fourier transform spectrometer*
- *Microscope (10-20 µm spots)*

Application (1)

- Probing a thin 3C-SiC layer on top of a thick n-type doped Si substrate.

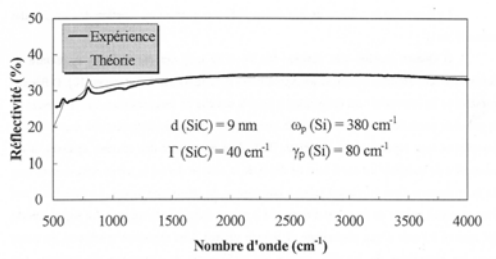

Figure III-6 : *Comparaison entre l'expérience et le spectre calculé pour une couche de carbonisation.*

Application (1-bis)

- The thickness is obtained from a comparison of the experimental and theoretical spectra using broadened dielectric functions as already displayed.

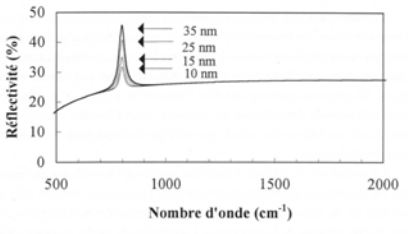

Figure III-5 : *Spectres théoriques calculés pour SiC/Si avec différentes épaisseurs de SiC. Afin de se rapprocher des spectres expérimentaux, le dopage du substrat de silicium a été pris en compte. Un paramètre d'élargissement de 20 cm-1 a été considéré dans chacun des cas.*

Applications (2)

Finding the experimental thickness of a growing or as-grown epitaxial layer, i.e. from in-situ Tg to RT (post-growth) investigation.

<u>In both cases</u>: Probe the interference pattern.

<u>Two requirements</u>:
- Work in a large transparency range (such that d < δ, whatever d);
- Have a sufficient difference in refractive index between the substrate, buffer(?) and active layer.

<u>Limitations</u>: Interface roughness (top and bottom) and/or a too thin or homoepitaxial layers with similar doping level.

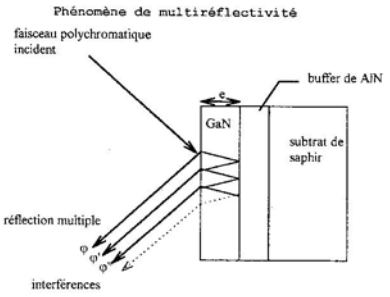

Results: GaN/saphire

From 2nd = kλ, considering «Δk » successive periods, one computes:

$d = (\lambda_1+\lambda_2)^2 \Delta k / 8n (\lambda_1-\lambda_2)$

This gives:

$d = 3.2\ (+/-\ 0.1)\ \mu m.$

$$e = 1\Big/ 2n\left(\frac{1}{\lambda_1}-\frac{1}{\lambda_2}\right)$$

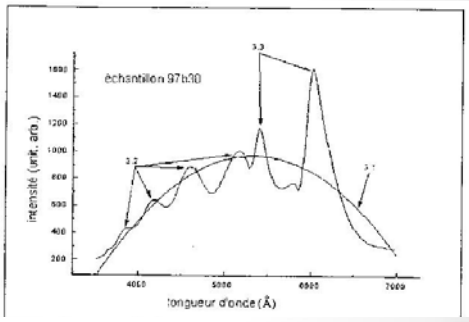

Has become a routine tool implemented on many growth set_up.

Interband transitions

Can be, either:

- High energy transitions at critical points E_1, $E_1+\Delta_1$ or E_2 of the BZ or
- Free exciton-polariton transitions probed (at LHT) in direct bandgap SC.

Exemple: GaN

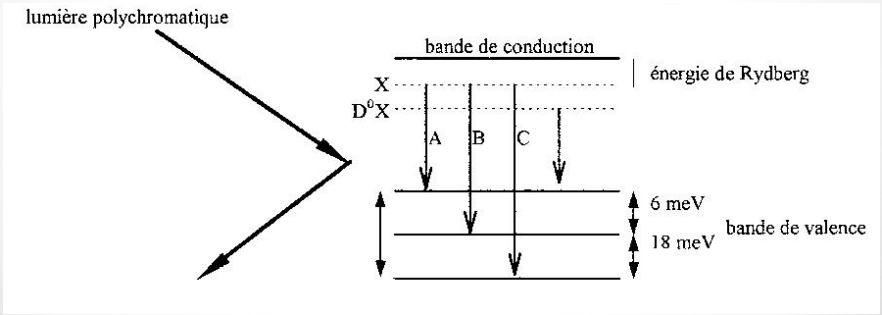

Threefold VB

3 VB give 3 M_0 c.p.,
i.e. 3 (A, B, C) exciton-polariton signatures.

They are clearly seen, superimposed on:

1: System response

2: Oscillations from multiple reflexions in the layer

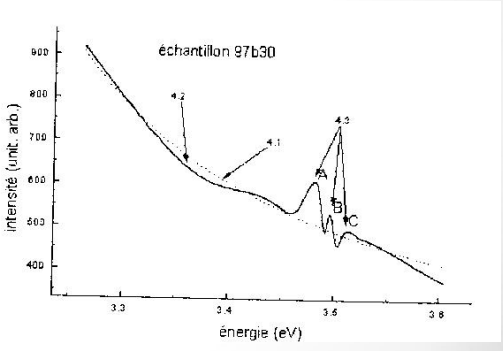

Conclusion (1)

Reflectivity is a versatile technique that:

- **Can be used on, both, very thin and very thick samples;**
- **Needs (almost) no surface preparation work.**

Many informations can be collected like:

- **Thin samples: Thickness;**
- **Thicker samples: Direct interband transition energies, IR-active phonon signatures.**

Absorption (1)

- **Basic « sample in - sample out » technique that measures the amount of transmitted light through a finite thickness sample.**
- **Main requirements are i) careful background corrections and ii) a careful sample preparation.**
- **Indeed, for a direct bandgap SC a can reach rapidly 5 to 10 thousand cm^{-1}. This means that the sample thickness « d » must be in the µm range.**

Absolute necessity of background corrections

Exemple: $CO_2(H_2O)$

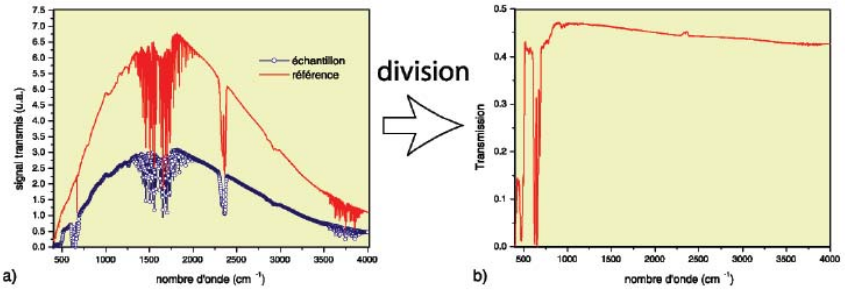

Figure III.10 : a) La division d'un spectre brut avec échantillon par un spectre de référence donne b) la transmission de l'échantillon. Les absorptions sur le spectre brut autour de 1500 cm^{-1} (2400 cm^{-1}) sont dues au CO_2 (H_20).

Once this is done: HMDSO

Hexamethyldisiloxane (HMDSO) cracking

Figure 5 : Spectres infrarouge de films réalisé par plasma de HMDSO

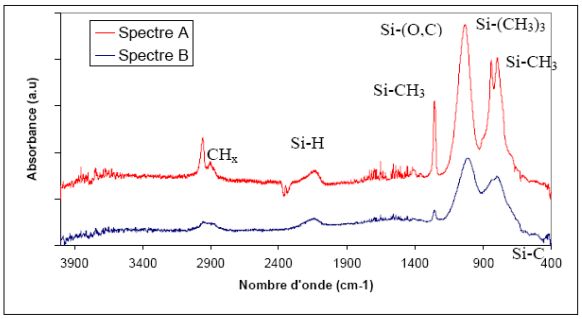

Un exemple est montré dans la figures 5. Sur cette figure nous avons représenté les spectres infrarouge de couches de type SiO_xC_y:H déposées par plasma d'héxaméthyldisiloxane ($(CH_3)_3Si\text{-}O\text{-}Si(CH_3)_3$) dans des conditions différentes. Le spectre A montre que la couche obtenue a conservé en partie la structure du précurseur avec la présence des liaisons $Si\text{-}CH_3$ et $Si\text{-}(CH_3)_3$ alors que sur le spectre B ces liaisons ont pratiquement disparu.
Si on fait le rapport Aire $Si\text{-}CH_3$ / Aire Si-(O,C) on obtient ainsi une grandeur caractérisant le caractère plus ou moins organique de la couche.

Grid oxyde evaluation

Un même groupe peut donner lieu à plusieurs types de vibrations et donc à des absorptions à différentes fréquences. Ainsi le silicium lié à 4 atomes d'oxygène de la silice donne trois type de vibrations : Si-O stretching (1080 cm^{-1}), Si-O bending (805 cm^{-1}), Si-O rocking (450 cm^{-1}) comme le montre la figure 4.

Figure 4 : Exemple de spectre infrarouge d'une couche de type silice

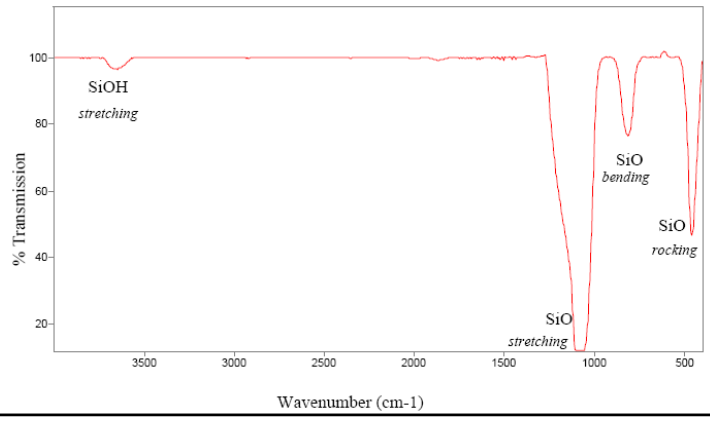

Interband transitions

GaAs (300K)

$$\alpha \propto \frac{m_r^{3/2}}{n\omega}\sqrt{\hbar\omega - E_g}$$

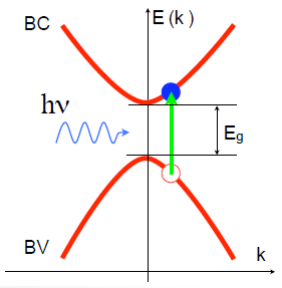

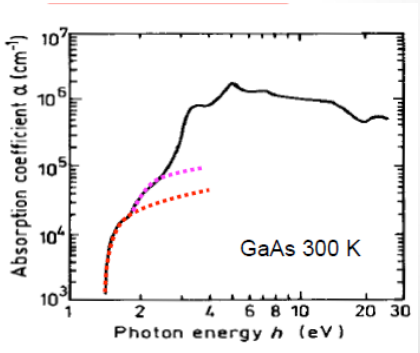

Conclusion (2)

Absorption is more difficult to use (and much less popular) than reflectivity:

- The main difficulty is to adjust the film thickness to the (unknown) value of the absorption coefficient (i.e. from few to thousand cm^{-1})
- Needs **careful** preparation work (CPM polishing or peeling).

The informations collected are:

- Direct absorption values (matrix elements) for interband transitions (no KK transformation necessary);
- Direct comparison with band structure calculations.

Photoluminescence (1)

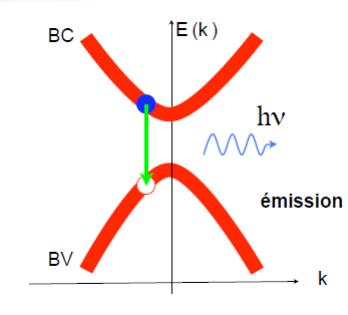

Simple process:

- a primary (e-h) pair is generated in the crystal.
- After thermalization it recombines radiatively, generating an emitted photon.
- Of course, to generate the primary pair an electronic excitation is needed.
- This excitation may have different forms, which are at the origin of the many possible variants.

Variants

The source is a direct injection of e-h pairs:
electroluminescence (LEDs).

Source is an e-beam (SEM):
cathodoluminescence.

Mechanic, chemic or thermic action:
Tribo or chemio or thermoluminescence.

Set-up (for WBG SCs)

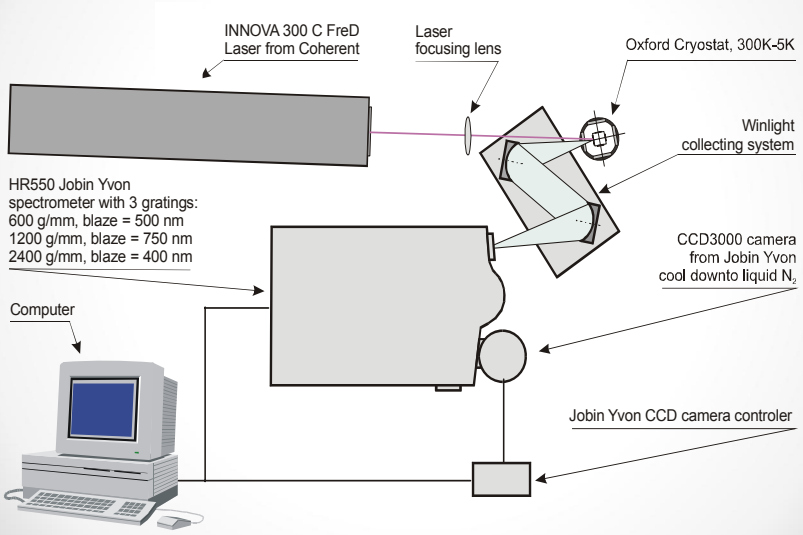

Collected intensity

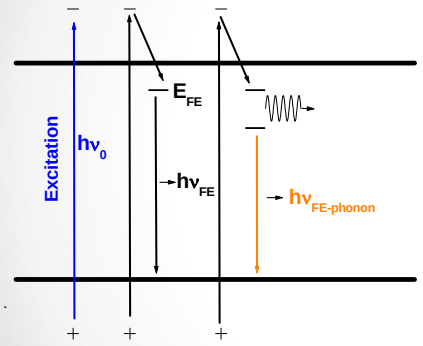

$$\frac{dn_{FE}}{dt} = g_{FE} - \left(\frac{1}{\tau^{r}_{FE}} + \frac{1}{\tau^{nr}_{FE}}\right) n_{FE}$$

$$I_{FE} = \frac{n_{FE}}{\tau^{r}_{FE}}$$

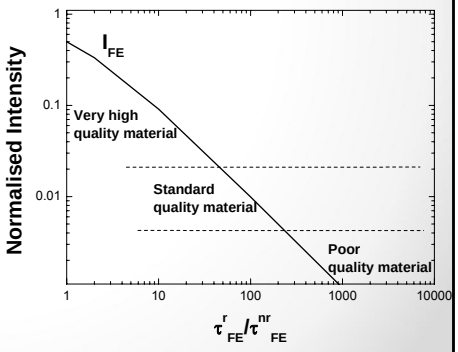

Results for 3C-SiC

- In 3C-SiC, from sample to sample there is more or less competition between the donor-bound exciton lines and the structural defects.

Results:

- Hopefully, the best TEM sample (R2, Lely-type) gives the best LTPL results;
- All other (seeded) samples like R1 (also grown by CF-PVT) or A, B and C (grown by SE) gave a lower intensity and a higher density of TEM defects.

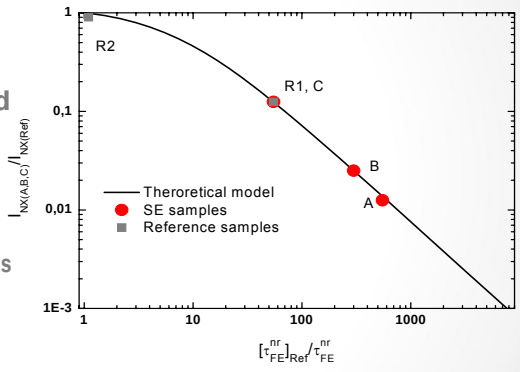

Note: A recent claim that record lifetimes have been obtained on a 750 µm thick SE layer by Chen and co-workers (APL 2012) could modify this hierarchy.

Results for GaN

In GaN:

•The threefold VB is an intrinsic feature;

•It appears clearly on both reflectivity spectra but, depending on the growth conditions, there is:

- More or less quenching of the radiative term for the A, B and C lines;

- More or less intensity of the associated LTPL features.

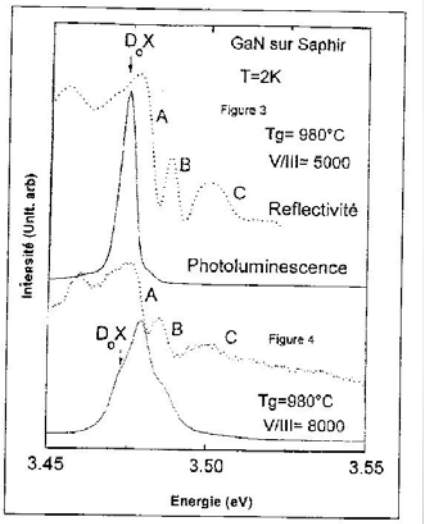

Growth optimization

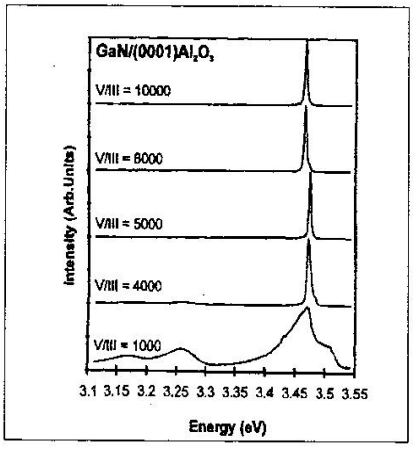

Exemple 2 (à gauche): Spectres de photoluminescence pour des croissances à 980°C sous des concentrations V/III différentes. On constate qu'a tous les taux sauf le plus bas les pics sont corrects. Au taux le plus bas les structures du bord de bande sont élargis et les paires donneurs-accepteurs sont visibles.

To optimize the growth conditions, focus on the intensity of the FE-polariton lines.

With 10^3 more signal intensity than SiC: r**outine tool**

Polytype identification

- From 4H to 6H, 15R and 3C

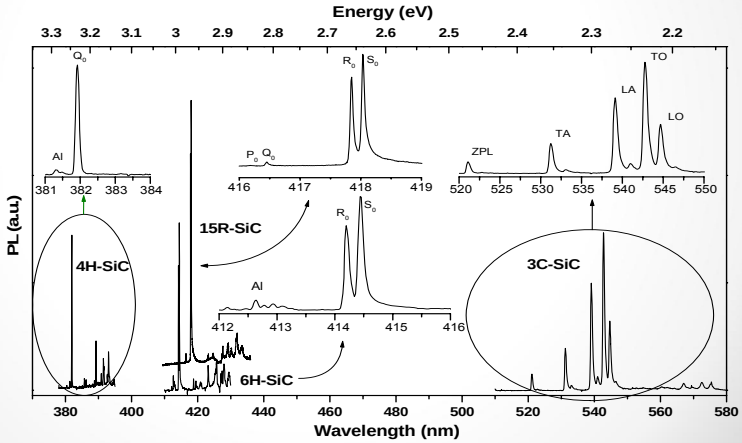

Free vs bound excitons

Low doped material (n type)

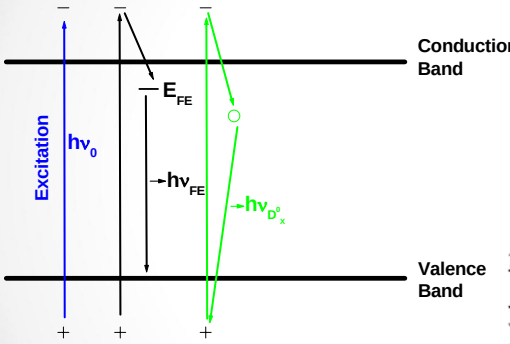

$$\frac{dn_{FE}}{dt} = g_{FE} - \left(\frac{1}{\tau^{r}_{FE}} + \frac{1}{\tau^{nr}_{FE}}\right) n_{FE} - t_{DX}$$

$$\frac{dn_{DX}}{dt} = t_{DX} - \left(\frac{1}{\tau^{r}_{DX}} + \frac{1}{\tau^{nr}_{DX}}\right) n_{DX}$$

FE: Free Exciton
DX: Exciton bound to neutral Donnor

O. Kordina ey al Phys. Stat. Sol. b 202 (1997), p. 321

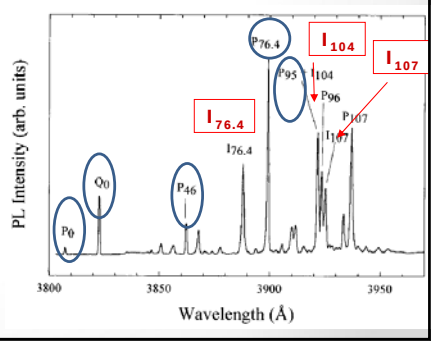

Increasing the [donor]

Steady state conditions:

$$\frac{dn_{FE}}{dt} = 0 \qquad \frac{dn_{DX}}{dt} = 0$$

2 LTPL intensities:

$$I_{FE} = \frac{n_{FE}}{\tau^r_{FE}} \qquad I_{DX} = \frac{n_{DX}}{\tau^r_{DX}}$$

$$\frac{I_{DX}}{I_{FE}} = \frac{\tau^r_{FE}}{\tau^r_{DX}} \frac{\tau^{nr}_{DX}}{} f_{FE} \frac{[D_{onor}]}{[S_{ites}]} = K[D_{onor}]$$

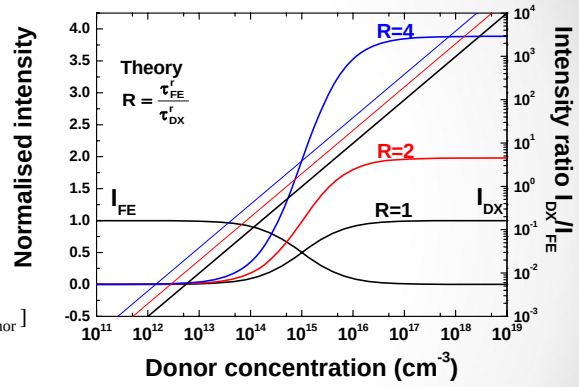

Application: optical calibration curves

J. Camassel, S. Juillaguet, M. Zielinski, C. Balloud. Chemical Vapor Deposition, 12, 549 (2006)

Well-known for Si

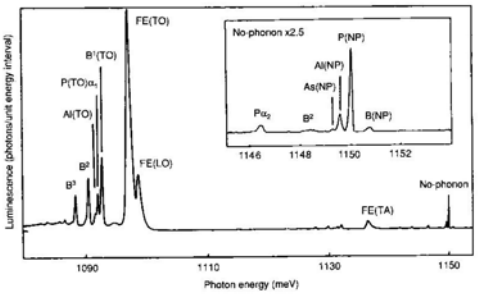

Fig. 5.10 Photoluminescence from high-resistivity (>20 kΩ-cm) near-intrinsic silicon. Fingerprint features from impurity boron, phosphorus, aluminum, and arsenic are marked. Their concentrations, in units of 10^{12} cm^{-3}, are 1.36, 1.69, 0.61, and 0.14 respectively. Free-exciton lines (FE) are visible. TO, LO and TA phonons participate as indicated. NP (no phonon) peaks come from bound excitons. Calibrations are discussed in the text and shown in Fig. 5.14. (After Lightowlers (1990).)

Impurity content

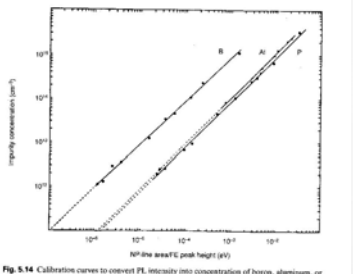

Fig. 5.14 Calibration curves to convert PL intensity into concentration of boron, aluminum, or phosphorus in silicon. This plot uses an internal calibration method. The area of the no-phonon (NP) peak for the particular impurity is ratioed against the height of the FE(TO) peak in the same spectrum (Fig. 5.11). (After Lightowlers (1990).)

Works the same for SiC:N

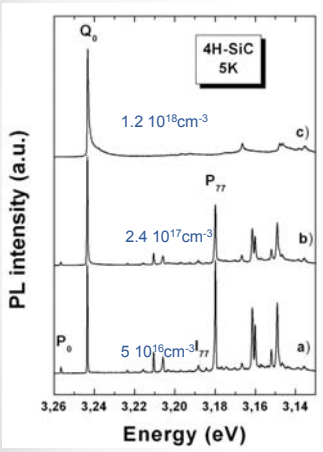

$$R = \frac{I_{DX}}{I_{FE}} = A\,\frac{[N]}{[C]}$$

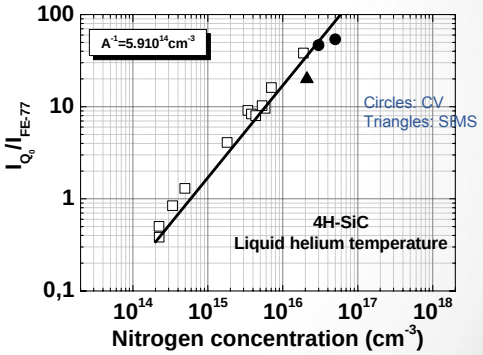

I.G. Ivanov et al J. Appl. Phys. Vol 80 (6), 3504 (1996).

Increasing the [N] level

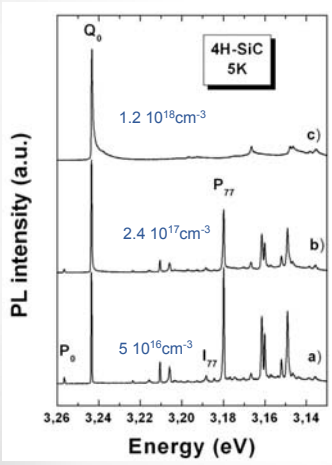

The intrinsic lines disappear.
New, intersite, competition.

$$\frac{I_{DX}^{C}}{I_{DX}^{H}} = R_0 + R_1[N] + R_2[N]^2$$

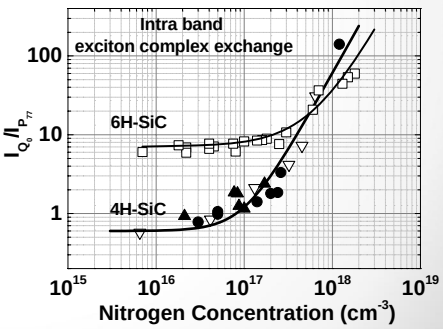

A. Henry, A. Ellison, U. Forsberg, B. Magnusson, G. Pozina and E. Janzen: Mater. Sci. Forum, 389-393, 593 (2002). R. Weingärtner, A. Albrecht, P.J. Wellmann and A. Winnacker. Mater. Sci. Forum, 433-436, 341 (2003).

With Al compensation

Low compensation

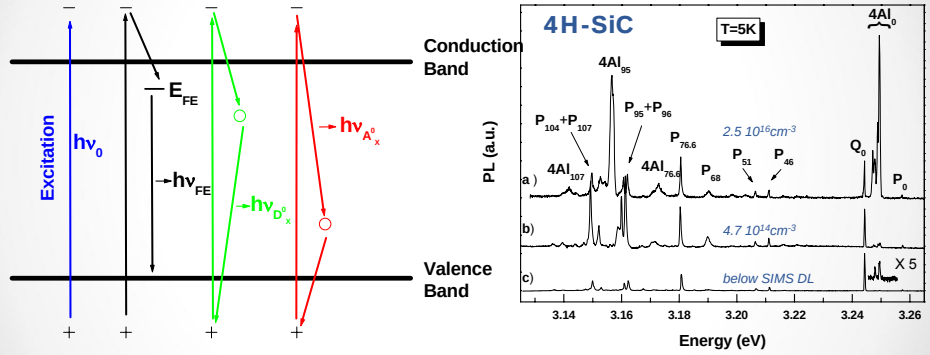

FE: Free Exciton (no longer to resolved)
DX: Exciton bound to neutral Donor
AX: Exciton bound to neutral Acceptor

S. Juillaguet, M. Zielinski, C. Balloud, C. Sartel, C. Consejo, B. Boyer, V. Soulière, J. Camassel and Y. Monteil. Mater. Sci. Forum Vols. 457-460, 775 (2004)

Al doping in 4H and 3C-SiC

$$\frac{dn_{AX}}{dt} = t_{AX} - \left(\frac{1}{\tau^r_{AX}} + \frac{1}{\tau^{nr}_{AX}}\right) n_{AX}$$

$$t_{AX} = n_{FE} f_{FE} \frac{[Al]}{[Si]}$$

Steady state conditions:

$$\frac{dn_{AX}}{dt} = 0 \qquad \frac{dn_{DX}}{dt} = 0$$

2 LTPL intensities:

$$I_{DX} = \frac{n_{DX}}{\tau^r_{DX}} \qquad I_{AX} = \frac{n_{AX}}{\tau^r_{AX}}$$

$$\frac{I_{AX}}{I_{DX}} = \frac{\tau^r_{DX}\tau^{nr}_{AX}}{\tau^{nr}_{DX}\tau^r_{AX}} \frac{[Al]}{[N]}$$

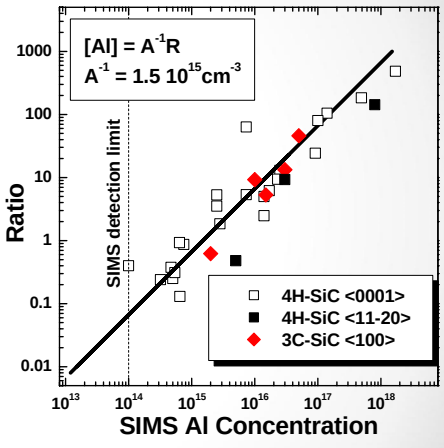

J. Camassel, S. Juillaguet, M. Zielinski ,C. Balloud Chemical Vapor Deposition, 12, 549 (2006)

High Al doping in 4H-SiC

Shift and broadening of the Al_0 line as a function of [Al]

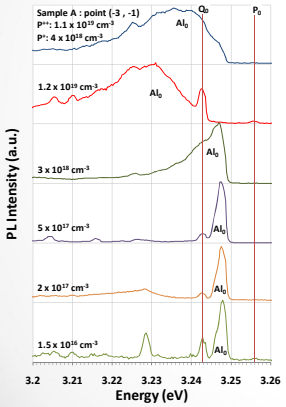

Corrélation with SIMS measurements
→ Calibration curve

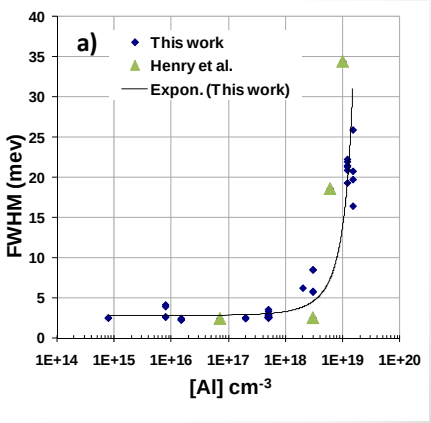

H. Peyre et al Mater. Scie. Forum 711, 164 (2012)

Conclusion (3)

PL is a very simple and popular technique:

- Can be used routinely from RT to LNT but, for detailed investigation, LHT is preferred.
- Does not necessitate any surface preparation but, in some (pathologic) cases, CPM polishing can be used.

The collected informations are:

- The overall signal intensity: a poor signal means a poor sample with numerous non-radiative centers.
- A list of the impurities present in the material with, in some cases, quantitative information on the concentration.

Raman (1)

- Consider again an incoming laser beam (ω_i):

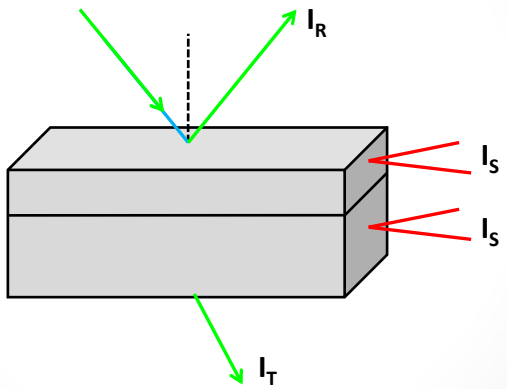

Raman (2)

- As already said, when travelling in the different media, the beam encounters:
- Linear response terms coming from the excitation of internal dipoles (polarization): $P = \varepsilon(\omega_i)\, E$
- P contains lattice vibration terms (phonons) at low frequency and electronic response terms (interband transitions) at higher frequency (laser frequency, for instance) .
- As already said, these linear response terms rule all the optical properties (R, a, T) from far IR to deep UV.

Raman (3)

- However, at laser frequency ω_i:
- Small additional perturbations exist in $\varepsilon(\omega_i)$ which come from the lattice vibrational modes $u(\Omega)$.
- They give non linear coupled terms (Raman signal components):

$$P = \varepsilon(\omega)\, E + d/du\, [\varepsilon(\omega)]\, u.E + d^2/du_2\, [\varepsilon(\omega)]\, [u.\, E]^2 + \ldots$$

- at low energy: Stokes shifted modes,
- at high energy, anti-Stockes shifted modes.

Raman (4)

In other words:

- For engineers: the (small) Raman signal is nothing but the results of a weak (10^{-6}) frequency modulation.
- For solid state physici

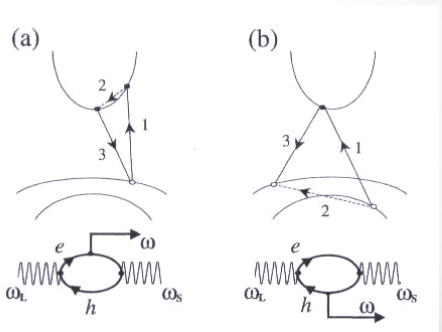

Raman (5)

- In both cases: « phase-matching » conditions.
- For well-ordered samples, they give standard selection rules:

$\omega_s = \omega_i +/- \Omega_{phonon}$ and $q_s = q_i +/- Q_{phonon}$

- which results in extremely precise Raman values:
  - C(diamond): 1332 cm^{-1} / Si: 520 cm^{-1} / Ge: 303 cm^{-1}
- For a weakly defective sample, partial relaxation of the selection rules (broadening and shift).
- For a strongly defective one, complete relaxation.

Set-up (a)

- **Routine Raman**
- **spectroscopy**

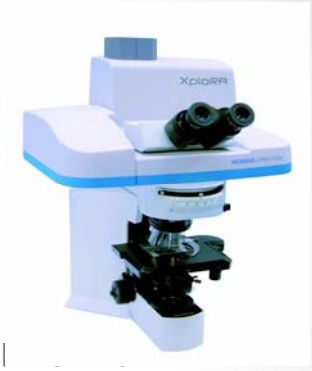

- Fast, non-destructive
- Extremely versatile
- Easy to use and calibrate
- Provides on-line control and mapping of ion-induced damage and recovery.

Set-up (b)

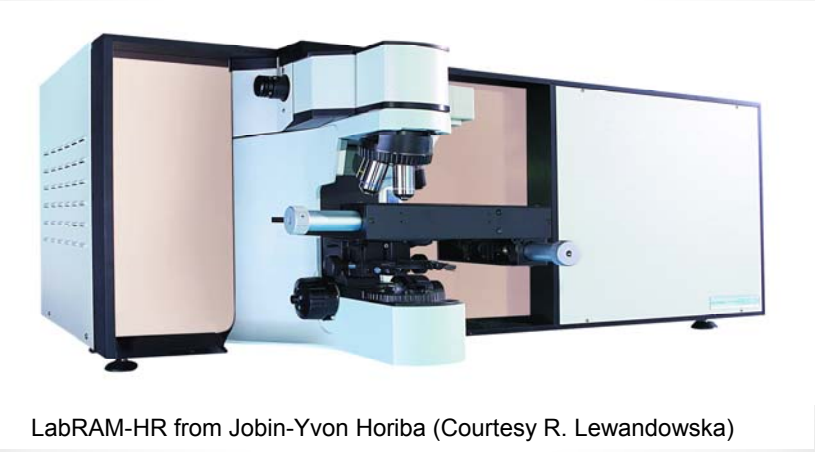

LabRAM-HR from Jobin-Yvon Horiba (Courtesy R. Lewandowska)

Best exemple is Si

From crystalline to µ-c and a-Si:

Three different Raman signatures

Three different micro-structure (from X-ray).

One average degree of crystallinity:

$$V_C = \frac{\sum A_c + A_{\mu-c}}{\sum A_c + A_{\mu-c} + A_a}$$

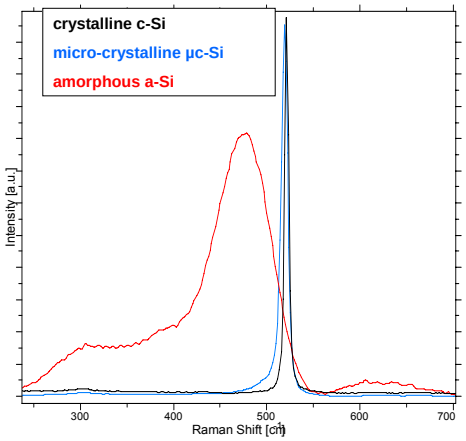

Limit of a-Si

c-Si: one Raman-active mode at 520 cm^{-1}

520 cm^{-1}

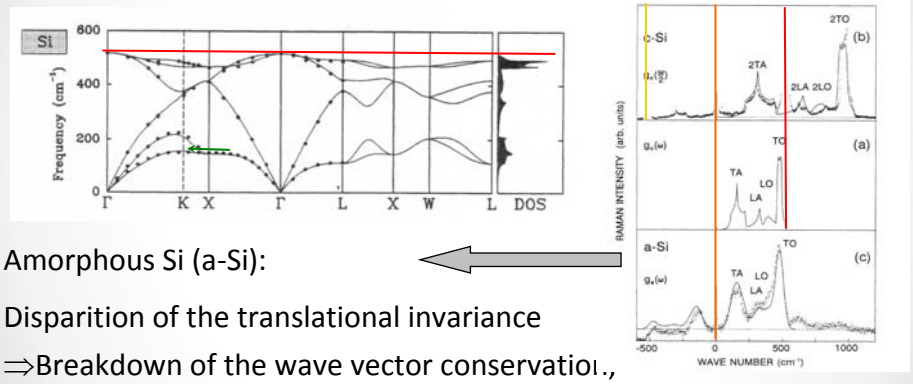

Amorphous Si (a-Si):

Disparition of the translational invariance

⇒Breakdown of the wave vector conservation,

⇒**q ≠ 0** modes become activated.

Carles *et al.*, PRB 93

Reversible behavior

- Application to «Process control» for Implantation damage reduction.

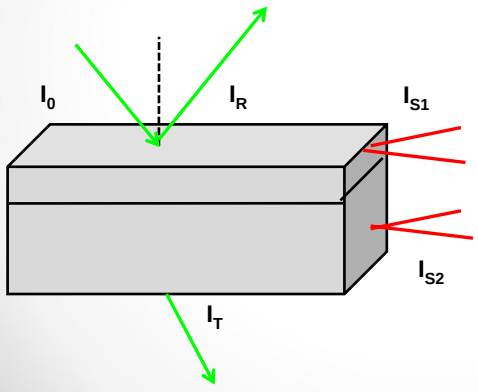

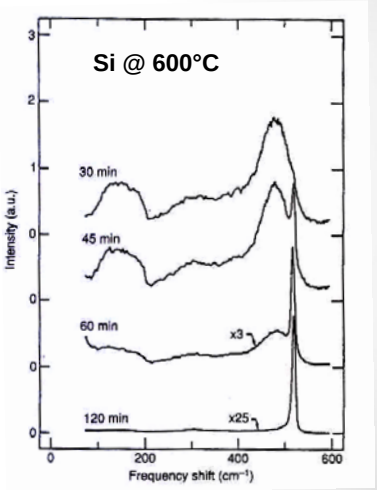

SiC

Low and high energy changes

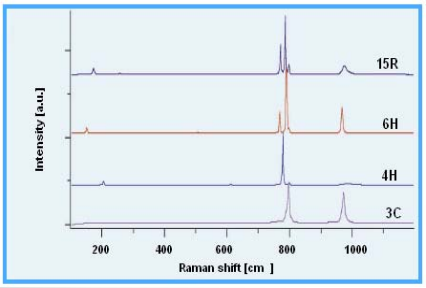

The stacking sequence of double layers of the three most common SiC polytypes

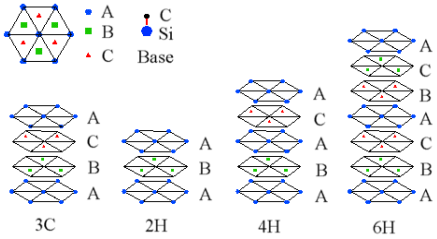

figure from http://www.ifm.liu.se/matephys/ew_page/research/sic/Chapter2.html

3C on 6H-SiC

3C contribution:

Proportional to 3C layer thickness (see insert)

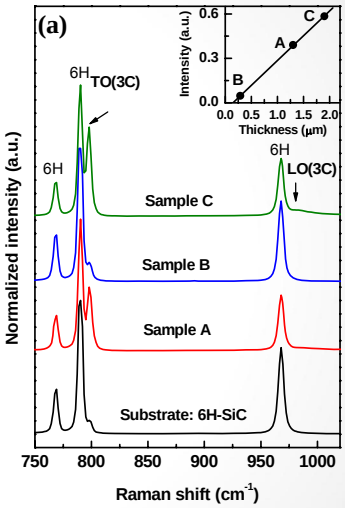

Graphene/Graphite

- Graphene is a single graphite layer.
- It can be exfoliated from a graphite sample or gro epitaxially on the Si or C faces of a SiC wafer.
- Commun defects are: C(diamond) fingerprint a
  - 1332 cm^{-1}
- To be compared with: C(graphite) fingerprint:
  - 1582 cm^{-1}

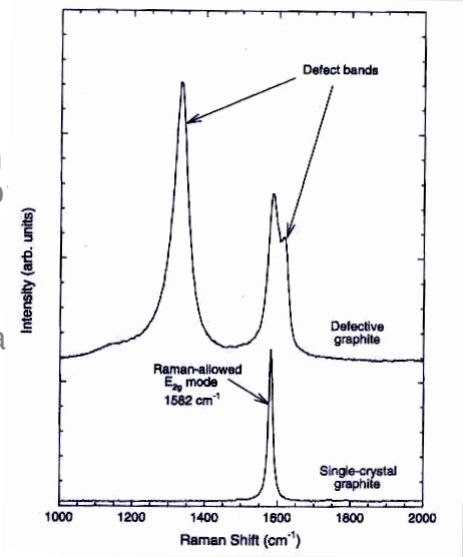

Graphene/SiC

- Micro-Raman spectroscopy coupled with transmission measurements
- Transmission (absorption ~1.2% per ML): direct thickness mapping
- Micro-Raman: thickness (G band) and stacking (2D band)

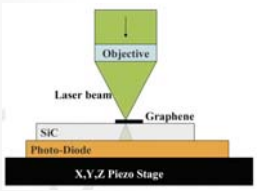

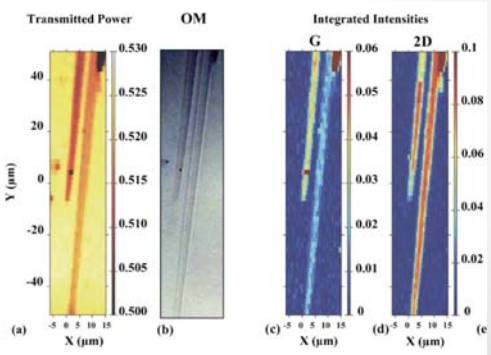

Raman

MLG on SiO_2/Si

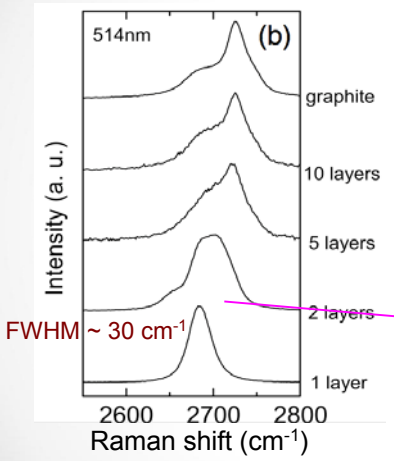

Ferrari et al., PRL **97**, 187401 (2006)

This work

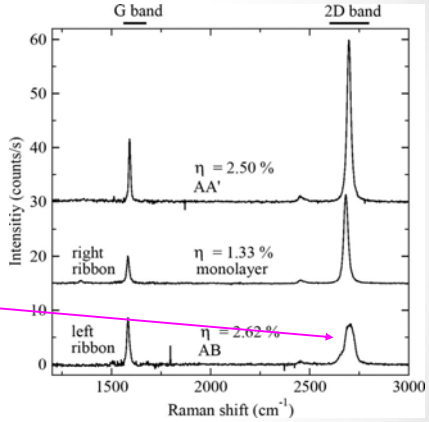

Camara et al., PR B**80**, 125410 (2009)

M2 FMPH

Absolute Raman intensities

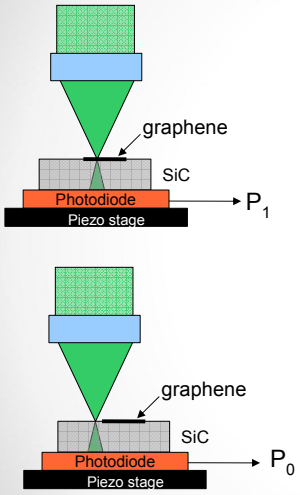

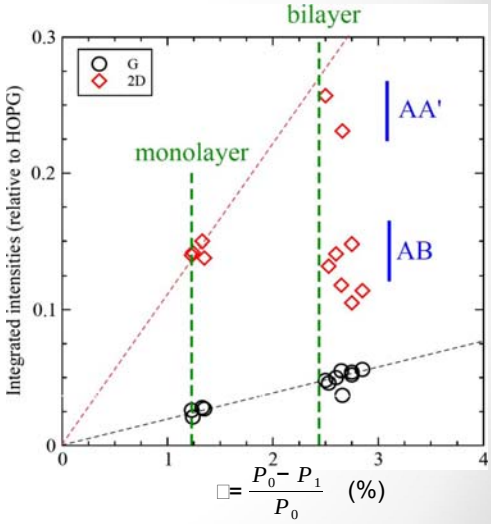

M2 FMPH

Conclusion (4)

- Raman is an extremelly versatile tool.
- It can be viewed (at the same time):
- - as a routine characterization tool (SiC);
- - and/or as a SoA research technique (graphene).

Thank you for your attention

OPTICAL PROPERTIES OF AS-GROWN STACKING FAULTS IN SIC

Sandrine Juillaguet

Laboratoire Charles Coulomb - CNRS
Département SMC – UMR 5221
MONTPELLIER

Outline

- Photoluminescence: application to SiC
- Stacking faults
- Correlation PL-TEM-Calculation on 2 samples
  - Local investigations CL, Micro-PL
- Conclusion

Summer School 3 Thessaloniki, July 15th, 2012

Experimental set-up

- Laser FreD (244nm 5eV) (200mW)
- CCD camera
- Spectrometer
- Cryostats with a Temperature range : 5K <T < 300K
  - Small samples T=5K
  - 2'' T = 15K
  - 4'' T=2K

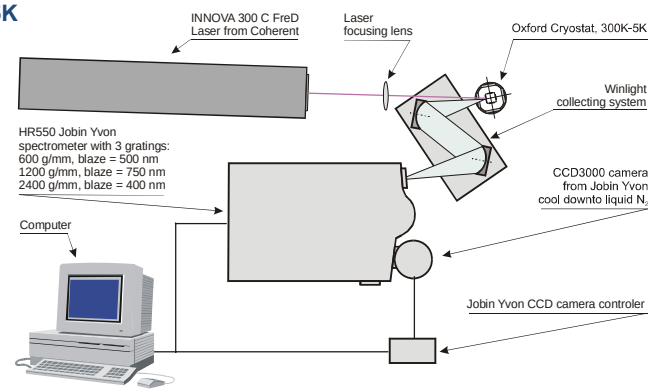

Summer School 4 Thessaloniki, July 15th, 2012

Experimental set-up

- CCD camera
- Cryostat T=5K

Cryostat 4'' T=2K

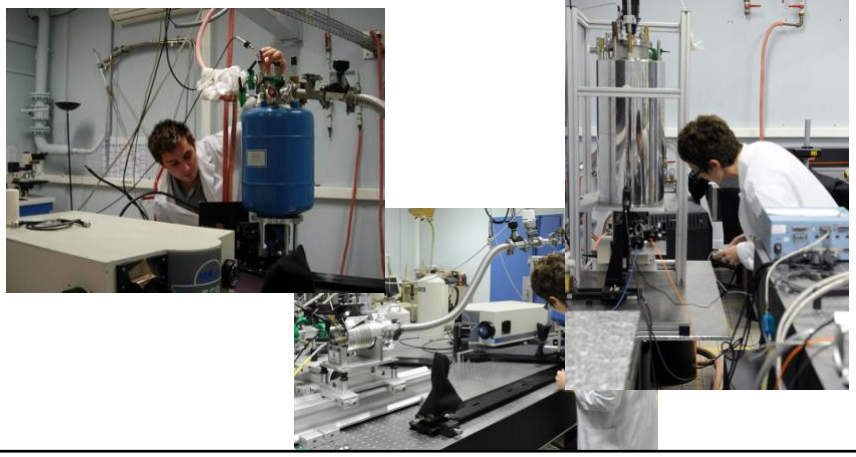

Summer School 5 Thessaloniki, July 15th, 2012

LTPL: background

Low temperature photoluminescence for what information ?

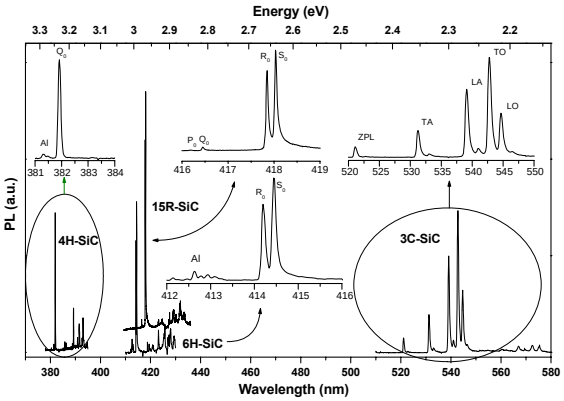

- Band gap energy depend of polytype :
- Variation of 1eV between 3C and 4H SiC

⇓

Identification of polytype

- Doping level
- impurities
- Defect

Summer School 6 Thessaloniki, July 14,2012

n type residual doping in 4H-SiC

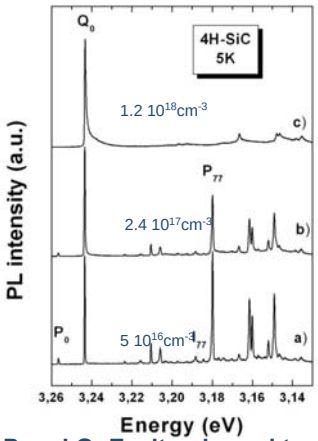

P and Q: Exciton bound to neutral Nitrogen and Phonons replicas

$$R = \frac{I_{DX}}{I_{FE}} = A \frac{[N]}{[C]}$$

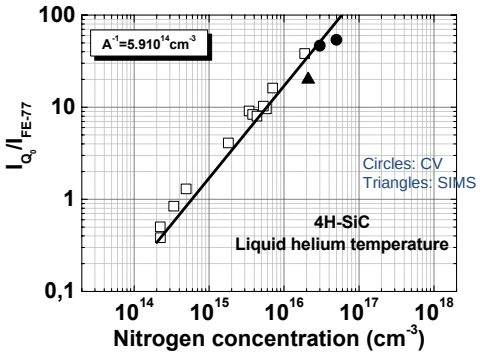

I_{FE}: intensity of the free exciton
I_{DX}: Intensity of the donor bound to an exciton

I.G. Ivanov et al J. Appl. Phys. Vol 80 (6), 3504 (1996).

Summer School 7 Thessaloniki, July 15th, 2012

N doping level increase in 4H-SiC

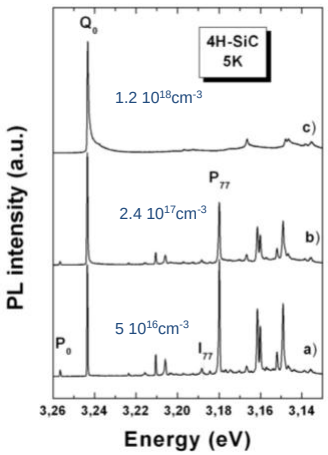

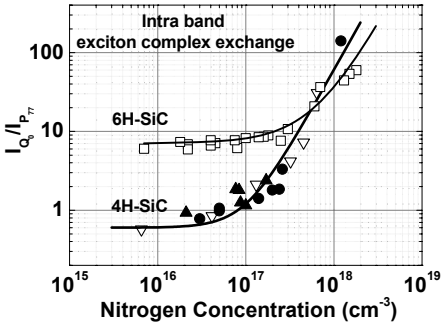

If [N] increase, the intrinsic line disappear
The ratio I_{Q0}/I_{P77} vary as the [N]

A. Henry, A. Ellison, U. Forsberg, B. Magnusson, G. Pozina and E. Janzen: Mater. Sci. Forum, 389-393, 593 (2002). R. Weingärtner, A. Albrecht, P.J. Wellmann and A. Winnacker. Mater. Sci. Forum, 433-436, 341 (2003).

Summer School 8 Thessaloniki, July 15th, 2012

Low compensation samples

Aluminum lines appear and increase with [Al]

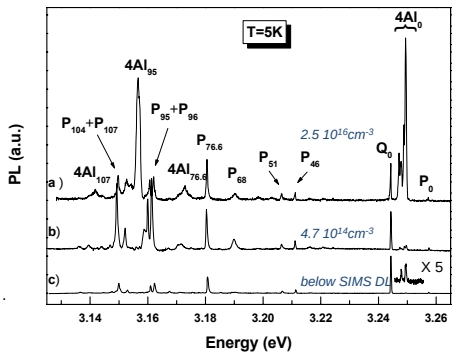

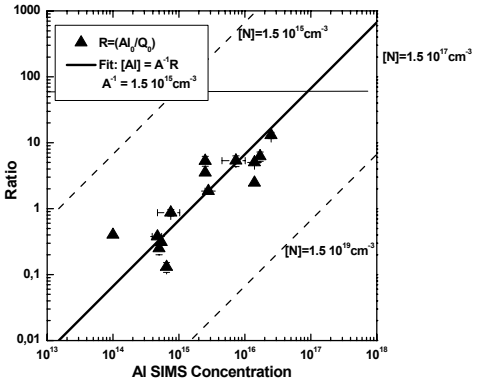

The ratio Al/Q depend of [N]
A set of calibration curves

S. Juillaguet et al Mater. Sci. Forum Vols. 457-460, 775 (2004)
J. Camassel et al Chemical Vapor Deposition, 12, 549 (2006)

Summer School 9 Thessaloniki, July 15th, 2012

Outline

- Photoluminescence: application to SiC
- Stacking faults
- Correlation PL-TEM-Calculation on 2 samples
  - Local investigations CL, Micro-PL
- Conclusion

Summer School 10 Thessaloniki, July 15th, 2012

SF Formation in 4H-SiC

- **under forward current injection**

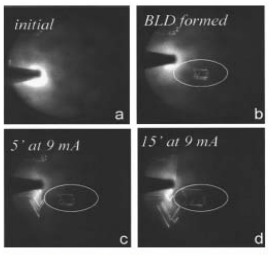

G. 2. Evolution of electroluminescence images in the course of 4*H*-Si ode degradation. All images were acquired at a diode current of 0.2 m/ e mesa size is 500 μm. After Ref. 20.

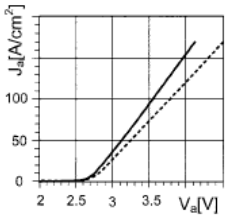

Increase voltage drop after testing 3C

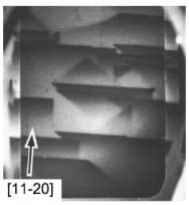

FIG. 5. Low-temperature panchromatic cathodoluminescence image of a stressed 4*H*-SiC diode. Triangular and rectangular features with reduced emission intensity (darker regions) are observed on stressed diodes. After Ref. 15.

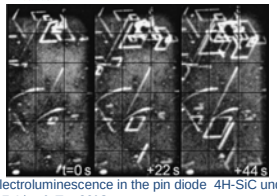

Electroluminescence in the pin diode 4H-SiC under J = 7 A/cm² T = 30°C

- **Oxydation process, doping, implantation, under high excitation power**
- **During the growth: as-grown SF**

Konstantinov at al APL 71 3700 (1997), M. Skowronski et al JAP 99 011101 (2006), Galeckas et al, Appl. Phys. Lett. 81 (2002)

Summer School 11 Thessaloniki, July 15th, 2012

Optical energetic signature of defects : SF

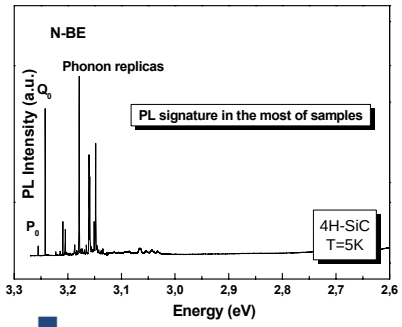

Typical 4H-SiC spectrum:
Near Band edge (NBE)

Summer School 12 Thessaloniki, July 15th, 2012

Optical energetic signature of defects : SF

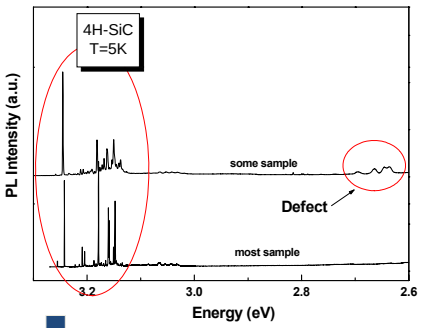

Typical 4H-SiC spectrum:
Near Band edge (NBE)

Summer School 13 Thessaloniki, July 15th, 2012

Optical energetic signature of defects : SF

•Large and regular phonon signatures*

4 phonon replicas :
46 - 75.5 - 94.5 – 104.5mev

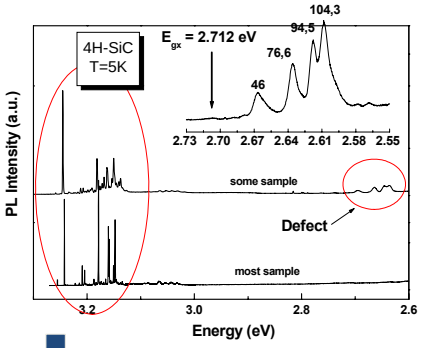

E_{gX}

E_{gX} : Optical energetic signature of the defect

Typical 4H-SiC spectrum:
Near Band edge (NBE)

* S.Bai et al. Materials Sci. Forum. Vol 389-393 (2002) 589

Summer School 14 Thessaloniki, July 15th, 2012

Large energetic dispersion

Particular PL spectra obtained in few cases

•Presence of 3C-SiC Micro inclusions

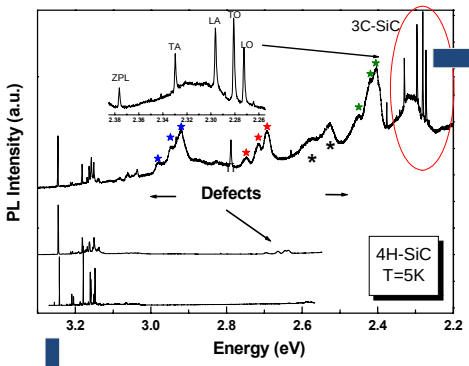

Defects appear on a large energy scale between 4H and -3C
3.1eV - 2.4eV

How can we explain this large energetic dispersion of defects?

Typical 4H-SiC signature

S. Juillaguet, et al Mater.. Sci. Forum Vols. 457-460, 577 (2004)

Summer School 15 Thessaloniki, July 15th, 2012

Stacking faults

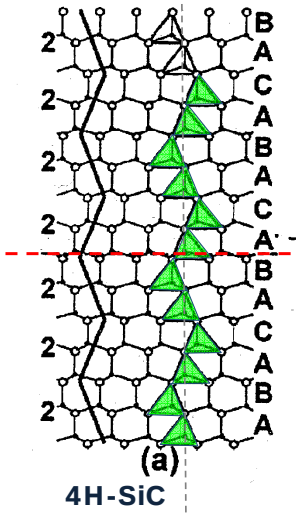

Fault in the sequence during the growth

Liu et al. Appl. Phys. Lett. 80, 2111, (2002)
H. Iwata et alJ. Appl. Phys. 93, 1577 (2003).

Summer School 16 Thessaloniki, July 15th, 2012

Stacking faults

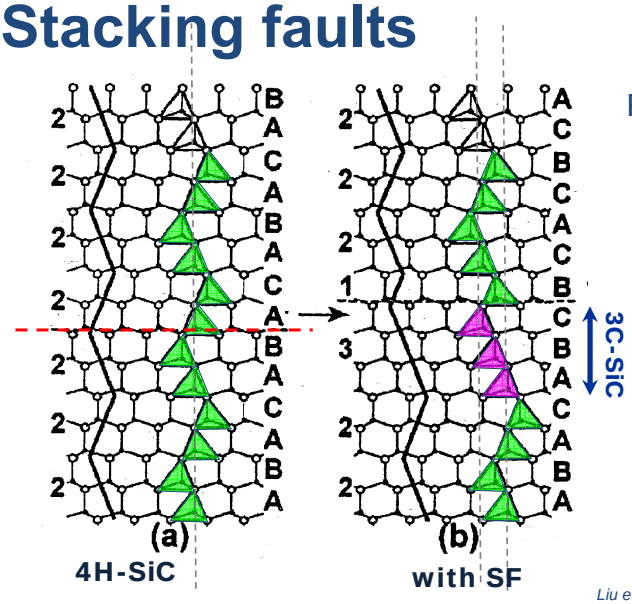

Fault in the sequence during the growth

Growth of other polytype

Optical signature of polytype to identify the SF?

Liu et al. Appl. Phys. Lett. 80, 2111, (2002)
H. Iwata et alJ. Appl. Phys. 93, 1577 (2003).

Summer School 17 Thessaloniki, July 15th, 2012

Energetic dispersion

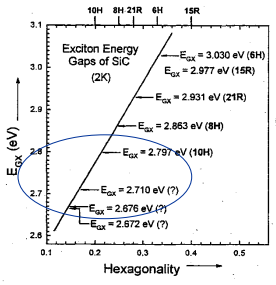

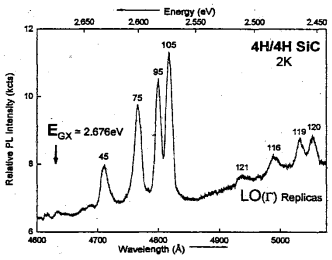

* S.Bai et al Materials Sci. Forum. Vol 389-393 (2002) p589

SF signature = Energy band gap of the polytype

No because it's difficult to explain some signatures!!

Summer School 18 Thessaloniki, July 15th, 2012

Model: Quantun well

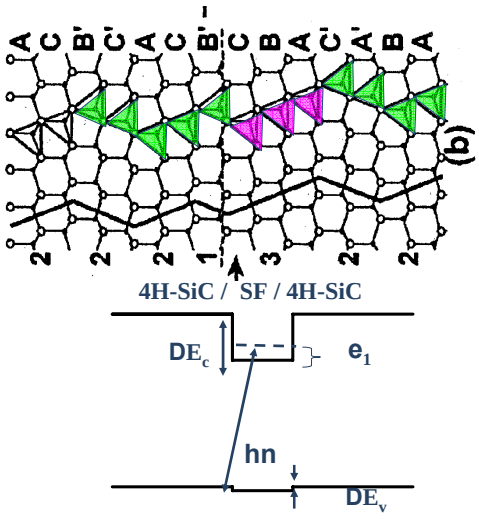

* S.Bai et al Materials Sci. Forum. Vol 389-393 (2002) p589

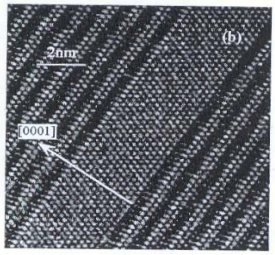

E_g4H : the highest energy band gap

Eg_{SF} other polytype with a lower energy band gap

Quantum well (intrinsic type II[a])

(a) F. Bechstedt et al Phys. Rev. Lett. 75 2180 (1995)

Summer School 19 Thessaloniki, July 15th, 2012

Model: Quantun well

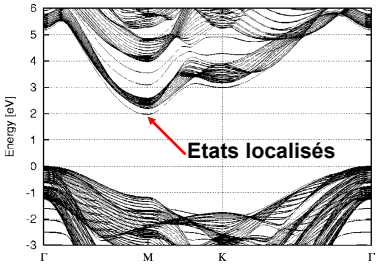

* Iwata et al, Phys. Rev. B 65 (2002)

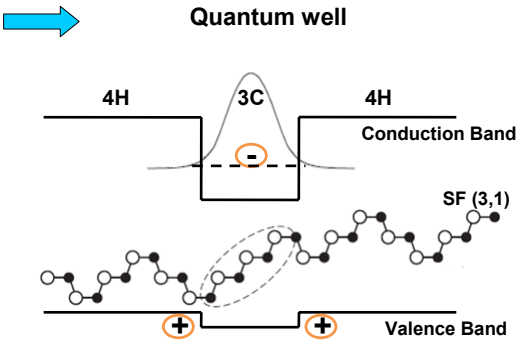

Iwata and al calculate the band structure of the SF with this model.
The SF is a trap for the electrons

Summer School 20 Thessaloniki, July 15th, 2012

Model: Quantum well

Increase the QW width

Decrease the optical SF signature

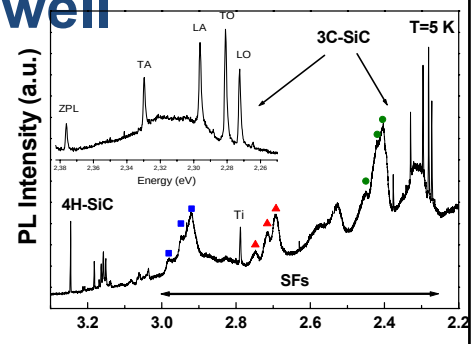

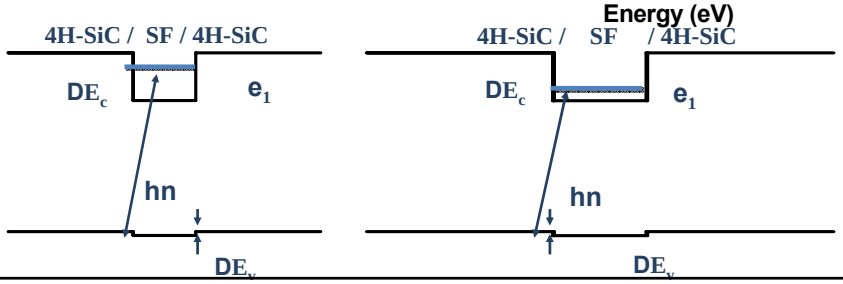

Summer School 21 Thessaloniki, July 15th, 2012

Stark effect

S. Bai et al Materials Sci. Forum. Vol 457-460, 573 (2004)

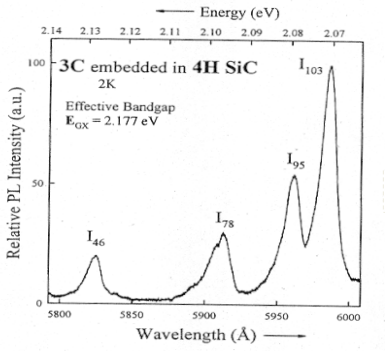

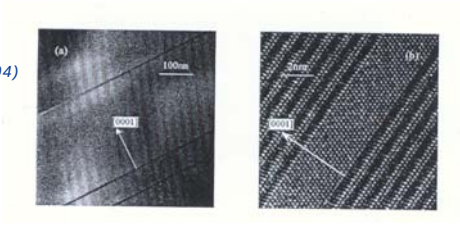

TEM Epaisseur : 3.25 nm

Eg(SF)=2.177eV 210meV < Eg(3C)

How we can explain SF signature 210 meV < Eg (3C) ?

Spontaneous polarisation* ➡ Electrical field ➡ Stark effect.

**A. Qteish et al Phys. Rev. Rev B45 6534 (1992)*

Summer School 22 Thessaloniki, July 15th, 2012

Spontaneous polarization

Spontaneous polarization on Hexagonal polytype :

inequivalent Si—C bonds
bond- to bonds transfer charge
electrical dipole

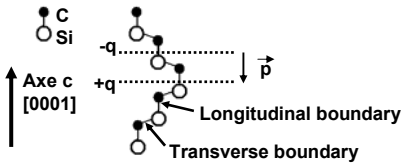

3C: no spontaneous polarization

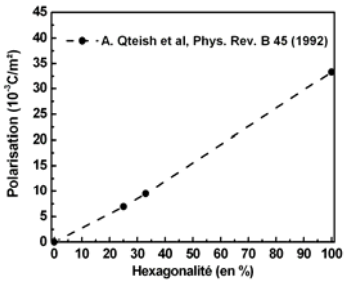

SF correspond to 2 different polytypes
a charge density is create at the interface which create an electrical field.

A. Qteish et al Phys. Rev. Rev B45 6534 (1992)

Summer School 23 Thessaloniki, July 15th, 2012

Model : Quantum well with Stark effect

4H-SiC / SF / 4H-SiC **4H-SiC / SF / 4H-SiC**

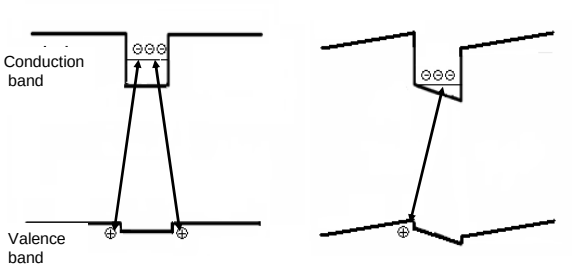

- Quantum well (type II[a])
- Electrical field [b]

- Electrons confinement on the QW
- Holes on the barriers

(a) F. Bechstedt et al Phys. Rev. Lett. 75 2180 (1995)
(b) A. Qteish et al Phys. Rev. Rev B45 6534 (1992)

Summer School 24 Thessaloniki, July 15th, 2012

Confined energies calculation : simple method

4H-SiC / SF / 4H-SiC

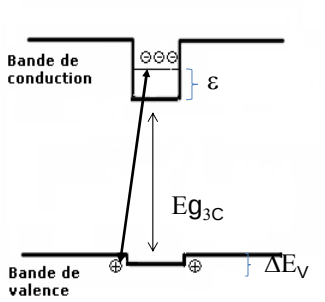

Simple model

Solve the Schrödinger equation in the envelope function approximation

V(z) = cte in the well

ε: confined energy of electrons

No electrical field $h\nu = Eg_{3C} + \varepsilon - \Delta E_V$

Summer School 25 Thessaloniki, July 15th, 2012

Confined energies calculation : simple method

4H-SiC / SF / 4H-SiC

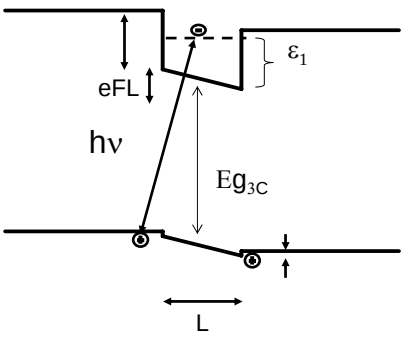

Simple model

Solve the Schrödinger equation in the envelope function approximation

V(z) = cte in the well

ε: confined energy of electrons

Taking into account about the electrical field

$$h\nu = Eg_{3C} + \varepsilon - \Delta E_F - eFL$$

Summer School 26 Thessaloniki, July 15th, 2012

Radiative recombination energies

4H-SiC / SF / 4H-SiC

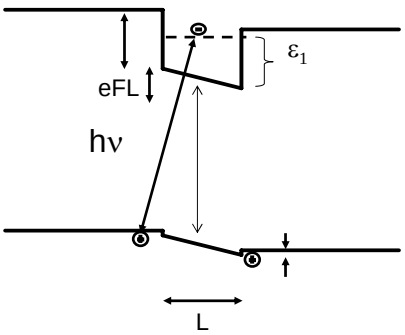

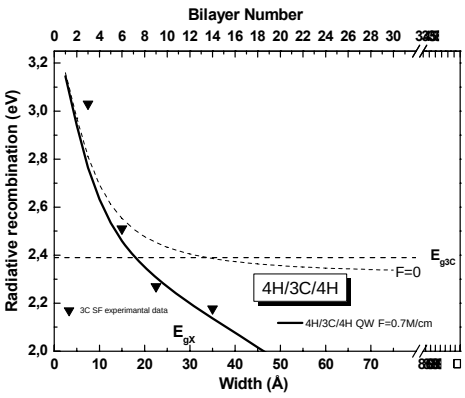

The electrical field is an adjust parameter

Using data from literature (PL and TEM data) to adjust F

F is below theoretical value (2,8MV/cm)

Summer School 27 Thessaloniki, July 15th, 2012

Matrix transfer method: Quantum well with Stark effect

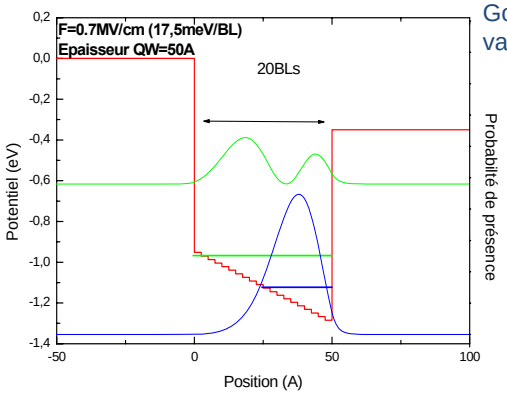

Goal: Taking into account about the variation of V(z) in the well

"cut" the QW in n parts with a constant potential in each.

Summer School 28 Thessaloniki, July 15th, 2012

Matrix transfer method: Quantum well with Stark effect

Wave function solution in the j region

$$\phi_j(z) = A_j \exp(ik_j z) + B_j \exp(-ik_j z)$$

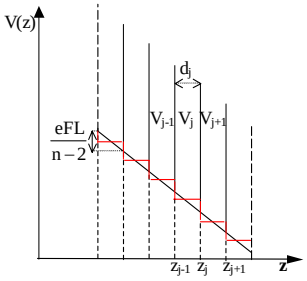

the boundaries conditions between j and j+1 regions

$$\begin{pmatrix} A_{j+1} \\ B_{j+1} \end{pmatrix} = M_j \begin{pmatrix} A_j \\ B_j \end{pmatrix}$$

For all regions:

$$\begin{pmatrix} A_n \\ B_n \end{pmatrix} = M_{n-1} M_{n-2} \ldots\ldots M_2 M_1 \begin{pmatrix} A_1 \\ B_1 \end{pmatrix} = \begin{pmatrix} M_{11} & M_{12} \\ M_{21} & M_{22} \end{pmatrix} \begin{pmatrix} A_1 \\ B_1 \end{pmatrix}$$

The confined energies of electrons :

$$M_{22}(E) = 0$$

Summer School 29 Thessaloniki, July 15th, 2012

Quantum well with Stark effect

4H-SiC / SF / 4H-SiC

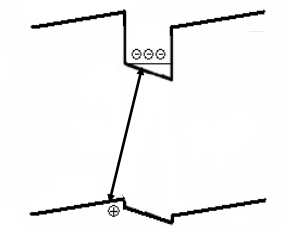

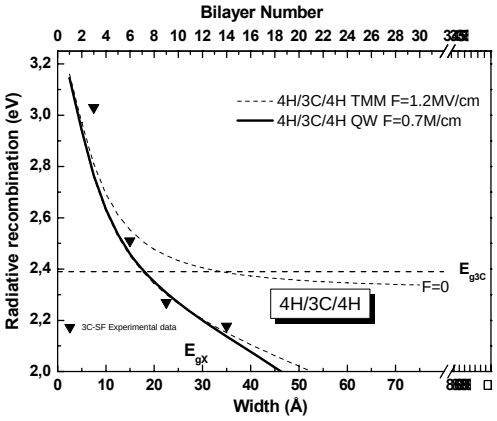

Summer School 30 Thessaloniki, July 15th, 2012

Quantum well with Stark effect

4H-SiC / SF / 4H-SiC

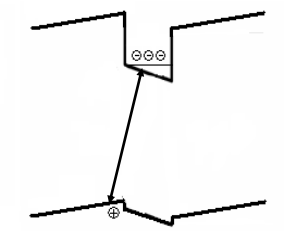

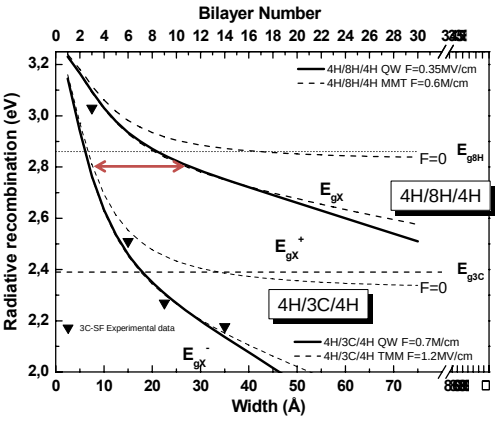

Problem :

SF Polytype ? → HR-TEM

thickness of the SF ?

Outline

- Photoluminescence: application to SiC
- Stacking faults
- Correlation PL-TEM-Calculation on 2 samples
  - Local investigations CL, Micro-PL
- Conclusion

Sample A: PL

A

4H-SiC sample
[N] = 10^{15} cm^{-3}

No 4H-SiC signature but a lot of SF signatures

Large energetic dispersion betwen 2.5 and 3 eV

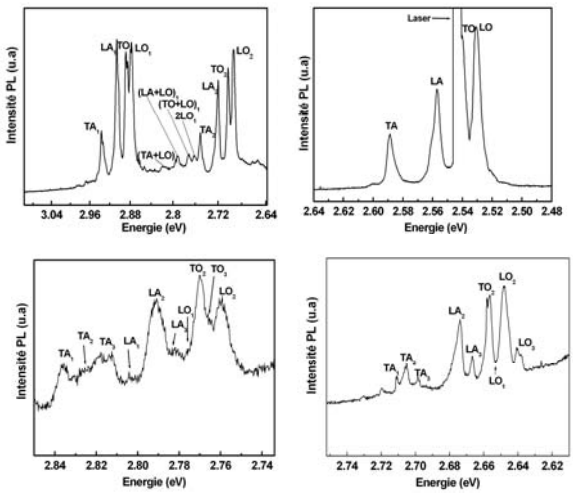

Egx(eV)	3.015	2.983	2.882	2.871	2.862	2.792	2.757	2.751	2.744	2.635	2.516

** T. Robert et al, Mater. Scie. Forum 645, 347 (2010)*

Sample A: HR-TEM

A

Defects made of a twisted arrangement of one or more threefold (+++) and (---) 3C-like lamellae in the Hägg notation, noticed SF(m) (m is an integer).

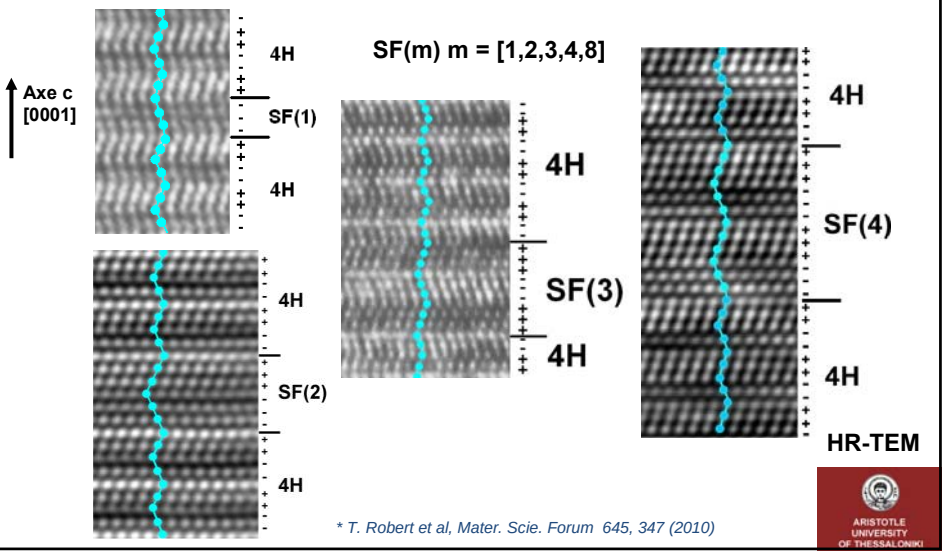

* T. Robert et al, Mater. Scie. Forum 645, 347 (2010)

Sample A: SF Calculation

A

Quantum well model: 4H/6H/4H and 4H/3C/4H

Corelation LTPL data with modelisation

SF lamellae

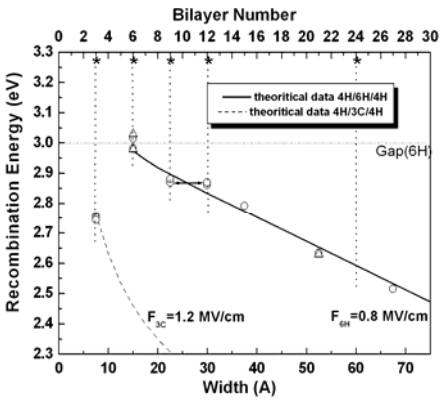

Optical signature (eV)	3.015	2.983	2.882	2.871	2.862	2.792	2.757	2.751	2.744	2.635	2.516
Lamella (SF(m))	SF(2)		SF(3)-SF(4)			SF(1)-SF(5)	SF(1)-SF(5)-SF(6)			SF(7)	SF(9)

* T. Robert et al, Mater. Scie. Forum 645, 347 (2010)

Summer School 35 Thessaloniki, July 15th, 2012 B

Sample B: PL

4H-SiC (0001) type n- grown by CVD thickness18mm

[N] = 10^{17} cm^{-3}

SF signature appear more or less intense, it depend on the position on the sample

SF signature : 2,672 eV

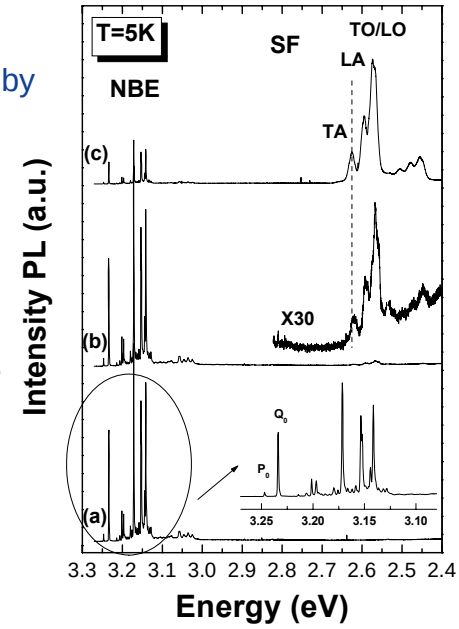

Summer School 36 Thessaloniki, July 15th, 2012 B

Sample B: HR-TEM

Low density of SF

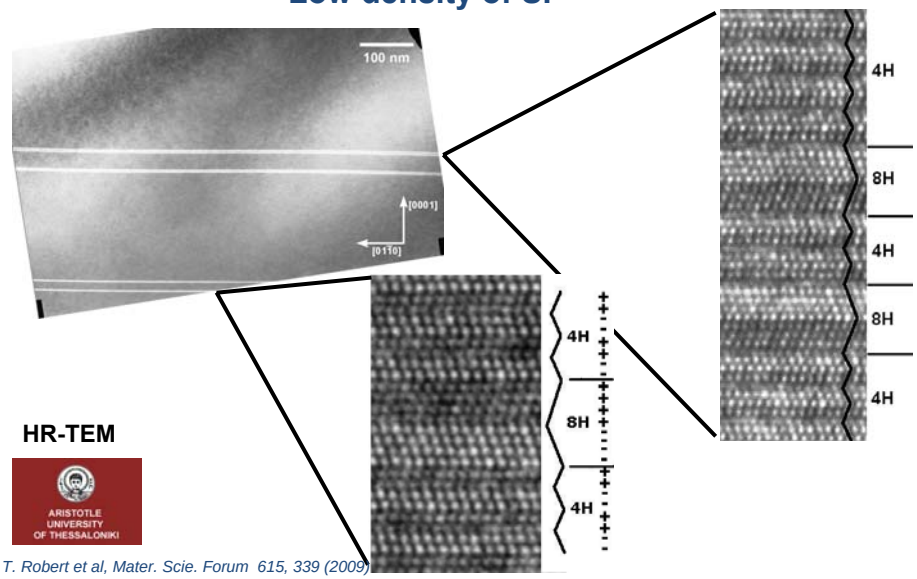

T. Robert et al, Mater. Scie. Forum 615, 339 (2009)

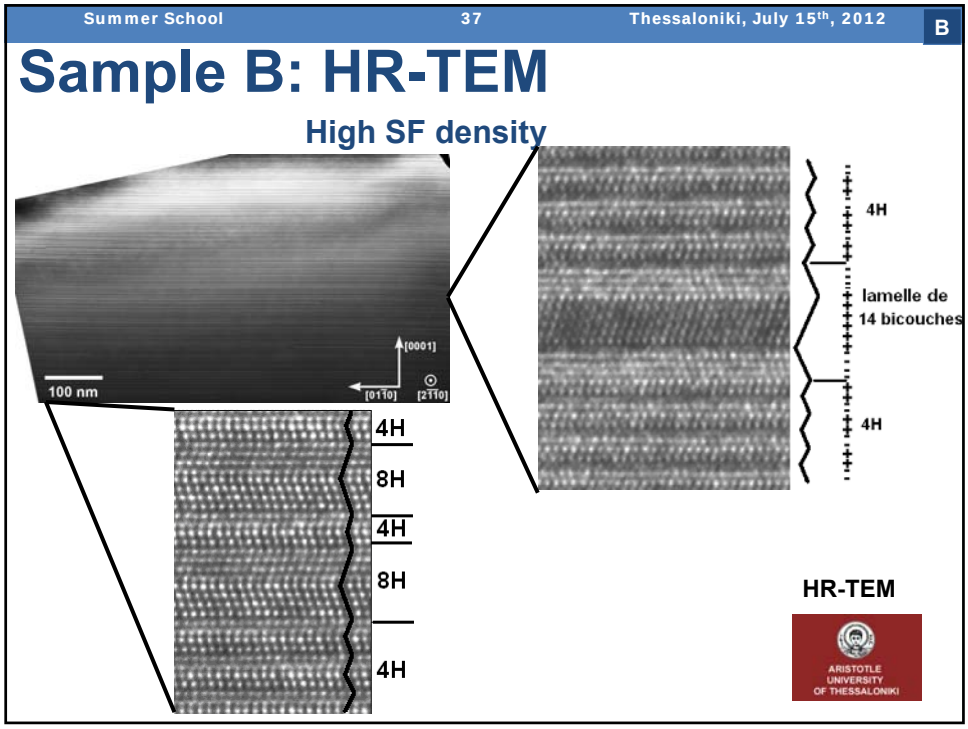
Summer School 37 Thessaloniki, July 15th, 2012 B
Sample B: HR-TEM
High SF density
100 nm
[0001]
[01$\bar{1}$0]
[2$\bar{1}\bar{1}$0]
4H
8H
4H
8H
4H
4H
lamelle de
14 bicouches
4H
HR-TEM
ARISTOTLE UNIVERSITY OF THESSALONIKI

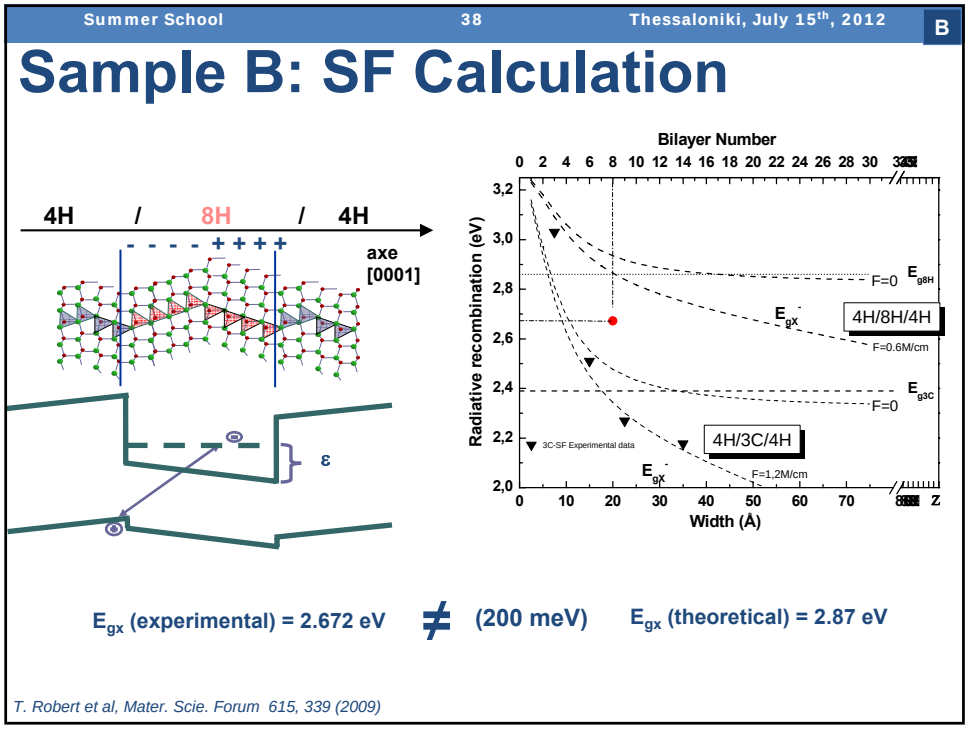
Summer School 38 Thessaloniki, July 15th, 2012 B
Sample B: SF Calculation
4H / 8H / 4H
axe [0001]
ε
Bilayer Number
Radiative recombination (eV)
Width (Å)
F=0
E_{g8H}
E_{gX}
4H/8H/4H
F=0.6M/cm
E_{g3C}
F=0
3C-SF Experimental data
4H/3C/4H
E_{gX}
F=1,2M/cm
E_{gx} (experimental) = 2.672 eV
≠
(200 meV)
E_{gx} (theoretical) = 2.87 eV
T. Robert et al, Mater. Scie. Forum 615, 339 (2009)

Summer School 39 Thessaloniki, July 15th, 2012 B

Sample B: SF Calculation

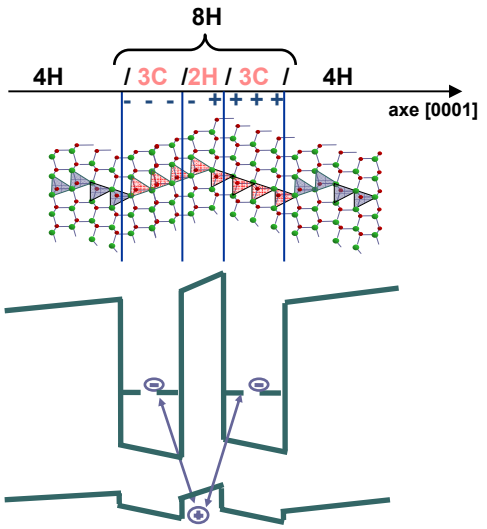

8H ≡ 3C / 2H/ 3C

The calculation (MMT)

E_{gx} (theoretical) = 2.68 eV

=

E_{gx} (experimental) = 2.672 eV

T. Robert et al, Mater. Scie. Forum 615, 339 (2009)

Summer School 40 Thessaloniki, July 15th, 2012

Outline

- Photoluminescence: application to SiC
- Stacking faults
- Correlation PL-TEM-Calculation on 2 samples
  - Local investigations CL, Micro-PL
- Conclusion

Summer School 41 Thessaloniki, July 15th, 2012 B

Local spectroscopy of SF

Sample B :

4H-SiC (0001) type n- grown by CVD
thickness18mm

Eg(SF)=2.672 eV
HR-TEM : 8H-SiC as SF

Cathodoluminescene
(*Montpellier and IKZ Berlin (LEA)*)

Micro-PL
(L2C Montpellier)

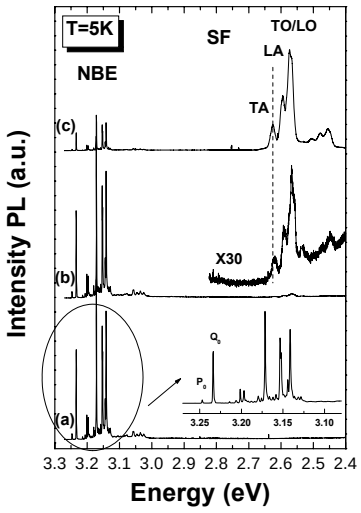

Summer School 42 Thessaloniki, July 15th, 2012 B

Cathodoluminescence

T=300K, Resolution 2μm

λ (SF) λ (NBE)

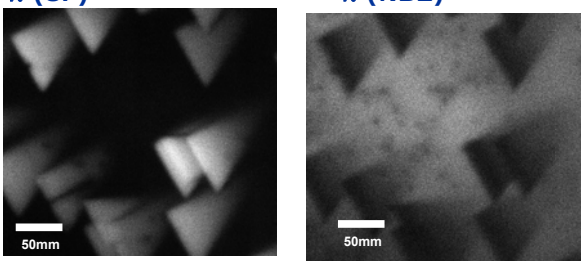

Focus on a zone with a Low density of defect

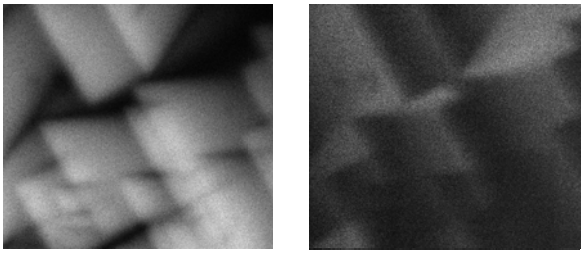

Focus on a zone with a high density of defect

Summer School 43 Thessaloniki, July 15th, 2012

8H SF in 4H-SiC

Fujiwara et al APL 87 051912 (2005)

N- epilayers 4H-SiC sample

PL signature : 2,56-2,7 eV

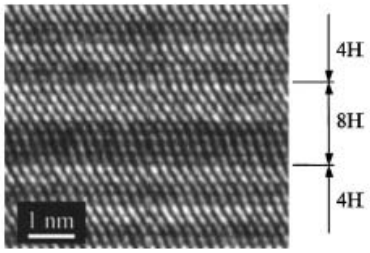

ross-sectional high-resolution TEM image of an in-grown stacking 4H–SiC epilayer.

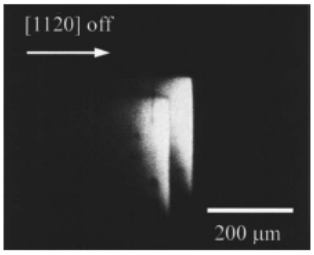

FIG. 1. Panchromatic CL image at room temperature taken from a 52-μm-thick 4H–SiC epilayer with stacking faults.

Summer School 44 Thessaloniki, July 15th, 2012

Cathodoluminescence

T=300K,

λ(SF) Resolution 2μm

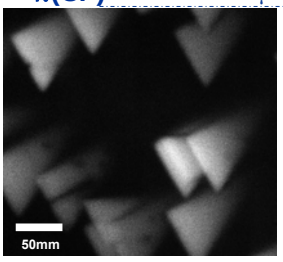

λ (NBE)

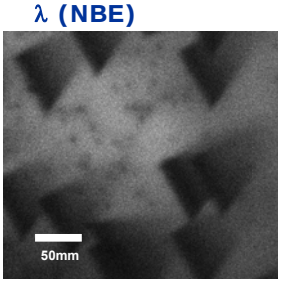

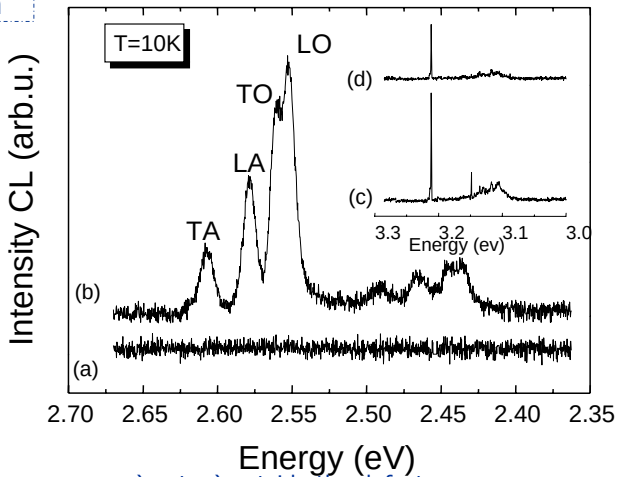

a) et c) outside the defect

b) et d) in the defect

Micro-PL

T=10K, Resolution 2μm
Constant Excitation power

SF emission

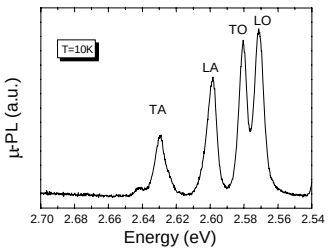

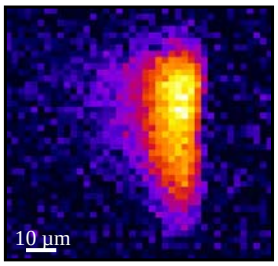

4H emission

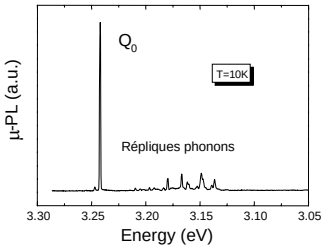

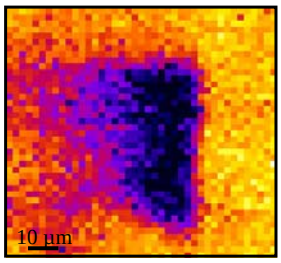

Micro-PL

T=10K, Resolution 2μm
Constant excitation Power

SF emission

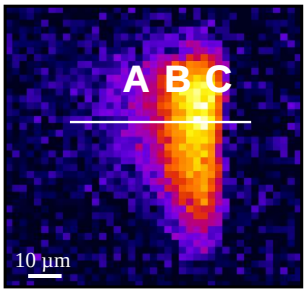

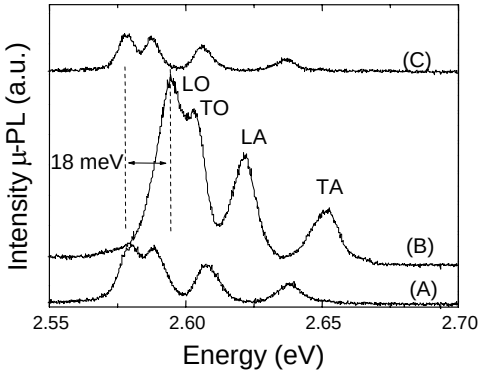

➡ Observation : blue shift at the SF center

A change on the hole-electron pairs and screening of the electrical field

Summer School 47 Thessaloniki, July 15th, 2012

Screening of the electrical field

Focus at the center of the SF , variation of the density of power excitation

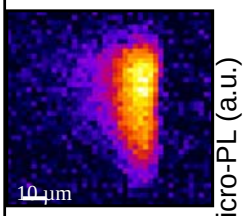

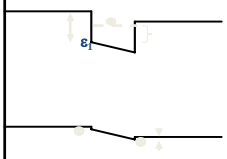

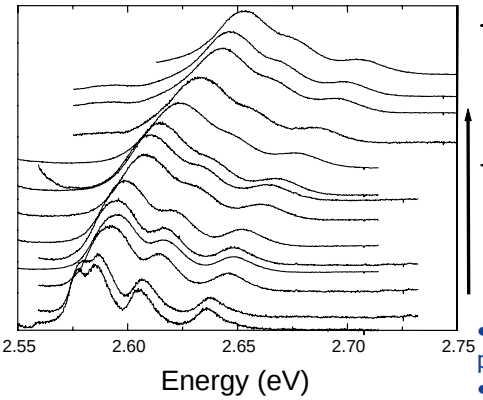

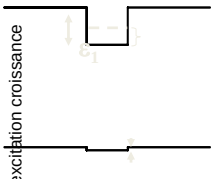

•Low excitation power
•No screening

•High excitation power
•Shift 70meV
• total screening ?

S.Juillaguet et al Mat. Science For. 556, 351 (2007)
S.Juillaguet et al Appl. Phys. Letters 90, 111902 (2007)

Summer School 48 Thessaloniki, July 15th, 2012

Screening of the electrical field

Focus at the center of the SF , variation of the density of power excitation

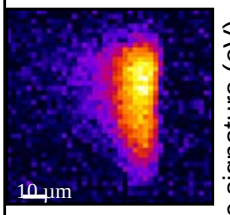

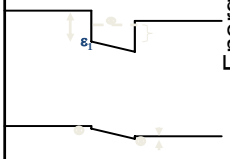

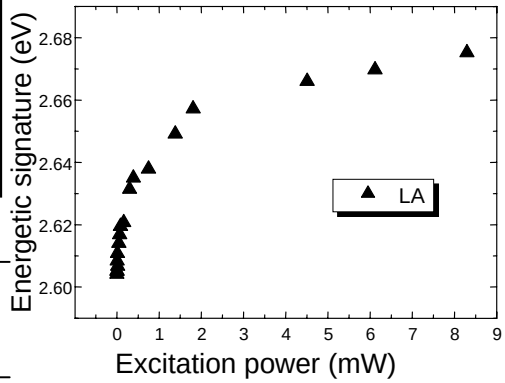

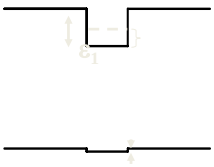

•Low excitation power
•No screening

•High excitation power
•Shift 70meV
• total screening ?

S.Juillaguet et al Mat. Science For. 556, 351 (2007)
S.Juillaguet et al Appl. Phys. Letters 90, 111902 (2007)

Summer School 49 Thessaloniki, July 15th, 2012

Micro PL on 6H lamella (sample A)

Microphotoluminescence (10K)

(λ) 4H

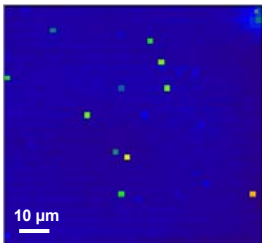

(λ) 6H Lamella

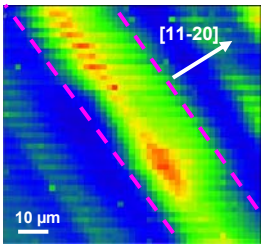

Low signature of 4H

No screening
Why?
High density of SF
Large dispersion of energetic signatures

Summer School 50 Thessaloniki, July 15th, 2012

Summarize ….

Polytype	Formation mechanism	Thickness	Optical signature	Measurement	Ref
3C-MQW	MBE growth	2.3nm	E_{gF}=2.27 eV (6K)	TEM, PL	**a, b**
3C	as grown	3SSF(14,2)	E_{gF}=2.177 eV (2K)	HR-TEM	**c**
3C	n^+ as grown + annealing	1SSF(3.1) 2SSF(6,2)	E_{gF}=3.03 eV (2K) E_{gF}=2.504 eV (1.8K)	HR-TEM, PL	**d-i**
3C	Compressive stress	2SSF(6,2)	BPD : 1.8 eV (77K)	HR-TEM, CL	**j**
3C	oxydation	7BLs (7,1)	E_{gF}=2.604 eV (300K)	HR-TEM, CL	**k, l**
8H	as grown (0001)	8 BLs (4,4)	Broad peak 2.56 – 2.7 eV	HR-TEM, CL	**l**
8H	**as grown** **(11-20)**	**8BLs (4,4)**	**2.62-2.68 eV** **E_{gF}=2.7232eV (9K)**	**HR-TEM** **PL**	**m**

J. Camassel et al J Phys. D. 40, 6267 (2007)

Outline

- Photoluminescence: application to SiC
- Stacking faults
- Correlation PL-TEM-Calculation on 2 samples
  - Local investigations CL, Micro-PL
- Conclusion

Conclusion

- Observation of SF optical signature by photoluminescence, cathodoluminescence and micro photoluminescence
- Model by QW
- Correlation with Optical measurements ad HR-TEM are necessary

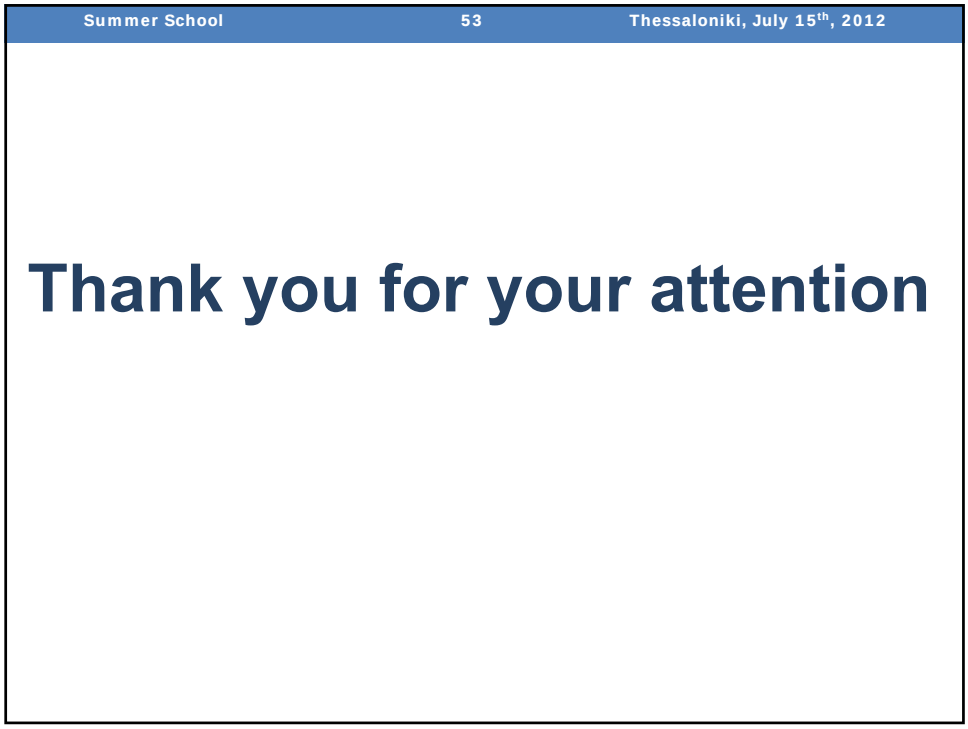
Summer School 53 Thessaloniki, July 15th, 2012
Thank you for your attention

Nanoscience at Silicon Carbide and Epitaxial Graphene using Scanning Tunneling Microscopy *(electrons/photons)*

Patrick Soukiassian - Πατριψκ Σοθκιασσιαν
Commissariat à l'Energie Atomique et aux Energies Alternatives, Saclay
and Université de Paris-Sud, Orsay, France



Summer School on Micro- and Nano-structural Characterization of Materials
July 11 – 15, 2012, Thessaloniki, Greece

Where are we coming from ?

What were the 1st "active" electronic components ?

The 1st Triode tube "Audion"

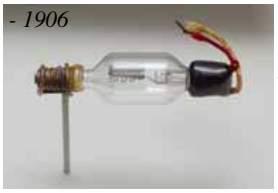

"Vacuum" approach

Patent sold to RCA

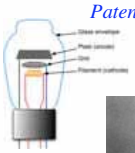

Lee De Forest

The 1st Transistor (based on Ge, not Si)

"Solid State" approach

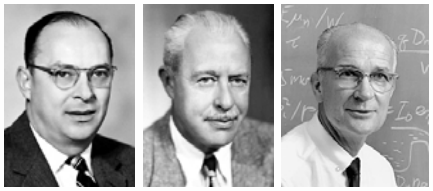

Bardeen Brattain Shockley
1956 Physics Nobel Prize Laureates

P. Soukiassian

Where are we?

Electronics Road Map

Number of Transistors per Microprocessor:
≈ 6 orders magnitude increase in 36 years

Intel:
1971 : 4004 : 2 300 transistors
1978 : 8086 : 29 000 transistors
1982 : 80286 : 275 000 transistors
1989 : 80486 : 1.16 millions transistors
1993 : Pentium : 3.1 millions transistors
1995 : Pentium Pro : 5.5 millions transistors
1997 : Pentium II : 27 millions transistors
2001 : Pentium 4 : 42 millions transistors
2004 : Pentium Extreme Edition : 169 millions transistors
2006 : Core 2 Duo : 291 millions transistors
2006 : Core 2 Quad : 582 millions transistors
2007 : Dual-Core Itanium 2 : 1.9 billion transistors

Others:
2006 : G80 (NVIDIA) : 681 millions transistors
2007 : POWER6 (IBM) : 291 millions transistors
2008 : GT200 (NVIDIA) : 1.4 billion transistors
2008 : RV770 (ATI) : 965 millions transistors

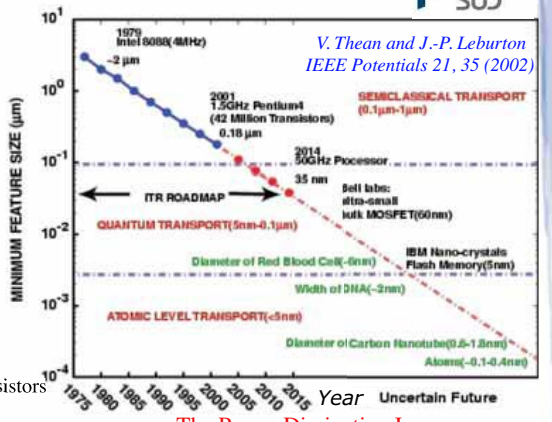

The Power Dissipation Issue

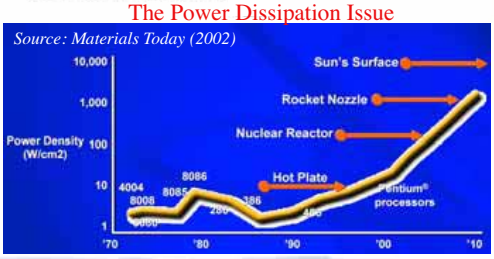

P. Soukiassian

Computer Speed *vs* Synchrotron Radiation Brilliance

Electrons vs Photons

***Moore's Law:* Integration density should double every 18 months**

Graphene on SiC wafer

SiC wafer

Diamond

Si wafer

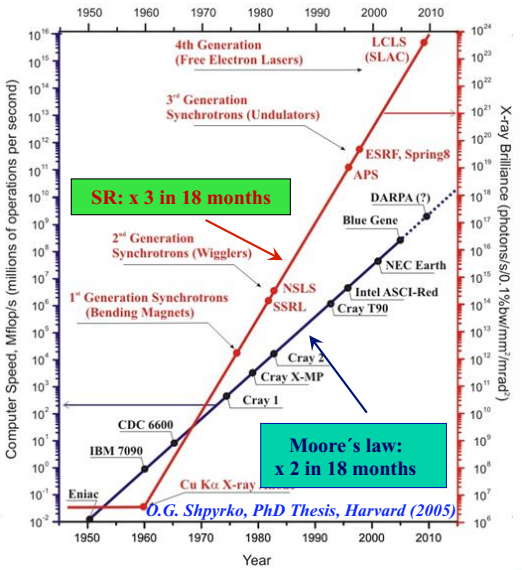

P. Soukiassian

Toward Smaller Objects: Why ?

- The number of information that needs to be stored or processed is increasing Dramatically !
- The transistor was discovered more than 65 years ago by
- So one has to increase the integration density ⟶ i.e.to built smaller objects
- Nano-Objects that not only need to be passive, but also active
- Today Billions transistors produced per year ! NOT ENOUGH ……
- Microelectronic Road Map up to ≈ 2015/2016 according to Moore's law: density of integration has to double every 18 months

How to do this ?

- the Top/Bottom or Bottom/Up Approach: 0 D, 1 D or 2 D Nano-Objects ?

P. Soukiassian

Toward Smaller Objects: How ?

- But we are reaching **fundamental limits**:
  1 - *Our ability to fabricate smaller e.g. with lithography using electrons/photons*
  2 - *At small scales, temperature becomes a Major problem because evacuating calories is a "challenge"*

- So, other approaches are necessary, like the **Bottom-Up** approach, e.g. starting from the elemental atom and built a desired pattern

- Also, one has to keep in mind that, at the atomic scale, the physical properties are very different

P. Soukiassian

Surface: What is this ?

Surface ⟶ *Single Crystal Material*

- It is the "interface" between a "bulk" material and the vacuum
- It is where everything "starts" or "ends"
- Controlling the Surface could favor a "reaction" (catalysis) with an adsorbate or prevent such a reaction to occur (passivation)
- Langmuir (Chemistry Nobel Prize in 1923) is the pionneer in Surface Science
- Understanding the structure of surfaces was initiated by diffraction techniques such as Low Energy Electron Diffraction (LEED) and other diffraction techniques
- The atomic structure of a surface differs from the bulk ⟶ Reconstruction

P. Soukiassian

What are the Tools that helped to make a Breakthrough at the bottom, i.e. at the atomic scale ?

- Near Field Scanning Tunneling and Force Microscopies – *STM, STS, AFM, Photoemission STM*
  Binning and Roher, 1986 Physics Nobel Laureates
- Transmission and Scanning Electron Microscopies – *TEM, SEM*
  Ruska, 1986 Physics Nobel Laureate
- Photoelectron Spectroscopies and X-rays Diffraction especially using Synchrotron Radiation related techniques
  Bloembergen, Schawlow and Siegbahn, 1981 Physics Nobel Laureates
- Theory using *ab-initio* approaches as e.g. Local Density Functional Theory (LDF)
  Kohn and Pople, 1998 Chemistry Nobel Laureate

P. Soukiassian

Scanning Tunneling Microscopy

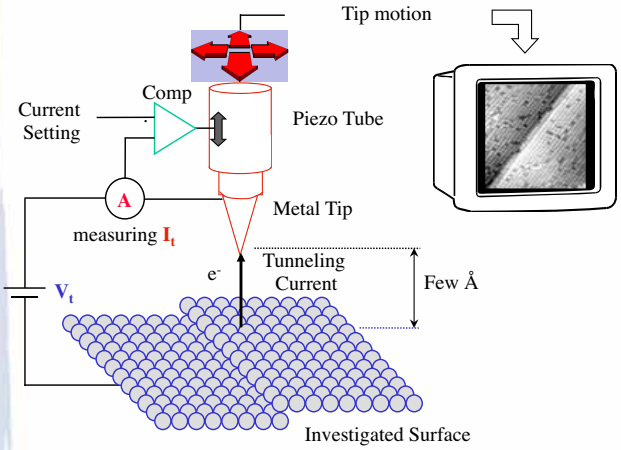

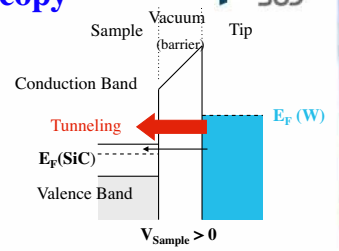

Empty Electronic States

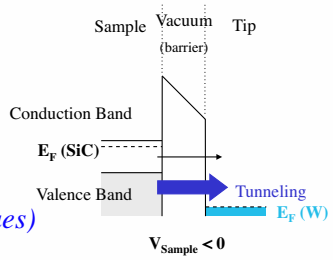

Filled Electronic States

STM is real space probe (unlike diffraction techniques)

- **But:** What you "see" with a STM is not necessarily what you "get" !
- **Why?** Because you "see" atoms trough their electronic properties

P. Soukiassian

Average Factors of Merit of Some Semiconductors

Si	GaAs	GaN	SiC	C (diamond)
1	1.5	≤ 500	≤ 1000	≤ 10,000

Main Advantages of SiC:

- Advanced Microelectronic Devices & Sensors
- Ceramic
- Very Inert Chemically
- Interesting Mechanical Properties (*hardness, composite materials*)
- Biocompatible
- Resistant to Radiation Damages (*suitable for hostile environments, e.g. in fuel rods for 3rd generation nuclear reactors*)
- Large high quality single crystal wafer
- Same native oxide as Si: SiO_2

High speed logic devices

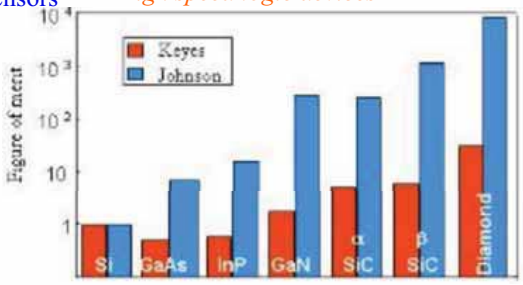

High power/high temperature devices

SiC is a IV-IV compound Wide Band Gap semiconductor (from 2.4 eV to 3.3 eV)
SiC has more than + 170 polytypes:
Hexagonal phase (α-SiC) 6H-SiC, 4H-SiC …. - Cubic phase (β-SiC) 3C-SiC
Stress/Strain driven surface structure: Lattice mismatch: -20% (*Si*) & +22% (*diamond*)

P. Soukiassian

Microwave characteristics of BARITT Diodes

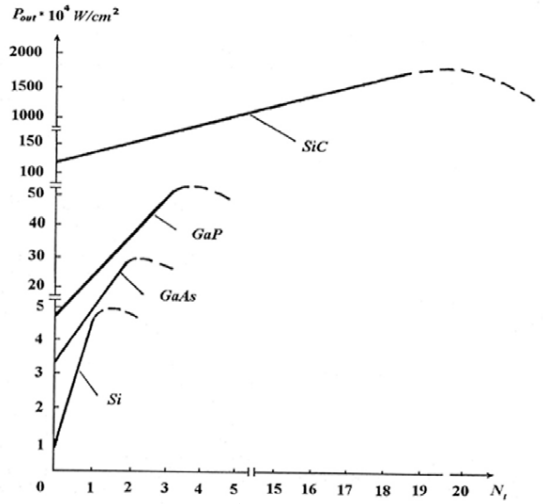

• *Aroutiounian, Buniatyan, Soukiassian,* ***Sol. Stat. Electronics 43****, 343 (1999)*
and ***IEEE Trans. on Electron Devices 46, Special Issue on SiC****, 585 (1999)*
• *Buniatyan, Aroutiounian in "Wide Band Gap Semiconductor: Present Status, Future Prospects and Frontiers"*
J. Phys D: Applied Physics 40*, 6355-6385 (2007)*

Yerevan State University — *P. Soukiassian*

Benefits of SiC in Microelectronics

Aeronautics

High Temperature Sensors and Control Electronics

- *weight savings*
- *increased performances*
- *increased reliability*

Energy

- *High Power Electronic Devices*
- *Energy Saving in Power Distribution*

Space


Ariane 5 - Kourou


Huygens: Titan


Soyouz - ISS

- *Reduction of spacecraft launch weights*
- *Satellite functional capacities increase*
- *Radiation resistant electronics*


Hubble: Nébuleuse de l'Aigle


Hubble: Galaxies Collision

Automobile and Transportation

- *High Temperature Sensors/Electronics*
- *Power Devices* • *Hybrid Cars*

better combustion monitoring and control

Communications and Radar

- *High Power Microwave Devices*


MOSFET Thales

P. Soukiassian

Outline

- **3C-SiC(100) Surfaces Reconstructions: from Si-rich to C-rich**
- **Massively Parallel Si Atomic Lines at SiC surfaces**
  - *including atomic lines imaged using "**photons**"*
- **From a Passive to an Active Massively Parallel Architecture**
  - *Negative differential resistance at Ag/Si nanowires*
- ***sp3* "*diamond-like*" SiC Surface Transformation**
- **Atomic Fracture at 6H and 3C Silicon Carbide Surfaces**
- **Nanochemistry at 3C-SiC(100) 3x2 and 6H-SiC(0001) 3x3 Surfaces**
  - *the 1st example of H/D-induced semiconductor surface metallization*
  - *Atomic scale initial O_2 interaction on Si-Rich SiC surfaces*
- ***sp2* SiC transformation: Epitaxial Graphene**
  - *Morphology and Electronic Properties*
  - *CNT and cracks defects at Graphene/SiC interfaces*
- **Manipulating Atoms and Molecules using STM**

Experimental Tools:

- ***Atom-resolved scanning tunneling microscopy & spectroscopy (electrons/photons)***
- *Synchrotron radiation-based photoelectron diffraction and spectroscopy*
- *Synchrotron radiation-based grazing incidence X-ray diffraction*

P. Soukiassian

Cubic Silicon Carbide: 3C-SiC(100)

- **Only 1 cubic polytype**
- **Zinc-blende structure**

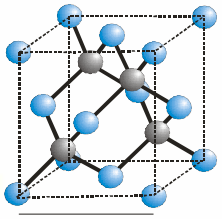

3C-SiC(100) thin film grown by CVD on a Si(100) wafer

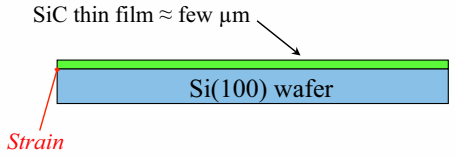

- The 3C-SiC(100) surface is polar unlike elementary group IV semiconductors
- In the [001] direction, stacking of **alternating C and Si planes**

→ (100) surface → C-rich surface
→ C-terminated surface
→ Si-terminated surface
→ Si-rich surface

→ **Existence of numerous different reconstructions**
(~ 10 in a 200°C temperature range)

P. Soukiassian

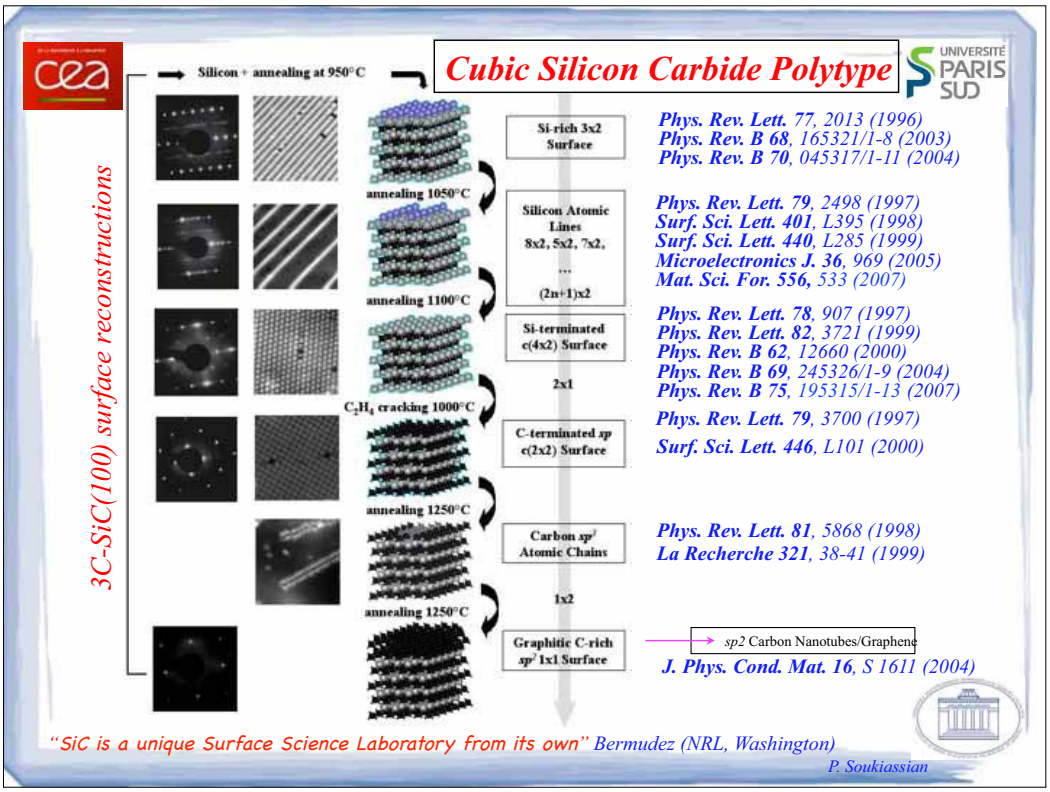
Cubic Silicon Carbide Polytype
UNIVERSITÉ PARIS SUD
3C-SiC(100) surface reconstructions
Silicon + annealing at 950°C
annealing 1050°C
annealing 1100°C
C_2H_4 cracking 1000°C
annealing 1250°C
annealing 1250°C
Si-rich 3x2 Surface
Silicon Atomic Lines 8x2, 5x2, 7x2, ... (2n+1)x2
Si-terminated c(4x2) Surface
2x1
C-terminated sp c(2x2) Surface
Carbon sp² Atomic Chains
1x2
Graphitic C-rich sp² 1x1 Surface
sp2 Carbon Nanotubes/Graphene
Phys. Rev. Lett. 77, 2013 (1996)
Phys. Rev. B 68, 165321/1-8 (2003)
Phys. Rev. B 70, 045317/1-11 (2004)
Phys. Rev. Lett. 79, 2498 (1997)
Surf. Sci. Lett. 401, L395 (1998)
Surf. Sci. Lett. 440, L285 (1999)
Microelectronics J. 36, 969 (2005)
Mat. Sci. For. 556, 533 (2007)
Phys. Rev. Lett. 78, 907 (1997)
Phys. Rev. Lett. 82, 3721 (1999)
Phys. Rev. B 62, 12660 (2000)
Phys. Rev. B 69, 245326/1-9 (2004)
Phys. Rev. B 75, 195315/1-13 (2007)
Phys. Rev. Lett. 79, 3700 (1997)
Surf. Sci. Lett. 446, L101 (2000)
Phys. Rev. Lett. 81, 5868 (1998)
La Recherche 321, 38-41 (1999)
J. Phys. Cond. Mat. 16, S 1611 (2004)
"SiC is a unique Surface Science Laboratory from its own" Bermudez (NRL, Washington)
P. Soukiassian

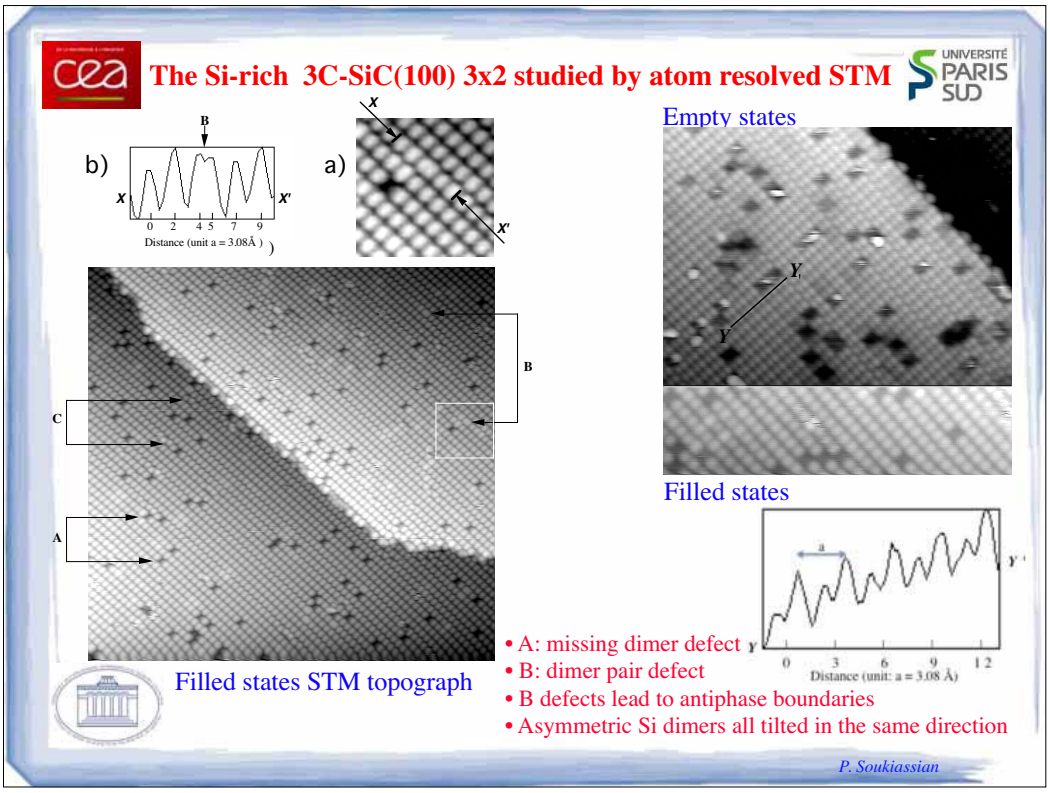
The Si-rich 3C-SiC(100) 3x2 studied by atom resolved STM
UNIVERSITÉ PARIS SUD
b)
a)
Distance (unit a = 3.08Å)
Empty states
Filled states
Filled states STM topograph
Distance (unit: a = 3.08 Å)
• A: missing dimer defect
• B: dimer pair defect
• B defects lead to antiphase boundaries
• Asymmetric Si dimers all tilted in the same direction
P. Soukiassian

Si-rich 3C-SiC(100)3x2 Structure by STM, GIX-Ray & Photoelectron Diffraction

Alternately Long & Short Dimers ALDS-TAADM Model

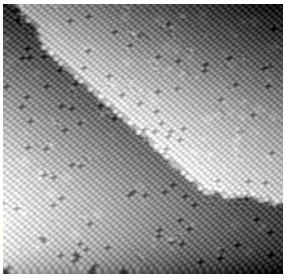

500 Å x 500 Å

1st layer
- A_U : up atom
- A_D : down atom

2nd layer
- D_L: long dimer
- D_S: short dimer

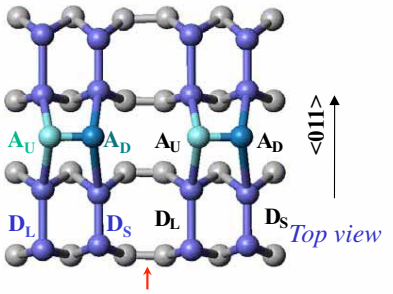

Top view

Si-Si dimer in the 3rd plane

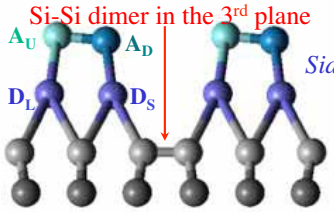

Side view

- *Complex Structure*
- *Strain Driven*

1st Si layer (1/3 ML) →
2nd Si layer (2/3 ML) →
3rd Si layer (1 ML) →
C layer →

*Semond, Soukiassian, Douillard, Mayne, Dujardin, Jaussaud, **Phys. Rev. Lett. 76**, 2013 (1996)*
*Lu, Krüger, Pollman, **Phys. Rev. B 60**, 2495 (1999) (theory)*
*Enriquez, D'angelo, Aristov, Derycke, Soukiassian, Renaud, Barbier, Semond, **J. Vac. Sci. Technol. B 21**, 1881 (2003)*
*D'angelo, Enriquez, Aristov, Soukiassian, Renaud, Barbier, Noblet, Chiang, Semond, **Phys. Rev. B 68**, 165321 (2003)*
*Tejeda, Dunham, García de Abajo, Denlinger, Rotenberg, Garcia-Michel, Soukiassian, **Phys. Rev. B 70**, 045317 (2004)*

P. Soukiassian

The Si-terminated 3C-SiC(100) c(4x2) surface studied by atom resolved STM

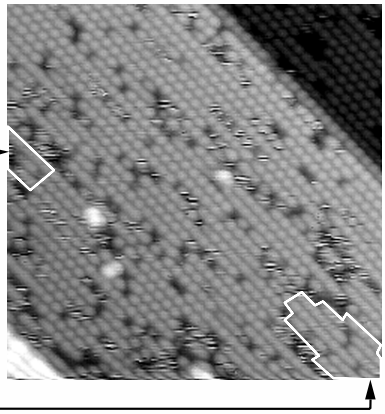

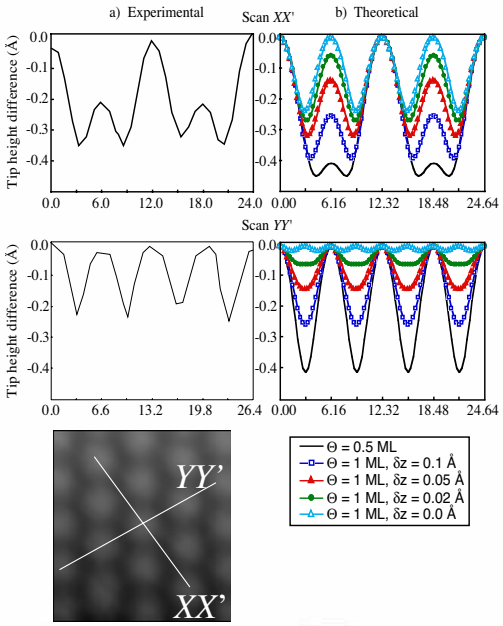

- Si-Si dimer rows having alternating heights
- Defects/contamination leads to a 2x1 array: dimers are coming at the same height

P. Soukiassian

Imaging the down dimers of 3C-SiC(100) c(4x2) by empty states STM topographs

Up-Dimer ○ Down-Dimer ●

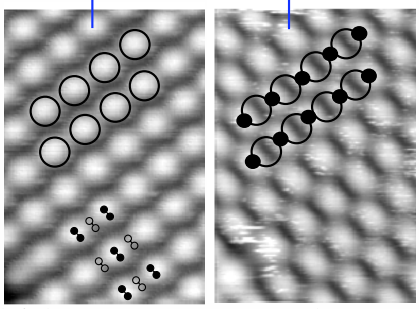

Filled Electronic States *Empty Electronic States*

Experimental STM topographs

P. Soukiassian

Si-terminated 3C-SiC(100) c(4x2) Surface by STM, PES, Theory & PED

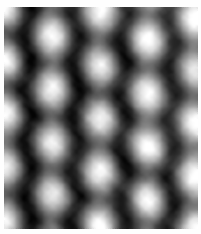

Experimental STM Topograph

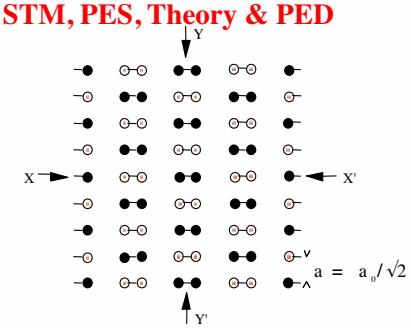

Up Si-Si Dimers

Down Si-Si Dimers

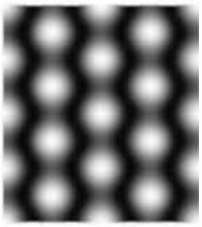

Calculated STM Image

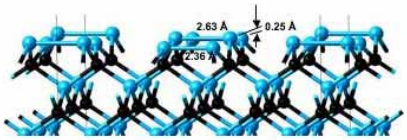

3% strain

Materials Design

- Alternately Up- and Down Dimers (AUDD) Rows
- Alternate lengths: Up/Long - Down/Short
- the AUDD array reduces the surface strain
- No c(4x2) & No AUDD without 3% strain

Soukiassian, Semond, Douillard, Mayne, Dujardin, Pizzagalli, Joachim, ***Phys. Rev. Lett. 78****, 907 (1997)*
Soukiassian, Aristov, Douillard, Semond, Mayne, Dujardin, Pizzagalli, Joachim, Delley, Wimmer ***Phys. Rev. Lett. 82****, 3721 (1999)*
Aristov, Enriquez, Derycke, Soukiassian, Le Lay, Grupp, Taleb-Ibrahimi, ***Phys. Rev. B 60****, 16553 (1999)*
Derycke, Fonteneau, Soukiassian, ***Phys. Rev. B 62****, 12660 (2000)*
Aristov, Soukiassian, Catellani, di Felice, Galli, ***Phys. Rev. B 69****, 245326 (2004)*
Tejeda, Wimmer, Soukiassian, Dunham, Denlinger, Rotenberg, Michel, ***Phys. Rev. B 75****, 195315 (2007)*

P. Soukiassian

Temperature-induced Semiconducting c(4x2) to Metallic 2x1 Reversible Phase Transition of Si-terminated 3C-SiC(100) surface

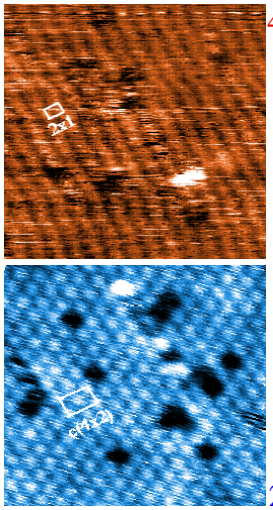

STS

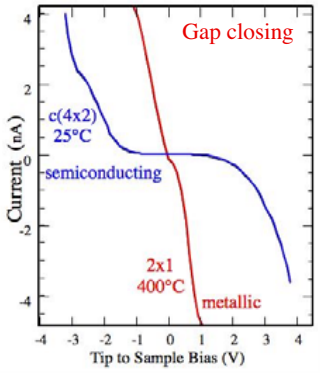

UV Photoemission

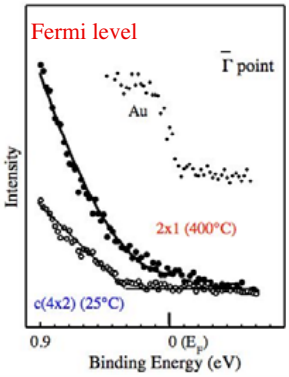

Non Fermi liquid behavior

25°C

*Aristov, Douillard, Fauchoux, Soukiassian, **Phys. Rev. Lett. 79**, 3700 (1997)*
*Enriquez, Derycke, Aristov, Soukiassian, Le Lay, Cricenti, Crotti, Ferrari, Perfetti **Appl. Surf. Sci. 162**, 559 (2000)*
*Soukiassian, Enriquez, **J. Phys. Cond. Mat. 16**, S 1611 - 1658 (2004)*

P. Soukiassian

From Single/Isolated- to Massively Parallel Atomic Lines

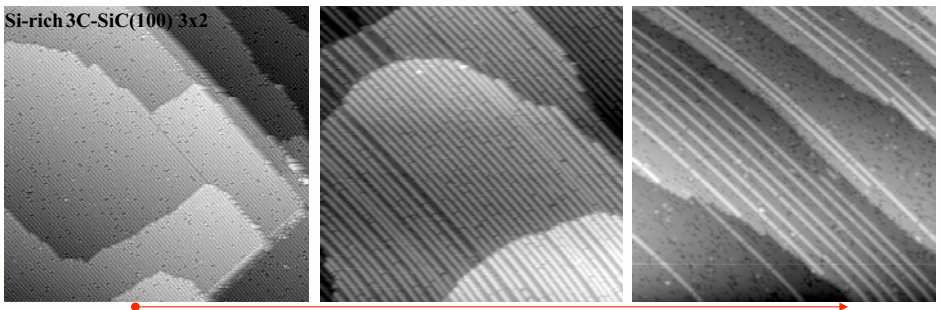

Annealings
@ ≈ 1150°C

800Å x 800Å

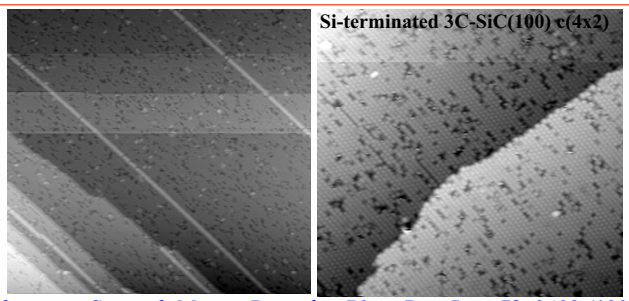

*Soukiassian, Semond, Mayne, Dujardin, **Phys. Rev. Lett. 79**, 2498 (1997)*

P. Soukiassian

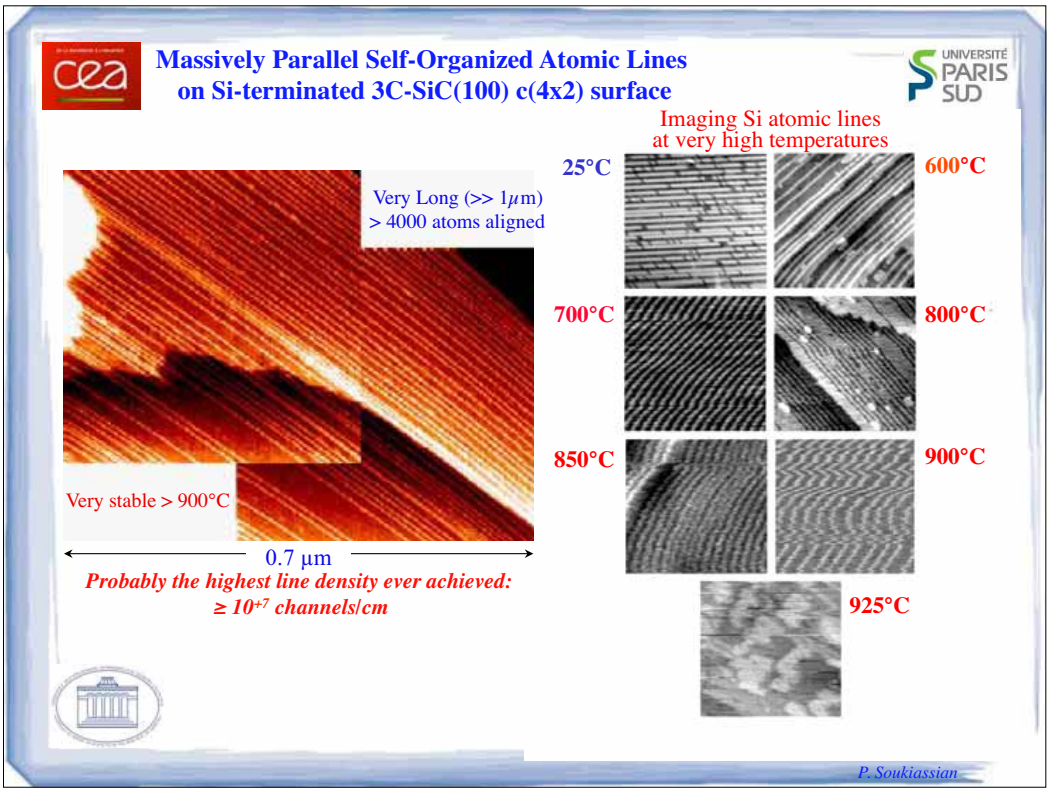
Massively Parallel Self-Organized Atomic Lines
on Si-terminated 3C-SiC(100) c(4x2) surface
UNIVERSITÉ PARIS SUD
Imaging Si atomic lines
at very high temperatures
25°C
600°C
700°C
800°C
850°C
900°C
925°C
Very Long (>> 1μm)
> 4000 atoms aligned
Very stable > 900°C
0.7 μm
Probably the highest line density ever achieved:
≥ 10+7 channels/cm
P. Soukiassian

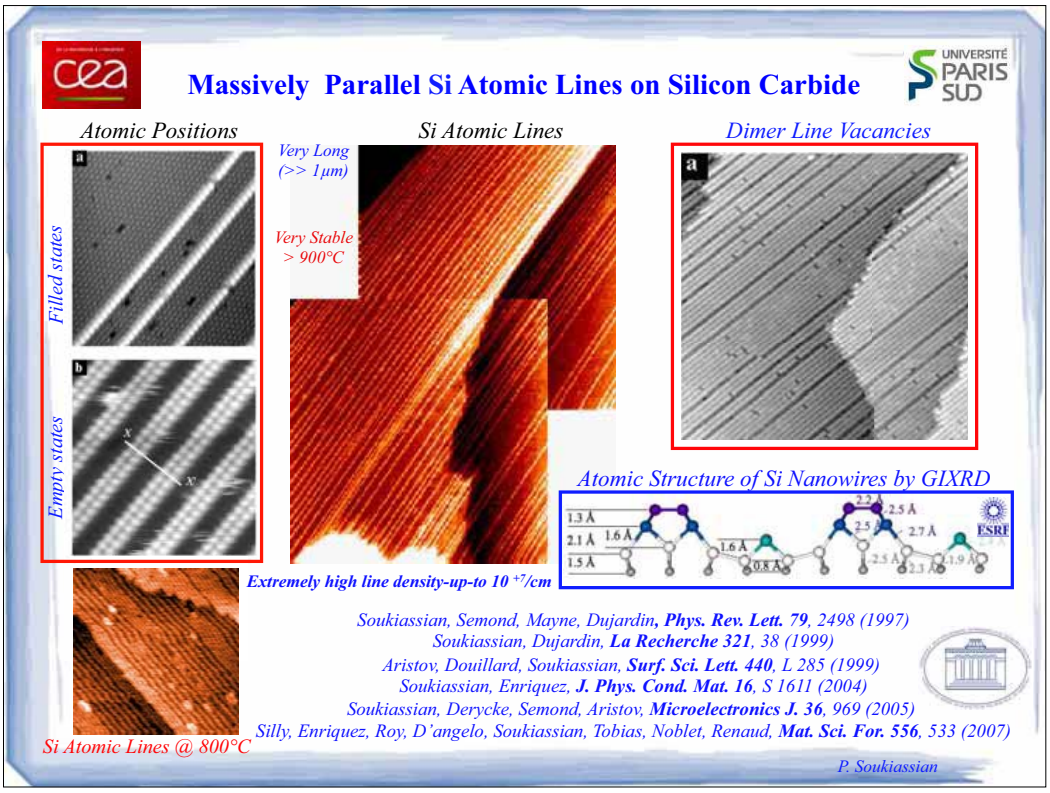
Massively Parallel Si Atomic Lines on Silicon Carbide
UNIVERSITÉ PARIS SUD
Atomic Positions
Si Atomic Lines
Dimer Line Vacancies
Filled states
Empty states
Very Long
(>> 1μm)
Very Stable
> 900°C
Atomic Structure of Si Nanowires by GIXRD
ESRF
Extremely high line density-up-to 10 +7/cm
Si Atomic Lines @ 800°C
Soukiassian, Semond, Mayne, Dujardin, Phys. Rev. Lett. 79, 2498 (1997)
Soukiassian, Dujardin, La Recherche 321, 38 (1999)
Aristov, Douillard, Soukiassian, Surf. Sci. Lett. 440, L 285 (1999)
Soukiassian, Enriquez, J. Phys. Cond. Mat. 16, S 1611 (2004)
Soukiassian, Derycke, Semond, Aristov, Microelectronics J. 36, 969 (2005)
Silly, Enriquez, Roy, D'angelo, Soukiassian, Tobias, Noblet, Renaud, Mat. Sci. For. 556, 533 (2007)
P. Soukiassian

20 L of H_2/Si atomic lines

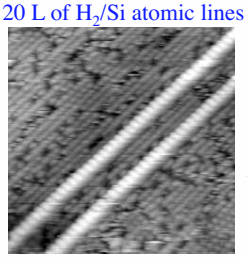

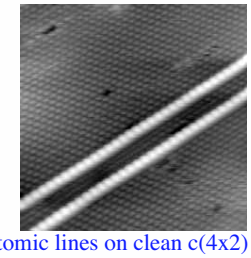

Si atomic lines on clean c(4x2) surface

- **Si atomic lines are not affected by hydrogen**
- **Allows to built Si atomic lines on H-passivated surface**

Derycke, Fonteneau, Pham, Soukiassian,
***Phys. Rev. B 63, Rap. Com.**, R 201305 (2001)*

Nb Ohmic Contact

Niobium Comb (lithography)

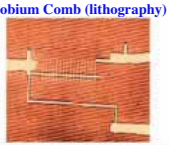

Branches: length 20 µm, width 200 nm, spacing 2 µm

10 µm x 10 µm

15 nm x 15 nm

Soukiassian, Derycke, Semond, Aristov
***Microelectronics J. 36**, 969 (2005)*

Device of the late 80's/early 90's

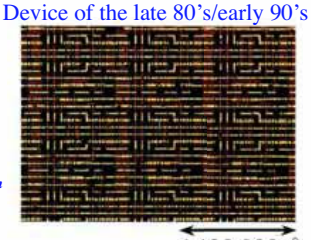

1.000.000 Å

Si atomic lines 100 Å

Surface 10^{-8} smaller !
Soukiassian, Dujardin
***La Recherche 321**, 38 (1999)*

P. Soukiassian

Negative Differential Resistance at Ag/Si Nanowires on SiC: From Passive to Active Massively Parallel Architecture

- Esaki discovered Negative Differential Resistance (NDR) known as the "Esaki-Diode" - microscopic scale
- Other examples of DNR at smaller scale (molecules, dopant)

Si atomic lines on β-SiC(100) | Ag-Si nanowires on β-SiC(100)

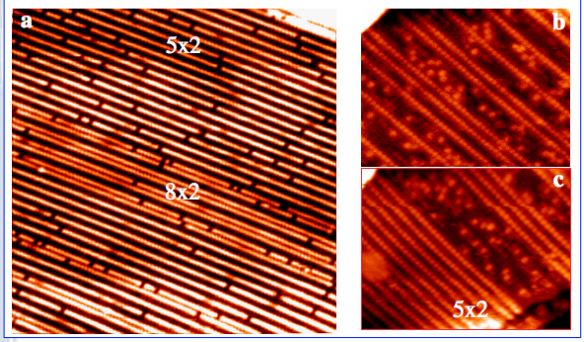

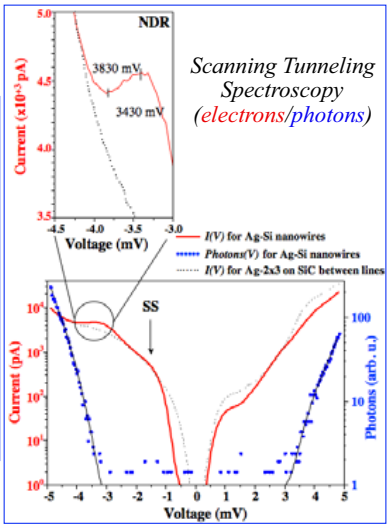

Scanning Tunneling Spectroscopy (electrons/photons)

- covering Si Nanolines by Ag atoms leads to Ag/Si nanowires
- exhibit a NDR behavior - from passive to active connectivity
- New surface state SS at Ag/Si nanowires yields to Double Tunnel Barrier

P. Soukiassian

Network of Massively Parallel of Ag/Si Nanowires having a NDR Behavior

Negative Differential Resistance

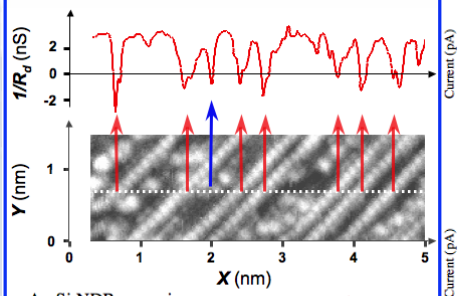

Scanning Tunneling Spectroscopy *I(V)* around E_F

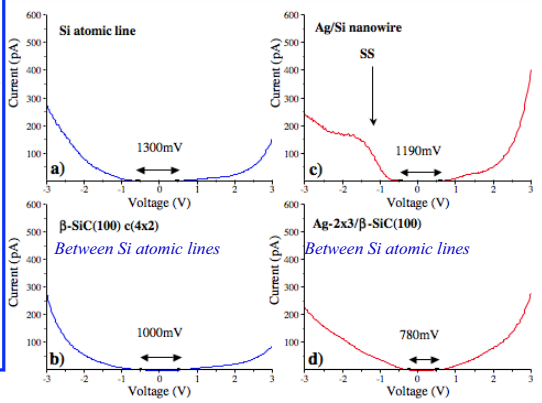

Potentially very interesting for TeraHertz Applications

Surface State SS ≈ 1eV below E_F specific of the Ag/Si nanowires

Silly, Charra, Soukiassian, ***Appl. Phys. Lett. 91****, 223111 (2007)*
D'angelo, Aristov, Soukiassian, ***Phys. Rev. B 76****, 045304 (2007)*

P. Soukiassian

The C-terminated 3C-SiC(100) c(2x2) Surface Structure

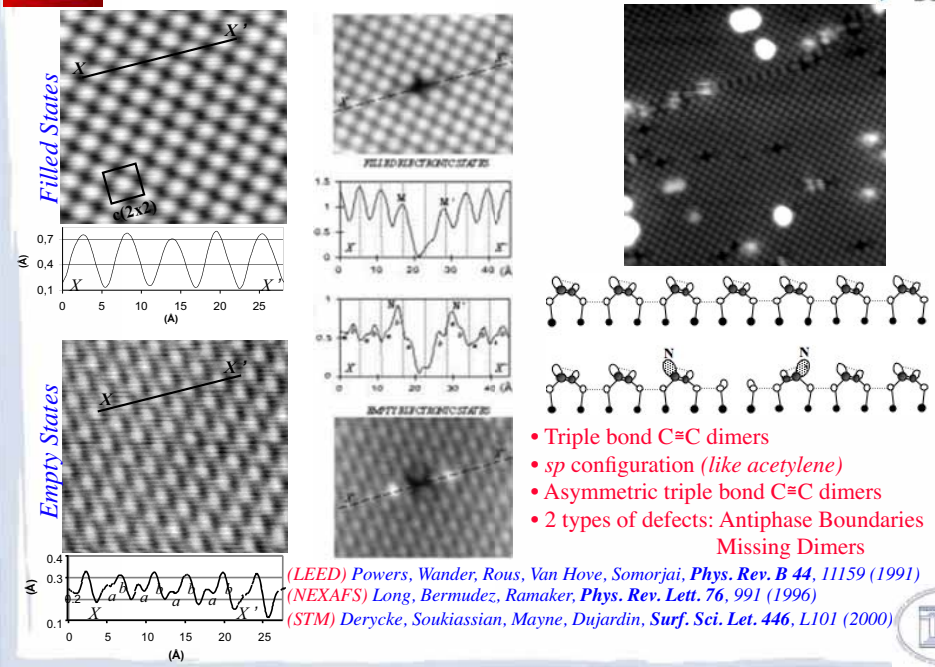

- Triple bond C≡C dimers
- *sp* configuration *(like acetylene)*
- Asymmetric triple bond C≡C dimers
- 2 types of defects: Antiphase Boundaries
  Missing Dimers

(LEED) Powers, Wander, Rous, Van Hove, Somorjai, ***Phys. Rev. B 44****, 11159 (1991)*
(NEXAFS) Long, Bermudez, Ramaker, ***Phys. Rev. Lett. 76****, 991 (1996)*
(STM) Derycke, Soukiassian, Mayne, Dujardin, ***Surf. Sci. Let. 446****, L101 (2000)*

P. Soukiassian

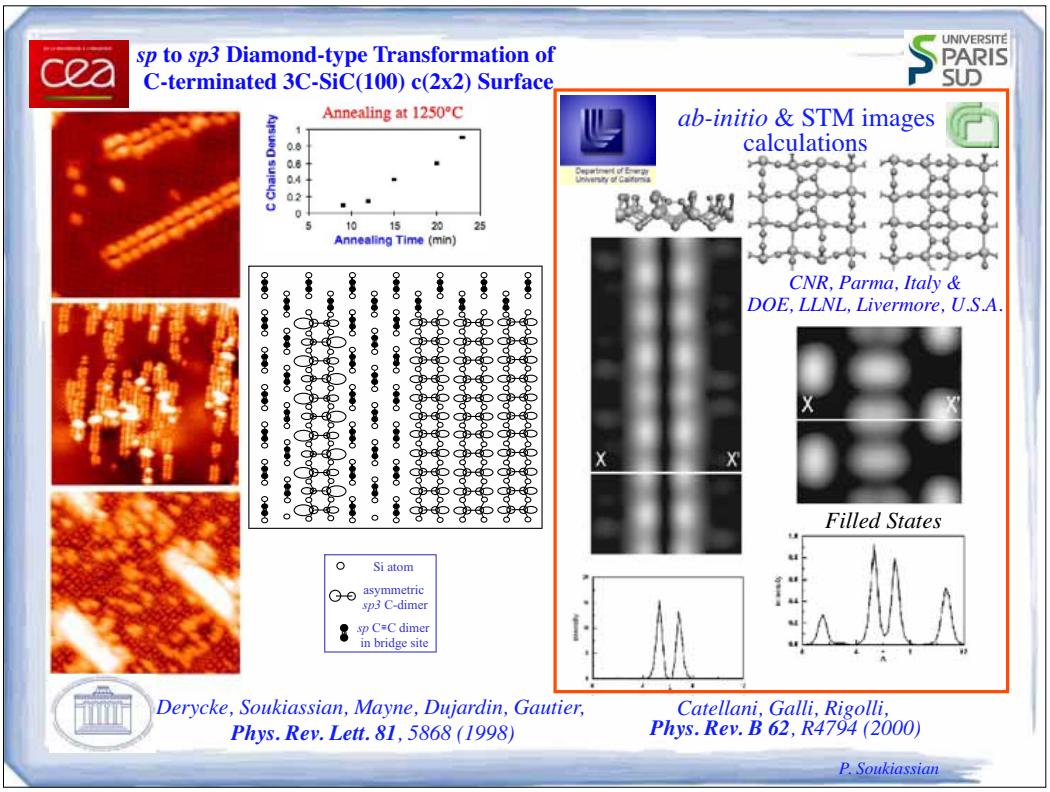
sp to sp3 Diamond-type Transformation of
C-terminated 3C-SiC(100) c(2x2) Surface
Annealing at 1250°C
C Chains Density
Annealing Time (min)
Si atom
asymmetric sp3 C-dimer
sp C≡C dimer in bridge site
ab-initio & STM images calculations
CNR, Parma, Italy &
DOE, LLNL, Livermore, U.S.A.
Filled States
Derycke, Soukiassian, Mayne, Dujardin, Gautier,
Phys. Rev. Lett. 81, 5868 (1998)
Catellani, Galli, Rigolli,
Phys. Rev. B 62, R4794 (2000)
P. Soukiassian


Fractures of Materials
Strong fundamental interest
Crucial importance in metals, concrete, glasses, semiconductors ….
• Mechanical engineering • Civil engineering • Geology & earth science • MEMS
• Nanofabrication • Aerospace industry • Automotive industry • Nuclear industry
Cracks at Kilauea Volcano
Crater Edge, Hawai
Cracks at glass surface
20 nm
Cracks at Al alloy surface
100 µm
Ice breaking Ienessi delta near Artic Ocean, Siberia
East Africa Afar Rift
Nanometers
Micrometers
10's Meters
10's Kilometers
1000's Kilometers
C is a "strained" material: Exploring possible fracture formation
P. Soukiassian

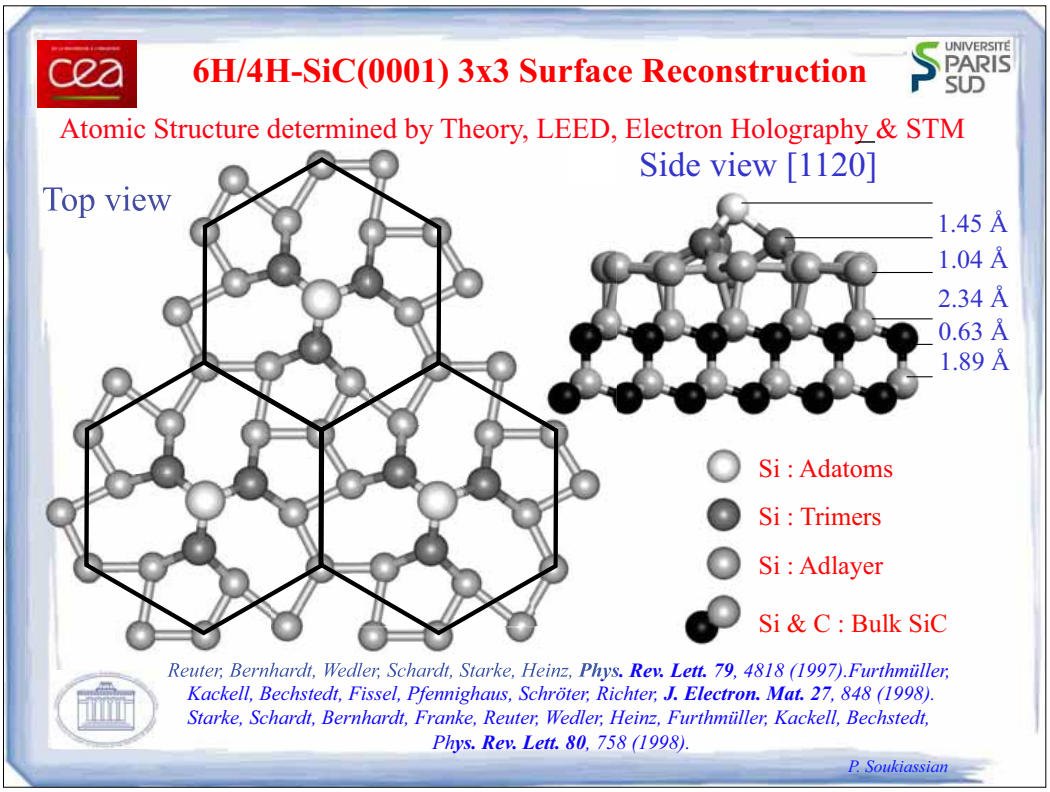
6H/4H-SiC(0001) 3x3 Surface Reconstruction
Atomic Structure determined by Theory, LEED, Electron Holography & STM
Top view
Side view [1120]
1.45 Å
1.04 Å
2.34 Å
0.63 Å
1.89 Å
Si : Adatoms
Si : Trimers
Si : Adlayer
Si & C : Bulk SiC
Reuter, Bernhardt, Wedler, Schardt, Starke, Heinz, Phys. Rev. Lett. 79, 4818 (1997).Furthmüller, Kackell, Bechstedt, Fissel, Pfennighaus, Schröter, Richter, J. Electron. Mat. 27, 848 (1998). Starke, Schardt, Bernhardt, Franke, Reuter, Wedler, Heinz, Furthmüller, Kackell, Bechstedt, Phys. Rev. Lett. 80, 758 (1998).
P. Soukiassian

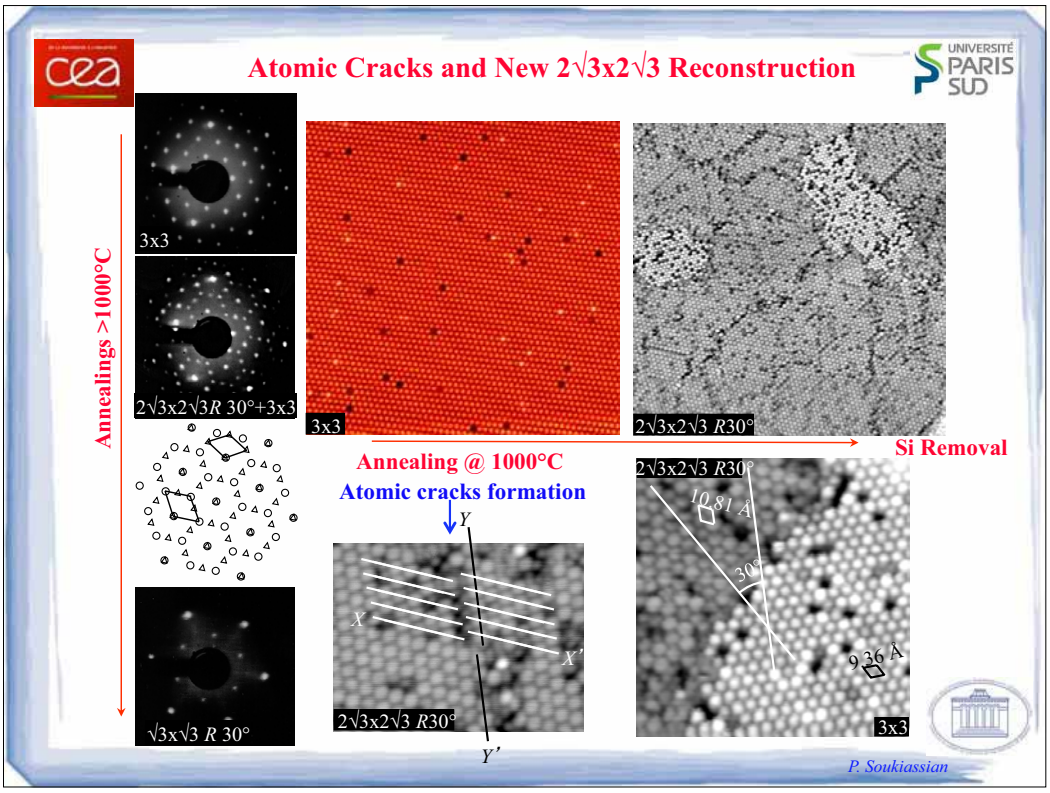
Atomic Cracks and New 2√3x2√3 Reconstruction
Annealings >1000°C
3x3
2√3x2√3R 30°+3x3
√3x√3 R 30°
3x3
2√3x2√3 R30°
Annealing @ 1000°C
Atomic cracks formation
Si Removal
2√3x2√3 R30°
10.81 Å
30°
9.36 Å
3x3
Y
X
X'
Y'
2√3x2√3 R30°
P. Soukiassian

Model of the 2√3x2√3 Surface Reconstruction

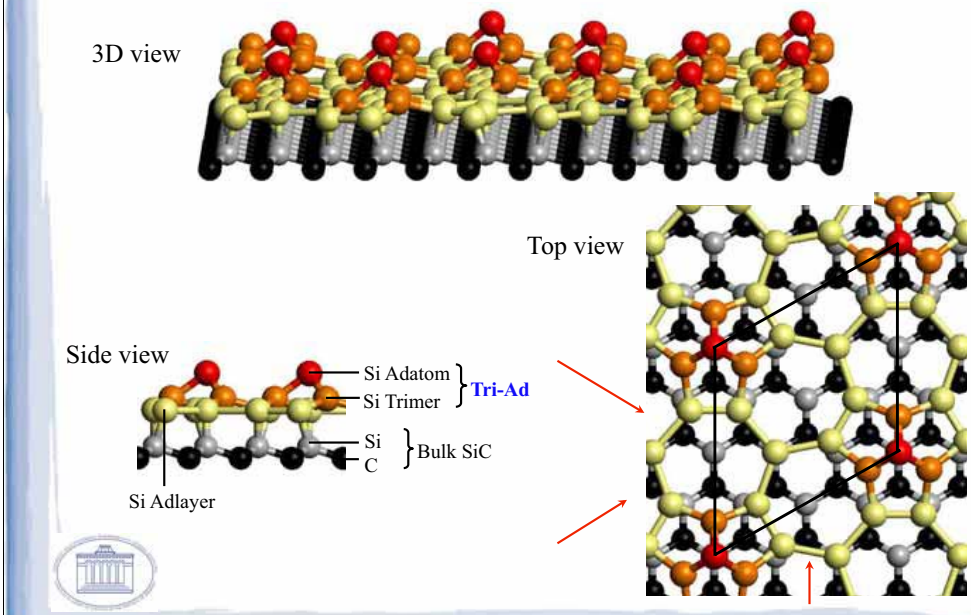

P. Soukiassian

Atomic Cracks *vs* Macroscopic One's

Cracks on Silicon Carbide

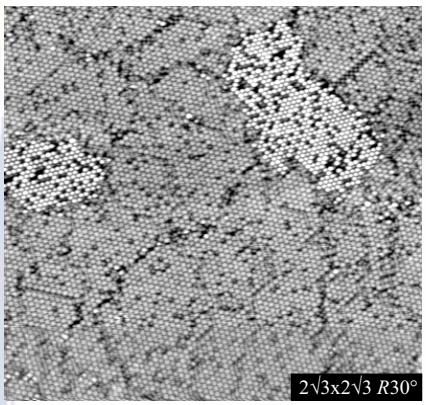

Ice breaking in artic region at spring:
Ienessi river delta near Artic Ocean, Siberia

≈ 12 orders of magnitude difference !

Amy, Soukiassian, Brylinski,
***Appl. Phys. Lett. 85**, 926 (2004)*

Renshaw, Schulson,
***Nature 412**, 897 (2001)*

P. Soukiassian

3C-SiC(100) Surface Morphology by LEEM

- 1x1 LEED - Graphitic
- Faceting and mesa formation
- Cracks are visible
- Brittle to ductile transition upon temperature

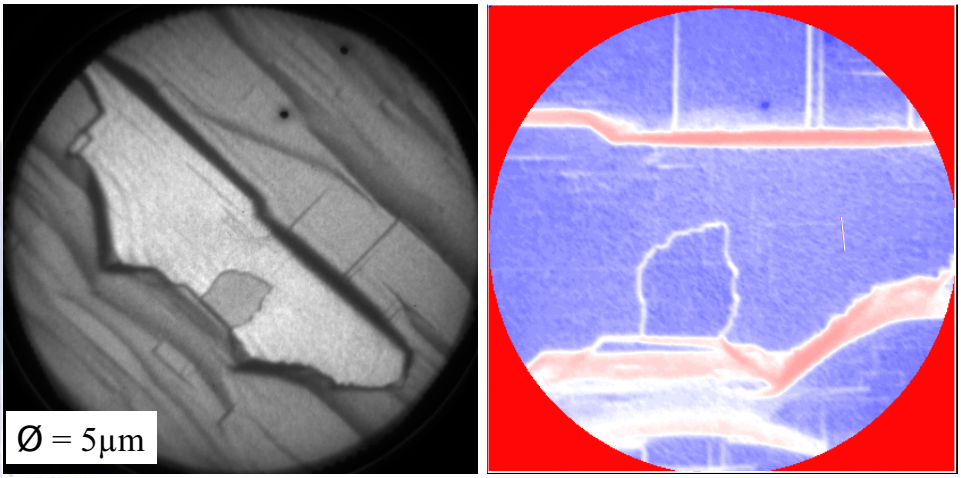

Soukiassian, Amy, Brylinski, Mentes, Locatelli, ***Mat. Sci. For.*** **556**, 481 (2007)

P. Soukiassian

Atomic cracks at 6H-SiC(0001) 2√3x2√3 Surface Reconstruction

- At 3x3 to √3x√3 phase transition: new 2√3x2√3 reconstruction
- 2√3x2√3 always coexists with the 3x3 reconstruction
- Atomic structure based on Trimer + Ad-Atom (**Tri-Ad**) clusters, as for 3x3 surface, but with a lower density
- Cracks originate in the Si atomic plane (stressed plane) and likely propagate in the C atomic plane (streched plane) located below the surface
- suggests that the **Tri-Ad** clusters tend to "stabilize" the surface
- **Tri-Ad** density decrease leads to charge redistribution, inter-atomic bond weakening and subsequent bond breaking - Result in atomic crack formation
- Brittle to ductile temperature-induce transition
- Surface faceting and mesa formation on cubic SiC
- these crack defects are likely highly relevant in the " high density of interface states" observed at SiO_2/6H-SiC(0001) interfaces

Amy, Soukiassian, Brylinski, ***Appl. Phys. Lett. 85****, 926 (2004)*
Soukiassian, Amy, Brylinski, Mentes, Locatelli, ***Mat. Sci. For.****,* **556**, 481 (2007)

P. Soukiassian

Nanochemistry at SiC surfaces and Interfaces

• Selective molecular hydrogen interaction on 3C-SiC surfaces

• Hydrogen atom-induced 3C-SiC surface metallization
The 1st example of H-induced semiconductor surface metallization

• Atomic scale oxidation of the Si-rich
3C-SiC(100) 3x2 and 6H-SiC(0001) 3x3 surfaces
Where & how the first O_2 molecules/atoms react with the surface ?

Experimental Tools
• Atom-resolved scanning tunneling microscopy & spectroscopy
• Synchrotron radiation-based photoelectron spectroscopies
• Infrared absorption spectroscopy

P. Soukiassian

Molecular H_2 interaction 3C-SiC(100) 3x2 and c(4x2) Reconstruction

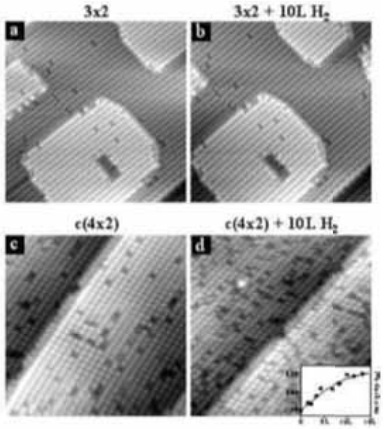

Scanning Tunneling Microscopy

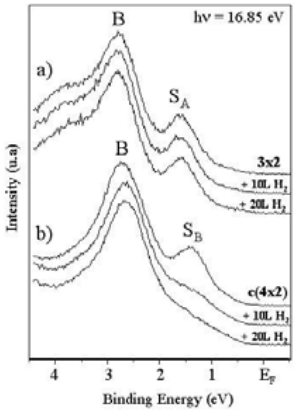

Valence Band Photoemission

• Si-rich 3C-SiC(100) 3x2 surface remains inert to molecular H_2
• In contrast, H_2 is highly reactive (dissociation) with Si-terminated 3C-SiC(100) c(4x2) and very high sticking probabilities, 10^{+8} higher than for Si surfaces
• H atom termination of Si dangling bonds leads to a 2x1 surface transformation

Derycke, Fonteneau, Pham, Soukiassian, ***Phys. Rev. B 63, RC****, R 201305 (2001)*

P. Soukiassian

H-induced 3C-SiC(100) 3x2 Surface Metallization

Scanning Tunneling Microscopy

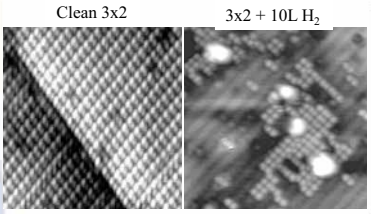

Photoemission Spectroscopy

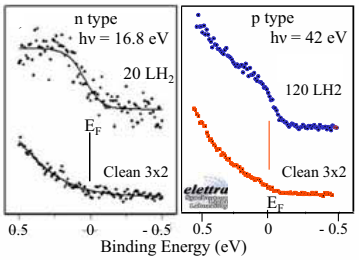

Upon H interaction

- S surface state quenched
- H-terminating top surface Si dangling bonds
- Fermi level build-up
- New surface state at E_F
- Band Gap Opening

Scanning Tunneling Spectroscopy

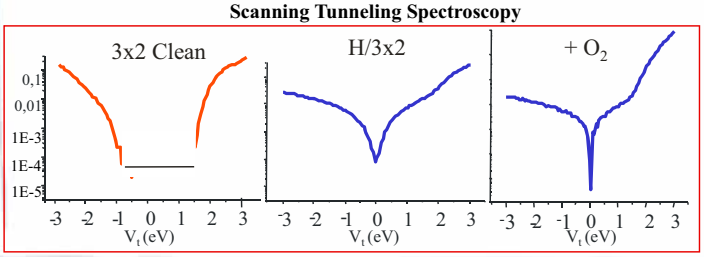

P. Soukiassian

Hydrogen interaction with a SiC surface

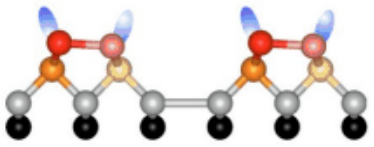

- H atoms bond to top surface dangling bonds (1st plane)
- Weakening of the back bonds
- Asymmetric attack on Si-dimer in 3rd plane
- H atom bonds to one of the Si atoms
- Lead to charge transfer
- **Metallization**

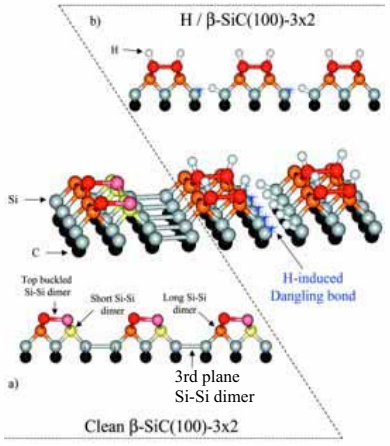

1st Example of H-induced semiconductor surface metallization

H atoms interact at & below the SiC surface

Derycke, Soukiassian, Amy, Chabal, D'angelo, Enriquez, Silly, ***Nature Materials 2****, 253 (2003)*
http://www.nature.com/nmat
Amy, Chabal, ***J. Chem. Phys. 119****, 6201 (2003)*
Silly, Radtke, Enriquez, Soukiassian, Gardonio, Moras, Perfetti, ***Appl. Phys. Lett. 85****, 4893 (2004)*
Soukiassian, ***Appl. Phys. A 86****, Special Issue on Surface Physics, 421 (2006)*
Roy, Aristov, Radtke, Jaffrennou, Enriquez, Soukiassian, Moras, Speziani, Crotti, Perfetti, ***Appl. Phys. Lett. 89****, 042114 (2006)*
D'angelo, Enriquez, Rodriguez, Aristov, Soukiassian, Tejeda, Michel, Pedio, Ottaviani, Perfetti
J. Chem. Phys. 147*, 164716 (2007)*

P. Soukiassian

SiC surface oxidation: a key issue device applications

VLSI-ULSI now requires:

- thin oxides films (< 50 Å)
- abrupt insulator/semiconductor interfaces
- SiC has the same native oxide than Si: SiO_2

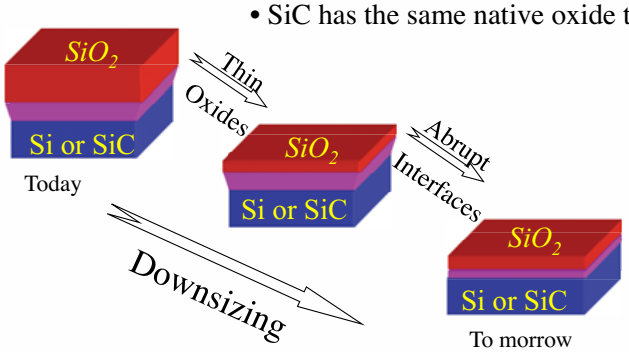

Problem: SiO_2/SiC interfaces have a high density of interface states, especially for the 4H polytype: detrimental for carrier mobility

Challenge: improving SiO_2/SiC interfaces

P. Soukiassian

O_2/3C-SiC(100) 3x2

Clean

+ 0.5 L O_2

Experimental

Simulation

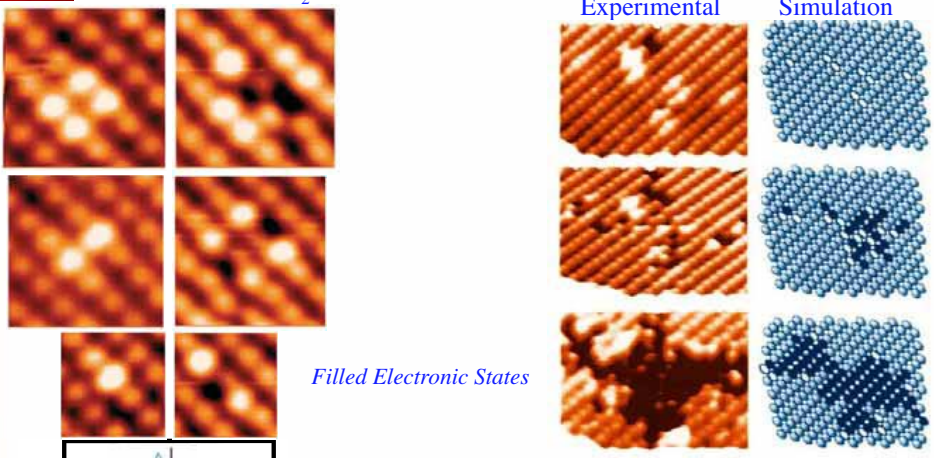

Filled Electronic States

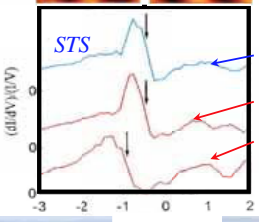

- Oxygen reacts at bright sites
- Creates new bright sites that become adsorption sites for oxygen

Mayne, Semond, Dujardin, Soukiassian,
***Phys. Rev. B 57**, RC, R 15108 (1998)*

P. Soukiassian

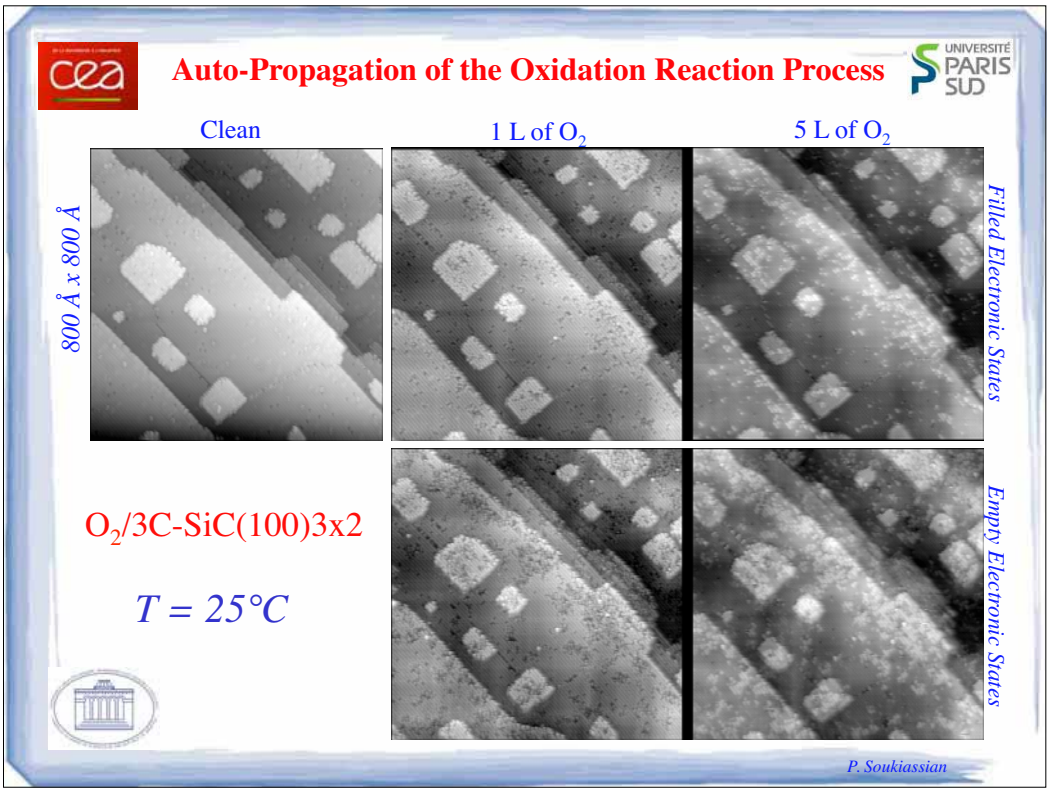
Auto-Propagation of the Oxidation Reaction Process
Clean
1 L of O2
5 L of O2
800 Å x 800 Å
Filled Electronic States
Empty Electronic States
O2/3C-SiC(100)3x2
T = 25°C
P. Soukiassian

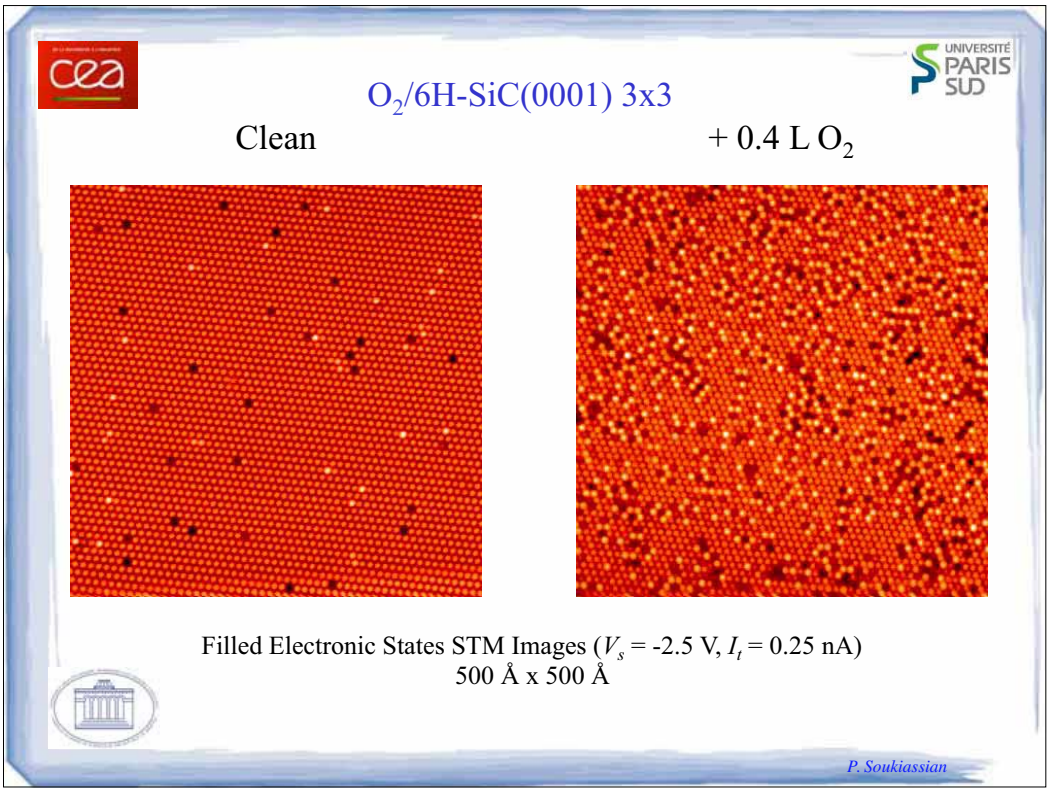
O2/6H-SiC(0001) 3x3
Clean
+ 0.4 L O2
Filled Electronic States STM Images (Vs = -2.5 V, It = 0.25 nA)
500 Å x 500 Å
P. Soukiassian

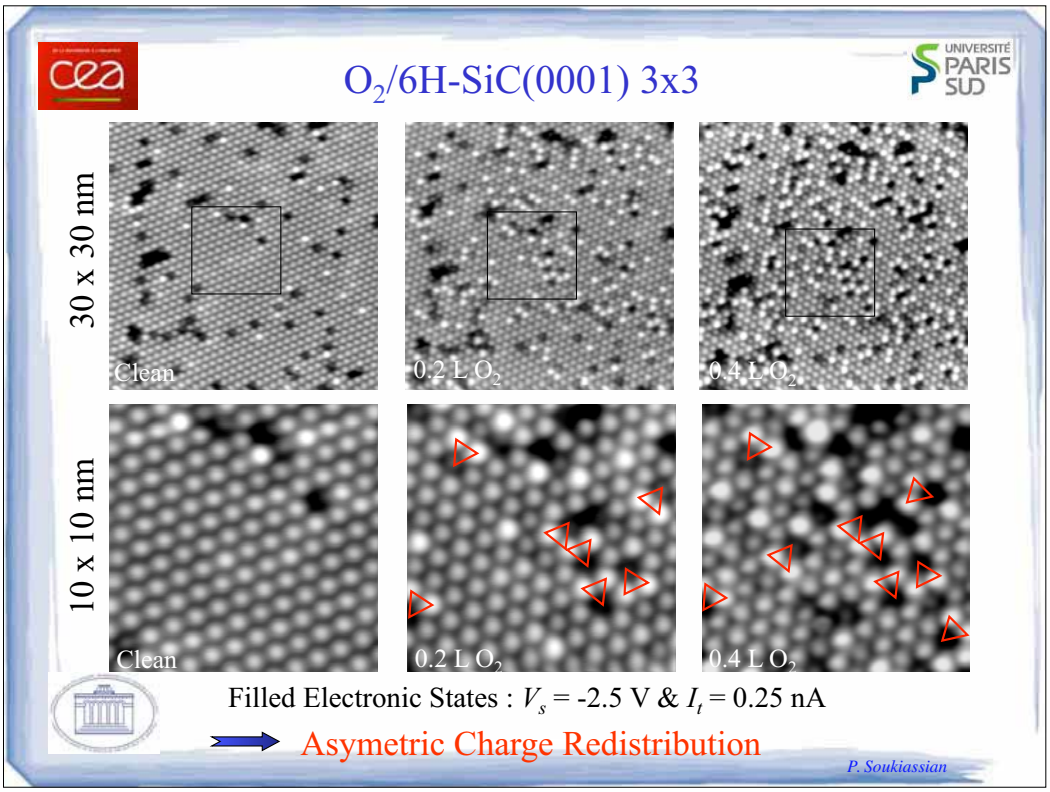
O_2/6H-SiC(0001) 3x3
30 x 30 nm
10 x 10 nm
Clean
0.2 L O_2
0.4 L O_2
Clean
0.2 L O_2
0.4 L O_2
Filled Electronic States : V_s = -2.5 V & I_t = 0.25 nA
Asymetric Charge Redistribution
P. Soukiassian

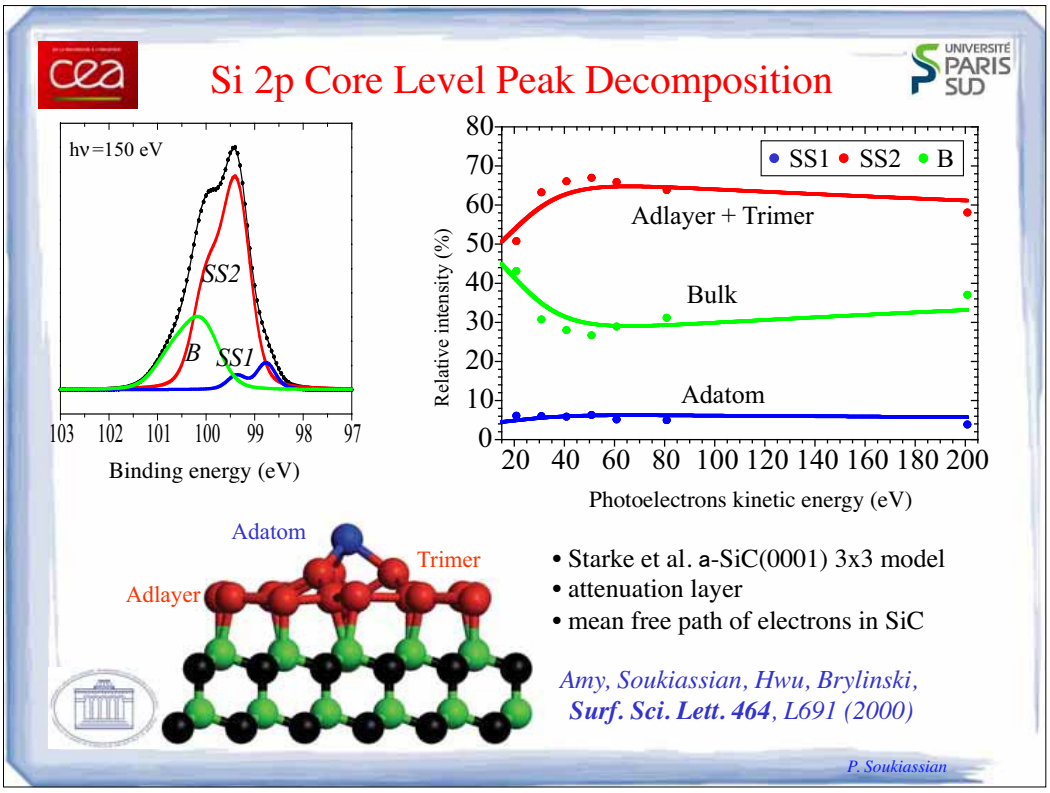
Si 2p Core Level Peak Decomposition
hν=150 eV
SS2
B
SS1
103 102 101 100 99 98 97
Binding energy (eV)
SS1 SS2 B
Adlayer + Trimer
Bulk
Adatom
Relative intensity (%)
Photoelectrons kinetic energy (eV)
Adatom
Trimer
Adlayer
• Starke et al. a-SiC(0001) 3x3 model
• attenuation layer
• mean free path of electrons in SiC
Amy, Soukiassian, Hwu, Brylinski,
Surf. Sci. Lett. 464, L691 (2000)
P. Soukiassian

Initial 6H-SiC(0001) 3x3 Surface Oxidation

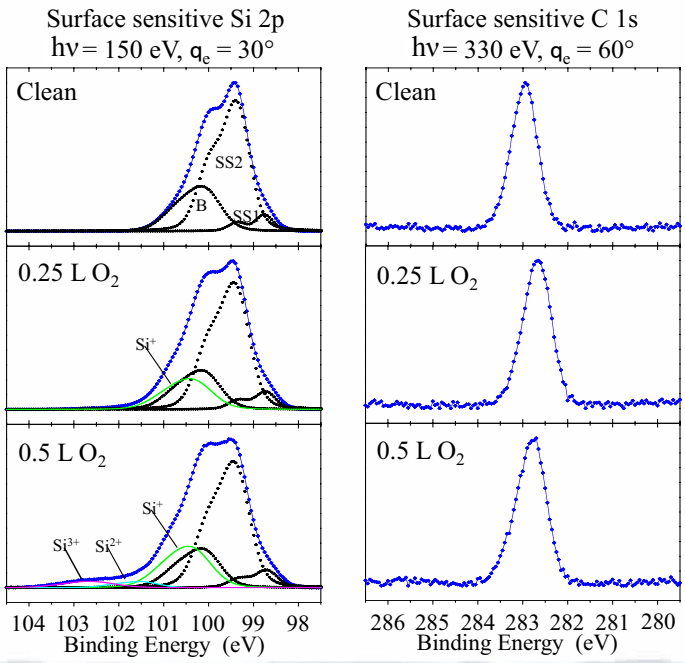

P. Soukiassian

Infrared Absorption Spectroscopy

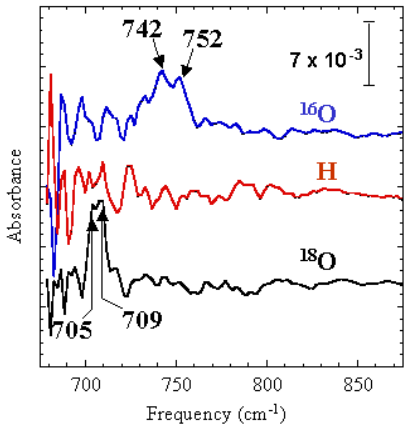

- UHV conditions
- 45° external reflection
- sensitivity to vibration modes normal to surface

Lucent Technologies

2 Adsorption sites for Oxygen
Fano : Adatoms + Trimers not affected

P. Soukiassian

Model for 6H-SiC(0001) 3x3 Surface Initial Oxidation

STM, XPS and IRAS results give converging evidences

Top view

Oxygen atom

Side view

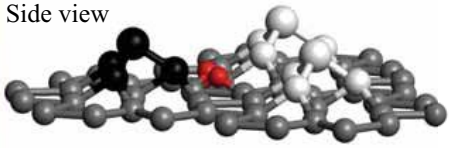

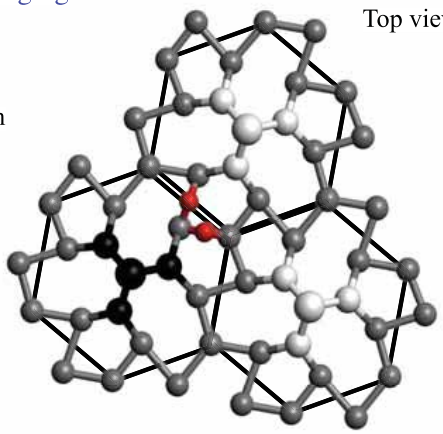

⟹ 2 Oxygen atoms bridge bonds Si adlayer atoms

Amy, Enriquez, Soukiassian, Storino, Chabal, Mayne, Dujardin, Hwu, Brylinski,
***Phys. Rev. Lett. 86**, 4342 (2001)*

P. Soukiassian

Graphene ?

A Zero Band Gap Semiconductor - Graphene - epitaxially grown on a Wide Band Gap Semiconductor - Silicon Carbide

Graphene is a single atomic layer of graphite – So Graphene is just "a Surface"

- **Nano-Objects at the Graphene/C-face-SiC(000-1) Interface**
- **Nano-Cracks at the Graphene/C-face-SiC(000-1) Interface**

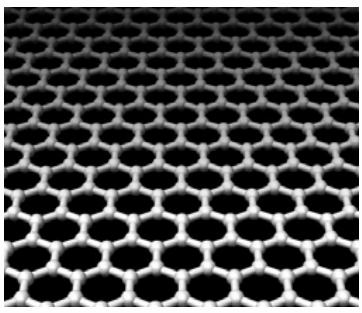

Experimental Tools:

- ***Atom-resolved scanning tunneling microscopy & spectroscopy (STM, STS)***
- ***Synchrotron radiation-based photoemission spectroscopy***

P. Soukiassian

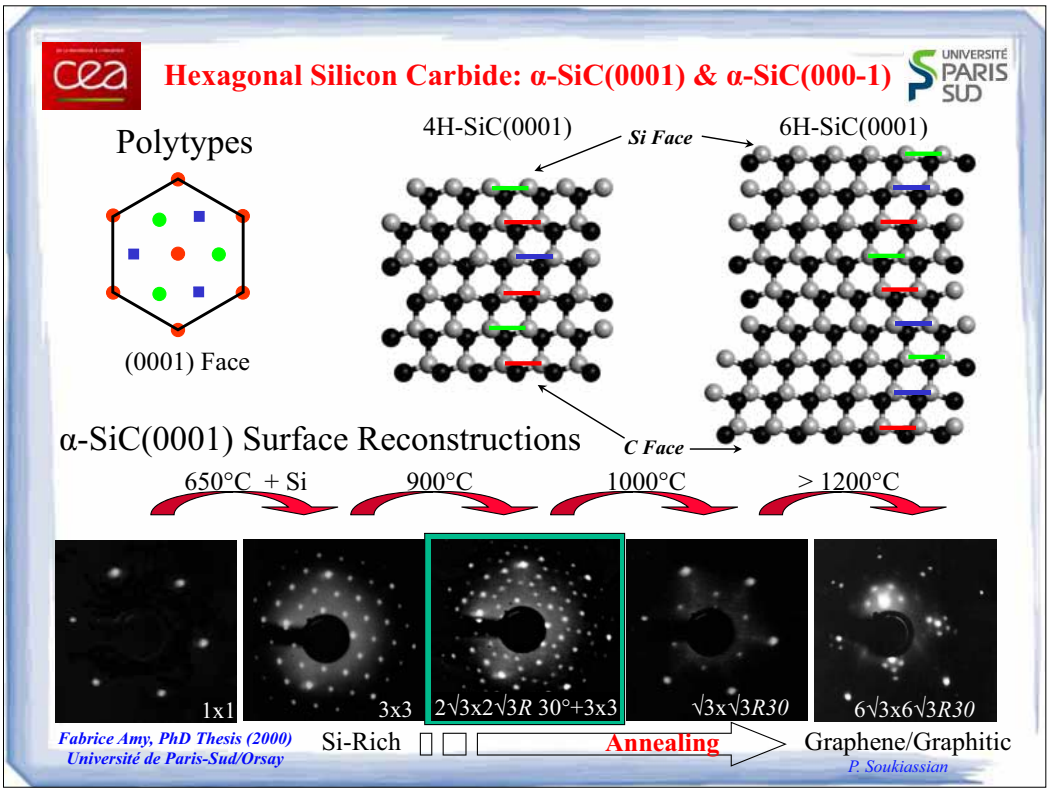
Hexagonal Silicon Carbide: α-SiC(0001) & α-SiC(000-1)
UNIVERSITÉ PARIS SUD
Polytypes
(0001) Face
4H-SiC(0001)
Si Face
6H-SiC(0001)
C Face
α-SiC(0001) Surface Reconstructions
650°C + Si
900°C
1000°C
> 1200°C
1x1
3x3
2√3x2√3R 30°+3x3
√3x√3R30
6√3x6√3R30
Fabrice Amy, PhD Thesis (2000)
Université de Paris-Sud/Orsay
Si-Rich
Annealing
Graphene/Graphitic
P. Soukiassian

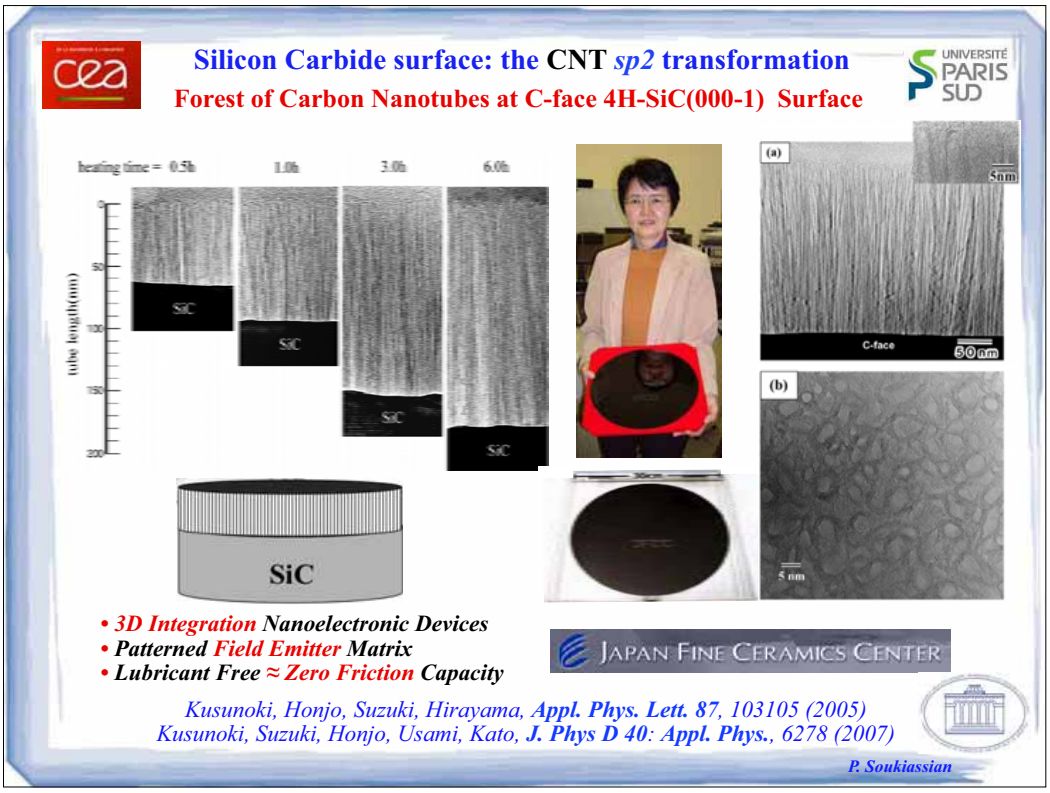
Silicon Carbide surface: the CNT sp2 transformation
Forest of Carbon Nanotubes at C-face 4H-SiC(000-1) Surface
UNIVERSITÉ PARIS SUD
heating time = 0.5h
1.0h
3.0h
6.0h
tube length(nm)
SiC
(a)
5nm
C-face
50 nm
(b)
5 nm
• 3D Integration Nanoelectronic Devices
• Patterned Field Emitter Matrix
• Lubricant Free ≈ Zero Friction Capacity
JAPAN FINE CERAMICS CENTER
Kusunoki, Honjo, Suzuki, Hirayama, Appl. Phys. Lett. 87, 103105 (2005)
Kusunoki, Suzuki, Honjo, Usami, Kato, J. Phys D 40: Appl. Phys., 6278 (2007)
P. Soukiassian

PHYSICAL REVIEW B VOLUME 58, NUMBER 24 15 DECEMBER 1998-II

Heteroepitaxial graphite on 6*H*-SiC(0001): Interface formation through conduction-band electronic structure

I. Forbeaux, J.-M. Themlin,* and J.-M. Debever
Groupe de Physique des Etats Condensés, UMR CNRS 6631, Case 901, Faculté des Sciences de Luminy, F-13288 Marseille Cedex 9, France
(Received 10 August 1998)

V. CONCLUSIONS

In summary, $k_{\parallel}$-resolved inverse photoemission spectroscopy applied to the $(6\sqrt{3}\times 6\sqrt{3})R30°$-reconstructed

growth of the first graphene sheet may proceed on top of adatoms characteristic of the $(\sqrt{3}\times\sqrt{3})R30°$ reconstruction which reduce the chemical reactivity of the substrate. This layer-by-layer growth opens up the possibility to isolate a single graphene sheet ''floating'' above the substrate. Fur-

ing plane with a lot of dangling bonds, suggests that the growth of the first graphene sheet may proceed on top of adatoms characteristic of the $(\sqrt{3}\times\sqrt{3})R30°$ reconstruction which reduce the chemical reactivity of the substrate. This layer-by-layer growth opens up the possibility to isolate a single graphene sheet ''floating'' above the substrate. Further STM work is currently in progress to understand more fully these mechanisms. This kind of van der Waals epitaxial

P. Soukiassian

Core Level Photoemission Spectroscopy on 3C-SiC(100) Surfaces

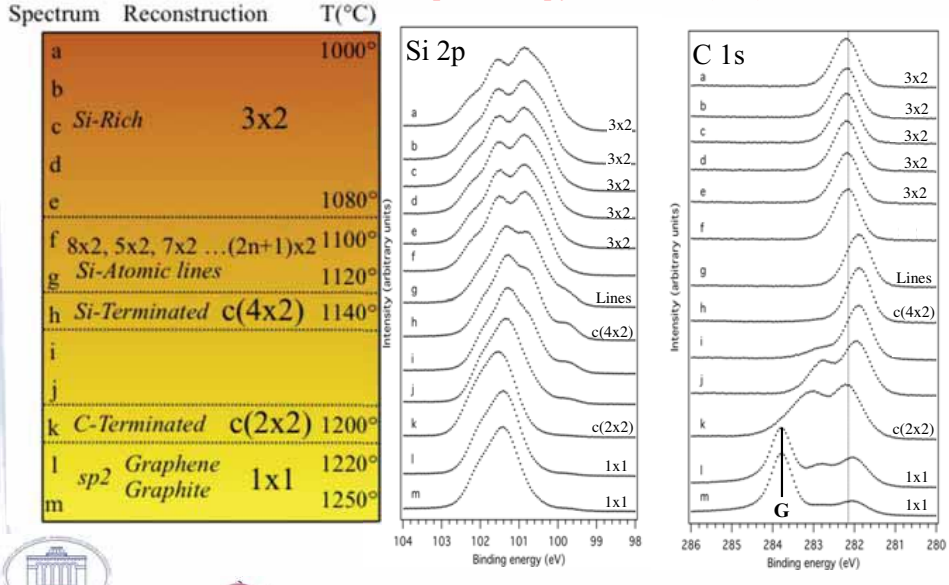

Tejeda, Dunham, Rotenberg, Denlinger, Soukiassian, ALS Experiments

P. Soukiassian

Silicon Carbide surface: the Graphene *sp2* transformation

Epitaxial Graphene on SiC: Exceptional Transport Properties

Electronic Confinement & Coherence

Quasiparticle Dynamics

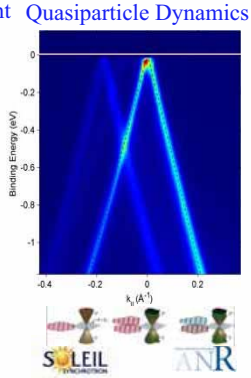

Morphology: Graphene on Si-terminated 6H-SiC(0001)

Graphene on Cubic 3C-SiC(100) & (111)

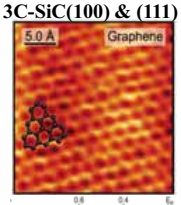

Walt de Heer
- **2009 Nanoscience Prize**
- **2010 MRS Medal**

- ***Very Large Phase Coherence Lengths:* > 1 µm at 4 K**
- ***Unprecedented High Mobilities:* µ = 250,000 cm²/V.s Si: 1,360 cm2/V.s**
- ***Charge carriers move at* ≈ *Zero Mass & Constant Velocity as Photons***

Graphene now on the "Road Map"

*Berger et al., **J. Phys. Chem. B108**, 19912 (2004) & **Science 312**, 1181 (2006); Rotenberg et al., **Science 313**, 951 (2006) & **Nat. Phys. 3**, 36 (2007); Lanzara et al., **Nat. Mat. 6**, 770 (2007); Veuillen et al., **PRB 76**, 041403R (2007); Conrad et al., **PRL 100**, 125504 (2008) & **J. Phys. D 43**, 374006 (2010); Potemski et al., **PRL 101**, 267601 (2008); Veuillen et al **PRL 101**, 206802 (2008); Virojanadara et al **PRB 78**, 245403 (2008); Haddon et al **JACS 131**, 1336 (2009), Seyller et al., **Nat. Mat. 8**, 203 (2009); Stroscio et al., **Science 324**, 924 (2009); Sprinkle et al. **PRL 103**, 226803 (2009); Suemitsu et al., **e-JSSNT** 7, 311 (2009) & **J. Phys. D 43**, 374012 (2010); Aristov et al., **Nano Lett 10**, 992 (2010)*

P. Soukiassian

C-Face: Multilayer Graphene decoupled one from each other

Graphene Layer Morphology by LEEM

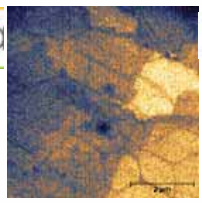

1st direct observation of nearly ideal Graphene Band Structure

Dirac Cones at Γ point for 3 rotated Graphene layers

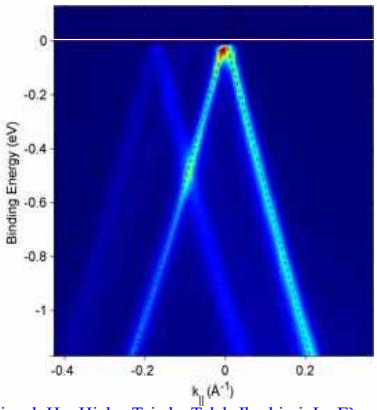

STM: Moiré pattern

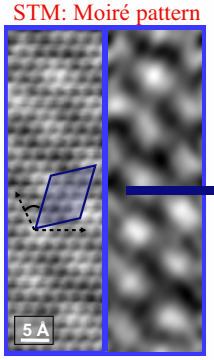

$(\sqrt{13} \times \sqrt{13})_G$ R46.1°

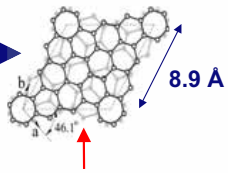

2 sheets with a relative rotation of 27.8⁰

Hass, Varchon, Millan-Otoya, Sprinkle, Sharma, de Heer, Berger, First, Magaud, Conrad, ***PRL 100***, *125504 (2008)*

Sprinkle, Siegel, Hu, Hicks, Tejeda, Taleb-Ibrahimi, Le Fèvre, Bertran, Vizzini, Enriquez, Chiang, Soukiassian, Berger, de Heer, Lanzara, Conrad, ***PRL 103***, *226803 (2009)*

P. Soukiassian

Epitaxial Graphene (1 or 2 Layer)/SiC Interface on the 4H-SiC(000-1) C face

interface ? → SiC ← Graphene

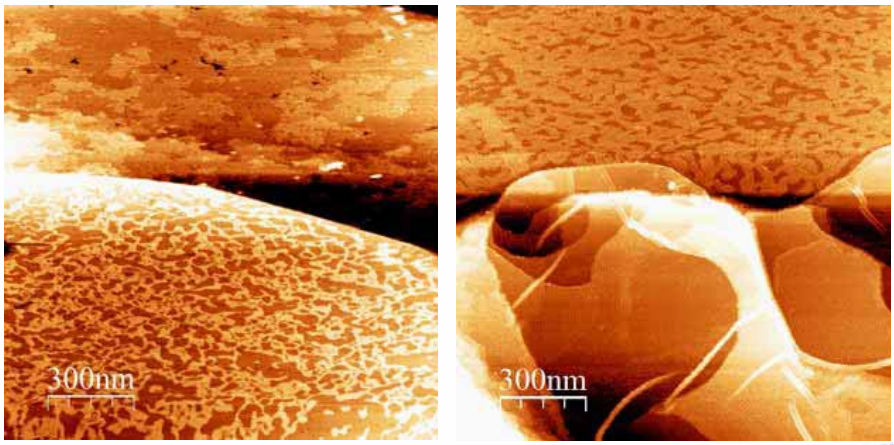

P. Soukiassian

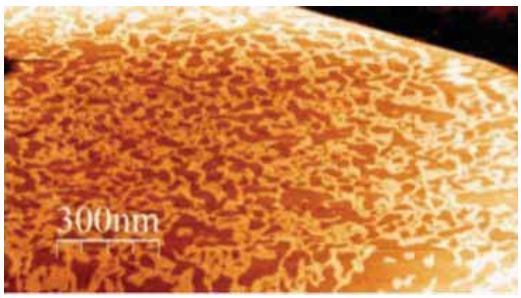

STM topograph of Nano-objects at Graphene/C-Face SiC(000-1) interface

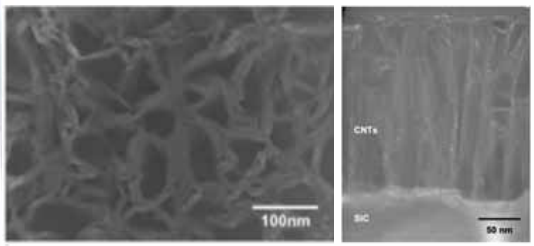

Top view *Side view*

TEM images of carbon nanotubes on top of C-Face SiC(000-1)

*Boeckl et al., **MSF 527-529**, 1579 (2006)*

P. Soukiassian

Nano-Objects at Epitaxial Graphene/SiC Interface

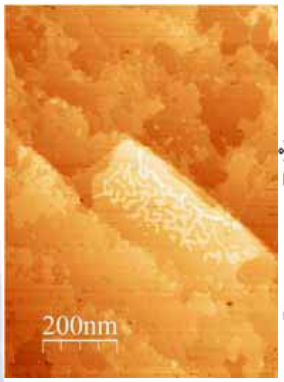

form mesas with steep sides

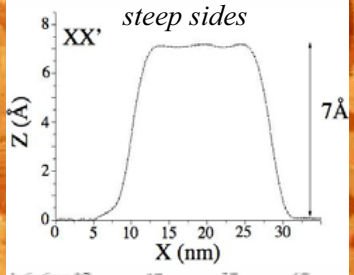

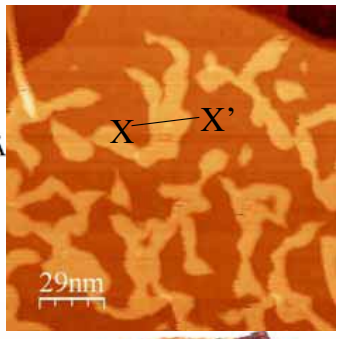

C Nanotubes ?

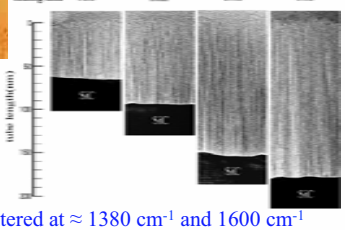

• Raman shows two bands centered at ≈ 1380 cm^{-1} and 1600 cm^{-1}
Hunztinger & Camassel • Consistent with CNT & damaged graphene
See - Boeckl, Mitchel, Weije Lu, Rigueur, ***Mat. Sci. For. 527****, 1579 (2006) and*
Dresselhaus, Jorio, Hofmann, Dresselhaus, Saito, ***Nanoletters 10****, 751 (2006)*

P. Soukiassian

Another look at these Nano-Objects as "Bushmen" paintings

Amazing
Art & Science !

Nano Ballerina

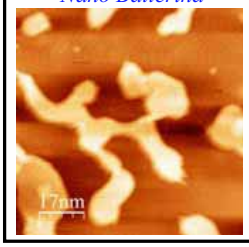

San "Lady" - Botswana

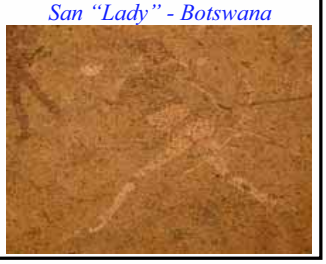

San painting-Zimbabwe

CNT Nano-Objects

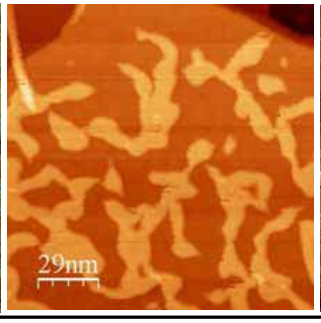

San painting - Namibia

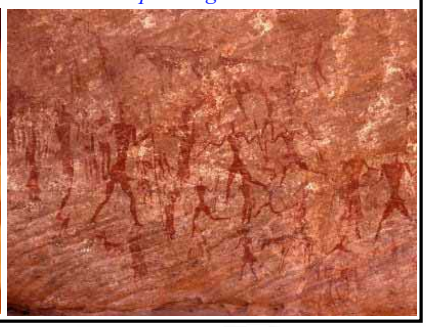

P. Soukiassian

Electronic Interface States

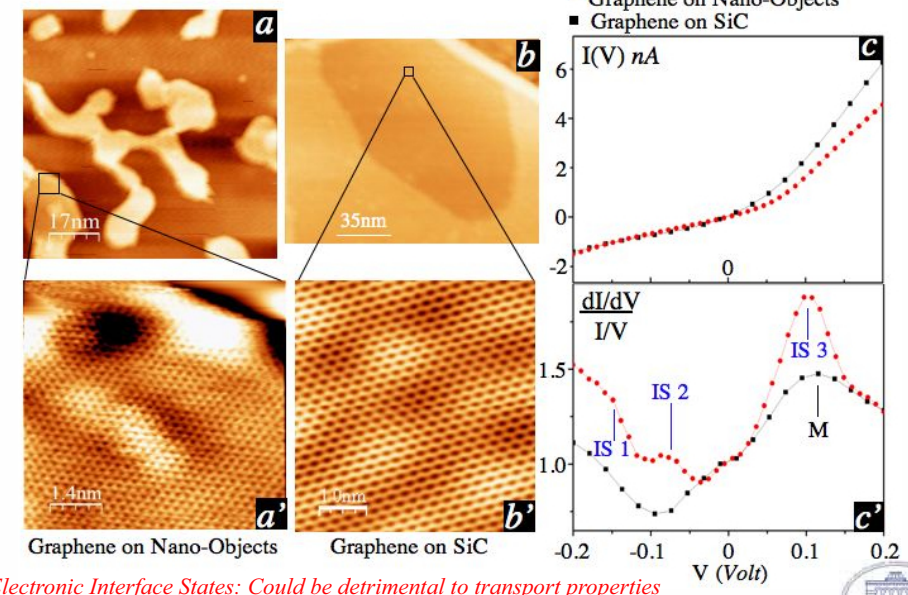

Electronic Interface States: Could be detrimental to transport properties

Vizzini, Enriquez, Oughaddou, Chiang, Soukiassian, ***Surf. Sci. Let. 605****, L6 (2011)*

P. Soukiassian

PRL 105, 085502 (2010) PHYSICAL REVIEW LETTERS week ending 20 AUGUST 2010

Epitaxial Graphene on SiC(0001): More than Just Honeycombs

Y. Qi, S. H. Rhim, G. F. Sun, M. Weinert, and L. Li*

Department of Physics and Laboratory for Surface Studies, University of Wisconsin, Milwaukee, Wisconsin 53211, USA

(Received 12 January 2010; revised manuscript received 19 May 2010; published 19 August 2010)

Using scanning tunneling microscopy with Fe-coated W tips and first-principles calculations, we show that the interface of epitaxial graphene/SiC(0001) is a warped graphene layer with hexagon-pentagon-heptagon ($H_{5,6,7}$) defects that break the honeycomb symmetry, thereby inducing a gap and states below E_F near the K point. Although the next graphene layer assumes the perfect honeycomb lattice, its interaction with the warped layer modifies the dispersion about the Dirac point. These results explain recent angle-resolved photoemission and carbon core-level shift data and solve the long-standing problem of the interfacial structure of epitaxial graphene on SiC(0001).

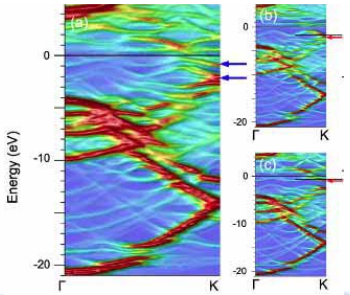

FLAPW Calculations

P. Soukiassian

Single Graphene Layer on Top of SiC Surface Nano-Cracks

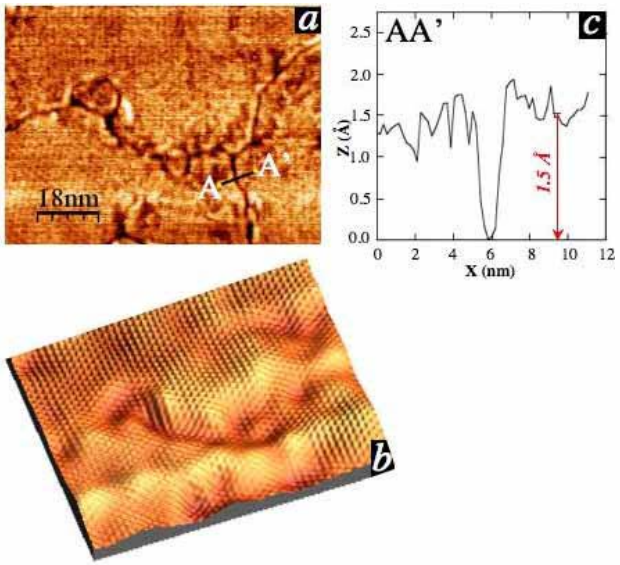

P. Soukiassian

Cracks at Graphene/SiC interface

Atomic cracks on 6H-SiC

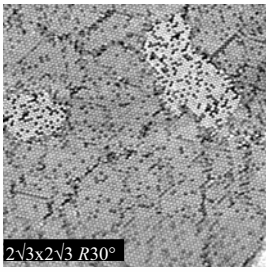

Amy, Soukiassian, Brylinski,
Appl. Phys. Lett 85, 926 (2004)

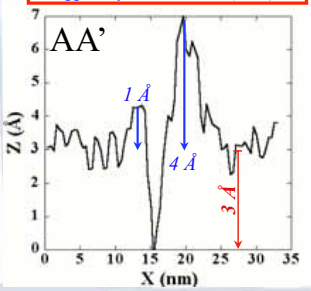

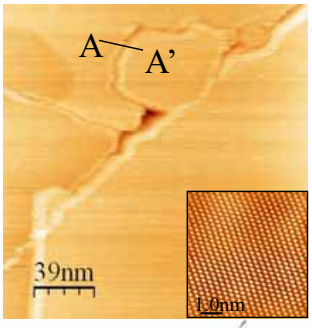

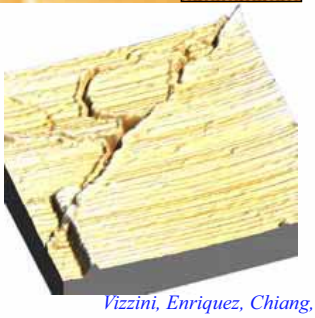

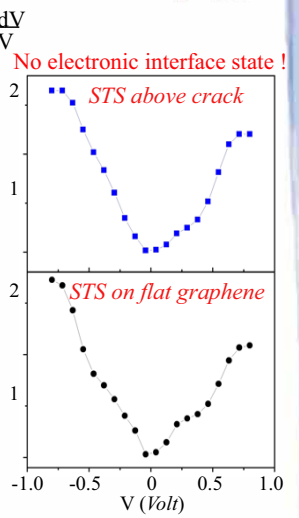

Vizzini, Enriquez, Chiang, Oughaddou, Soukiassian
Surf. Sci. Let. 605, L6 (2011)

P. Soukiassian

SCIENCE VOL 321 18 JULY 2008 385

Measurement of the Elastic Properties and Intrinsic Strength of Monolayer Graphene

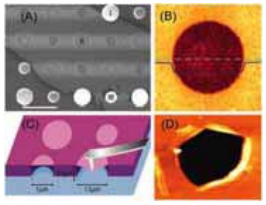

Changgu Lee,[1,2] Xiaoding Wei,[1] Jeffrey W. Kysar,[1,3] James Hone[1,2,4]*

We measured the elastic properties and intrinsic breaking strength of free-standing monolayer graphene membranes by nanoindentation in an atomic force microscope. The force-displacement behavior is interpreted within a framework of nonlinear elastic stress-strain response, and yields second- and third-order elastic stiffnesses of 340 newtons per meter (N m^{-1}) and −690 N m^{-1}, respectively. The breaking strength is 42 N m^{-1} and represents the intrinsic strength of a defect-free sheet. These quantities correspond to a Young's modulus of E = 1.0 terapascals, third-order elastic stiffness of D = −2.0 terapascals, and intrinsic strength of σ_{int} = 130 gigapascals for bulk graphite. These experiments establish graphene as the strongest material ever measured, and show that atomically perfect nanoscale materials can be mechanically tested to deformations well beyond the linear regime.

P. Soukiassian

Graphene: Steps and Applications

A -Growth
1-Mechanical Exfoliation
2 –Epitaxy on SiC
3–CVD on Metal or Insulator
4–Transfer on Insulator
5–Chemical exfolation

B-Functionalization
1 – Band Gap Monitoring
2 – Doping
3 – Metal Graphene Interface
4 – Interface Passivation
5 – Graphene Nanoribbons

?

C-Applications II
3 – "Touch" screen technology
4 – Infrared/THz & lasers

C-Applications I
1 – Electronic Devices
2 – Spintronics
5 – Graphene in Metrology
6 – Sensors
7 – NEMS

The key points:
- A2, A3 - Growth of high quality wafer size graphene
- A4
- B1, B2, B3, B5
- CI-1, CI-2, CI-6 ……..
- CII-4 ……

P. Soukiassian

STM not only used as an Eye but also as a Hand

- **Nanochemistry using the STM Tip**
- **Creating Atomic Wires and Logic Gate by STM-induced selective H Atom Desorption**
- **Moving Atoms One by One**
- **Manipulating Molecules One by One**

P. Soukiassian

Nanochemistry and Nano-Device

AFM Oxidation

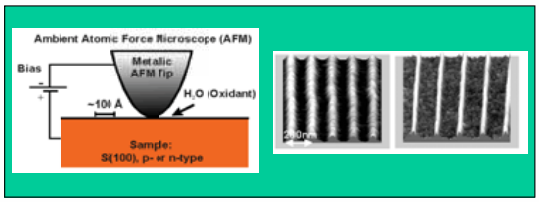

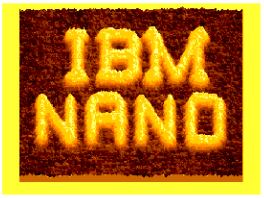

Current-induced local oxidation (CILO)

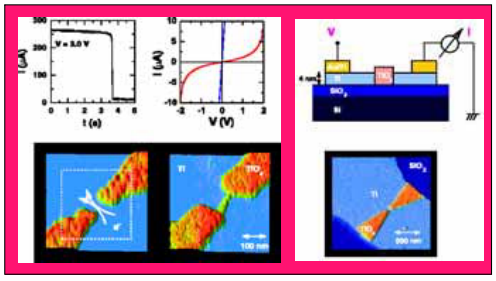

Avouris, Martel, Derycke et al., IBM Yorktown Heights
http://www.research.ibm.com/nanoscience/

Nanotube field-effect transistor

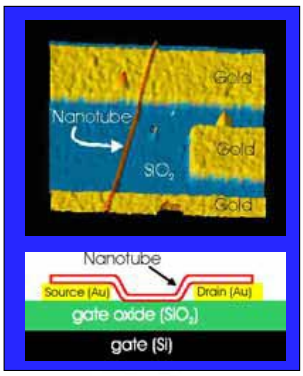

P. Soukiassian

Creating Atomic Wires and Logic Gate by STM-induced H Atom Desorption

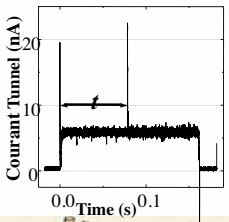

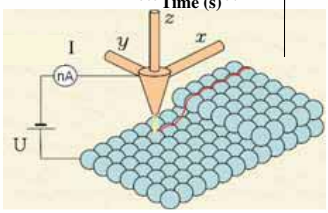

H terminated Si(100)

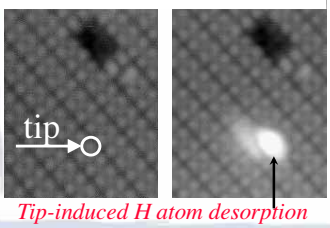

Tip-induced H atom desorption

Dangling bond lines created by tip-induced H atom desorption

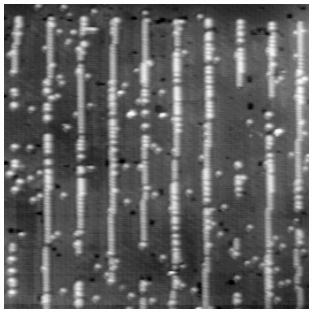

"OR" Logic Gate

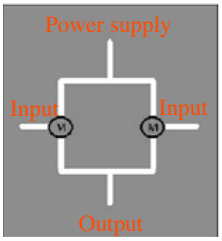

Laetitia Soukiassian, Mayne, Carbone, Dujardin,
***Phys. Rev. B 68**, 035303 (2003); **Surf. Sci. 528**, 121 (2003)*

P. Soukiassian

Individual Atom Manipulation

Iron atoms on Copper (111): atomic corrals

T ≈ few K !

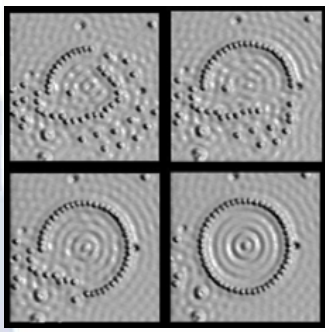

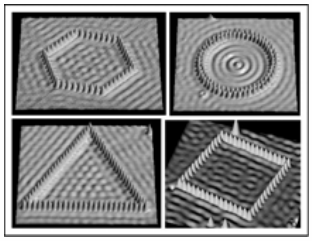

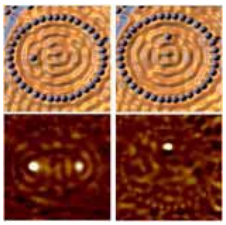

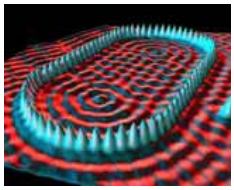

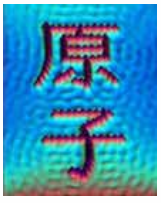

Xenon atoms on Nickel (110)

Eigler, Crommie, Lutz, Zeppenfeld et al., IBM Almaden
http://www.almaden.ibm.com/

P. Soukiassian

TRIMA Molecule Manipulation on Si(100) by STM Tip

Bending on one side | Reaction at the center | Dissociation

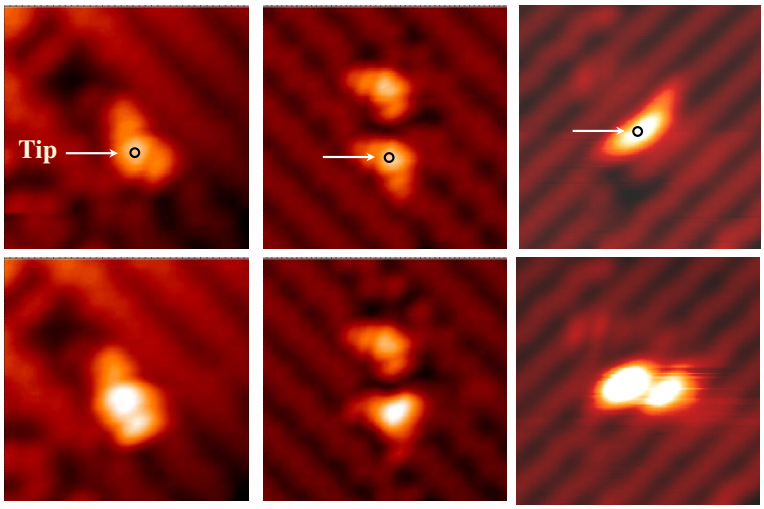

Mayne, Laetitia Soukiassian, Commaux, Comtet, Dujardin, ***Appl. Phys. Lett. 85****, 5379 (2004)*

P. Soukiassian

STM ?

- STM is a **Real Space** experimental technique
- STM is a **Very Versatile** experimental technique

BUT what you see is not necessarily what you get !
We look at the atomic structure ***through*** *the electronic properties*

So we can look at « atoms »

We can probe the local electronic structure

We can use STM for selective surface engineering

P. Soukiassian

Conclusions

- **Strain-driven 3C-SiC(100) Surfaces Reconstructions**
  - *Leads for each of them to have very different properties and reactivity*
- **Nanochemistry at 3C-SiC(100) 3x2 Surface**
  - *THE 1st example of H/D-induced semiconductor surface metallization*
  - *Especially exciting for interfacing with biology*
- **Massively Parallel Si Atomic Lines at SiC surfaces**
  - *Unsurpassed high integration density - Unsurpassed temperature resistance – up to 900°C*
- **From a Passive to an Active Massively Parallel Architecture**
  - *Negative differential resistance at Ag/Si nanowires – Interest in THz technology*
- ***sp - sp3* "*diamond-like*" SiC Surface Transformation**
- ***sp2* SiC Surface Transformation: Epitaxial Graphene**
  - *Morphology and Electronic Properties*
  - *Ideal graphene electronic band structure measurements*
- **Nano-Objects at the Graphene/SiC Interface**
  - *Carbon Nanotubes grown on SiC surface - Only very few area covered*
  - *Leads to electronic interface states - May have detrimental effects to the transport properties*
- **Nano-Cracks Defects at the Graphene/SiC Interface**
  - *The graphene layer is not broken - No electronic interface state – No detrimental effec*
- **STM not only used as an Eye but also as a Tool to Engineer Surfaces**

P. Soukiassian

So, Where are we heading to ?

What are the materials that marked their Century ?

- **Carbon (Coal)** was the material of the 19th century
- **Silicon** was the material of the 20th century

Bardeen, Brattain, Shockley ***(1956 Physics Nobel Prize Laureates)***
von Klitzing ***(1985 Physics Nobel Prize Laureate)***
Kilby ***(2000 Physics Nobel Prize Laureate)***

What could be The Material of 21th Century ?

P. Soukiassian

Still **Silicon ?**

Would it be **Silicon Carbide ?**

Organic Semiconductors ? ***Heeger (2000 Chemistry Nobel Prize Laureate)***

Magnetic Materials (GMR, ….) *the electron spin* **?** ***(Fert 2005 Nanoscience Prize, Fert & Grünberg 2007 Japan Prize and 2007 Physics Nobel Prize Laureates)***

or may-be **Carbon** back again **?**

Diamond ?

Fullerenes ? ***Curl, Kroto, Smalley (1996 Chemistry Nobel Prize Laureates)***

Nanotubes ? ***Iijima (2003 NanoScience Laureate)***

or Graphene ? ***Geim & Novosolov (2009 Physics Nobel Prize Laureates), de Heer (2009 NanoScience Prize & 2010 MRS Medal Laureate)***

…… so, may be the is not Bright …. the Future is Black …… !

But then, we will not only need more Moore, but more than Moore and then much more than Moore i.e. Much More Physics and Materials Science !

P. Soukiassian

Acknowledgements

PhD Students:

Fabrice Amy	*Air Products Inc., Allentown, PA, U.S.A.*
Marie D'angelo	*Université Pierre et Marie Curie, Paris, France*
Vincent Derycke	*CEA, Saclay, France*
Fabrice Semond	*CNRS-Sophia Antipolis, France*
Mathieu Silly	*Synchrotron SOLEIL, Saint Aubin, France*
Antonio Tejeda	*CNRS-Nancy & Synchrotron SOLEIL, Saint Aubin, France*

Visiting Scientists on sabbatical leave:

Victor Aristov	*Russian Academy of Sciences, Moscow-Chernogolovka, Russia*
Vladimir Aroutiounian	*Yerevan State University, Armenia*
Shirley Chiang	*U. California-Davis, U.S.A.*

Collaborations:

C. Berger, E. Conrad, W. de Heer, M. Sprinkle	*Georgia Institute of Technology, Atlanta, U.S.A*
C. Brylinski	*Thales and Université Claude Bernard, Lyon, France*
V. Buniatyan	*Yerevan Polytechnic University, Armenia.*
J. Camassel, J.R. Huntzinger	*LC2-CNRS, U. Montpellier-II, France*
A. Catellani, G. Galli	*CNR-Parma, Italy & Lawrence Livermore National Laboratory, U.S.A.*
Y. Chabal	*U. Texas-Austin, U.S.A.*
F. Charra, L. Douillard, D. Martinotti	*CEA, Saclay, France*
H. Enriquez	*Université de Paris-Sud/Orsay, France*
A. Mayne	*ISMO-CNRS, Orsay, France*
A. Nicolaou, A. Taleb-Ibrahimi	*Synchrotron SOLEIL, Cassiopée Beam line, Saint Aubin, France*
H. Oughaddou	*Université de Cergy-Pontoise*
P. Moras, C. Crotti, A. Locatelli, O. Mentes, M. Pedio	*Elettra Sincrotrone, Trieste, Italy*
S. Vizzini	Fmr *Post-Doc @ CEA, France*
E. Wimmer	*Materials Design SARL, Le Mans, France & Taos, NM, U.S.A*

EU-RU.NET European Project

ANR ***GraphSiC***

P. Soukiassian

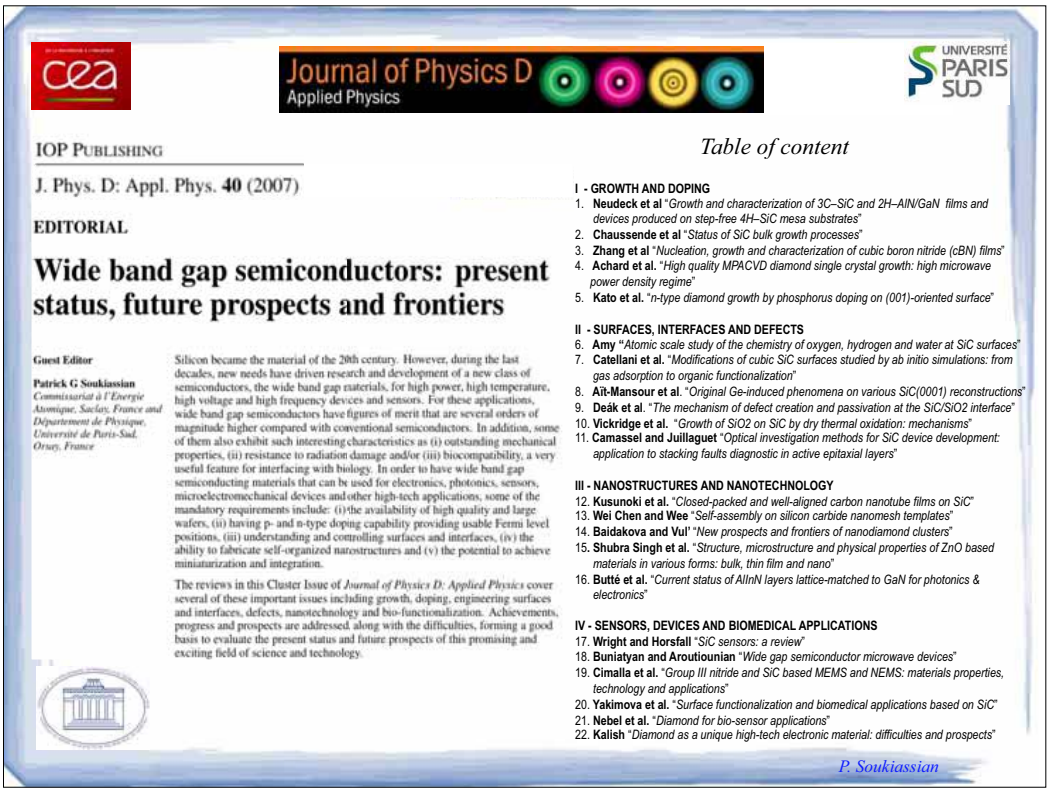

Journal of Physics D
Applied Physics

IOP PUBLISHING

J. Phys. D: Appl. Phys. **40** (2007)

EDITORIAL

Wide band gap semiconductors: present status, future prospects and frontiers

Guest Editor

Patrick G Soukiassian
Commissariat à l'Energie Atomique, Saclay, France and Département de Physique, Université de Paris-Sud, Orsay, France

Silicon became the material of the 20th century. However, during the last decades, new needs have driven research and development of a new class of semiconductors, the wide band gap materials, for high power, high temperature, high voltage and high frequency devices and sensors. For these applications, wide band gap semiconductors have figures of merit that are several orders of magnitude higher compared with conventional semiconductors. In addition, some of them also exhibit such interesting characteristics as (i) outstanding mechanical properties, (ii) resistance to radiation damage and/or (iii) biocompatibility, a very useful feature for interfacing with biology. In order to have wide band gap semiconducting materials that can be used for electronics, photonics, sensors, microelectromechanical devices and other high-tech applications, some of the mandatory requirements include: (i)the availability of high quality and large wafers, (ii) having p- and n-type doping capability providing usable Fermi level positions, (iii) understanding and controlling surfaces and interfaces, (iv) the ability to fabricate self-organized nanostructures and (v) the potential to achieve miniaturization and integration.

The reviews in this Cluster Issue of *Journal of Physics D: Applied Physics* cover several of these important issues including growth, doping, engineering surfaces and interfaces, defects, nanotechnology and bio-functionalization. Achievements, progress and prospects are addressed along with the difficulties, forming a good basis to evaluate the present status and future prospects of this promising and exciting field of science and technology.

Table of content

I - GROWTH AND DOPING
1. **Neudeck et al** "*Growth and characterization of 3C–SiC and 2H–AlN/GaN films and devices produced on step-free 4H–SiC mesa substrates*"
2. **Chaussende et al** "*Status of SiC bulk growth processes*"
3. **Zhang et al** "*Nucleation, growth and characterization of cubic boron nitride (cBN) films*"
4. **Achard et al.** "*High quality MPACVD diamond single crystal growth: high microwave power density regime*"
5. **Kato et al.** "*n-type diamond growth by phosphorus doping on (001)-oriented surface*"

II - SURFACES, INTERFACES AND DEFECTS
6. **Amy "***Atomic scale study of the chemistry of oxygen, hydrogen and water at SiC surfaces*"
7. **Catellani et al.** "*Modifications of cubic SiC surfaces studied by ab initio simulations: from gas adsorption to organic functionalization*"
8. **Aït-Mansour et al**. "*Original Ge-induced phenomena on various SiC(0001) reconstructions*"
9. **Deák et al**. "*The mechanism of defect creation and passivation at the SiC/SiO2 interface*"
10. **Vickridge et al.** "*Growth of SiO2 on SiC by dry thermal oxidation: mechanisms*"
11. **Camassel and Juillaguet** "*Optical investigation methods for SiC device development: application to stacking faults diagnostic in active epitaxial layers*"

III - NANOSTRUCTURES AND NANOTECHNOLOGY
12. **Kusunoki et al.** "*Closed-packed and well-aligned carbon nanotube films on SiC*"
13. **Wei Chen and Wee** "*Self-assembly on silicon carbide nanomesh templates*"
14. **Baidakova and Vul'** "*New prospects and frontiers of nanodiamond clusters*"
15. **Shubra Singh et al.** "*Structure, microstructure and physical properties of ZnO based materials in various forms: bulk, thin film and nano*"
16. **Butté et al.** "*Current status of AlInN layers lattice-matched to GaN for photonics & electronics*"

IV - SENSORS, DEVICES AND BIOMEDICAL APPLICATIONS
17. **Wright and Horsfall** "*SiC sensors: a review*"
18. **Buniatyan and Aroutiounian** "*Wide gap semiconductor microwave devices*"
19. **Cimalla et al.** "*Group III nitride and SiC based MEMS and NEMS: materials properties, technology and applications*"
20. **Yakimova et al.** "*Surface functionalization and biomedical applications based on SiC*"
21. **Nebel et al.** "*Diamond for bio-sensor applications*"
22. **Kalish** "*Diamond as a unique high-tech electronic material: difficulties and prospects*"

P. Soukiassian

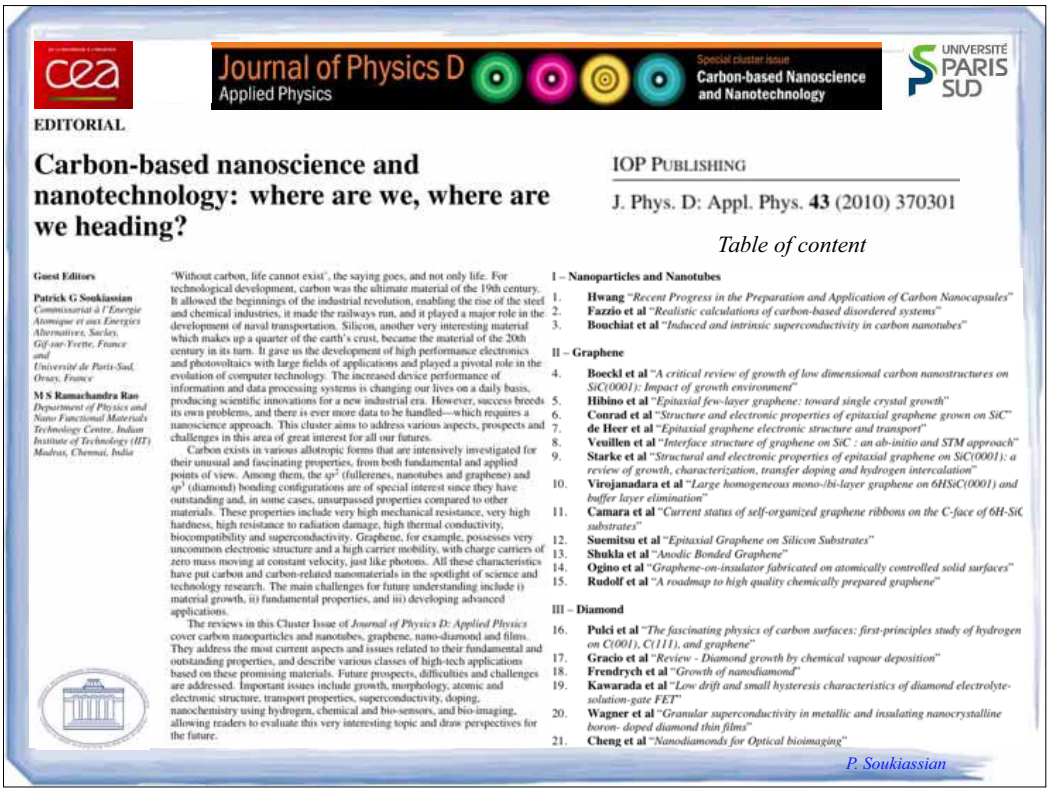

Journal of Physics D
Applied Physics

Special cluster issue
Carbon-based Nanoscience and Nanotechnology

EDITORIAL

Carbon-based nanoscience and nanotechnology: where are we, where are we heading?

Guest Editors

Patrick G Soukiassian
Commissariat à l'Energie Atomique et aux Energies Alternatives, Saclay, Gif-sur-Yvette, France and Université de Paris-Sud, Orsay, France

M S Ramachandra Rao
Department of Physics and Nano Functional Materials Technology Centre, Indian Institute of Technology (IIT) Madras, Chennai, India

"Without carbon, life cannot exist", the saying goes, and not only life. For technological development, carbon was the ultimate material of the 19th century. It allowed the beginnings of the industrial revolution, enabling the rise of the steel and chemical industries, it made the railways run, and it played a major role in the development of naval transportation. Silicon, another very interesting material which makes up a quarter of the earth's crust, became the material of the 20th century in its turn. It gave us the development of high performance electronics and photovoltaics with large fields of applications and played a pivotal role in the evolution of computer technology. The increased device performance of information and data processing systems is changing our lives on a daily basis, producing scientific innovations for a new industrial era. However, success breeds its own problems, and there is ever more data to be handled—which requires a nanoscience approach. This cluster aims to address various aspects, prospects and challenges in this area of great interest for all our futures.

Carbon exists in various allotropic forms that are intensively investigated for their unusual and fascinating properties, from both fundamental and applied points of view. Among them, the sp^2 (fullerenes, nanotubes and graphene) and sp^3 (diamond) bonding configurations are of special interest since they have outstanding and, in some cases, unsurpassed properties compared to other materials. These properties include very high mechanical resistance, very high hardness, high resistance to radiation damage, high thermal conductivity, biocompatibility and superconductivity. Graphene, for example, possesses very uncommon electronic structure and a high carrier mobility, with charge carriers of zero mass moving at constant velocity, just like photons. All these characteristics have put carbon and carbon-related nanomaterials in the spotlight of science and technology research. The main challenges for future understanding include i) material growth, ii) fundamental properties, and iii) developing advanced applications.

The reviews in this Cluster Issue of *Journal of Physics D: Applied Physics* covet carbon nanoparticles and nanotubes, graphene, nano-diamond and films. They address the most current aspects and issues related to their fundamental and outstanding properties, and describe various classes of high-tech applications based on these promising materials. Future prospects, difficulties and challenges are addressed. Important issues include growth, morphology, atomic and electronic structure, transport properties, superconductivity, doping, nanochemistry using hydrogen, chemical and bio-sensors, and bio-imaging, allowing readers to evaluate this very interesting topic and draw perspectives for the future.

IOP PUBLISHING

J. Phys. D: Appl. Phys. **43** (2010) 370301

Table of content

I – Nanoparticles and Nanotubes
1. **Hwang** "*Recent Progress in the Preparation and Application of Carbon Nanocapsules*"
2. **Fazzio et al** "*Realistic calculations of carbon-based disordered systems*"
3. **Bouchiat et al** "*Induced and intrinsic superconductivity in carbon nanotubes*"

II – Graphene
4. **Boeckl et al** "*A critical review of growth of low dimensional carbon nanostructures on SiC(0001): Impact of growth environment*"
5. **Hibino et al** "*Epitaxial few-layer graphene: toward single crystal growth*"
6. **Conrad et al** "*Structure and electronic properties of epitaxial graphene grown on SiC*"
7. **de Heer et al** "*Epitaxial graphene electronic structure and transport*"
8. **Veuillen et al** "*Interface structure of graphene on SiC : an ab-initio and STM approach*"
9. **Starke et al** "*Structural and electronic properties of epitaxial graphene on SiC(0001): a review of growth, characterization, transfer doping and hydrogen intercalation*"
10. **Virojanadara et al** "*Large homogeneous mono-/bi-layer graphene on 6HSiC(0001) and buffer layer elimination*"
11. **Camara et al** "*Current status of self-organized graphene ribbons on the C-face of 6H-SiC substrates*"
12. **Suemitsu et al** "*Epitaxial Graphene on Silicon Substrates*"
13. **Shukla et al** "*Anodic Bonded Graphene*"
14. **Ogino et al** "*Graphene-on-insulator fabricated on atomically controlled solid surfaces*"
15. **Rudolf et al** "*A roadmap to high quality chemically prepared graphene*"

III – Diamond
16. **Pulci et al** "*The fascinating physics of carbon surfaces: first-principles study of hydrogen on C(001), C(111), and graphene*"
17. **Gracio et al** "*Review - Diamond growth by chemical vapour deposition*"
18. **Frendrych et al** "*Growth of nanodiamond*"
19. **Kawarada et al** "*Low drift and small hysteresis characteristics of diamond electrolyte-solution-gate FET*"
20. **Wagner et al** "*Granular superconductivity in metallic and insulating nanocrystalline boron- doped diamond thin films*"
21. **Cheng et al** "*Nanodiamonds for Optical bioimaging*"

P. Soukiassian


physicsworld.com
Graphene comes of age
UNIVERSITÉ PARIS SUD
Graphene comes of age
P. Soukiassian interviewed by James Dacey
from PhysicsWorld
See also: Epitaxial Graphene
J. Phys. D: Applied Physics 44 150301 (2012)
Walt de Heer and Claire Berger Guest Editors
EDITORIAL
Epitaxial graphene
Guest Editors
Walt A de Heer
School of Physics, Georgia Institute of Technology, USA
Claire Berger
School of Physics, Georgia Institute of Technology, USA and CNRS-Institut Néel, Grenoble, France
Graphene is widely regarded as an important new electronic material with interesting two-dimensional electron gas properties. Not only that, but graphene is widely considered to be an important new material for large-scale integrated electronic devices that may eventually even succeed silicon. In fact, there are countless publications that demonstrate the amazing applications potential of graphene.
In order to realize graphene electronics, a platform is required that is compatible with large-scale electronics processing methods. It was clear from the outset that graphene grown epitaxially on silicon carbide substrates was exceptionally well suited as a platform for graphene-based electronics, not only because the graphene sheets are grown directly on electronics-grade silicon carbide (an important semiconductor in its own right), but also because these sheets are oriented with respect to the semiconductor. Moreover, the extremely high temperatures involved in production assure essentially defect-free and contamination-free materials with well-defined interfaces.
See: http://physicsworld.com/cws/article/multimedia/2012/may/17/graphene-comes-of-age
P. Soukiassian


Summer School on
Micro- and Nano- structural characterization of materials
focused on electron microscopy
July 11-15, 2012, Thessaloniki, Greece
Closing
NetFISiC funded by the European Commission FP7 GA n.264613
ARISTOTLE UNIVERSITY OF THESSALONIKI


Scientific Program
29 hours of lectures
6-hour hands-on training
at the Electron Microscopy Lab
of AUTH
participants' presentations


19 lecturers from 12 universities, institutions and companies
Aix-Marseille University, France
Aristotle University of Thessaloniki, Greece
Centre for Research and Technology Hellas, Greece
JEOL, Japan
Lyon Ingénierie Projets, France
NanoMEGAS, Belgium
National Centre for Scientific Research "Demokritos", Greece
The Institute of Photonic Sciences, Spain
University of Ioannina, Greece
University of Montpellier 2, France
University of Paris-Sud, France
University of Silesia, Poland
Many thanks to all of them


39 participants from 12 countries
France
Germany
Greece
Hungary
India
Italy
Lithuania
Romania
Russia
Spain
Sweden
Turkey
Thank you all for your participation


Special Thanks to
Nikos Frangis
Christos Lioutas
Nikos Vouroutzis
Dimitris Evangelinos
Archontis Michtaris
Alkioni Mantzari
Aria Andreadou
Katerina Breza
Maya Marinova
Eleni Sarakinou
Naren Chandran
Eleni Polychroniadou
for their help in the organization of the school


Summer School on
Micro- and Nano- structural characterization of materials
focused on electron microscopy
July 11-15, 2012, Thessaloniki, Greece
Goodbye
NetFISiC funded by the European Commission FP7 GA n.264613
ARISTOTLE UNIVERSITY OF THESSALONIKI

Université Claude Bernard Lyon 1

netFISiC

Germanium incorporation inside 4H-SiC 8 ° off-axis seed

Kassem AlAssaad

*Dr. Gabriel Ferro **
Dr. Veronique Souliere

Laboratoire des Multimatériaux et Interfaces - UMR 5615
Université Claude Bernard UCBL-Lyon1

Summer school on Micro- and Nano- structural characterization of materials, focused on electron microscopy, 11th – 15th July, 2012, Thessaloniki, Greece

LMI

Objective

Search for the best way towards implementing Ge incorporation inside 4H-SiC layers

Work on the *growth conditions*

- GeH4 flux
- Growth rate / SiH4 flux
- C/Si ratio
- Growth Time
- Growth temperature

Properties of the resulting layers

- surface morphology
- Nitrogen Doping
- Incorporated [Ge]
- surface roughness

for DLTS measurements and MOS capacitors
to evaluate material quality
to evaluate electronic properties through optical methods
to evaluate optical properties and doping
SiC/SiO_2 and/or SiC/metal interfaces

netFISiC SUMMER SCHOOL ON MICRO- AND NANO-STRUCTURAL CHARACTERIZATION Wednesday, July 11, 2012 2 Lyon 1

Home made CVD

Preliminary Characterization

- Optical Microscope
- C-V measurement
- Infrared spectrometry
- Scanning electron microscope (SEM)

Further Characterization

- Particle Induced X-ray Emission (PIXE)
- Atomic force microscopy (AFM)

SUMMER SCHOOL ON MICRO- AND NANO-STRUCTURAL CHARACTERIZATION Wednesday, July 11, 2012 3

Sampling

	C/Si	Gr (µm/h)	Temperature (°C)	GeH_4 (sccm)	Time (h)
Set1 / Set2	2 3.5 5	6	1500	0/0.2	2
Set3	3.5	6	1500 1550 1600	0.2	1
Set4	3.5	2 4 6	1500	0.2	3.00 1.66 1.00

- Check the absence or presence of any memory effect
- Counting of the triangular defect (*at the center*)

SUMMER SCHOOL ON MICRO- AND NANO-STRUCTURAL CHARACTERIZATION Wednesday, July 11, 2012 4

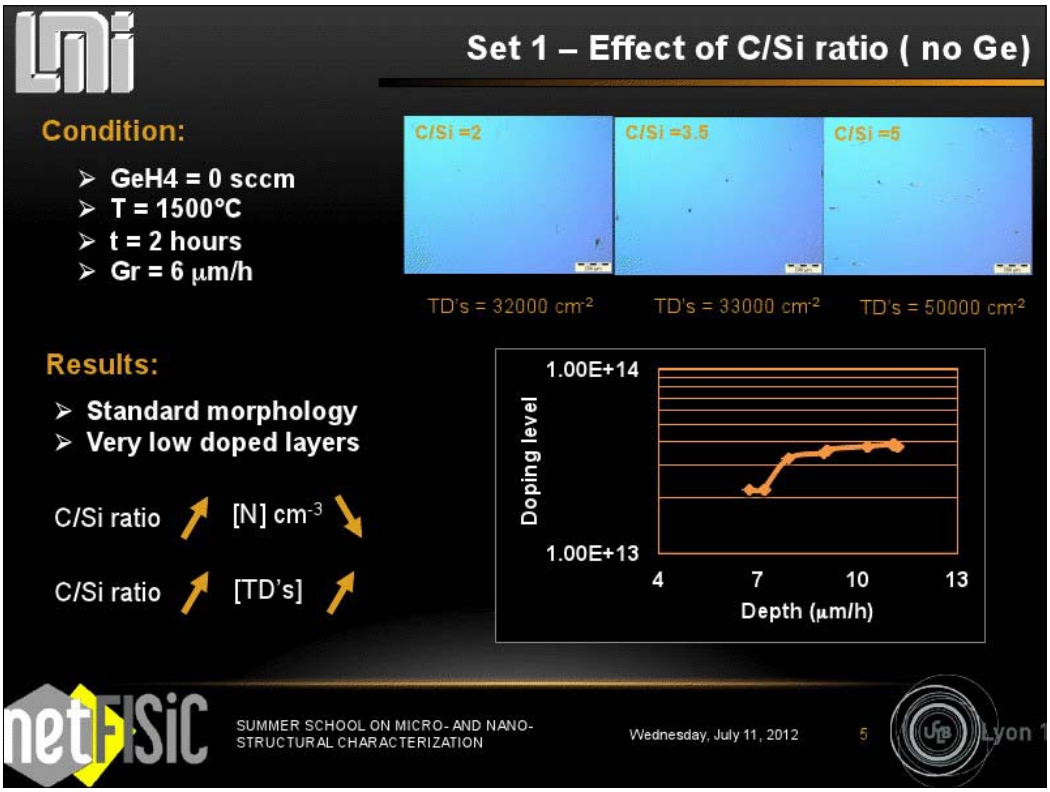
Set 1 – Effect of C/Si ratio (no Ge)
Condition:
GeH4 = 0 sccm
T = 1500°C
t = 2 hours
Gr = 6 µm/h
C/Si =2
C/Si =3.5
C/Si =5
TD's = 32000 cm-2
TD's = 33000 cm-2
TD's = 50000 cm-2
Results:
Standard morphology
Very low doped layers
C/Si ratio [N] cm-3
C/Si ratio [TD's]
1.00E+14
1.00E+13
Doping level
4
7
10
13
Depth (µm/h)
SUMMER SCHOOL ON MICRO- AND NANO-STRUCTURAL CHARACTERIZATION
Wednesday, July 11, 2012
5

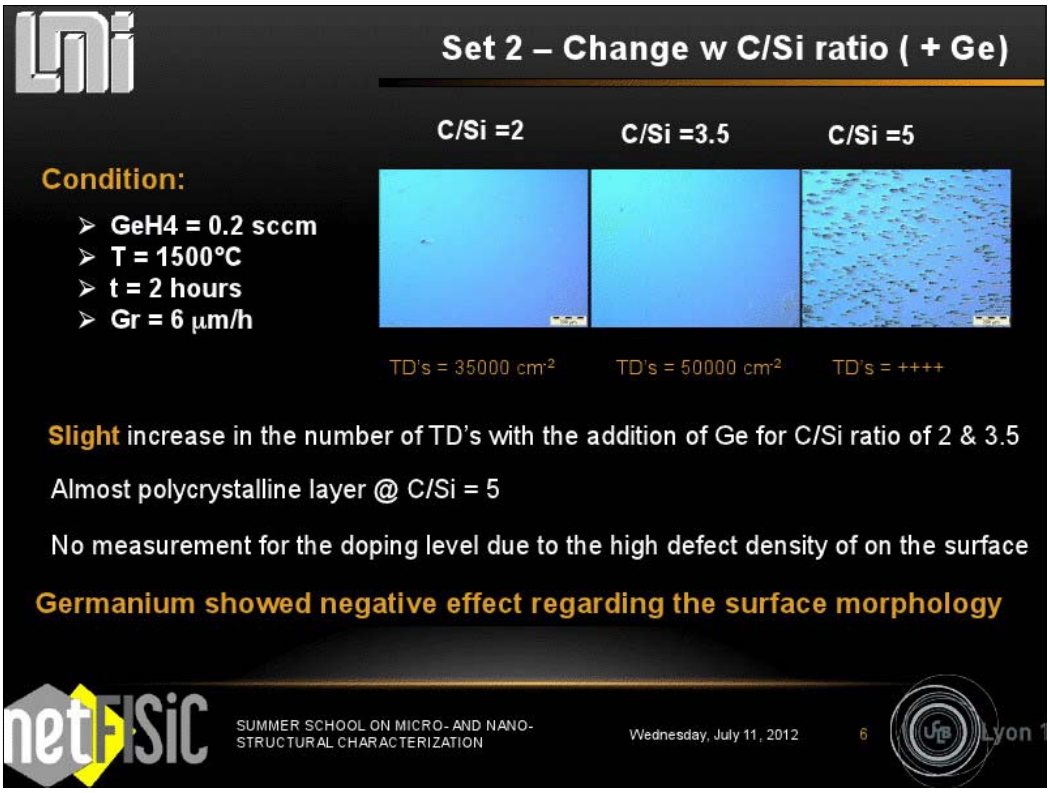
Set 2 – Change w C/Si ratio (+ Ge)
Condition:
GeH4 = 0.2 sccm
T = 1500°C
t = 2 hours
Gr = 6 µm/h
C/Si =2
C/Si =3.5
C/Si =5
TD's = 35000 cm-2
TD's = 50000 cm-2
TD's = ++++
Slight increase in the number of TD's with the addition of Ge for C/Si ratio of 2 & 3.5
Almost polycrystalline layer @ C/Si = 5
No measurement for the doping level due to the high defect density of on the surface
Germanium showed negative effect regarding the surface morphology
SUMMER SCHOOL ON MICRO- AND NANO-STRUCTURAL CHARACTERIZATION
Wednesday, July 11, 2012
6

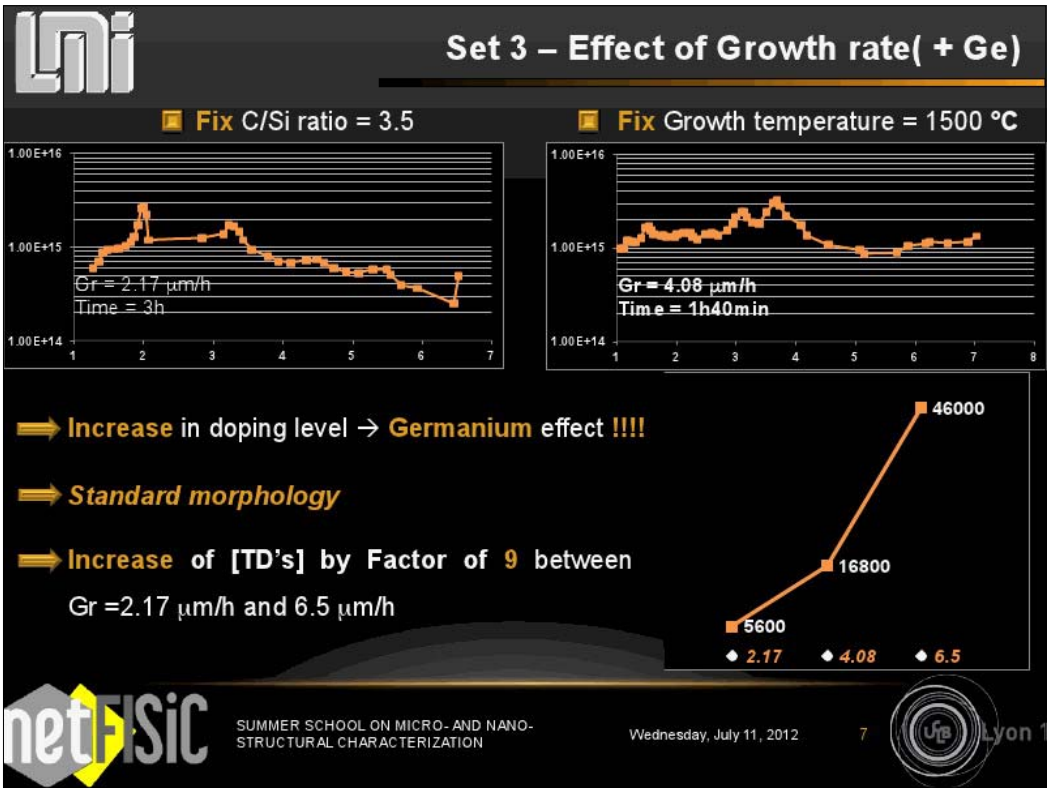
Set 3 – Effect of Growth rate(+ Ge)
Fix C/Si ratio = 3.5
Fix Growth temperature = 1500 °C
1.00E+16
1.00E+15
1.00E+14
Gr = 2.17 µm/h
Time = 3h
Gr = 4.08 µm/h
Time = 1h40min
Increase in doping level → Germanium effect !!!!
Standard morphology
Increase of [TD's] by Factor of 9 between
Gr =2.17 µm/h and 6.5 µm/h
46000
16800
5600
2.17
4.08
6.5
SUMMER SCHOOL ON MICRO- AND NANO-STRUCTURAL CHARACTERIZATION
Wednesday, July 11, 2012
7

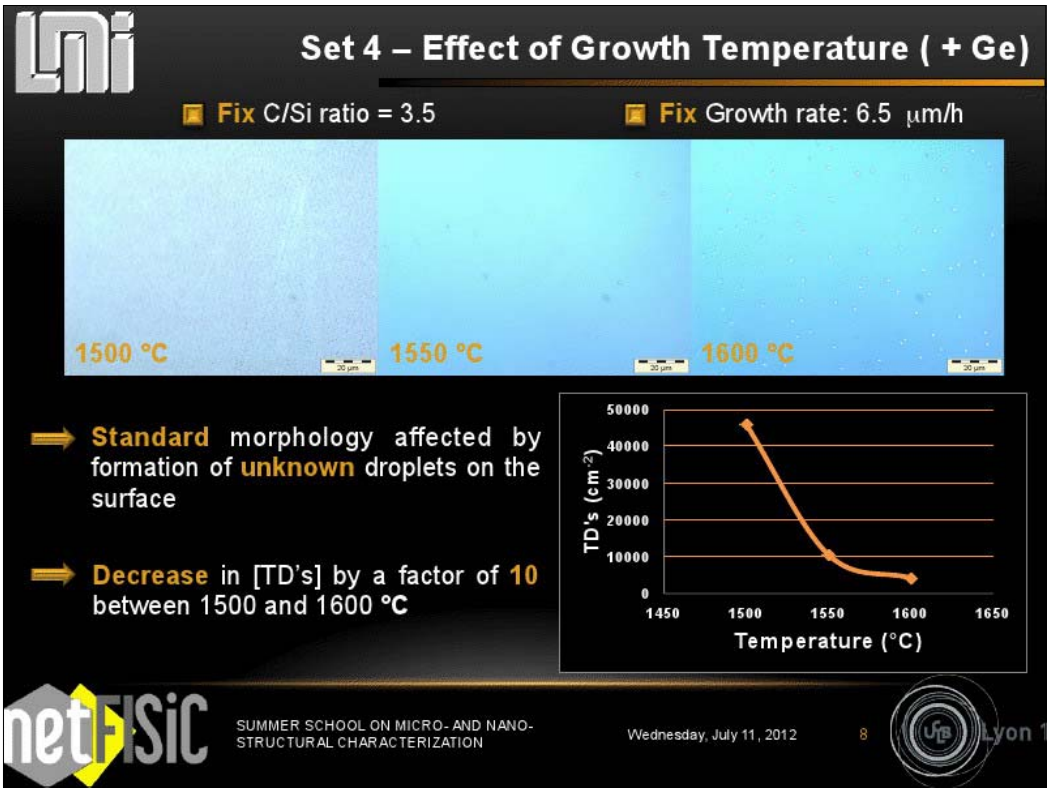
Set 4 – Effect of Growth Temperature (+ Ge)
Fix C/Si ratio = 3.5
Fix Growth rate: 6.5 µm/h
1500 °C
1550 °C
1600 °C
Standard morphology affected by formation of unknown droplets on the surface
Decrease in [TD's] by a factor of 10 between 1500 and 1600 °C
TD's (cm-2)
50000
40000
30000
20000
10000
0
1450
1500
1550
1600
1650
Temperature (°C)
SUMMER SCHOOL ON MICRO- AND NANO-STRUCTURAL CHARACTERIZATION
Wednesday, July 11, 2012
8

SEM – Checking particle's shape and composition

C/Si =2
Growth Temperature = 1500 °C
Growth rate = 6.5 µm/h

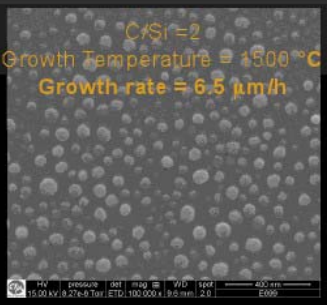

C/Si =3.5
Growth Temperature = 1600 °C
Growth rate = 6.0 µm/h

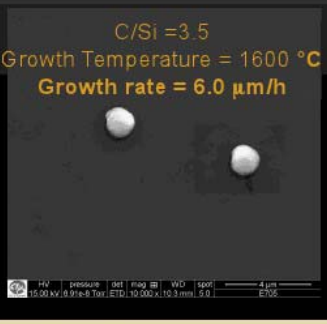

1500 °C	1600 °C
Nano-metric	Micrometric

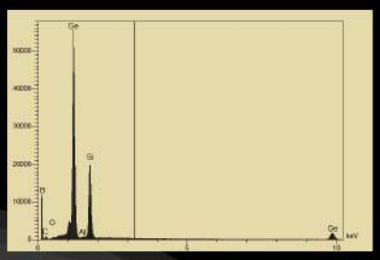

Coalescence @ higher Temperature

Germanium containing droplets

Modifications and Obstacles

Memory Effect

- No **morphological** memory effect
- Incorporated **Ge** element !!!!!!

Wet etching [$HFHNO_3$}

⟹ Improve the growth procedure ←→ Carbonization step / annealing

- *Reduce defect density*
- *Avoid Ge containing droplets*

⟹ Technical Obstacles

- Deposit on the side wall
- Detroit of the susceptor

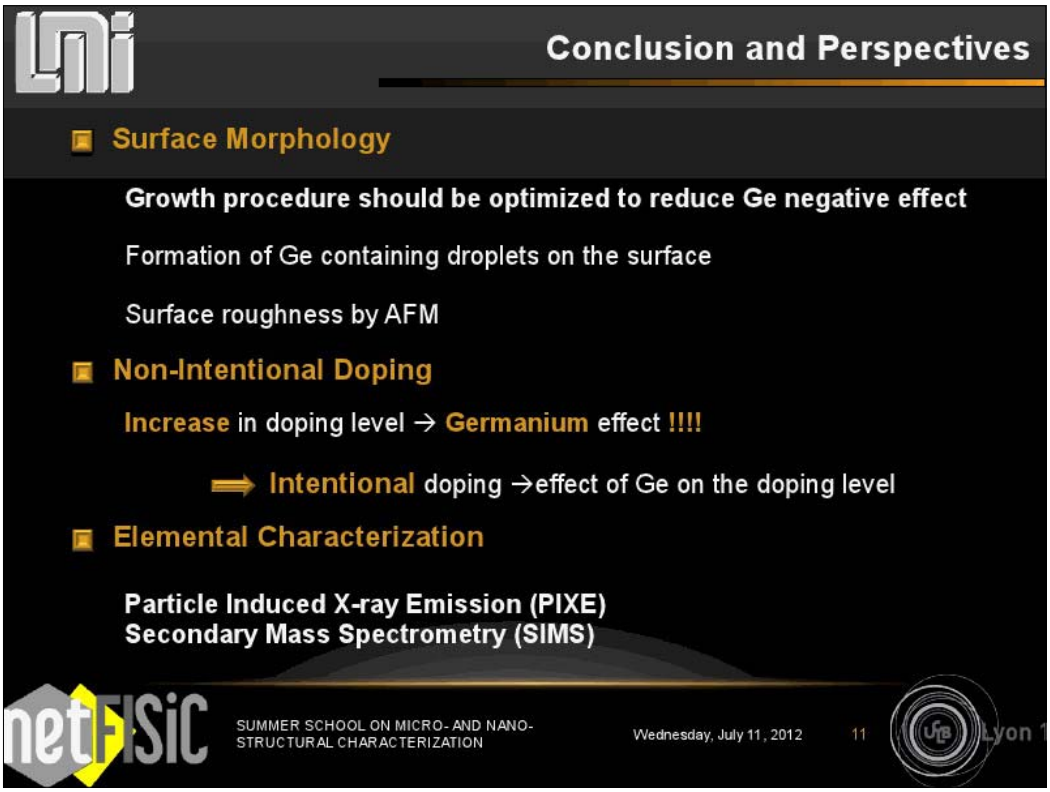
Conclusion and Perspectives
Surface Morphology
Growth procedure should be optimized to reduce Ge negative effect
Formation of Ge containing droplets on the surface
Surface roughness by AFM
Non-Intentional Doping
Increase in doping level → Germanium effect !!!!
⟹ Intentional doping →effect of Ge on the doping level
Elemental Characterization
Particle Induced X-ray Emission (PIXE)
Secondary Mass Spectrometry (SIMS)
netFISiC
SUMMER SCHOOL ON MICRO- AND NANO-STRUCTURAL CHARACTERIZATION
Wednesday, July 11, 2012
11
Lyon 1

Synthesis and Characterization of SiC-SiO_2 Core shell nanowires

Sathish Chander Dhanabalan
IMEM-CNR
Parma, Italy
ESR fellow in European Project Nanowiring

Introduction

3C-SiC nanowires:

- High surface/volume ratio of 3C SiC nanowires
- Carrier quantum confinement.
- Unique electronic, field-emitting, hydrophobic and optical propeties
- Thermal , chemical and mechanical properties

SiC-SiO_2 nanowires:

- Surface functionalization
- High photocatalytic activity
- High Biocompatibility for biomedical applications

Projects

Nanowiring - Marie Curie Initial Training Network

sensing applications

Nanowires as bio-sensors

energy harvesting

Thermoelectric devices

BioNiMed (Innovative Hybrid Nanosystem s for biomedical applications)

Nanomedicine

Surface functionalized NWs
with magnetic nanoparticles
for bio-medical applications

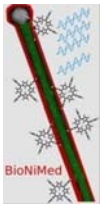

First phase of the projects to optimize the synthesis procedures for such applications.

State of the Art - SiC/SiO_2 core shell

Our group succeded to grow with nickel catalyst

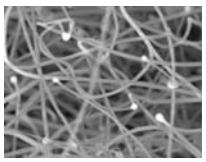

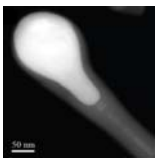

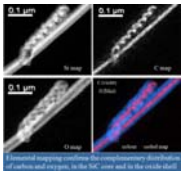

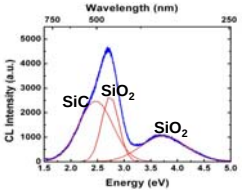

Diameter: ~60 nm Length: ~10 µm
core Diameter: ~20 nm
Core: 3C-SiC with <111> direction of growth
Shell: SiO2 amorphous
Particle tip: alloy Ni-Si

Synthesis of SiC/SiO_2 core shell NWs

Parameters we changed and optimized

T_{growth}, precursors, catalyst

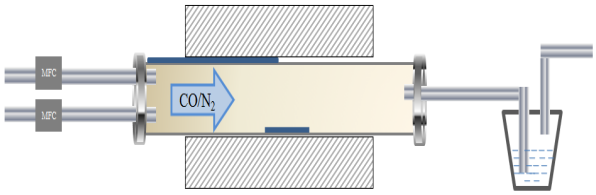

Thermal CVD: Experimental Conditions:

Si, $Ni(NO_3)_2$, $Fe(NO_3)_3$
T: 1050, 1070, 1100, 1150 °C
Growth time: 5 – 60 min.
CO, N_2

CVD grown Fe catalyzed SiC/SiOx NWs

Fe compounds are less Cytotoxic than Ni componds

Avg. Diameter: ~70 nm,
Length: ~10 µm

Core thickness: 19 nm

Fe-Si Alloy on tip

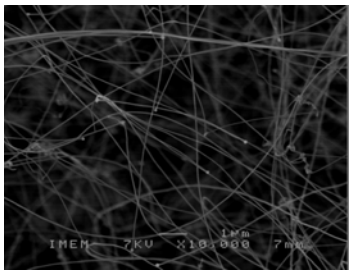

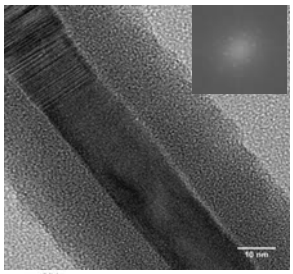

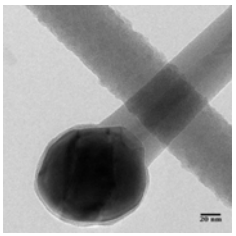

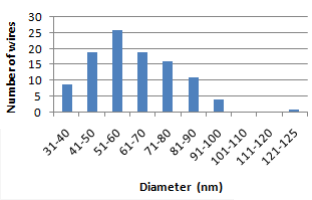

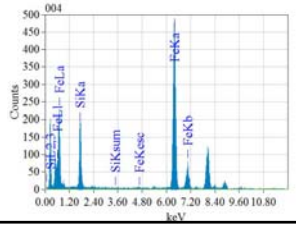

Temperature effect of SiC/SiO_2 Core shell NWs

Study of temperature interval to form core shell structure

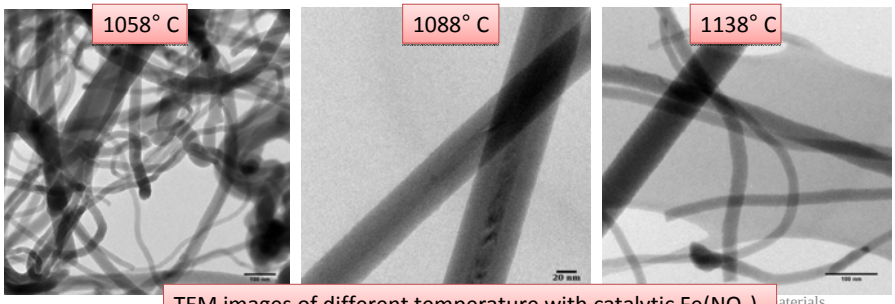

TEM images of different temperature with catalytic $Fe(NO_3)_3$

nanowiring sensing · lighting · energy · electronics

imem

Growth Mechanism for SiC/SiO_2 Core shell NWs

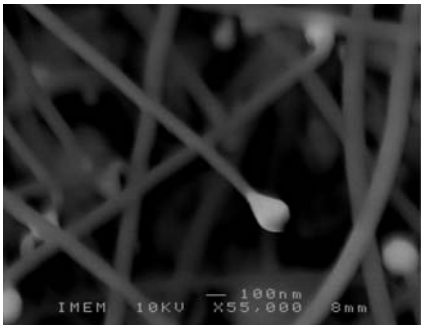

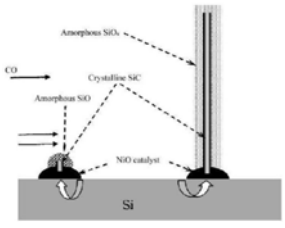

Park, B., Ryu, Y., & Yong, K. (2004). Surface Review and Letters, 11(4-5), 373-378.

nanowiring sensing · lighting · energy · electronics

imem

Conclusions

- Sucessfully grown SiC/SiO_2 core shell NWs - Fe as catalytic tip for nanomeical (bio sensing) applications.
- Optimised the growth paramaters for SiC/SiO_2 core shell NWs .

Acknowledgements

Prof. Giancarlo Salviati, Dr. Giovanni Attolini, Dr. Marco Negri,
Dr. Francesca Rossi, Dr. Marco Campanini,,Dr. Filippo Fabbri,
Dr.Tullo Besagni, Dr.Elena Bedogni, Prof. Franca Bigi, Dr. Elisa Buffagni
Dr. Matteo Bosi, Dr. Joice Sophia Ponraj, Prof. Alessandra Catellani ,
Prof. Andrea Zappettini, Dr. Davide Calestani, Dr. Marco Villani,
Mr. Giacomo Benassi, Mr. Nicola Zambelli, Dr. Nicola Coppedè,

THANKS FOR YOUR KIND ATTENTION

Microstructural design of coatings produced by powder spraying

Dina V. Dudina
Institute of Solid State Chemistry and Mechanochemistry SB RAS, Novosibirsk, Russia,
E-mail: dina1807@gmail.com

Abstract

The microstructure of coatings produced by spraying of powder particles depends on the feedstock characteristics as well as on the spraying parameters. During thermal spraying, when chemical reactions of the sprayed particles with the spraying atmosphere are allowed and the particle temperature is varied, interesting microstructural features of the coatings emerge. In cold spraying, in which the compositional and phase changes are avoided thanks to the use of high velocities rather than high temperatures for efficient deposition, the microstructural design of the coatings is possible through the ex-situ variation of the microstructure of the feedstock powder particles.

Examples of microstructural design

Modern detonation spraying facilities allow precise control over the amounts of fuel and oxidizer as well as their ratio [1]. As the latter is varied, reducing or oxidizing conditions of spraying can be created. At the same time, the fuel to oxidizer ratio and the explosive charge affect the particle temperature upon deposition presenting thereby chemical and thermal "tools" useful in the design of composite coatings.

We have found that in composite coatings TiO_2-Ag produced by the detonation spraying method, the coalescence of Ag droplets occurs if titanium dioxide remains solid during the spraying. However, when the two components are in a molten state, dispersion of the droplets of the lower-melting temperature component is favored. At an explosive charge of 30%, titanium dioxide does not melt while silver particles experience melting. The molten silver droplets coalesce, which results in the formation of Ag agglomerates in the coatings several microns in size. At an explosive charge of 60%, the sprayed composite particles are in a molten or semi-molten state [2]. These conditions favor dispersion of silver molten droplets into submicron and nanoparticles as is seen from Fig.1. Bright particles distinguished in the back-scattered electron image of the surface of the TiO_2-2.5vol.%Ag coatings correspond to the silver phase.

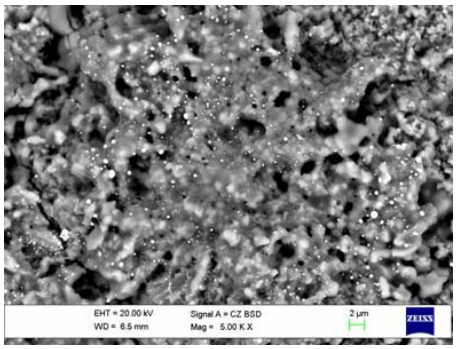

Fig.1. Back-scattered electron image of the surface the TiO_2-2.5vol.%Ag coating formed by detonation spraying at an explosive charge of 60% and O_2/C_2H_2 =1.05.

Coatings produced by detonation spraying of Ti_3Al powders in an oxidizing atmosphere were composed of titanium oxides and possessed a lamellar microstructure [3]. Distinct alternating bright and dark layers can be distinguished in the back-scattered electron image of the deposit (Fig.2) confirming the presence of at least two oxide phases differing in the Ti/O ratio. This can be explained as a result of flattening of the particles still having an inner core with a higher Ti/O ratio compared to that of an outer layer, which has been more severely oxidized.

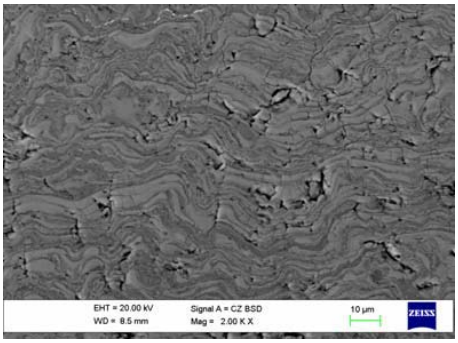

Fig.2. Back-scattered electron image of the microstructure of the coating formed by detonation spraying of Ti_3Al at an explosive charge of 50% and O_2/C_2H_2 =1.50.

In cold spraying, for which chemical reactions involving the sprayed material are not typical [4], the microstructural design of the coatings is possible through the ex-situ preparation of the composite particles of a particular structure. Particles of a softer matrix can be surface-decorated by the particles of a harder phase, which will determine the distribution of the harder-phase particles in the cold sprayed coating.

Acknowledgements

This work is supported by Program V.36.4 of SB RAS (2010-2012) and Integration Project №15 of SB RAS (2012-2014).

References

[1] V.Ulianitsky, V.Shtertser, S.Zlobin, I.Smurov. **Computer-controlled detonation spraying: from process fundamentals toward advanced applications.** Journal of Thermal Spray Technology 20 (2011) 791-801.

[2] D.V.Dudina, S.B. Zlobin, N.V. Bulina, A.L.Bychkov, V. N.Korolyuk, V.Yu.Ulianitsky, O.I.Lomovsky. **Detonation spraying of TiO_2-2.5vol.%Ag powders in a reducing atmosphere.** Journal of the European Ceramic Society 32 (2012) 815-821.

[3] D.V. Dudina, M.A. Korchagin, S.B. Zlobin, V.Yu. Ulianitsky, O.I. Lomovsky, N.V. Bulina, I.A. Bataev, V.A. Bataev. **Compositional variations in the coatings formed by detonation spraying of Ti_3Al at different O_2/C_2H_2 ratios.** Intermetallics 29 (2012) 140-146.

[4] A.Sova, D.Pervushin, I.Smurov. **Development of multimaterial coatings by cold spray and gas detonation spraying.** Surface & Coatings Technology 205 (2010) 1108-1114.

"Heating efficacy of bimetallic FePt magnetic nanoparticles"

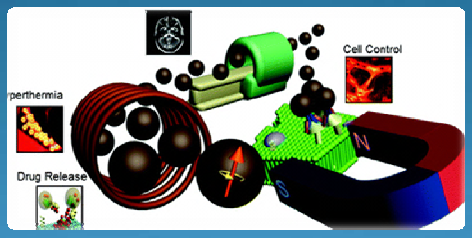

Makrygiannis Evangelos
Undergraduate student
Department of Physics, Aristotle University of Thessaloniki

TABLE OF CONTENTS

- Magnetic nanoparticles
- Properties
- Biomedical Applications
- Bachelor Thesis: *Heating efficacy of bimetallic FePt magnetic nanoparticles*
  - *Introduction*
  - *Hyperthermia*
  - *Experimental procedures*
- Conclusions

Magnetic nanoparticles

Magnetic nanoparticle: Spheres with diameter < 50 nm, < 100.000 atoms

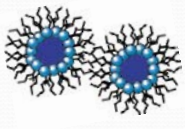

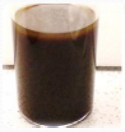


- The last 20 years following the novel properties, enhanced features of magnetic multilayers, scientists aimed their efforts to analogous system with 3 nanodimensions.
- Initially metallic nanoparticles of Ni, Fe, Co randomly oriented in solution or on substrates.
- Gradually, bimetallic particles with varying **stochiometry**, **morphological** features and **tunable** nano-, micro- & macro- scopic **magnetic** behavior.

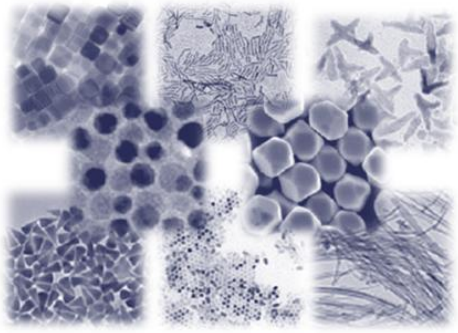

Properties

Bulk vs Nano

- **Region between bulk and atomic scale**
  - Increase of surface atoms
  - Surface structure modulation
  - Tunable electronic, optic, magnetic and catalytic properties
- **Reduced dimensionality effects**
  - Mono-Multidomain Limit
  - Superpamagnetic Limit
- **Surface effects**
  - Magnetization tuning
  - Magnetic anisotropy increase(shape, interface)
  - Magnetic coupling effects (intra, or inter particle)

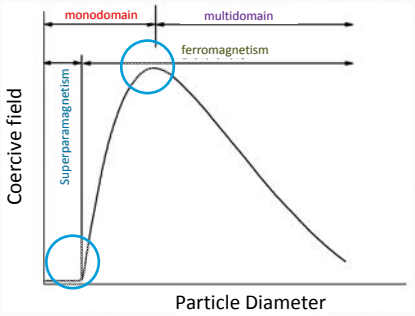

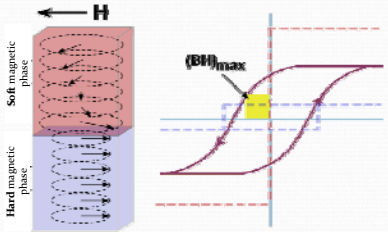


Biomedical Applications
Cell Regeneration
Magnetic Hyperthermi
Drug Delivery
Therapy
Cellural Proteomic
Cell Capture
MRI
Diagnosis
Handling
Bioseparation
Cell Tracing
BioSensing

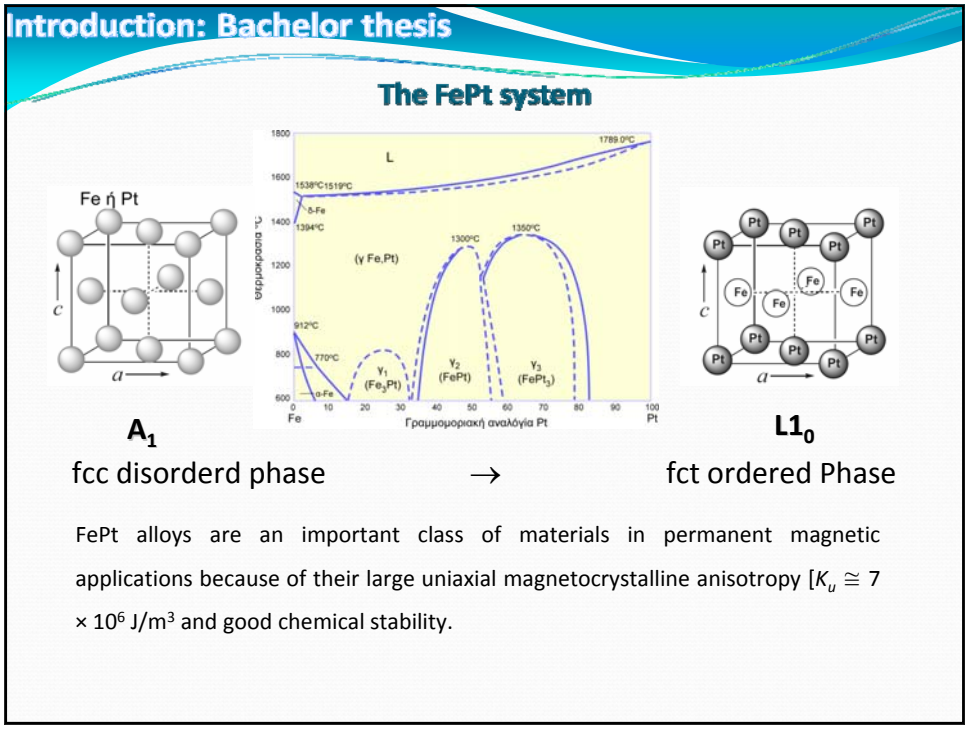
Introduction: Bachelor thesis
The FePt system
Fe ή Pt
L
(γ Fe,Pt)
Γ1 (Fe3Pt)
Γ2 (FePt)
Γ3 (FePt3)
Γραμμομοριακή αναλόγια Pt
A1
L10
fcc disorderd phase → fct ordered Phase
FePt alloys are an important class of materials in permanent magnetic applications because of their large uniaxial magnetocrystalline anisotropy [$K_u \cong 7 \times 10^6$ J/m^3 and good chemical stability.

Hyperthermia: Bachelor thesis

Hyperthermia types

- **Whole body hyperthermia** : the systemic temperature has to be carefully controlled to ~41.8 ◦C by a heat bath.
- **Local hyperthermia**: the temperature increase with respect to standard temperature of the human body is considered to be therapeutically useful over a relatively broad temperature range where different mechanisms of cell damaging occur with increasing temperature.



- **Local intracorporal heat generation by**: microwave radiation, capacitive or inductive coupling of radiofrequency fields, implanted electrodes, ultrasound, lasers.

- **Hyperthermia:** Treatments at temperatures of 41–45 ◦C for up to few hours—actually denoted as hyperthermia—need a combination with other assisting toxic agents (mostly irradiation or chemotherapy) for reliable damage of tumor cells.
- **Thermoablation:** aims for the thermal killing of all tumor cells by applying temperatures in excess of at least 50 ◦C in the tumor region for exposure times of at least few minutes.

Hyperthermia: Bachelor thesis

Magnetically Mediated Hyperthermia

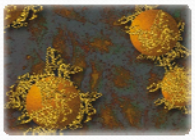
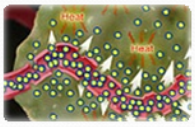

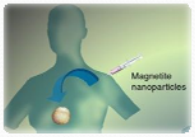

- Deposit of magnetic material in the tumor which is heated by means of an external alternating magnetic field.
- macroscopic magnetic implants (‘seeds’) currently in clinical use
- magnetic nanoparticles currently in clinical trials
  - **heat generation potential** appears beneficial
  - **direct tumor targeting** through blood circulation
  - **localized heat generation**
  - **self-limitation of the temperature** enhancement by suitable Curie temperature

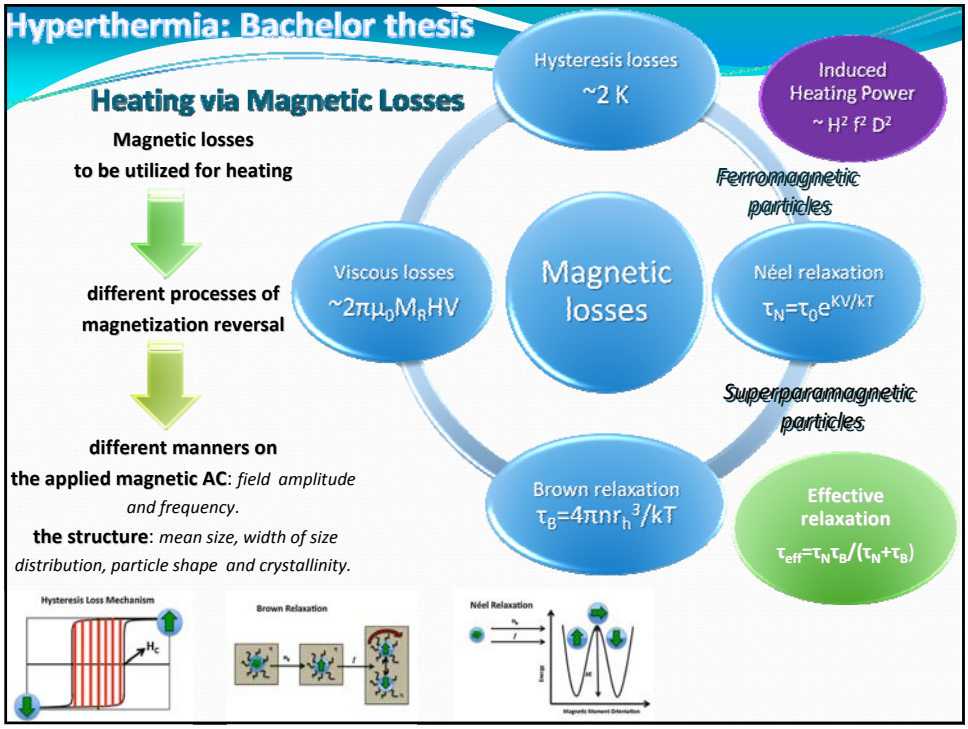

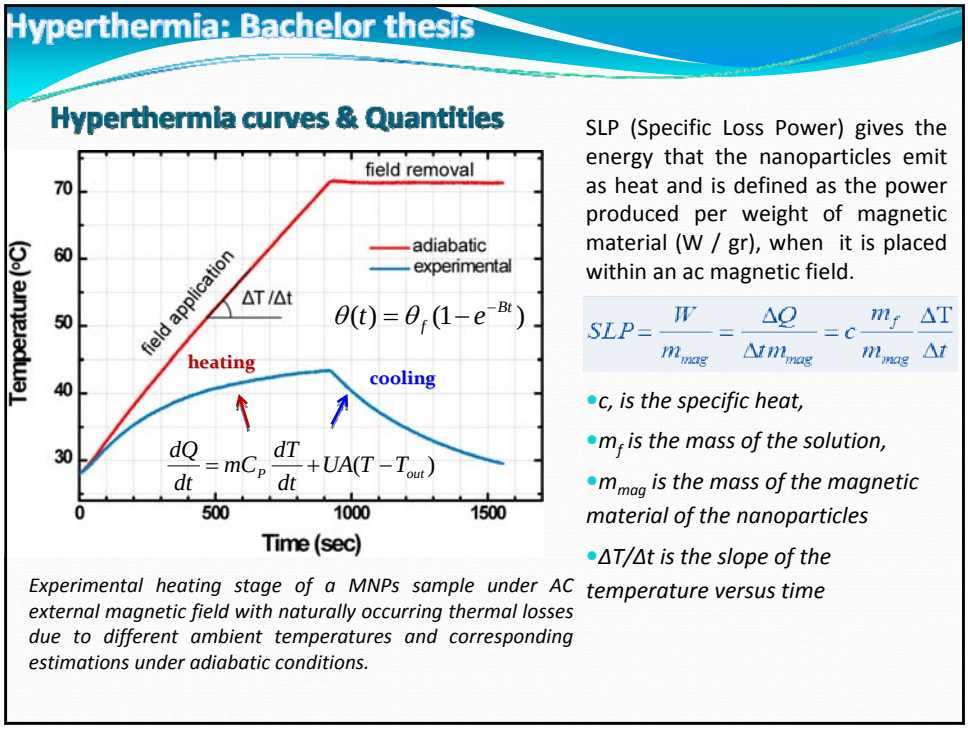

Experimental heating stage of a MNPs sample under AC external magnetic field with naturally occurring thermal losses due to different ambient temperatures and corresponding estimations under adiabatic conditions.

SLP (Specific Loss Power) gives the energy that the nanoparticles emit as heat and is defined as the power produced per weight of magnetic material (W / gr), when it is placed within an ac magnetic field.

$$SLP = \frac{W}{m_{mag}} = \frac{\Delta Q}{\Delta t\, m_{mag}} = c\,\frac{m_f}{m_{mag}}\,\frac{\Delta T}{\Delta t}$$

- *c, is the specific heat,*
- *m_f is the mass of the solution,*
- *m_{mag} is the mass of the magnetic material of the nanoparticles*
- *$\Delta T/\Delta t$ is the slope of the temperature versus time*

Experimental Procedures: Bachelor thesis

Synthesis of FePt: Thermal Decomposition

- Platinum acetylacetonate (197 mg, 0.5 mmol), 1,2-tetradecanediol (345mg, 1.5 mmol) and dioctyl ether (20 mL) were mixed and heated to 100°C under airless conditions.
- At this temperature, oleic acid (0.16 mL, 0.5 mmol), oleylamine (0.17mL, 0.5mmol) and $Fe(CO)_5$ (0.13 mL, 1 mmol) were injected, and the mixture was further heated to reflux (295°C).
- The refluxing was continued for 30 min.
- Then the reaction mixture was cooled to room temperature.
- The black product was precipitated by adding toluene (10 ml) and ethanol (60 ml), and separated by centrifugation.
- The black precipitate was redissolved in toluene (~10 ml) in the presence of oleic acid (10 μL) and oleylamine (10 μL), and centrifuged to remove any insoluble species.
- Then the product was additionally precipitated by adding 30-40 ml ethanol and centrifuging.
- The particles were redispered in toluene containing oleic acid (5μL) and oleylamine (5μL) and stored for further use.

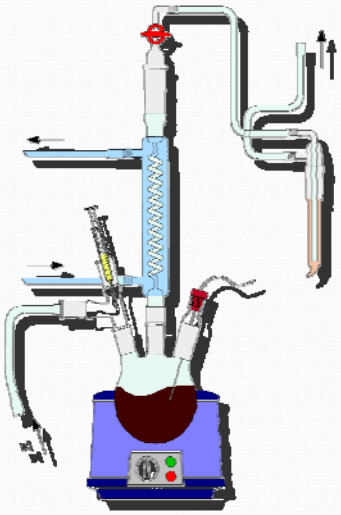

Experimental Procedures: Bachelor thesis

Structure & Magnetism

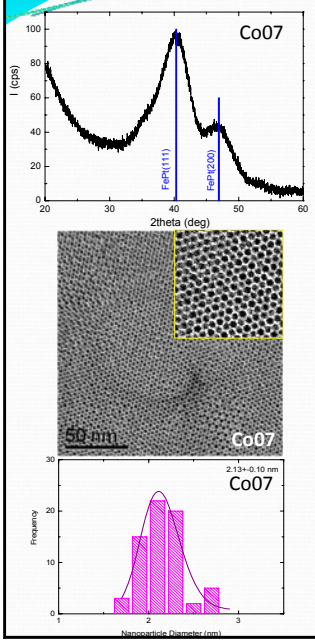

- X-ray diffraction (XRD) measurements and transmission electron microscopy (TEM) imaging are used to verify the obtained crystal structure, the actual particles size and the monodispersity.
- The magnetic properties of the nanoparticles are evaluated at room temperature using static magnetometry (VSM & SQUID). ZFC-FC and hysteresis loops were recorded.

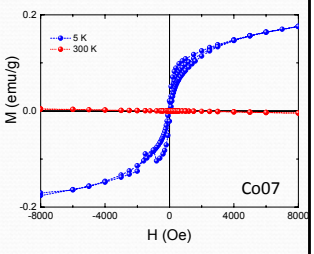

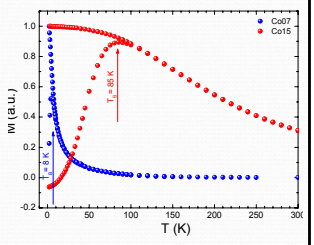

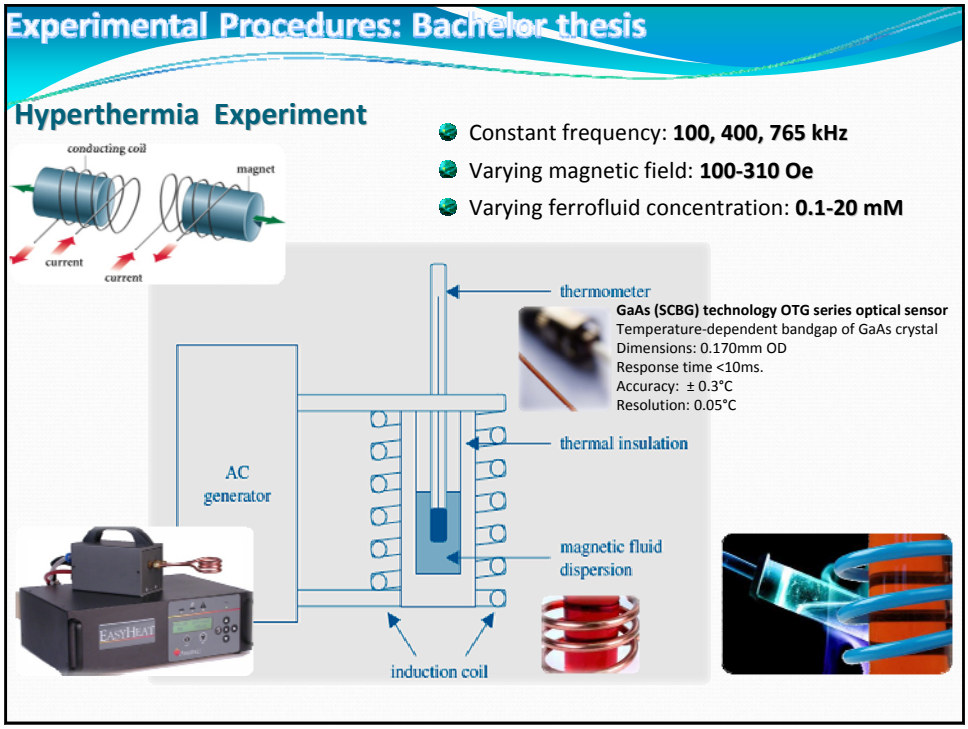
Experimental Procedures: Bachelor thesis
Hyperthermia Experiment
Constant frequency: 100, 400, 765 kHz
Varying magnetic field: 100-310 Oe
Varying ferrofluid concentration: 0.1-20 mM
conducting coil
magnet
current
current
thermometer
GaAs (SCBG) technology OTG series optical sensor
Temperature-dependent bandgap of GaAs crystal
Dimensions: 0.170mm OD
Response time <10ms.
Accuracy: ± 0.3°C
Resolution: 0.05°C
thermal insulation
AC
generator
magnetic fluid
dispersion
induction coil

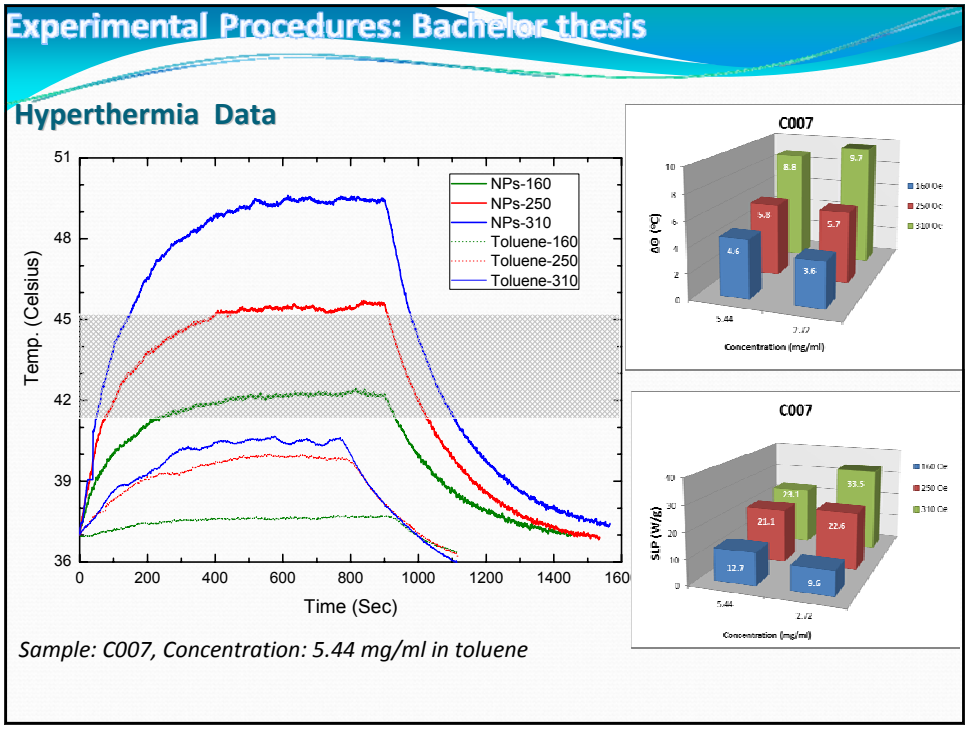
Experimental Procedures: Bachelor thesis
Hyperthermia Data
Temp. (Celsius)
Time (Sec)
NPs-160
NPs-250
NPs-310
Toluene-160
Toluene-250
Toluene-310
C007
ΔΘ (°C)
Concentration (mg/ml)
C007
SLP (W/g)
Concentration (mg/ml)
Sample: C007, Concentration: 5.44 mg/ml in toluene

Conclusions

- *Controllable sizes ranging from **a few up to tens of nanometres**,*
- *they can be coated with biological molecules to make them **interact with or bind to a biological entity**, thereby providing a controllable means of 'tagging' or addressing it.*
- *They '**act from a distance**', combined with the intrinsic penetrability of magnetic fields into human tissue, opens up new therapy pathways.*

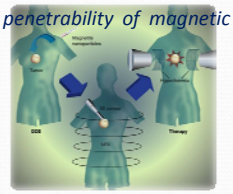

May be used as hyperthermia agents

- *as can be made to **resonantly respond to a time-varying magnetic field**, with advantageous results related to the transfer of energy from the exciting field to the nanoparticle.*
- *satisfy the request for **high-enough thermal efficiency** and **minimum treatment duration***
- ***Tunable particle properties**, electromagnetic field parameters for **reliable cancer therapy**.*
- *Magnetic hyperthermia may act synergistically with chemotherapy and radiotherapy.*

Synthesis and characterization of silicon carbide nanowires

Marco Negri

Università degli Studi di Parma
Facoltà di Scienze MM. FF. NN.

CNR – Imem institute
Institute for materials
for electronics and magnetism

Summer school on micro- and nano- structural characterization of materials

Why SiC nanowires?

SiC

- high temperature stability
- thermal conductivity
- Hardness
- chemical stability
- biocompatibility

high temperature and high power devices which can operate in harsh environments

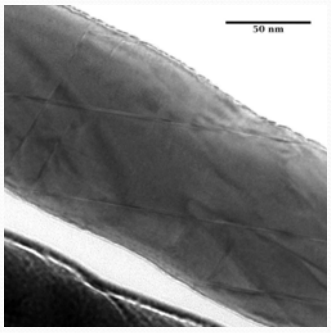

Nanowires 1-D nanostructures

Device miniaturization in nano-electronics and nano-optoelectronics
Superior mechanical properties
elasticity and strength of a single nanowire are much higher than that of bulk SiC

[E. W. Wong, P. E. Sheenhan and C. M. Lieber, Science, 277, 1971-1975 (1997)]

High surface/volume ratio → Sensing
Quantum confinement effects → fundamental research
Nanomedical applications

Vapour phase epitaxy

Advantages:
High purity, possibility to grow at low pressure, reducing athmospere

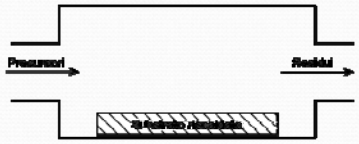

«Cold wall» reactor

Precursors: Silane (SiH_4), propane (C_3H_8) 3% in H_2
Carrier gas: Hydrogen
Substrate: Silicon
Catalyst: Ni layer sputtered on the substrate
Growth temperature: 1100°C

Self assembly growth mechanism of nanowires

Vapour-Liquid-Solid
Vapour phase precursors
Solid-Liquid-Solid
Solid phase precursors
Vapour-Solid
Catalyst and precursors from vapour phase

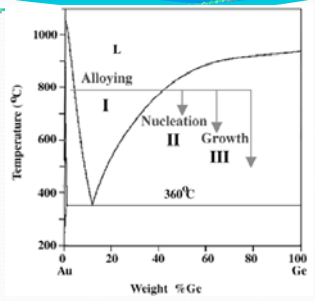

In-situ observation of VLS growth
(Ge NWs grown with Au catalyst)

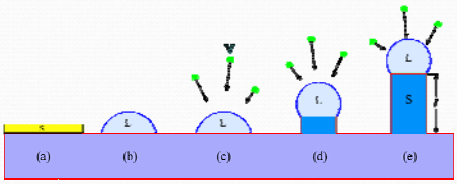

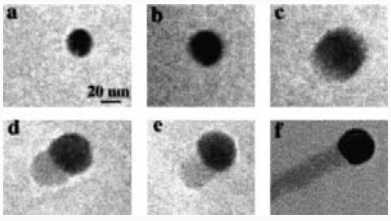

Stach EA, Pauzauskie PJ, Kuykendall T, Goldberger J, He R, Yang P. Nano Letters. 2003;3(6):867-9

SiC NWs: dewetting

dewetting

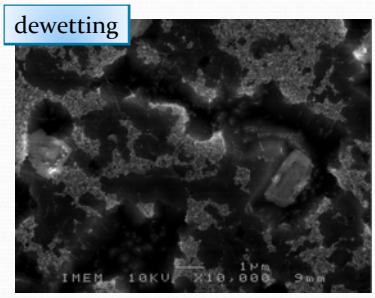

Growth

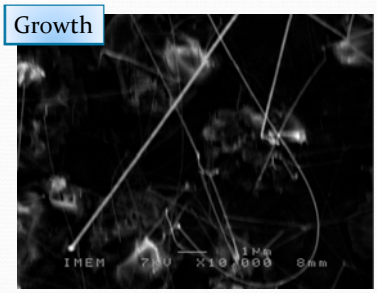

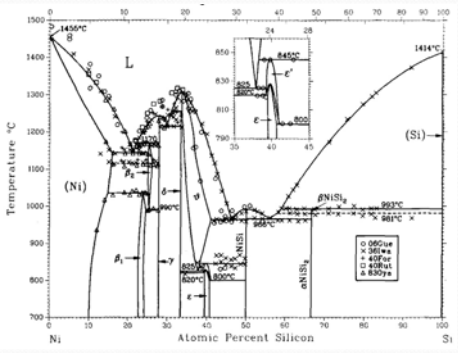

Eutectic points: 1143°C, 1215°C, 964°C and 966°

SiC nanowires

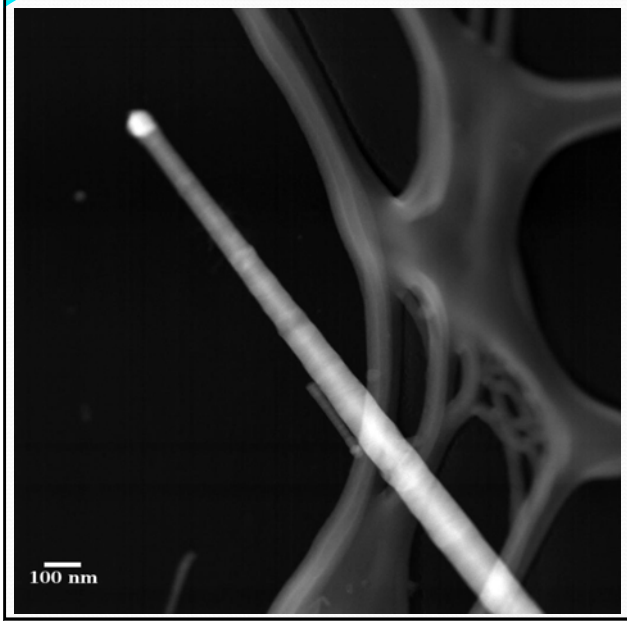

Base diameter: ~60-130 nm
Length: ~10 μm

SiC nanowires

3C-SiC with <111> axis parallel to growth direction

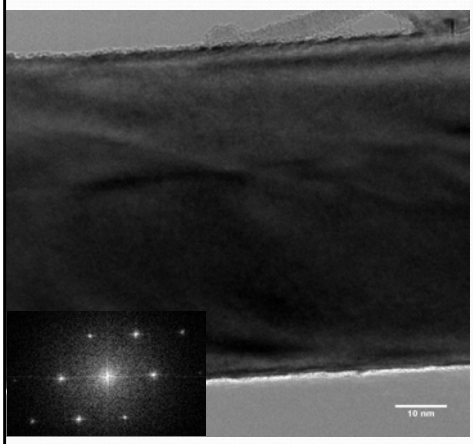

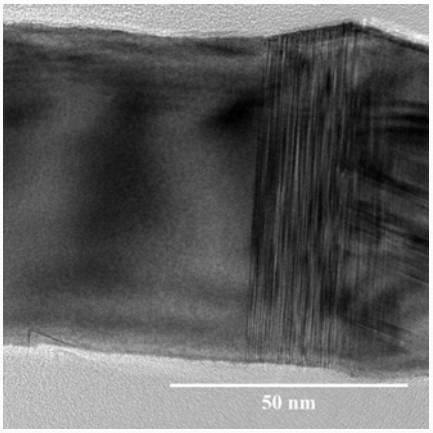

highly crystalline wires
presence of planar defects (stacking faults and twins) parallel to (111) planes

SiC nanowires: growth temperature

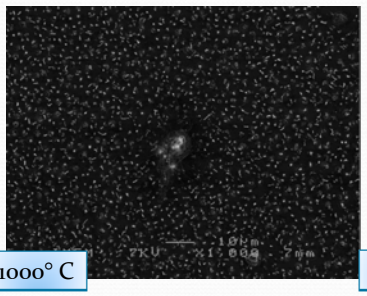

1000° C

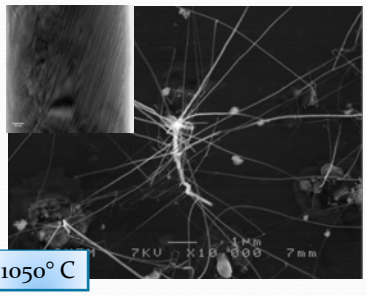

1050° C

Conclusions

Epitaxial growth of SiC nanowires

Possibility to achieve a control on the shape and distribution of nanowires on the substrate

Summer school on micro- and nano- structural characterization of materials

Thank you for your kind attention

Thanks to:

Dr. Francesca Rossi and Dr. Marco Campanini for TEM images

Prof. Giancarlo Salviati, Dr. Giovanni Attolini, Dr. Filippo Fabbri, Dr. Sathish Chander Dhanabalan, Dr. Matteo Bosi, Dr. Marco Campanini, Prof. Franca Bigi, Dr. Elena Bedogni, Dr. Antonio Mega, Dr. Elisa Buffagni, Dr. Tullo Besagni